The RASS-SDSS Galaxy Cluster Survey.

Correlating X-ray and optical properties of Galaxy Clusters

DISSERTATION
der fakultät für Physik der
Ludwigs-Maximilians-Universität
München
zur Erlangung des Grades
Doktor der Naturwissenschaften
Dr. rer. nat.

vorgelegt von

Paola Popesso
aus Padua, Italien

München, den 27. April 2006

The RASS-SDSS Galaxy Cluster Survey

Correlating X-ray and optical properties of Galaxy Clusters

Ph.D. Student: Paola Popesso
Advisor: Prof. Hans Böhringer
München, den 27. April 2006

Contents

Chapter 1

Introduction

1.1 Introduction

The galaxy clusters are the largest gravitationally bound systems in the universe. Clusters consist of three components: galaxies, gas, and dark matter. The galaxies themselves contribute the least, at most a few percent, to the total mass (Sarazin 1988). The remainder consists of diffuse, hot gas at densities between 10^{-4} and 10^{-2} cm^{-3} and temperatures of $10^7 - 10^8$ K (the intracluster medium, or ICM) and an unseen, presumably collisionless component which is needed to explain the gravitational stability of clusters (the dark matter). Through its X-ray emission, the ICM, which contributes from 10% to 20% of the total mass needed to bind most clusters, yields the highest-quality observational data concerning a cluster's dynamical state. As example, Fig. 1.1 shows the optical (left-hand panel) and the X-ray (right-hand panel) appearance of the Coma cluster, one of the nearest rich clusters of galaxies.

The two most obvious means of studying clusters of galaxies are by observing the optical light emitted from the constituent galaxies or the X-ray emission from the hot intracluster gas. Clusters of galaxies, bound ensambles of hundreds of galaxies like our own, are an ideal environment to study galaxy evolution and to learn how this is affected by different physical processes: gravity, starbursts and star formation, interactions with the intergalactic medium and energy emitted from black holes. Since the very early works of Hubble in the thirties, it has been recognized that galaxies in dense environments differ systematically from those in low-density regions in their morphological types, stellar populations and gaseous content. In the local universe spiral galaxies, gas rich and star forming, are abundant in the low-density field, while S0 and elliptical galaxies (spheroidals with almost no gas and ongoing star formation) dominate the densest regions of the Universe in the cores of galaxy clusters. When during the history of the Universe and why such environmental differences were established is currently one of the subjects of most intensive investigation in the international astrophysical community.

Two general paradigms have been proposed in the last twenty years to account for the statistical properties of the local galaxies along the Hubble sequence, and for the specific features of the faint, high-redshift galaxies unveiled by deep surveys.

In the picture of monolithic collapse, galaxies form at a given epoch, when the physical conditions of the universe are favorable, and evolve at different rates which are fixed by the initial conditions. In this prospect, the influence of environment, such as galaxy merging or cannibalism, is only considered as a correction to the main evolutionary stream.

In the picture of hierarchical collapse, on the contrary, bigger galaxies form from the merging of smaller ones, and in turn merge to form still bigger galaxies, and so on. The beginning of the process took place at some early redshift z $\sim$ 30 to 10, when the first objects cooled and the first stars probably formed (and reionized the gas of the universe), and the formation is still going on now. As a result, the "epoch of galaxy formation" can be defined e.g. as the epoch when the first stars formed, when 50% of the stars have formed,

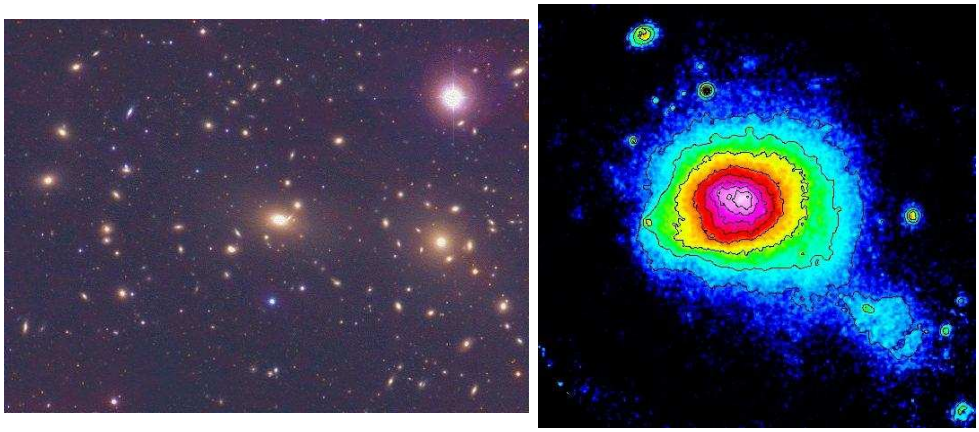

Figure 1.1: *Left: optical appareance of the Coma Cluster. Right: X-ray appareance of the same object.*

or when the morphology was fixed after the last major merging event. In this prospect, the influence of environment dominates the evolution, and the very notions of galaxy formation and evolution appear as closely intertwined.

Moreover, clusters can teach us a great deal about cosmology. As shown in Fig. 1.2, galaxies are not smoothly distributed across the sky. There are small regions of high galaxy density and large areas encompassing only relatively few galaxies. The distributions of galaxies on the sky shows a net-like structure in which thin walls and filaments surround large voids. The galaxy clusters are the nodes of this network. Therefore, clusters trace out the Large-Scale Structure (LSS) of the universe just as do galaxies and can be used to study the LSS distribution and formation. However, there are several cluster properties that are interesting by themselves. If clusters provide a 'fair sample' of the universe, then the fraction of their mass in baryons should equal the universal baryon fraction, known as Ω_b/Ω_M. The present number density of clusters is a measure of the amplitude of fluctuations in the universe on scales of around 8Mpc. The evolution of this number density (vs mass or temperature) with redshift can determine the mass density parameter, known as Ω_M, and possibly determine the equation of state (and nature) of the dark energy believed to be causing the expansion of the universe to accelerate.

From this brief introduction it emerges that the galaxy clusters have a twofold importance: first as laboratories of galaxy formation and evolution, and second as cosmological tool. The aim of this thesis is to study galaxy clusters from these two perspectives. For this purpose we use the largest optical and X-ray surveys ever realized, the Sloan Digital Sky Survey (SDSS) and the Rosat All Sky Survey (RASS), respectively, to conduct a multiwavelenght study of the properties of galaxy clusters. The project is called RASS-SDSS Galaxy Cluster Survey reflecting the name of the two big surveys used for this work. All the analises

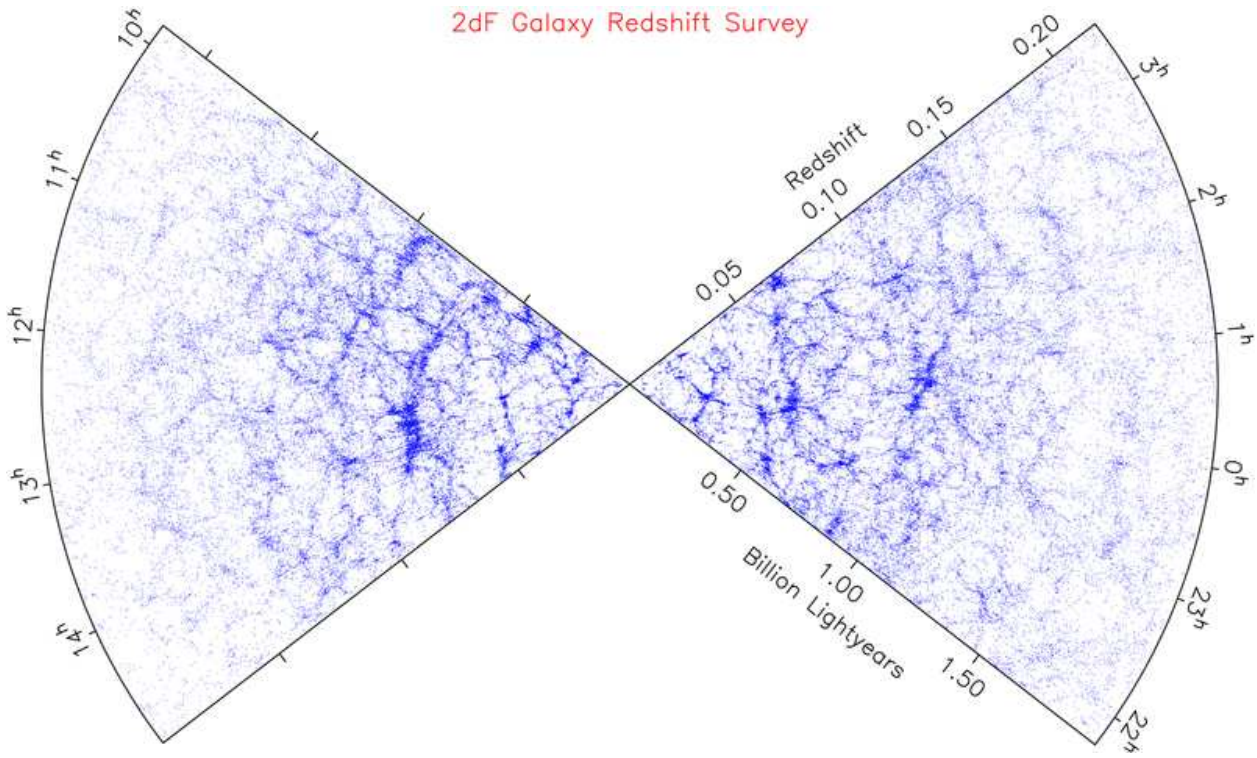

Figure 1.2: *Cone diagram illustrating the clustering pattern seen in a 4 deg slice of the 2dF Galaxy Redshift Survey.*

are performed on two clusters samples specially created for the survey: the RASS-SDSS galaxy cluster catalog, which comprises 130 X-ray selected clusters spanning a large mass range from the low mass groups to the very massive clusters; a subsample of 137 optically selected, isolated and spectroscopically confirmed Abell clusters.

In the first part of the project, we use cluster of galaxies as laboratories of galaxies formation. The aim of the work is to understand which role play the gravitational processes on large scale, the galaxy merger and collisions and the interaction with the hot X-ray emitting Intracluster Medium in the process of galaxy formation and evolution. For this porpuse, we use the SDSS photometric and spectroscopic data to calculate several properties of the cluster galaxy population such as the galaxy Luminosity Function (LF), the morphological type mix, the integrated and mean Star Formation Rate (SFR) and the galaxy spatial distribution in clusters. The high statistical significance of the cluster samples used in the analysis (the RASS-SDSS sample and the Abell cluster sample) in terms of their mass and X-ray luminosity allows us to follow the variation of those galaxy properties as a function of the cluster mass, velocity dispersion and X-ray luminosity. We interpret any dependence of the properties of the cluster galaxy population on a cluster global property as a link between the galaxy formation and evolution processes and a particular environmental effect. Moreover, we compare the results of this analysis with the predictions of the two main theoretical scenarios of galaxy formation, the hierarchical and the monolithic models, to discriminate between the two pictures.

In the second part of the RASS-SDSS survey, galaxy clusters are considered as cosmological tool. All the cosmological tests applied to clusters of galaxies require cluster samples highly complete in mass. The cluster dynamical mass is not an observable and, therefore, the detection and selection methods have to be based on other cluster observable properties such as their optical or X-ray emission. So far the X-ray selection methods were the most used for creating samples of galaxy clusters due to the assumption that the X-ray luminosity L_X is an excellent tracer of the cluster mass. Is this assumption correct? The aim of this work is to elucidate which component, galaxies or ICM, traces better the cluster mass in order to understand wheter different selection methods select the same cluster population. This will clarify which bias is introduced by the different cluster selection methods in the results of the cosmological tests applied to galaxy clusters. For this porpuse, we use the optical/X-ray multiwavelenght approach of the RASS-SDSS survey to study the relation of optical and X-ray appearance of galaxy clusters, expressed by the optical (L_{op}) and the X-ray (L_X) luminosities, respectively, with the cluster mass (M). First we analyse the slope and the scatter of the $L_{op} - M$ and $L_X - M$ relations in the X-ray selected RASS-SDSS cluster sample. The main motivation in deriving these dependences is to evaluate L_{op} and L_X, as predictors of the cluster mass and to compare the quality of the two quantities as predictors. The same analysis is applied to the optically selected Abell cluster sample. The results of the two analyses are, then, compared to study the variations introduced by the different cluster selection methods in the slope and in the scatter of the considered relations. As a

second step, we compare directely the X-ray and the optically selected cluster samples to investigate the presence of clusters which are luminous in the X-rays and particularly faint or undetected in the optical wavebands and viceversa. This could reveal whether the different selection criteria are able to identify the same cluster population above a given dynamical mass threshold.

The 'RASS-SDSS Galaxy Clusters Survey' series comprises 7 scientific papers which are inserted as part of the thesis. Four of the papers are accepted for pubblication on a scientific Journal ('Astronomy & Astrophysics') and three are submitted.

1.2 The theoretical framework

The finding of COBE of very small fluctuations in the temperature of the microwave background radiation, and its interpretation in terms of slight variations of the gravitational potential at the surface of last scattering, is a remarkable confirmation of the general theoretical framework of 'gravitational instability' for cosmic structure formation. According to this theory the early universe was almost perfectly smooth except for tiny density variations with respect to the general background density of the universe and related tiny velocity perturbations with respect to the general Hubble expansion. Because slight density enhancements exert a slightly stronger gravitational attraction on the surrounding matter, they start to accrete material from its surroundings as long as pressure forces are not sufficient to counteract this infall. In this way the overdensity becomes even more overdense, and their gravitational influence even stronger. The denser it becomes the more it will accrete, resulting in an instability which can ultimately cause the collapse of a density fluctuation to a gravitationally bound object. The size and mass of the object is of course dependent on the scale of the fluctuation. For example, galaxies are thought to have formed out of fluctuations on a scale of $\approx 0.5h^{-1}$Mpc, while clusters of galaxies have emerged out of fluctuations on a larger scale of $\approx 4h^{-1}$Mpc. The formation of voids fits in the same general scheme, having grown out of primordial underdensities in the matter distribution.

Given the size of the fluctuations, their total mass is determined by the average cosmological density, parametrized by Ω. The very low value of the amplitude of the primordial density fluctuations inferred from the COBE MWB measurements is a strong argument in favor of a high overall density of the universe. The value of Ω has the important implication that most likely the major share of matter in the universe does not consist of familiar baryons and leptons but of one or more as yet unidentified species of "dark matter".

The nature and amount of dark matter is also of substantial influence in determining the character of the initial density and fluctuation field, probably the most crucial issue in the structure formation saga. Hot dark matter, eg. neutrinos, is relativistic and smoothes any small density perturbations in the early universe. Hence, the consequence is a top-down scenario, where the first structures to form are the largest superclusters. These would

then fragment into smaller and smaller substructures resulting in clusters and individual galaxies. However, the most popular models at present are based on cold dark matter (i.e. not thermalized, non-baryonic, collisionless dust). In this scenario, the Cold Dark Matter (CDM) causes a hierarchical or "bottom-up" build-up of structure, where small objects that formed first merge into larger structures, which themselves merge to form galaxies, cluster of galaxies, and so on. A simple scheme of this structure formation scenario is given in Fig. 1.3, where the growth of a halo is proposed as a 'merger three'. The large scale density fluctuations will have an amplitude high enough such that by the time small scale clumps have completely collapsed the large scale structure in which they are embedded will already have contracted substantially. In those cases we expect to see more or less coherent walls and filaments in which the small scale clumps stand out like beads on a string. A large variety of models which are based on the hierarchical clustering hypothesis have been extensively studied using N-body simulations as well as analytical approximations. The Cold Dark Matter with a cosmological constant, the so called Λ Cold Dark Matter scenario (ΛCDM), represents the current concordance model of big bang cosmology that explains cosmic microwave background observations, as well as large scale structure observations and supernovae observations of the accelerating expansion of the universe. It is the simplest model that is in agreement with all the observations. Fig. 1.4 reproduces the standard result of a numerical simulation of the evolution of the structure in the hierarchical scenario. The small dark halo masses, on galactic scale, collapse first, and then merge to form bigger systems as galaxy clusters, which merge as well to form the so called superclusters. The filamentary large scale structure distribution obtained at low redshift mimic the galaxy distribution observed in the most recent galaxy redshift survey, like 2dF, as shown above in the Fig. 1.2.

1.2.1 Clusters as a cosmological tool

Galaxy clusters are the rare high peaks of the primordial density perturbations in the hierarchical clustering scenario for the formation of cosmic structures. They are relatively young objects, formed after the merger of smaller systems, galaxy groups or low mass clusters. Cosmic baryons, which represent approximately 10–15% of the mass content of the Universe, follow the dynamically dominant dark matter during the collapse. As a result of adiabatic compression and of shocks generated by supersonic motions during shell crossing and virialization, a thin hot gas permeating the cluster gravitational potential well is formed. For a typical cluster mass of 10^{14}–$10^{15} M_{\odot}$ this gas reaches temperatures of several 10^7 K, becomes fully ionized and, therefore, emits via thermal bremsstrahlung in the X-ray band.

As high peaks of the primordial density perturbations, clusters of galaxies are good tracers of the large scale structure mass distributions. They offer an alternative cosmological tool to the usual analysis of the galaxy distribution shown in Fig. 1.2. In fact, the cosmological tests are based on the direct comparison between the measurements and the prediction of

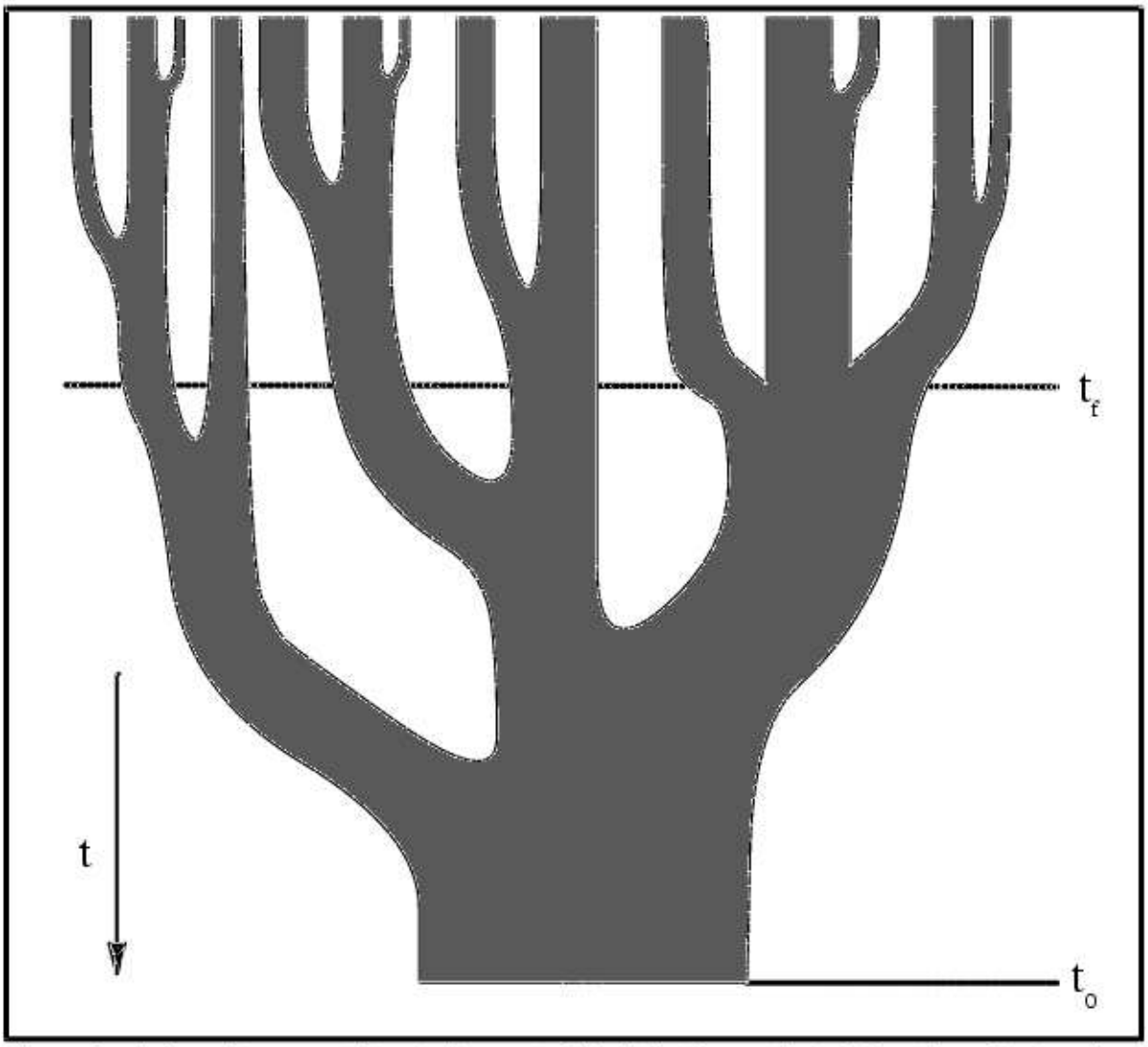

Figure 6. A schematic representation of a "merger tree" depicting the growth of a halo as the result of a series of mergers. Time increases from top to bottom in this figure and the widths of the branches of the tree represent the masses of the individual parent halos. Slicing through the tree horizontally gives the distribution of masses in the parent halos at a given time. The present time t_0 and the formation time t_f are marked by horizontal lines, where the formation time is defined as the time at which a parent halo containing in excess of half of the mass of the final halo was first created.

Figure 1.3:

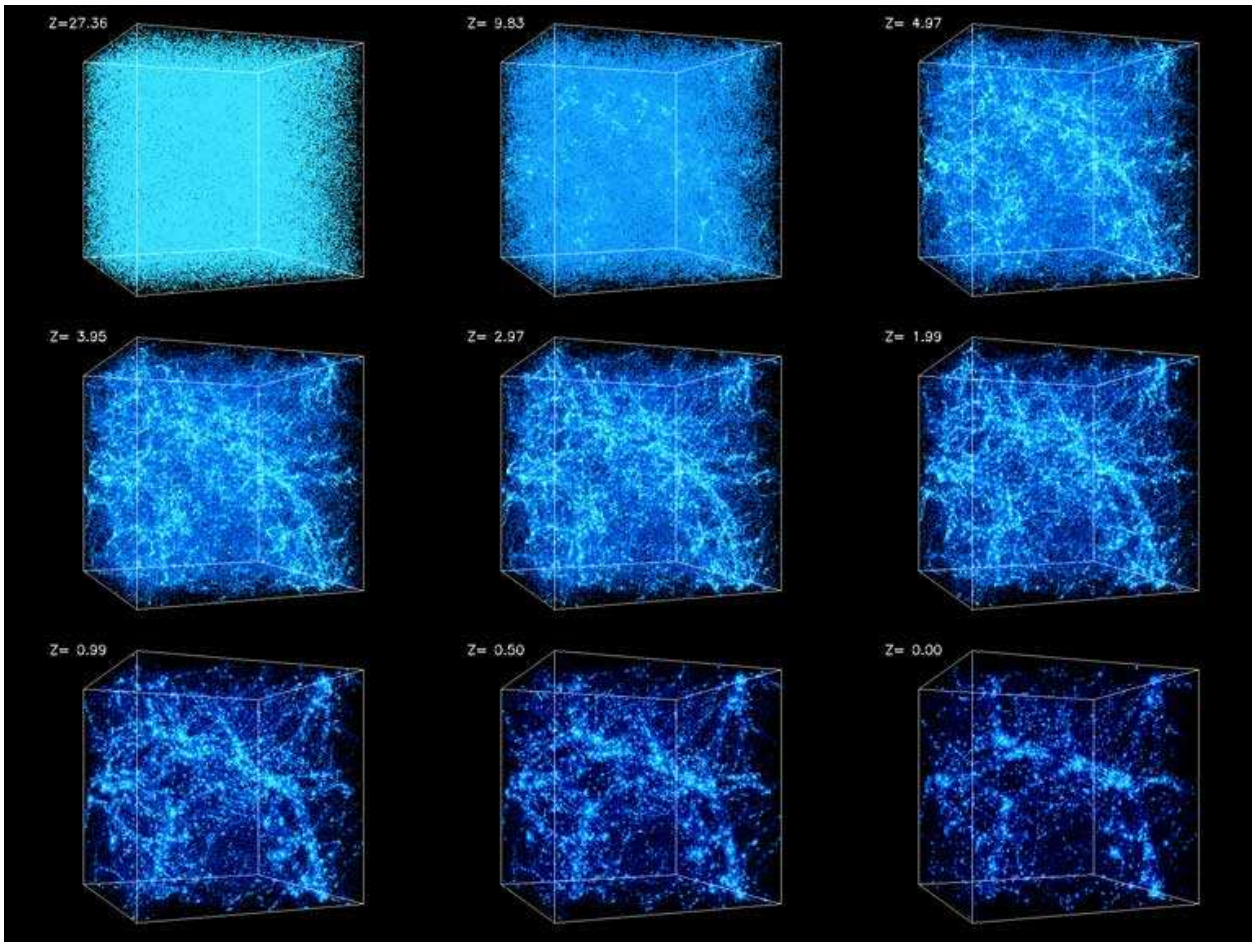

Figure 1.4: *Simulation of the formation and evolution of the dark matter halos in a numerical simulation. The 'z' in the picture corresponds to the redshift of the Hubble Law. The particular filamentary distribution of the dark matter in the low redshift box reproduces the large scale structure distribution observed in the 2dF survey of Fig. 1.2.*

the cosmological models. However, measurements give the spatial distribution of light and not the fluctuations of the underlying matter field. For the galaxies the connection between mass and the presence of stellar systems is complicated because nonlinear gravitational, dissipative, and radiative processes could lead to a nonlinear biasing up to rather large scales (e.g. Bertshinger et al. 1997 and references given therein). For rich clusters the relations between the mass and the presence of the hot intracluster medium is expected to be governed by comparatively simple biasing schemes (e.g. Kaiser 1984; Bardeen et al. 1986; Mo & White 1996), mainly driven by gravitation, and only slightly modified by dissipative processes. In this sense, rich clusters of galaxies are much easier to model and thus 'better' traces of the large scale distribution of matter.

The mass distribution of dark matter halos undergoing spherical collapse in the framework of hierarchical clustering is described by the Press-Schechter distribution (PS, Press &Schechter 1974). The number of such halos in the mass range $[M, M+dM]$ can be written as

$$n(M,z)dM \;=\; \frac{\bar{\rho}}{M}\, f(\nu)\, \frac{d\nu}{dM}\, dM \tag{1.1}$$

where $\bar{\rho}$ is the cosmic mean density. The function f depends only on the variable $\nu = \delta_c(z)/\sigma_M$, and is normalized so that $\int f(\nu)\, d\nu = 1$. $\delta_c(z)$ is the linear–theory overdensity extrapolated to the present time for a uniform spherical fluctuation collapsing at redshift z. This quantity conveys information about the dynamics of fluctuation evolution in a generic Friedmann background. It is convenient to express it as $\delta_c(z) = \delta_0(z=0)\,[D(0)/D(z)]$, where $D(z)$ is the linear fluctuation growth factor, which depends on the density parameters contributed by matter, Ω_m and by cosmological constant, Ω_Λ (e.g. Peebles 1993). The quantity $\delta_0(z)$ has a weak dependence on Ω_m and Ω_Λ (e.g. Kitayama & Suto 1997). For a critical–density Universe it is $\delta_0 = 1.686$, independent of z.

The r.m.s. density fluctuation at the mass scale M, σ_M, is connected to the fluctuation power spectrum, $P(k)$, by the relation

$$\sigma_M^2 \;=\; \frac{1}{2\pi^2} \int_0^\infty dk\, k^2\, P(k)\, W^2(kR)\,. \tag{1.2}$$

The dependence of the power spectrum on the wavenumber k is usually written as $P(k) \propto k^{n_{pr}} T^2(k)$, where $T(k)$ is the transfer function, which depends both on the cosmological parameters of the Friedmann background and on the cosmic matter constituents (e.g. fraction of cold, hot and baryonic matter, number of relativistic species; see Kolb & Turner 1989). The amplitude of $P(k)$ is usually expressed in terms of σ_8, the r.m.s. density fluctuation within a top–hat sphere of $8\,h^{-1}$Mpc radius. Finally, in Equation 1.2 $W(x)$ is the Fourier representation of the window function, which describes the shape of the volume from which the collapsing object is accreting matter. The comoving fluctuation size R is connected to the mass scale M as $R = (3M/4\pi\bar{\rho})^{1/3}$ for the top–hat window, i.e. $W(x) = 3(\sin x - x\cos x)/x^3$.

In their original derivation of the cosmological mass function, Press &Schechter (1974) obtained the expression $f(\nu) = (2\pi)^{-1/2} \exp(-\nu^2/2)$ for Gaussian density fluctuations. De-

spite its subtle simplicity (e.g., Monaco 1998), the PS mass function has served for more than a decade as a guide to constrain cosmological parameters from the mass function of galaxy clusters. Only with the advent of the last generation of N–body simulations, which are able to span a very large dynamical range, significant deviations of the PS expression from the exact numerical description of gravitational clustering have been noticed (e.g. Gross et al. 1998, Governato et al. 1999, Jenkins et al. 2001, Evrard et al. 2002). Such deviations are interpreted in terms of corrections to the PS approach (Sheth & Tormen 1999).

In practical applications, the observational mass function of clusters is usually determined over about one decade in mass. Therefore, it probes the power spectrum over a relatively narrow dynamical range, and does not provide strong constraints on the shape Γ of the power spectrum. Using only the number density of nearby clusters of a given mass M, one can constrain the amplitude of the density perturbation at the physical scale $R \propto (M/\Omega_m \rho_{crit})^{1/3}$ containing this mass. Since such a scale depends both on M and on Ω_m, the mass function of nearby ($z \lesssim 0.1$) clusters is only able to constrain a relation between σ_8 and Ω_m. Determinations of the cluster mass function in the local Universe using a variety of samples and methods indicate that $\sigma_8 \Omega_m^{\alpha} = 0.4 - 0.6$, where $\alpha \simeq 0.4 - 0.6$, almost independent of the presence of a cosmological constant term providing spatial flatness (e.g. Bahcall & Cen 1993, Eke et al. 1996, Girardi et al. 1998, Viana & Liddle 1999, Blanchard et al. 2000, Pierpaoli et al. 2001, Reiprich & Böhringer 2002, Seljak 2002, Viana et al. 2002). It is worth pointing out that formal statistical uncertainties in the determination of σ_8 from the different analyses are always far smaller, $\lesssim 5\%$, than the above range of values. This suggests that current discrepancies on σ_8 are likely to be ascribed to systematic effects, such as sample selection and different methods used to infer cluster masses. We comment more on such differences in the following section. Completely independent constraints on a similar combination of σ_8 and Ω_m can be obtained with measurements of the cosmic gravitational lensing shear (e.g. Mellier 1999). The most recent results give $\sigma_8 \Omega_m^{0.6} = 0.45 \pm 0.05$ (van Waerbecke et al. 2001, and references therein). A Powerful way to break the degeneracy between σ_8 and Ω_m, is to follow the evolution of the number density of clusters. In fact, the growth rate of the density perturbations depends primarily on Ω_m and, to a lesser extent, on Ω_Λ, at least out to $z \sim 1$. This is shown and quantified in Fig. 1.5: models with different values of Ω_m, which are normalized to yield the same number density of nearby clusters, predict cumulative mass functions that progressively differ by up to orders of magnitude at increasing redshifts.

The fundamental aspect of all these cosmological tests is that they need to be applied to cluster samples highly complete in dynamical mass. From the observational point of view it is quite difficult to create a detection and selection method able to create such cluster samples. Obviously this is due to the fact that the cluster dynamical mass is not an observable and, therefore, the detection and selection methods have to be based on other cluster observable properties such as their optical or X-ray emission. So far, as we will show in section 1.5.2, the X-ray selection methods were the most used for creating samples of galaxy clusters.

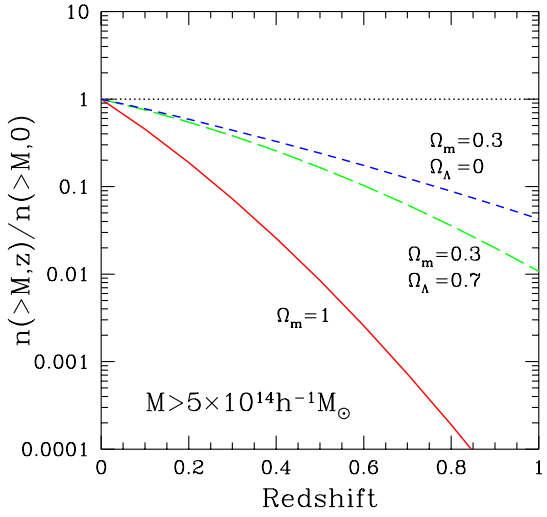

Figure 1.5: *Evolution of the number of clusters* $n(>M,z)$ *for* $M > 5\times10^{14}H^{-1}M_{\odot}$ *for three cosmologies, with* $\sigma_8 = 0.5$ *for the* $\Omega_m = 1$ *case and* $\sigma_8 = 0.8$ *for the low-density models.*

The X-ray approach is favorite due to the assumption that the X-ray luminosity, L_X, is an excellent tracer of the cluster mass. That is, a very tight relation exists between L_X and the cluster mass. As a consequence a cluster sample highly complete in X-ray luminosity is highly complete in mass. Verifying this assumption is one of the goal of the thesis.

1.2.2 Models of galaxy formation and evolution

Due to the success of the ΛCDM scenario in reproducing the large scale structure distribution, more and more work focused on smaller structures in order to embed galaxy formation into the hierarchical picture. In analogy to the galaxy cluster formation, the individual galaxies are the merger products of smaller systems. In such scenario the small dark matter halos are the oldest systems in the Universe and they are the building-blocks of the today's giant galaxies.

One successful approach has been semi-analytical or phenomenological models (Kauffmann, White & Guiderdoni, 1993; Cole et al., 1994). These models use the extended Press-Schechter theory to predict abundances and merger rates of halos as a function of mass and redshift. Physically motivated recipes are used to model how gas cools, how it settles at the center of dark matter halos and how it is transformed into stars. This phenomenological ansatz provides at comparably low computational cost a very efficient method to predict

the formation and evolution of the galaxy population. This models do not make predictions on the detailed formation history of individual galaxies, but provides some useful statistical predictions on the formation epoch, the galaxy type mix, the clustering and the luminosity distribution of the galaxy population.

In the hierarchical merging scenario, galaxies end up as spirals or ellipticals depending on the details of their merger history. In particular, typical elliptical galaxies form from the merging of intermediate-mass disks at lower redshifts (e.g. Kauffmann, Charlot & White 1996; Baugh, Cole & Frenk 1996). As a result, the model predicts that the number of the high mass galaxies should decrease with increasing redshift (that is, decreasing age) in favour of the number of smaller systems.

One of the most important results of the hierarchical models of structure formation is that the mass distribution of the subhalos is universal and well approximated by a power law, $dN(m_{sub})/dm \propto m_{sub}^{-1.9}$ (see De Lucia et al. 2004 and Gao et al. 2004 for the most recent simulations). Its shape is independent of the mass of the parent halo, from the massive clusters to the small galaxy groups. Due to the very steep slope, -1.9, of the power law, the hierarchical mass function predicts the existence of a large number of dwarf subhalos. Moreover, it is quite well established that the ratio of massive halos to low mass halos is larger in dense regions. This is due to the fact that the merging efficiency is higher in the high density region as the cluster core, than in the low density region as the field.

Probing the shape of the subhalos mass function and the predicted dependence on the large scale environment are two of the major tests of the hierarchical models of galaxy formation and evolution. Since the subhalo mass is not an observable, the shape and the universality of this mass function cannot be probed directly by observations. The semyanalitical models provide the only way to transform this theoretical mass function into the observable galaxy luminosity function. The basic physical mechanisms which determine the form of the luminosity function were first described by Rees & Ostriker (1977) and White & Rees (1978). In this picture, galaxy formation is regulated by the rate at which gas is able to cool in the parent dark matter halos. These authors suggested that the sharp cut-off in the galaxy luminosity function arose from the long cooling times of gas in high mass halos (or high mass protogalaxies in the case of Rees & Ostriker). The model has been developed by many authors to follow in great detail the formation of galaxies in a hierarchical universe. Key improvements are the inclusion of galaxy merging and the evolution of stellar populations (White & Frenk 1991; Cole 1991; Kauffmann, White & Guideroni 1993; Lacey et al. 1993; Cole et al. 1994; Kauffmann et al. 1999; Somerville & Primark 1999; Cole et al. 2000; Benson et al. 2002). Such models are now being tested by high-precision measurements of the galaxy luminosity function from large redshift surveys such as 2dF, 2Mass and SDSS (the present work).

While the key physics of gas cooling and merging are now thought to be modeled with reasonable accuracy (Benson et al. 2001, 2002; Yoshida et al. 2002; Helly et al. 2002; Voit et al. 2002), other physics crucial to establishing the shape of the luminosity function remain

poorly understood. The main uncertainty is the metal pollution, ('feedback') needed to regulate the formation of dwarf galaxies, and hence reconcile the rather shallow slope of the faint end of the observed luminosity function with the relatively steep mass function of dark matter halos. All current models of galaxy formation, calculated using either gas-dynamical simulations (Pearce et al. 2001; Kay et al. 2002; Weinberg et al. 2003) or semi-analytic techniques (e.g. Kauffmann et al. 1999; Somerville & Primack 1999, Cole et al. 2000), exhibit strong gas cooling in the central regions of groups and clusters. This leads to the formation of extremely bright galaxies, which are never seen in reality, unless some additional suppression of the gas cooling is assumed.

A further prediction of the hierarchical model is the Halo Ocupation model. Recently, the Halo Occupation Distribution (HOD) has emerged as a powerful framework for describing galaxy bias and modeling galaxy clustering (e.g. Ma & Fry 2000; Peacock & Smith 2000; Seljak 2000; Scoccimarro et al. 2001; Berlind & Weinberg 2002). It characterizes the bias between galaxies and mass in terms of the probability distribution, P(N|M), that a halo of virial mass M contains N galaxies of a given type, together with relative spatial and velocity distributions of galaxies and dark matter within halos. The HOD is a fundamental prediction of hierachical galaxy formation theory (e.g. Kauffmann et al. 1997, Kauffmann et al. 1999; White, Hernquist & Springel 2001; Yoshikawa et al. 2001; Berlind et al. 2003; Kravtsov et al. 2004) and it can be extremely useful to compare the observational results with the theoretical models. Due to the universality of the mass distribution of the subhalos predicted by the hierarchical model of structure formation, the number of subhalos, N_{sub}, above a given dynamical mass threshold is directly proportional to the parent halo mass, $N_{sub} \propto M$. The HOD provides the number of galaxies above a given luminosity threshold, N_{gal}, as a function of the parent halo mass. Then, if the galaxy formation efficiency is the same in all the cluster mass dark halos, we should expect $N_{gal} \propto M$. If the massive clusters form galaxies more efficiently than the low mass systems, then, we expect $N_{gal} \propto M^{\gamma}$, with $\gamma > 1$. If the massive clusters form galaxies less efficiently than the low mass systems, we expect $N_{gal} \propto M^{\gamma}$, with $\gamma < 1$. Semianalytic models predict $\gamma \sim 0.8 - 0.9$ (Sheth & Diaferio 2001; White et al. 2001; Berlind et al. 2003). Smoothed particle hydrodynamic simulations of a ΛCDM cosmological model predict halo occupation function with $\gamma \sim 0.55 - 0.74$ for cluster mass halos, similar to the values for a different set of semianalytic models (Berlind et al. 2003). Therefore, the more massive a cluster, the lower its efficiency in forming galaxies.

The general interpretation of these results is based on the different evolutionary pattern of the galaxy populations of the low mass systems in comparison to the massive clusters. Kobayashi (2005) show in particular that elliptical galaxies, which are the dominant cluster galaxy population, have larger mass to light ratio when they undergo a major merger. In the hierarchical picture, the galaxies in the high density regions as the cluster core are more likely to undergo a significant merger activity in comparison to the group galaxies. As a consequence, the more massive a clusters the larger on average the M/L of its galaxy (elliptical) population. Hence, at given luminosity treshold the number of cluster galaxies

per unit cluster mass decreases with the cluster mass, as observed. This also explaines why the high mass clusters have a lower star formation efficiency than the low mass systems (Springel & Hernquist 2003) and, thus, the fraction of cluster stellar mass is decreasing with the halo mass (Borgani et al. 2004).

In contrast to the hierarchical models of galaxy formation there is an alternative scenario. In the monolithic collapse scenario, all galaxies were formed in a single event, through the gravitational collapse of a cloud of primordial gas, very early in the history of the universe. In the monolithic collapse scenario, galaxies of different morphological types are born intrinsically different. The rotational characteristics of Spiral and Elliptical galaxies are different. Spiral galaxy disks have well organized rotational structure whereas elliptical galaxies are dominated by random orbits. A rotating cloud of protogalactic gas would certainly contract more slowly than one without rotation and could only contract along the rotation axes, forming a disk as we see in spiral galaxies. It is plausible to suppose that a non-rotating, freely collapsing protogalaxy would reach higher densities at earlier times, using up its gas rapidly in a time of order a billion years. As the rotating protogalaxy contracts more slowly to a disk shape, it would not reach such high densities, star-formation would proceed more slowly, preserving gas for future epochs of star formation. As a result, the model predicts that the number of galaxies of a given type should be approximately conserved at all redshifts (that is, throughout the history of the universe).

Attempts to discriminate between the two models focus mostly on elliptical galaxies, which are easier to study than spiral ones. However, none of the observational tests so far performed were able to discriminate convincingly among the two models. Thus, how galaxies form and evolve is still an unanswered question in the modern astrophysics.

1.3 Optical properties of galaxy clusters

Clusters span a size range from rich, with several thousand galaxies, to poor, with only 20 or 30 members. The richest nearby cluster is Virgo, 60 million light years from the Milky Way. It contains about 2500 galaxies, mostly ellipticals. The physical size of these systems ranges from 0.5 Mpc for the small groups to few Mpc for the very massive systems. The cluster mean redshift is obtained from the mean radial velocity of galaxies in clusters. In fact the radial velocities of individual galaxies are distributed around this mean. Statistical tests reveal that this distribution is consistently fitted by a Gaussian distribution as for systems in dynamical equilibrium. The typical dispersion of the velocity distribution is around 500 kms^{-1} for the poor clusters and 1000 kms^{-1} for the rich systems, revealing that galaxy clusters are associated with a deep potential well. Moreover, the Gaussian velocity distribution found in clusters suggest that they are at least partially relaxed systems.

Clusters of galaxies are classified by their properties: richness (number of members), galactic content (spiral-rich,spiral-poor, or elliptical-rich), their shape (spherical,flattened,

or irregular) or their mass.

1.3.1 The cluster galaxy content

The Hubble Sequence

In the early thirties, Hubble developed a classification scheme for galaxies which, with minor revisions remains in use today. Hubble divided galaxies into two principal categories Elliptical and Spiral, with a third "Irregular" category left to catch those galaxies which defied regular classification. Elliptical galaxies, which essentially consist of only a nuclear bulge component are subdivided among seven ellipticity classes from E0 (circular) to E7 (cigar shaped). Numerically the ellipticity is given by 10(a-b)/a, where a is the length of the major axis and b is the length of the minor axis. Of course, the Hubble Classification does not tell us the true shape of the galaxy (e.g. an E0 could be a "cigar" seen down its barrel). Statistical arguments suggest that the distribution of galaxies among the ellipticities is roughly uniform.

Spiral galaxies are subdivided among three classes Sa, Sb, Sc, with a parallel sequence for Barred Spirals SBa, SBb, SBc . (More modern classifications add a class Sd and subdivide among the classes Sab, Sbc, Scd.) The three criteria are: the size of nuclear bulge (Sa=large; Sc= small), the openness of spiral pattern (Sa=tightly wound; Sc= open), the resolution of arms into supergiant stars and HII regions (Sa=smooth, few small HII regions; Sc=clumpy, lots of bright supergiants and HII regions). Upon completion of the scheme Hubble realized that he needed to allow for an intermediate classification between Elliptical and Spiral S0 and SB0. Traditionally the classification scheme is arranged in a "tuning fork diagram". Irregular galaxies come in two types:Irr I which are in some sense a logical extension of the Hubble tuning fork, having characteristics "beyond" those of class Sc - high gas content, dominant presence of a young population. Irr I galaxies may show bar-like structures and incipient spiral structure like the Large Magellanic Cloud, below. Such galaxies are sometimes referred to as "Magellanic Irregular" galaxies. Irr II which are galaxies which defy classification because of some form of disturbance. M82, shown below, is undergoing an intense period of star-formation.

Particular attention should be devoted to the cD galaxies. They compose a peculiar class of objects that lie at the center of rich clusters. A defining characteristic of cD galaxies is that in their inner regions they have surface brightness profiles like those of ellipticals, but in the outer regions (which can be truly gigantic) they decline much more slowly. That is, cDs have giant luminous halos or envelopes, which can contain as much light as the rest of the galaxy. the studies of Schombert (1987, 1988, and references therein) of the surface brightness distributions of 342 bright cluster ellipticals substantiate and quantify these general statements. According to the galactic cannibalism theory, while the cD precursor may well have been the largest galaxy to form in the center of the cluster (or subcluster, see Merritt

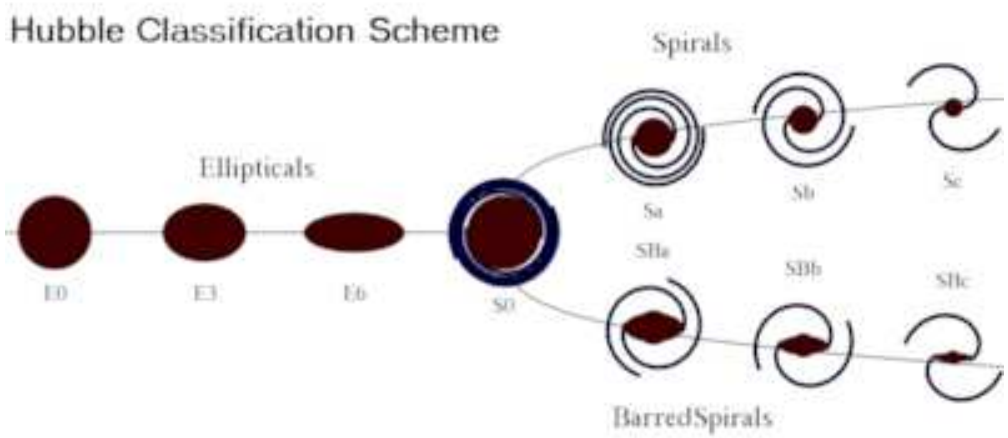

Figure 1.6: *The Hubble sequence is a classification of galaxy types developed by Edwin Hubble in 1936. It is also called the tuning-fork diagram as a result of the shape of its graphical representation.*

1984), the halo developed by the disruption and merger of numerous smaller galaxies.

The unique relationship between the Hubble Class and other properties, most especially stellar populations suggests that the Hubble Class is fundamentally related to the way in which galaxies form and evolve. For some reason elliptical galaxies formed all their stars a long time ago, using up all their gas, so that new stars are no longer forming, there is virtually no young stellar population nor gas nor dust. Spirals, on the other hand, have retained much of their gas and are continuing to form stars.

The morphology-density relation

Morphological types show striking differences between various environments. If we tabulate the percentages of various galaxy types in rich and poor clusters and in the "field", a clear distinction emerges: E and S0 galaxies favor rich environments, and cD systems even more so. This is sometimes expressed in terms of spiral fraction, evaluated for lots of clusters but somewhat subjective when determined only from Sky Survey material. It has long been known as well that spirals and irregulars favor clusters of irregular (rather than centrally concentrated) form, but this is likely to reflect a nearly universal relation between morphology and local galaxy density (see Dressler 1980). One frequently finds this relation within a single cluster, with galaxies in the core being only E/S0.

Many explanations have been proposed for the origin of the systematic variation in galactic content with the environment. In general, these theories fall into two broad classes. In the first class, the proportion of galaxy types is set by the conditions when the galaxies form,

and once the galaxies form, they do not alter their morphology. Thus, more ellipticals than spiral galaxies are formed in protoclusters. This has trouble if many clusters are just now collapsing out of the Hubble flow. The Monolithic collapse models belong to this class. In the second group of theories, galaxies may form with the same distribution of morphological types everywhere, but physical processes that depend on the environment cause galaxies to alter their morphology. In this case there are two competing scenarios. Spirals turn into elliptical galaxies via mergers, according to the hierarchical scenario of galaxy formation discussed in the previous section. Otherwise spirals turn into S0s if they are stripped either by ram pressure of the intracluster gas or by direct collision with other bright galaxies, including in both cases "galaxy harassment" (Moore et al. 1996).

The transformation of spiral galaxies into S0 or ellipticals seems to be supported by several indications. Gas deficiency has been inferred from H I measurements for spirals in clusters. The most deficient spirals are found in cluster cores. This suggests removal of the gas for those galaxies that come close to the dense core. A spectacular result was obtained by Cayatte et al. 1990, who mapped the whole Virgo Cluster core in H I, showing that the outer disks are missing in central stripped spirals. A further suggestive correlation exists between the fraction of H I - deficient galaxies in a cluster and its hot gas content, measured through its X-ray luminosity (Giovanelli and Haynes 1985). This strongly suggests a dominant role for ram-pressure stripping rather than collisions, since the ram pressure (perhaps amplified by turbulence at the ISM-IGM interface) varies with location in the cluster and is stronger in the cluster core. Other authors in the literature do note, however, that some stripped galaxies do seem to be undergoing tidal encounters, so that ram pressure isn't necessarily the whole story. Looking at nearby spirals claimed to show evidence for stripping, one usually finds that tidal effects are at least as likely to be involved, although the combination might make stripping work in places where it couldn't happen by itself. One such candidate is NGC 3312 in the Hydra I cluster (Abell 1060). As noted by Gallagher 1978, this giant spiral shows diffuse matter that appears to be streaming away from part of the disk, and is projected quite close to the center of the cluster. NGC 2276 and NGC 1961 were once good candidates, but more detailed work showed that their oddities look more like weak tidal disturbances (in particular the stars and gas share the same disk geometry). Perhaps more convincing is the bizarre H I distribution in NGC 4438 (see Cayatte et al.), but a strong tidal encounter is also involved here so that the interpretation is not so clear-cut.

The overall effect of tidal stripping of stars has been sought in the form of diffuse cluster light, not associated with any single galaxy, which is a tough observational challenge, the so called IntraCluster Light (ICL). A remarkable step here was the recent discovery by Ferguson et al. (1998) of an intergalactic population of red giants in the Virgo cluster, giving a direct measure of the density of intergalactic stars (which have, in only a few instances, been previously traced by supernovae). This was complemented by the ground-based detection of planetary nebulae in the Virgo cluster and other galaxy systems (Feldmeier, Ciardullo, & Jacoby 1998, Feldmeier et al. 2004; Murante et al. 2004; Willman et al. 2004). The

fraction of stars implied not to belong to individual galaxies is nontrivial, of order 1/3 the total in the cluster.

In contrast to the evidence for spirals, explained above, elliptical galaxies, once produced, show little environmental influence. Their colors show a strikingly consistent color-absolute magnitude relation, often called cluster red sequence, which is well accounted for just by metallicity changes, allowing very little recent star formation. Many studies in the literature looked for these signs of recent star formation in just-formed ellipticals in clusters. The analysis often concentrates on spectral features such as Hd, as the last strong absorption line to disappear as a young population ages and fades. Somewhat younger systems, soon after cessation of star formation presumed to accompany gas removal, are the "E+A" systems, spectroscopically resembling a mix of E galaxy and A-star spectra.

The Butchler-Oemler effect

The most direct test of the hypothesis that spiral galaxies evolve to become elliptical galaxies, both in the hierarchical and the 'harassment' scenarios of galaxy formation is the observation of spiral galaxies in high redshift clusters which may be undergoing this transformation. Butcher and Oemler (1978a, 1984a, b) showed that a number of moderately high redshift (z approx 0.4) clusters apparently contained a high proportion of blue galaxies. The blue galaxies lie at larger projected distances from the cluster center than the redder galaxies. When redshift effects were removed, these blue galaxies had colors indistinguishable from those of nearby spiral galaxies. No such population of blue galaxies occurs in nearby compact clusters (Butcher and Oemler, 1978b). These blue galaxies in high redshift clusters probably contain substantial quantities of gas and may be undergoing star-formation; they may indeed be spiral galaxies. If so, we would have fairly direct evidence that galactic populations evolve in rich clusters.

Later studies have confirmed the prevalence of such populations in clusters at modest redshift (for example, Dressler et al. 1985) though there is some evidence that the blue galaxies are frequently in tight, perhaps interacting clumps (Lavery and Henry 1988). HST imaging (e.g. Oemler et al. 1997) makes it clear that many of the anomalous blue galaxies are respectably normal spirals, with these clusters being quite rich in spirals. While some mergers and tidal interactions are seen, they cannot be the whole story, so these data make it clear that in clusters, we are dealing with the wholesale transformation of spirals into E/S0 systems within the last few 10^9 years. Study of a cluster at z=0.83 by van Dokkum et al. (2000) adds the interesting wrinkle that the merger remnants which may by now have formed ellipticals can be distinguished in color, and that the fraction of spirals has reached 39% (not found for any rich cluster in our neighborhood). More recently, Rakos and Shombert (2004) found that the fraction of blue galaxies increases from 20% at $z \sim 0.4$ to 80% at $z = 0.9$, suggesting a very strong evolution in the cluster galaxy types mix.

The Butcher-Oemler effect is not solely redshift dependent, although it is nearly universal

at z $\sim$ 0.4. There are a few very rich clusters of red galaxies at about z=0.4 (Cl 0024+1654, for example, Schneider, Dressler, & Gunn 1989), and rich clusters like Abell 2125 at z=0.25 (an HST detail of part of this cluster is shown below) which are unusually rich in spiral members, so that the density history of a cluster may be more important than redshift.

Recently, as a modern version of the Butcher-Oemler effect, the evolution of the SFR in clusters has been actively debated (e.g. Kodoma & Bower 2001, Homeier et al. 2005). Postman et al. (1998, 2001) found that a large number of cluster members show high levels of star formation activity, and that the average SFR is higher in $z \sim 0.9$ clusters than in low redshift systems. Finn et al. 2004 studied the H_α derived star formation rates of the cluster CL0023+0423B and found that the integrated SFR normalized to the cluster mass is 10 times higher than in low redshift clusters.

All these studies could be affected by strong selection effects. In fact, Newberry et al. (1988) measured the velocity dispersions and surface densities of galaxies in clusters, and found a marked difference between local clusters and intermediate redshift clusters. More recently, Andreon and Ettori (1999) measured the X-ray brightness profiles, sizes and luminosities of the Buchter-Oemler sample of clusters and concluded that the sample is not uniform. Moreover, Margoniner et al. (2001) and Goto et al. (2003) found a dependence of the blue galaxy fraction on the cluster richness. Since more distant clusters tend to be more massive due to selection effect, a Malmquist-bias type could imply an erroneously weaker redshift trend. Therefore, it is not clear yet if the variation of the cluster blue galaxy fraction and SFR is caused by cluster mass or redshift evolution.

There is a rich literature about the types of environmental processes which could affect the evolution of the SFR in clusters. There are processes which affect mainly the gaseous content of a galaxy, such as ICM-ISM interactions (van Gorkom 2004), starvation (Larson et al. 1980), and gas accretion (Kenney et al. 2004). Gravitational processes, which affect both the gaseous and the stellar properties of a galaxy, range from low-velocity tidal interactions and mergers, to high-velocity interactions between galaxies and/or clusters (Struck 1999; Mihos 2005). Despite a number of recent studies of nearby and distant clusters, it is not yet clear which processes, if any, are dominant. Only a detailed study of the dependence of the SFR on the global cluster properties such as, mass, velocity dispersion, X-ray luminosity and galaxy surface density, if any, would help in understanding.

1.3.2 The luminosity function

The galaxy luminosity function (LF) provides one of the most direct observational tests of theories of galaxy formation and evolution. Clusters of galaxies are ideal systems within which to measure the galaxy LF for the large number of galaxies at the same distance. There are two main purposes in the study of the cluster LF: the comparison of the galaxy LF in clusters and field and thus the study of the influence of the environment on the global statistical properties of galaxies, and the search for differences in the LF of different clusters

as indicators of differences in the galaxy formation due to environmental effects or dynamical processes.

The luminosity function of galaxies in a cluster gives the number distribution of the luminosities of the galaxies. the integrated luminosity function $N(L)$ is the number of galaxies with luminosities greater than L, while the differential luminoisty function $n(L)dL$ is the number of galaxies with luminosity in the range L to $L+dL$. Schechter (1976) proposed an analytic approximation for the differential luminosity function

$$n(L)dL = N^*(L/L^*)^{-\alpha}exp(\mathrm{L}/L^*)d(L/L^*) \tag{1.3}$$

where L^* is a characteristic luminosity, $N^*\Gamma(1-\alpha,1)$ is the number of galaxies with $L > L^*$, and $\Gamma(\alpha, x)$ is the incomplete gamma function. Schechter derives a value for the faint end slope $\alpha = 1.25$. The integrated luminosity function corresponding to eq. 1.3 is $N(L) = N^*\Gamma(1-\alpha, L/L^*)$. The advantages of the Schechter function are that it is analytic and continuous and is a statistical distribution function. The Schechter function fits the observed distribution in many clusters reasonably well from the faint to the bright end, as long as the very brightest galaxies, the cD galaxies, are excluded (Schechter 1976). These can have luminosities as large as $10L^*$, and thus are extremely improbably if eq. 1.3 holds exactly. However, cD galaxies have a number of distinctive morphological characteristics which suggest that they were formed by special processes which occur primarily in the center of rich clusters. In any case, equation 1.3 can be taken to be the non-cD luminosity function.

The parameter N^* in the Schechter function is a useful measure of the richness of the cluster. If the luminosity function is an adequate approximations, then fitting the LF to determine N^* ought to give a more accurate measure of richness than counting galaxies in magnitude range. Note that while the total number predicted by the Schecter LF diverges at the faint end, the total luminosity is finite and is given by $L_{op} = N^*\Gamma(2-\alpha)L^*$.

Is the cluster LF universal or does it depend on the global properties of the systems, such as richness, mass, X-ray or optical luminosity and ICM temperature? In other words, is the LF environment-dependent? Much work has been done on this issue, with various groups finding differences in the shape of the cluster LF and its faint-end slope. Different techniques have been used to measure LFs of individual clusters or to make a composite LF from individual clusters LFs (e.g. Dressler 1978; Lugger 1986, 1989; Colless 1989; Biviano et al. 1995; Lumsden et al. 1997; Valotto et al. 1997; Rauzy et al. 1998; Garilli et al. 1999; Paolillo et al. 2001; Goto et al. 2002; Yagi et al. 2002). Whether the LF of cluster galaxies is universal or not, and whether it is different from the LF of field galaxies are still debated issues. Several authors (Dressler 1978; Lumdsen et al. 1997; Valotto et al. 1997; Garilli et al. 1999; Goto et al. 2002; Christlein & Zabludoff 2003) have found significant differences between the LFs of different clusters as well as between the LFs of cluster and field galaxies, while others (Lugger 1986, 1989; Colless 1989; Rauzy et al. 1998; Trentham 1998; Paolillo et al. 2001; Andreon 2004) have concluded that the galaxy LF is universal in all environments.

Another debated issue is the slope of the faint end of the LF of cluster galaxies (see, e.g., Driver et al. 1994; Lobo et al. 1997; Smith et al. 1997; Phillipps et al. 1998; Boyce et al. 2001; Beijersbergen et al. 2001; Trentham et al. 2001; Sabatini et al. 2003; Cortese et al. 2003). The LF of cluster galaxies is typically observed to steepen faint-ward of $M_g \sim -18$, with power-law slopes $\alpha \sim -1.8 \pm 0.4$. This corresponds to the debated upturn of the cluster LF due to an excess of dwarf galaxies relative to the field LF. The effect may be real, and due to cluster environmental effects, but it could also be generated by systematics in the detection techniques of faint, low surface-brightness galaxies.

The environmental dependence of the luminosity function is often studied also in terms of the LF per morphological type. Since the morphological type fraction of galaxies depends on the environment, this should affect also the general LF. Fig. 1.7 shows the pioneering work pf Bingelli et al. (1988) on the LF of the Virgo cluster in comparison with the field LF. The figure shows that the Schechter function is an approximation of the real LF at very faint magnitudes. The faint end of the Virgo cluster seems to be steeper than the field LF. Different types have clearly different LFs. The spirals galaxies dominate the field while the ellipticals are more common in the cluster regions. There is a clear distinction between elliptical galaxies and dwarf ellipticals, which are not a scaled version of the former ones. Dwarf elliptical galaxies are recognized to have distinct spectrophotometric properties with regard to giant ellipticals. Their contribution to the general LF seems to depend on the environment, being much more significant in the Virgo cluster than in the field where the dwarf Irregulars dominate. Is Virgo representative of the cluster LF, or is it a particular case? So far a detailed study of the cluster LF down to very faint magnitudes has been conducted only on few individual clusters like Virgo. The lack of very deep and extensive optical survey data did not allow to perform this kind of analysis on a statistically significant sample of clusters.

From the theoretical point of view, a steep mass function of galactic halos is a robust prediction of currently popular hierarchical clustering theories for the formation and evolution of cosmic structure (e.g. Kauffmann et al. 1993; Cole et al. 1994, see also previous section). Nevertheless, as explained in the previous section, the hierarchical models predict that the ratio of low mass halos to massive halos is larger in low-density regions, such as the field, than in the dense cluster regions. Thus, the flat LF observed in the field and the steeper LF observed in several nearby clusters are inconsistent with the predictions. Several solutions are proposed in the literature. According to Menci et al. (2002), merging processes are responsible for the flattening of the field LF; the environmental dependence arises because mergers are more common in the field (or group) environment than in clusters, where they are inhibited by the high velocity dispersion of galaxies. According to Tully et al. (2002), instead, the LF flattening in the field is due to inhibited star formation in dark matter halos that form late, i.e. after photoionization of the intergalactic medium has taken place. Since dark matter halos form earlier in higher density environments, a dependence of the observed LF slope on the environment is predicted. On the other hand, if reionization happens very

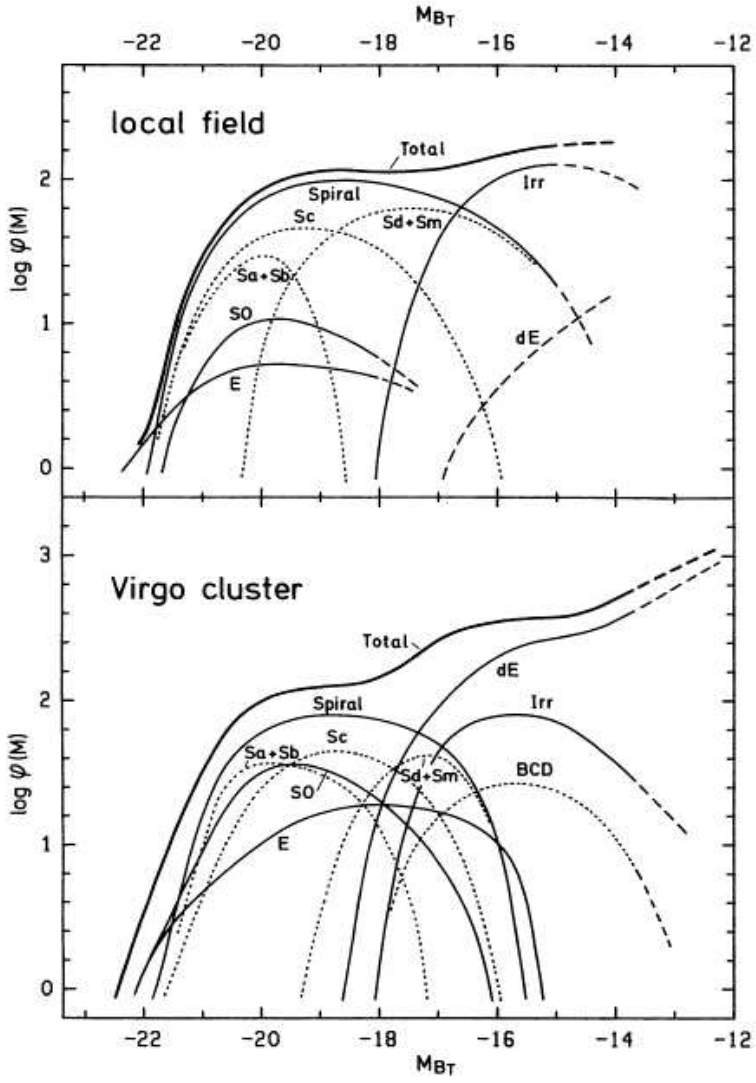

Figure 1 The LF of field galaxies (top) and Virgo cluster members (bottom). The zero point of $\log \varphi(M)$ is arbitrary. The LFs for individual galaxy types are shown. Extrapolations are marked by dashed lines. In addition to the LF of all spirals, the LFs of the subtypes Sa+Sb, Sc, and Sd+Sm are also shown as dotted curves. The LF of Irr galaxies comprises the Im and BCD galaxies; in the case of the Virgo cluster, the BCDs are also shown separately. The classes dS0 and "dE or Im" are not illustrated. They are, however, included in the total LF over all types (heavy line).

Figure 1.7:

early in the Universe, this scenario may not work (Davies et al. 2005). Other physical processes are, however, at work in the cluster environment, such as ram-pressure stripping (Gunn & Gott 1972) and galaxy harassment (e.g. Moore et al. 1996, 1998), which are able to fade cluster galaxies, particularly the less massive ones. In particular, the evolution of spirals into dwarf spheroidals is a prediction of the 'galaxy harassment' scenario, as explained in a previous paragraph. In this scenario, close, rapid encounters between galaxies can lead to a radical transformation of the galaxy morphology. Gas and stars are progressively stripped out of the disk systems, eventually leaving a spheroidal remnant, that resembles an S0 galaxy or a dwarf spheroidal, depending on the size of the progenitor. Direct support for the harassment scenario comes from the discoveries of disks or even spiral arms in dwarf early-type cluster galaxies (Jerjen et al. 2000; Barazza et al. 2002; Graham et al. 2003). Indirect support comes from the similar velocity distribution of dwarf cluster galaxies (Drinkwater et al. 2001) and gas-rich spirals and irregulars (Biviano et al. 1997), both suggesting infalling orbits. However, whether the outcome of these processes should be a steepening or a flattening of the LF faint-end is still unclear.

1.3.3 The cluster optical shape

The cluster optical shape can provides information on the dynamical state of the systems. Moreover, if the galaxies are distributed in the same way as the dark matter, their projected radial distribution can reveals the distribution of the underlying dominant dark matter component. Until fairly recently, the projected galaxy density in rich galaxy clusters was generally described by King or Hubble profiles. In these profiles, the logarithmic slope of the mass distribution is essentially zero near the cluster center. The King Profile is the most used model. The 3D and the projected King profiles are given, respectively, by:

$$\rho(r) = \frac{n_0}{(1 + (r/r_c)^2)^{3/2}} \tag{1.4}$$

$$\sigma(b) = \frac{\sigma_0}{(1 + (b/r_c)^2)} \tag{1.5}$$

where r_c is the core radius and $\sigma_0 = 2n_0 r_c$ is the normalization (Sarazin 1981). The core radius which is the characteristic scale of the distribution, was sometimes also regarded as the distance which more or less separates dynamically distinct regions in a cluster or, more in general, to scale the radius in order to distinguish regiorns dominated by different physical processes. From the kinematics of the galaxy population it appears that in clusters the relaxation time is significantly shorter than the Hubble time *only* in the very central region within at most a few core radii (see e.g. den Hartog and Katgert 1996).

The concept of cores in clusters has been seriously challenged, on observational grounds (e.g. Beers & Tonry 1986) and as a result of numerical simulations. Navarro, Frenk and White (1995, 1996) found in the similations that the equilibrium density profiles of dark

matter halos in universes with dominant hierarchical clustering all have the same shape, which is essentially independent of the mass of the halo, the spectrum of initial density fluctuations, or the values of the cosmological parameters. The NFW profile is given by:

$$\rho(r) = \frac{\delta_0}{r/r_s(1+(r/r_s)^2)} \tag{1.6}$$

where r_s is the characteristic radius ($r_s = cr_{200}$ with c concentration parameter) and δ_0 is the normalization. The surface density profile is then an integration of the three-dimensional profile (see Bartelmann et al. 1996).This 'universal' density profile does not have a core, but has a logarithmic slope of –1 near the centre which, at large radii, steepens to –3, and thus closely resembles the Hernquist (1990) profile except for the steeper slope of the latter at large radii of –4.

Navarro, Frenk and White (1997) argue that the apparent variations in profile shape, as reported before, can be understood as being due to differences in the characteristic density (or mass) of the halo, which sets the linear scale at which the transition of the flat central slope to the steep outer slope occurs. They also argued that the existence of giant arcs in clusters requires that the mass distributions in clusters does not exhibit a flat core in the centre. In other words: if clusters have cores, the lensing results require that the core radii are very small, at least quite a bit smaller than the values usually quoted.

It is not clear that galaxy clusters should have cores; after all, the dynamical structure of galaxy clusters is quite different from that of globular clusters, for which Michie & Bodenheimer (1963) and King first proposed density profiles with cores, in particular the King profile (see e.g. King 1962). The X-ray data for clusters are quite consistent with the existence of a core in the density distribution (Pratt & Arnoud 2005). On the other hand, similarly, the galaxy surface density in clusters is generally found to be consistent with a King profile. For galaxy clusters, little use has been made of the de Vaucouleurs profile to describe the galaxy density, even though the latter was found to arise quite naturally in N-body simulations of the collapse of isolated galaxy systems (e.g. van Albada 1982).

1.3.4 The cluster mass and mass-to-light ratio

The crossing time for a cluster of size R can be defined as

$$t_{\rm cr} = \frac{R}{\sigma_v} \simeq 1 \left(\frac{R}{1{\rm Mpc}}\right) \left(\frac{\sigma_v}{10^3\,{\rm km\,s^{-1}}}\right)^{-1} {\rm Gyr}\,. \tag{1.7}$$

Where R is the gravitational radius and σ_v is the cluster veocity dispersion. Therefore, in a Hubble time, $t_H \simeq 10\,h^{-1}$ Gyr, such a system has enough time in its internal region, $\lesssim 1\,h^{-1}$Mpc, to dynamically relax – a condition that can not be attained in the surrounding, ~ 10 Mpc, environment. Assuming that cluster of galaxies are bound, gravitating systems

in virial equilibrium, the typical cluster mass is

$$M \simeq \frac{R\sigma_v^2}{G} \simeq \left(\frac{R}{1\,h^{-1}\mathrm{Mpc}}\right)\left(\frac{\sigma_v}{10^3\,\mathrm{km\,s^{-1}}}\right)^2 10^{15}\,h^{-1}M_\odot\,. \tag{1.8}$$

Smith (1936) first noticed in his study of the Virgo cluster that the mass implied by cluster galaxy motions through the virial theorem was largely exceeding that associated with the optical light component. This was confirmed by Zwicky (1937), and was the first evidence of the presence of dark matter. These analyses give surprisingly large masses for clusters, particularly when compared to the total luminosity of a cluster $L_{tot} \sim 10^{13}L_\odot$. The conventional method of quantifying this comparison is to calculate the mass-to-light ratio of a system in solar unit $(M_{tot}/L_{tot})/(M_\odot/L_\odot)$. Obviously, any system composed solely of stars like our sun would have a mass to light ratio of unit. Mass to light ratio have been derived for a large sample of galaxy clusters in many optical bands. Typically one finds $(M/L_V)_{tot} \sim 250(M_\odot)/L_\odot$. More recent analyses have shown that, in general, M/L increases with the cluster mass. Assuming a relation of the type $M/L \propto M^\alpha$, and adopting the usual scaling relations between mass and X-ray temperature or velocity dispersion, when needed, most authors have found $\alpha \simeq 0.25 \pm 0.1$, in both optical and near-infrared bands, and over a very large mass range, from loose groups to rich clusters of galaxies (Adami et al. 1998; Bahcall & Comerford 2002; Girardi et al. 2002; Lin et al. 2003, 2004; Rines et al. 2004; Ramella et al. 2004; see however Kochanek et al. 2003 for a discordant result). This indicates that massive clusters are less luminous per unit mass than the smaller systems like the galaxy groups.

1.4 X-ray properties of clusters

Observations of galaxy clusters in the X-ray band have revealed a substantial fraction, $\sim$15%, of the cluster mass to be in the form of hot diffuse gas, permeating its potential well. If this gas shares the same dynamics as member galaxies, then it is expected to have a typical temperature

$$k_BT \simeq \mu m_p\sigma_v^2 \simeq 6\left(\frac{\sigma_v}{10^3\,\mathrm{km\,s^{-1}}}\right)^2\,\mathrm{keV}\,, \tag{1.9}$$

where m_p is the proton mass and μ is the mean molecular weight ($\mu = 0.6$ for a primordial composition with a 76% fraction contributed by hydrogen). Observational data for nearby clusters (e.g. Wu et al. 1999) and for distant clusters (see Figure 1.8 left-hand side panel) actually follow this relation, although with some scatter and with a few outliers. This correlation indicates that the idealized picture of clusters as relaxed structures in which both gas and galaxies feel the same dynamics is a reasonable representation. There are some exceptions that reveal the presence of a more complex dynamics.

At the high energies implied by Equation 1.9, the ICM behaves as a fully ionized plasma, whose emissivity is dominated by thermal bremsstrahlung. The emissivity for this process

at frequency ν scales as $\epsilon_\nu \propto n_e n_i g(\nu, T)\, T^{-1/2} \exp(-h\nu/k_B T)$, where n_e and n_i are the number density of electrons and ions, respectively, and $g(\nu, T) \propto \ln(k_B T/h\nu)$ is the Gaunt factor. Whereas the pure bremsstrahlung emissivity is a good approximation for $T \gtrsim 3$ keV clusters, a further contribution from metal emission lines should be taken into account when considering cooler systems (e.g. Raymond & Smith 1977). By integrating the above equation over the energy range of the X-ray emission and over the gas distribution, one obtains X-ray luminosities $L_X \sim 10^{43}$–$10^{45}\,\mathrm{erg\,s^{-1}}$. These powerful luminosities allow clusters to be identified as extended sources out to large cosmological distances.

Assuming spherical symmetry, the condition of hydrostatic equilibrium connects the local gas pressure p to its density $\rho_{\rm gas}$ according to

$$\frac{dp}{dR} = -\frac{GM(<R)\rho_{\rm gas}(R)}{R^2}\,. \tag{1.10}$$

By inserting the equation of state for a perfect gas, $p = \rho_{\rm gas} k_B T/\mu m_p$ into Equation (1.10), one can express, $M(<R)$, the total gravitating mass within R as

$$M(<R) = -\frac{k_B T R}{G\mu m_p}\left(\frac{d\,\log\rho_{\rm gas}}{d\log R} + \frac{d\,\log T}{d\log R}\right)\,. \tag{1.11}$$

If R is the virial radius, then at redshift z we have $M \propto R^3 \bar{\rho}_0 (1+z)^3 \Delta_{vir}(z)$, where $\bar{\rho}_0$ is the mean cosmic density at present time and $\Delta_{vir}(z)$ is the mean overdensity within a virialized region (see also Equation 13, below). For an Einstein–de-Sitter cosmology, Δ_{vir} is constant and therefore, for an isothermal gas distribution, Equation (1.11) implies $T \propto M^{2/3}(1+z)$.

Such relations show how quantities, such as $\rho_{\rm gas}$ and T, which can be measured from X-ray observations, are directly related to the cluster mass. Thus, in addition to providing an efficient method to detect clusters, X-ray studies of the ICM allow one to measure the total gravitating cluster mass, which is the quantity predicted by theoretical models for cosmic structure formation. Fig. 1.8 shows the correlation the X-ray luminosity, L_X, in the ROSAT energy band ($0.1 - 2.4$ keV) and the cluster mass. The $L_X - M_C$ relation is relatively tight (see for more details Reiprich & Böhringer 2002) and allows to select clusters according to their mass.

A popular description of the gas density profile is the β–model,

$$\rho_g(r) = \rho_{g,0}\left[1 + \left(\frac{r}{r_c}\right)^2\right]^{-3\beta/2}\,, \tag{1.12}$$

which was introduced by Cavaliere & Fusco–Femiano (1976; see also Sarazin 1988, and references therein) to describe an isothermal gas in hydrostatic equilibrium within the potential

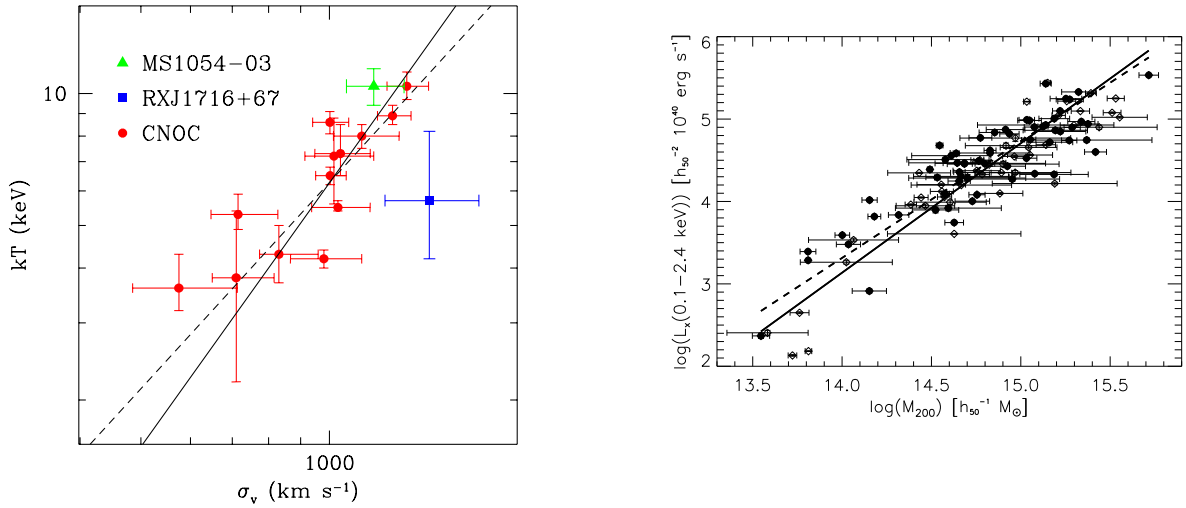

Figure 1.8: *Left The relation between galaxy velocity dispersion, σ_v, and ICM temperature, T, for distant ($z > 0.15$) galaxy clusters (from Rosati, Borgani & Norman 2001). The solid line shows the relation $k_B T = \mu m_p \sigma_v^2$, and the dashed line is the best–fit to the low–z T–σ_v relation from Wu et al. (1999). Right The low-z relation between X-ray luminosity and the mass contained within the radius encompassing an average density $200\rho_c$ (from Reiprich & Böhringer 2002). The two lines are the best log–log linear fit to two different data sets indicated with filled and open circles.*

well associated with a King dark-matter density profile. The parameter β is the ratio between kinetic dark-matter energy and thermal gas energy (see Equation 1.9). This model is a useful guideline for interpreting cluster emissivity, although over limited dynamical ranges. Now, with the *Chandra* and *Newton-XMM* satellites, the X-ray emissivity can be mapped with high angular resolution and over larger scales. These new data have shown that Equation 1.12 with a unique β value cannot always describe the surface brightness profile of clusters (e.g. Allen et al. 2001).

Kaiser (1986) described the thermodynamics of the ICM by assuming it to be entirely determined by gravitational processes, such as adiabatic compression during the collapse and shocks due to supersonic accretion of the surrounding gas. As long as there are no preferred scales both in the cosmological framework (i.e. $\Omega_m = 1$ and power–law shape for the power spectrum at the cluster scales), and in the physics (i.e. only gravity acting on the gas and pure bremsstrahlung emission), then clusters of different masses are just a scaled version of each other. Because bremsstrahlung emissivity predicts $L_X \propto M \rho_{\rm gas} T^{1/2}$, $L_X \propto T_X^2 (1+z)^{3/2}$ or, equivalently $L_X \propto M^{4/3} (1+z)^{7/2}$. Furthermore, if we define the

gas entropy as $S = T/n^{2/3}$, where n is the gas density assumed fully ionized, we obtain $S \propto T(1+z)^{-2}$.

It was soon recognized that X-ray clusters do not follow these scaling relations. The observed luminosity–temperature relation for clusters is $L_X \propto T^3$ for $T \gtrsim 2$ keV, and possibly even steeper for $T \lesssim 1$ keV groups. This result is consistent with the finding that $L_X \propto M^\alpha$ with $\alpha \simeq 1.8 \pm 0.1$ for the observed mass–luminosity relation (e.g. Reiprich & Böhringer 2002; see right panel of Figure 1.8). Furthermore, the low-temperature systems are observed to have shallower central gas-density profiles than the hotter systems, which turns into an excess of entropy in low–T systems with respect to the $S \propto T$ predicted scaling (e.g. Ponman et al. 1999).

A possible interpretation for the breaking of the scaling relations assumes that the gas has been heated at some earlier epoch by feedback from a non-gravitational astrophysical source (Evrard & Henry 91). This heating would increase the entropy of the ICM, place it on a higher adiabat, prevent it from reaching a high central density during the cluster gravitational collapse and, therefore, decrease the X-ray luminosity (e.g. Balogh et al. 1999, Tozzi & Norman 2001, and references therein). For a fixed amount of extra energy per gas particle, this effect is more prominent for poorer clusters, i.e. for those objects whose virial temperature is comparable with the extra–heating temperature. As a result, the self–similar behavior of the ICM is expected to be preserved in hot systems, whereas it is broken for colder systems. Both semi–analytical works (e.g. Cavaliere et al. 1998, Balogh et al. 1999, Wu et al. 2000; Tozzi et al. 2001) and numerical simulations (e.g. Navarro et al. 1995, Brighenti & Mathews 2001, Bialek et al. 2001, Borgani et al. 2001a) converge to indicate that ~ 1 keV per gas particle of extra energy is required. The effect of extra energy injection is to decrease the gas density in central cluster regions and to erase the small gas clumps associated with accreting groups. More recently a mixture of heating and cooling is used to reproduce the entropy profile (see Voit et al. 2004 review for more details).

1.5 The observational framework

1.5.1 Optically-based Cluster Surveys

Abell (1958) provided the first extensive, statistically complete sample of galaxy clusters. Based on pure visual inspection, clusters were identified as enhancements in the galaxy surface density on Palomar Observatory Sky Survey (POSS) plates, by requiring that at least 50 galaxies were contained within a metric radius $R_A = 3h_{50}^{-1}$ Mpc and a predefined magnitude range. Clusters were characterized by their *richness* and estimated distance. The Abell catalog has been for decades the prime source for detailed studies of individual clusters and for characterizing the large scale distribution of matter in the nearby Universe. The sample was later extended to the Southern hemisphere by Corwin and Olowin (Abell, Corwin

& Olowin, 1989) by using UK Schmidt survey plates. Another comprehensive cluster catalog was compiled by Zwicky and collaborators (Zwicky et al. 1966), who extended the analysis to poorer clusters using criteria less strict than Abell's in defining galaxy overdensities.

Several variations of the Abell criteria defining clusters were used in an automated and objective fashion when digitized optical plates became available. The Edinburgh-Durham Southern Galaxy Catalog, constructed from the COSMOS scans of UK Schmidt plates around the Southern Galactic Pole, was used to compile the first machine-based cluster catalog (Lumsden et al. 1992). In a similar effort, the Automatic Plate Measuring machine galaxy catalog was used to build a sample of ~ 1000 clusters (Maddox et al. 1990, Dalton et al. 1997).

Projection effects in the selection of cluster candidates have been much debated. Filamentary structures and small groups along the line of sight can mimic a moderately rich cluster when projected onto the plane of the sky. In addition, the background galaxy distribution against which two dimensional overdensities are selected, is far from uniform. As a result, the background subtraction process can produce spurious low-richness clusters during searches for clusters in galaxy catalogs. N-body simulations have been extensively used to build mock galaxy catalogs from which the completeness and spurious fraction of Abell-like samples of clusters can be assessed (e.g. van Haarlem et al. 1997). All-sky, X-ray selected surveys have significantly alleviated these problems and fueled significant progress in this field as discussed below.

Optical plate material deeper than the POSS was successfully employed to search for more distant clusters with purely visual techniques (Couch et al. 1991, Gunn et al. 1986). By using red-sensitive plates, Gunn and collaborators were able to find clusters out to $z \simeq 0.9$. These searches became much more effective with the advent of CCD imaging. Postman et al. (1996) were the first to carry out a V&I-band survey over 5 deg^2 (the Palomar Distant Cluster Survey, PDCS) and to compile a sample of 79 cluster candidates using a matched-filter algorithm. This technique enhances the contrast of galaxy overdensities at a given position, utilizing prior knowledge of the luminosity profile typical of galaxy clusters. Olsen et al. (1999) used a similar algorithm to select a sample of 35 distant cluster candidates from the ESO Imaging Survey I-band data. A simple and equally effective counts-in-cell method was used by Lidman & Peterson (1996) to select a sample of 104 distant cluster candidates over 13 deg^2. All these surveys, by using relatively deep I-band data, are sensitive to rich clusters out to $z \sim 1$.

Dalcanton (1996) proposed another method of optical selection of clusters, in which drift scan imaging data from relatively small telescopes is used to detect clusters as positive surface brightness fluctuations in the background sky. Gonzalez et al. (2001) used this technique to build a sample of ~ 1000 cluster candidates over 130 deg^2. Spectroscopic follow-up observations will assess the efficiency of this technique.

The advantage of carrying out automated searches based on well-defined selection criteria (e.g. Postman et al. 1996) is that the survey selection function can be computed, thus

enabling meaningful statistical studies of the cluster population. For example, one can quantify the probability of detecting a galaxy cluster as a function of redshift for a given set of other parameters, such as galaxy luminosity function, luminosity profile, luminosity and color evolution of cluster galaxies, and field galaxy number counts. A comprehensive report on the performance of different cluster detection algorithms applied to two-dimensional projected distributions can be found in Kim et al. (2002).

The success rate of finding real bound systems in optical surveys is generally relatively high at low redshift ($z < 0.3$, Holden et al. 1999), but it degrades rapidly at higher redshifts, particularly if only one passband is used, as the field galaxy population overwhelms galaxy overdensities associated with clusters. The simplest way to counteract this effect is to observe in the near-infrared bands ($\gtrsim 1\mu m$). The cores of galaxy clusters are dominated by red, early-type galaxies at least out to $z \simeq 1.3$ for which the dimming effect of the K-correction is particularly severe. In addition, the number counts of the field galaxy population are flatter in the near-IR bands than in the optical. Thus, by moving to z, J, H, K bands, one can progressively compensate the strong K-correction and enhance the contrast of (red) cluster galaxies against the background (blue) galaxy distribution. An even more effective way to enhance the contrast of distant clusters is to use some color information, so that only overdensities of galaxies with peculiar red colors can be selected from the field. With a set of two or three broad band filters, which sample the rest frame UV and optical light at different redshifts, one can separate out early type galaxies which dominate cluster cores from the late type galaxy population in the field. The position of the cluster red sequence in color-magnitude diagrams, and red clumps in color-color diagrams can also be used to provide an accurate estimate of the cluster redshift, by modeling the relatively simple evolutionary history of early-type galaxies.

The effectiveness of this method was clearly demonstrated by Stanford et al. (1997), who found a significant overdensity of red galaxies with $J - K$ and $I - K$ colors typical of $z > 1$ ellipticals and were able to spectroscopically confirm this system as a cluster at $z = 1.27$ (c.f. see also Dickinson 1997). With a similar color enhancement technique and follow-up spectroscopy, Rosati et al. (1999) confirmed the existence of an X-ray selected cluster at $z = 1.26$. Gladders & Yee (2000) applied the same technique in a systematic fashion to carry out a large area survey in R and z bands (the Red Sequence Survey), which is currently underway and promises to unveil rare, very massive clusters out to $z \sim 1$.

By increasing the number of observed passbands one can further increase the efficiency of cluster selection and the accuracy of their estimated redshifts. In this respect, a significant step forward in mapping clusters in the local Universe will be made with the five-band photometry provided by the Sloan Digital Sky Survey (York et al. 2000). The data will allow clusters to be efficiently selected with photometric redshift techniques, and will ultimately allow hundreds of clusters to be searched directly in redshift space. The next generation of wide field (>100 deg^2) deep multicolor surveys in the optical and especially the near-infrared will powerfully enhance the search for distant clusters.

1.5.2 X-ray Cluster Surveys

The *Uhuru* X-ray satellite, which carried out the first X-ray sky survey (Giacconi et al. 1972), revealed a clear association between rich clusters and bright X-ray sources (Gursky et al. 1971, Kellogg et al. 1971). *Uhuru* observations also established that X-ray sources identified as clusters were among the most luminous X-ray sources in the sky (10^{43-45} erg s^{-1}), were extended and showed no variability. Felten et al. (1966) first suggested the X-ray originated as thermal emission from diffuse hot intra-cluster gas (Cavaliere et al. 1971). This was later confirmed when the first high quality X-ray spectra of clusters were obtained with the HEAO-1 A2 experiment (e.g. Henriksen and Mushotzsky, 1986). These spectra were best fit by a thermal bremsstrahlung model, with temperatures in the range $2 \times 10^7 - 10^8$ keV, and revealed the 6.8 keV iron K α line, thus showing that the ICM was a highly ionized plasma pre-enriched by stellar processes.

The HEAO-1 X-ray Observatory (Rothschild et al. 1979) performed an all-sky survey with much improved sensitivity compared to *Uhuru* and provided the first flux-limited sample of extragalactic X-ray sources in the 2-10 keV band, with a limiting flux of 3×10^{-11} erg cm^{-2} s^{-1} (Piccinotti et al. 1982). Among the 61 extragalactic sources discovered outside the galactic plane ($|b| > 20°$), 30 were identified as galaxy clusters, mostly in the Abell catalog. This first X-ray flux-limited sample allowed an estimate of the cluster X-ray luminosity function (XLF) in the range $L_X = 10^{43} - 3 \cdot 10^{45}$ erg s^{-1}. The derived space density of clusters (all at $z < 0.1$) is fairly close to current values. An earlier determination of the XLF based on optically selected Abell clusters (McKee et al. 1980) and the same HEAO-1 A2 data gave similar results.

The Piccinotti et al. sample was later augmented by Edge et al. (1990), who extended the sample using the *Ariel V* catalog (McHardy et al. 1981) and revised the identifications of several clusters using follow-up observations by the *Einstein Observatory* and *EXOSAT*. With much improved angular resolution, these new X-ray missions allowed confused sources to be resolved and fluxes to be improved. The resulting sample included 55 clusters with a flux limit a factor of two fainter than in the original Piccinotti catalog.

Confusion effects in the large beam ($\gtrsim 1°$) early surveys, such as *HEAO-1* and *Ariel V*, had been the main limiting factor in cluster identification. With the advent of X-ray imaging with focusing optics in the 80's, particularly with the *Einstein Observatory* (Giacconi et al. 1979), it was soon recognized that X-ray surveys offer an efficient means of constructing samples of galaxy clusters out to cosmologically interesting redshifts.

First, the X-ray selection has the advantage of revealing physically-bound systems, because diffuse emission from a hot ICM is the direct manifestation of the existence of a potential well within which the gas is in dynamical equilibrium with the cool baryonic matter (galaxies) and the dark matter. Second, the X-ray luminosity is well correlated with the cluster mass (see right panel of Figure 1.8). Third, the X-ray emissivity is proportional to the square of the gas density, hence cluster emission is more concentrated than the optical

bidimensional galaxy distribution. In combination with the relatively low surface density of X-ray sources, this property makes clusters high contrast objects in the X-ray sky, and alleviates problems due to projection effects that affect optical selection. Finally, an inherent fundamental advantage of X-ray selection is the ability to define flux-limited samples with well-understood selection functions. This leads to a simple evaluation of the survey volume and therefore to a straightforward computation of space densities. Nonetheless, there are some important caveats described below.

Pioneering work in this field was carried out by Gioia et al. (1990) and Henry et al. (1992) based on the *Einstein Observatory* Extended Medium Sensitivity Survey (EMSS, Gioia et al. 1990b). The EMSS survey covered over 700 square degrees using 1435 imaging proportional counter (IPC) fields. A highly complete spectroscopic identification of 835 serendipitous sources lead to the construction of a flux-limited sample of 93 clusters out to $z = 0.8$. By extending significantly the redshift range probed by previous samples (e.g. Edge et al. 1990), the EMSS allowed the cosmological evolution of clusters to be investigated. Several follow-up studies have been undertaken such as the CNOC survey (e.g. Yee et al. 1996), and gravitational lensing (Gioia & Luppino 1994).

The *ROSAT* satellite, launched in 1990, allowed a significant step forward in X-ray surveys of clusters. The *ROSAT-PSPC* detector, in particular, with its unprecedented sensitivity and spatial resolution, as well as low instrumental background, made clusters high contrast, extended objects in the X-ray sky. The *ROSAT* All-Sky Survey (RASS, Trümper 1993) was the first X-ray imaging mission to cover the entire sky, thus paving the way to large contiguous-area surveys of X-ray selected nearby clusters (e.g. Ebeling et al. 1997, 1998, 2000, 2001; Burns et al. 1996; Crawford et al. 1995; De Grandi et al. 1999; Böhringer et al. 2000, 2001). In the northern hemisphere, the largest compilations with virtually complete optical identification include, the Bright Cluster Sample (BCS, Ebeling et al. 1998), its extension (Ebeling et al. 2000b), and the Northern *ROSAT* All Sky Survey (NORAS, Böhringer et al. 2000). In the southern hemisphere, the *ROSAT*-ESO flux limited X-ray (REFLEX) cluster survey (Böhringer et al. 2004) has completed the identification of 447 clusters, the largest, homogeneous compilation to date. Another on-going study, the Massive Cluster Survey (MACS, Ebeling et al. 2001) is aimed at targeting the most luminous systems at $z > 0.3$ which can be identified in the RASS at the faintest flux levels. The deepest area in the RASS, the North Ecliptic Pole (NEP, Henry et al. 2001) which *ROSAT* scanned repeatedly during its All-Sky survey, was used to carry out a complete optical identification of X-ray sources over a 81 deg^2 region. This study yielded 64 clusters out to redshift $z = 0.81$.

In total, surveys covering more than 10^4 deg^2 have yielded over 1000 clusters, out to redshift $z \simeq 0.5$. A large fraction of these are new discoveries, whereas approximately one third are identified as clusters in the Abell or Zwicky catalogs. For the homogeneity of their selection and the high degree of completeness of their spectroscopic identifications, these samples are now becoming the basis for a large number of follow-up investigations and cosmological studies.

After the completion of the all-sky survey, *ROSAT* conducted thousands of pointed observations, many of which (typically those outside the galactic plane not targeting very bright or extended X-ray sources) can be used for a serendipitous search for distant clusters. It was soon realized that the good angular resolution of the *ROSAT-PSPC* allowed screening of thousands of serendipitous sources and the selection of cluster candidates *solely* on the basis of their flux and spatial extent. In the central 0.2 deg^2 of the *PSPC* field of view the point spread function (PSF) is well approximated by a Gaussian with FWHM$= 30 - 45$ arcsec. Therefore a cluster with a canonical core radius of 250 h^{-1}kpc (Forman & Jones 1982) should be resolved out to $z \sim 1$, as the corresponding angular distance always exceeds 45 arcsec for current values of cosmological parameters (important surface brightness biases are discussed below).

ROSAT-PSPC archival pointed observations were used for serendipitous searches of distant clusters. These projects, which are now completed or nearing completion, include: the RIXOS survey (Castander et al. 1995), the *ROSAT* Deep Cluster Survey (RDCS, Rosati et al. 1995, 1998), the Serendipitous High-Redshift Archival *ROSAT* Cluster survey (SHARC, Collins et al. 1997, Burke et al. 1997), the Wide Angle *ROSAT* Pointed X-ray Survey of clusters (WARPS, Scharf et al. 1997, Jones et al. 1998, Perlman et al. 2002), the 160 deg^2 large area survey (Vikhlinin et al. 1998b), the *ROSAT* Optical X-ray Survey (ROXS, Donahue et al. 2001). *ROSAT*-HRI pointed observations, which are characterized by a better angular resolution although with higher instrumental background, have also been used to search for distant clusters in the Brera Multi-scale Wavelet catalog (BMW, Campana et al. 1999).

A principal objective of all these surveys has been the study of the cosmological evolution of the space density of clusters. In Figure 1.9, we give an overview of the flux limits and surveyed areas of all major cluster surveys carried out over the last two decades. RASS-based surveys have the advantage of covering contiguous regions of the sky so that the clustering properties of clusters (e.g. Collins et al. 2000, Mullis et al. 2001), and the power spectrum of their distribution (Schuecker et al. 2001a) can be investigated. They also have the ability to unveil rare, massive systems albeit over a limited redshift and X-ray luminosity range. Serendipitous surveys, or general surveys, which are at least a factor of ten deeper but cover only a few hundreds square degrees, provide complementary information on lower luminosities, more common systems and are well suited for studying cluster evolution on a larger redshift baseline. The deepest pencil-beam surveys, such as the Lockman Hole with *XMM* (Hasinger et al. 2001) and the Chandra Deep Fields (Giacconi et al. 2002, Bauer et al. 2002), allow the investigation of the faintest end of the XLF (poor clusters and groups) out to $z \sim 1$.

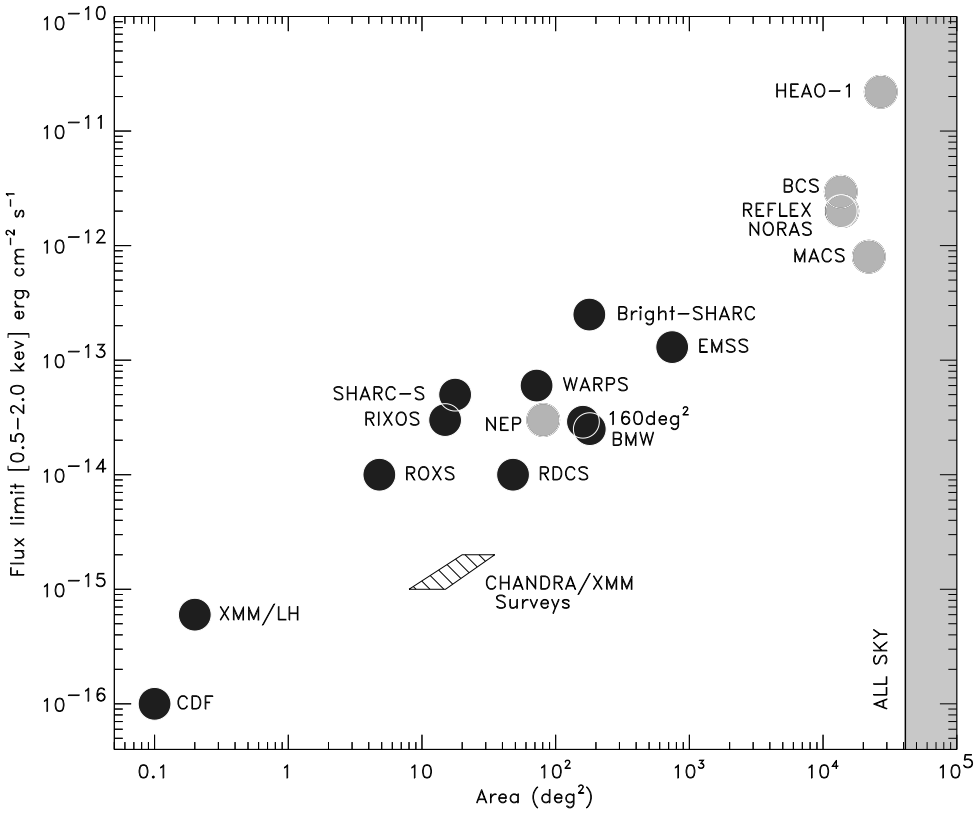

Figure 1.9: *Solid angles and flux limits of X-ray cluster surveys carried out over the last two decades. References are given in the text. Dark filled circles represent serendipitous surveys constructed from a collection of pointed observations. Light shaded circles represent surveys covering contiguous areas. The hatched region is a predicted locus of future serendipitous surveys with Chandra and Newton-XMM.*

1.5.3 Optical vs. X-ray selection

As explained in the previous sections, most of the cosmological studies involving galaxy clusters require counting the number of clusters of a given mass per unit volume at different redshifts. Therefore, three essential tools are required for application of clusters in the cosmological tests: *i)* an efficient method to find clusters over a wide redshift range; *ii)* an observable estimator of the cluster mass and *iii)* a method to compute the selection function or equivalently the survey volume within which clusters are found. The X-ray selection is thought to fulfill the three requirements above much better than how the optical selection does. In fact, L_X is known to correlate with the cluster mass, while the optical luminosity-mass relation is not well studied. The X-ray selection method are not affected by projection problems typical of the optical surveys. Moreover, the X-ray selection allows to compute the

selection function, which is difficult to know in the optical selection methods.

However, any cluster selection method introduces a bias in the definition of the cluster samples. There are some indications in the literature that the X-ray and the optical selection methods would allow to select different classes of objects. Castander et al. (1995) used ROSAT to observe cluster candidates in the redshift range 0.7-0.9 from the 3.5 square degree subsample of Gunn et al.(1986) optical cluster catalog and found surprisingly weak X-ray emission ($\sim 10^{43}$ erg s^{-1}). Bower et al. (1994) undertook ROSAT X-ray observations of optically selected clusters from the Couch et al. (1991) catalog. From this 46 deg^2 catalog, Bower et al. (1994) took clusters with reliable spectroscopic follow up and X-ray data in the redshift range 0.15 to 0.66, assuming this to be a random subsample of the full catalog. The X-ray luminosity of almost all the clusters was found to be surprisingly weak - less than 5×10^{43} erg s^{-1}. The observed decrease with respect to the locally measured value of the X-ray luminosity was attributed to the evolution of the X-ray luminosity function between $z = 0$ and $z \sim 0.4$. On the other side, the existence of X-ray underluminous clusters at low redshift suggests this effect is not due to evolution. The same results were obtained by Holden et al. (1997). Donahue et al. (2002) using the ROSAT Optical X-ray Survey (ROXS), found that using both X-ray and optical methods to identify clusters of galaxies, the overlap was poor. About 20% of the optically selected clusters were found in X-rays while 60% of the X-ray clusters were identified also in the optical sample. Furthermore, not all of their X-ray detected clusters had a prominent red-sequence, a fact that could introduce a bias in constructing cluster samples using only color information (Goto et al. 2002, Gladders et al. 2000). Ledlow at al. (2003) analyzed the X-ray properties of a sample of nearby bright Abell clusters with the ROSAT All-Sky Survey (RASS). They found an X-ray detection rate of 83%. Gilbank at al. (2004) explored the biases due to optical and X-ray cluster selection techniques in the X-ray Dark Cluster Survey (XDCS). They found that a considerable fraction of the optically selected clusters do not have a clear X-ray counterpart. Moreover, spectroscopic follow-up of a subsample of X-ray underluminous systems confirmed they reality. Lubin et al. (2004) analyzed the first XMM-Newton results of two optically selected clusters at $z \geq 0.7$. They found that their X-ray luminosity and temperature are low for their measured velocity dispersion. Similar results were obtained in the XMM-2dF Survey of Basilakos et al. (2004). They found many more optical cluster candidates than X-ray ones. Moreover, they found that using deeper XMM data many of the optically selected clusters are faint X-ray emitters with fluxes below the limit of their shallow survey. Thus, are there X-ray (optical) underluminous clusters, that is clusters extremely faint in X-rays (optical) and normally bright in the optical (X-rays)?

These results would suggest that the X-ray selection criteria do not allow to select the whole cluster population but only a class of them. Moreover, it is not known whether it is the X-ray or the optical luminosity that correlates better with the cluster mass. Therefore, it is not clear at which level these selection criteria allow to select clusters according to their mass. Hence, understanding the selection effects and the biases due to the different cluster

selection techniques is crucial for understanding the scientific results obtained from such different cluster samples.

1.6 Purpose of the thesis

In the previous analysis of the cluster properties has emerged the twofold importance of galaxy clusters first as laboratories of galaxy formation and evolution, and second as cosmological tool. The aim of this thesis is to study galaxy clusters from these two perspectives. For this porpuse we use the largest optical and X-ray surveys ever realized, the Sloan Digital Sky Survey (SDSS) and the Rosat All Sky Survey (RASS), respectively, to conduct a multiwavelenght study of the properties of galaxy clusters. The multiwavelenght approach allows us to perform two parallel analyses.

The first part of the thesis concerns the analysis of the processes that regulates the observed dependence of the galaxy morphological type mix on the environment. In particular we study which role play in the galaxy formation processes the interaction with the ICM, the gravitational processes on large scale (e.g. the dynamical state of the cluster) and the galaxy merger and collisions. A key point of the project is the statistics. The SDSS provides high quality photometric and spectroscopic data for a complete sample of galaxies down to very faint magnitudes, and its size allows to study the optical properties of an extremely large sample of clusters. Moreover, our multiwavelenght approach allowed us to construct two cluster samples statistically rapresentative of the X-ray and optical cluster properties and covering the whole dynamical range in cluster mass. Therefore, for the first time it is possible to study with great detail the galaxy population of a statistically significant sample of clusters and to follow the variation of the properties of cluster galaxies as a function of the environmental conditions and the cluster global properties.

In the second part of this thesis we use the optical/X-ray multiwavelenght approach to study the relation of optical and X-ray appearance of galaxy clusters with the cluster mass, to understand which component, galaxies or ICM, traces better the cluster mass. So far the ICM was considered the best tracer of the cluster mass and the cluster X-ray luminosity is known to correlate relatively well the cluster mass. Instead the optical luminosity-mass relation is not well studied. This is due mainly to the difficulty in measuring the cluster optical luminosity. The lack of optical wide field surveys in the past did not allow to measure in the proper way the optical luminosity in galaxy systems. Until now the uncertainties in luminosity determination came from the corrections for the calibration of inhomogeneous photometric data, background galaxy contamination and the need to extrapolate the sum of measured luminosities of galaxy members to include faint galaxies and the outer parts of the systems, beyond the region studied. The use of the SDSS for the optical data allows us to overcome all the problems related to the optical luminosity estimation. Moreover, the use of the RASS and the SDSS together allows us to define both the X-ray and optical properties

in a completely homogeneous way. The analysis is performed separately on a X-ray selected cluster sample and on a optically selected cluster sample constructed on the same sky region in common between the SDSS and the RASS. This allows to compare in detail the X-ray and the optically selected cluster populations and to explore the existence of optical/X-ray underluminous clusters. The analysis will reveal which is the bias introduced by different criteria of cluster selection in the results of the cosmological tests.

In the rest of this section we present a brief description of the two cluster samples based on X-ray and the optically selection methods, respectively, and specially created for this project. Then, we briefly summarize the analysis performed in the two parts of the thesis. The thesis is, then, organized as a collection of papers. All the papers belong to the series *'RASS-SDSS Galaxy Cluster Survey'*. The list of the papers with the abstracts is presented at the end of the section.

1.6.1 The dataset

To compare the X-ray and the optical cluster selection criteria and to take under control the consequent selection effects, we use two different cluster samples: an X-ray and an optically selected cluster sample. Before describing the two samples, we briefly describe the optical and the X-ray surveys used for the construction of the samples.

The optical and X-ray data

The optical photometric data are taken from the SDSS DR2 (Fukugita 1996, Gunn et al. 1998, Lupton et al. 1999, York et al. 2000, Hogg et al. 2001, Eisenstein et al. 2001, Smith et al. 2002, Strauss et al. 2002, Stoughton et al. 2002, Blanton et al. 2003 and Abazajian et al. 2003). The SDSS consists of an imaging survey of π steradians of the northern sky in the five passbands u, g, r, i, z, in the entire optical range from the atmospheric ultraviolet cutoff in the blue to the sensitivity limit of silicon in the red. The survey is carried out using a 2.5 m telescope, an imaging mosaic camera with 30 CCDs, two fiber-fed spectrographs and a 0.5 m telescope for the photometric calibration. The imaging survey is taken in drift-scan mode. The imaging data are processed with a photometric pipeline (PHOTO, Lupton et al. 2001) specially written for the SDSS data. For each cluster we defined a photometric galaxy catalog as described in Section 3 of Popesso et al. (2004, paper we hereafter, see also Yasuda et al. 2001). The SDSS photometric sample comprises data for more than one million galaxies.

For the analysis in this work we use only SDSS Model magnitudes. Due to a bug of PHOTO, found during the completion of DR1, the model magnitudes were systematically under-estimated by about 0.2-0.3 magnitudes for galaxies brighter than 20th magnitude, and accordingly the measured radii were systematically too large. This problem has been fixed in the SDSS DR2, therefore the model magnitude can be considered a good estimate

of the galaxy total luminosity at any magnitude and is not dependent on the seeing as the Petrosian magnitudes.

The spectroscopic component of the survey is carried out using two fiber-fed double spectrographs, covering the wavelength range 3800–9200 Å, over 4098 pixels. They have a resolution $\Delta\lambda/\lambda$ varying between 1850 and 2200, and together they are fed by 640 fibers, each with an entrance diameter of 3 arcsec. The fibers are manually plugged into plates inserted into the focal plane; the mapping of fibers to plates is carried out by a tiling algorithm (Blanton et al. 2003) that optimizes observing efficiency in the presence of large-scale structure. The finite diameter of the fiber cladding prevents fibers on any given plate from being placed closer than 55 arcsec apart. For any given plate, a series of fifteen-minute exposures is carried out until the mean signal to noise ratio (S/N) per resolution element exceeds 4 for objects with fiber magnitudes (i.e., as measured through the 3 aperture of the fiber) brighter than $g = 20.2$ and $i = 19.9$, as determined by preliminary reductions done at the observing site. Under good conditions (dark, clear skies and good seeing), this typically requires a total of 45 minutes of exposure. In analogy to the photometric survey, the spectroscopic data are reduced by a pipeline specially written for the SDSS spectroscopic survey. The SDSS spectroscopic survey comprises more than 250.000 galaxies.

The X-ray data are taken from the ROSAT All Sky Survey. The RASS was conducted mainly during the first half year of the ROSAT mission in 1990 and 1991 (Trümper 1988). The ROSAT mirror system and the Position Sensitive Proportional counter (PSPC) operating in the soft X-ray regime (0.1-2.4 keV) provided optimal conditions for the studies of celestial objects with low surface brightness. In particular, due to the unlimited field of view of the RASS and the low background of the PSPC. This dataset is ideal to investigate the properties of nearby clusters of galaxies.

The X-ray selected cluster sample

For the analysis of this work we use the RASS-SDSS galaxy cluster sample, which is an X-ray selected sample of objects in a wide range of X-ray luminosity. The updated version of the RASS-SDSS galaxy cluster catalog comprises 130 systems detected in the common sky region of the RASS and the SDSS. The X-ray cluster properties and the cluster redshifts have been taken from a variety of X-ray catalogs, that allow to cover the whole L_X spectrum. The X-ray intermediate and bright clusters have been selected from three ROSAT based cluster samples: the ROSAT-ESO flux limited X-ray cluster sample (REFLEX, Böhringer et al. 2002), the Northern ROSAT All-sky cluster sample (NORAS, Böhringer et al. 2000), the NORAS 2 cluster sample (Retzlaff 2001). The X-ray faint clusters and the groups have been selected from two catalogs of X-ray detected objects: the ASCA Cluster Catalog (ACC) from Horner (2001) and the Group Sample (GS) of Mulchaey et al. (2003). The RASS-SDSS galaxy cluster sample comprises only nearby systems at the mean redshift of 0.1. The sample covers the entire range of masses and X-ray luminosities, from very low-mass and X-ray faint

groups ($10^{13} M\odot$ and $10^{42} ergs^{-1}$) to very massive and X-ray bright clusters ($5 \times 10^{15} M\odot$ and $5 \times 10^{44} ergs^{-1}$).

For each X-ray selected cluster, we look for the optical counterpart in the SDSS photometric data. The optical counterpart of the cluster is identified as an overdensity of galaxies in the cluster region with regard to the galaxy background. For each X-ray system we found a clear optical counterpart.

The optically selected cluster sample

The optically selected cluster sample considered in this work is a subsample of the Abell cluster catalog (Abell, 1958). we have selected all the Abell clusters in the region covered by the 2^{nd} data release (DR2) of the Sloan Digital Sky Survey (SDSS). The Abell catalog is based on a visual inspection of galaxy overdensity. Therefore, it is affected by the presence of spurious detections due to projection effects. To exclude the spurious clusters from the catalog, we have considered only the clusters with a spectroscopic 3D confirmation of the galaxy overdensity. The SDSS spectroscopic catalog provides spectra and redshifts for more than 250000 galaxies with petrosian magnitude $r_{petro} \leq 17.77$. we have used the redshifts of the galaxies in the region of each Abell cluster to study its redshift distribution and confirm the presence of a three-dimensional galaxy overdensity. We have finally selected all the Abell clusters with at least 10 galaxy members, which is the minimum number of cluster members in order to calculate in a reasonable way the cluster mass and velocity dispersion. Among the 280 Abell clusters in the region covered by DR2, 179 fulfill the requirements. We have further excluded from our analysis all the clusters with contamination problems due to the presence of a close companion or a second system on the same line of sight at different redshift. we have found 42 systems among the 179 Abell clusters with problems of contamination or misclassification.

In this thesis we consider the remaining 137 Abell isolated clusters. we point out also that not for all the Abell clusters there is a clear X-ray detection. In case of insecure X-ray detection the X-ray center cannot be accurately defined. In those cases we consider the optical center as center of the cluster.

For each optically selected cluster we look for the X-ray counterpart in the RASS data. The X-ray luminosity has been calculated with the growth curve analysis (GCA) method used for the NORAS and REFLEX cluster surveys (Böhringer et al. 2000) based on the RASS3 data base (Voges et al. 1999). The GCA method is optimized for the detection of the extended emission of clusters by assessing the plateau of the background subtracted cumulative count rate curve.

1.6.2 Part I: clusters as laboratories of galaxy formation

The aim of the first part of the project is to explore the nature of the processes of galaxy formation and evolution and their relation with the environment. For this porpuse, we follw the variations of several properties of the cluster galaxy population such as the galaxy luminosity and spatial distribution, the morphological type mix, the Star Formation Rate (SFR) and stellar mass with the environmental conditions and the cluster global properties. Moreover we analyse the Halo Occupation Distribution of our cluster sample to verify the prediction of the hierarchical models of galaxy formation.

We analyse the individual and the mean cluster Luminosity Function (LF) of the RASS-SDSS galaxy cluster sample using the second and third release of the Sloan Digital Sky survey (SDSS DR2, Abazajian et al. 2004). The excellence of the SDSS DR2 in terms of its size, depth and sky coverage and the accurate photometry in 5 different optical wavebands gives unprecedented advantages in comparison to the previous studies. Firstly, the sky coverage gives us the possibility to overcome the well known problem of the statistical subtraction of the galaxy background. We used large areas of the survey to define a mean global galaxy background and a region close to the clusters to determine the local galaxy background in order to check for systematics in the field subtraction. Secondly, the apparent magnitude limit of the SDSS DR2 in all the five bands is sufficiently deep (e.g. $r_{lim} = 22.2$, 95% completeness) that, at the mean redshift of our cluster sample ($z \sim 0.10$), the cluster LF can extend and cover a significant part of the dwarf region, going deeper than in all previous studies of the composite luminosity function (more than 6 magnitudes fainter than M*). Thirdly, the high accuracy of the SDSS photometry in all bands gives us the possibility to measure in a statistically significant way the individual cluster LF with the consequent opportunity to check directly the universality of the LF. Furthermore, the accurate multi-color photometry allows us to use several objectively-measured galaxy properties like galaxy morphology.

The cluster LF is analysed from several different perspectives. We test the universality of the cluster LF through the comparison of the individual and the composite (mean) LF. We analyse the variation of the shape and of the Dwarf to Giant Ratio (DGR) of the individual cluster LFs as a function of the cluster global properties such as the mass, velocity dispersion, and X-ray luminosity. We study the cluster LF per morphological type and its dependence on the environment. In addition we compare the cluster LF with the field LF. A fully detailed discussion of this analysis and its results can be found in paper II and IV of the RASS-SDSS galaxy cluster survey series.

As a second step, we investigate whether the total cluster SFR, stellar mass and the fraction of star forming galaxies depends on the cluster global properties. The analysys is performed on a combined sample of X-ray and optically selected clusters at very low redshift ($z < 0.1$) taken, respectively, from the RASS-SDSS galaxy cluster catalog (paper I) and the Abell cluster sample (paper IV). The SFRs and the stellar masses of the cluster galaxies

are taken from the SFR catalog of Brinchmann et al. (2004), based on SDSS spectra. The results provide a basis for the comparison of the star formation rate in cluster and field galaxies. Moreover we provide an important constraint on the effects of the physical mechanism associated with the cluster mass, tidal disruption and galaxy-ICM interplay on the star forming galaxies in clusters. In addition our analysis provides an important basis in studying the redshift evolution of the cluster SFR using high redshift clusters. This analysis can be found in the paper VI of the RASS-SDSS series.

As a third step, we perform the analysis of the Halo Occupation Distribution of the combined RASS-SDSS and the Abell cluster catalogs. The number of cluster galaxies above a given luminosity threshold and within the virial region is calculated using the SDSS photometric data. Moreover, in order to account for projection effects, we study the galaxy surface number density profile in our cluster sample. This study allows us to correct the observed projected number of cluster galaxies to the value within the virial sphere. In addition it provides pretious information on the dynamical status of the considered clusters.

The observed HOD is compared to the predictions of the hierarchical models of galaxy formation. For this porpuse, we relate the observed HOD to the cluster LF and the Ellipticals Fundamental Plane in galaxy clusters to constraint the scenario of galaxy formation and evolution. This analysis can be found if the paper VII of the RASS-SDSS series.

1.6.3 Part II: Optical versus X-ray properties

The aim of the second part of the project is to elucidate which component, galaxies or ICM, traces better the cluster mass in order to understand wheter different selection methods select the same cluster population. For this porpuse, we investigate in great detail the relation of optical and X-ray apparence of galaxy clusters to the cluster mass. This is done through the analysis of the relation between the optical (L_{op}) and the X-ray (L_X) luminosity, respectively, with the dynamical properties of the clusters such as the total mass, the velocity dispersion and the X-ray temperature. The main motivation in deriving these dependences is to evaluate L_{op} and L_X, as predictors of the other quantities and to compare the quality of the two quantities as predictors. These evaluation is done through the comparison of the scatter in the $L_{op} - M$ and $L_X - M$ relations in order to understand which of the two observables, L_{op} and L_X, shows the best correlation with the cluster mass.

The analysis described above is performed in two steps. First, it is applied to the X-ray selected RASS-SDSS Galaxy Cluster sample. The best $L_X - M$, $L_X - \sigma_V$ and $L_X - T_X$ relations are estimated and the possible sources of scatter are well studied. The same is done for the $L_{op} - M$, $L_{op} - \sigma_V$ and $L_{op} - T_X$ relations. As a second step we applied the same analysis to the sample of spectroscopically selected Abell clusters. The comparison of the results obtained with samples of optically and X-ray selected clusters allows to study how the slope and the scatter of the considered relations depend on the selection criteria. As a second step, we compare directely the X-ray and the optically selected cluster samples to

investigate the presence of clusters which are luminous in the X-rays and particularly faint or undetected in the optical wavebands and viceversa. Moreover, we analyze in detail the properties of these clusters in their virialized and infall regions to highlight the differences and the similarities with the clusters which have standard X-ray and optical properties. We use the spectrophotometric properties of the cluster galaxy spectroscopic members to look for the aspects which can reveal the particular nature of these X-ray/optical underluminous systems. In particular we compare their galaxy luminosity function, the galaxy spatial profile, the velocity distribution, the presence of optical substructures and the red sequence of these systems with the clusters of the same mass with standard X-ray/optical properties. The analysis summarized in this subsection can be found in the papers III and V of the RASS-SDSS Galaxy Cluster Survey.

1.6.4 List of the papers

- 'RASS-SDSS Galaxy CLuster Surevy. I. The Catalog and the correlation of X-ray and optical properties.', Popesso, P., Böhringer, H., Brinkmann, J., Voges, W.; York, D. G, 2004, A&A, 423, 449
  Abstract:'For a detailed comparison of the appearance of cluster of galaxies in X-rays and in the optical, we have compiled a comprehensive database of X-ray and optical properties of a sample of clusters based on the largest available X-ray and optical surveys: the ROSAT All Sky Survey (RASS) and the Sloan Digital Sky Survey (SDSS). The X-ray galaxy clusters of this RASS-SDSS catalog cover a wide range of masses, from groups of $10^{12.5}$ $M_\odot$ to massive clusters of 10^{15} $M_\odot$ in the redshift range 0.002-0.45. The RASS-SDSS sample comprises all the X-ray selected objects already observed by the Sloan Digital Sky Survey (114 clusters). For each system we have uniformly determined the X-ray (luminosity in the ROSAT band, bolometric luminosity, center coordinates) and optical properties (Schechter luminosity function parameters, luminosity, central galaxy density, core, total and half-light radii). For a subsample of 53 clusters we have also compiled the temperatures and the iron abundances from the literature. The total optical luminosity can be determined with a typical uncertainty of 20% independent of the choice of local or global background subtraction. We searched for parameters which provide the best correlation between the X-ray luminosity and the optical properties and found that the z band luminosity determined within a cluster aperture of 0.5 Mpc h_{70}^{-1} provides the best correlation, with a scatter of about 60-70%. The scatter decreases to less than 40% if the correlation is limited to the bright X-ray clusters. The resulting correlation of L_X and L_{op} in the z and i bands shows a logarithmic slope of 0.38, a value not consistent with the assumption of a constant M/L. Consistency is found, however, for an M/L increasing with luminosity as suggested by other observations. We also investigated the correlation between L_{op} and the X-ray temperature, obtaining the same result.'

- 'RASS-SDSS Galaxy Clusters Survey. II. A unified picture of the Cluster Luminosity Function.',Popesso, P., Böhringer, H., Romaniello, M., Voges, W., 2005, A&A, 433, 415
  Abstract:'We constructed the composite luminosity function (LF) of clusters of galaxies in the five SDSS photometric bands u,g,r,i and z from the RASS-SDSS galaxy cluster catalog. Background and foreground galaxies are subtracted using both a local and a global background correction to take in account the presence of large scale structures and variations from field to field, respectively. The composite LF clearly shows two components: a bright-end LF with a classical slope of -1.25 in each photometric band, and a faint-end LF steeper ($-2.1 \leq \alpha \leq -1.6$) in the dwarf galaxy region. The observed upturn of the faint galaxies has a location ranging from -16 +5log(h) in the g band to -18.5 +5log(h) in the z band. To study the universality of the cluster LF we

compare the individual cluster LFs with the composite luminosity function. We notice that, in agreement with the composite LF, a single Schechter component is not a good fit for the majority of the clusters. We fit a Schechter function to the bright-end of the individual clusters LFs in the magnitude region brighter than the observed upturn of the dwarf galaxies. We observe that the distributions of the derived parameters is close to a Gaussian around the value of the composite bright-end LF parameters with a dispersion compatible with the statistical errors. We conclude that the bright-end of the galaxy clusters is universal. To study the behavior of the individual faint-end LF we define the Dwarf to Giant galaxy Ratio (DGR) of the single clusters. We notice that the distribution of DGR has a spread much larger than the statistical errors. Our conclusion is that the cluster luminosity function is not universal since the cluster faint-end, differently from the bright-end, varies from cluster to cluster.'

- 'RASS-SDSS Galaxy Cluster Survey. III. Scaling relations of galaxy clusters.', Popesso, P., Böhringer, H., Romaniello, M., Voges, W., 2005, A&A, 433, 431
  Abstract:'We use the RASS-SDSS galaxy cluster sample to compare the quality of optical and X-ray luminosities as predictors of other cluster properties such as their masses, temperatures, and velocity dispersions. We use the SDSS spectroscopic data to estimate the velocity dispersions and the virial masses of a subsample of 69 clusters within r_{500} and r_{200}. The ASCA temperature of the intra-cluster medium, T_X, is retrieved from the literature for a subsample of 49 clusters. For this subsample we estimate the cluster masses also by using the mass-temperature relation. We show that the optical luminosity, L_{op}, correlates with the cluster mass much better than the X-ray luminosity, L_X. L_{op} can be used to estimate the cluster mass with an accuracy of 40% while L_X can predict the mass only with a 55% accuracy. We show that correcting L_X for the effect of a cool core at the center of a cluster, lowers the scatter of the $L_X - M$ relation only by 3%. We find that the scatter observed in the $L_{op} - L_X$ relation is determined by the scatter of the $L_X - M$ relation. The mass-to-light ratio in the SDSS i band clearly increases with the cluster mass with a slope 0.2 ± 0.08. The optical and X-ray luminosities correlate in excellent way with both T_X and σ_V with an orthogonal scatter of 20% in both relations. Moreover, L_{op} and L_X can predict with the same accuracy both variables. We conclude that the cluster optical luminosity is a key cluster parameter since it can give important information about fundamental cluster properties such as the mass, the velocity dispersion, and the temperature of the intra-cluster medium.'

- 'RASS-SDSS Galaxy Cluater survey. IV. An ubiquitous dwarf galaxy population in clusters.', Popesso, P., Biviano, A., Böhringer, H., Romaniello, M., 2006, A&A, 445, 29
  Abstract:'We analyze the Luminosity Functions (LFs) of a subsample of 69 clusters from the RASS-SDSS galaxy cluster catalog. When calculated within the cluster phys-

ical sizes, given by r_{200} or r_{500}, all the cluster LFs appear to have the same shape, well fitted by a composite of two Schechter functions with a marked upturn and a steepening at the faint-end. Previously reported cluster-to-cluster variations of the LF faint-end slope are due to the use of a metric cluster aperture for computing the LF of clusters of different masses.

We determine the composite LF for early- and late-type galaxies, where the typing is based on the galaxy $u - r$ colors. The late-type LF is well fitted by a single Schechter function with a steep slope ($\alpha = -2.0$ in the r band, within r_{200}). The early-type LF instead cannot be fitted by a single Schechter function, and a composite of two Schechter functions is needed. The faint-end upturn of the global cluster LF is due to the early-type cluster galaxies. The shape of the bright-end tail of the early-type LF does not seem to depend upon the local galaxy density or the distance from the cluster center. The late-type LF shows a significant variation only very near the cluster center. On the other hand, the faint-end tail of the early-type LF shows a significant and continuous variation with the environment.

We provide evidence that the process responsible for creating the excess population of dwarf early type galaxies in clusters is a threshold process that occurs when the density exceeds ~ 500 times the critical density of the Universe.

We interpret our results in the context of the 'harassment' scenario, where faint early-type cluster galaxies are predicted to be the descendants of tidally-stripped late-type galaxies.'

- ‚RASS-SDSS Galaxy Cluster survey. V. The Abell X-ray Underlumious Clusters.', P. Popesso, A. Biviano, H. Böhringer, M. Romaniello, 2007, A&A, 461, 397
  Abstract:'In this paper we consider a large sample of optically selected clusters, in order to elucidate the physical reasons for the existence of X-ray underluminous clusters. For this purpose we analyzed the correlations of the X-ray and optical properties of a sample of 137 spectroscopically confirmed Abell clusters in the SDSS database. We searched for the X-ray counterpart of each cluster in the ROSAT All Sky Survey. We find that 40% of our clusters have a marginal X-ray detection or remain undetected in X-rays. These clusters appear too X-ray faint on average for their mass as determined by velocity dispersion; i.e. they do not follow the scaling relation between X-ray luminosity and virial mass traced by the other clusters. On the other hand, they do follow the general scaling relation between optical luminosity and virial mass. We refer to these clusters as the X-ray-underluminous Abell clusters (AXU clusters, for short) and designate as 'normal' the X-ray detected Abell systems. We separately examined the distributions and properties of the galaxy populations of the normal and the AXU clusters. The AXU clusters are characterized by leptokurtic (more centrally concentrated than a Gaussian) velocity distribution of their member galaxies in the outskirts ($1.5 < r/r_{200} \leq 3.5$), as expected for the systems in accretion. In addition,

the AXU clusters have a higher fraction of blue galaxies in the external region and show a marginally significant paucity of galaxies at the center. Our results seem to support the interpretation that the AXU clusters are systems in formation undergoing a phase of mass accretion. Their low X-ray luminosity should be due to the still accreting intracluster gas or to an ongoing merging process.'

- 'RASS-SDSS Galaxy Cluster survey. VI. The dependence of the cluster SFR on the cluster global properties.', P. Popesso, A. Biviano, M. Romaniello, H. Böhringer, 2007, A&A, 461, 411
  Abstract: ,To quantify the relationships between star formation in cluster galaxies and global cluster properties. Using a subsample of 79 nearby clusters from the RASS-SDSS galaxy cluster catalogue of Popesso et al. (2005a), we perform a regression analysis between the cluster integrated star formation rate (ΣSFR) the cluster total stellar mass ($M_\star$), the fractions of star forming (f_{SF}) and blue (f_b) galaxies and other cluster global properties, namely its richness (N_{gal}, i.e. the total number of cluster members within the cluster virial radius, corrected for incompleteness), velocity dispersion (σ_v), virial mass (M_{200}), and X-ray luminosity (L_X). All cluster global quantities are corrected for projection effects before the analysis. Galaxy SFRs and stellar masses are taken from the catalog of Brinchmann et al. (2004), which is based on SDSS spectra. We only consider galaxies with $M_r \leq -20.25$ in our analysis, and exclude AGNs. We find that both ΣSFR and $M_\star$ are correlated with all the cluster global quantities. A partial correlation analysis show that all the correlations are induced by the fundamental one between ΣSFR and N_{gal}, hence there is no evidence that the cluster properties affect the mean SFR or $M_\star$ per galaxy. The relations between ΣSFR and $M_\star$, on one side, and both N_{gal} and M_{200}, on the other side, are linear, i.e. we see no evidence that different clusters have different SFR or different $M_\star$ per galaxy and per unit mass. The fraction f_{SF} does not depend on any cluster property considered, while f_b does depend on L_X. We note that a significant fraction of star-forming cluster galaxies are red ($\sim 25\%$ of the whole cluster galaxy population). We conclude that the global cluster properties are unable to affect the SF properties of cluster galaxies, but the presence of the X-ray luminous intra-cluster medium can affect their colors, perhaps through the ram-pressure stripping mechanism.'

- 'RASS-SDSS Galaxy Cluster survey. VII. On the Cluster Mass to Light ratio and Halo Occupation Number.' P. Popesso, A. Biviano, M. Romaniello, H. Böhringer, 2007, astro-ph/0606260, A&A in press
  Abstract:'We explore the mass-to-light ratio in galaxy clusters and its relation to the cluster mass. We study the relations among the optical luminosity (L_{op}), the cluster mass (M_{200}) and the number of cluster galaxies within r_{200} (N_{gal}) in a sample of 217 galaxy clusters with confirmed 3D overdensity. We correct for projection effect, by determining the galaxy surface number density profile in our cluster sample. This is

best fitted by a cored King profile in low and intermediate mass systems. The core radius decreases with cluster mass, and, for the highest mass clusters, the profile is better represented by a generalized King profile or a cuspy Navarro, Frenk & White profile. We find a very tight proportionality between L_{op} and N_{gal}, which, in turn, links the cluster mass-to-light ratio to the Halo Occupation Distribution N_{gal} vs. M_{200}. After correcting for projection effects, the slope of the $L_{op} - M_{200}$ and $N_{gal} - M_{200}$ relations is found to be 0.92 ± 0.03, close, but still significantly less than unity. We show that the non-linearity of these relations cannot be explained by variations of the galaxy luminosity distributions and of the galaxy M/L with the cluster mass. We suggest that the nonlinear relation between number of galaxies and cluster mass reflects an underlying nonlinear relation between number of subhaloes and halo mass.

Bibliography

[1] Abell G.O. 1958, ApJS,3,211

[2] Abell G.O., Corwin H.G.Jr., Olowin D.P. 1989, ApJS, 70, 1

[3] Adami, C., Mazure, A., Biviano A., Katgert, P., & Rhee, G. 1998, A&A, 331, 493

[4] Allen S.W., Schmidt R.W., Fabian A.C. 2001, MNRAS, 328, 37

[5] Andreon S. & Ettori S. 1999 ApJ, 516, 647

[6] Andreon, S. 2004, A&A, 416, 865

[7] Bahcall N.A. & Cen R. 1993, ApJ, 407, 49

[8] Bahcall, N.A., & Comerford, J.M.2002, ApJ, 565, L5

[9] Balogh M.L., Morris S.L., Yee H.K.C., Carlberg R.G., Ellingson E. 1999, MNRAS, 307, 463

[10] Bardeen, J. M., Bond, J. R., Kaiser, N.. Szalay, A. S. 1986, ApJ, 304, 15

[11] Bartelmann, M. 1996, A&A, 313, 697

[12] Basilakos S., Plionis M., Georgakakis A., Georgantopoulos I., Gaga T., Kolokotronis V., Stewart G.C. 2004, MNRAS, 351, 989

[13] Bauer F.E., Alexander D.M., Brandt W.N., Hornschemeier A.E., Miyaji T., Garmire D.P. 2002, AJ, 123, 1163

[14] Baugh C.M., Cole S., Frenk C.S. 1996, MNRAS, 283, 1361

[15] Beijersbergen, M., Hoekstra, H., van Dokkum, P.G., & van der Hulst, T. 2002, MNRAS, 329, 385

[17] Benson A. J., Ellis R.S., Menanteau F. 2002, MNRAS, 336, 564

[17] Berlind A.A., Weinberg D.H. 2002, ApJ, 575, 587

[18] Berlind A.A., Weinberg D.H., Benson A.J., Baugh C.M., Cole S., Dav R., Frenk C.S., Jenkins A., Katz, N., Lacey C.G. 2003, ApJ, 593, 1

[19] Bialek J.J., Evrard A.E., Mohr J.J. 2001, ApJ, 555, 597

[20] Binggeli B., Sandage A., Tammann G.A. 1988, ARA&A, 26, 509

[21] Biviano, A., Durret, F., Gerbal, D., et al. 1995, A&A, 297, 610

[22] Biviano, A., Katgert, P., Mazure, A., et al. 1997, A&A, 321, 84

[23] Blanchard A., Sadat R., Bartlett J.G., Le Dour M. 2000, A&A, 362, 809

[24] Borgani S., Governato F., Wadsley J., Menci N., Tozzi P., Lake G., Quinn T., Stadel J. 2001, ApJ, 559, 71

[25] Böhringer H., Voges W., Huchra J.P., McLean B., Giacconi R., et al. 2000, ApJS, 129, 435

[26] Boyce, P.J., Phillips, S., Jones, J.B., et al. 2001, MNRAS, 328, 277

[27] Bower R.G., Bohringer H., Briel U.G., Ellis R.S., Castander F.J., Couch W.J .1994, MNRAS, 268, 345

[28] Bower R.G., Castander F.J., Ellis R.S., Couch W.J., Boehringer H. 1997, MNRAS, 291, 353

[29] Brighenti F. & Mathews W.G. 2001, ApJ, 553, 103

[30] Burke D.J., Collins C.A., Sharples R.M., Romer A.K., Holden B.P., Nichol, R.C., et al. 1997, ApJL, 488, 83

[31] Butcher H. & Oemler A.Jr. 1978a, ApJ, 219, 18

[32] Butcher H. & Oemler A.Jr. 1978b, ApJ, 226, 559

[33] Butcher H. & Oemler A.Jr. 1984a, ApJ, 285, 426

[34] Butcher H. & Oemler A.Jr. 1984b, Natur, 310, 31

[35] Campana S., Lazzati D., Panzera M.R., Tagliaferri G. 1999, ApJ, 524, 423

[36] Castander F.J., Bower R.G., Ellis R.S., Aragon-Salamanca A., Mason K.O., et al. 1995, Nature, 377, 39

[37] Cavaliere A., Gursky H., Tucker W.H. 1971. Nature, 231, 437

[38] Cavaliere A. & Fusco-Femiano R. 1976, A&A, 49, 137

[39] Cavaliere A., Menci N., Tozzi P. 1998, ApJ, 501, 493

[40] Cayatte V., van Gorkom J.H., Balkowski C., Kotanyi, C. 1990, AJ, 100, 604

[41] Christlein D. & Zabludoff, A. 2003, ApJ, 591, 764

[42] Cole S. 1991, ApJ, 367, 45

[43] Cole S., Aragon-Salamanca A., Frenk C.S., Navarro J.F., Zepf S.E. 1994, MNRAS, 271, 781

[44] Cole S., Lacey C. G., Baugh C. M., Frenk C. S. 2000, MNRAS, 319, 168

[45] Colless M. 1989, MNRAS, 237, 799

[46] Collins C.A., Burke D.J., Romer A.K., Sharples R.M., Nichol R.C. 1997, ApJL, 479, 117

[47] Collins C.A., Guzzo L., Böhringer H., Schücker P., Chincarini G., et al. 2000, MNRAS, 319, 939

[48] Cortese L., Gavazzi, G., Boselli, A., et al. 2003, A&A, 410, L25

[49] Couch W.J., Ellis R.S., MacLaren I., Malin D.F. 1991, MNRAS, 249, 606

[50] Dalcanton J.J. 1996, ApJ, 466, 92

[51] Dalton G.B., Maddox S.J., Sutherland W.J., Efstathiou G. 1997, MNRAS, 289, 263

[52] Davies, J.I., Roberts, S., & Sabatini, S. 2005, MNRAS, 356, 794

[53] Dickinson M., 1997, in *The Early Universe with the VLT,* ed. J. Bergeron, (Springer: Berlin) p.274

[54] Donahue M., Mack J., Scharf C., Lee P., Postman M., et al. 2001, ApJL, 552, 93

[55] Dressler, A., 1978, ApJ, 223, 765

[56] Dressler A. 1980 ApJ, 236, 351

[57] Dressler A., Thompson I.B., Shectman S.A. 1985, ApJ, 288, 481

[58] Drinkwater, M.J., Gregg, M.D., & Colless, M. 2001, ApJ, 548, L139

[59] Driver, S.P., Phillips, S., Davies, J.I., Morgan, I., & Disney, M.J. 1994, MNRAS, 268, 393

[60] Edge A.C., Stewart G.C., Fabian A.C., Arnaud K.A., 1990, MNRAS, 245, 559

[61] Ebeling H., Voges W., Böhringer H., Edge A.C., Huchra J.P., Briel U.G.. 1996, MNRAS, 281, 799

[62] Ebeling H., Edge A.C., Fabian A.C., Allen S.W., Crawford C.S., Böhringer H. 1997, ApJL, 479, 101

[63] Ebeling H., Edge A.C., Bohringer H., Allen S.W., Crawford C.S., et al. 1998, MNRAS, 301, 881

[64] Ebeling H., Jones L.R., Perlman E., Scharf C., Horner D., et al. 2000a, ApJ, 534, 133

[65] Ebeling H., Edge A.C., Allen S.W., Crawford C.S., Fabian A.C., Huchra J.P. 2000b, MNRAS, 318, 333

[66] Ebeling H., Edge A.C., Henry J.P. 2001, ApJ, 553, 668

[67] Eke V.R., Cole S., Frenk C.S., 1996, MNRAS, 282, 263

[68] Evrard A. E. & Henry J. P. 1991, ApJ, 383, 95

[69] Evrard A.E., MacFarland T.J., Couchman H.M.P., Colberg J.M., Yoshida N., White S.D.M., Jenkins A., Frenk C.S., Pearce F.R., Peacock J.A. Thomas P. A. 2002, ApJ, 573, 7

[70] Feldmeier J.J., Ciardullo R., & Jacoby G.H. 1998, ApJ, 503, 109

[71] Feldmeier J.J., Ciardullo R., Jacoby G.H., Durrell P.R. 2004, ApJ, 615, 196

[72] Felten J.E., Gould R.J., Stein W.A., Woolf N.J.. 1966. ApJ, 146, 955

[73] Ferguson A.M.N., Wyse R.F.G., Gallagher J.S., Hunter D.A. 1998, Nature, 391, 461

[74] Forman W. & Jones C. 1982, ARA&A,, 20, 547

[75] Gallagher J. S. 1978, ApJ, 223, 386

[76] Garilli, B., Maccagni, D., & Andreon, S. 1999, A&A, 342, 408

[77] Giacconi R., Branduardi G., Briel U., Epstein A., Fabricant D. et al. 1979 ApJ, 230, 540

[78] Giacconi R., Zirm A., JunXian W., Rosati P., Nonino M., et al. 2002, ApJS, 139, 369

[79] Gilbank D.G., Bower R.G., Castander F.J., Ziegler B.L. 2004, MNRAS, 348, 551

[80] Gioia I.M., Henry J.P., Maccacaro T., Morris SL, Stocke J.T., Wolter A. 1990, ApJL, 356, 35

[81] Gioia I.M. & Luppino G.A.. 1994, ApJS, 94, 583

[82] Girardi M., Borgani S., Giuricin G., Mardirossian F., Mezzetti M. 1998, ApJ, 506, 45

[83] Girardi, M., Manzato, P., Mezzetti, M. et al. 2002, ApJ, 569, 720

[84] Giovanelli R. & Haynes M.P. 1985, ApJ, 292, 404

[85] Gladders M.D.& Yee H.K.C. 2000, AJ, 120, 2148

[86] Gonzalez A.H., Zaritsky D., Dalcanton J.J., Nelson A. 2001, ApJS, 137, 117

[87] Goto, T., Sekiguchi, M., Nichol, R.C., et al. 2002, AJ, 123, 1807

[88] Governato F., Babul A., Quinn T., Tozzi P., Baugh C.M., Katz N., Lake G. 1999 MNRAS, 307, 949

[89] Gross, M.A.K., Somerville R.S., Primack J.R., Holtzman J., Klypin A. 1998, MNRAS, 301, 81

[90] Gunn, J.E., & Gott, J.R.III 1972, ApJ, 176, 1

[91] Gunn J.E., Hoessel J.G., Oke J.B. 1986, ApJ, 306, 30

[92] Gursky H., Kellogg E., Murray S., Leong C., Tananbaum H., Giacconi R. 1971. ApJ, 167, 81

[93] Hasinger G., Altieri B., Arnaud M., Barcons X., Bergeron J., et al. 2001, A&A, 365, 45

[95] Henry J.P., Gioia I.M., Maccacaro T., Morris S.L., Stocke J.T., Wolter A. 1992, ApJ, 386, 408

[95] Henry J.P., Gioia I.M., Mullis C.R., Voges W., Briel U.G., et al. 2001. ApJL, 553, 109

[96] Henriksen M.J., Mushotzky R.F. 1986. ApJ, 302, 287

[97] Hernquist L. 1990, ApJ, 356, 359

[98] Holden B.P., Romer A.K., Nichol R.C., Ulmer M.P. 1997, AJ, 114, 1701

[99] Holden B.P., Nichol R.C., Romer A.K., Metevier A., Postman M., et al. 1999. AJ 118, 2002

[100] Homeier N. L., Demarco R., Rosati P., Postman M., Blakeslee J.P. et al. 2005, ApJ, 621, 651

[101] Jenkins A., Frenk C.S., White S.D.M., Colberg J.M., Cole S., Evrard A.E., Couchman H.M.P., Yoshida N. 2001, MNRAS, 321, 372

[102] Jones L.R., Scharf C., Ebeling H., Perlman E., Wegner G., et al. 1998, ApJ, 495, 100

[103] Kaiser N. 1984, ApJ, 284,9

[104] Kaiser N. 1986, MNRAS, 222, 323

[105] Kauffmann G., White S. D. M., Guiderdoni B. 1993, MNRAS, 264, 201

[106] Kauffmann G., Charlot S., White S.D.M., 1996, MNRAS, 283, 117

[107] Kauffmann G., Nusser A., Steinmetz M. 1997, MNRAS, 286, 795

[108] Kauffmann G., Colberg J.M., Diaferio A., White S.D.M. 1999, MNRAS, 307, 529

[109] Kay S.T., Pearce F.R., Frenk C.S., Jenkins A. 2002, MNRAS, 330, 113

[110] Kellogg E., Gursky H., Leong C., Schreier E., Tananbaum H., Giacconi R. 1971. ApJ, 165, 49

[111] Kenney J.D.P., van Gorkom J.H., Vollmer B. 2004, AJ, 127, 3361

[112] Kim R.S.J., Kepner J.V., Postman M., Strauss M.A., Bahcall N.A., et al. 2002. AJ, 123, 20

[113] King I. 1962, AJ, 67, 274

[114] Kitayama T., Suto, Y., 1997, ApJ,490, 557

[115] Kochanek, C. S., White, M., Huchra, J. et al. 2003, ApJ, 585, 161

[116] Kodoma T. & Bower R.G. 2001, MNRAS, 321, 18

[117] Kravtsov A.V., Gnedin O.Y., Klypin A.A. 2004, ApJ, 609, 482

[120] Lacey C. & Cole S. 1993, MNRAS, 262, 627

[119] Larson R.B., Tinsley B.M., Caldwell C.N. 1980, ApJ, 237, 692

[120] Lavery R.J. & Henry J.P. 1988, ApJ, 330, 596

[121] Ledlow M.J., Voges W., Owen F.N., Burns J.O. 2003, AJ, 126, 2740

[122] Lin, Y.-T., Mohr, J.J., & Stanford, S.A. 2003, ApJ, 591, 749

[123] Lidman C.E & Peterson B.A. 1996, AJ, 112, 2454

[124] Lobo, C., Biviano, A., Durret, F., et al. 1997, A&A, 317, 385

[125] Lugger, P.M. 1986, ApJ, 303, 535

[126] Lugger, P.M. 1989, ApJ, 343, 572

[127] Lumsden S. L., Nichol R.C., Collins C.A., Guzzo L. 1992, MNRAS, 258, 1

[128] Lumsden, S.L., Collins, C.A., Nichol, R.C., Eke, V.R, & Guzzo, L. 1997, MNRAS, 290, 119

[129] Ma, C.P. & Fry J.N. 2000, ApJ, 543, 503

[130] McHardy I.M., Lawrence A., Pye J.P., Pounds K.A. 1981. ApJ, 197, 893

[131] Maddox S. J., Efstathiou G., Sutherland W.J. 1990, MNRAS, 246, 433

[132] Margoniner, V.E., de Carvalho, R.R., Gal, R.R., et al. 2001, ApJ, 548, L143

[133] Mellier Y. 1999, ARA&A, 37, 127

[134] Menci, N., Cavaliere, A., Fontana, A., Giallongo, E. & Poli, F. 2002, ApJ, 575, 18

[135] Merritt, D. 1984, ApJ, 280, 5

[136] Michie R. W. & Bodenheimer P.H. 1963, MNRAS, 126, 269

[137] Mihos J.C, Harding P., Feldmeier J., Morrison H. 2005, ApJ, 631, 41

[138] Mo, H. J.& White, S. D. M. 1996, MNRAS, 282, 347

[139] Monaco, P., 1998, Fundamentals of Cosmic Physics,19, 157-317.

[140] Moore B., Katz N., Lake G., Dressler A., Oemler A.Jr. 1996 Nature 379, 613

[141] Moore, B., Lake, G., & Katz, N. 1998, ApJ, 495, 139

[142] Mullis C.R., Henry J.P., Gioia I.M., Böhringer H., Briel U.G., et al. 2001, ApJL, 553, 115

[143] Murante G., Arnaboldi M., Gerhard O., Borgani S., Cheng L.M., Diaferio A., Dolag K., Moscardini L., Tormen G., Tornatore L., Tozzi P. 2004, ApJ, 607, 83

[144] Navarro J.F., Frenk C.S., White S.D.M. 1995, MNRAS, 275, 720

[145] Navarro, J. F., Frenk, C. S., White, S. D.M. 1996, ApJ, 462, 563

[146] Navarro, J. F., Frenk, C. S., White, S. D.M. 1997, ApJ, 490, 493

[147] Newberry M.V., Kirshner R.P., Boroson T.A. 1988, ApJ 335, 629

[148] Oemler A.Jr., Dressler A., Butcher H.R. 1997, ApJ, 474, 561

[149] Olsen L.F, Scodeggio M., da Costa L., Benoist C., Bertin E., Deul E., Erben T., Guarnieri M.D., Hook R., Nonino M. 1999, A&A, 345, 681

[150] Paolillo, M., Andreon, S., Longo, G., et al. 2001, A&A, 367, 59

[151] Peacock J.A. & Smith R.E. 2000, MNRAS, 318, 1144

[152] Pearce F.R., Jenkins A., Frenk C.S., White S.D.M., Thomas P.A., Couchman H.M.P., Peacock J.A., Efstathiou G 2001, MNRAS, 326, 649

[153] Peebles, P. J. E., 1993, Principles of physical cosmology, Princeton University Press

[154] Perlman E.S., Horner D.J., Jones L.R., Scharf C.A., Ebeling H., et al. 2002, ApJS, 140, 265

[155] Piccinotti G., Mushotzky R.F., Boldt E.A., Holt S.S., Marshall F.E., et al. 1982. ApJ, 253, 485

[156] Pierpaoli E., Scott D., White M. 2001, MNRAS, 325, 77

[157] Phillips, S., Driver, S.P., Couch, W.J., & Smith, R.M. 1998, ApJ, 498, L119

[158] Ponman T.J., Cannon D.B. Navarro J.F. 1999, Natur, 397, 135

[159] Postman M., Lubin L.M., Gunn J.E., Oke J.B., Hoessel J.G., Schneider D.P., Christensen J.A. 1996 AJ, 111, 615

[160] Pratt G.W. & Arnaud M. 2005, A&A, 429, 791

[161] Press W. H., Schechter P. 1974, ApJ, 187, 425

[162] Raymond J.C. & Smith B.W. 1977, ApJS, 35, 419

[163] Rakos K. & Shombert J. 2004, AJ, 127, 1502

[164] Ramella, M., Boschin, W., Geller, M.J., Mahdavi, A., & Rines, K., AJ, in press, astro-ph/0407640

[165] Rauzy, S., Adami, C., & Mazure, A. 1998, A&A, 337, 31

[166] Rees M.J., Ostriker J.P. 1977, MNRAS, 179, 541

[167] Reiprich T.H. & Bhringer H. 2002, ApJ, 567, 716

[168] Rines, K., Geller, M. J., Diaferio, A., et al. 2004, AJ, 128, 1078

[169] Rosati P., Della Ceca R., Burg R., Norman C., Giacconi R. 1995, ApJL, 445, 11

[170] Rosati P., Della Ceca R., Burg R., Norman C., Giacconi R. 1998, ApJL, 492, 21

[171] Rosati P., Borgani S., Della Ceca R., Stanford S.A., Eisenhardt P.R., Lidman C. 2000. In *Large Scale Structure in the X–ray Universe*, ed M Plionis, I Georgantopoulos, p.13. Paris, France: Atlantisciences

[172] Rosati P., Borgani S., Norman, C., 2002, ARA&A, 40, 539

[173] Rothschild R. et al. 1979 *Space Sci. Instr.* 4:265

[174] Sabatini, S., Davies, J., Scaramella, R., et al. 2003, MNRAS, 341, 981

[175] Sarazin, C. L., 1988 'X-Ray Emission from Clusters of Galaxies', BRITISH ASTRON. ASSOC. JNL. V. 98, NO. 4, P.212

[176] Scharf C.A., Jones L.R., Ebeling H., Perlman E., Malkan M., et al. 1997, ApJ, 477, 79

[177] Schechter, P., 1976, ApJ,203,297

[178] Schneider D.P., Dressler A., & Gunn J.E. 1989, AJ, 92, 523

[179] Schombert J.M. 1987, ApJS, 64, 643

[180] Schombert J.M. 1988, ApJ, 328, 475

[181] Scoccimarro R., Sheth R.K., Hui L., Jain B. 2001, ApJ, 546, 20

[182] Seljak U. 2000, MNRAS 318, 203

[183] Seljak U. 2002, MNRAS, 337, 769

[184] Sheth R.K. & Tormen G. 1999, MNRAS, 308, 119

[185] Smith S. 1936, ApJ, 83, 23

[186] Smith R.M., Driver S.P. & Phillips S. 1997, MNRAS, 287, 415

[187] Somerville R.S. & Primack J.R. 1999, MNRAS, 310, 1087

[188] Stanford S.A., Elston R., Eisenhardt P.R., Spinrad H., Stern D., Dey A. 1997. AJ 114, 2232

[189] Struck C. 1999, PhR, 321, 1

[190] Tozzi P.& Norman C. 2001, ApJ, 546, 63

[191] Tozzi P., Rosati P., Nonino M., Bergeron J., Borgani S., Gilli R., Gilmozzi R., Hasinger G. Grogin N., Kewley L. et al. 2001, ApJ, 562, 42

[192] Trentham, N. 1998, MNRAS, 295, 360

[193] Trentham, N., Tully, R. B., & Verheijen, M.A.W. 2001, MNRAS, 325, 385

[194] Trümper J. 1993, Science, 260, 1769

[195] Tully, R.B., Somerville, R.S., Trentham, N., & Verheijen, M.A. 2002, ApJ, 569, 573

[196] Valotto, C., Nicotra, M.A., Muriel, H., & Lambas, D.G. 1997, ApJ, 479, 90

[197] van Albada T.S. 1982, MNRAS, 201, 939

[198] van Haarlem M.P., Frenk C.S., White S.D.M. 1997, MNRAS, 287, 817

[200] van Dokkum P.G., Franx M., Fabricant D., Illingworth G.D., Kelson D.D. 2000 ApJ, 541, 95

[200] van Dokkum P.G., Franx M., Frster S. et al. 2004, ApJ, 611, 703

[201] Viana P.T.P. & Liddle A.R. 1999, MNRAS, 303, 535

[202] Viana P.T.P., Nichol R.C., Liddle A.R. 2002, ApJ, 569L, 75

[203] Vikhlinin A., McNamara B.R., Forman W., Jones C. Hornstrup A., Quintana H., et al. 1998a, ApJL, 498, 21

[204] Vikhlinin A., McNamara B.R., Forman W., Jones C., Quintana H., Hornstrup A. 1998b, ApJ, 502, 558

[205] Voit G.M. 2004, astro-ph/0410173, Rev.Mod.Ohys. in press

[206] Yagi, M., Kashikawa, N., Sekiguchi, M., et al. 2002 AJ, 123, 87

[207] Yee H.K.C., Ellingson E., Carlberg R.G. 1996. ApJS, 102, 269

[208] York D.G., Adelman J., Anderson J.E.Jr., Anderson S.F., Annis J., et al. 2000., AJ, 120, 1579

[209] Yoshikawa K., Taruya A., Jing Y.P., Suto Y. 2001, ApJ, 558, 520

[210] White, S. D. M.; Rees, M. J. 1978, MNRAS, 183, 341

[211] White S.D.M. & Frenk C.S. 1991, ApJ, 379, 52

[212] White M., Hernquist L., Springel V., 2001, ApJ, 550, 129

[213] Willman B., Governato F., Wadsley J., Quinn T. 2004, MNRAS, 355, 159

[214] Wu X., Xue Y., Fang L. 1999, ApJ, 524, 22

[215] Wu K.K.S., Fabian A.C., Nulsen P.E.J. 2000, MNRAS, 318, 889

[216] Zwicky F. 1937, ApJ, 86, 217

[217] Zwicky, F.& Karpowicz M. 1966, ApJ, 146, 43

Chapter 2

Summary of the results

2.1 Part I: Clusters as laboratories of galaxy formation.

2.1.1 The Cluster Luminosity Function

The general CLuster LF

We analyze the Luminosity Functions (LFs) of a subsample of 69 clusters from the RASS-SDSS galaxy cluster catalog. We have presented a detailed analysis of the cluster individual and composite luminosity functions down to -14 mag in all the Sloan photometric bands. First, we calculate the individual and the composite cluster LF within a metric aperture of 1 Mpc for all the ssystems. The LF clearly shows a bimodal behavior with an upturn and a evident steepening in the faint magnitude range in any SDSS band. The LF is well fitted

by the sum of two Schechter functions. The results are well confirmed by different methods of background subtraction. The observed upturn of the faint galaxies has a location ranging from -16 +5log(h) in the g band to -18.5 +5log(h) in the z band. The bright end LF shows the classical slope of -1.25 in each photometric band, while M^* is brighter in the red bands than in the blue bands. The distribution of the Schechter parameters obtained fitting only the bright end of the individual cluster LF is close to a Gaussian around the corresponding value of the composite bright-end LF. We check the dependence of the Schecter parameters of the composite LF on the clustercentric distance calculating the LF within different cluster apertures. We do not find any significant variation of the results with different apertures. Therefore, we conclude that the bright-end of the galaxy clusters is universal in different cluster environments, both in different systems and in different locations within the same cluster.

The faint end LF is much steeper than the bright end LF with slope $-2.5 \leq \alpha \leq -1.6$. We apply different tests to check whether the observed faint end in the single clusters is due to the presence of background large scale structures or a second cluster on the line of sight. To check the first possibility we measure the individual cluster LF with a color cut method to identify the cluster members. We obtain the same slope observed with the statistical background subtraction. Moreover, we observe that the faint population is dominated by galaxies with colors compatible with late type galaxies at the cluster redshift. We, then, conclude that the observed steepening of the cluster LF is due to the presence of a real population of faint cluster galaxies.

In order to analyze the behavior of the composite LF faint-end as a function of waveband and clustercentric distance, we define the number ratio of dwarf to giant galaxies, DGR, as the ratio between the number of faint ($-18 \leq M \leq -16.5$) and bright ($M < -20$) galaxies in the cluster LF. In each waveband the DGR seems to slightly increase from the very center 0.3 Mpc h^{-1} to 1.0 Mpc h^{-1}. When the DGRs are computed within a fixed metric radius, they are found to vary also from cluster to cluster, more than expected from statistical errors. These variations are not random however. The DGRs are significantly anti-correlated with several cluster global properties, i.e. the cluster velocity dispersions, masses, and X-ray and optical luminosities. All the correlations are very significant ($1–5 \times 10^{-5}$, according to a Spearman correlation test). The more massive a cluster, the lower its fraction of dwarf galaxies. The correlation between cluster DGRs and cluster masses is most likely due to the choice of a fixed metric aperture for all the clusters. In fact, a fixed metric aperture samples larger (smaller) fractions of the virialized regions of clusters of smaller (respectively, larger) masses, and DGR is known to increase with clustercentric distance. If the cluster LF is calculated within the physical size of the system, as the virial radius (r_{500} or r_{200}), the differences due to aperture effects disappear and the individual cluster LF is well represented by the composite LF. Therefore, we conclude that the shape of the cluster LF is universal in all the magnitude ranges.

The CLuster LF per morphological type

We use the $u-r$ color to study the color distribution of the faint cluster galaxies. The color distribution confirms that the contamination due to background galaxies is due to field-to-field variance of the background. We apply the color cut at $u-r=2.22$ suggested by Strateva et al. (2001) to separate early-type from late-type galaxies and study the composite LF by morphological type. We observe that the upturn at the faint magnitudes shown by the complete LF is due to early-type galaxies while the late-type LF is well represented by a single Schechter function.

We study the cumulative and the differential radial profile of the faint early- and late-type galaxies in clusters. The faint early-type galaxies are concentrated in the central regions while the faint late-type galaxies dominate the outskirts of the systems. The analysis of the color-density relation in a reference sample of nearby galaxies selected from the SDSS spectroscopic sample suggests that red galaxies could be a typical cluster galaxy population. Our analysis show that the bright red population seems to have a luminosity distribution absolutely independent from the behavior of the faint red galaxies in different environments. We observe a fading of the LF upturn toward the cluster core.

Comparison with the field LF

It is also interesting to compare our composite cluster LFs with the LF of field galaxies. Blanton et al. (2005) have recently derived the LF of field SDSS galaxies down to -12 mag. Their LF have a very weak upturn, much shallower and at a fainter carachteristic magnitude than in our cluster LF. The faint-end slope of their LF is -1.3, but could be steeper (-1.5) if a correction is applied to account for low surface-brightness selection effects. The LF of *blue* field galaxies is even steeper, but the authors do not report the value of the faint-end slope. A similar faint-end slope (-1.5) has also been found by Madgwick et al. (2002) for the LF of field galaxies from the 2dF survey. They also noticed an upturn in the LF, due to an overabundance of early-type galaxies, making it impossible to fit the LF adequately with a single Schechter function. A previous determination of the SDSS field LF was obtained by Nakamura et al. (2003). They found a slope of ~ -1.9 for dIrr, consistent with the value found by Marzke et al. (1994) for the CfA survey.

The faint-end slope of our late-type cluster galaxies LF is steeper than most field LFs for the same galaxy type (see Table 3 in Paper II) but consistent with those of Nakamura et al. (2003) and Marzke et al. (1994). Given the large variance of results for the field LFs, possibly due to the different magnitude limits adopted, or to poor statistics in the fainter bins of the LF (see de Lapparent 2003 for a thorough discussion on this topic), we conclude there is no significant difference between the late-type LF in clusters and the field.

Hierarchical clustering theories of galaxy formation generically predict a steep mass function of galactic halos (Kauffmann, White & Guideroni 1993; Cole et al. 1994). This is in

conflict with the flat galaxy LF measured in the field and in diffuse local groups, but not with the steep LF measured in many clusters. However in the hierarchical universe, clusters form relatively recently from the accretion of smaller systems. The dynamical processes that operate in clusters are destructive. Ram pressure stripping (e.g. Moore & Bauer 1999) and gravitational tides/galaxy harassment (e.g. Moore et al. 1996, 1998) will both tend to fade galaxies by removing gas or stripping stars. These processes are most effective for less massive, less bound systems. Hence, we might expect to see a flattening of the faint end slope in clusters compared to the field, rather than the observed steepening.

The dwarf galaxy population in clusters

There are many observations and theoretical models in the literature that try to explain the formation and evolution of cluster galaxies, red dwarf galaxies in particular. According to the hierarchical picture for structure formation, small dark matter haloes form before large ones. If one identifies the dwarf galaxies with the small dark matter haloes, they are predicted to origin soon after the structure formation began. Dwarf ellipticals would then be old, passively evolved galaxies. This scenario seems to be inconsistent with the observations of a large spread in age and metallicity in the clusters dwarf early-type galaxies (Conselice et al. 2001,2003; Rakos et al. 2001). Hence, dwarf ellipticals must have had a delayed star formation epoch. The delay could be originated by the intense ultraviolet background intensity at high redshift, keeping the gas of the dwarf galaxies photoionized until $z \sim 1$, or, perhaps by the intra-cluster medium confinement. The intra-cluster medium pressure could avoid dwarf galaxies losing their gas content by SN ejecta. However, this possibility would require a much more centrally concentrated distribution of dwarf ellipticals in clusters than is observed.

In alternative, the excess of dwarf early-type galaxies in clusters could origin from the evolution of field dIrr when they are accreted by the clusters. The evolution of dIrr into dwarf early-type galaxies is supported by the result of van Zee et al. (2004), namely that there is significant similarity in the scaling relations and properties of dIrr and dEs. A scenario where *all* dwarf early-type galaxies evolve from dIrr via disk fading does not however seem possible, because many dEs in the Virgo and Fornax clusters are brighter than the dIrr (Conselice et al. 2001).

Perhaps, some dwarf early-type galaxies evolve from dIrr and some evolve from spirals. The evolution of spirals into dwarf spheroidals can occur via the process of 'galaxy harassment' proposed by Moore et al. (1996,1998). In this scenario, close, rapid encounters between galaxies can lead to a radical transformation of a galaxy morphology. Gas and stars are progressively stripped out of the disk systems, eventually leaving a spheroidal remnant, that resembles an S0 galaxy or a dwarf spheroidal, depending on the size of the progenitor. Direct support for the harassment scenario comes from the discoveries of disks or even spiral arms in dwarf early-type cluster galaxies (Jerjen et al. 2000; Barazza et al. 2002; Graham

et al. 2003). Indirect support comes from the similar velocity distribution of dwarf cluster galaxies (Drinkwater et al. 2001) and gas-rich spirals and irregulars (Biviano et al. 1997), both suggesting infalling orbits.

Is the harassment scenario still viable in view of our results? We can draw the following conclusions from our observational results. First, the universality of the cluster LF suggests that whatever shapes the cluster LF is not strictly dependent on the cluster properties. Second, the difference between the cluster and field LF seems to be related to an excess of dwarf early-type galaxies in clusters. Hence, there is a cluster-related process that leads to the formation of dwarf early-type galaxies, regardless of the cluster intrinsic properties. The process cannot be related, e.g., to the intra-cluster gas density, or the cluster velocity dispersion, or the cluster mass, hence, a process like ram-pressure would seem to be ruled out.

The density dependence of the relative number of early- and late-type dwarfs suggests that the shaping of the cluster LF is related to the excess mean density relative to the field, which is the same for all clusters if, as we have done, the cluster regions are defined within a fixed overdensity radius (r_{200} in our case). In other words, the transformation of spirals, and perhaps, dIrr, into dwarf spheroidals or dEs, seems to be a threshold process that occurs when the local density exceeds a given threshold. Judging from Fig. **??**, this threshold seems to occur at a clustercentric distance of ~ 0.6–$0.7\ r_{200}$.

We have also found that the relative number of dwarf early- and late-type galaxies increases with decreasing clustercentric distance (and increasing density). Galaxies near the cluster center are probably an older cluster population, accreted when the cluster was smaller, according to the hierarchical picture of cluster formation and evolution. Hence, these centrally located galaxies have had more time to accomplish the morphology transformation than galaxies located in the cluster outskirts, which are more recent arrivals.

On the other hand, very near the cluster center, an additional process must be at work to explain our observed fading of the upturn of the cluster early-type LF, and the decrease of both the early- and the late-type dwarf-to-giant galaxy ratio with decreasing clustercentric distance. High-velocity dispersions in clusters inhibit merging processes (e.g. Mihos 2004), hence it is unlikely that dwarf galaxies merge to produce bigger galaxies at the cluster centers. Consistently, we find that the shape of the bright-end of the early-type LF does not depend on the environment, which suggests that bright early-type galaxies are not a recent product of the cluster environment. In fact, the luminosity density profile of bright early-type galaxies has not evolved significantly since redshift $z \sim 0.5$ (Ellingson 2003).

The most likely explanation for the lack of dwarf galaxies near the cluster center is tidal or collisional disruption of the dwarf galaxies. The fate of the disrupted dwarfs is probably to contribute to the intra-cluster diffuse light (e.g. Feldmeier et al. 2004; Murante et al. 2004; Willman et al. 2004).

The difference between the cluster and field LF could thus be explained as a difference in morphological mix, plus a density-dependent dwarf early-type galaxies LF, that, added

to an invariant bright early-type LF, produces a more or less important and bright upturn, depending on the density of the environment.

Whether galaxies evolve from one type to another, in response to the local density, to create the morphology-density relation, or whether the relation is established when the galaxies form, is still an open issue (see, e.g., Dressler 2004). Photometric data alone cannot provide conclusive indications about the nature and the origin of the dwarf population in cluster. In this respect, it would be very useful to sample the velocity distributions of a large set of dwarf galaxies in clusters, in order to constrain their orbital characteristics as it has recently been done for bright cluster galaxies (Biviano & Katgert 2004). If the dwarf early-type galaxies evolve from spirals, radially elongated orbits are expected, while if dwarf early-type galaxies are a more pristine cluster population, their orbits should resemble the isotropic orbits of ellipticals. Additional insights may come from higher accuracy spectroscopy of the dwarf galaxies, allowing to deduce information about their internal velocity dispersion and metallicity, which could be used to put constraints on their age (see, e.g., Kauffmann et al. 2004; Carretero et al. 2004).

2.1.2 The cluster Star Formation Rate as a function of the cluster properties

We have presented a detailed analysis of the dependence of the cluster integrated SFR and stellar mass on the cluster global properties. For the first time we observe a very tight positive correlation between the integrated SFR and the cluster mass and velocity dispersion. The increse of ΣSFR as a function of the cluster mass (velocity dispersion) is due to the observed proportionality between ΣSFR and N_{gal}, the number of cluster galaxies within the virial radius. Massive clusters have an higher integrated SFR because they contain an higher number of galaxies and proportionally an higher number of star forming galaxies. The best relation between the integrated SFR calculated within the virial radius and the cluster mass is a power law, $\Sigma SFR \propto M_{200}^{\beta}$ with $\beta = 0.86 \pm 0.06$. We analyse the relation between the cluster ΣSFR and the X-ray luminosity of the systems. A positive correlation does exist but with a lower significance than in the previous cases.

The same analysis is performed on the relation between the total cluster stellar mass within r_{200} and the cluster global properties. We find that the cluster M_{star} mimics perfectely the behavior of the ΣSFR with regard to the considered properties such as the cluster mass, velocity dispersion and X-ray luminosity. It is interesting to note that to total cluster M_{star} is the integral of the cluster ΣSFR over. We could speculate that, due to the surprising similarity between the behavior of M_{star} and ΣSFR, at least the slope of the relation between the integrated SFR with the cluster properties did not evolve significantly.

For both quantities relations , $\Sigma SFR - M_{200}$ and $M_{star} - M_{200}$, the slope of the power law is smaller than 1. As a consequence, we find and highly significant anti-correlation between the mass normalized cluster ΣSFR and the fraction M_{star}/M_{200} with the cluster

mass (velocity dispersion). The massive clusters have a lower integrated SFR per unit mass and a lower farction of mass in form of stars. Nevertheless, to explain the observed anti-correlation it is not necessary to appeal to processes of SFR truncation or inefficiency in the galaxy members of the massive clusters. This aspect has been analyzed from two point of view. First, we show clearly that the mean cluster SFR is nearly constant throughout our cluster sample and it does not depend on the properties of the systems such as mass, velocity dispersion, X-ray luminosity and galaxy surface density. Second, there is a very poor relation between the fraction of blue and star forming systems with the mass and the velocity dispersion. Instead, we suggest that because of the well observed proportionality between ΣSFR and the number of cluster galaxies, the physical reason of the decrease of $\Sigma SFR/M_{200}$ as a function of the mass is ascribable to the the slope of the $N_{gal} - M_{200}$ relation. In fact, many works in the literature show that $N_{gal} \propto M^{0.7-0.9}$ (Marinoni & Hudson 2002; Pisani et al.2003; Yang et al.2005). These results are consistent with the values of the slope found for the $\Sigma SFR - M_{200}$ and $M_{star} - M_{200}$ relations.

As a last point of our analysis we study the relation between the fraction of blue galaxies with the cluster properties considered so far. We select among the spectroscopic cluster members the blue galaxies using the color cut of Strateva et al. 2001. As mentioned above, we do not find any significant correlation between f_b and the cluster mass and velocity dispersion. We observe a clear anti-correlation between the fraction of blue galaxies and the X-ray luminosity. Moreover, we find an highly significant anti-correlation between f_b and cluster galaxy surface density.

The study of the galaxy SFR as a function of the galaxy color reveals that the color cut of Strateva et al. (2001) is not able to distinguish clearly star forming from non-star forming systems. We observe a large population of red galaxies with SFR similar to the blue galaxies. To distinguish quiescent from star-forming galaxies we use the SFR cut at $SFR/m^* = 10^{-10.5} yr^{-1}$ and define the fraction of star forming systems f_{SF} on the basis of this cut. f_{SF} does not show any significant correlation with the cluster properties considered so far.

A preliminary visual inspection of a small sample of these red star forming systems reveals that they are late type galaxies with a pronounced red central bulge and a small blue disk with some spots of star formation. This very preliminary result suggests that the red star forming could be the results of the trasformation of late type galaxies into red remnants. We consider two possible scanarios : the 'harassmet scenario' of Moore et al. (1996,1998) and the ram pressure stripping scenario. In the former scenario, close, rapid encounters between galaxies can lead to a radical transformation of a galaxy morphology eventually leaving a spheroidal remnant. In the ram pressure stripping scenario the dense Intracluster Medium (ICM) is able to strip the outer part of the galaxies passing through the cluster center with high velocity. The inverse correlation of the fraction of blue galaxies with the X-ray luminosity would suggest this second scenario. On the other hand, the inverse correlation between the f_b and the surface galaxy density would support the role of the

galaxy-galaxy encounters of the harassment scenario. Our data do not allow us to make conclusions on the competitive or complementary role of the ram pressure stripping and the galaxy-galaxy interaction in the transformation of the properties of the cluster star forming galaxies. We can only conclude that the gravitational processes are not likely to affect directly the star formation rate of the cluster galaxies since there is no relation between f_b (f_{SF}) with the cluster mass and velocity dispersion. Instead, the interaction with the ICM ($f_b - L_X$ relation) and the galaxy-galaxy encounters ($f_b - \rho_{gal}$ relation) are more likely responsible of the variations of the star formation in the cluster members.

2.1.3 The Cluster Mass to Light Ratio and the Halo Occupation Number

We have studied the $L - M$ and the $N - M$ relations in the 4 SDSS bands, g, r, i, z for a sample of 217 galaxy clusters with confirmed 3D overdensity in the SDSS DR3 spectroscopic catalog. All the quantities are measured within the cluster characteristic radius r_{200}. We pointed out the direct connection between the two relations due to the proportionality of the cluster optical luminosity and the number of cluster galaxies.

We have studied the galaxy surface number density profile in five bin of cluster mass and discovered that the profile has a strong dependence on the cluster mass. In the low and intermediate mass systems the best fit is provided by a King profile. The core radius of the best fit is decreasing as a function of the cluster mass, while the central galaxy density is increasing. This causes that the profile becomes more centrally concentrated at higher cluster mass, until, in the highest mass bins the simple King profile does not provide an excellent fit and a even more concentrated generalized King profile or a cuspy NFW profile provide the best fit. Using the best fit profile in each mass bin, we have converted the observed number of cluster galaxies to the value within the virial sphere. This fact that clusters of different masses exhibit different surface density profiles, implies that the correction decreases with the cluster mass. Applying a statistical. mass-dependent, correction affects the $L - M$ and $N - M$ relations, by increasing the slope of 10% to the value of 0.92 ± 0.03. As a consequence, the slope of the corrected $M/L - M$ relation is 0.18 ± 0.04. It is, therefore, important to notice that neglecting the dependence of the correction on the cluster mass, would lead to underestimating the slope of the $L_{op} - M_{200}$ and $N_{gal} - M_{200}$ relations. In fact, the corrected $L_{op} - M_{200}$ and $N_{gal} - M_{200}$ relations have a slope steeper than the value of 0.70 typically found in previous works in the literature (see previous subsection for the references) where an average, mass independent, correction is used. Our $N - M$ and the $L - M$ relation are only marginally consistent at the 3σ level with unity, i.e. direct proportionality between cluster mass and number of cluster galaxies. At a face fact, we should conclude that the massive clusters have a smaller number of galaxies per unit mass than the low mass systems. It is, however, important to note that our derived slope could still be underestimated, because we can only apply a statistical correction which may not be sufficient to remove completely the

systematic effect due to projection.

On the basis of these results, it is important to note that all the cluster properties, like to integrated cluster star formation rate (ΣSFR) and the total stellar mass (M_{star}), which are found to be proportional to N_{gal} (see Popesso et al. 2005e) should be converted to the value within the virial sphere. Therefore, in analogy to the $L_{op} - M_{200}$ relation, the corrected $\Sigma SFR - M_{200}$ and $M_{star} - M_{200}$ studied in Popesso et al. (2005e) should be steeper than what observed.

We have compared the properties of our clusters with the prediction of the hierarchical models of structure formation. These models naturally predict that $N \propto M^{\gamma}$ with $\gamma < 1$. This result is generally interpreted as the indication that the galaxies in the low mass systems are older and more luminous per unit mass than the galaxies in high mass clusters. The consequence of this point is a variation of the shape of the cluster LF and of the elliptical fundamental plane with the cluster mass. We have shown that these predictions is inconsistent with our results. In fact, the cluster luminosity functions calculated in cluster of different masses are consistent with each other, confirming the universality of the shape of the cluster LF. Moreover, we have shown that the best fit Schechter function of the composite LF can accurately locate the magnitude of the three brightest cluster galaxies given the normalization of the considered cluster. This result indicated that the BCGs are extracted from the same parent distribution of the composite cluster LF.

On the basis of these results, we point out that the universality of the mass distribution of the sudhalos in the parent halo, predicted by the hierarchical model of galaxy formation, and the observational evidence of a universal luminosity distribution in clusters within r_{200}, are inconsistent with an Halo Occupation Number $\gamma < 1$. We conclude that, on the assumption that our result on the universality of the cluster LF is correct, there are only two possible solutions to the problem. An option is that the mass distribution of the sudhalos in the parent halo is not universal and also $N_{sub} \propto M_{halo}^{\beta}$ with $\beta < 1$. An alternative possibility is that, as suggested above, the statistical correction applied to observed number of cluster galaxies may not be sufficient to remove completely the systematic effect due to projection and the real value of the Halo Occupation Number is 1.

We conclude this paper with the following considerations. From the observational point of view, the mean cluster luminosity function and the $N-M$ or the $L-M$ relation determine completely the luminosity distribution of cluster galaxies. The mean cluster LF constraints with high accuracy the shape of the luminosity distribution in clusters, while the $N - M$ relation, calculated in a given magnitude range, fixes the normalization of the LF as a function of the cluster mass. We point out that the new models of galaxy formation should be able to reproduce simultaneously this cluster properties in order to understand the processes of galaxy formations in the cluster mass halo.

2.2 Part II: X-ray versus Optical cluster properties

2.2.1 Results on the X-ray selected cluster sample

We used the RASS-SDSS galaxy cluster sample to compare the quality of the optical and X-ray luminosity as predictors of other cluster properties such as the mass within r_{500} and r_{200}, the velocity dispersion and the ICM temperature. The optical luminosity turns out to be a better predictor of the cluster mass than the X-ray luminosity. The knowledge of L_{op} allows to estimate the cluster mass with an average accuracy of 40%, while L_X can be used to predict the mass with an average accuracy of 55%. We investigated the nature of the scatter of the $L_X - M$ relation using a sample of clusters with X-ray luminosity corrected for the effect of cool core at the center of the system. We concluded that this kind of effect can affect the scatter of the relation by at most 3% and, thus, it cannot explain the dispersion in the observed $L_X - M$ relation, which is probably related with the variation in the compactness of the galaxy clusters. We conclude that a cluster optical luminosity is a better estimator of its mass than its X-ray luminosity. The optical luminosity is clearly a very useful and rather cheap estimator (in terms of observational resources required) given that it can be determined from ground-based photometric data only.

We also analysed the relations of the optical and X-ray luminosities with cluster velocity dispersions and X-ray temperatures. We found that both luminosities are strongly correlated with these cluster properties, and can be used to predict them with an average accuracy of 20%. Using a sample of clusters with L_X and T_X corrected for the cool core effect, we find that the scatter in the $L_X - T_X$ relation is decreased by 5%. Such a decrease is almost exclusively due to the correction applied to the X-ray temperature, since the cool-core correction has a negligible effect on the X-ray luminosity. Therefore, we expect a similar decrease of the scatter of the $L_{op} - T_X$ relation, when the X-ray temperatures are corrected for the same cool-core effect. Unfortunately we cannot verify this expectation on our sample, since we lack the information to apply the cool-core correction to the clusters with known L_{op}. We conclude that L_{op} and L_X can be used to predict the ICM temperature and the cluster velocity dispersion, at a similar level of accuracy.

The most important conclusion of our analysis is that the optical luminosity is a key measure of the fundamental properties of a galaxy cluster, such as its mass, velocity dispersion, and temperature. In this respect, the optical luminosity performs even better than the X-ray luminosity, which suggests that the mass distribution of a cluster is better traced by cluster galaxies rather than by intracluster gas (see, e.g., the discussion in Biviano & Girardi 2003). The poorer performance of L_X as a cluster mass predictor, relative to L_{op}, is probably related to the variation in the compactness of the galaxy clusters.

Our conclusion is clearly in agreement with Lin et al. (2003) result, namely that the K-band luminosity is a good estimator of the cluster mass. On the other hand, our conclusion is at odds with the generally accepted view that a cluster main physical properties are more

easily revealed in the X-ray than in the optical (e.g. Donahue et al. 2002). Such a view was established at an epoch when the lack of optical wide field surveys precluded a reliable determination of the optical luminosities of a large sample of clusters. With the advent of the Sloan Digital Sky survey, this problem is now overcome, and L_{op} can now be used to infer the fundamental physical properties of the many clusters being discovered within large optical surveys with improved cluster finding techniques (such as, e.g., the Red-Sequence Cluster Survey, Barrientos et al. 2003). In this context L_{op} becomes a very powerful mean to do cosmological studies with galaxy clusters without the need of optical or X-ray spectroscopy.

Finally, we showed that the relation between mass and luminosity implies an increasing mass-to-light ratio, M/L, with increasing cluster mass. The dependence we found is in excellent agreement with previous results (Adami et al. 1998; Bahcall & Comerford 2002; Girardi et al. 2002; Lin et al. 2003, 2004; Rines et al. 2004; Ramella et al. 2004), and confirms the achromaticity of the effect. Hence, the effect cannot be explained by the different ages of the galaxies stellar populations in clusters of different masses (Bahcall & Comerford 2002), but, rather, seems to indicate that the star formation efficiency decreases as the cluster mass increases (Lin et al. 2003).

The results obtained in this paper are applicable to nearby clusters since the RASS-SDSS galaxy cluster catalog comprises only X-ray clusters at $z \leq 0.3$. It would be very interesting to conduct the same analysis on a sample of high redshift clusters to study the evolution of the analysed relations and to compare again the quality of L_{op} and L_X as predictors of the other cluster properties.

The analysis conducted in this work is based on a sample of clusters all detected in the X-ray, 90% of which are taken from X-ray-selected galaxy cluster catalogs. It seems that optically bright clusters exist which are faint in the X-ray (Donahue et al. 2002). Hence, the selection criteria of the RASS-SDSS galaxy cluster catalog could in principle affects our results (see, e.g., Gilbank et al. 2004). To check how the selection criteria affect the correlations studied in this part of the work, we repeat the same analyses on a sample of optically-selected clusters, as shown in the next section.

2.2.2 Results on the otically selected cluster sample

We have studied the X-ray and optical properties of 138 isolated Abell clusters. Each object has a confirmed three-dimensional overdensity of galaxies. We have looked for the X-ray counterpart of each system in the RASS data. Three classes of objects have been identified, where the classification is based on the quality of the X-ray detection. 88 clusters out of the 138 Abell systems have a clear X-ray detection and are considered normal X-ray emitting clusters (the 'normal Abell clusters'). 27 systems have a X-ray detection of low significance (less the 3σ) and 23 do not have clear X-ray detection (a rough estimate of L_X is provided but with huge statistical errors).

The normal Abell clusters follow the same scaling relasions observed in the X-ray selecetd

RASS-SDSS clusters. The $23 + 27$ Abell clusters with unsecure X-ray detection appear to be outliers in the $L_X - M_{200}$ relation determined for X-ray luminous clusters. Their X-ray luminosity is on average one order of magnitude fainter than would be expected for their mass . A carefull analysis of the 3D galaxy overdensity of these systems reveals that the individual galaxy velocity distributions in the virial region are gaussian in 90% of the clusters and are not ascribable to the superposition of smaller interacting systems. We conclude that these Abell clusters with unsecure X-ray detection in RASS are not spurious detections in the redshift distribution, but represent a distinct class of objects. Due to their location with regard to the RASS-SDSS $M - L_X$ relation we call them 'Abell X-ray Underluminous clusters' or AXU clusters for short. Several AXU clusters are confirmed to be very faint X-ray objects in the literature. Their X-ray flux is probably too low to be detected in the RASS survey. Yet, AXU clusters are not outliers from the $L_{op} - M_{200}$ relation, i.e. they have a normal optical luminosity given their mass. Hence, the distinctive signature of AXU clusters seems to lie in an X-ray luminosity which is unexpectedly low.

We have looked for other properties of AXU clusters that make them different from normal Abell clusters. We have shown that AXU clusters do not have more substructures than normal Abell clusters. The galaxy luminosity functions within the virial region of the two cluster samples are very similar to eachother. Rather similar are their galaxy number density profiles, even if the AXU clusters seem to lack galaxies near the core, relative to normal Abell clusters (but the significance of this result is low). The fractions of blue galaxies in the two kinds of clusters are also marginaly different, AXU clusters being characterized by a higher fraction.

The main difference between the two classes of objects lies in the velocity distribution of their member galaxies. The galaxy velocity distribution of the normal Abell clusters is perfectly fitted by a Gaussian both in the inner, virialized region ($\leq 1.5\, r_{200}$), and also in the external region ($1.5\, r_{200} \leq r \leq 3.5\, r_{200}$). The AXU clusters instead have a Gaussian velocity distribution only within the virial region. In the external region, their velocity distribution is significantly more peaked than a Gaussian. The analysis of its shape by comparison with dynamical models available in the literature (van der Marel et al. 2000), suggests a radially anisotropic galaxy orbital distribution. However, the galaxies in this external region need not be in dynamical equilibrium with the cluster potential. As a matter of fact, a leptokurtic shape of the velocity distribution is a typical signature of the external, infall regions of dark matter haloes (Wojtak et al. 2005).

The analysis of the velocity distribution of the AXU clusters in their outer regions hence suggests the presence of an unvirialized component of the galaxy population, still in the process of accretion onto the cluster. This infalling population would be mainly composed of field, hence blue, galaxies, which could then explain the excess of blue galaxies in AXU clusters, relative to normal Abell clusters. On the other hand, the Gaussian velocity distribution in the inner region suggests that there the galaxy population is dynamically more evolved, and probably virialized.

By a similar analysis on a different sample of X-ray underluminous clusters, Bower et al. (1997) came to propose two different scenarios. AXU clusters could be severely affected by projection effects arising from surrounding large-scale structure filaments elongated along the line-of-sight. Their velocity dispersion, and hence their virial masses would then be severely overestimated by interlopers in the filaments. In the alternative scenario AXU clusters could be clusters not yet formed, or in the phase of forming, or, at least, caught at a particular stage of their evolution, while they are undergoing a rapid mass growth.

Should the former of the two scenarios apply, we would expect AXU clusters to be X-ray underluminous for they mass, but they could still be optically luminous because we partly see the light of the filament projected onto the cluster. However, contamination by interlopers does affect the optical luminosity estimate, but not so much as the virial mass estimate, and not so much in the i band, where contamination by the field (hence blue) galaxies should be small. Therefore, in such scenario it would be surprising that the clusters obey so well the Lopt - M200 relation, which requires that the effects of the filament on the dynamical mass estimate and the optical light in the aperture both conspire not to produce an offset from the relation. It would also be surprising that the AXU clusters show a galaxy LF perfectely consistent with the steep LF found in galaxy clusters (see Popesso et al. paper II and IV) and not the flat LF observed in the field (Blanton et al. 2005). Instead AXU clusters are not outliers from the $L_{op} - M_{200}$ relation. If anything, AXU clusters are overluminous in the optical for their mass. In fact, the biweight-average (see Beers et al. 1990) i-band mass-to-light ratios of normal Abell clusters and AXU clusters are $150 \pm 10\, M_{\odot}/L_{\odot}$, and $110 \pm 10\, M_{\odot}/L_{\odot}$, respectively.

As a further test, we have re-calculated the virial masses of all clusters by considering only red cluster members belonging to the red sequence in the $u - i$ vs. i color-magnitude diagram. In this way contamination by interlopers is strongly reduced (see, e.g., Biviano et al. 1997). The cluster masses do not change significantly when only red-sequence members are used to calculate them, suggesting a low level of contamination by interlopers.

The results of our analyses therefore supports Bower et al.'s alternative scenario, namely AXU clusters are systems in the stage of formation and/or of significant mass accretion. If AXU clusters are still forming, the intra-cluster gas itself may still be infalling or have not yet reached the virial temperature. In addition, for AXU clusters undergoing massive accretion, it is to some degree possible that the continuous collisions of infalling groups is affecting the gas distribution, lowering its central density (such as in the case of the so called 'bullet cluster', see Barrena et al. 2002 and Clowe et al. 2004). In both cases the X-ray luminosity would be substantially lower than predicted for the virial mass of the system, because of its dependence on the square of the gas density. We note however that a virialized cluster undergoing a strong collision with an infalling group would show up as a substructured cluster, yet the AXU clusters do not show an increased level of substructures when compared to normal Abell clusters. It is then more natural to suppose that AXU clusters are clusters where virialization has been reached by their member galaxies, but only

in the central region, and not by their intracluster gas.

In summary, we know that the X-ray emission is very much dominated by the central region whereas the optical properties are more global. Therefore it could well be that we see a rough relaxation on the large scale of the galaxy system reflected by a rough Gaussian galaxy velocity distribution, while the central region has not yet settled to reach the high density and temperatures of the luminous X-ray clusters.

In order to explore this further, we need much more detailed information on the distribution of the density and temperature of the intracluster gas in AXU clusters, something that cannot be done with the RASS data, but requires the spatial resolution and sensitivity of XMM-Newton.

Our results give supports to the conclusion of Donahue et al. (2002) concerning the biases inherent in the selection of galaxy clusters in different wavebands. While the optical selection is prone to substantial projection effects, also the X-ray selection is not perfect or not simple to characterize. The existence of X-ray underluminous clusters, even with large masses, makes it difficult to reach the needed completeness in mass for cosmological studies. Moreover, as discussed in Paper III, the relation between the X-ray luminosity and mass is not very tight even for the X-ray bright clusters, and the relation between cluster masses and optical luminosities is as tight or perhaps even tighter. Clearly, a multi-waveband approach is needed for optimizing the completeness and reliability of clusters samples.

On the other hand, it becomes clear that for precision cosmology we also need a more observationally oriented prescription of cluster selection from theory, rather than a mear counting of "relaxed" dark matter halos. Predicted distribution functions closer to the observational parameters like temperature or velocity dispersion distribution functions and their relations to X-ray and optical luminosity are needed.

Bibliography

[1] Adami, C., Biviano, A., & Mazure, A. 1998c, A&A, 331, 439

[2] Bahcall, N.A., & Comerford, J.M. 2002, ApJ, 565, L5

[3] Barazza, F.D., Binggeli, B., & Jerjen, H. 2002, A&A, 391, 823

[4] Barrientos, F., Gladders, M., Yee, H., Ellingson, E., Hall, P., & Infante, L. 2003, Messenger, 112, 40

[5] Beers, T.C., Flynn,K., Gebhardt 1990, AJ, 100, 32

[6] Biviano, A., Katgert, P., Mazure, A., et al. 1997, A&A, 321, 84

[7] Biviano, A., & Girardi, M. 2003, ApJ, 585, 205

[8] Biviano, A., & Katgert, P. 2004, A&A, 424, 779

[9] Bower, R. G., Castander, F. J., Ellis, R. S., et al. 1997, MNRAS, 291, 353

[10] Blanton M.R., Lupton R.H., Schlegel D.J., Strauss M.A., Brinkmann J., Fukugita M., Loveday J. 2005, ApJ, 631, 208

[11] Carretero, C., Vazdekis, A., Beckman, J.E., Sánchez-Blázquez, P., & Gorgas, J. 2004, ApJ, 609, L45

[12] Cole S., Aragon-Salamanca A., Frenk C.S., Navarro J.F., Zepf S.E. 1994, MNRAS, 271, 781

[13] Conselice, C.J., Gallagher, J.S III, & Wyse, R.F.G. 2001, ApJ, 559, 791

[14] Conselice, C.J., Gallagher, J.S. III, & Wyse, R.F.G. 2003, AJ, 125, 66

[15] de Lapparent, V. 2003, A&A, 408, 845

[16] Donahue, M., Scharf, C.A., Mack, J. et al. 2002, ApJ, 569, 689

[17] Dressler, A., 2004, in 'Clusters of Galaxies: Probes of Cosmological Structure and Galaxy Evolution', Cambridge University Press, J.S. Mulchaey, A. Dressler, and A. Oemler Jr., eds., p. 206.

[18] Drinkwater, M.J., Gregg, M.D., & Colless, M. 2001, ApJ, 548, L139

[19] Ellingson, E. 2003, Ap&SS, 285, 9

[20] Feldmeier, J.J., Ciardullo, R., Jacoby, G.H. & Durrell, P.R. 2004, ApJ, 615, 196

[21] Gilbank, D.G., Bower, R.G., Castander, F.J., & Ziegler, B.L. 2004, MNRAS, 348, 551

[22] Girardi, M., Manzato, P., Mezzetti, M. et al. 2002, ApJ, 569, 720

[23] Graham, A.W., Jerjen, H., & Guzmán, R. 2003, AJ, 126, 1787

[24] Kauffmann G., White S. D. M., Guiderdoni B. 1993, MNRAS, 264, 201

[25] Kauffmann, G., White, S.D.M., Heckman, T.M., et al. 2004, MNRAS, 353, 713

[26] Jerjen, H., Kalnajs, A., & Binggeli, B. 2000, A&A, 358, 845

[27] Lin, Y.-T., Mohr, J.J., & Stanford, S.A. 2003, ApJ, 591, 749

[28] Lin, Y.-T., Mohr, J.J., & Stanford, S.A. 2004, ApJ, 610, 745

[29] Madgwick D.S., Lahav, O., Baldry, I.K., et al. 2002 MNRAS, 333, 133

[30] Marinoni, C. & Hudson, M. J 2002, ApJ, 569, 101

[31] Marzke, R.O., Geller, M.J., Huchra, J.P., & Corwin, H.G.Jr. 1994, AJ, 108, 437

[32] Mihos, J.C., 2004, in 'Clusters of Galaxies: Probes of Cosmological Structure and Galaxy Evolution', Cambridge University Press, J.S. Mulchaey, A. Dressler, and A. Oemler Jr., eds., p. 277.

[33] Moore B., Katz N., Lake G., Dressler A., Oemler A.Jr. 1996 Nature 379, 613

[34] Moore, B., Lake, G., & Katz, N. 1998, ApJ, 495, 139

[35] Murante, G., Arnaboldi, M., Gerhard, O., et al. 2004, ApJ, 607, L83

[36] Nakamura, O., Fukugita, M., Yasuda, N., et al. 2003, AJ, 125, 1682

[37] Pisani, A., Ramella, M., Geller, M. J. 2003, AJ,126, 1677

[38] Rakos, K., Schombert, J., Maitzen, H.M., Prugovecki, S., & Odell, A. 2001, AJ, 121, 1974

[39] Ramella, M., Boschin, W., Geller, M.J., Mahdavi, A., & Rines, K., AJ, in press, astro-ph/0407640

[40] Rines, K., Geller, M. J., Diaferio, A., et al. 2004, AJ, 128, 1078

[41] Strateva, I., Ivezić, Z., Knapp, G., et al. 2001 AJ, 122, 1861

[42] van der Marel, R.P., Magorrian, J., Carlberg, R.G., Yee, H.K.C., & Ellingson, E. 2000, AJ, 119, 2038

[43] van Zee, L., Skillman, E.D., & Haynes, M.P. 2004 AJ, 128, 121

[44] Willman, B., Governato, F., Wadsley, J., & Quinn, T. 2004, MNRAS, 355, 159

[45] Wojtak, R., Łokas, E.L., Gottlöber, S., & Mamon, G.A. 2005, MNRAS, 361, L1

[46] Yang, X., Mo, H. J., van den Bosch, F. C. 2005, MNRAS, 358, 217

A&A 423, 449–467 (2004)
DOI: 10.1051/0004-6361:20035818

Astronomy & Astrophysics

RASS-SDSS Galaxy clusters survey

I. The catalog and the correlation of X-ray and optical properties⋆

P. Popesso[1], H. Böhringer[1], J. Brinkmann[2], W. Voges[1], and D. G. York[3]

[1] Max-Planck-Institut fur extraterrestrische Physik, 85748 Garching, Germany
e-mail: popesso@mpe.mpg.de
[2] Apache Point Observatory, PO Box 59, Sunspot, NM 88349, USA
[3] Department of Astronomy and Astrophysics, University of Chicago, 5640 South Ellis Avenue, Chicago, IL 60637, USA

Received 8 December 2003 / Accepted 4 March 2004

Abstract. For a detailed comparison of the appearance of cluster of galaxies in X-rays and in the optical, we have compiled a comprehensive database of X-ray and optical properties of a sample of clusters based on the largest available X-ray and optical surveys: the ROSAT All Sky Survey (RASS) and the Sloan Digital Sky Survey (SDSS). The X-ray galaxy clusters of this RASS-SDSS catalog cover a wide range of masses, from groups of $10^{12.5}$ $M_{\odot}$ to massive clusters of 10^{15} $M_{\odot}$ in the redshift range 0.002−0.45. The RASS-SDSS sample comprises all the X-ray selected objects already observed by the Sloan Digital Sky Survey (114 clusters). For each system we have uniformly determined the X-ray (luminosity in the ROSAT band, bolometric luminosity, center coordinates) and optical properties (Schechter luminosity function parameters, luminosity, central galaxy density, core, total and half-light radii). For a subsample of 53 clusters we have also compiled the temperatures and the iron abundances from the literature. The total optical luminosity can be determined with a typical uncertainty of 20% independent of the choice of local or global background subtraction. We searched for parameters which provide the best correlation between the X-ray luminosity and the optical properties and found that the *z* band luminosity determined within a cluster aperture of 0.5 Mpc h_{70}^{-1} provides the best correlation, with a scatter of about 60−70%. The scatter decreases to less than 40% if the correlation is limited to the bright X-ray clusters. The resulting correlation of $L_{\rm X}$ and $L_{\rm op}$ in the *z* and *i* bands shows a logarithmic slope of 0.38, a value not consistent with the assumption of a constant *M/L*. Consistency is found, however, for an *M/L* increasing with luminosity as suggested by other observations. We also investigated the correlation between $L_{\rm op}$ and the X-ray temperature, obtaining the same result.

Key words. galaxies: clusters: general – galaxies: luminosity function, mass function – methods: observational

1. Introduction

Clusters of galaxies are the largest well defined building blocks of our Universe. They form via gravitational collapse of cosmic matter over a region of several megaparsecs. Cosmic baryons, which represent approximately 10−15% of the mass content of the Universe, follow dynamically the dominant dark matter during the collapse. As a result of adiabatic compression and of shocks generated by supersonic motions, a thin hot gas permeates the cluster gravitational potential. For a typical cluster mass of 10^{14} $M_{\odot}$ the intracluster gas reaches a temperature of the order of 10^7 keV and, thus, radiates optically thin thermal bremsstrahlung and line radiation in the X-ray band. In 1978, the launch of the first X-ray imaging telescope, the *Einstein* observatory, began a new era of cluster discovery, as clusters proved to be luminous ($\geq 10^{42-45}$ erg s^{-1}), extended ($r \sim 1-5$ Mpc) X-ray sources, readily identified in the X-ray sky. Therefore, X-ray observations of galaxy clusters provide an efficient and physically motivated method of identification of these structures. The X-ray selection is more robust against contamination along the line of sight than traditional optical methods since the richest clusters are relatively rare and since X-ray emission, which is proportional to the gas density squared, is far more sensitive to physical overdensities than the projected number density of galaxies in the sky. In fact the existence of diffuse, very hot X-ray emitting gas implies the existence of a massive confining dark matter halo. Moreover, selection according to X-ray luminosity is also an efficient way to find the highest mass concentrations due to well defined correlation between the X-ray luminosity and the total cluster mass (Reiprich & Bhöringher 2002). In addition to allowing the identification of galaxy clusters, X-ray observations provide a wealth of information on the intracluster medium itself, e.g. its metal abundance, radial density distribution and

⋆ Full Tables 1–3 are only available in electronic form at the CDS via anonymous ftp to cdsarc.u-strasbg.fr (130.79.128.5) or via
http://cdsweb.u-strasbg.fr/cgi-bin/qcat?J/A+A/423/449

temperature profile. These latter quantities, in turn, can be used to reliably estimate the *total mass* of the system.

In addition to the hot, diffuse component, baryons are also concentrated in the individual galaxies within the cluster. These are best studied through photometric and spectroscopic optical surveys, which provide essential information about luminosity, morphology, stellar population and age. Solid observational evidence indicates a strong interaction between the two baryonic components, as galaxies pollute the intracluster medium expelling metals via galactic winds producing the observed metal abundances in clusters (De Grandi et al. 2002; Finoguenov et al. 2001). On the other hand, the evolution of galaxies in clusters is influenced by processes due to the hot gas (e.g. gas stripping by ram pressure, etc.) and also by internal processes like star formation, galactic winds, supernovae explosions etc., operating inside the galaxies themselves (Dressler et al. 1997; Fasano et al. 2000; van Dokkum et al. 2000; Lubin et al. 2002; Kelson et al. 1997, 2000; Ziegler & Bender 1997; Gomez et al. 2003). In conclusion, understanding the complex physics at play in clusters of galaxies requires combined X-ray and optical observation of a statistically significant sample of these objects.

On the basis of these considerations, we have created a large database of clusters of galaxies based on the largest available X-ray and optical surveys: the ROSAT All Sky Survey (RASS), the only X-ray all sky survey ever realized using an imaging X-ray telescope, and the Sloan Digital Sky Survey (SDSS), which the whole Northern Galactic Cap and part of the Southern Galactic Cap is observed in five wide optical bands covering the entire optical range. By carefully combining the data of the two surveys we have created the RASS-SDSS galaxy cluster catalog. Although two galaxy cluster catalogs from the SDSS already exist, the Cut and Enhance Galaxy Cluster Catalog of Goto et al. (2002a) and the Merged Cluster Catalog of Bahcall et al. (2003, see also Kim et al. 2002), we preferred to compile a new cluster catalog by selecting the systems in the X-ray band for which we have reliable X-ray characteristics, for the reasons explained above. The X-ray-selected galaxy clusters cover a wide range of masses, from groups of $10^{12.5}$ $M_{\odot}$ to massive clusters of 10^{15} $M_{\odot}$ in a redshift range from 0.002 to 0.45. The RASS-SDSS sample comprises all the X-ray detected objects already observed in the sky region covered by the Sloan Digital Sky Survey.

One of the first goals is the comparison of the X-ray and the optical appearance of the clusters. We want in particular find optical parameters that provide the closest correlation to the X-ray parameters, such that we can predict within narrow uncertainty limits the X-ray luminosity from these optical parameters and vice versa. So far optical and X-ray cluster surveys have been conducted independently without much intercomparison. Therefore, the empirical relationship between the X-ray luminosity and optical luminosity of clusters is not so well defined, in large part because of the difficulties inherent in measuring the cluster optical luminosity and in getting a homogeneous set of total optical luminosities for a large number of clusters. Edge & Stewart (1991) found that the bolometric X-ray luminosity of a local sample of X-ray-selected clusters correlated very roughly with Abell number and somewhat better with the Bahcall galaxy density (number of bright galaxies within 0.5 h^{-1} Mpc; Bahcall 1977, 1981) for the small subsample that had Bahcall galaxy densities. Arnaud et al. (1992) made an heroic effort in computing cluster optical luminosities at low redshift from a heterogenous literature. The first joint X-ray/optical survey of galaxy clusters was the ROSAT Optical X-ray Survey (ROXS, Donahue et al. 2002). They observed 23 ROSAT pointings for a total of 5 square degrees in the I band and partially in the V band. The X-ray selection and the optical selection of cluster candidates were done independently, with the wavelets algorithm in the former, and with a matched filter algorithm in the latter case. They found X-ray and optical coincident detections for 26 galaxy clusters. Donahue et al. (2001) studied the relation between the X-ray luminosity and the matched filter parameter $\Lambda_{\rm cl}$, which is approximately equivalent to the number of L^* galaxies in the system (Postman et al. 1998). They found a marginally significant correlation between the two quantities with a significant scatter. Yee & Ellingson (2003) defined a new richness parameter as the number of cluster galaxies within some fixed aperture, scaled by a luminosity function and a spatial distribution function. They analysed a sample of 15 clusters from the CNOC1 Cluster Redshift Survey, and found a very poor correlation between this parameter and other cluster properties such as the X-ray luminosity, temperature and the velocity dispersion.

In the present paper we describe the properties and the information contained in the RASS-SDSS catalog and the resulting correlations between the X-ray and optical properties in the sample. In Sect. 2 we explain how the cluster sample has been created by X-ray selecting the systems from the available X-ray cluster and group catalogs. In Sect. 3 we describe the method for calculating the X-ray cluster properties. We describe in Sect. 4 the optical data and in Sect. 5 the data reduction method. We analyse and discuss the correlations between the optical luminosity and the X-ray properties in Sect. 6. We summarize and discuss the catalog properties and the results in Sect. 7.

For all derived quantities, we have used $H_0 = 70\ \mathrm{km\,s^{-1}\,Mpc^{-1}}$, $\Omega_{\rm m} = 0.3$ and $\Omega_{\lambda} = 0.7$.

2. The construction of the sample

In order to correlate optical and X-ray galaxy cluster properties it is necessary to have a large statistical sample and to cover the whole mass range of the systems considered. Since the X-ray observations provide a robust method of identification of galaxy clusters and the X-ray luminosity is a good estimator of the system total mass, in principle the best approach should be to construct a cluster catalog of X-ray selected objects in a wide range of X-ray luminosity. While for intermediate and high X-ray luminosity (mass), several complete catalogs of X-ray selected clusters already exist (NORAS and REFLEX), in the low mass range a systematic X-ray survey of groups has still to be carried out. As a consequence, it is impossible at the moment to construct a strictly X-ray selected cluster sample, which covers a wide range of masses from very poor groups to rich clusters. A reasonable compromise in order to fill the low mass range of the spectrum is to select all the low mass

clusters and groups X-ray detected to date, even if they are selected in other wavebands. This compromise is acceptable for our purposes, since we do not want to carry out an X-ray survey of galaxy clusters, but a systematic analysis of the correlation between X-ray and optical properties of those systems.

By following these criteria, the intermediate mass and high mass clusters have been selected from three ROSAT based cluster samples: the ROSAT-ESO flux limited X-ray cluster sample (REFLEX, Böhringer et al. 2002), the Northern ROSAT All-sky cluster sample (NORAS, Böhringer et al. 2000) and the NORAS 2 cluster sample (Retzlaff 2001). REFLEX is a complete sample of clusters detected in 13 924 deg^2 in the southern hemisphere down to a flux limit of 3×10^{-12} erg s^{-1} cm^{-2} in the 0.1−2.4 keV energy bandcomprising 448 clusters. The NORAS galaxy cluster survey contains 495 clusters showing extended emission in the RASS in the northern hemisphere with count rates $C_X \geq 0.06$ counts s^{-1} in the 0.1−2.4 keV energy band. NORAS 2 is the continuation of the NORAS project and aims at a complete survey of X-ray galaxy clusters, in 13 598 deg^2 of the northern hemisphere, down to a flux limit of 2×10^{-12} erg s^{-1} cm^{-2} in the same X-ray band, which gives rise to an expected total of about 800 clusters. The samples are based on an MPE internal X-ray source catalog extracted with a detection likelihood ≥7.

The low mass clusters and the groups have been selected from two catalogs of X-ray detected objects: the ASCA Cluster Catalog (ACC) from Horner et al. (2001) and the Group Sample (GS) of Mulchaey et al. (2003). The ACC is a collection of all the clusters retrieved from the ASCA archive and discovered with different selection strategies. It contains measured luminosities, average temperatures, and metal abundances for 273 clusters and groups. The GS is a heterogeneous collection of 66 ROSAT systems, especially optically selected, with velocity dispersions less than 600 km s^{-1} or an intragroup medium temperature less than 2 keV.

The RASS-SDSS galaxy cluster sample comprises all the X-ray clusters of the cited catalogs in the area covered by the Sloan Digital Sky Survey up to February 2003. For each X-ray system in the common RASS-SDSS area we found an optical counterpart. The sample includes 114 galaxy clusters, 14 of which come from REFLEX, 72 from NORAS and NORAS 2, 8 from Mulchaey's sample and 20 from ACC. The RASS-SDSS galaxy cluster sample, therefore, cannot be considered strictly an X-ray "selected" cluster sample, but should be defined more precisely an X-ray "detected" cluster sample because of the heterogeneous selection of the low mass range systems.

3. The X-ray data

To create a homogeneous catalog of X-ray cluster properties, we have calculated all X-ray parameters using only RASS data for all clusters in the sample. The X-ray luminosity has been calculated with the growth curve analysis (GCA) method used for REFLEX and NORAS 2, based on the RASS3 database (Voges et al. 1999). The GCA method was applied to RASS3 at the position of the clusters. The method allowed for a small adjustment of the position to center on the X-ray maximum. Since within the GCA aperture the measured flux is underestimated typically by an amount of 7−10% (Böhringer et al. 2000) the missing flux is estimated by assuming an X-ray luminosity scaled cluster model (Böhringer et al. 2001) and corrected for. A first approximate unabsorbed flux is calculated for each X-ray source from the observed count rate, by assuming a thermal spectrum with a temperature of 5 keV and a metallicity of 0.3 solar and without a K-correction. Then an iterative computation uses the redshift and the unabsorbed X-ray flux to give a first estimate of the luminosity. With the luminosity-temperature relation of Markevitch (1998, without correction for cooling flows) a better temperature estimate is obtained, and the count rate-flux conversion factor is recomputed including the appropriate K-correction for the redshift, resulting in a corrected flux and a new X-ray luminosity. The X-ray luminosities as used in this paper are calculated in the ROSAT (0.1−2.4) keV energy band in the cluster rest frame for a Λ cosmology with the parameters given above. The GCA also returns for each source many physical parameters like improved source position, background brightness, spectral hardness ratio, and KS probability for source extent.

The X-ray bolometric luminosity is derived from the X-ray luminosity in the ROSAT (0.1−2.4) keV energy band. A first estimation of the cluster temperature is calculated using the $L_X - T_X$ relation of Xue & Wu (2000) to estimate the appropriate bolometric correction.

For a subsample of 53 galaxy clusters we have also compiled from the literature the ASCA and XMM temperature and iron abundance of the intracluster medium in the system.

4. Optical data

The optical photometric data were taken from the SDSS (York et al. 2000; Stoughton et al. 2002). The SDSS consists of an imaging survey of π steradians of the northern sky in the five passbands u, g, r, i, z, in the entire optical range from the atmospheric ultraviolet cutoff in the blue to the sensitivity limit of silicon in the red (Fig. 1). The survey is carried out using a 2.5 m telescope, an imaging mosaic camera with 30 CCDs, two fiber-fed spectrographs and a 0.5 m telescope for the photometric calibration. The imaging survey is taken in drift-scan mode. The imaging data are processed with a photometric pipeline (PHOTO) specially written for the SDSS data.

4.1. The galaxy sample

To study the optical cluster properties, we have created a complete galaxy sample for each cluster by selecting the galaxies in an area centered on the X-ray source position and within a radius of 1.5 deg. We used the selection criteria of Yasuda et al. (2001) to define our galaxy sample from the photometric catalog produced by PHOTO. We have selected only objects flagged with PRIMARY, to avoid multiple detections in the overlap between adjacent scan lines in two strips and between adjacent frames. Objects with multiple peaks (parent) are divided by the deblender into different components (children); if the objects can not be deblended, they are additionally flagged as NODEBLEND. Only isolated objects, child objects and NODEBLEND flagged objects are used in

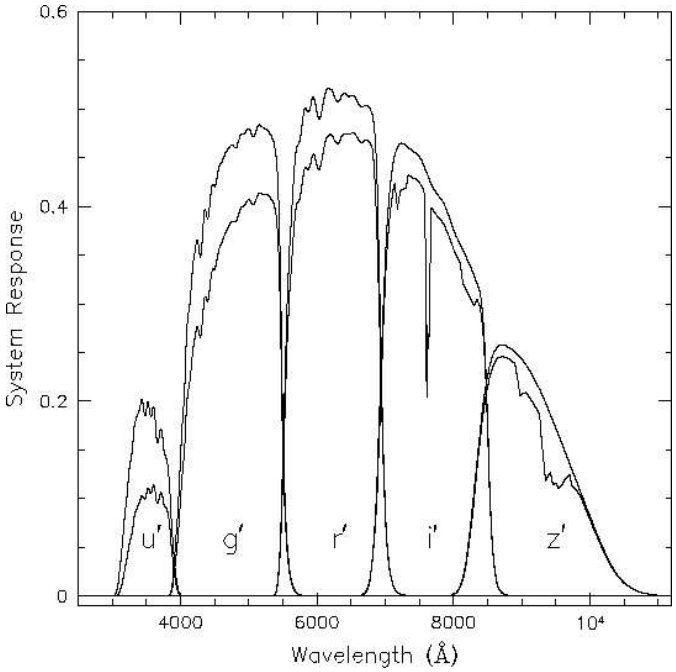

Fig. 1. Response function of the SDSS photometric system. Dashed curves indicate the response function including atmospheric transmission at 1.2 airmass at the altitude of Apache Point Observatory.

constructing our galaxy sample. The star-galaxy separation is performed in each band using an empirical technique based on the difference between the model and the PSF magnitude. An object is classified as galaxy if the model magnitude and the Point Spread Function (PSF) magnitude differ by more than 0.145. This method seems to be robust for $r \leq 21$ mag, which is also the completeness limit of the survey in the Northern Galactic cap. Since saturated pixels and diffraction spikes can compromise the model-fitting algorithm, some stars can be misclassified as galaxies. Therefore we have rejected all object with saturated pixels and which are flagged as BRIGHT. Furthermore, we have classified an object as a galaxy only if PHOTO classified it as a galaxy in at least two of the three photometric bands *g*, *r*, *i*. After a visual inspection of a sample of galaxies with $r \leq 16$ mag, Yasuda et al. (2001) concluded that the described selection criteria give a sample completeness of 97%, and the same completeness is found for the sample at $16 \leq r \leq 21$ mag after comparison with the Medium Deep Survey catalog (MDS) constructed using WFPC2 parallel images from HST. The major reason of missing real galaxies is the rejection of galaxies blended with saturated stars, while spurious galaxy detections are double stars or shredded galaxies with substructures.

4.2. SDSS Galaxy photometry

Since the galaxies do not have sharp edges or a unique surface brightness profile, it is nontrivial to define a flux for each object. PHOTO calculates a number of different magnitudes for each object: model magnitude, Petrosian magnitudes and PSF magnitudes. The model magnitudes are calculated by fitting de Vaucouleurs and exponential model, convolved with the local PSF, to the two dimensional images of the galaxies in the *r* band. The total magnitude is determined from which of the two shape functions fits best. Galaxy colors are measured by applying the best fit model of an object in the *r* band to the other bands, measuring the flux within the same effective aperture. However, due to a bug in PHOTO found during the completion of DR1, the model magnitudes are systematically underestimated by about 0.2 mag for galaxies brighter than 20th magnitude, and accordingly the measured radii are systematically too large (`http://www.sdss.org/DR1/products/catalogs/index.html`). This error does not affect the galaxy colors but makes the model magnitudes useless for the determination of the galaxy total luminosities.

The Petrosian flux is defined by

$$F_{\rm p} = 2\pi \int_0^{f_2 r_{\rm P}} I(r){\rm d}r, \tag{1}$$

where $I(r)$ is the surface brightness profile of the galaxy, and $r_{\rm P}$ is the Petrosian radius satisfying the equation:

$$f_1 = \frac{2\pi \int_{0.8r_{\rm P}}^{1.25r_{\rm P}} \frac{I(r)r{\rm d}r}{\pi[(1.25r_{\rm P})^2 - (0.8r_{\rm P})^2]}}{2\pi \int_0^{r_{\rm P}} \frac{I(r)r{\rm d}r}{(\pi r_{\rm p}^2)}}. \tag{2}$$

The Petrosian aperture is set to $2r_{\rm P}$, and it encompasses 99% of the galaxy total light in case of an exponential profile and 82% in case of a de Vaucouleurs profile (Blanton et al. 2001). The Petrosian ratio f_1 is set to 0.2; at smaller values PHOTO fails to measure the Petrosian ratio, since the *S/N* is too low. For faint objects the effect of the seeing on the Petrosian magnitude is not negligible. As the galaxy size becomes comparable to the seeing disk, the fraction of light measured by the Petrosian quantities approaches the fraction for a PSF, about 95%, in which case the flux is reduced for a galaxy with an exponential profile and increased for a galaxy with a de Vaucouleurs profile (Strauss et al. 2002). Thus the Petrosian magnitudes are the best measure of the total light for bright galaxies, but fail to be a good measure for faint objects. In the data analysis of this paper we used the Petrosian magnitudes for galaxies brighter than 20 mag and the psf magnitudes for objects fainter than 20 mag.

5. Optical luminosity from SDSS data

5.1. Background subtraction

The total optical luminosity of a cluster has to be calculated after the subtraction of the foreground and background galaxy contamination. Since we have used only photometric data from the SDSS galaxy catalog, we have no direct information on the cluster galaxy memberships. There are two different approaches to overcome this problem. Since galaxy clusters show a very well defined red sequence in the color magnitude diagram, a galaxy color cut could be use to define the cluster membership (Gladders et al. 2000). On the other hand the background subtraction can be based on the number counts of the projected field galaxies outside the cluster. We chose the latter approach since the former method may introduce a bias against bluer cluster members.

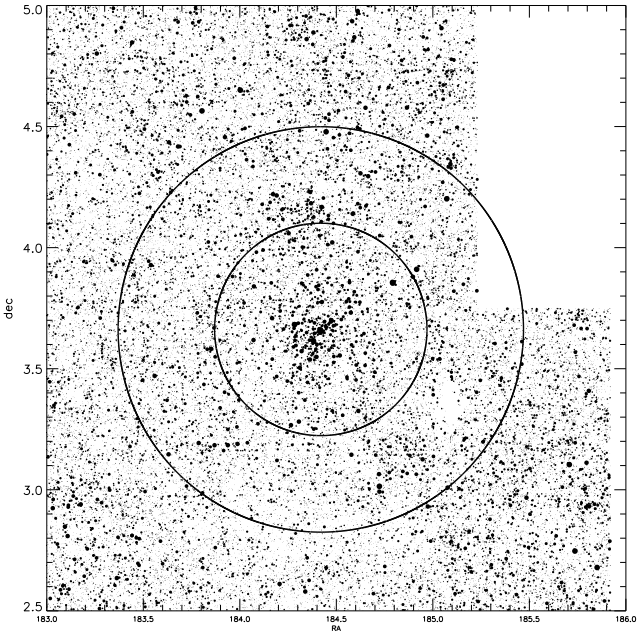

Fig. 2. The plot shows a cluster region with the local background. The dots represent the galaxies in the sample. The biggest dots correspond to the brightest galaxies in apparent r magnitude. The local background number counts have been calculated inside the annulus with inner radius equal to $r_{200} + 0.2$ deg and a width of 0.5 degree. The regions with voids due to lack of data or with close clusters have to be discarded in the background estimation.

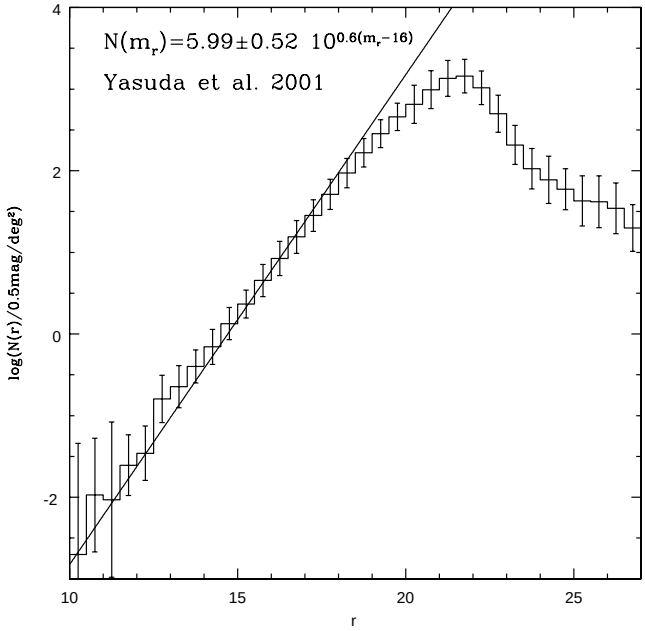

Fig. 3. Global background number counts as a function of magnitude in the r band. The error bars include the contribution of large scale structure. The line shows the counts-magnitude relation expected for a homogeneous galaxy distribution in a universe with Euclidean geometry: $N(r) = A_r \times 10^{0.6(r-16)}$. The value of $A_r = 5.99 \pm 0.52(0.5\ \mathrm{mag})^{-1}\ \mathrm{deg}^{-2}$ is the result of the fit in Yasuda et al. (2001) for $12 \leq r \leq 17$.

We have considered two different approaches to the statistical subtraction of the galaxy background. First we have calculated a local background. The $M_{200} - L_X$ relation of Reiprich & Böringher (2002) was used to compute the r_{200} radius (where the cluster mass density is 200 times the critical cosmic mass density), as a pragmatic approximation of the virial radius. Then, we defined an annulus centered on the cluster X-ray center, with an inner radius equal to r_{200} + 0.2 deg and a width of 0.5 degree (Fig. 2). In this way the galaxy background has been estimated well outside the cluster but still locally. The annulus was then divided into 20 sectors (analogous to the approach in Böhringer et al. 2001) and those featuring a larger than 3σ deviation from the median galaxy density were discarded from the further calculation. In this way other clusters close to the target or voids are not included in the background correction. We have computed the galaxies number counts $N^l_{\rm bg}(m)\mathrm{d}m$ per bin of magnitude (with a bin width of 0.5 mag) and per square degree in the remaining area of the annulus. The statistical source of error in this approach is the Poissonian uncertainty of the counts, given by $\sqrt{(N^l_{\rm bg}(m))}$.

As a second method we have derived a global background correction. The galaxy number counts $N^{\rm g}_{\rm bg}(m)\mathrm{d}m$ were derived from the mean of the magnitude number counts determined in five different SDSS sky regions, each with an area of 30 deg^2 (Fig. 3). The source of uncertainty in this second case is systematic and originates in the presence of large-scale clustering within the galaxy sample, while the Poissonian error of the galaxy counts is small due to the large area involved. We have estimated this error as the standard deviation of the mean global number counts, $\sigma^{\rm g}_{\rm bg}(m)$, in the comparison of the five areas. To take into account this systematic source of error also for the local background we have estimated the background number counts error as $\sigma_{\rm bg}(m) = \max(\sqrt{(N^l_{\rm bg}(m))}, \sigma^{\rm g}_{\rm bg}(m))$ (Lumdsen et al. 1997) for all the derived quantities.

After the background subtraction we found that the signal to noise in the u band was too low to be useful, and performed our analysis on the 4 remaining Sloan photometric bands g, r, i, z.

5.2. Luminosity function

For each cluster and in all photometric bands we have assumed that the distribution function of galaxies in magnitude can be described by the Schechter Luminosity function (LF):

$$\phi(m)\mathrm{d}m = 0.4\ \ln(10)\ N_{\rm clu}\ \phi^*\ 10^{-0.4\ (m-m^*)\ (\alpha-1)} \times \exp\left(-10^{-0.4\ (m-m^*)}\right)\ \mathrm{d}m. \quad (3)$$

In the equation $N_{\rm clu}$ is the number of cluster galaxies and was computed as the difference between the total number of galaxies in the cluster region and the expected number of interlopers, estimated from the local (global) background galaxy density. ϕ^* is the normalization of the Schechter Luminosity function, given by the inverse of the integral of the LF over the considered magnitude range. To determine the remaining parameters M^* and α we fitted the Schechter LF to the data with a Maximum Likelihood Method (MLM, Sarazin 1980). Since we have no information about the cluster membership, we have considered the observed galaxy magnitude distribution in the

cluster region as the sum of the Schechter Luminosity function ($\phi(m)$) plus a background contribution ($b(m)$):

$$\Phi(m) = \frac{\phi(m) + b(m)}{N_{\rm tot}}. \quad (4)$$

$\Phi(m)$ is normalized to unity when integrated over the considered range of magnitudes.

To perform an ML analysis, the background contribution has to be specified at any magnitude. To estimate the $b(m)$, one can try to fit the background number counts by a model. While the behavior of the $N(m) - m$ relation is well know at the bright end (in the log $N(m)$ – log m it is a line with slope 0.6, Fig. 3), it is not well understood at the faint end (Yasuda et al. 2001; Lumdsen et al. 1997). Therefore instead of using a specific functional form, we simply have used a spline to interpolate the background galaxy number counts and estimated $b(m)$ at any magnitude.

The probability that the assumed distribution gives a galaxy at the magnitudes m_k is thus $\Phi(m_k)$. Therefore, if the observed galaxies are statistically independent, the combined probability that the assumed distribution gives the observed galaxies at the magnitude m_k (with $k = 1, n$) is:

$$L = \prod_{\kappa=1}^{n} \Phi(m_k). \quad (5)$$

The best-fit parameters are those that maximize the likelihood L. In practice we have minimized the log-likelihood $-2\ln(L)$. This minimization was performed with the CERN software package MINUIT. We used the variable metric method MIGRAD (Fletchter 1970) for the convergence at the minimum, and the MINOS routine to estimate the error parameters in case of non-linearities. We also have placed constraints on the values of m^* and α that the fitting routine can accept, to avoid being trapped in a false minimum ($M*$ in the range between −18 and −26 mag and α between 0 and −2.5, Lumdsen et al. 1997). Figure 7 gives an example of the LF derived with the MLM in each of the Sloan photometric bands for a cluster. Figures 4 and 5 show the comparison between the fit parameters calculated with different backgrounds $b(m)$ (local and global). Figure 6 shows the correlation between the fit parameters M^* and α.

The great advantage of the MLM is that the method does not require the data to be binned and does not depend on the bin size, but uses all the available information. On the other hand, the MLM provides no information about the goodness of the fit. Therefore, we have performed a statistical test. Since the routine procedure uses a unbinned set of data to perform the fit, in principle the Kolmogorov Smirnov test should be applicable to our case. Nevertheless since the KS probability is not easy to interpret, we have applied a χ^2 test, by comparing the background subtracted magnitude number counts of the cluster with the Schechter luminosity function fitted to the data. Figure 8 shows the distribution of the reduced χ^2 in the cluster sample. Almost 90% of the fitted LFs are a good fit to the data having a reduced $\chi^2 \leq 1$.

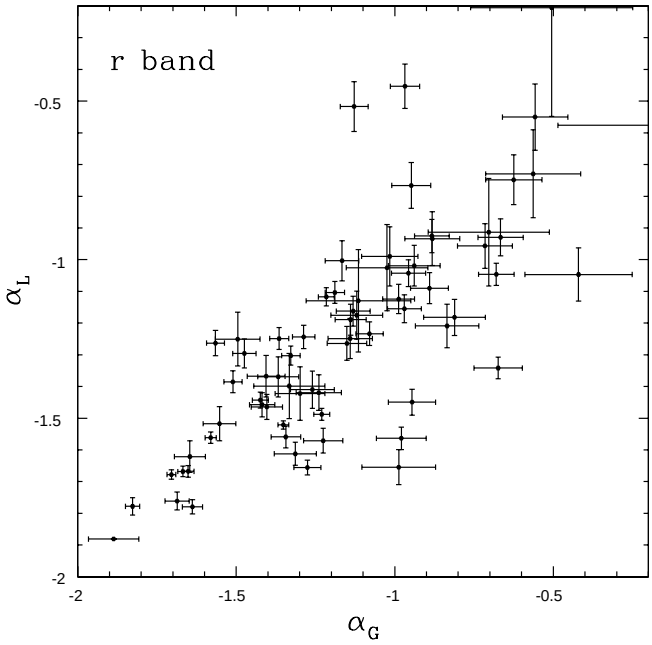

Fig. 4. Comparison of the α parameter (slope) of the individual Schechter luminosity functions. α_L is calculated using the local background correction, while α_G is the result of the global background correction. The different background subtractions give consistent results. The error bars in the plot are at the 68% confi dence level.

5.3. The total luminosity

To calculate the total cluster luminosity we have calculated first the absolute magnitude

$$M = m - 25 - 5\log_{10}(D_L/1\ {\rm Mpc}) - A - {\rm K}(z) \quad (6)$$

where D_L is the luminosity distance, A is the Galactic extinction and K(z) is the K-correction. We deredden the Petrosian and model magnitudes of galaxies using the Galactic map of Schlegel et al. (1998) in each photometric band. We used the K-correction supplied by Fukugita et al. (1995) for elliptical galaxies, assuming that the main population of our clusters are the old elliptical galaxies at the cluster redshift. The transformation from absolute magnitudes to absolute luminosity in units of solar luminosities is performed using the solar absolute magnitude obtained from the color transformation equation from the Johnson-Morgan-Cousins system to the SDSS system of Fukugita et al. (1996). We have calculated the optical luminosity of each cluster with two different methods. First, we have estimated L by using the (background corrected) magnitude number counts of the cluster galaxies with the following prescription:

$$L = \sum_{i}^{N} N_i(m) l_i(m) + \int_{m_{\rm lim}}^{\infty} \phi(m) {\rm d}m. \quad (7)$$

The sum on the right side is performed over all the N magnitude bins with galaxy number $N_i(m)$ and mean luminosity $l_i(m)$. The integral is an incompleteness correction due to the completeness limit of the galaxy sample at $m_{\rm lim} = 21$ mag in the five Sloan photometric bands. $\phi(m)$ is the individual Schechter

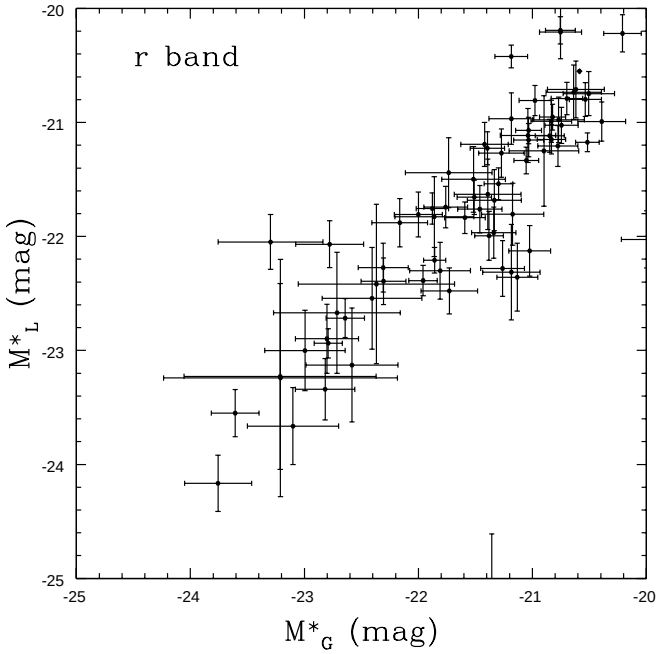

Fig. 5. Comparison of the $M*$ parameter (knee) of the individual Schechter luminosity functions. $M*_{\rm L}$ is calculated using the local background correction, while $M*_{\rm G}$ is the result of the global background correction. The different background subtractions give consistent results, as they do for the slope. The error bars in the plot are at 68% confidence level.

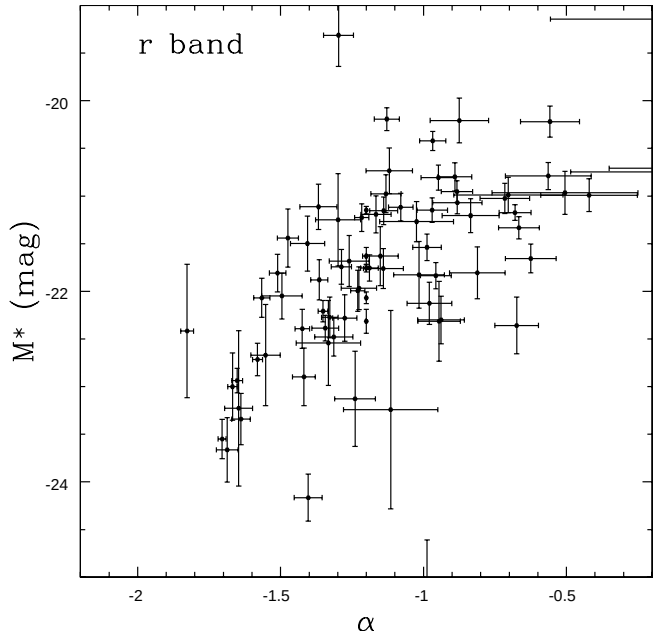

Fig. 6. Fit parameters of the individual Schechter luminosity functions in the *r* band. The fitting procedure is performed using the local background magnitude number counts. The parameters show a slight correlation. The error bars in the plot are at the 68% confidence level.

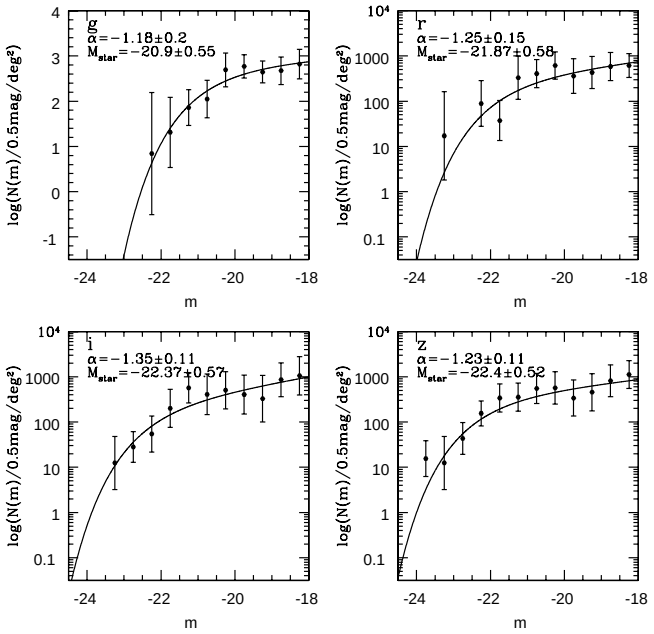

Fig. 7. Example of the individual fitted luminosity function of a cluster in 4 Sloan photometric bands. The values of the fitted parameters are indicated in each panel.

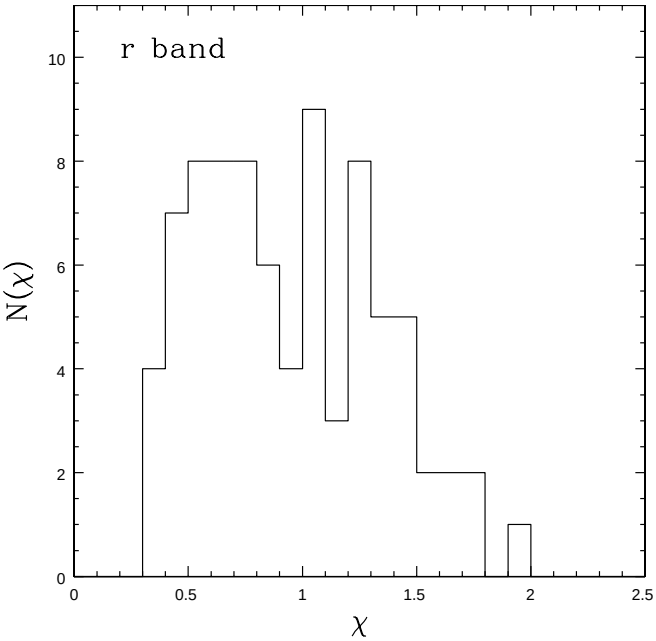

Fig. 8. Distribution of the reduced χ^2 of the individual Schechter luminosity functions. Since the MLM allows us to perform a fit without binning the data but does not give information about the goodness of the fit, we have performed the fitting procedure with MLM and checked the goodness of our fitted luminosity functions with a χ^2 test. All clusters are well represented by the individual fitted luminosity functions.

luminosity function fitted to the galaxy sample of each cluster. The incompleteness correction is of the order of 5−10% in the whole cluster sample, as shown in Fig. 9. This means that the galaxies below the magnitude limit do not give a significant contribution to the total optical luminosity. Therefore the most important source of error is due to the contribution of the background galaxy number counts. The uncertainty in each bin of magnitude is given by the Poissonian error of the bin counts ($\sqrt{N^i_{\rm tot}(m)}$, with $i = 1, ..., N$) and the background subtraction in each magnitude bin ($\sigma^i_{\rm bg}(m)$, with $i = 1, ..., N$, see previous

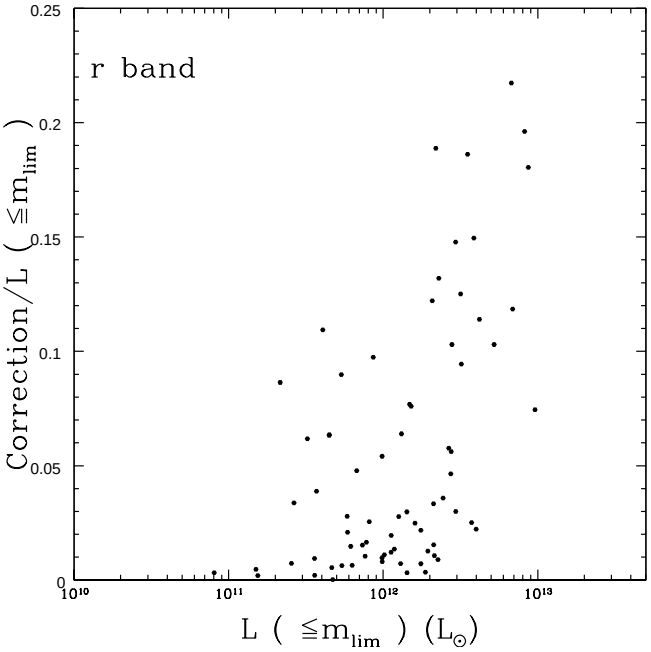

Fig. 9. The plot shows the correction to the total optical luminosity for incompleteness. The completeness magnitude limit is 21 mag in each Sloan photometric band. The correction is of the order of 5% for 50% of the clusters in the sample, while it is less than 10% for 85% of the sample. The trend in the plot is due to a selection effect, since the most distant clusters are also the most luminous ones.

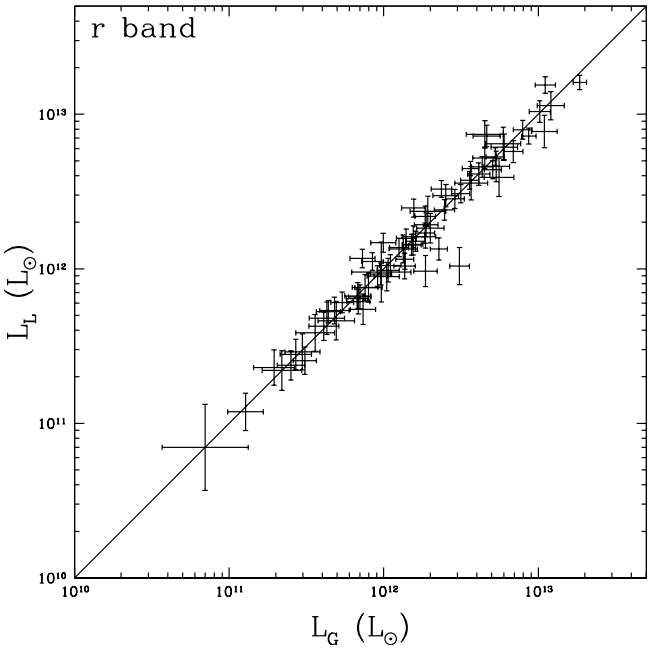

Fig. 10. Comparison of the cluster optical luminosities calculated from the cluster magnitude number counts with different background corrections. $L_{\rm L}$ is calculated with the local, and L_G with the global background subtraction. The different corrections do not affect the cluster luminosity estimation. The error bars in the plot are at the 68% confidence level.

section for the definition). Since the galaxy counts in the bins are independent, the error in the luminosity is given by:

$$\Delta L = \left(\sum_{i}^{N} \left(N^{i}_{\rm tot}(m) + \sigma^{i}_{\rm bg}(m)^2 \right) \right)^{\frac{1}{2}} . \quad (8)$$

Figure 10 shows the comparison between the luminosity calculated from the local background corrected and global background corrected magnitude number counts. The difference between the two methods is much smaller than the statistical error.

In the second case we have taken advantage of the individual fitted luminosity function. If MIGRAD has converged successfully to the minimum, we calculate the total luminosity as

$$L = L^{*} N_{\rm clu} \phi^{*} \Gamma(2+\alpha) \quad (9)$$

where L^{*} and α are the fit parameters estimated from the data and $N_{\rm clu}$ is the total number of cluster galaxies. There are different sources of errors in this calculation. The major source of errors comes from the background which affects both the number of cluster galaxies $N_{\rm clu}$ and the result of the fitting procedure. A second kind of error is due to the uncertainty of the fit parameters. Since all these errors are not independent, we can not treat their contributions separately. Therefore the luminosity errors were calculated by varying the fit parameter values, M^{*} and α, along their 68% confidence level error ellipse and using the upper and lower bound of the quoted background number counts ($b(m)$) range. The statistical luminosity error was then defined as half of the difference between the minimum and maximum luminosity. With this method we can take into account statistical and systematic errors due to the background, and their effects on the fit parameters as well. Note that a simple error propagation applied to Eq. (9) would underestimate the error in the luminosity, since it would not take into account the error of the galaxy background.

Figure 11 shows the comparison of the two optical luminosities (fit-based and count-based), which are consistent within the errors. For 70% of the clusters in the sample the luminosity based on counts is systematically brighter than that based based on fit, as shown in Fig. 12. In the former case, indeed, the method includes in the calculation of $L_{\rm op}$ the Bright Cluster Galaxies (BCG) which are usually excluded by the Schechter luminosity function. The error bars in the fit-based luminosity are larger than in the count-based luminosity. In fact in the former case there are two main sources of error: the uncertainty due to the galaxy background subtraction and the statistical errors in the fit parameters of the luminosity function. In the latter case, instead, only the subtraction of the galactic background plays a crucial role. The mean error in the fit-based luminosity is around 30%, while it is around 20% with the count-based method.

The great advantage of the count-based optical luminosity is that it can be easily computed, if the cluster *S/N* is high enough. On the other hand, the fit-based luminosity depends on the success of the fitting procedure. Therefore, it is sensitive not only to the *S/N* but also to the chosen model and the goodness of the fit. The uncertainty in the count-based method is smaller than in the fit-based method. Moreover, while the count-based method provides the optical luminosity for any system and at

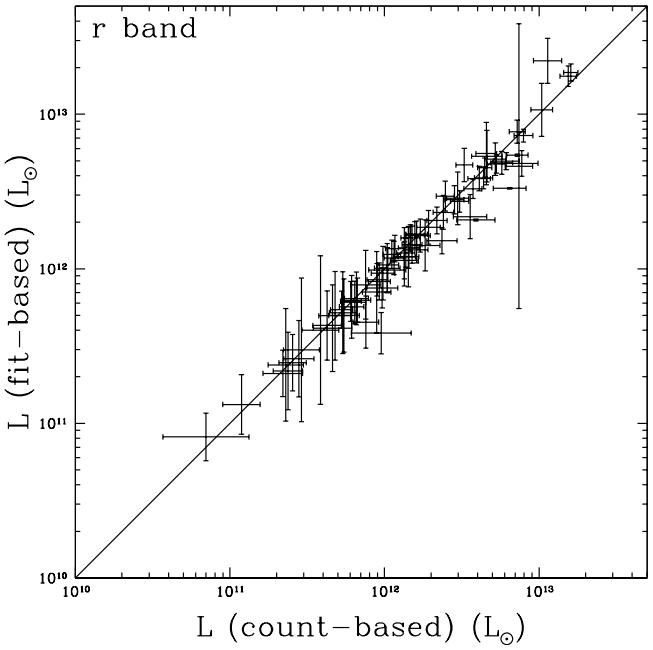

Fig. 11. Comparison of the cluster luminosities determined with count-based and fit-based methods. The error bars in the plot are at the 68% confidence level.

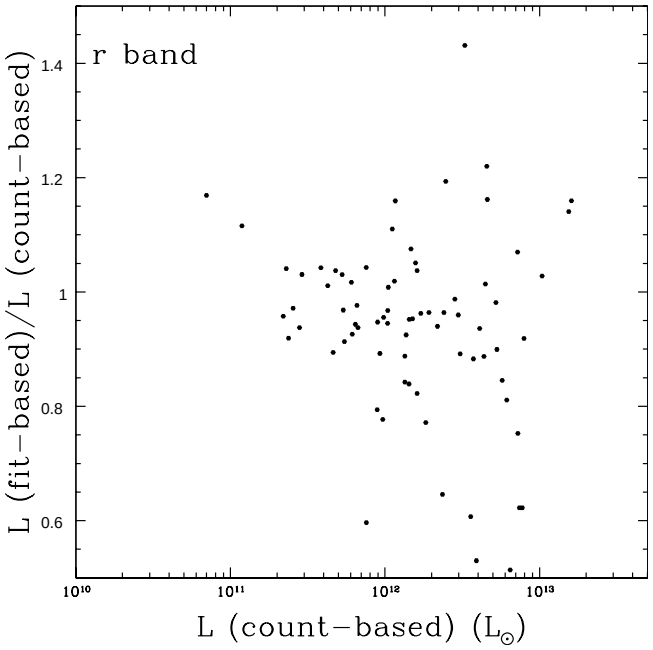

Fig. 12. Comparison of the count-based and fit-based cluster luminosities. The plot shows the ratio of these two versus the count-based luminosity. For 70% of the sample the ratio $L_{\rm fit-based}/L_{\rm count-based}$ is less than 1.1, indicating that the fit-based luminosity is systematically less bright the count-based luminosity. This is due to the Bright Cluster Galaxies (BCG): they are included in the computation of the count-based luminosity but not in the estimation of the fit-based luminosity.

any cluster aperture, the number of failures in the fitting procedure is an increasing function of the cluster aperture. In fact the fit-based method fails to fit the data for 15% of the clusters at 0.35 Mpc h_{70}^{-1} and up to 35% at 2.0 Mpc h_{70}^{-1}. In consequence, the count-based $L_{\rm op}$ has to be preferred to the fit-based one in the study of the correlation between optical and X-ray properties. The count-based method also reflects what we actually observe.

On the basis of this analysis we can conclude that the behavior of the optical luminosities calculated with different background subtraction is stable for variant approaches and the main source of errors is due to the necessary background subtraction (Fig. 10). Moreover, since the two different methods (count-based and fit-based) give consistent results, our measure of $L_{\rm op}$ seems to be a good estimation of the cluster total optical luminosity.

5.4. The optical structure parameters

To study the spatial distribution of galaxies in cluster we have analysed the projected radial galaxy distributions of all clusters in the sample. The analysis is performed in the *g*, *r*, *i* and *z* bands. As for the luminosity functions, we have used a Maximum Likelihood method to fit a King profile to the data

$$P(r) = \frac{\sigma_0}{\left(1+\left(\frac{r}{r_{\rm c}}\right)^2\right)^{\beta}} + \sigma_{\rm b}. \quad (10)$$

In Eq. (10), σ_0 is the central galaxy density, $r_{\rm c}$ the core radius, β the profile exponent, and $\sigma_{\rm b}$ the background density. $P(r)$ has to be normalized through:

$$\int_A P(r){\rm d}(\pi r^2) = N_{\rm tot} \quad (11)$$

where A is the relevant cluster area and $N_{\rm tot}$ is the total number of galaxies within that area. In agreement with Sect. 5.2 the Likelihood is given by:

$$L = \prod_{\kappa=1}^{n} P(r_\kappa) \quad (12)$$

where r_κ is the projected galaxy distance from the X-ray center. We regarded β, $r_{\rm c}$ and $\sigma_{\rm b}$ as fitting parameters, while σ_0 is a dependent variable and its value is derived from the likelihood normalization, Eq. (11). The fitting method worked successfully on average for 95% of the sample in any photometric band; it failed for groups, where the overdensity in comparison to the background density is too low to fit a profile. As shown in Fig. 13, there are no correlations of the parameters σ_0, $r_{\rm c}$, and β with the background density $\sigma_{\rm b}$. Furthermore the histogram of the β values in the same figure shows that the mean value of the profile exponent is around 0.8 with a very large dispersion of 0.5 around the peak.

We have estimated from the King profile the physical size of each cluster, $r_{\rm tot}$. We have assumed that this quantity is given by the radial distance from the X-ray center, where the galaxy number density of the cluster becomes *n* times the error of the background galaxy density (the cross in Fig. 14). To search for the best value of *n*, we have estimated the total radius with different values of n ($n = 1, ..., 5$) and calculated the total optical luminosity within that radius; *n* was then fixed to 3, since the differences in the luminosities calculated within different total radii are smaller than the luminosity uncertainties due to background subtraction.

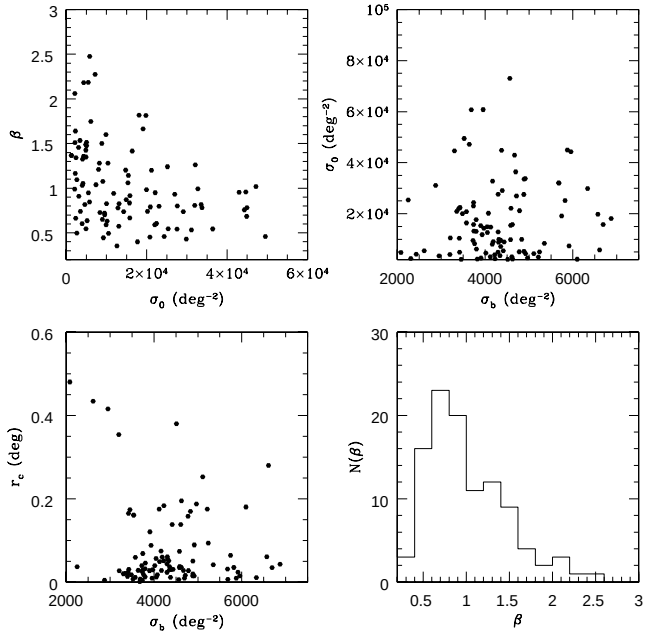

Fig. 13. The four panels show the behavior of the fit parameters in the King profile fit procedure. The first three panels show that there is no correlation between the parameters, while the bottom right panel presents the histogram of the exponent β of the King profile.

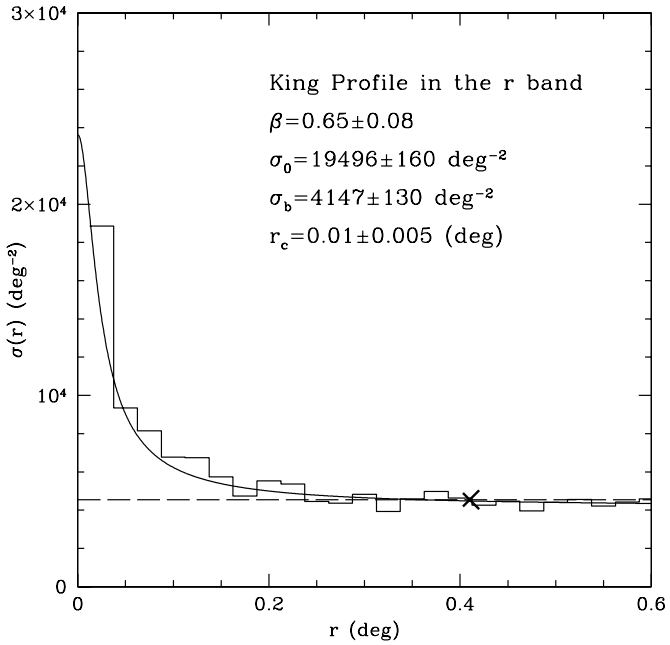

Fig. 14. The physical total size (the cross) of each cluster is estimated as the radius where the galaxy number density within the cluster becomes 3 times the error in the statistical background galaxy number density (the dashed line).

We assumed that the cluster total optical luminosity in a band is the luminosity calculated within $r_{\rm tot}$ estimated in the given filter. To calculate then the half-light radius, which encircles half of the total cluster luminosity, we estimated in each band the luminosity of the cluster within 20 increasing apertures centered in the X-ray center. We obtained the cluster cumulative luminosity profile interpolating in each filter the 20 values of the luminosity calculated within increasing apertures. Finally we used the cluster cumulative luminosity profile to find the radius which corresponds to half of the total cluster luminosity.

5.5. The catalog

In the following we present the catalog of the 114 RASS-SDSS galaxy clusters. Tables 1−3 list all the X-ray and optical properties of the sample computed as explained in the previous sections. The sample tables show the results for the first 35 clusters in the sample. The complete tables are available in electronic form.

Table 1 gives the X-ray properties of the cluster derived from the ROSAT data. Columns 1 and 2 put the ROSAT and the alternative cluster name respectively. Columns 3 and 4 contain the equatorial coordinates of the X-ray cluster center used for the region selection for the epoch J2000 in decimal degrees. Column 5 contains the heliocentric cluster redshift. Column 6 presents the flux in the energy band 0.1−2.4 keV in units of 10^{-11} erg s^{-1} cm^{-2}. Column 7 gives the corrected flux for a temperature derived from the $L_{\rm X} - T$ relation including the K-correction for an assumed cluster temperature of 5 keV. Column 8 contains the relative 1 σ Poissonian error of the count rate, the flux and the luminosity in percents. Column 9 gives the luminosity in the energy range 0.1−2.4 keV in units of $h_{70}^{-2} \times 10^{44}$ erg s^{-1}. Column 10 contains the count rate in units of counts s^{-1}. Column 11 gives the outer radius within which the flux and the luminosity are estimated, in units of arc minutes.

Table 2 provides the optical parameters of the luminosity function and the luminosities of each cluster calculated using the local galaxy background. Listed are results in the r band. All the quantities are calculated within a fixed cluster aperture of 1.0 Mpc h_{70}^{-1}. Column 1 presents the ROSAT name of the cluster. Columns 2 and 3 show the resulting fit parameters of a Schechter luminosity function. α is the slope of the LF, while $M*$ is the magnitude knee of the distribution. Column 4 gives the galaxy number density within the cluster region selected to perform the fit, in units of deg^{-2}. Column 5 shows the reduced χ^2 of the fitted luminosity function. Column 6 provides the cluster optical luminosity in units of 10^{12} $L_{\odot}$, calculated on the basis of the fitted luminosity function. Column 7 lists the cluster optical luminosity in units of 10^{12} $L_{\odot}$, calculated on the basis of the cluster magnitude number counts. All the errors in the table are at 68% confidence level. The full catalog, which is an extended version of this table, is available online. Similar tables exist, listing the parameters and the luminosities relative to 22 different cluster apertures: 20 fixed apertures ranging from 0.05 to 4.0 Mpc h_{70}^{-1}, 2 variable apertures as the core radius and the half-light radius. All the data are provided in each of the 4 Sloan photometric bands g, r, i and z, and for both local and global galaxy background correction.

Table 3 provides the information concerning the radial distribution of the projected galaxy density in the region of the cluster. Column 1 presents the ROSAT name of the cluster. Column 2 gives the cluster central galaxy number density in

Table 1. Example of the table containing the X-ray cluster properties of the whole cluster sample. The table show the results for the first 35 cluster in the sample.

Name	Alternative Name	RA	Dec	z	F_X	$F_X{}^*$	Error	L_X	Count rate	R_{out}
(1)	(2)	(3)	(4)	(5)	(6)	(7)	(8)	(9)	(10)	(11)
RXC J0041.8-0918	*A*0085	10.4587	–9.3019	0.052	67.612	67.905	3.0	7.87	3.25	18.0
RXC J 0114.9+0022	*A*0168	18.7350	0.3746	0.047	8.725	8.484	8.7	0.81	0.42	14.0
RXC J0119.6+1453	*A*0175	19.9072	14.8931	0.129	3.124	3.114	29.1	2.23	0.14	9.5
RXC J0137.2-0912	...	24.3140	–9.2028	0.039	7.275	7.071	8.4	0.46	0.35	9.5
RXC J0152.7+0100	*A*0267	28.1762	1.0126	0.227	4.257	4.276	12.1	9.32	0.20	9.0
RXC J0736.4+3925	...	114.1040	39.4329	0.117	8.239	8.239	9.5	4.81	0.36	13.0
RXC J0747.0+4131	...	116.7537	41.5314	0.028	3.201	2.431	15.0	0.08	0.14	9.5
RXC J0753.3+2922	...	118.3291	29.3741	0.062	6.414	0.062	9.6	1.04	0.30	9.0
RXC J0758.4+3747	*Ngc*2484	119.6172	37.7888	0.041	0.605	0.431	32.1	0.03	0.02	7.0
RXC J0800.9+3602	*A*0611	120.2445	36.0469	0.288	2.536	2.545	16.9	8.85	0.11	6.0
RXC J0809.6+3455	...	122.4177	34.9262	0.080	5.208	5.164	13.2	1.43	0.24	7.5
RXC J0810.3+4216	...	122.5942	42.2669	0.064	2.974	2.893	13.8	0.51	0.13	6.0
RXC J0822.1+4705	*A*0646	125.5417	47.0995	0.130	7.236	7.236	9.0	5.25	0.34	8.0
RXC J0824.0+0326	*MS* 0821.5 + 0337	126.0209	3.4383	0.347	0.297	0.294	78.6	1.57	0.01	2.5
RXC J0825.4+4707	*A*0655	126.3652	47.1196	0.126	7.235	7.235	15.1	4.92	0.34	12.0
RXC J0828.1+4445	...	127.0278	44.7634	0.145	4.501	4.501	11.2	4.04	0.21	6.0
RXC J0842.9+3621	*A*0697	130.7401	36.3625	0.282	5.821	5.858	16.0	19.42	0.28	8.0
RXC J0845.3+4430	*HGC*35	131.3434	44.5115	0.054	0.082	0.057	100.0	0.00	0.00	0.5
RXC J0850.1+3603	*CL*0847.2 + 3617	132.5499	36.0614	0.373	2.742	2.75	18.7	15.87	0.13	9.5
RXC J0913.7+4056	*CL*09104 + 4109	138.4411	40.9339	0.442	1.756	1.769	30.1	14.16	0.09	8.5
RXC J0913.7+4742	*A*0757	138.4446	47.7021	0.051	6.202	6.022	13.3	0.68	0.31	15.0
RXC J0917.8+5143	*A*0773	139.4637	51.7223	0.217	5.961	5.998	9.2	11.85	0.30	9.0
RXC J0943.0+4700	*A*0851	145.7600	47.0038	0.406	1.014	1.017	30.8	7.10	0.05	4.5
RXC J0947.1+5428	...	146.7862	54.4754	0.046	5.241	15.090	2.6	0.46	0.27	14.0
RXC J0952.8+5153	...	148.2009	51.8888	0.214	4.196	4.216	10.6	8.13	0.21	8.0
RXC J0953.6+0142	...	148.4231	1.7118	0.098	2.389	2.322	24.3	0.97	0.11	9.5
RXC J1000.5+4409	...	150.1260	44.1550	0.154	2.775	2.766	12.6	2.83	0.14	5.0
RXC J1013.7-0006	...	153.4368	–0.1085	0.093	3.382	3.353	28.4	1.25	0.16	8.0
RXC J1017.5+5933	*A*0959	154.3960	59.5577	0.353	4.079	4.109	11.4	21.15	0.21	13.0
RXC J1022.5+5006	...	155.6283	50.1030	0.158	5.389	5.403	9.0	5.77	0.27	8.0
RXC J1023.6+0411	...	155.9125	4.1873	0.285	8.562	8.617	8.1	29.21	0.42	7.5
RXC J1023.6+4908	*A*0990	155.9212	49.1349	0.144	8.180	8.202	7.3	7.23	0.42	10.0
RXC J1053.7+5452	...	163.4349	54.8726	0.075	4.024	3.907	11.5	0.96	0.20	11.0
RXC J1058.4+5647	...	164.6097	56.7922	0.136	7.661	7.682	7.0	6.09	0.40	8.5

units of deg^{-2} (σ_0 is not a fit parameter, therefore the error is not provided). Column 3 lists the background galaxy number density around the cluster in units of deg^{-2}. Column 4 shows the core radius estimated from the fit, in units of Mpc. Column 5 provides the cluster total radius, extrapolated from the King profile, in units of Mpc. Column 6 gives the half-light radius in units of Mpc. All the errors in the table are at 68% confidence level.

The full set of extended tables is available in electronic form.

6. Correlating X-ray and optical properties

For a cluster in which mass traces optical light (M/L_{op} is constant), the gas is in hyrostatic equilibrium ($T \propto M^{2/3}$), and $L_X \propto T^3$ (Xue & Wu 2000), we expect the X-ray bolometric luminosity to be related to the optical luminosity as $L_{op} \propto L_X^{0.5}$ and to the intracluster medium temperature as $L_{op} \propto T_X^{1.5}$.

We now have an optimal data base to test these scaling relations. In a first step we look for those optical parameters which are best suited for a correlation analysis and use these in a second step in the test of the scaling relations.

In this section we show that tight correlations exist between the total optical cluster luminosity and the X-ray cluster properties such as the X-ray luminosity and the intracluster medium temperature.

To search for the best correlation between optical and X-ray properties and to optimally predict for example the X-ray luminosity from the optical appearance, we are interested in an optical characteristic that shows a minimum scatter in the

Table 2. Example of the table containing optical properties of the whole cluster sample in the *r* band. The table show the results for the first 35 clusters in the sample.

Name	α	$M*$	ρ	χ/ν	L_F	L_C
RXC J0041.8-0918	-1.52 ± 0.18	-22.19 ± 0.31	2227	1.2	1.81 ± 0.22	1.87 ± 0.06
RXC J0114.9+0022	-1.28 ± 0.12	-22.01 ± 0.35	759	0.9	1.27 ± 0.18	1.34 ± 0.04
RXC J0119.6+1453	-1.07 ± 0.26	-21.92 ± 0.24	2848	0.9	4.12 ± 1.22	2.55 ± 0.23
RXC J0137.2-0912	-1.78 ± 0.12	-23.33 ± 0.33	1036	1.5	0.69 ± 0.11	0.70 ± 0.13
RXC J0152.7+0100	0.00 ± 0.00	0.00 ± 0.00	0	0	0.00 ± 0.00	3.02 ± 1.24
RXC J0736.4+3925	-0.87 ± 0.18	-20.84 ± 0.42	1274	0.8	1.06 ± 0.31	0.82 ± 0.09
RXC J0747.0+4131	-2.50 ± 0.00	-18.02 ± 0.00	263	0.8	0.12 ± 0.07	0.00 ± 0.00
RXC J0753.3+2922	-1.59 ± 0.11	-22.85 ± 0.26	1763	1.6	1.38 ± 0.20	1.42 ± 0.08
RXC J0758.4+3747	0.00 ± 0.00	0.00 ± 0.00	0	0.0	0.00 ± 0.00	0.05 ± 0.04
RXC J0800.9+3602	-0.90 ± 0.17	-21.33 ± 0.43	5523	1.2	4.81 ± 2.13	2.62 ± 0.14
RXC J0809.6+3455	-1.45 ± 0.17	-21.57 ± 0.32	2041	0.5	1.09 ± 0.18	1.16 ± 0.10
RXC J0810.3+4216	-1.61 ± 0.18	-22.56 ± 0.81	1120	0.6	0.72 ± 0.18	0.76 ± 0.09
RXC J0822.1+4705	-0.71 ± 0.10	-21.37 ± 0.76	1422	0.8	1.52 ± 0.27	1.49 ± 0.08
RXC J0824.0+0326	0.00 ± 0.00	0.00 ± 0.00	0	0	0.00 ± 0.00	0.95 ± 0.25
RXC J0825.4+4707	-0.71 ± 0.18	-20.57 ± 0.50	3518	0.6	2.30 ± 0.35	2.09 ± 0.06
RXC J0828.1+4445	-1.71 ± 0.14	-23.50 ± 0.44	2885	0.5	1.40 ± 0.36	1.79 ± 0.21
RXC J0842.9+3621	-1.54 ± 0.16	-21.71 ± 0.50	7211	0.2	2.40 ± 0.37	3.92 ± 0.27
RXC J0845.3+4430	0.00 ± 0.00	0.00 ± 0.00	0	0	0.00 ± 0.00	0.17 ± 0.12
RXC J0850.1+3603	-0.58 ± 0.18	-21.31 ± 0.31	8955	0.2	4.52 ± 0.67	5.21 ± 0.17
RXC J0913.7+4056	-0.01 ± 0.02	-20.69 ± 0.37	1235	0.4	1.20 ± 0.92	0.79 ± 0.14
RXC J0913.7+4742	-1.29 ± 0.19	-21.66 ± 1.34	319	0.8	0.41 ± 0.11	0.41 ± 0.03
RXC J0917.8+5143	-1.07 ± 0.17	-21.42 ± 0.27	8128	0.6	4.02 ± 0.53	3.86 ± 0.14
RXC J0943.0+4700	-1.29 ± 0.11	-21.87 ± 0.54	6627	1.3	4.27 ± 1.01	5.46 ± 0.30
RXC J0947.1+5428	0.00 ± 0.00	-20.24 ± 0.32	64	0.6	0.40 ± 0.12	0.34 ± 0.30
RXC J0952.8+5153	-0.13 ± 0.20	-20.15 ± 0.43	2041	0.3	0.84 ± 0.24	0.80 ± 0.05
RXC J0953.6+0142	-1.73 ± 0.14	-26.00 ± 0.68	1051	0.5	1.18 ± 0.60	1.16 ± 0.07
RXC J1000.5+4409	-1.35 ± 1.05	-22.11 ± 0.28	542	0.4	0.34 ± 0.19	0.31 ± 0.08
RXC J1013.7-0006	-1.05 ± 0.14	-20.80 ± 0.31	1324	0.6	1.00 ± 0.22	0.85 ± 0.16
RXC J1017.5+5933	-1.44 ± 0.18	-23.07 ± 0.47	6321	1.6	4.40 ± 0.87	5.53 ± 0.30
RXC J1022.5+5006	-1.19 ± 0.10	-21.55 ± 0.38	4271	0.7	2.38 ± 0.36	2.25 ± 0.10
RXC J1023.6+0411	-0.98 ± 0.15	-20.81 ± 0.25	5696	0.1	1.97 ± 0.44	2.25 ± 0.12
RXC J1023.6+4908	-0.84 ± 0.10	-20.85 ± 0.25	2664	0.4	1.65 ± 0.32	1.46 ± 0.06
RXC J1053.7+5452	-1.43 ± 0.17	-22.19 ± 0.37	1320	0.8	1.06 ± 0.17	1.08 ± 0.05
RXC J1058.4+5647	-1.59 ± 0.25	-22.26 ± 0.23	4433	1.1	2.15 ± 0.42	2.15 ± 0.28

X-ray/optical correlation. Therefore, we perform a correlation using 4 of the 5 SDSS optical band, *g*, *r*, *i* and *z*, to find out which filter should be used in the prediction. The *u* band was not used since the cluster S/N in that band is too low to calculate the cluster total luminosity. We used a fixed aperture to calculate the optical luminosities for all the clusters, in order to make no a priori assumption about the cluster size. Moreover, to check whether the scatter in the correlation depends on the cluster aperture, we did the same analysis several times using optical luminosities calculated within different radii, ranging from 0.05 to 4 Mpc h_{70}^{-1} from the X-ray center. To quantify the $L_{op} - L_X$ and the $L_{op} - T_X$ relations, a linear regression in log-log space was performed using two methods for the fitting: a numerical orthogonal distance regression method (ODRPACK) and the bisector method (Akritas & Bershady 1996). The fits are performed using the form

$$\log(L_{op}/L_\odot) = \alpha \log(P_X) + \beta \quad (13)$$

where P_X is the X-ray property, and the errors of each variable are transformed into log space as $\Delta \log(x) = \log(e)(x^+ - x^-)/(2x)$, where x^+ and x^- denote the upper and lower boundary of the error range of the quantity, respectively. To exclude the outliers in the fitting procedure we apply a σ clipping method. After a first fit all the points featuring a larger than 3σ deviation from the relation, were excluded and the fitting procedure was repeated (see discussion below).

Figures 15 and 16 show the scatter of the $L_{op} - L_X$ and the $L_{op} - T_X$ relations, respectively, versus the cluster aperture used to calculate the optical luminosity. The scatter in the plot is the orthogonal scatter estimated from the best fit given by ODRPACK. In any photometric band the scatter has a clear dependence on the cluster aperture showing a minimum in the very center of the cluster, between 0.2 Mpc h_{70}^{-1} and 0.8 Mpc h_{70}^{-1}, and increasing at larger radii. The scatter is partially due to the method used to calculate the optical luminosity. Our method is simply based on the overdensity of the

Table 3. Example of the table containing the optical properties of the whole cluster sample in the *r* band. The table shows the results for the first 35 cluster of the sample.

Name	β	σ_0	σ_b	r_c	r_{tot}	r_h
RXC J0041.8-0918	0.88 ± 0.16	5731	2295 ± 456	1.15 ± 0.04	2.33	1.00 ± 0.37
RXC J0114.9+0022	1.61 ± 0.48	2281	4540 ± 106	0.51 ± 0.07	0.78	0.36 ± 0.09
RXC J0119.6+1453	0.44 ± 0.14	17803	4051 ± 896	0.08 ± 0.04	0.67	0.22 ± 0.16
RXC J0137.2-0912	1.68 ± 0.33	4955	5256 ± 37	0.20 ± 0.03	0.59	0.22 ± 0.14
RXC J0152.7+0100	0.78 ± 0.21	12846	4297 ± 607	0.40 ± 0.07	1.34	0.87 ± 0.16
RXC J0736.4+3925	1.49 ± 0.40	4834	2083 ± 594	0.57 ± 0.12	2.52	1.27 ± 0.26
RXC J0747.0+4131	0.00 ± 0.00	0	0 ± 0	0.00 ± 0.00	0.00	0.00 ± 0.00
RXC J0753.3+2922	1.06 ± 0.25	5076	4314 ± 270	0.48 ± 0.05	1.03	0.43 ± 0.10
RXC J0758.4+3747	0.00 ± 0.00	0	0 ± 0	0.00 ± 0.00	0.00	0.00 ± 0.00
RXC J0800.9+3602	0.40 ± 0.131	30806	3649 ± 1807	0.11 ± 0.05	0.96	0.75 ± 0.35
RXC J0809.6+3455	0.18 ± 0.212	23059	3860 ± 2779	0.00 ± 0.03	0.02	0.00 ± 0.00
RXC J0810.3+4216	0.46 ± 0.16	9392	3998 ± 536	0.07 ± 0.03	0.48	0.36 ± 0.14
RXC J0822.1+4705	0.83 ± 0.20	8734	3817 ± 262	0.26 ± 0.05	1.09	0.52 ± 0.13
RXC J0824.0+0326	0.76 ± 0.26	32273	5369 ± 588	0.08 ± 0.04	0.56	0.23 ± 0.24
RXC J0825.4+4707	0.90 ± 0.13	15229	4130 ± 292	0.32 ± 0.03	1.54	0.64 ± 0.18
RXC J0828.1+4445	1.12 ± 0.13	46498	5262 ± 108	0.11 ± 0.02	1.02	0.42 ± 0.14
RXC J0842.9+3621	0.54 ± 0.08	50832	4247 ± 606	0.09 ± 0.03	1.96	1.57 ± 0.21
RXC J0845.3+4430	0.59 ± 0.51	6690	3060 ± 974	0.04 ± 0.03	0.07	0.00 ± 0.00
RXC J0850.1+3603	2.05 ± 0.30	24289	6445 ± 178	0.64 ± 0.06	1.50	0.63 ± 0.31
RXC J0913.7+4056	0.62 ± 0.21	31255	3200 ± 581	0.08 ± 0.05	0.84	0.31 ± 0.13
RXC J0913.7+4742	1.23 ± 0.43	3911	4558 ± 65	0.15 ± 0.04	0.48	0.32 ± 0.10
RXC J0917.8+5143	0.89 ± 0.09	43660	4508 ± 308	0.23 ± 0.03	2.01	0.55 ± 0.23
RXC J0943.0+4700	0.46 ± 0.111	54863	2903 ± 1315	0.07 ± 0.04	1.21	0.65 ± 0.18
RXC J0947.1+5428	0.00 ± 0.00	0	0 ± 0	0.00 ± 0.00	0.00	0.00 ± 0.00
RXC J0952.8+5153	0.94 ± 0.18	16193	3828 ± 207	0.21 ± 0.05	1.16	0.58 ± 0.20
RXC J0953.6+0142	1.30 ± 0.55	4345	4761 ± 157	0.28 ± 0.07	0.59	0.28 ± 0.12
RXC J1000.5+4409	0.81 ± 0.16	20092	3245 ± 199	0.10 ± 0.03	0.88	0.27 ± 0.14
RXC J1013.7-0006	0.77 ± 0.13	16004	4101 ± 223	0.11 ± 0.03	0.90	0.22 ± 0.19
RXC J1017.5+5933	1.21 ± 0.13	44927	3836 ± 193	0.30 ± 0.04	1.77	0.71 ± 0.27
RXC J1022.5+5006	0.79 ± 0.10	33560	4690 ± 263	0.14 ± 0.02	1.45	0.55 ± 0.20
RXC J1023.6+0411	0.55 ± 0.07	97158	4280 ± 429	0.04 ± 0.02	2.07	1.49 ± 0.72
RXC J1023.6+4908	0.91 ± 0.14	14311	3679 ± 222	0.28 ± 0.04	1.50	0.33 ± 0.09
RXC J1053.7+5452	3.00 ± 0.00	2855	5201 ± 41	0.60 ± 0.09	0.82	0.34 ± 0.11
RXC J1058.4+5647	1.14 ± 0.12	24980	4836 ± 151	0.26 ± 0.03	1.48	0.91 ± 0.22

cluster with respect of the galaxy background. In fact if the central region in which L_{op} is measured is too small (0.05 Mpc h_{70}^{-1} in Figs. 15 and 16), the value of the galaxy density is low and the measurement becomes more uncertain. On the other hand, at larger radii the density contrast between cluster and background decreases progressively. Instead, within a cluster aperture between 0.2 Mpc h_{70}^{-1} and 0.8 Mpc h_{70}^{-1}, the optical luminosity of both groups and massive clusters can be easily measured. In fact in both cases the radial aperture is small enough to show an high density contrast and therefore a high cluster S/N, and still large to enclose enough galaxies for the luminosity calculation.

After a more accurate analysis, we noted also that the low luminosity systems (both in the optical and in the X-ray band) are the main source of scatter at any cluster aperture. This could be due to different reasons. From the technical point of view the groups have a lower surface density contrast, and this causes problems in calculating the optical luminosity with a method based on the overdensity contrast. Moreover, the low mass systems could have a larger scatter in the optical and X-ray properties.

Furthermore, the galaxy groups could be responsible for the behavior of the scatter shown in Fig. 15. In fact at large cluster apertures the galaxy density contrast can be very low for the small systems and still very high for the massive and larger clusters. The large error introduced by the low density contrast in the calculation of the optical luminosity of galaxy groups could explain the increment of the scatter at larger apertures. To study in more detail the nature of the scatter of our correlation, and to investigate the role of the less luminous systems, we carried out the analysis explained above with the low mass systems removed. We limited the analysis to the subsample of the X-ray selected REFLEX-NORAS clusters, which occupy the intermediate and high luminosity region. Figure 17 shows the behavior of the scatter as a function of the cluster aperture in this second analysis. After removing the low mass systems the

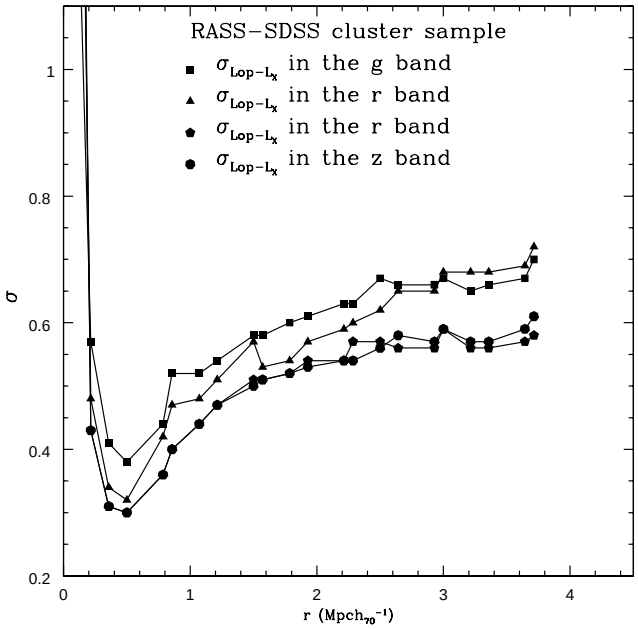

Fig. 15. Orthogonal scatter to the best fit of the $L_{op} - L_X$ relation obtained with the orthogonal method, as a function of the cluster aperture. The scatter shows a minimum in the region $0.2 \leq r \leq 0.8$ Mpc h_{70}^{-1}. Different symbols relate to the different photometric bands in which L_{op} is calculated: squares for the *g* band, triangles for the *r* band, hexagons for *i* band and filled circles for the *z* band. The *i* and *z* bands clearly show the smallest scatter at any aperture.

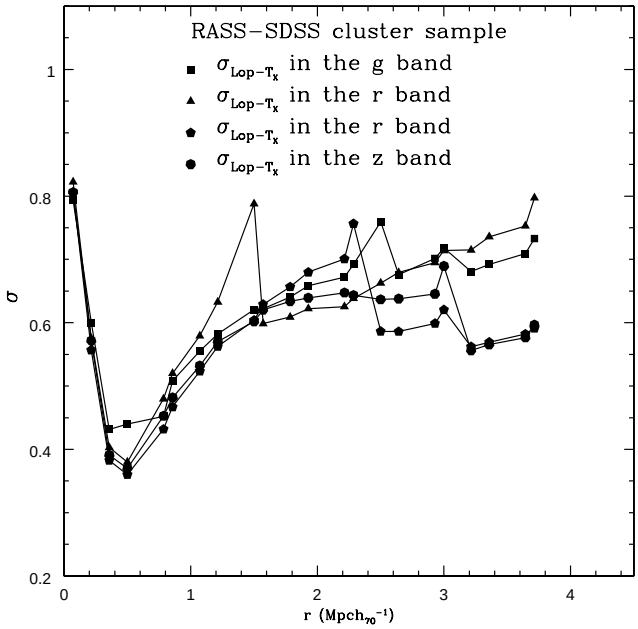

Fig. 16. Orthogonal scatter to the best fit of the $L_{op} - T_X$ relation obtained with the orthogonal method, as a function of the cluster aperture. The scatter shows a minimum in the region $0.2 \leq r \leq 0.8$ Mpc h_{70}^{-1}. Different symbols relate to the different photometric bands in which L_{op} is calculated: squares for the *g* band, triangles for the *r* band, hexagons for *i* band and filled circles for the *z* band. The *i* and *z* bands clearly show the smallest scatter at any aperture.

scatter decreases by about 30% for any aperture (from 0.3 dex to 0.2 dex in the region of minimum scatter and from 0.6 dex on average to 0.4 dex at larger apertures). Nevertheless the behavior of the scatter at increasing aperture is exactly the same observed in the analysis carried out on the overall RASS-SDSS galaxy cluster sample. This means that groups are responsible for part of the scatter but cannot explain the existence of the region of minimum scatter between 0.2 and 0.8 Mpc h_{70}^{-1}. A possible explanation for the behavior of the scatter at different cluster apertures could be the cluster compactness. As L_X depends not only on the cluster mass but also on the compactness of the cluster, the optical luminosity should also reflect somehow the cluster properties, mass and concentration. Thus, there should be an optimal aperture radius within which to measure L_{op}. We found that in all photometric bands, the minimum scatter is around 0.5 Mpc h_{70}^{-1}.

Figures 18 and 19 show the $L_{op} - L_X$ and $L_{op} - T_X$ relation respectively, at the radius of minimum scatter, 0.5 Mpc h_{70}^{-1}, in the *z* band. In fact the *i* and the *z* bands have a slightly smaller scatter than the other optical bands at any radius. Both plots show, as an outlier, the cluster RXC J0845.3+4430, which features a deviation larger than 3σ from the best fit. The system is a nearby group with a density contrast too low to estimate the optical luminosity reliably. The X-ray luminosity of this system has a 100% error. In $L_{op} - T_X$ there is another outlier: the cluster RXC J1629.6+4049. This system is not a source of scatter in the $L_{op} - L_X$ relation and the error in the X-ray and optical luminosities is 8% and 35% respectively. This can suggests that the optical luminosity is well measured, and it questions the estimate of the temperature. In fact, the X-ray luminosity of RXC J1629.6+4049 is 2.78×10^{43} erg s^{-1}, and the temperature, estimated from Horner et al. (2001), is 1 keV, while the $L_X - T_X$ relation of Xue & Wu (2000), predicts at least a T_X of 4.3 keV at that L_X.

With the σ clipping method those clusters were excluded from the estimation of the best fit. The best fit parameters of the orthogonal and bisector methods, in the *i* and *z* photometric bands, are shown in Tables 4 and 5 for the $L_{op} - L_X$ relation for the ROSAT X-ray luminosity and the bolometric X-ray luminosity, respectively. Table 6 shows the same results for the $L_{op} - T_X$ relation. Table 7 provides the results for the $L_{op} - L_X$ relation in the *i* and *z* band for the subsample of X-ray selected REFLEX-NORAS clusters. The tables also give the estimated orthogonal scatter and the estimated scatter in the two variables. The best fits in the *z* band for the $L_{op} - L_X$ and the $L_{op} - T_X$ relations at the radius of minimum scatter for the whole RASS-SDSS galaxy cluster sample are respectively:

$$L_{op}/L_\odot = 10^{11.79\pm0.02} L_X(ROSAT)^{0.45\pm0.03} \quad (14)$$

$$L_{op}/L_\odot = 10^{11.75\pm0.02} L_X(\mathrm{Bol})^{0.38\pm0.02} \quad (15)$$

$$L_{op}/L_\odot = 10^{11.42\pm0.06} T_X^{1.12\pm0.08}. \quad (16)$$

The value of the exponent in the power law for the $L_{op} - L_X$(Bol) relation is around 0.38 in the region of minimum, as indicated in Table 4. The values are not consistent within the errors with the value of 0.5 predicted under the assumption of hydrostatic equilibrium and constant mass to light ratio. The same conclusion can be reached for the $L_{op} - T_X$ relation and from

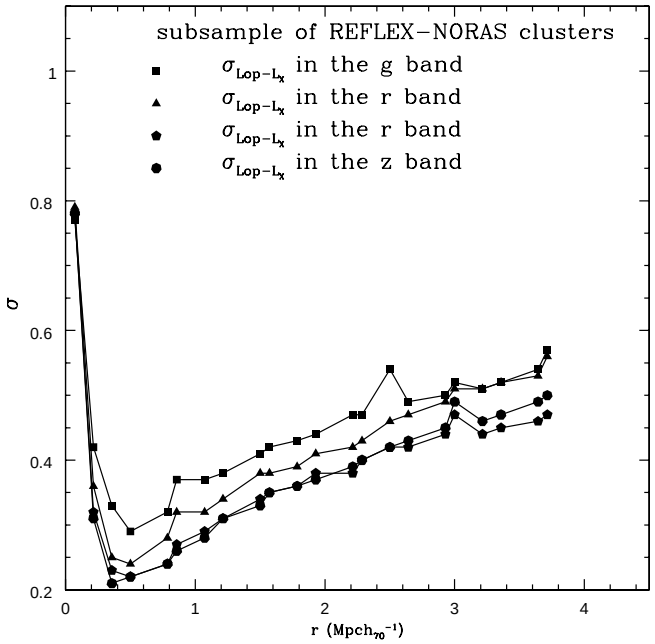

Fig. 17. Orthogonal scatter to the best fit of the $L_{\rm op} - L_{\rm X}$ relation obtained with the orthogonal method, as a function of the cluster aperture for the subsample of *REFLEX − NORAS* clusters. The scatter shows again a minimum in the region $0.2 \leq r \leq 0.8$ Mpc h_{70}^{-1}. Different symbols relate to the different photometric bands in which $L_{\rm op}$ is calculated: squares for the *g* band, triangles for the *r* band, hexagons for *i* band and filled circles for the *z* band. The *i* and *z* bands clearly show the smallest scatter at any aperture.

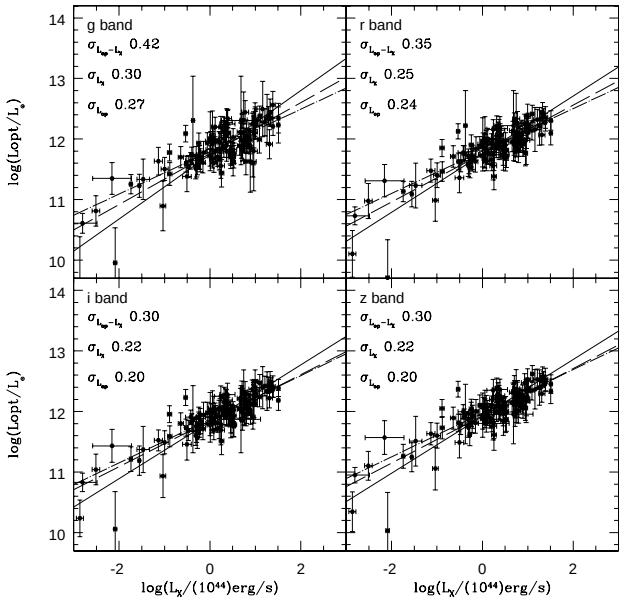

Fig. 18. Correlation between optical luminosities and X-ray luminosities. The fit is performed with a linear regression in the $\log(L_{\rm op}) - \log(L_{\rm X})$ space for each of the 4 optical bands. The solid and the dashed lines are the results of the orthogonal and the bisector method respectively over the whole RASS-SDSS galaxy cluster sample. The dot-dashed line is the best fit result of the orthogonal method applied to the subsample of strictly X-ray selected REFLEX-NORAS clusters. The error bars are at the 68% confidence level in both variables.

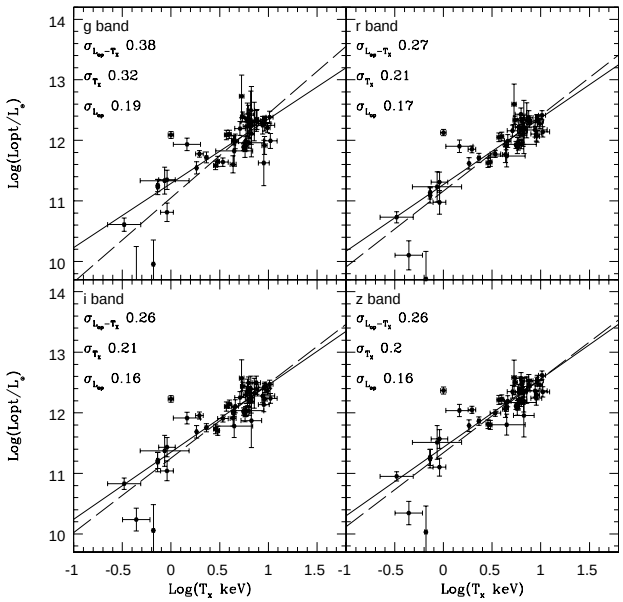

Fig. 19. Correlation between optical luminosities and ICM temperature. The fit is performed with a linear regression in the $\log(L_{\rm op}) - \log(T_{\rm X})$ space for each of the 4 optical bands. The solid and the dashed lines are the results of the orthogonal and the bisector method respectively. The error bars are at the 68% confidence level in both variables.

the $L_{\rm op} - L_{\rm X}$ for the subsample of X-ray selected REFLEX-NORAS clusters. A simple reason for the disagreement could be the assumption of a constant mass to light ratio. In fact, Girardi et al. (2002) analysed in detail the mass to light ratio in the *B* band of a sample of 294 clusters and groups, finding $M/L \propto L^{0.33\pm0.03}$. The same result was found by Lin et al. (2003) in the *K* band. Thus if we combine this dependence of *M/L* from the optical luminosity with the assumptions of hydrostatic equilibrium, the new expected relations between the optical luminosity and the X-ray luminosity and temperature are $L_{\rm op} \propto L_{\rm X}^{0.4}$ and $L_{\rm op} \propto T_{\rm X}^{1.25}$, respectively, which are in good agreement with our results.

The scatter in the $L_{\rm op} - L_{\rm X}$ relation for the aperture with the best correlation (0.5 Mpc h_{70}^{-1}), in the $L_{\rm op}$ variable is 0.20, and the scatter in the $L_{\rm X}$ variable is 0.22 in the correlations obtained in the *i* and *z* bands as shown in Table 4. Therefore, by calculating the total cluster luminosity in the central part of the system, one can use the *i* or *z* band to predict the X-ray luminosity from the optical data with a mean error of 60%. In the same way the optical luminosity can be derived from $L_{\rm X}$ with the same uncertainty. As indicated in Table 7, the uncertainty in the prediction of the two variables decreases to less than 40% if the correlation is limited to the REFLEX-NORAS cluster subsample. Table 6 shows that analogous results are obtained for the $L_{\rm op} - T_{\rm X}$ relation.

Since the observational uncertainties in the optical and in the X-ray luminosity are about 20%, the scatter of 60% of the overall sample in both relations and of 40% in the REFLEX-NORAS cluster subsample for the $L_{\rm op} - L_{\rm X}$ relation should be intrinsic.

Table 4. The table presents the results of the best fit for the *i* and *z* bands in the region of minimum scatter, $0.2 \leq r \leq 1.0$ Mpc h_{70}^{-1} for the $L_{\rm op} - L_{\rm X}(ROSAT)$ relation. We show the results for the two methods applied: the orthogonal distance regression (ODRPACK) and the bisector method, which is the line bisecting the best fit results of the vertical and horizontal minimization. The α and β parameters are given for several apertures with 95% confidence errors. The orthogonal scatter and the scatter in $\log(L_{\rm X}(0.1-2.4\ {\rm keV}))$ and in $\log(L_{\rm op})$ to the best fit line are given by σ, $\sigma_{L_{\rm X}}$, and $\sigma_{L_{\rm op}}$, respectively.

$L_{\rm op} - L_{\rm X}(ROSAT)$ relation in the *I* band										
	Orthogonal method					Bisector method				
r	α	β	σ	$\sigma_{L_{\rm X}}$	$\sigma_{L_{\rm op}}$	α	β	σ	$\sigma_{L_{\rm X}}$	$\sigma_{L_{\rm op}}$
0.2	0.50 ± 0.04	11.41 ± 0.03	0.43	0.32	0.30	0.32 ± 0.01	11.44 ± 0.03	0.36	0.23	0.28
0.3	0.46 ± 0.03	11.70 ± 0.02	0.31	0.23	0.21	0.36 ± 0.01	11.71 ± 0.02	0.29	0.18	0.23
0.5	0.47 ± 0.03	11.83 ± 0.02	0.30	0.22	0.20	0.38 ± 0.01	11.85 ± 0.02	0.27	0.18	0.20
0.7	0.56 ± 0.03	11.94 ± 0.03	0.36	0.26	0.25	0.47 ± 0.01	11.96 ± 0.02	0.32	0.22	0.24
0.8	0.61 ± 0.04	11.99 ± 0.03	0.40	0.29	0.28	0.51 ± 0.01	12.01 ± 0.03	0.36	0.24	0.26
1.0	0.65 ± 0.04	12.05 ± 0.03	0.44	0.31	0.31	0.54 ± 0.01	12.07 ± 0.03	0.39	0.27	0.28
$L_{\rm op} - L_{\rm X}(ROSAT)$ relation in the *Z* band										
	Orthogonal method					Bisector method				
r	α	β	σ	$\sigma_{L_{\rm X}}$	$\sigma_{L_{\rm op}}$	α	β	σ	$\sigma_{L_{\rm X}}$	$\sigma_{L_{\rm op}}$
0.2	0.50 ± 0.04	11.50 ± 0.03	0.43	0.31	0.31	0.31 ± 0.01	11.54 ± 0.03	0.35	0.23	0.26
0.3	0.45 ± 0.03	11.79 ± 0.02	0.31	0.23	0.21	0.37 ± 0.01	11.80 ± 0.02	0.29	0.18	0.23
0.5	0.47 ± 0.03	11.92 ± 0.02	0.30	0.22	0.20	0.39 ± 0.01	11.93 ± 0.02	0.28	0.18	0.21
0.7	0.56 ± 0.03	12.03 ± 0.03	0.36	0.26	0.25	0.47 ± 0.01	12.04 ± 0.02	0.33	0.22	0.24
0.8	0.60 ± 0.04	12.08 ± 0.03	0.40	0.29	0.27	0.51 ± 0.01	12.10 ± 0.03	0.36	0.24	0.26
1.0	0.65 ± 0.04	12.14 ± 0.03	0.44	0.31	0.31	0.54 ± 0.01	12.15 ± 0.03	0.39	0.27	0.28

Table 5. The table presents the results of the best fit for the *i* and *z* bands in the region of minimum scatter, $0.2 \leq r \leq 1.0$ Mpc h_{70}^{-1} for the $L_{\rm op} - L_{\rm X}(Bolometric)$ relation. We show the results for the two methods applied: the orthogonal distance regression (ODRPACK) and the bisector method, which is the line bisecting the best fit results of the vertical and horizontal minimization. The α and β parameters are given for several apertures with 95% confidence errors. The orthogonal scatter and the scatters in $\log(T_{\rm X})$ and in $\log(L_{\rm op})$ to the best fit line are given by σ, $\sigma_{T_{\rm X}}$, and $\sigma_{L_{\rm op}}$, respectively.

$L_{\rm op} - L_{\rm X}(Bolometric)$ relation in the *I* band										
	Orthogonal method					Bisector method				
r	α	β	σ	$\sigma_{L_{\rm X}}$	$\sigma_{L_{\rm op}}$	α	β	σ	$\sigma_{L_{\rm X}}$	$\sigma_{L_{\rm op}}$
0.2	0.38 ± 0.03	11.25 ± 0.04	0.41	0.31	0.27	0.27 ± 0.01	11.31 ± 0.03	0.37	0.24	0.28
0.3	0.36 ± 0.02	11.54 ± 0.03	0.31	0.23	0.20	0.30 ± 0.01	11.57 ± 0.02	0.29	0.18	0.23
0.5	0.38 ± 0.02	11.66 ± 0.03	0.30	0.22	0.20	0.32 ± 0.01	11.70 ± 0.02	0.27	0.18	0.21
0.7	0.38 ± 0.02	11.66 ± 0.03	0.30	0.22	0.20	0.32 ± 0.01	11.70 ± 0.02	0.27	0.18	0.21
0.8	0.49 ± 0.03	11.77 ± 0.04	0.41	0.30	0.28	0.42 ± 0.01	11.82 ± 0.03	0.37	0.25	0.27
1.0	0.53 ± 0.03	11.81 ± 0.04	0.44	0.32	0.31	0.45 ± 0.01	11.86 ± 0.03	0.40	0.27	0.29
$L_{\rm op} - L_{\rm X}(Bolometric)$ relation in the *Z* band										
	Orthogonal method					Bisector method				
r	α	β	σ	$\sigma_{L_{\rm X}}$	$\sigma_{L_{\rm op}}$	α	β	σ	$\sigma_{L_{\rm X}}$	$\sigma_{L_{\rm op}}$
0.2	0.38 ± 0.03	11.34 ± 0.04	0.41	0.30	0.28	0.26 ± 0.01	11.42 ± 0.03	0.35	0.23	0.27
0.3	0.35 ± 0.02	11.63 ± 0.03	0.30	0.24	0.19	0.31 ± 0.01	11.65 ± 0.02	0.29	0.18	0.23
0.5	0.38 ± 0.02	11.75 ± 0.03	0.30	0.23	0.20	0.32 ± 0.01	11.78 ± 0.02	0.28	0.18	0.21
0.7	0.38 ± 0.02	11.75 ± 0.03	0.30	0.23	0.20	0.32 ± 0.01	11.78 ± 0.02	0.28	0.18	0.21
0.8	0.49 ± 0.03	11.86 ± 0.04	0.40	0.29	0.28	0.42 ± 0.01	11.90 ± 0.03	0.37	0.25	0.27
1.0	0.52 ± 0.03	11.90 ± 0.04	0.44	0.32	0.31	0.44 ± 0.01	11.95 ± 0.03	0.40	0.28	0.29

7. Summary and conclusions

We created a database of clusters of galaxies based on the largest available X-ray and optical surveys: the ROSAT All Sky Survey (RASS) and the Sloan Digital Sky Survey (SDSS). The RASS-SDSS galaxy cluster catalog is the first catalog which combines X-ray and optical data for a large number (114) of galaxy clusters. The systems are X-ray selected, ranging from groups of $10^{12.5}$ $M_{\odot}$ to massive clusters of 10^{15} $M_{\odot}$ in a redshift range from 0.002 to 0.45. The X-ray (luminosity in the

Table 6. The table presents the results of the best fit for the *i* and *z* bands in the region of minimum scatter, $0.2 \leq r \leq 1.0$ Mpc h_{70}^{-1}. We show the results for the two methods applied: the orthogonal distance regression (ODRPACK) and the bisector method, which is the line bisecting the best fit results of the vertical and horizontal minimization. The α and β parameters are given for several apertures with 95% confidence errors. The orthogonal scatter and the scatters in $\log(T_X)$ and in $\log(L_{op})$ to the best fit line are given by σ, σ_{T_X}, and $\sigma_{L_{op}}$, respectively.

$L_{op} - T_X$ relation in the *I* band										
Orthogonal method						Bisector method				
r	α	β	σ	σ_{T_X}	$\sigma_{L_{op}}$	α	β	σ	σ_{T_X}	$\sigma_{L_{op}}$
0.2	0.97 ± 0.17	11.05 ± 0.12	0.53	0.39	0.36	1.22 ± 0.22	10.80 ± 0.16	0.54	0.39	0.37
0.3	1.06 ± 0.09	11.21 ± 0.06	0.32	0.27	0.17	1.17 ± 0.18	11.12 ± 0.14	0.31	0.18	0.25
0.5	1.11 ± 0.08	11.33 ± 0.06	0.26	0.20	0.16	1.13 ± 0.10	11.30 ± 0.08	0.25	0.17	0.19
0.7	1.20 ± 0.11	11.43 ± 0.08	0.30	0.23	0.19	1.40 ± 0.12	11.27 ± 0.09	0.29	0.20	0.21
0.8	1.20 ± 0.12	11.51 ± 0.09	0.33	0.26	0.20	1.51 ± 0.13	11.26 ± 0.10	0.33	0.23	0.24
1.0	1.21 ± 0.14	11.60 ± 0.10	0.39	0.32	0.23	1.62 ± 0.16	11.26 ± 0.12	0.39	0.27	0.28
$L_{op} - T_X$ relation in the *Z* band										
Orthogonal method						Bisector method				
r	α	β	σ	σ_{T_X}	$\sigma_{L_{op}}$	α	β	σ	σ_{T_X}	$\sigma_{L_{op}}$
0.2	0.97 ± 0.18	11.18 ± 0.13	0.54	0.37	0.40	1.16 ± 0.18	10.95 ± 0.13	0.55	0.42	0.35
0.3	1.06 ± 0.08	11.31 ± 0.06	0.31	0.27	0.16	1.18 ± 0.19	11.20 ± 0.15	0.31	0.18	0.25
0.5	1.12 ± 0.08	11.42 ± 0.06	0.25	0.20	0.16	1.12 ± 0.10	11.39 ± 0.08	0.25	0.16	0.19
0.7	1.20 ± 0.11	11.52 ± 0.08	0.30	0.24	0.19	1.40 ± 0.12	11.34 ± 0.09	0.30	0.20	0.23
0.8	1.21 ± 0.12	11.60 ± 0.09	0.34	0.27	0.20	1.51 ± 0.13	11.34 ± 0.10	0.33	0.23	0.24
1.0	1.22 ± 0.14	11.68 ± 0.10	0.39	0.32	0.23	1.62 ± 0.15	11.34 ± 0.11	0.39	0.27	0.28

Table 7. The table presents the results of the best fit for the *i* and *z* bands in the region of minimum scatter, $0.2 \leq r \leq 1.0$ Mpc h_{70}^{-1} for the $L_{op} - L_X(ROSAT)$ relation in the subsample of REFLEX and NORAS X-ray selected clusters. We show the results for the orthogonal distance regression (ODRPACK) method. The α and β parameters are given for several apertures with 95% confidence errors. The orthogonal scatter and the scatters in $\log(L_X(0.1{-}2.4\ \mathrm{keV}))$ and in $\log(L_{op})$ to the best fit line are given by σ, σ_{L_X}, and $\sigma_{L_{op}}$, respectively.

$L_{op} - L_X(ROSAT)$ relation for REFLEX-NORAS clusters only										
Orthogonal method										
i band						*z* band				
r	α	β	σ	σ_{L_X}	$\sigma_{L_{op}}$	α	β	σ	σ_{L_X}	$\sigma_{L_{op}}$
0.2	0.28 ± 0.04	11.48 ± 0.03	0.32	0.23	0.22	0.27 ± 0.04	11.57 ± 0.03	0.31	0.23	0.21
0.3	0.33 ± 0.03	11.74 ± 0.02	0.23	0.16	0.15	0.34 ± 0.03	11.83 ± 0.02	0.21	0.16	0.15
0.5	0.36 ± 0.03	11.87 ± 0.02	0.22	0.16	0.15	0.36 ± 0.03	11.97 ± 0.02	0.22	0.16	0.14
0.7	0.36 ± 0.03	12.01 ± 0.02	0.24	0.18	0.16	0.37 ± 0.03	12.11 ± 0.02	0.24	0.17	0.16
0.8	0.37 ± 0.03	12.08 ± 0.03	0.27	0.20	0.17	0.37 ± 0.03	12.17 ± 0.02	0.26	0.20	0.17
1.0	0.37 ± 0.04	12.18 ± 0.03	0.29	0.23	0.18	0.37 ± 0.04	12.28 ± 0.03	0.28	0.22	0.18

ROSAT band, bolometric luminosity, redshift, center coordinates) and optical properties (Schechter luminosity function parameters, luminosity, central galaxy density, core, total and half-light radii) are computed in a uniform and accurate way. The catalog also contains temperatures and iron abundances for a subsample of 53 clusters from the Asca Cluster Catalog and the Group Sample. The resulting RASS-SDSS galaxy cluster catalog constitutes an important database to study the properties of galaxy clusters and in particular the relation of the galaxy population seen in the optical to the properties of the X-ray luminous ICM.

The first investigations reported have shown a tight correlation between the X-ray and optical properties, when the choice of the measurement aperture for the optical luminosity and the optical wavelength band are optimized. We find that the optical luminosity calculated in the *i* and in the *z* band correlates better with the X-ray luminosity and the ICM temperature, than is the case for the other Sloan photometric bands. Thus the red optical bands, which are more sensitive to the light of the old stellar population and therefore to the stellar mass of cluster galaxies, have tight correlations with the X-ray properties of the systems.

Moreover, we found that the scatter in the $L_{op} - L_X$ and $L_{op} - T_X$ relations can be minimized if the optical luminosity is measured within a cluster aperture between 0.2–0.8 Mpc h_{70}^{-1}, with an absolute minimum of the scatter at 0.5 Mpc h_{70}^{-1}. The best aperture for the measurement of the optical luminosity is due to the fact that it is a good compromise for assessing simultaneously the total richness and the compactness of the cluster.

Finally, using the relations obtained from the *z* band, we demonstrated that, given the optical properties of a cluster, we can predict the X-ray luminosity and temperature with an accuracy of 60% and vice versa. By restricting the correlation analysis to the subsample of X-ray detected REFLEX-NORAS clusters, the minimum scatter decreases to less than 40% for the $L_{\rm op} - L_{\rm X}$ relation. Since the observational uncertainties in the optical and in the X-ray luminosity are about 20%, the observed scatter in both relations should be intrinsic.

The resulting logarithmic slope for the $L_{\rm op} - L_{\rm X}$ relation with the minimum scatter is 0.38 ± 0.02, while the value for the $L_{\rm op} - T_{\rm X}$ relation is 1.12 ± 0.08. These results are not consistent with the assumption of hydrostatic equilibrium and constant *M/L*. If we assume that *M/L* depends on the luminosity with a power law $M/L \propto L^{0.3}$ (Girardi et al. 2002), our results are in very good agreement with the expected values under the assumption of hydrostatic equilibrium.

The analysis carried out in this paper on the correlation between X-ray and optical appearance of galaxy clusters is completely empirical. In principle, the best way to proceed in this kind of study is to measure the optical luminosity within the physical size of the cluster, i.e. whitin the virial radius. Without optical spectroscopic data or accurate temperature measurements, the cluster virial radius can be calculated assuming a theoretical model relating the optical luminosity to the cluster mass. At this stage of the work, we preferred to tackle the cluster X-ray-optical connection with the empirical method explained in the paper, in order to have model-independent results. On the other hand, not taking into account the different cluster sizes could have affected both the slope and the scatter of the given relations (Eqs. (14)–(16)). Therefore, for a better understanding of the important connection between the X-ray and optical appearance of galaxy clusters, the optical luminosity has to be calculated within the physical size of the cluster. This work is in progress and will be published in the second paper of this series on the RASS-SDSS galaxy cluster sample. The next step will be the study of the fundamental plane of galaxy clusters. Through this kind of analysis we will find out if the observed scatter in the correlations between the optical and X-ray properties depends on another parameter related to the cluster compactness. Moreover, because of the link between the galaxy cluster fundamental plane and the *M/L* parameter, we will connect directly the slope of two relations to the behavior of *M/L*.

Acknowledgements. Funding for the creation and distribution of the SDSS Archive has been provided by the Alfred P. Sloan Foundation, the Participating Institutions, the National Aeronautics and Space Administration, the National Science Foundation, the US Department of Energy, the Japanese Monbukagakusho, and the Max Planck Society. The SDSS Web site is `http://www.sdss.org/`. The SDSS is managed by the Astrophysical Research Consortium (ARC) for the Participating Institutions. The Participating Institutions are The University of Chicago, Fermilab, the Institute for Advanced Study, the Japan Participation Group, The Johns Hopkins University, Los Alamos National Laboratory, the Max-Planck-Institute for Astronomy (MPIA), the Max-Planck-Institute for Astrophysics (MPA), New Mexico State University, University of Pittsburgh, Princeton University, the United States Naval Observatory, and the University of Washington.

References

Abazajian, K., Adelman, J., Agueros, M., et al. 2003, AJ, 126, 2081 (Data Release One)
Adami, C., Mazure, A., Katgert, P., et al. 1998, A&A, 336, 63
Akritas, M., Mazure, A., Katgert, P., et al. 1996, ApJ, 470, 706
Arnaud, M., Rothenflug, R., Boulade, O., et al. 1992, A&A, 254, 49
Bahcall, N. 1977, ApJ, 217, L77
Bahcall, N. 1981, ApJ, 247, 787
Bahcall, N., McKay, T. A., Annis, J., et al. 2003, ApJS, 148, 253
Blanton, M. R., Dalcanton, J., Eisenstein, D., et al. 2001, AJ, 121, 2358
Blanton, M. R., Lupton, R. H., Maley, F. M., et al. 2003, AJ, 125, 2276 (Tiling Algorithm)
Böhringer, H., Voges, W., Huchra, J. P., et al. 2000, ApJS, 129, 435
Böhringer, H., Schuecker, P., Guzzo, L., et al. 2001, A&A, 369, 826
Böhringer, H., Collins, C. A., Guzzo, L., et al. 2002, ApJ, 566, 93
De Grandi, S., & Molendi, S. 2002, ApJ, 567, 163
De Propris, R., Colless, M., Driver, S. P., et al. 2003, MNRAS, 342, 725
Donahue, M., Mack, J., Scharf, C., et al. 2001, ApJ, 552, L93
Donahue, M., Scharf, C. A., Mack, J., et al. 2002, ApJ, 569, 689
Dressler, A., Oemler, A. Jr., Couch, W. J., et al. 1997, ApJ, 490, 577
Edge, A. C., & Stewart, G. C. 1991, MNRAS, 252, 428
Eisenstein, D. J., Annis, J., Gunn, J. E., et al. 2001, AJ, 122, 2267
Fasano, G., Poggianti, B. M., Couch, W. J., et al. 2000, ApJ, 542, 673
Finoguenov, A., Arnaud, M., & David, L. P. 2001, ApJ, 555, 191F
Finoguenov, A., Reiprich, T. H., & Böhringer, H. 2001, A&A, 368, 749
Fletcher, R. 1970, Comput. J., 13, 317
Fukugita, M., Shimasaku, K., & Ichikawa, T. 1995, PASJ, 107, 945
Fukugita, M., Ichikawa, T., & Gunn, J. E. 1996, AJ, 111, 1748
Girardi, M., Borgani, S., Giuricin, G., et al. 2000, ApJ, 530, 62
Girardi, M., Manzato, P., Mezzetti, M., et al. 2002, ApJ, 569, 720
Gladders, M., & Yee, H. K. C. 2000, AJ, 120, 2148
Gomez, P., Nichol, R. C., Miller, C. J., et al. 2003, ApJ, 584, 210
Goto, T., Sekiguchi, M., Nichol, R. C., et al. 2002a, AJ, 123, 1807
Goto, T., Okamura, S., McKay, T. A., et al. 2002b, PASP, 123, 1807
Gunn, J. E., Carr, M. A., Rockosi, C. M., et al. 1998, AJ, 116, 3040 (SDSS Camera)
Hogg, D. W., Finkbeiner, D. P., Schlegel, D. J., & Gunn, J. E. 2001, AJ, 122, 2129
Horner, D. 2001, Ph.D. Thesis, University of Maryland
Ikebe, Y., Reiprich, T. H., Böhringer, H., et al. 2002, A&A, 383, 773
Isobe, T., Feigelson, E. D., Akritas, M. G., et al. 1990, ApJ, 364, 104
Kelson, D., van Dokkum, P. G., Franx, M., et al. 1997, ApJ, 478, 13
Kelson, D., Illingworth, G. D., van Dokkum, P. G., & Franx, M. 2000, ApJ, 531, 137
Kim, R., Seung, J., & Kepner, J. V. 2002, AJ, 123, 20
Kochanek, C. S., Pahre, M. A., Falco, E. E., et al. 2001, ApJ, 560, 566
Lin, Y., Mohr, J. J., & Stanford, S. A. 2003, ApJ, 591, 749
Lubin, L., Oke, J. B., & Postman, M. 2002, AJ, 124, 1905
Lumsden, S. L., Collins, C. A., Nichol, R. C., et al. 1997, MNRAS, 290, 119
Lupton, R. H., Gunn, J. E., & Szalay, A. S. 1999, AJ, 118, 1406
Lupton, R., Gunn, J. E., Ivezić, Z., et al. 2001, in Astronomical data analysis software and systems X, ed. F. R. Harnden, Jr., F. A. Primini, & H. E. Payne (San Francisco: Astr. Soc. Pac.), ASP Conf. Ser., 238, 269 [arXiv:astro-ph/0101420]
Markevitch, M. 1998, ApJ, 504, 27

Mulchaey, J. S., Davis, D. S., Mushotzky, R. F., & Burstein, D. 2003, ApJSS, 145, 39
Pier, J. R., Munn, J. A., Hindsley, R. B., et al. 2003, AJ, 125, 1559 (Astrometry)
Poggianti, B., Bridges, T. J., Komiyama, Y., et al. 2004, ApJ, 601, 197
Postman, M., Lubin, L. M., & Oke, J. B. 1998, AJ, 116, 560
Reiprich, T. H., & Böringher, H. 2002, ApJ, 567, 716
Retzlaff, J. 2001, XXIst Moriond Astrophysics Meeting, March 10−17, 2001 Savoie, France, ed. D. M. Neumann, & J. T. T. Van
Rosati, P., Borgani, S., & Norman, C. 2002, ARA&A, 40, 539
Sarazin, C. 1980, ApJ, 236, 75
Schlegel, D., Finkbeiner, D. P., & Davis, M. 1998, ApJ, 500, 525
Shimasaku, K., Fukugita, M., Doi, M., et al. 2001, AJ, 122, 1238
Smith, J. A., Tucker, D. L., Kent, S. M., et al. 2002, AJ, 123, 2121
Stoughton, C., Lupton, R. H., Bernardi, M., et al. 2002, AJ, 123, 485
Strateva, I., Ivezić, Z., Knapp, G. R., et al. 2001, AJ, 122, 1861
Strauss, M. A., Weinberg, D. H., Lupton, R. H., et al. 2002, AJ, 124, 1810
van Dokkum, S., Franx, M., Fabricant, D., et al. 2000, ApJ, 541, 95V
Voges, W., Aschenbach, B., Boller, Th., et al. 1999, A&A, 349, 389
Xue, Y., & Wu, X. 2000, ApJ, 538, 65
Yasuda, N., Fukugita, M., Narayanan, V. K., et al. 2001, AJ, 122, 1104
Yee, H. K. C., & Ellingson, E. 2003, ApJ, 585, 215
York, D. G., Adelman, J., Anderson, J. E., et al. 2000, AJ, 120, 1579
Ziegler, B., & Bender, R. 1997, MNRAS, 291, 527

A&A 433, 415–429 (2005)
DOI: 10.1051/0004-6361:20041870

Astronomy & Astrophysics

RASS-SDSS galaxy cluster survey

II. A unified picture of the cluster luminosity function

P. Popesso[1], H. Böhringer[1], M. Romaniello[2], and W. Voges[1]

[1] Max-Planck-Institut fur extraterrestrische Physik, 85748 Garching, Germany
e-mail: popesso@mpe.mpg.de
[2] European Southern Observatorty, Karl Scharzschildstr. 2, 85748 Garching b. München, Germany

Received 20 August 2004 / Accepted 1 December 2004

Abstract. We constructed the composite luminosity function (LF) of clusters of galaxies in the five SDSS photometric bands *u*, *g*, *r*, *i* and *z* from the RASS-SDSS galaxy cluster catalog. Background and foreground galaxies are subtracted using both a local and a global background correction to take in account the presence of large scale structures and field to field variations, respectively. The composite LF clearly shows two components: a bright-end LF with a classical slope of −1.25 in each photometric band, and a steeper faint-end LF ($-2.1 \leq \alpha \leq -1.6$) in the dwarf galaxy region. The observed upturn of the faint galaxies has a location ranging from $-16 + 5\log(h)$ in the *g* band to $-18.5 + 5\log(h)$ in the *z* band. To study the universality of the cluster LF we compare the individual cluster LFs with the composite luminosity function. In agreement with the composite LF, a single Schechter component is not a good fit for the majority of the clusters. We fit a Schechter function to the bright-end of the individual cluster LFs in the magnitude region brighter than the observed upturn of the dwarf galaxies. The bright-end of the galaxy clusters shows the same shape in all the systems. To study the behavior of the individual faint-end LF we define the Dwarf to Giant galaxy Ratio (DGR) of the single clusters. The distribution of DGR has a spread much larger than the statistical errors. The DGR clearly anti-correlates with both X-ray and optical cluster luminosities. This anti-correlation is most likely due to the choice of a fixed metric aperture for all the clusters. Therefore, because of this effect, the different cluster physical sizes must be taken into account before comparing the LF of different clusters.

Key words. galaxies: clusters: general – galaxies: general

1. Introduction

The galaxy luminosity function (LF) is one of the most direct observational test of theories of galaxy formation and evolution. Clusters of galaxies are ideal systems within which to measure the galaxy LF for the large number of galaxies at the same distance. There are two main purposes for the study of the cluster LF: the comparison of the galaxy LF in clusters and field and thus the study of the influence of the environment on the global statistical properties of galaxies, and the search for differences in the LF of different clusters as indicators of differences in the galaxy formation due to environmental effects or dynamical processes.

The cluster galaxy over-density with respect to the surrounding field is sufficiently high to efficiently identify members either photometrically through the statistical removal of foreground and background galaxies or spectroscopically. These techniques have been used to measure LFs for individual clusters or to form a composite LF, in order to eliminate the peculiarity of the individual LFs and enhance the underlying possibly universal LF (Dressler 1978; Lugger 1986; Colless 1989; Lugger 1989; Lumsden et al. 1997; Valotto et al. 1997; Rauzy et al. 1998; Garilli et al. 1999; Paolillo et al. 2001; Goto et al. 2002b; Yagi et al. 2002). Many of these studies do not agree on the exact form of the LF. Several authors (Dressler 1978; Lumdsen 1997; Valotto et al. 1997; Garilli et al. 1999; Goto et al. 2002b) found differences between the LFs of different clusters and between cluster and field, while others (Lugger 1986; Colless 1989; Lugger 1989; Rauzy 1998; Trentham 1998; Paolillo et al. 2001) concluded that the galaxy LF is universal in all environments. However, all these works used different techniques and selections to check the universality of the cluster LF. Therefore, it is difficult to understand if their conclusions depend on the different tests beeing applied or to actual physical distinctions. Table 1 summarizes the variations between previous studies in the same color and their σ error limits for the Schechter parameters M^* and α. We have transformed magnitudes to $H_0 = 100\,\mathrm{km\,s^{-1}\,Mpc^{-1}}$ without changing their cosmology.

So far, the majority of the studies on the cluster composite LF has concentrated on the slope at the relatively bright end of the cluster LF ($M_g \leq -17$) without taking into account the behavior of the dwarf galaxy population in clusters. Instead, much work has been done in recent years in measuring the faint

Table 1. Schechter parameters fitted to the Composite LF retrieved in the literature.

Reference	M^*	α	Band	Ncluster	Luminosity range
Goto et al. (2002b)	-20.84 ± 0.26	-1.40 ± 0.11	u	204	$-24 \leq M_u \leq -18$
Schechter (1976)	-19.9 ± 0.50	-1.24	b_j	13	$-22.5 \leq M_{b_j} \leq -18.5$
Dressler (1978)	-19.7 ± 0.50	-1.25	F	12	$-23.5 \leq M_F \leq -18.5$
Colless (1989)	-20.10 ± 0.07	-1.25	b_j	14	$-22.5 \leq M_{b_j} \leq -17$
Lumsden et al. (1997)	-20.16 ± 0.02	-1.22 ± 0.04	b_j	46	$-21 \leq M_{b_j} \leq -18$
Valotto et al. (1997)	-20.00 ± 0.10	-1.40 ± 0.10	b_j	55	$-21 \leq M_{b_j} \leq -17$
Rauzy et al. (1998)	-20.91 ± 0.21	-1.50 ± 0.11	b_j	28	$-21 \leq M_{b_j} \leq -17$
Garilli et al. (1999)	-20.30 ± 0.10	-0.94 ± 0.07	g	65	$-22.5 \leq M_g \leq -15.5$
Paolillo et al. (2001)	-20.22 ± 0.15	-1.07 ± 0.08	g	39	$-24.5 \leq M_g \leq -16.5$
Goto et al. (2002b)	-21.24 ± 0.11	-1.00 ± 0.06	g	204	$-24 \leq M_g \leq -18$
De Propris et al. (2003)	-20.07 ± 0.07	-1.28 ± 0.03	b_j	60	$-22.5 \leq M_{b_j} \leq -16$
Lugger et al. (1989)	-21.31 ± 0.13	-1.21 ± 0.09	R	9	$-23 \leq M_R \leq -18.5$
Garilli et al. (1999)	-20.66 ± 0.16	-0.95 ± 0.07	r	65	$-22.5 \leq M_r \leq -15.5$
Paolillo et al. (2001)	-20.67 ± 0.16	-1.11 ± 0.08	r	39	$-24.5 \leq M_r \leq -16.5$
Yagi et al. (2002)	-21.30 ± 0.20	-1.31 ± 0.05	R_C	10	$-23.5 \leq M_{R_C} \leq -16$
Goto et al. (2002b)	-21.44 ± 0.05	-0.85 ± 0.03	r	204	$-24 \leq M_r \leq -18$
Paolillo et al. (2002)	-20.85 ± 0.20	-1.09 ± 0.11	i	39	$-24 \leq M_i \leq -17$
Goto et al. (2002b)	-21.54 ± 0.08	-0.70 ± 0.05	i	204	$-24 \leq M_i \leq -18$
Goto et al. (2002b)	-21.59 ± 0.06	-0.58 ± 0.04	z	204	$-24 \leq M_z \leq -18$

end ($-18 \leq M_g \leq -10$) of the galaxy LF in several nearby clusters (e.g. Driver 1994; Smith et al. 1997; Phillipps et al. 1998; Boyce et al. 2001; Beijersbergen et al. 2001; Sabatini et al. 2002; Trentham 2003; Cortese et al. 2004). The LF of these clusters typically steepens faintward of about $M_g \sim -18$ showing the debated upturn of the dwarf galaxies . The faint end slope α of the LF in this range of magnitudes typically lies in the range -1.4 to -2.2. Phillipps et al. (1998) noted that the steepness of the faint end slope appears to depend on the cluster density, with dwarfs being more common in lower density environments. This is possibly because the various dynamical processes which can destroy dwarf galaxies act preferentially in dense environments.

In this paper we present the analysis of the cluster composite LF based on the second release of the Sloan Digital Sky survey (SDSS DR2, Abazajian et al. 2004). The excellence of the SDSS DR2 in terms of its size, depth and sky coverage and the accurate photometry in 5 different optical wavebands gives unprecedented advantages in comparison to the previous studies. Firstly, the sky coverage (3324 deg^2) gives us the possibility to overcome the well-known problem of the statistical subtraction of the galaxy background. We used large areas of the survey to define a mean global galaxy background and a region close to the clusters to determine the local galaxy background in order to check for systematics in the field subtraction. Secondly, the apparent magnitude limit of the SDSS DR2 in all the five bands is sufficiently deep (e.g. $r_{\rm lim} = 22.2$, 95% completeness) that, at the mean redshift of our cluster sample ($z \sim 0.15$), the cluster LF can extend and cover a significant part of the dwarf region, going deeper than in all previous studies of the composite luminosity function (more than 6 mag fainter than M^*). Thirdly, the high accuracy of the SDSS photometry in all bands gives us the possibility to measure in a statistically significant way the individual cluster LF with the consequent opportunity to check directly the universality of the LF. Furthermore, the accurate multi-color photometry allows us to use several objectively-measured galaxy properties like galaxy morphology. Finally, our comparison of the cluster and field LFs can done within the SDSS data.

To calculate the cluster composite LF we used the RASS-SDSS galaxy cluster sample (Popesso et al. 2004), which includes 130 systems observed in X-rays. The use of the RASS-SDSS galaxy cluster catalog ensures that none of the systems is a simple projection of large scale structure along the line of sight.

The paper is organized as follows: in Sect. 2 we describe the properties of the cluster sample and the optical galaxy photometry; in Sect. 3 we explain the methods used in constructing the individual cluster LFs and the methods of the background subtraction, in Sect. 4 we describe the methods used for building the Composite LF, in Sect. 5 we describe in detail our results. Section 6 contains our conclusions. Throughout the paper we use $H_0 = 100$ km s^{-1} Mpc^{-1}, $\Omega_{\rm m} = 0.3$ and $\Omega_\lambda = 0.7$.

2. The data

The RASS-SDSS galaxy cluster catalog comprises 130 systems detected in the ROSAT All Sky Survey (RASS). The X-ray cluster properties and the cluster redshift have been taken from different X-ray catalogs: the ROSAT-ESO flux limited X-ray cluster sample (REFLEX, Böhringer et al. 2003), the Northern ROSAT All-sky cluster sample (NORAS, Böhringer et al. 2000), the NORAS 2 cluster sample (Retzlaff 2001), the ASCA Cluster Catalog (ACC) from Horner et al. (2001) and

the Group Sample (GS) of Mulchaey et al. (2003). In constructing the composite LF we restricted our selection to clusters with $z \leq 0.25$ in order to sample well below the predicted M^*, and used therefore 97 clusters out of 130 systems in the catalog.

The optical photometric data are taken from the SDSS DR2 (York et al. 2000; Stoughton et al. 2002; and Abazajian et al. 2004). The SDSS consists of an imaging survey of π steradians of the northern sky in the five passbands *u*, *g*, *r*, *i*, *z*, in the entire optical range from the atmospheric ultraviolet cutoff in the blue to the sensitivity limit of silicon in the red. The survey was carried out using a 2.5 m telescope, an imaging mosaic camera with 30 CCDs, two fiber-fed spectrographs and a 0.5 m telescope for the photometric calibration. The imaging survey is taken in drift-scan mode. The imaging data are processed with a photometric pipeline (PHOTO) especially written for the SDSS data. For each cluster we defined a photometric galaxy catalog as describe in Sect. 3 of Popesso et al. (2004).

For the analysis in this paper we use only SDSS Model magnitudes. Due to a bug of PHOTO, found during the completion of DR1, the model magnitudes are systematically underestimated by about 0.2–0.3 mag for galaxies brighter then 20th magnitude, and accordingly the measured radii are systematically too large. This problem has been fixed in the SDSS DR2, therefore the model magnitude can be considered a good estimate of the galaxy total luminosity at any magnitude and are not dependent on the seeing as the Petrosian magnitudes. Figures 1 and 2 show the difference in the quality of the galaxy photometry between the DR1 and the DR2 data. For this study we only use the revised DR2 for the complete cluster sample.

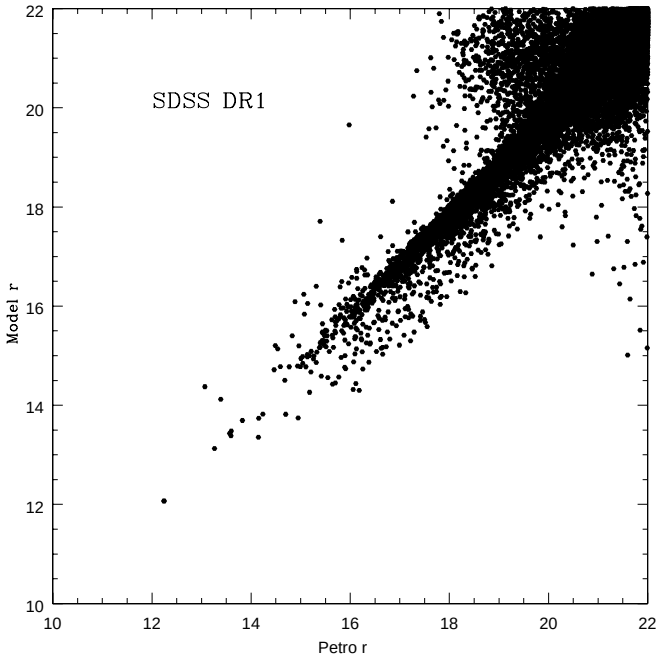

Fig. 1. Petrosian magnitude versus Model magnitude in the Data Release 1 (DR1).

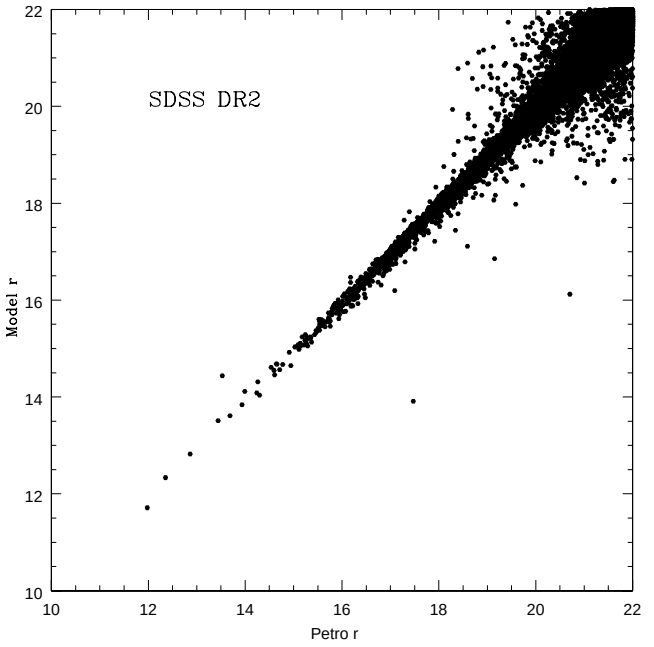

Fig. 2. Petrosian magnitude versus Model magnitude in the Data Release 2 (DR2).

3. The individual luminosity functions

3.1. Background subtraction

We consider two different approaches to the statistical subtraction of the galaxy background. First we calculate a local background in an annulus with inner radius of 3 Mpc h^{-1} from the X-ray cluster center and width of 0.5 deg. The annulus is divided in 20 sectors (Popesso et al. 2004) and those featuring a larger than 3σ deviation from the median galaxy density are discarded from further calculations. In this way other clusters close to the target or voids are not included in the background correction. We compute the galaxies number counts $N^{\rm l}_{\rm bg}(m)\mathrm{d}m$ per bin of magnitude (with a bin width of 0.5 mag) and per squared degree in the remaining area of the annulus. The statistical source of error in this approach is the Poissonian uncertainty of the counts, given by $\sqrt{N^{\rm l}_{\rm bg}(m)}$.

As a second method we derive a global background correction. The galaxy number counts $N^{\rm g}_{\rm bg}(m)\mathrm{d}m$ is derived from the mean of the magnitude number counts determined in five different SDSS sky regions, each with an area of 30 deg^2. The source of uncertainty in this second case is systematic and originates from the presence of large-scale clustering within the galaxy sample, while the Poissonian error of the galaxy counts is small due to the large area involved. We estimate this error as the standard deviation of the mean global number counts, $\sigma^{\rm g}_{\rm bg}(m)$, in the comparison of the five areas. To take into account this systematic source of error also for the the local background, we estimate the background number counts error as $\sigma_{\rm bg}(m) = \max(\sqrt{N^{\rm l}_{\rm bg}(m)}, \sigma^{\rm g}_{\rm bg}(m))$ (Lumdsen et al. 1997) for all the derived quanties. For a detailed comparison of the results of the local and global background estimates see Popesso et al. (2004).

3.2. Luminosity function

We derive the individual cluster luminosity function by subtracting from the galaxy counts measured in a certain region

the local or the global field counts rescaled to the cluster area. We calculate the individual cluster LF within different radii, from 0.3 to 2 Mpc h^{-1}, to study possible dependences of the LF on the clustercentric distance and thus on the density. Following previous works, we exclude from the individual cluster LFs the Brightest Cluster Galaxies (BCG).

To build the Composite LF we transform the apparent magnitude in absolute magnitude according to:

$$M = m - 25 - 5\log_{10}(D_L/1\ \mathrm{Mpc}) - A - K(z) \quad (1)$$

where D_{L} is the luminosity distance, A is the Galactic extinction and $K(z)$ is the K-correction. We deredden the Petrosian and model magnitudes of galaxies using the Galactic map of Schlegel et al. (1998) in each photometric band. We use the K-correction supplied by Fukugita et al. (1995) for elliptical galaxies, assuming that the main population of our clusters are the old elliptical galaxies at the cluster redshift.

Due to the high accuracy of the SDSS multi-color photometry, the quality of the individual cluster LF is very high. Therefore, to compare the Schechter parameters of the individual LF with those of the composite luminosity function, we fit a Schechter luminosity function to the single clusters by using the fitting method described in the Sect. 4 of Popesso et al. (2004).

4. The composite luminosity function

The composite LF is not only a good method to calculate with high accuracy the cluster LF when the quality of the individual cluster LFs is too low, but it is also a tool to check for the LF universality. The composite LF can be easily interpreted as a mean cluster LF. Therefore, if the LF is universal in all the cluster environments, the distribution of the individual LF parameters should be Gaussian around the corresponding value of the Composite LF parameters. A good description of the calculation of the composite LF can be found in Colless (1989). Following these prescriptions, the Composite LF is built by summing the cluster galaxies in absolute magnitude bins and scaling by the richness of their parent clusters:

$$N_{\mathrm{c}j} = \frac{N_{\mathrm{c}0}}{m_j} \sum_i \frac{N_{ij}}{N_{i0}} \quad (2)$$

where $N_{\mathrm{c}j}$ is the number of galaxies in the jth absolute magnitude bin of the composite LF, N_{ij} is the number in the jth bin of the ith cluster LF, N_{i0} is the normalization used for the ith cluster LF, m_j is the number of clusters contributing to the jth bin and $N_{\mathrm{c}0}$ is the sum of all the normalizations:

$$N_{\mathrm{c}0} = \sum_i N_{i0}. \quad (3)$$

Since all the systems in the cluster sample cover the magnitude region $M \leq -19$ in the five wavebands, we choose that region for the normalization according to the treatment in the literature.

The formal error in the $N_{\mathrm{c}j}$ is computed according to:

$$\delta N_{\mathrm{c}j} = \frac{N_{\mathrm{c}0}}{m_j} \left[\sum_i \left(\frac{\delta N_{ij}}{N_{i0}} \right)^2 \right]^{(1/2)} \quad (4)$$

where the $\delta N_{\mathrm{c}j}$ and δN_{ij} are the formal errors in the jth bin of the Composite LF and of the ith cluster LF. Since the ith cluster LF bin is given by the galaxy counts corrected by the field subtraction, the formal error δN_{ij} is calculated as the quadratic sum of the Poissonian error in the counts and the background error.

It is easy to note that in the Colless (1989) prescriptions the jth bin of the Composite LF represents just the mean fraction of galaxies, with respect to the normalization region, of all the clusters contributing to the jth bin.

There are three caveats in the use of the Colless method described above. Firstly, the magnitude limit of all the clusters has to be at least fainter than the limit of the region of normalization ($M < -19$ mag in our case). Secondly, the normalization region has to be large enough to be representative of the richness of the cluster and, thirdly, that the number of clusters contributing to each bin of magnitude has to be statistically significant. If these requirements are satisfied, the Colless (1989) prescriptions can be used to build a Composite LF which extends to the faintest magnitude limit of the cluster sample, with an efficient use of the available data. Therefore, we use the whole magnitude range available with our cluster sample and we include in the Composite LF all the bins with at least 10 contributing clusters.

An alternative method has been recently proposed by Garilli et al. (1999):

$$N_{\mathrm{c}j} = \frac{1}{m_j} \sum_i N_{ij} w_i^{-1} \quad (5)$$

where $N_{\mathrm{c}j}$ and N_{ij} have the same meaning as in the former case, while m_j is the number of clusters with the limiting magnitude deeper than the jth bin and w_i is the weight of each cluster, given by the ratio of the number of galaxies of the ith cluster to the number of galaxies brighter than its magnitude limit in all clusters with fainter magnitude limits (Andreon private communication). The formal error in the Composite LF is computed as:

$$\delta N_{\mathrm{c}j} = \frac{1}{m_j} \sqrt{\sum_i N_{ij} w_i^{-2}}. \quad (6)$$

The important difference of the latter method with regard to the Colless (1989) prescriptions is that the Composite LF is not a simple mean of the galaxy fraction in each bin (multiplied by a normalization constant), but a weighted mean of the cluster galaxy number in each bin of magnitude.

5. Results

Figure 3 shows the Composite LF obtained with the Colless (1989) prescription with a global and local background corrections. In both cases, the Composite LF shows a clear bimodal behavior, showing the upturn of the dwarf galaxies in the magnitude region $-18 \leq M \leq -16$, depending on the waveband. We apply two different approaches in fitting the Composite LF. We divide the Composite LF in two components, a "brigh-end" and a "faint-end" Composite LF, locating by eye the upturn of the dwarf galaxies. We, then, fit the two components separately

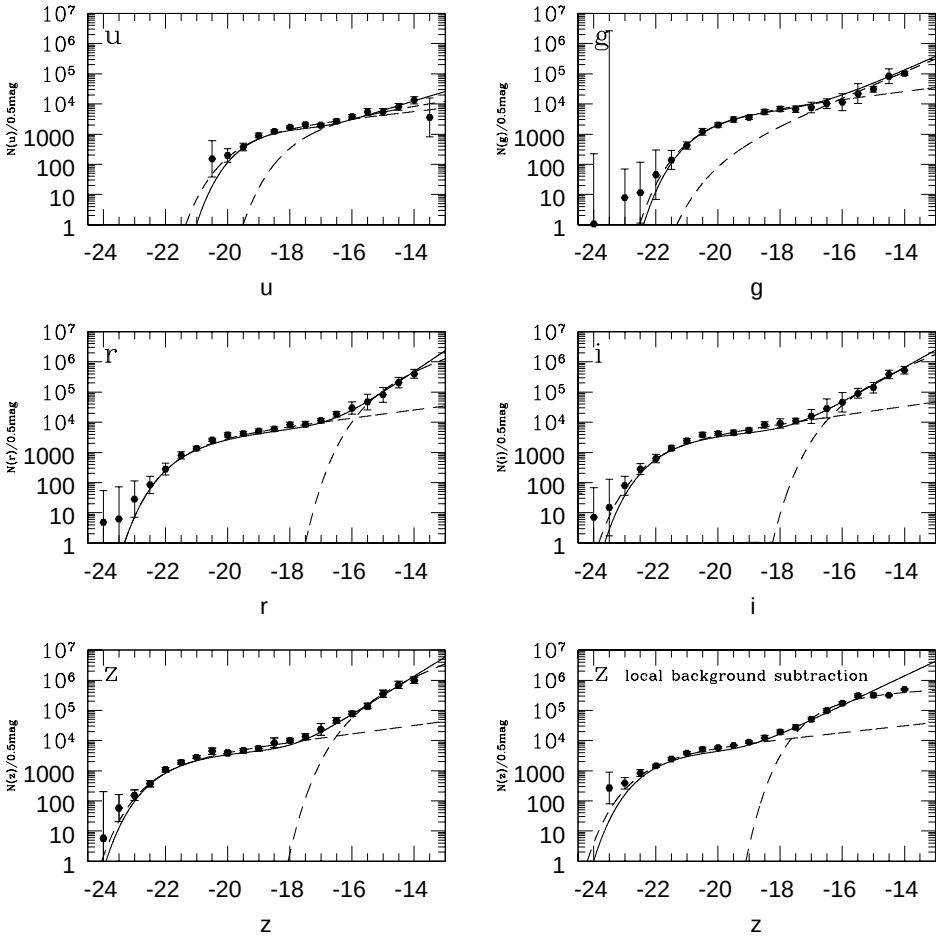

Fig. 3. The Composite LF in the five Sloan bands calculated within 1 Mpc h^{-1} aperture and with a global background correction. For comparison we show also the composite LF in the *z* band calculated with a local background subtraction. The solid line in each plot is the result of the two Schechter components fit (2Scf), while the dashed line are obtained with the single Schechter component fit (SScf) at the bright and at the faint end of the LF. The 2Scf fit perfectly reproduces the sum of the two single bright and faint components.

using a Single Schechter component fit (SScf). As a second approach, we fit the whole available range of magnitude of the Composite LF with the sum of the two Schechter components (2 Schechter components fit, 2Scf). The dashed lines in Fig. 3 are the results of the SScf method, while the solid line is the fit resulting from the 2Scf procedure. There is a very good agreement between the results of the methods applied. Table 2 lists the values of the Schechter parameters of the bright and the faint LF components obtained with different fitting procedures. The Composite LFs are calculated using different background subtractions and within different cluster radii (from 0.5 to 2.0 Mpc h^{-1}). Figure 4 shows the individual cluster LFs for a subsample of 25 systems of the RASS-SDSS galaxy cluster catalog. We overplotted the results of the SScf method applied to the corresponding Composite LF.

For comparison we also applied the method proposed by Garilli et al. (1999). The plot on the left side in Fig. 5 shows the results obtained applying that method. It is clear that the upturn in the faint magnitude region has disappeared completely and the composite LF is well fitted by a single Schechter function. The results obtained with the Garilli et al. (1999) prescription do not agree within the errors with the results obtained with the Colless method, and show a much flatter LF with a fainter M^* in all the wavebands. Instead, there is a very good agreement (1σ) with the Schechter parameters obtained by Garilli et al. (1999) and Paolillo et al. (2001), who applied the same method to derive the composite LF. The Composite LF obtained with this prescription is not a good representation of the mean cluster LF since it does not reproduce the features visible in the individual cluster LFs (see Fig. 4). The reason of the disagreement between the Composite LF obtained with the Garilli's method and the individual LFs is due to the different weighting method applied by Garilli et al. (1999). As shown in the plot on the right side of Fig. 5, the weight in the Garilli et al. (1999) method depends strongly on the cluster magnitude limits. The weight w_i^{-1} is a decreasing function of the cluster $M_{\rm lim}$, therefore, the clusters with fainter $M_{\rm lim}$, which contribute to the faint magnitude bins, are heavily down-weighted. This bias explains the lack of the dwarf upturn in the Composite LF.

In the following analysis we consider only the results obtained with the Colless (1989) prescription.

5.1. The bright end

The Schechter parameters α and M^* obtained for the Composite LF derived with the Colless (1989) prescriptions

Table 2. Schechter parameters of the Composite LF.

	u		g		r		i		z	
r	α_u	M^*_u	α_g	M^*_g	α_r	M^*_r	α_i	M^*_i	α_z	M^*_z
SScf – Bright component, global background subtraction										
0.5	-1.31 ± 0.16	-19.59 ± 0.85	-1.18 ± 0.05	-20.52 ± 0.26	-1.29 ± 0.09	-21.54 ± 0.39	-1.20 ± 0.06	-21.77 ± 0.30	-1.23 ± 0.07	-22.09 ± 0.30
1.0	-1.15 ± 0.15	-19.11 ± 0.48	-1.19 ± 0.04	-20.39 ± 0.15	-1.30 ± 0.06	-21.35 ± 0.19	-1.07 ± 0.08	-21.62 ± 0.15	-1.16 ± 0.06	-21.86 ± 0.18
1.5	-1.16 ± 0.14	-18.92 ± 0.39	-1.33 ± 0.04	-20.59 ± 0.20	-1.33 ± 0.06	-21.57 ± 0.21	-1.22 ± 0.06	-21.76 ± 0.17	-1.28 ± 0.06	-22.04 ± 0.25
2.0	-1.39 ± 0.13	-19.44 ± 0.61	-1.44 ± 0.04	-20.83 ± 0.22	-1.34 ± 0.07	-21.63 ± 0.22	-1.25 ± 0.06	-22.19 ± 0.25	-1.25 ± 0.07	-22.11 ± 0.22
SScf – Bright component, local background subtraction										
0.5	-1.28 ± 0.15	-19.38 ± 0.63	-1.25 ± 0.04	-20.64 ± 0.23	-1.41 ± 0.07	-21.81 ± 0.43	-1.33 ± 0.05	-22.13 ± 0.33	-1.33 ± 0.05	-22.44 ± 0.27
1.0	-1.34 ± 0.08	-18.93 ± 0.18	-1.44 ± 0.05	-20.76 ± 0.19	-1.33 ± 0.06	-21.40 ± 0.20	-1.25 ± 0.06	-21.63 ± 0.16	-1.28 ± 0.06	-21.99 ± 0.18
1.5	-1.37 ± 0.17	-19.30 ± 1.03	-1.24 ± 0.10	-20.49 ± 0.19	-1.40 ± 0.05	-21.71 ± 0.19	-1.47 ± 0.04	-22.14 ± 0.18	-1.35 ± 0.06	-22.07 ± 0.16
2.0	-1.38 ± 0.10	-19.40 ± 0.71	-1.02 ± 0.16	-20.35 ± 0.21	-1.51 ± 0.06	-21.93 ± 0.24	-1.54 ± 0.03	-22.31 ± 0.16	-1.51 ± 0.05	-22.46 ± 0.19
	SScf – Faint component, global background subtraction					SScf – Faint component, local background subtraction				
r	α_u	α_g	α_r	α_i	α_z	α_u	α_g	α_r	α_i	α_z
0.5	-1.50 ± 0.35	-1.98 ± 0.38	-1.96 ± 0.24	-1.81 ± 0.15	-1.80 ± 0.16	-1.60 ± 0.25	-2.16 ± 0.09	-2.18 ± 0.04	-1.98 ± 0.08	-2.18 ± 0.03
1.0	-1.40 ± 0.14	-1.88 ± 0.24	-1.54 ± 0.50	-1.61 ± 0.08	-2.24 ± 0.10	-1.50 ± 0.33	-2.45 ± 0.47	-1.83 ± 0.06	-2.27 ± 0.07	-1.72 ± 0.05
1.5	-1.69 ± 0.07	-1.73 ± 0.25	-2.11 ± 0.37	-1.74 ± 0.21	-2.27 ± 0.05	-1.73 ± 0.03	-1.73 ± 0.05	-1.53 ± 0.07	-1.90 ± 0.07	-1.78 ± 0.05
2.0	-1.53 ± 0.06	-2.05 ± 0.20	-1.74 ± 0.11	-2.09 ± 0.11	-2.44 ± 0.11	-1.66 ± 0.03	-1.64 ± 0.13	-2.08 ± 0.06	-1.91 ± 0.05	-2.35 ± 0.02
2Scf – Bright component, global background subtraction										
0.5	-0.92 ± 0.13	-18.00 ± 0.50	-1.30 ± 0.13	-20.75 ± 0.46	-1.30 ± 0.12	-21.50 ± 0.51	-1.09 ± 0.13	-21.54 ± 0.41	-1.23 ± 0.11	-22.19 ± 0.44
1.0	-1.59 ± 0.13	-19.24 ± 0.53	-0.55 ± 0.17	-19.67 ± 0.20	-1.03 ± 0.13	-20.90 ± 0.26	-1.14 ± 0.11	-21.56 ± 0.26	-1.07 ± 0.12	-21.73 ± 0.27
1.5	-1.27 ± 0.22	-19.40 ± 0.23	-1.41 ± 0.16	-20.80 ± 0.46	-1.39 ± 0.07	-21.50 ± 0.23	-1.20 ± 0.04	-21.98 ± 0.26	-1.06 ± 0.16	-21.69 ± 0.38
2.0	-1.50 ± 0.17	-20.59 ± 0.09	-1.58 ± 0.15	-21.53 ± 0.82	-1.06 ± 0.10	-21.24 ± 0.37	-0.94 ± 0.22	-21.61 ± 0.49	-1.29 ± 0.03	-22.17 ± 0.36
2Scf – Bright component, local background subtraction										
0.5	-0.68 ± 0.18	-18.32 ± 0.33	-1.24 ± 0.16	-20.62 ± 0.46	-1.23 ± 0.19	-21.36 ± 0.60	-1.16 ± 0.19	-21.79 ± 0.62	-1.22 ± 0.12	-22.14 ± 0.44
1.0	-0.95 ± 0.23	-19.53 ± 0.30	-1.23 ± 0.11	-20.39 ± 0.27	-1.05 ± 0.13	-20.95 ± 0.27	-1.17 ± 0.13	-21.64 ± 0.29	-1.06 ± 0.12	-21.70 ± 0.26
1.5	-1.71 ± 0.13	-20.36 ± 0.26	-0.91 ± 0.28	-20.23 ± 0.34	-0.76 ± 0.13	-20.86 ± 0.20	-1.11 ± 0.09	-21.51 ± 0.21	-1.02 ± 0.12	-21.71 ± 0.21
2.0	-0.96 ± 0.49	-18.75 ± 0.76	-0.99 ± 0.23	-20.15 ± 0.35	-1.03 ± 0.14	-21.19 ± 0.23	-1.27 ± 0.11	-21.82 ± 0.26	-1.46 ± 0.06	-22.41 ± 0.26
2Scf – Faint component, global background subtraction										
0.5	-0.88 ± 0.18	-18.92 ± 0.45	-2.44 ± 0.25	-16.99 ± 0.31	-2.38 ± 0.15	-17.76 ± 0.23	-2.09 ± 0.07	-18.34 ± 0.19	-2.28 ± 0.08	-18.59 ± 0.21
1.0	0.00 ± 0.00	-18.09 ± 0.37	-2.04 ± 0.03	-17.89 ± 0.11	-2.01 ± 0.05	-18.40 ± 0.15	-2.36 ± 0.05	-18.86 ± 0.16	-2.22 ± 0.06	-19.09 ± 0.17
1.5	-2.65 ± 0.90	-15.43 ± 0.44	-2.54 ± 0.18	-17.18 ± 0.25	-2.79 ± 0.14	-17.40 ± 0.18	-2.83 ± 0.07	-18.00 ± 0.14	-2.70 ± 0.07	-18.71 ± 0.12
2.0	0.00 ± 0.05	-17.31 ± 0.01	-2.52 ± 0.30	-17.52 ± 0.57	-2.03 ± 0.08	-18.63 ± 0.21	-2.21 ± 0.08	-18.91 ± 0.23	-2.76 ± 0.05	-18.64 ± 0.14
2Scf – Faint component,local background subtraction										
0.5	0.00 ± 0.00	-15.63 ± 0.26	-2.23 ± 0.25	-17.26 ± 0.32	-2.18 ± 0.18	-18.12 ± 0.26	-2.17 ± 0.19	-18.51 ± 0.22	-2.34 ± 0.12	-18.57 ± 0.20
1.0	-1.64 ± 0.25	-19.79 ± 4.04	-2.84 ± 0.13	-17.27 ± 0.13	-2.02 ± 0.05	-18.42 ± 0.15	-2.45 ± 0.13	-18.96 ± 0.17	-2.21 ± 0.06	-19.08 ± 0.16
1.5	-0.76 ± 5.46	-18.71 ± 0.87	-1.86 ± 0.07	-18.49 ± 0.26	-1.92 ± 0.03	-18.94 ± 0.13	-2.13 ± 0.03	-19.07 ± 0.13	-2.25 ± 0.05	-19.45 ± 0.13
2.0	-1.62 ± 0.04	-18.71 ± 2.17	-2.26 ± 0.07	-18.26 ± 0.18	-2.22 ± 0.04	-19.06 ± 0.15	-2.54 ± 0.10	-19.21 ± 0.14	-2.61 ± 0.06	-19.16 ± 0.12

The Schechter parameters of the bright and the faint end of the composite LF. The results are obtained with a single Schechter component fit (SScf) and with a two Schechter components fit (2Scf). For each case the fit procedure was applied to the composite LF calculated within 4 different clustercentric distances, 0.5, 1.0, 1.5 and 2.0 Mpc h^{-1} and with different background corrections.

with the local and global background corrections agree very well at any radius (in the worse cases within 1.5σ). There is also a very good agreement within the errors for M^* obtained with different fitting procedures. The slope of the bright component calculated with the SScf method is systematically steeper than the slope obtained with the 2Scf procedure. This is due to the fact that in the 2Scf method the fitting function is the sum of two components. Consequently, the slope of the bright component does not represent only the bright galaxies population but depends also on the slope and M^* of the second (faint) component. Therefore, in the following analysis we consider the parameters of the bright component obtained with the SScf method as representative of the bright galaxies population in clusters.

Figure 6 shows the error contours of these Schechter parameters calculated for the Composite LFs measured within 3 different cluster radii, 1.0, 1.5 and 2.0 Mpc h^{-1} in the case of a global background correction. α and M^* do not seem to depend on the clustercentric distance since the error contours overlap in all wavebands, except for the g band. However, the behavior of the Schechter parameters in this band is not confirmed by the same Composite LF calculated with the local background subtraction. Therefore, we can conclude that there is no significant difference in the bright end LF measured in different aperture radii.

To check the universality of the cluster LF, we compare the Schechter parameters of the bright component of Composite LF with the Schechter parameters derived by fitting the individual cluster LFs. Figure 7 shows the distributions of M^* and α of the individual cluster LFs derived in the z band within 1 Mpc h^{-1} from the cluster center and with a global background correction. The vertical dashed lines in the plots show the value of the corresponding Composite LF parameter and the 3σ error interval. The plots a and b in the Fig. 7 show the distributions of M^* and α when a single Schechter luminosity function is fitted to the galaxies in the whole available magnitude range of each cluster (including the dwarf region). It is clear from those distributions that the "bright end" Composite LF is not a good representation of the mean behavior of the individual LFs: the individual LFs seems to be systematically steeper and the dispersion of M^* is larger than 2 mag. The distributions of both parameters change drastically if the galaxies in the dwarfs region are excluded from the fits. Plots c and d of the Fig. 7 clearly show that the distributions become in both cases close to

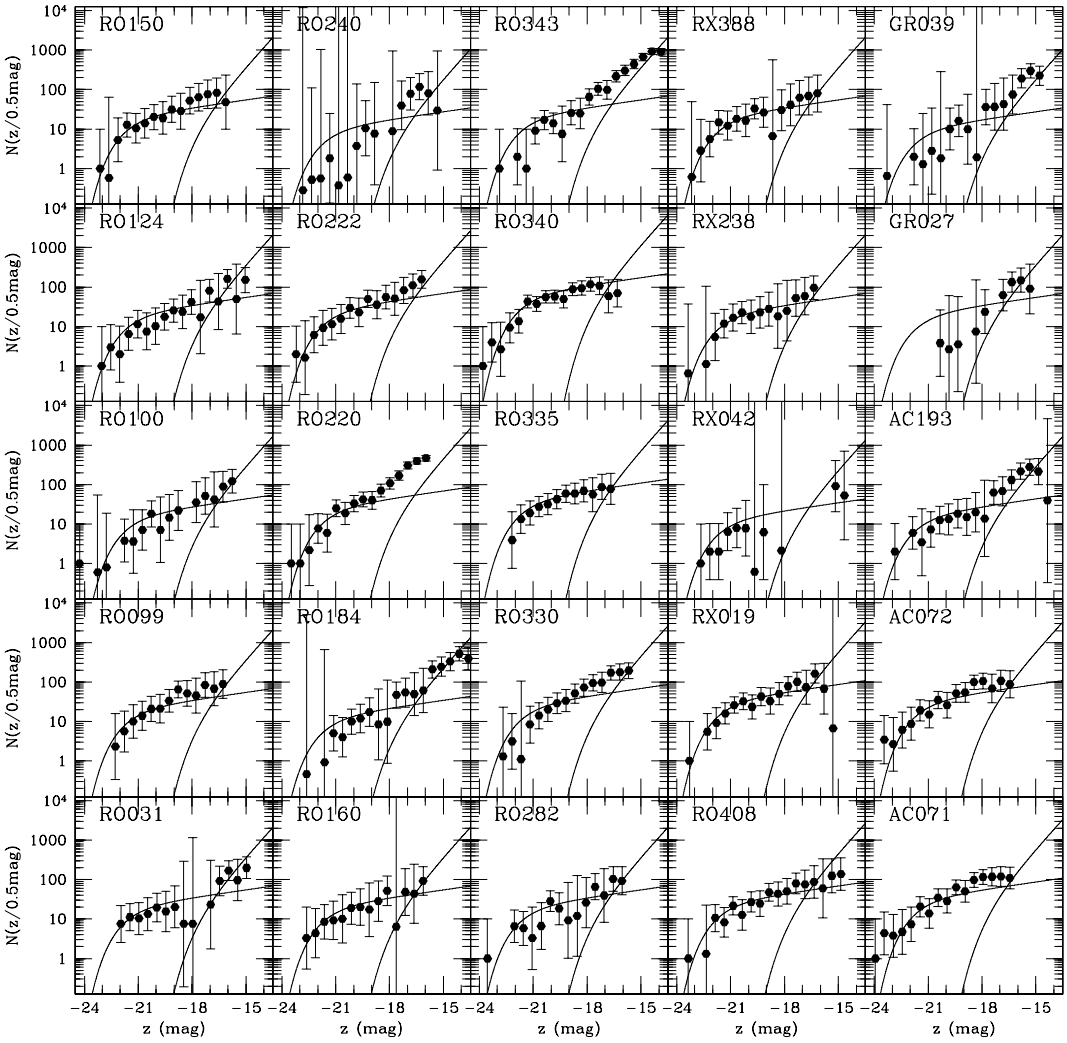

Fig. 4. The individual cluster luminosity functions for 25 clusters of the RASS-SDSS galaxy cluster catalog, calculated within 1 Mpc h^{-1} aperture and with a global background subtraction. The solid line in the plots are the results of the SSfc method applied to the corresponding Composite LF. The upturn of the dwarf and the steepening of the LFs at the faint end is evident in several clusters.

a Gaussian with the maximum coincident with the value of the corresponding Composite LF parameter. The dispersion of the distribution of α seems to be larger than the 3σ error interval of the Composite LF parameter. Therefore, we conclude that the Composite LF is a very good representation of the mean behavior of the individual cluster "bright end" LFs, but it is not universal. Nevertheless, we assume that the dwarf upturn of all the clusters in the sample has the same location observed in the Composite LF ($M_z \sim -18$). A brighter upturn could give a steeper individual LF and, therefore, it could explain the excess of clusters in the region $\alpha \leq -1.3$ in the plot *d* of Fig. 7.

5.2. The faint end

The results obtained for the fits of the faint LF components with different fitting procedures, background corrections and cluster apertures are listed in Table 2. For the SScf method we report only the slope of the faint-end component in each band and not the values of M^*. In fact, the faint end of the composite LF does not contain a sufficient number of points to constrain in a meaningful way the characteristic magnitude, and the statistical errors of M^* are larger than 1 mag. We listed in the same table α and M^* measured with the 2Scf method. In this case the characteristic magnitude of the faint end is constrained by the slope of the bright component.

As Table 3 shows, the "faint end" Composite LF is much steeper than the "bright end" LF at any radius and in any passband with both fitting procedures. There is a discrepancy between the values of the slope of the SScf and the 2Scf methods in all the analysed cases. The reason of the disagreement is the same observed for the slopes of the bright component. The mean value of α derived with the SScf method in the case of a global background correction is 1.60 in *u*, 1.84 in *g*, 1.81 in *r*, 1.76 in *i* and 2.07 in *z*. The slope do not show a dependence on the waveband and on the distance from the cluster center. The result is confirmed also by the values given by the 2Scf procedure.

Valotto et al. (2001) use a numerical simulation of a hierarchical universe to show that many "clusters" identified from two dimensional galaxy distributions might result principally

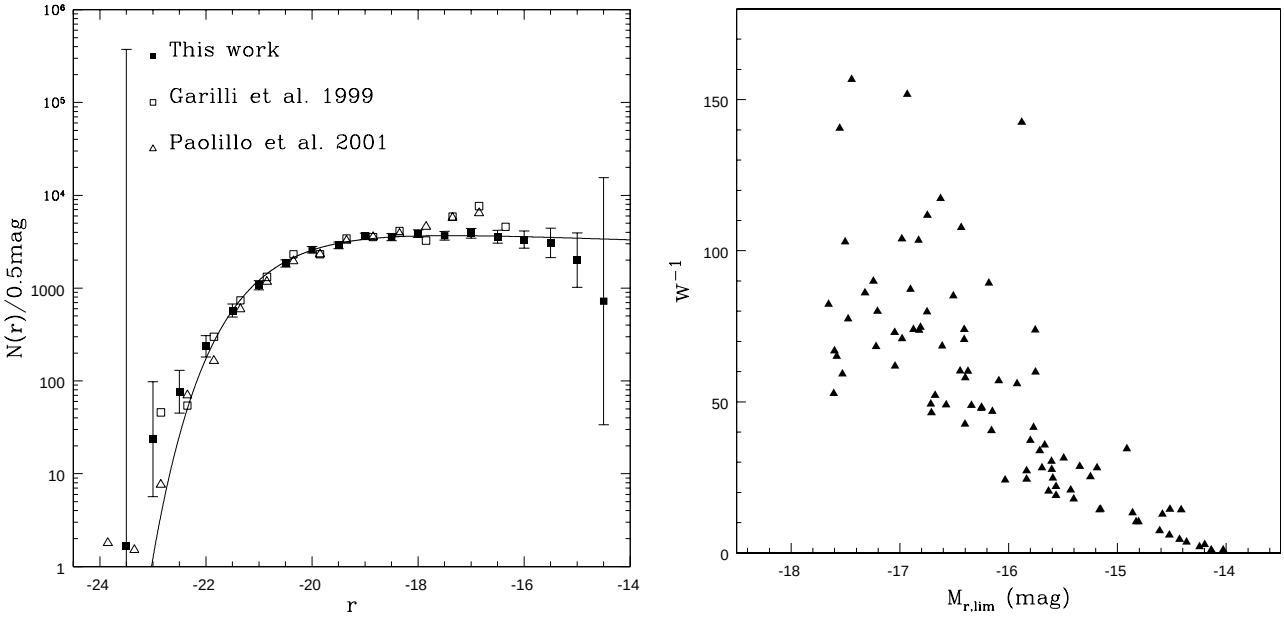

Fig. 5. The results obtained applying the Garilli et al. (1999) method. The plot on the left side shows the Composite LF in the *r* Sloan band (filled squares). For comparison we plot also the Composite LF obtained by Garilli et al. (1999) (empty squares) and by Paolillo et al. (2001) (empty triangles). The three LFs agree very well (within 1σ) in the characteristic magnitude and in the faint end slope. However the Composite cluster LFs obtained with this prescription do not reproduce the main features observed in the individual cluster LFs (see Fig. 4). The reason for the disagreement is the weighing method in the Garilli's prescription. The plot on the right side shows the dependence of the weight w_i on the magnitude limit of the single cluster. The systems with very faint $M_{\rm lim}$, which contribute to the faint magnitude bins in the composite LF, are heavily down-weighted. The bias explains the lack of the upturn in the dwarf magnitude range observed in the individual cluster LFs.

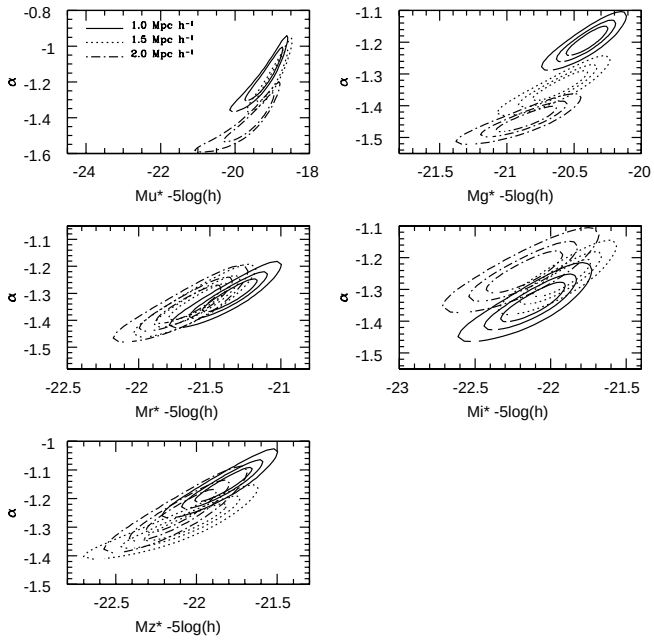

Fig. 6. 1, 2 and 3σ contours of the best fit Schechter parameters for the bright component of the Composite LF. The contours are derived with the SScf method applied to the bright end of the Composite LF. The LF is calculated with a global background subtraction within 1, 1.5 and 2 Mpc h^{-1} apertures.

from the projection of a large-scale structure alone the line of sight. They suggest that attempts to derive the LF for these "clusters" using the standard background subtraction procedure lead to deriving an LF with a steep faint-end slope, despite the fact that the actual input LF had a flat faint-end. Since the RASS-SDSS galaxy cluster sample comprises only clusters detected in X-rays, all the systems contributing to the "faint-end" Composite LF (26 clusters with $M_{z\rm lim} \geq -16$) are not a projection effect but are real clusters. Moreover, the use of a local background subtraction, which takes into account the presence of large-scale structure, confirms the steepening of the Composite LF observed with the global background subtraction. Valotto et al. (2004) compare the composite luminosity function of a optically selected sample of clusters with an X-ray selected sample of systems from the RASS1 bright clusters catalog of De Grandi et al. (1999). They show that the composite LF of the former sample presents a steep faint end due to projection effects, while the composite LF of the X-ray selected sample is flat with a slope of -1.1 in the magnitude range $M_{\rm b_J} \leq -16.5$. Our results are still in agreement with Valotto et al. (2004), since we are observing a much fainter population with $-16 \leq M_{\rm g} - 5\log(h) \leq -14$. Nevertheless, one could still suspect that the observed steepening of the faint end in the individual clusters is due to a baclground object at higher redshift and the same line of sight. In fact, in this case, both the global and local background corrections would fail to subtract this contribution. To test this possibility, we use the SDSS spectroscopic redshifts to check the presence of galaxy overdensities at higher redshift and in the same line of sight of the systems of interest. Only RO184 shows a second object in background while all the others clusters with and without

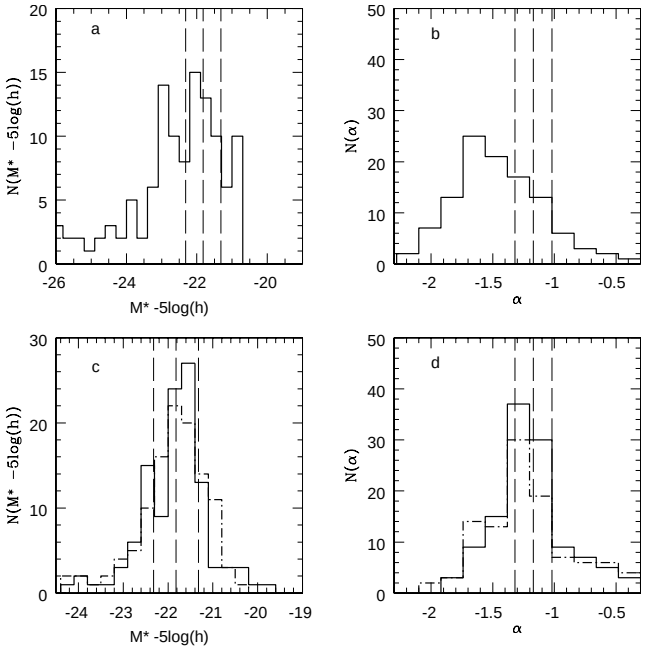

Fig. 7. Distribution of the Schechter parameters α and M^* of the individual cluster LFs in the sample, calculated in the z band within 1 Mpc h^{-1} and with a global background correction. Plots *a* and *b* show the distribution of M^* α, respectively, obtained by fitting a single Schechter luminosity function to the galaxies in the whole available magnitude range of each cluster. Plots *c* and *d* show the distribution of M^* and α , respectively, obtained by fitting a single Schechter luminosity function to the galaxies brighter than the magnitude of the dwarf upturn $M_Z \leq -18$. The dashed lines in plots *c* and *d* are the distributions obtained from the fits with α and M^* being free parameters. The solid line in plots *c* is the distribution of M^* when α is fixed to the value of the corresponding bright component of the Composite LF calculated with the SScf method. The solid line in plot *d* is the distribution of α when M^* is fixed to the value of the Composite LF. The vertical dashed lines in each plots indicate the value of the corresponding parameters of the bright component in the Composite LF and its 3σ error interval.

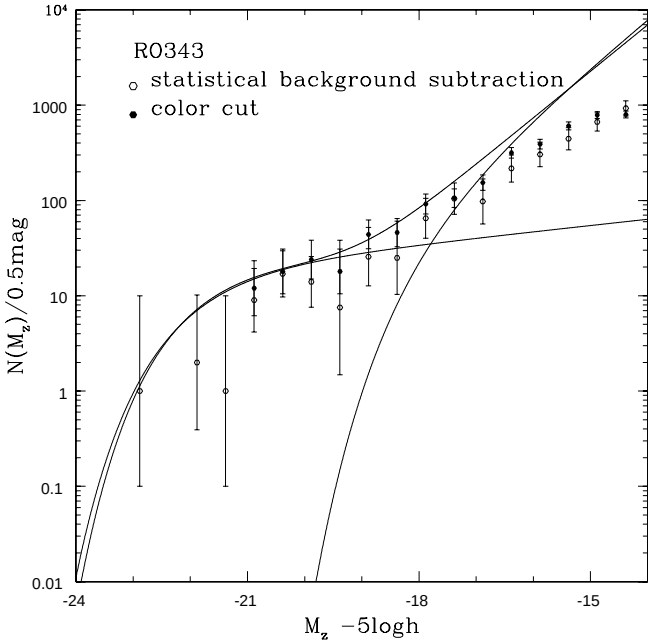

Fig. 8. The two different methods of background subtraction. The cluster RO343 is one of the clusters showing a significant steepening of the LF in the faint magnitude range. The filled points indicate the cluster LF obtained with a cut in the $g - r - r - i$ plane (Garilli et al. 1999). The empty points are the LF obtained with the statistical local background correction applied to obtain the composite LF analysed in the paper. The methods of background subtraction agree perfectly within the errors. The error bars in the color-cut method are the Poissonian error in the galaxy counts. The color cut method excludes all the galaxies redder than the color of an elliptical galaxy at the cluster redshift. Therefore, the steepening in the faint end can not be due to galaxies at higher redshift in a second cluster or in the large scale structure behind the cluster, but should be due to the presence of a real cluster population. A bluer color cut deletes the contribution of the bright elliptical cluster galaxies leaving the faint end LF. This implies that the faint end LF is dominated by late-type galaxies.

steepening in the individual LF present the same single peak redshift distribution.

As an additional test we have measured the individual cluster LF with a color cut method in the same way as Garilli et al. (1999). We use the $g - r$ and $r - i$ galaxy colors defined in Fukugita et al. (1995). We define our color cut in order to exclude all the galaxies redder than the expected color of the ellipticals at the cluster redshift, and the late type galaxies in foreground. We observe that the systems with a significant steepening in the individual LF obtained with a statistical background subtraction show the same feature also with the color cut method (Fig. 8). This implies that we are not observing the contribution of large scale structures but a real cluster faint population. Moreover, we observe that the faint-end of those clusters is due to galaxies with colors compatible with spiral galaxies at the redshift of the cluster. In conclusion, then, the observed steepening of the Composite LF in the considered magnitude range is real.

Even if the Schechter function with the values reported in Table 2 offers a very good fit to the data (reduced $\chi^2 \leq 1.5$ in the worst case), the "faint end" Composite LF contains only few points. Therefore, the slope α has to be considered as a good indicator of the steepening of the LF in this magnitude region, but does not allow a detailed analysis of the behavior of the Composite LF. To study in more detail the behavior of the "fain-end" Composite LF as a function of the waveband and of the distance from the center, we define the Dwarf to Giant Ratio (DGR) in each band as the ratio between the number of galaxies of the "faint end" Composite LF to the number of galaxies of the "bright end" Composite LF. We define DGR as the ratio between the number of galaxies in the magnitude range $-18 \leq M \leq -16.5$ and the number of galaxies brither than -20 mag (except in the u band where we count the galaxies brighter than -19 mag). Figure 9 shows the behavior of DGR in each band as a function of the clustercentric distance. The filled points are derived in the case of a global background subtraction, while the empty points in the case of a local background subtraction. The two results do not agree perfectly on the DGR value, but they reproduce the same dependence on the clustercentric distance. In each waveband the DGR seems to slightly increase from the very center,

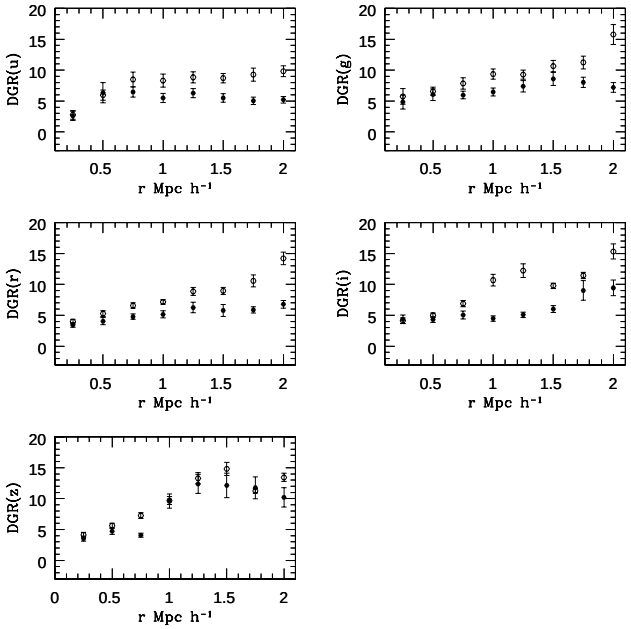

Fig. 9. Dwarf to Giant Ratio (DGR) as a function of the cluster radii in the 5 wavebands. DGR is derived from the Composite LF calculated with a global background correction (filled points) and a local background correction (empty points).

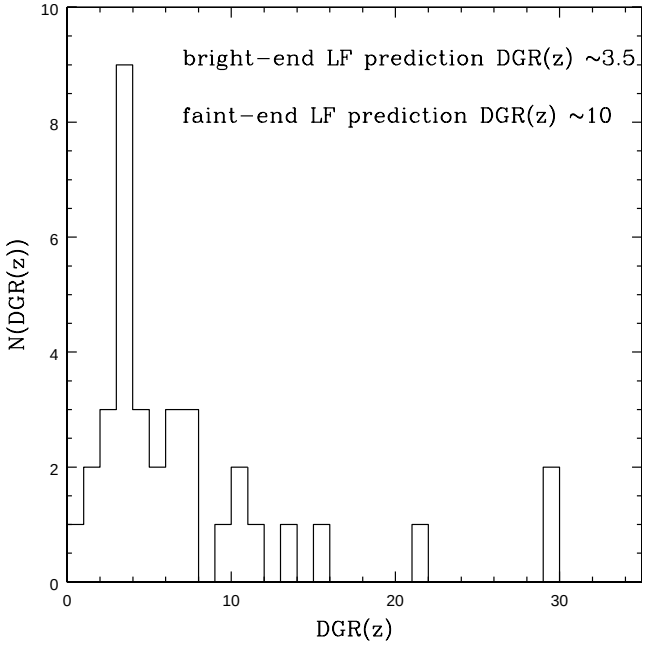

Fig. 10. Distribution of the DGR(z). DGR(z) defined as as the ratio between the number of galaxies brighter than −20 mag and the number of galaxies in the magnitude range $-18. \leq M_z \leq -16.5$. The faint magnitude range in the definition of DGR(z) is large enough to be representative of the dwarf population while the number of clusters with magnitude limits fainter than −16.5 mag is still large (35 systems) to be statistically significant. The value of DGR(z) predicted by the "bright end" Composite LF (without the dwarf population) is 3.5, while the value predicted with the presence of the "faint-end" Composite LF if around 10.

0.3 Mpc h^{-1}, to 1.0 Mpc h^{-1}. The mean value of DGR increases from the u band (5) to the z band (10).

To test whether the "faint-end" Composite LF is a standard representation of the dwarf population of galaxy clusters or if it is due to the contribution of few particular clusters, we define a DGR for the individual objects and compare it to the DGR of the Composite LF. Figure 10 shows the distribution of the DGR calculated for the single clusters in the z band. The faint magnitude range in the definition of DGR(z) is large enough to be representative of the dwarf population while the number of clusters with magnitude limits fainter than −16.5 mag is still large (35 systems) to be statistically significant. It is important to stress that the value of DGR(z) predicted by the "bright end" Composite LF (without the dwarf population) is 3.5, while the value predicted with the presence of the "faint-end" Composite LF is around 10. As shown in Fig. 10, there is a large spread in the distribution of DGR(z). The histogram in the figure shows a clear peak around the value predicted by the "bright end" LF (3.5), and a large number of objects (1/2) at values larger than this. This result indicates that the behavior of the faint end LF in not universal. We conclude that there seem to exist two different kinds of cluster populations depending on the excess of the dwarf galaxies.

To study the spread of the distribution in DGR(z), we plot DGR(z) versus the cluster richness and versus the M^* of the individual cluster bright-end LF, as shown in Figs. 11 and 12, respectively. We do not find any correlation between the parameters. The Spearman's rank coefficient is very low in both cases and with a probability of non correlation close to 1. However Fig. 13 shows that DGR(z) is significantly anti-correlated with several cluster global properties, i.e. the X-ray and optical luminosities (all the correlations are very significant, 1×10^{-4}–1×10^{-5}, according to a Spearman correlation test). Since L_X correlates with the cluster mass (Reiprich & Böhringer 2001), we conclude that the more massive a cluster, the lower its fraction of dwarf galaxies. The anti-correlation between cluster DGRs and cluster luminosities is most likely due to the choice of a fixed metric aperture for all the clusters. In fact, a fixed metric aperture samples larger (smaller) fractions of the virialized regions of clusters of smaller (respectively, larger) masses, and DGR is known to decrease with cluster-centric distance as showed in Fig. 9 of this section. Therefore, because of this effect, the different cluster physical sizes must be taken into account before comparing different cluster LFs.

In our analysis we do not take into account possible low surface brightness selection effects. Unfortunately, the analysis of the completness limits in surface brightness of the SDSS galaxy photometric sample is not yet completed. Therefore, the luminosity function analysed in this paper should be considered as a lower limit of the true cluster LF, since we could miss low surface brightness galaxies especially at the faint end. Bernstein et al. (1995), Ulmer et al. (1996) and Adami et al. (2000) explore these issues in a series of papers on the faint LF of the Coma cluster and conclude that LSB galaxies in Coma were inconsequential. Moreover, Cross et al. (2004) compare the completeness limits in magnitude and surface brightness of SDSS-EDR and SDSS-DR1 with the Millennium Galaxy Catalogue (MCG). MCG is a deep survey with a limit

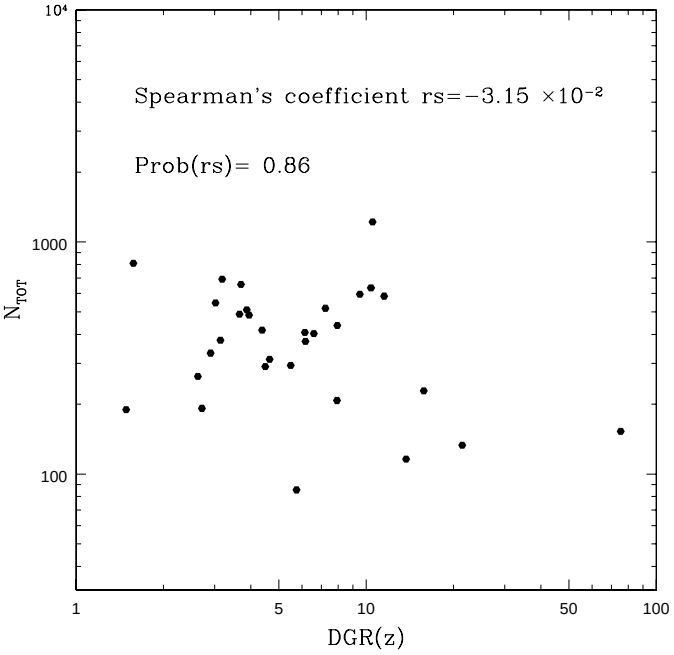

Fig. 11. DGR versus the cluster richness in the z band within 1 Mpc h^{-1} in the case of global background subtraction.

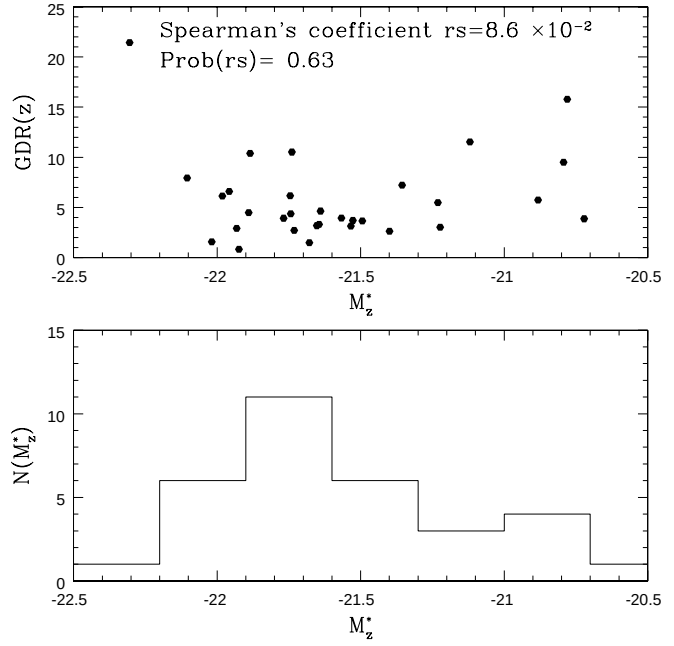

Fig. 12. The upper panel shows DGR versus the characteristic magnitude of the individual bright component LF derived within 1 Mpc h^{-1} in the case of global background subtraction. The bottom panel shows the histogram of M^* for the subsample of clusters. The histogram mimics the behavior of the whole sample showed in the panel c) of Fig. 7.

in surface brightness of 26 mag arcsec^{-2}. They use the MCG bright galaxy catalogue with galaxies in the magnitude range $16 \leq B \leq 20$ (where $B = g + 0.39(g - r) + 0.21$ for DR1 magnitudes) for the comparison with the SDSS-EDR-DR1 catalog. They show that in the range $21 \leq \mu_e \leq 25$ mag arcsec^{-2} the incompleteness of SDSS-EDR is less than 5% and is around 10% in the range $25 \leq \mu_e \leq 26$ mag arcsec^{-2}. In the present work, for most of the clusters the galaxies contributing to the DGR are faint galaxies in the magnitude range $19 \leq r \leq 21$ mag. In this region of magnitudes 65% of the objects lie at $\mu_e \leq 23$ mag arcsec^{-2}, 30% in the range $23 < \mu_e \leq 24$ mag arcsec^{-2}, and 5% at $\mu_e \geq 25$ mag arcsec^{-2}. If we can apply also in this range of magnitude the results of Cross et al. (2004), the incompleteness correction for low surface brightness selection effects should be around 5%. Therefore we expect that the LSB galaxies do not contribute in a egregious way to our luminosity function and cannot change signifi cantly the DGR calculated in the paper.

5.3. Comparison with previous work

The results obtained by previous works are listed in Table 1. All the works in the literature analyse only the relatively bright end of the cluster LF. In Fig. 14 is shown the very good agreement between our results in the g band and the Composite LF of De Propris et al. (2003), who use the 2df spectroscopic data to defi ne the cluster membership. It is clear in the fi gure that even the 2df composite LF is not enough deep to cover the dwarf galaxy region analysed in this work. Therefore, we can compare only our bright end composite LF with the results found in the literature.

We consider mainly the luminosity function in the g band since there is a large number of b and g band cluster composite LFs in the literature to compare with. After correcting the absolute magnitudes for the different cosmology and for colors, our M^*_g perfectly agrees with almost all the the previous results except for Goto et al. (2002b). The disagreement with this work is larger than 3σ. The reason for the discrepancy with previous work based on SDSS data is ascribable to the different quality of the photometry between the last data release (DR2), used in this work, and the Early Data Release (EDR) used in Goto et al. (2002a).

The slopes of the Composite LF in the g band retrieved from the literature lie in a very large range of values from –1.50 to –0.94. Therefore, there is not an overall agreement in the literature about the slope of the cluster composite LF. Nevertheless, several of the works retrieved in the literature should not be taken into account in this comparison. In fact, the results of Garilli et al. (1999) and Paolillo et al. (2001) should be excluded from our analysis , since we discussed in a previous paragraph that their results depend on the method applied to derive the composite LF. Moreover, we would exclude from our analysis also the results of Goto et al. (2002b) for two different reasons. First, Goto et al. (2002a) use a different SDSS dataset (EDR) with lower quality in the photometry. Secondly, in that work the background is calculated locally in an annulus around the cluster center with outer radius of 1.3 Mpc h^{-1} and inner radius of 1.0 Mpc h^{-1}. Since the background is calculated within the cluster region (within an Abell radius of 1.5 Mpc), where the fraction of cluster galaxies could be very high, such background correction would subtract to a substantial degree the contribution of that cluster galaxy population from the individual and the Composite LF. This suspicious background subtraction could explain the very fl at LF obtained by

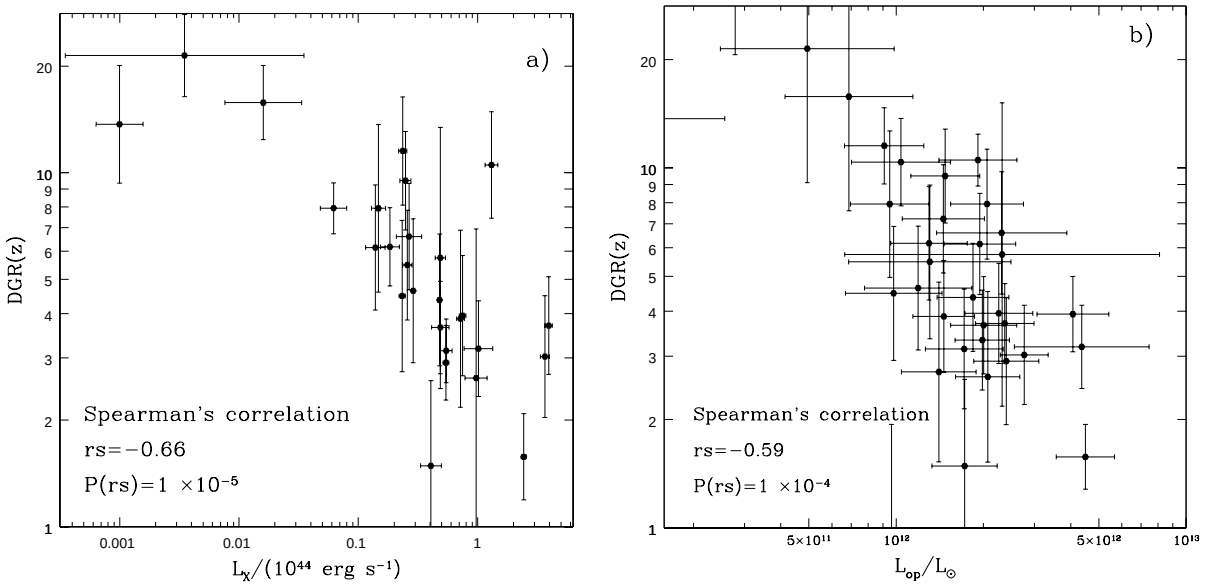

Fig. 13. The correlation between DGR(z) and the X-ray (panel **a)** and optical (panel **b)**) luminosities. DGR(z) clearly anticorrelates with the cluster luminosities as confirmed by a Spearman's test. Since DGR(z) increases with the clustercentric distance as confirmed in the previous sections, the anti-correlation between cluster DGRs and cluster luminosities is most likely due to the choice of a fixed metric aperture for all the clusters.

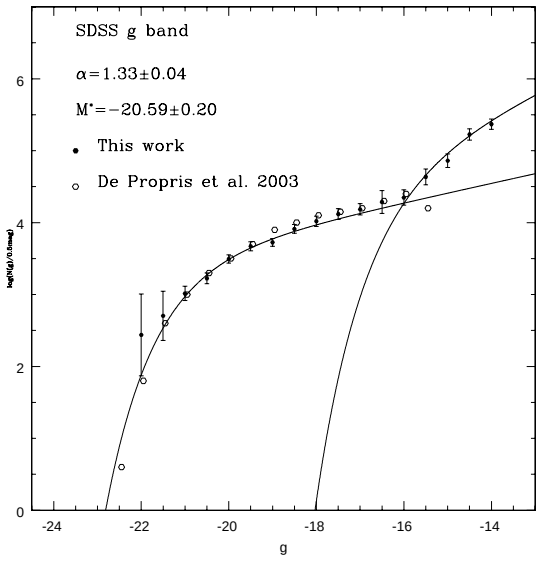

Fig. 14. The Composite LF calculated with the prescription of Colless (1989) with a global background correction and within 1.5 Mpc h^{-1} in the g band (filled points) and the De Propris et al. (2003) Composite LF in the b band derived from the 2df spectroscopic data (empty points).

Goto et al. (2002b) in all the Sloan wavebands. In conclusion, if we exclude the works of Garilli et al. (1999), Paolillo et al. (2001) and Goto et al. (2002b) from our analysis, the range of α is reduced significantly to the values between –1.50 and –1.22. All the values of the slope of our g band composite LF perfectly fit in this range of results.

5.4. Comparison with the field

One of the most important and interesting aspects of the luminosity function is the comparison of the LFs derived in different environments. The SDSS field luminosity function is given by Blanton et al. (2003). In this work the absolute magnitude limit is around $-16+5\log(h)$ in the g and r bands and $-17+5\log(h)$ in the i and z bands. Therefore, the field LF is not studied in the magnitude range of the dwarf galaxies. We compare, then, only the bright end of the cluster luminosity function with the SDSS field LF. The result of the comparison with the field LF of Blanton et al. (2003) is that the field LF is systematically flatter than the cluster LF in any band, while the cluster M^* is brighter than the field M^* of about 0.5 mag. However, there is not an overall agreement in the literature about the values of slope and M^* in the field luminosity function. As Table 3 shows, most of the results reveal a very poor agreement only within 3σ, while several values (see, e.g., the CfA2 LF of Marzke et al. 1994) do not agree at all with the results of the other surveys. For example, if we compare our cluster lf with the 2df field lf, we should conclude, in agreement with De Propris et al. (2002), that the slope of the cluster lf is consistent with the field lf, while the characteristic magnitute is about 0.5 mag brighter than the field M^*. In conclusion, the rather large scatter of the results in the literature does not allow us to a conclusive comparison between the luminosity function of different environments.

Since the magnitude range of our faint end cluster LF is not covered by the SDSS field LF, we have to compare our results with other surveys. Loveday (1997) in the Stromlo-APM survey finds that the number of faint galaxies seen in projection on the sky is much larger than expected for a flat faint-end Schechter function. Moreover, they show that the best fit function for the field luminosity function is a "double

Table 3. Schechter parameters fitted to the Composite LF retrieved from the literature.

Survey		band	$m_{\rm lim}$	M^*	α	ϕ^* ($\times 10^{-2}\,h^3$ Mpc^{-1})	evolution correction	Reference
AUTOFI		b_j	−14	-19.30 ± 0.13	-1.16 ± 0.05	2.45 ± 0.35	no	(1)
Stromlo-APM		b_j	−15	-19.50 ± 0.13	-0.97 ± 0.15	1.40 ± 0.17	no	(2)
SSRS2		$m_{B(0)}$	−14	-19.45 ± 0.08	-1.16 ± 0.07	1.09 ± 0.30	no	(3)
CfA2		m_Z	−16.5	-18.8 ± 0.3	-1.0 ± 0.2	$4. \pm 1$	no	(4)
EPS	all	b_j	−12.4	-19.61 ± 0.06	-1.22 ± 0.06	2.0 ± 0.4	no	(5)
	early type	b_j	−12.4	-19.62 ± 0.09	-0.98 ± 0.09	1.1 ± 0.2	no	
	late type	b_j	−12.4	-19.47 ± 0.10	-1.40 ± 0.09	1.0 ± 0.2	no	
2dF	all	b_j	−13	-19.79 ± 0.04	-1.19 ± 0.01	1.59 ± 0.14	no	(6)
	early type	b_j	−17	-19.58 ± 0.05	-0.54 ± 0.02	0.99 ± 0.05	no	
	late type	b_j	−13	-19.15 ± 0.05	-1.50 ± 0.03	0.24 ± 0.02	no	
2dF		b_j	−16.5	-19.66 ± 0.07	-1.21 ± 0.03	1.61 ± 0.08	yes	(7)
LCRS		r	−17.5	-20.29 ± 0.02	-0.70 ± 0.05	1.9 ± 0.1	no	(8)
CNOC2	early type	$R_{\rm C}$	−17	-20.50 ± 0.12	-0.07 ± 0.14	1.85 ± 0.37	yes	(9)
	late type	$R_{\rm C}$	−16	-20.11 ± 0.18	-1.34 ± 0.12	0.56 ± 0.30	yes	
SDSS		$u^{0.1}$	−15.54	-17.93 ± 0.03	-0.92 ± 0.07	3.05 ± 0.33	yes	(10)
DR1		$g^{0.1}$	−16.10	-19.39 ± 0.02	-0.89 ± 0.03	2.18 ± 0.08	yes	
		$r^{0.1}$	−16.11	-20.44 ± 0.01	-1.05 ± 0.01	1.49 ± 0.04	yes	
		r	−16.11	−20.54	−1.15	1.77	no	
		$i^{0.1}$	−17.07	-20.82 ± 0.02	-1.00 ± 0.02	1.47 ± 0.04	yes	
		$z^{0.1}$	−17.34	-21.18 ± 0.02	-1.08 ± 0.02	1.35 ± 0.04	yes	

References: (1) Loveday et al. (1992); (2) Ellis et al. (1996); (3) Marzke & Da Costa (1997); (4) Marzke et al. (1994); (5) Zucca et al. (1997); (6) Madgwick et al. (2002); (7) Norberg et al. (2002); (8) Lin et al. (1996); (9) Lin et al. (1999); (10) Blanton et al. (2003).

power-law" Schechter function. Lin et al. (1996) finds in the Las Campana Redshift Survey (LCRS) that the Schechter function is a good approximation of the magnitude range $-23 \leq M_r - 5\log(h) \leq -15.5$ for the field LF, but there is a significant excess relative to the Schechter fit at the faint end $M_r \geq -17.5$. Zucca et al. (1997) finds a steepening of the field LF at $M_{\rm b_J} \leq -17.5 + 5\log(h)$ from the ESO Slice Project (ESP) galaxy redshift survey. A Schechter function is an excellent representation of their data points at $M_{\rm b_J} \leq -16 + 5\log(h)$, but at fainter magnitude it lies below all the points down to $M_{\rm b_j} = -12.4 + 5\log(h)$. They find that the best fit to the data is a two-law fit given by a Schechter function plus a power law with slope −1.5. They conclude that the faint end steepening is almost completely due to galaxies with emission lines. In fact, dividing the galaxies in two samples (i.e. galaxies with and without emission lines) they find very significant differences in their luminosity functions. Galaxies with emission lines show a significantly steeper faint end slope and a slightly fainter M^*. However, it is noteworthy that in their results the Schechter function is a inadequate fit especially for the galaxies without emission lines, which show a significant evidence of an upturn in the dwarf region, while the LF of galaxies with emission lines is much more compatible with a steep Schechter function. A similar difference in the best fit parameters of galaxies with and without emission lines has been found also in the LCRS, Lin et al. (1996), although for each subsample their best fit is significantly flatter than the corresponding slope in the EPS survey.

A partially different result comes from the 2dF survey, which shows for the first time significant evidence for the presence of a substantial passive dwarf population. In fact, Madgwick et al. (2002) find that the Schechter function provides an inadequate fit of the LF calculated over the magnitude range $-22 \leq M_{\rm b_J} - 5\log(h) \leq -13$, especially for the most passive and star-forming galaxies. They conclude that a Schechter function is not a good fit to the data over the entire $M_{\rm b_J}$ magnitude range and that this is mostly due to an overabundance of the faint passive star-forming galaxies relative to the bright objects. In fact, their sample of passive galaxies clearly show a very significant increase in the predicted number density of faint galaxies. Moreover, they argue that the small size of the other surveys has meant that only a statistically insignificant number of galaxies have contributed to the faint magnitude range. Hence previous studies could not determine if the features observed at the faint end were real or a consequence of the small volume being sample at these magnitudes.

Our results are more in agreement with the results of the ESP survey of Zucca et al. (1997). As mentioned in Sect. 5.2, the faint end of our clusters should be due to a significant number of very faint late type galaxies in clusters, which should be compatible with the emission line galaxies observed by Zucca et al. (1997). There is also a qualitative good agreement with the results of the 2dF survey of Madgwick et al. (2002), since the late type galaxies in their sample seem to have a steeper LF than the early type galaxies, even if they conclude that the incompatibility of a Schechter function with the global field LF

should be due to the passive galaxies. However, it is important to stress that we can compare only qualitatively our cluster LF with the field LF retrieved from the literature since we are using different wavebands and we are covering different magnitude range. Therefore, a quantitative comparison between the different environments requires absolutely the measure of the field luminosity function in the Sloan waveband and in the faint magnitude region.

6. Conclusion

The main conclusions of our analysis are as follows:

- we determine the composite LF of galaxies in clusters from the SDSS data. The LF clearly shows a bimodal behavior with an upturn and a evident steepening in the faint magnitude range in any SDSS band. The LF is well fitted by the sum of two Schechter functions. The results are confirmed by different methods of background subtraction. The observed upturn of the faint galaxies has a location ranging from $-16+5\log(h)$ in the g band to $-18.5+5\log(h)$ in the z band.
- The bright end LF shows the classical slope of -1.25 in each photometric band, while M^* is brighter in the red bands than in the blue bands. The distribution of the Schechter parameters obtained fitting only the bright end of the individual cluster LF is close to a Gaussian around the corresponding value of the composite bright-end LF. We check the dependence of the Schecter parameters of the composite LF on the clustercentric distance calculating the LF within different cluster apertures. We do not find any significant variation of the results with different apertures. Therefore, we conclude that the bright-end of the galaxy clusters is universal in different cluster environments, both in different systems and in different locations within the same cluster.
- The faint end LF is much steeper than the bright end LF with slope $-2.5 \leq \alpha \leq -1.6$. We apply different tests to check whether the observed faint end in the single clusters is due to the presence of background large scale structures or a second cluster on the line of sight. To check the first possibility we measure the individual cluster LF with a color cut method to identify the cluster members. We obtain the same slope observed with the statistical background subtraction. Moreover, we observe that the faint population is dominated by galaxies with colors compatible with late type galaxies at the cluster redshift. We then conclude that the observed steepening of the cluster LF is due to the presence of a real population of faint cluster galaxies.
- We defined the Dwarf to Giant galaxy Ratio DGR as the ratio between the number of galaxies in the magnitude range $-18 \leq M \leq -16.5$ and the number of galaxies brighter than -20 mag. In each waveband the DGR seems to slightly increase from the center 0.3 Mpc h^{-1} to 1.0 Mpc h^{-1}. The distribution of DGR of the single clusters has a peak around the value predicted by the composite bright-end and and a large spread at larger values. We check the relation between the DGR and the cluster richness and between the DGR and M^* through the Spearman rank coefficient and we do not find any correlation between the parameters. However DGR(z) clearly anti-correlates with both the X-ray and the optical cluster luminosities. The anti-correlation between cluster DGRs and cluster luminosities is most likely due to the choice of a fixed metric aperture for all the clusters. Therefore, because of this effect, the different cluster physical sizes must be taken into account before any conclusion about the universality of the shape of the cluster faint end LF is reached.

We compare the above results with the field LF calculated in the Sloan Digital Sky Survey and in other surveys. The magnitude range covered by the SDSS field LF allows us to compare only the bright end of the cluster luminosity function with the field LF. Unfortunately there is no good agreement between the results retrieved in the literature. Therefore we cannot perform a conclusive comparison between the LF of the different environments. Moreover, several surveys find evidence for the presence of an upturn at the faint end of the field luminosity function in agreement with our results for the cluster LF. In particular Zucca et al. (1997) find in the ESP field LF evidence for the presence of a late type galaxy population dominating the faint end of the field luminosity function. However, it is important to stress that this is only a qualitative comparison and does not allow us to draw any conclusion about the nature of the faint population in clusters and in the field. We can only conclude that the faint end of the cluster LF is systematically steeper than the field LF, although the field LF seems to show some evidence of an excess of galaxies in the faint magnitude range relative to a Schechter function.

Hierarchical clustering theories of galaxy formation generally predict a steep mass function of galactic halos (Kauffmann et al. 1993; Cole et al. 1994). This is in conflict with the flat galaxy LF measured in the field and in diffuse local groups, but not with the steep LF measured in many clusters. However in the hierarchical universe, clusters form relatively recently from the accretion of smaller systems. The dynamical processes that operate in clusters are destructive. Ram pressure stripping (e.g. Moore & Bauer 1999) and gravitational tides/galaxy harassment (e.g. Moore et al. 1996, 1998) will tend to fade galaxies by removing gas or stripping stars. These processes are most effective for less massive, less bound systems. Hence, we might expect to see a flattening of the faint end slope in clusters compared to the field, rather than the observed steepening.

Understanding the nature of the observed faint galaxy population requires a more detailed study of the galaxy population in the clusters through the analysis of the morphological type, the colors and the study of the relation between the fraction of dwarf galaxies and the cluster parameters such as the cluster mass, velocity dispersion or the X-ray luminosity. Moreover, the origin of this faint population can be understood only if a conclusive comparison between cluster and field is possible. At the moment, as we discussed above, the SDSS field LF based on the Sloan spectroscopic galaxy sample does not allow to an exhaustive comparison and analysis of the different environments.

It is clear from our results and from the existing work in the literature that the composite bright end of the cluster LF can

give useful information on the global cluster properties (such as the total optical luminosity, which is dominated by the very bright cluster galaxies), but it does not provide useful information on the cluster galaxy population as a whole. Equally it is clear that a Schechter function is a good fit of the cluster LF only in a very restricted magnitude range (the bright end). The photometric data available now should make it possible to consider non-parametric comparisons between the individual and the composite cluster LFs using the full range of the available data. Our results on the dwarf galaxy fraction are a first step in this direction, but it should be possible to devise a test that does not require a split in bright and faint galaxies but considers the cluster galaxy population as a whole.

Acknowledgements. We would like to thank the referee, S. Lumsden, for the useful comments which significantly improved the paper.
Funding for the creation and distribution of the SDSS Archive has been provided by the Alfred P. Sloan Foundation, the Participating Institutions, the National Aeronautics and Space Administration, the National Science Foundation, the U.S. Department of Energy, the Japanese Monbukagakusho, and the Max Planck Society. The SDSS Web site is `http://www.sdss.org/`. The SDSS is managed by the Astrophysical Research Consortium (ARC) for the Participating Institutions. The Participating Institutions are The University of Chicago, Fermilab, the Institute for Advanced Study, the Japan Participation Group, The Johns Hopkins University, Los Alamos National Laboratory, the Max-Planck-Institute for Astronomy (MPIA), the Max-Planck-Institute for Astrophysics (MPA), New Mexico State University, University of Pittsburgh, Princeton University, the United States Naval Observatory, and the University of Washington.

References

Abazajian, K., Adelman, J., Agueros, M., et al. 2003, AJ, 126, 2081 (Data Release One)
Adami, C., Ulmer, M. P., Durret, F., et al. 2000, A&A, 353, 930
Beijersbergen, M., Hoekstra, H., & Van Dokkum, P. G. 2002, MNRAS, 329, 385
Bernstein, G. M., Nichol, R. C., Tyson, J. A., et al. 1995, AJ, 110, 1507
Blanton, M. R., Dalcanton, J., Eisenstein, D., et al. 2001, AJ, 121, 2358
Blanton, M. R., Hogg, D. W., Bahcall, N. A., et al. 2003, ApJ, 592, 819
Böhringer, H., Voges, W., Huchra, J. P., et al. 2000, ApJS, 129, 435
Böhringer, H., Schuecker, P., Guzzo, L., et al. 2001, A&A, 369, 826
Böhringer, H., Collins, C. A., Guzzo, L., et al. 2002, ApJ, 566, 93
Boyce, P. J., Phillips, S., Bryn Jones, J., et al. 2001, MNRAS, 328, 277
Cole, S., Aragon-Salamanca, A., Frenk, C. S., et al. 1994, MNRAS, 271, 781
Colless, M. 1989, MNRAS, 237, 799
Cortese, L. 2003, A&A, 410, L25
Cross, N. J. G., Driver, S. P., Liske, J., et al. 2004, MNRAS, 349, 576
De Grandi, S., Böhringer, H., & Guzzo, L. 1999, ApJ, 514, 148
De Propris, R., Colless, M., Driver, S. P., et al. 2003, MNRAS, 342, 725
Dressler, A. 1978, ApJ, 223, 765
Driver, S. P., Phillips, S., Davies, J. I., et al. 1994, MNRAS, 268, 393
Ellis, R. S., Colless, M., Broadhurst, T., et al. 1996, MNRAS, 280, 235
Fukugita, M., Shimasaku, K., & Ichikawa, T. 1995, PASJ, 107, 945
Fukugita, M., Ichikawa, T., & Gunn, J. E. 1996, AJ, 111, 1748
Garilli, B., Maccagni, D., Stefano, A., et al. 2001, A&A, 342, 408
Goto, T., Sekiguchi, M., Nichol, R. C., et al. 2002a, AJ, 123, 1807
Goto, T., Okamura, S., McKay, T. A., et al. 2002b, PASP, 54, 515
Gunn, J. E., Carr, M. A., Rockosi, C. M., et al. 1998, AJ, 116, 3040 (SDSS Camera)
Hogg, D.W., Finkbeiner, D. P., Schlegel, D. J., & Gunn, J. E. 2001, AJ, 122, 2129
Horner, D. 2001, Ph.D. Thesis, University of Maryland
Kauffmann, G., White, S. D. M., & Guideroni, B. 1993, MNRAS, 264, 201
Kochanek, C. S., Pahre, M. A., Falco, E. E., et al. 2001, ApJ, 560, 566
Lin, H., Kirshner, R. P., Shectman, S. A., et al. 1996, ApJ, 464, 60
Lin, H., Yee, H. K. C., Carlberg, R. G., et al. 1999, ApJ, 518, 533
Loveday, J., Peterson, B. A., Efstathiou, G., et al. 1992, ApJ, 390,338
Loveday, J. 1997, ApJ, 489, 29
Lugger, P. M. 1986, ApJ, 303, 535
Lugger, P. M. 1989, ApJ, 343, 572
Lumsden, S. L., Collins, C. A., Nichol, R. C., et al. 1997, MNRAS, 290, 119
Lupton, R. H., Gunn, J. E., & Szalay, A. S. 1999, AJ, 118, 1406
Lupton, R., Gunn, J. E., Ivezić, Z., et al. 2001, in Astronomical Data Analysis Software and Systems X, ed. F. R. Harnden, Jr., F. A. Primini, & H. E. Payne (San Francisco: ASP), ASP Conf. Ser., 238, 269 [arXiv:astro-ph/0101420]
Madgwick, D. S., Lahav, O., Baldry, I. K., et al. 2002, MNRAS, 333, 133
Marzke, R. O., Huchra, J. P., & Geller, M. J. 1994, ApJ, 428,43
Marzke, R. O., & Da Costa, L. N. 1997, AJ, 113, 185
Moore, B., Katz, N., Lake, G., et al. 1996, Nature, 379, 613
Moore, B., lake, G., & Katz, N. 1998, ApJ, 495, 139
Mulchaey, J. S., Davis, D. S., Mushotzky, R. F., & Burstein, D. 2003, ApJS, 145, 39
Norberg, P., Cole, S., Baugh, C. M., et al. 2002, MNRAS, 336, 907
Paolillo, M., Andreon, S., Longo, G., et al. 2001, A&A, 367, 59
Phillips, S., Driver, S. P., Couch, W. J., et al. 1998, ApJ, 498, L119
Popesso, P., Böhringer, H., Brinkmann, J., et al. 2004, A&A, 423, 449
Reiprich, T., & Böhringer, H. 2002, ApJ, 567, 740 (R02)
Retzlaff, J. 2001, XXIst Moriond Astrophysics Meeting, March 10–17, 2001 Savoie, France, ed. D. M. Neumann, & J. T. T. Van
Rauzy, S., Adami, C., Mazure, A., et al. 1998, A&A, 337, 31
Sabatini, S., Davies, J., Scaramella, R., et al. 2003, MNRAS, 341, 981
Schechter, P. 1976, ApJ, 203, 297
Schlegel, D., Finkbeiner, D. P., & Davis, M. 1998, ApJ, 500, 525
Shimasaku, K., Fukugita, M., Doi, M., et al. 2001, AJ, 122, 1238
Smith, R. M., Driver, S. P., Phillips, S., et al. 1997, MNRAS, 287, 415
Smith, J. A., Tucker, D. L., Kent, S. M., et al. 2002, AJ, 123, 2121
Stoughton, C., Lupton, R. H., Bernardi, M., et al. 2002, AJ, 123, 485
Strauss, M. A., Weinberg, D. H., Lupton, R. H., et al. 2002, AJ, 124, 1810
Trentham, N. 1998, MNRAS, 295,360
Ulmer, M. P., Bernstein, G. M., Martin, D. R., et al. 1996, AJ, 112, 2517
Valotto, C., Nicotra, M. A., Muriel, H., et al. 1997, ApJ, 479, 90
Valotto, C., Moore, B., & Lambas, D. 2001, ApJ, 479, 90
Valotto, C., Muriel, H., Moore, B., et al. 2004, ApJ, 479, 90
Yagi, M., Kashikawa, N., Sekiguchi, M., et al. 2002, AJ, 123, 87
Yasuda, N., Fukugita, M. Narayanan, V. K., et al. 2001, AJ, 122, 1104
York, D. G., Adelman, J., Anderson, J. E., et al. 2000, AJ, 120, 1579
Zucca, E., Zamorani, G., Vettolani, G., et al. 1997, A&A, 326, 477

A&A 433, 431–445 (2005)
DOI: 10.1051/0004-6361:20041915

Astronomy & Astrophysics

RASS-SDSS galaxy cluster survey

III. Scaling relations of galaxy clusters

P. Popesso[1], A. Biviano[2], H. Böhringer[1], M. Romaniello[3], and W. Voges[1]

[1] Max-Planck-Institut fur extraterrestrische Physik, 85748 Garching, Germany
e-mail: popesso@mpe.mpg.de
[2] INAF - Osservatorio Astronomico di Trieste, via G. B. Tiepolo 11, 34131 Trieste, Italy
[3] European Southern Observatory, Karl Scharzschildstr. 2, Garching b. München, Germany

Received 27 August 2004 / Accepted 16 November 2004

Abstract. We use the RASS-SDSS galaxy cluster sample to compare the quality of optical and X-ray luminosities as predictors of other cluster properties such as their masses, temperatures, and velocity dispersions. We use the SDSS spectroscopic data to estimate the velocity dispersions and the virial masses of a subsample of 69 clusters within r_{500} and r_{200}. The ASCA temperature of the intra-cluster medium, $T_{\rm X}$, is retrieved from the literature for a subsample of 49 clusters. For this subsample we estimate the cluster masses also by using the mass-temperature relation. We show that the optical luminosity, $L_{\rm op}$, correlates with the cluster mass much better than the X-ray luminosity, $L_{\rm X}$. $L_{\rm op}$ can be used to estimate the cluster mass with an accuracy of 40% while $L_{\rm X}$ can predict the mass only with a 55% accuracy. We show that correcting $L_{\rm X}$ for the effect of a cool core at the center of a cluster lowers the scatter of the $L_{\rm X} - M$ relation only by 3%. We find that the scatter observed in the $L_{\rm op} - L_{\rm X}$ relation is determined by the scatter of the $L_{\rm X} - M$ relation. The mass-to-light ratio in the SDSS *i* band clearly increases with the cluster mass with a slope 0.2 ± 0.08. The optical and X-ray luminosities correlate in an excellent way with both $T_{\rm X}$ and σ_V with an orthogonal scatter of 20% in both relations. Moreover, $L_{\rm op}$ and $L_{\rm X}$ can predict variables with the same accuracy both. We conclude that the cluster optical luminosity is a key cluster parameter since it can give important information about fundamental cluster properties such as the mass, the velocity dispersion, and the temperature of the intra-cluster medium.

Key words. X-rays: galaxies: clusters – surveys

1. Introduction

Clusters of galaxies are the most massive gravitationally bound systems in the universe. The mass is the most important property of these systems. The cluster mass function and its evolution provide constraints on the evolution of large-scale structure and important cosmological parameters such as $\Omega_{\rm m}$ and σ_8. The mass-to-light ratio of clusters provides one of the most robust determinations of $\Omega_{\rm m}$ in connection with the observed light density in the Universe via the Oort (1958) method. For these reasons, over the last 70 years (starting with Zwicky 1933, 1937; and Smith 1936), much effort has been spent on measuring the mass of clusters using a number of techniques. These include: (i) dynamical methods applied to the galaxy distributions derived from redshift surveys; or (ii) X-ray observations of the distribution and temperature of the diffuse hot gas in the intracluster medium (ICM); (iii) gravitational lensing; and (iv) observations of the Sunyaev-Zeldovich effect. All these methods are in general quite expensive in terms of the observational resources required, especially for high redshift clusters.

In the literature several comparisons have been made between the different methods for determining the mass of the clusters. These include comparisons between the X-ray and strong-lensing methods (see, e.g., Wu 2000) in cores of clusters, between X-ray and weak lensing methods (see, e.g., Smail et al. 1997), and between the dynamical and the X-ray methods (see, e.g., Wu 2000). In particular, Girardi et al. (1998) and Rines et al. (2003) have shown that consistent results can be obtained from these last two methods.

The existence of a fundamental plane for the global properties of galaxy clusters (Schaeffer et al. 1993; Adami et al. 1998; Fujita & Takahara 1999) naturally implies that other properties, such as cluster luminosities, velocity dispersions, X-ray temperatures, can be used to infer the cluster masses. It is not known which correlates better with the cluster mass, the X-ray or the optical luminosity. Reiprich & Böhringer (2002, R02 hereafter) showed that a tight correlation exists between the X-ray total luminosity of the clusters and the mass, with a scatter of 60%. Girardi et al. (2000, 2002) analysed the relation between mass and optical luminosity in the blue band, and detetrmined the mass-to-light ratio for a sample of 162 clusters using inhomogeneous photometric data.

Yee & Ellingson (2003) analysed a sample of 16 X-ray luminous clusters from the *Canadian Network for Observational Cosmology* (CNOC) survey. They used the cluster optical richness, rather than the optical luminosity, and showed that it is well correlated with other global properties of galaxy clusters as their velocity dispersion such as their intracluster gas temperature, and their total mass. Lin et al. (2003) analysed a sample of 27 clusters with near-infrared data from the Two Micron All Sky Survey (2MASS) and available X-ray temperature. They showed that the *K*-band luminosity of a cluster can be used to estimate its mass with 45% accuracy.

Analysing the relation between optical luminosity and cluster mass is not an easy task. The lack of optical wide field surveys in the past did not allow measuring in the proper way the optical luminosity in galaxy systems. Until now the uncertainties in luminosity determination came from the corrections for the calibration of inhomogenous photometric data, background galaxy contamination and the need to extrapolate the sum of measured luminosities of galaxy members to include faint galaxies and the outer parts of the systems, beyond the region studied. The use of the *Sloan Digital Sky Survey* (SDSS) for the optical data allows us to overcome all the problems related to the optical luminosity estimation.

In this paper we use the RASS-SDSS galaxy cluster sample (Popesso et al. 2004) to study the correlations between the optical luminosity and other important properties of galaxy clusters such as their mass, line-of-sight velocity dispersion, temperature and X-ray luminosity. Moreover, the RASS-SDSS galaxy cluster sample allows us to compare the correlations of the optical and the X-ray luminosity with other global properties of the systems. The excellence of the second release of the SDSS (SDSS-DR2, Abazajian et al. 2004) in terms of its size, depth and sky coverage, the accurate photometry in 5 different optical wavebands, and the detailed spectroscopy for more than 260 000 galaxies give us unprecedented advantages in comparison to the previous studies. Firstly, the sky coverage (3324 deg^2) gives us the possibility of studying a large sample of clusters with completely homogeneous photometric data. Secondly, the accurate estimation of the spectroscopic redshift for a large subsample of galaxies allows us to define an accurate membership for any cluster and, thus, perform a detailed dynamical analysis of the system within the same survey. Thirdly, the sky coverage of the survey also makes it possible to overcome the well known problem of the statistical subtraction of the galaxy background. We use large areas of the survey to define a mean global galaxy background, and a region close to the clusters to determine the local galaxy background in order to check for systematics in the field subtraction. Finally, the magnitude limit of the SDSS DR2 in all the five bands is sufficiently deep (e.g. $r_{\rm lim} = 22.2$, 95% completeness) that, at the mean redshift of our cluster sample ($z \sim 0.10$), the cluster luminosity function (LF) is sampled down to a significant part of the faint end. Moreover, the use of the *ROSAT All Sky Survey* (RASS) allows us to define also the X-ray properties in a homogeneous way for all the systems and perform a detailed comparison with the optical luminosity.

In this paper we show that the optical luminosity, $L_{\rm op}$, is strongly correlated with the other global properties of a galaxy cluster, allowing its use as an estimator for quantities such as the velocity dispersion, the mass, and the intra-cluster gas temperature, $T_{\rm X}$. We demonstrate that $L_{\rm op}$ is a better predictor of the virial mass than the X-ray luminosity, which makes $L_{\rm op}$ an important defining parameter of galaxy clusters, and an extremely useful cosmological tool. Throughout this paper we use $H_0 = 70$ km s^{-1} Mpc^{-1} in a flat cosmology with $\Omega_0 = 0.3$ and $\Omega_\Lambda = 0.7$ (e.g. Tegmark et al. 2004).

2. The cluster sample and the data

The ROSAT-SDSS galaxy cluster catalog comprises 130 systems detected in the ROSAT All Sky Survey (RASS). The X-ray cluster properties and the redshifts have been taken from different catalogs of X-ray selected clusters: the ROSAT-ESO flux limited X-ray cluster sample (REFLEX, Böhringer et al. 2001, 2002), the Northern ROSAT All-sky cluster sample (NORAS, Böhringer et al. 2000), the NORAS 2 cluster sample (Retzlaff 2001), the ASCA Cluster Catalog (ACC) from Horner et al. (2001) and the Group Sample (GS) of Mulchaey et al. (2003).

The optical photometric data are taken from the SDSS DR2 (Fukugita 1996; Gunn et al. 1998; Lupton et al. 1999; York et al. 2000; Hogg et al. 2001; Eisenstein et al. 2001; Smith et al. 2002; Strauss et al. 2002; Stoughton et al. 2002; Blanton et al. 2003; Abazajian et al. 2003). The SDSS consists of an imaging survey of π steradians of the northern sky in the five passbands u, g, r, i, z, in the entire optical range from the atmospheric ultraviolet cutoff in the blue to the sensitivity limit of silicon in the red. The survey is carried out using a 2.5 m telescope, an imaging mosaic camera with 30 CCDs, two fiber-fed spectrographs and a 0.5 m telescope for the photometric calibration. The imaging survey is taken in drift-scan mode. The imaging data are processed with a photometric pipeline (PHOTO, Lupton et al. 2001) specially written for the SDSS data. For each cluster we defined a photometric galaxy catalog as described in Sect. 3 of Popesso et al. (2004; see also Yasuda et al. 2001).

For the analysis in this paper we use only SDSS Model magnitudes. Because of a bug in PHOTO, found during the completion of DR1, the model magnitudes were systematically under-estimated by about 0.2–0.3 mag for galaxies brighter than 20th magnitude, and accordingly the measured radii were systematically too large. This problem has been fixed in the SDSS DR2, therefore the model magnitude can be considered a good estimate of the galaxy total luminosity at any magnitude and is not dependent on the seeing, like the Petrosian magnitudes.

The spectroscopic component of the survey is carried out using two fiber-fed double spectrographs, covering the wavelength range 3800–9200 Å, over 4098 pixels. They have a resolution $\Delta\lambda/\lambda$ varying between 1850 and 2200, and together they are fed by 640 fibers, each with an entrance diameter of 3 arcsec. The fibers are manually plugged into plates inserted into the focal plane; the mapping of fibers to plates is carried out by a tiling algorithm (Blanton et al. 2003) that optimizes observing efficiency in the presence of large-scale structure. The finite diameter of the fiber cladding prevents fibers on any

given plate from being placed less than 55 arcsec apart. For any given plate, a series of fifteen-minute exposures is carried out until the mean signal to noise ratio (S/N) per resolution element exceeds 4 for objects with fiber magnitudes (i.e., as measured through the 3 aperture of the fiber) brighter than $g = 20.2$ and $i = 19.9$, as determined by preliminary reductions done at the observing site. Under good conditions (dark, clear skies and good seeing), this typically requires a total of 45 min of exposure.

To create a homogeneous catalog of X-ray cluster properties, we have computed the X-ray luminosity using only RASS data for all clusters in the sample. The X-ray luminosity has been calculated with the growth curve analysis (GCA) method used for the NORAS and REFLEX cluster surveys (Böhringer et al. 2000) based on the RASS3 data base (Voges et al. 1999). The GCA method is optimized for the detection of the extended emission of clusters by assessing the plateau of the background subtracted cumulative count rate curve. We use as final result the total flux inside the radius r_{200} which is corrected for the missing flux estimated via the assumption of a standard β-model for the X-ray surface brightness (see Böhringer et al. 2000 for more details). The correction is typically only 8–10% illustrating the high effectiveness of the GCA method for sampling the flux of extended sources. For a subsample of 49 galaxy clusters we have also compiled from the literature the ASCA temperature of the ICM.

3. The cluster optical luminosity

The total optical luminosity of a cluster has to be computed after the subtraction of the foreground and background galaxy contamination. We consider two different approaches to the statistical subtraction of the galaxy background. We compute the local background number counts in an annulus around the cluster and a global background number counts from the mean of the magnitude number counts determined in five different SDSS sky regions, each with an area of 30 deg^2. In our analysis we show the results obtained using the optical luminosity estimated with the second method. The optical luminosity is then computed following the prescription of Popesso et al. (2004). The reader is referred to that paper for a detailed discussion about the comparison between optical luminosities calculated with different methods.

4. Cluster members selection and mass estimation

To select the members of each system and estimate the mass we use the redshifts in the SDSS spectroscopic sample. The SDSS spectroscopic pipeline (spectro1d) assigns a final redshift to each object spectrum by choosing the emission or cross-correlation redshift with the highest confidence level. The emission-redshift is obtained by matching the list of candidate emission lines against a list of common galaxy and quasar emission lines. The cross-correlated redshift is estimated by cross-correlating the spectrum with stellar, emission-line galaxy, and quasar template spectra.

In order to select the cluster members, we proceed in two steps. In the first step we follow the method of Girardi et al. (1993). Namely, we select only galaxies within a circle of one Abell radius (2.15 Mpc), and eliminate those with redshift $|cz - cz_{\rm cluster}| > 4000$ km s^{-1}, where $z_{\rm cluster}$ is the mean cluster redshift as given in the X-ray catalogues (see Sect. 2). We then define the weighted gaps (see also Beers et al. 1990) in the z-distribution of the remaining galaxies, and reject galaxies separated from the main cluster body by a weighted gap $\geq$4. This allows us to define the cluster limits in velocity space.

In the second step of our procedure for membership selection, we consider all galaxies (not only those within an Abell radius) with a velocity within the limits defined with the gapper procedure, and apply the method of Katgert et al. (2004) to these galaxies. The method takes into account both the velocities and the clustercentric positions of the galaxies (we take the X-ray center as the dynamical center of the cluster). The method is identical to that of den Hartog & Katgert (1996) when the cluster sample contains at least 45 galaxies, and it is a simplified version of it for smaller samples (for more details, see Appendix A in Katgert et al. 2004).

The virial analysis (see, e.g., Girardi et al. 1998) is then performed on the clusters with at least 10 member galaxies. The velocity dispersion is computed using the biweight estimator (Beers et al. 1990). The virial masses are corrected for the surface pressure term (The & White 1986) by adopting a profile of Navarro et al. (1996, 1997; NFW) with concentration parameter $c = 4$ (this profile has been found to describe the average mass profile of rich clusters by Katgert et al. 2004). Correction for the surface term requires knowledge of the r_{200} radius, for which we adopt Carlberg et al.'s (1997a) definition (see Eq. (8) in that paper), as a first guess. After the virial mass has been corrected for the surface pressure term, we refine our r_{200} estimate using the virial mass density itself. Let $M_{\rm vir}$ be the virial mass (corrected for the surface term) contained in a volume of radius equal to the clustercentric distance of the most distant cluster member in the sample, i.e. the aperture radius $r_{\rm ap}$. The radius r_{200} is then given by:

$$r_{200} \equiv r_{\rm ap}\ [\rho_{\rm vir}/(200\rho_{\rm c})]^{1/2.4} \qquad (1)$$

where $\rho_{\rm vir} \equiv 3M_{\rm vir}/(4\pi r_{\rm ap}^3)$ and $\rho_{\rm c}(z)$ is the critical density at redshift z in the adopted cosmology. The exponent in Eq. (1) is the one that describes the average cluster mass density profile near r_{200}, as estimated by Katgert et al. (2004) for an ensemble of 59 rich clusters. Similarly, r_{500} is estimated by setting 500 instead of 200 in Eq. (1). Finally, a $c = 4$ NFW profile is used to interpolate (or, in a few cases, extrapolate) the virial mass $M_{\rm vir,\,c}$ from $r_{\rm ap}$ to r_{200} and r_{500}.

Our clusters span a wide range in mass; since clusters of different masses have different concentrations (see, e.g. Dolag et al. 2004) we should in principle compute the cluster masses, M, using a different concentration parameter c for each cluster. According to Dolag et al. (2004), $c \propto M^{-0.102}$. Taking $c = 4$ for clusters as massive as those analysed by Katgert et al. (2004), $M \simeq 2\times10^{15}\ M_\odot$, Dolag et al.'s scaling implies that our clusters span a range $c \simeq 3$–6. Using $c = 6$ instead of $c = 4$ makes the mass estimates 4% and 10% higher at, respectively, r_{200} and r_{500}, while using $c = 3$ makes the mass estimates lower by the same factors. This effect clearly being much smaller than

the observational uncertainties, we assume the same $c = 4$ in the analysis for all clusters.

Even if the completeness level of the SDSS spectroscopic sample is very high, in the central regions of galaxy clusters this level is likely to drop because fibers cannot be placed closer than 55 arcsec. We estimate that the spectroscopic completeness drops to ∼70% in the central ∼0.1 Mpc. This affects the observed number density profile of a cluster, and hence our estimate of the projected mean harmonic pairwise separation s$\langle R_{ij}^{-1}\rangle$, and, as a consequence, also our virial mass estimates (see, e.g., Beers et al. 1984). Using the average cluster number density profile, and the relation between the core radius of this profile and $\langle R_{ij}^{-1}\rangle$, as given by Girardi et al. (1995, 1998), we estimate that this effect of incompleteness translates into an average over-estimate of the virial mass of only ∼5%. Since the effect is very small, and much smaller than the observational uncertainties, we neglect this correcting factor in the following analysis.

There are several indications that cluster galaxies of later morphological and/or spectral type, have wider velocity distributions than early-type cluster galaxies (Moss & Dickens 1977; Biviano et al. 2002, and references therein). As a consequence, we also estimate the virial masses by considering only cluster members along the red sequence in the $u - i$ vs. i colour–magnitude diagram. When only the red-sequence cluster members are used to compute the virial masses, these masses are ∼25% smaller than when all the cluster members are used. A similar effect has been discussed by Biviano et al. (1997) for the galaxy clusters of the *ESO Nearby Abell Cluster Survey*, and by Carlberg et al. (1997b) for the galaxy clusters of the CNOC. The effect is generally interpreted as evidence for ongoing accretion of blue field galaxies onto the cluster, before complete virialization (see, e.g., the discussion in Biviano & Katgert 2003). Since this effect is not negligible, in the following we consider both the mass estimates obtained using only the red-sequence galaxies, and the mass estimates obtained using all the cluster members. However, for the sake of conciseness, we only plot results for the mass estimates obtained using all the cluster members.

To check the consistency of our mass estimates with those obtained from X-ray data, we retrieve the latter from R02, for a subsample of 10 clusters with optical mass estimates. Figure 1 shows the overall agreement between the X-ray mass from R02 and the optical mass calculated in this work (empty squares). The figure shows also the comparison between optical mass and the mass obtained from the $M - T$ relation for 6 more clusters with know ASCA temperature but with unknown X-ray mass (filled squares). It is mainly for the systems with evident substructures in the redshift distribution (the empty and filled squares surrounded by big triangles in the figure) that the two mass estimates are in disagreement, as expected. In the following analysis we do not consider these clusters with strong optical substructures. We omit in Fig. 1 the comparison between the mass estimated from the $M - T_X$ relation (see Eq. (2) below) and the direct measure of the X-ray mass (R02). They are in very good agreement since the $M - T_X$ relation is derived from R02 data, and the scatter in the relation is very small as shown by the errors in Eq. (2) and Fig. 3.

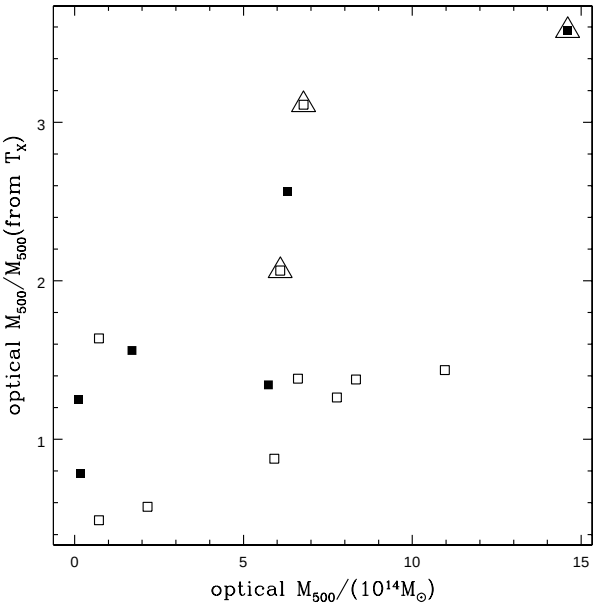

Fig. 1. Comparison of M_{500} estimated from X-ray data with the mass estimated from the dynamical analysis of the optical data. We know the temperature for 16 clusters of the subsample with known optical mass. For 10 of them the measure of the X-ray mass is given by R02. We compare the optical mass with the X-ray mass of R02, when available, and with the mass derived from the $M - T_X$ relation (Eq. (2)) in the other case. The empty squares are the ratio between the optical mass and the mass given by R02. The filled squares are the ratio between the optical mass and the mass derived from the $M - T_X$ relation (Eq. (2)). The squares surrounded by big triangles are clusters with known optical substructures.

4.1. Masses estimated from the $M - T_X$ relation

We use the $M - T_X$ relation to estimate the mass for the subsample of 49 clusters with known ASCA temperature. First, we consider the $M - T_X$ relations provided by Finoguenov et al. (2001, hereafter F01). F01 provided several $M - T_X$ relations that had been estimated using different samples of systems: the cluster sample of R02 (HIFLUGCS + 60 more clusters) and a sample of 39 clusters with known temperature profile from ASCA data (Markevitch et al. 1998). We notice that the masses estimated with the $M - T_X$ relation of F01 obtained from clusters with known temperature profile are systematically smaller by a factor 1.5–2 than both the virial masses obtained from the analysis of the galaxy distribution, and also the X-ray masses of R02. The F01 sample comprises only 9 of the 45 clusters included in the R02 sample with temperature higher than 5 keV. The masses of these 9 clusters are in good agreement with the masses estimated in R02 (which assumes the isothermality of the ICM) but, as shown in Fig. 2, the high-mass region is not well sampled. Moreover, the presence of 4 systems in the low mass regime with $\beta \sim 0.3$ (where β is the exponent of the β-model used to calculate the X-ray mass, see F01 or R02 for more details) implies both a steepening of the $M - T_X$ relation and a decrease of its normalization.

Therefore, instead of using the $M - T_X$ relation of F01, we prefer to recalibrate the $M - T_X$ relation using the data of R02 in order to obtain both the $M_{500} - T_X$ and the $M_{200} - T_X$

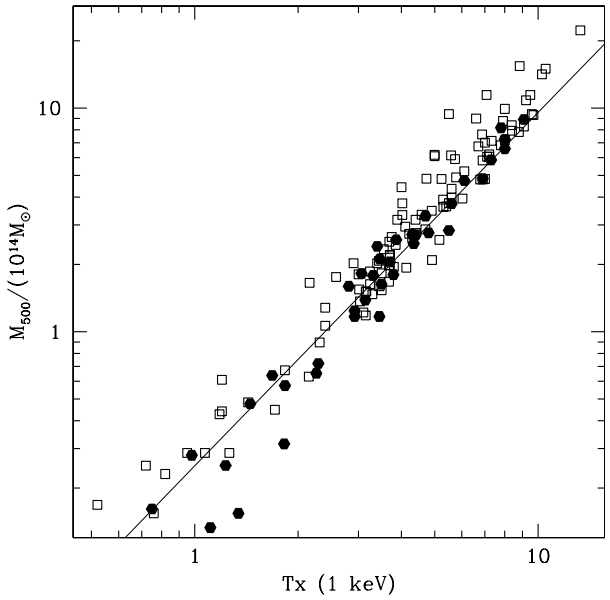

Fig. 2. Relation between mass and temperature. The mass is calculated using a β-model and the temperature of the ICM. The empty squares are the clusters of R02, while the filled hexagons are taken from F01. The solid line in the figure is the best fit line given by F01.

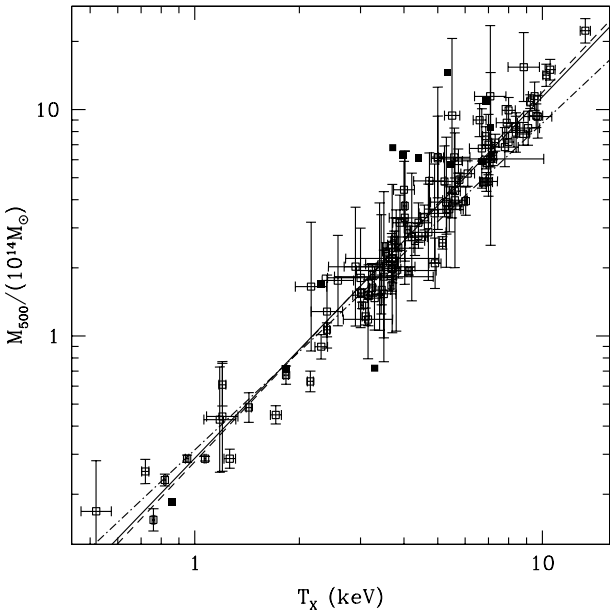

Fig. 3. Mass-temperature relation calibrated with the cluster mass and temperature used in R02. The new normalization in the $M-T_X$ relation is 60% higher than in the classical $M-T_X$ relation of F01. The solid line is the best fit line obtained using the enlarged sample of R02. The dotted line is the best fit line obtained fitting the clusters with T_X higher than 4.5 keV, while the dashed-dotted line is the best fit line derived from the fit of systems with temperature lower than 4.5 keV.

relations. The data are fitted with the ODRPACK routine (Akritas & Bershady 1996) and the errors are calculated using a bootstrap method. In the following analysis the mass is calculated from the temperature with the following relations:

$$M_{500} = 2.89 \pm 0.29 \times 10^{13} T_X^{1.59\pm0.04} \quad (2)$$

$$M_{200} = 4.69 \pm 0.36 \times 10^{13} T_X^{1.59\pm0.05}. \quad (3)$$

The normalization of the $M-T_X$ relation in Eq. (2) is 60% higher than that of the usual $M-T_X$ relation of F01 estimated with the sample with known T_X profiles. There is much better agreement (within 1σ) with the relation of F01 estimated excluding from the sample the groups with β lower than 0.4. Figure 3 shows the best fit for the enlarged sample of R02 while Fig. 4 shows the comparison of our best fit with the relation predicted by the hydrodynamical simulations.

5. Correlation of the optical and X-ray luminosities with the cluster global properties

In this section we examine the correlation of the optical luminosity L_{op} and the X-ray luminosity L_X with quantities derived from the optical and X-ray data, such as the total mass, the velocity dispersion, the X-ray temperature, r_{500}, and r_{200}. The main motivation in deriving these dependences is to use L_{op} and L_X, as predictors of the other quantities. Moreover, we will compare the quality of the two quantities L_{op} and L_X as predictors. To quantify all the dependences, a linear regression in log-log space is performed using a numerical orthogonal distance regression method (ODRPACK). The fits are performed using the form

$$\log\left(L_{op}/\left(10^{12}L_\odot\right)\right) = \alpha \times \log(P_C) + \beta \quad (4)$$

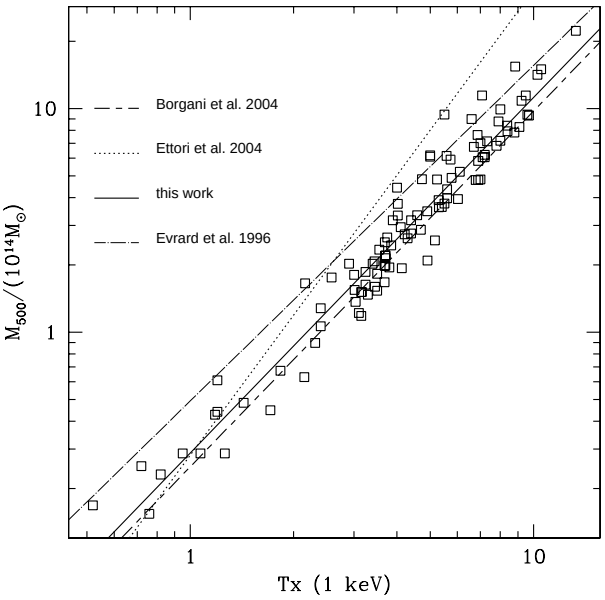

Fig. 4. Comparison of the $M-T_X$ relation obtained with the sample from R02 and the theoretical prediction from Borgani et al. (2004), Ettori et al. (2004), Evrard et al. (1996).

$$\log\left(L_X/\left(10^{44}\ \mathrm{erg\,s^{-1}}\right)\right) = \alpha \times \log(P_C) + \beta \quad (5)$$

where P_C is the cluster global property, and the errors of each variable are transformed into log space as $\Delta\log(x) = \log(e)(x^+ - x^-)/(2x)$, where x^+ and x^- denote the upper and lower boundary of the error range of the quantity, respectively. In all the correlations we analyse separately the sample with masses derived from the dynamical analysis (69 clusters) and

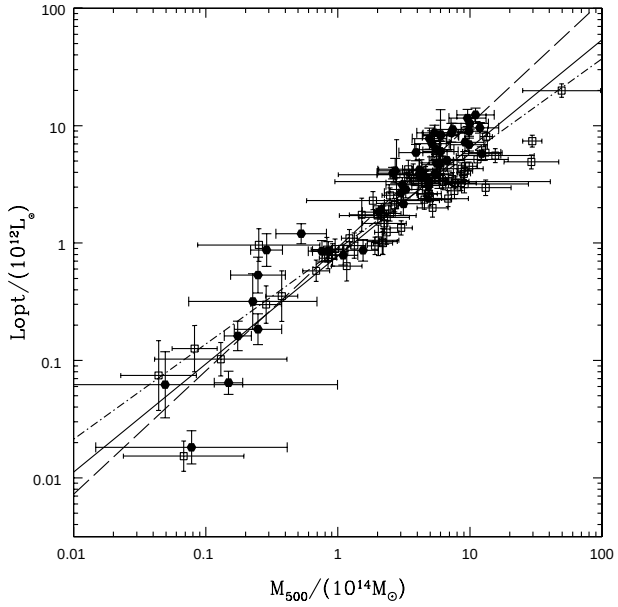

Fig. 5. $L_{op} - M_{500}$ relation in the *i* Sloan band. The empty squares in the figure indicate clusters with mass estimated from the dynamical analysis of the Sloan spectroscopic data. The filled points indicate systems with mass estimated from the $M - T_X$ relation. The dot-dashed line is the best fit line obtained for the O sample. The dashed line is the best fit line for the X sample and the solid line is the result obtained from the E sample.

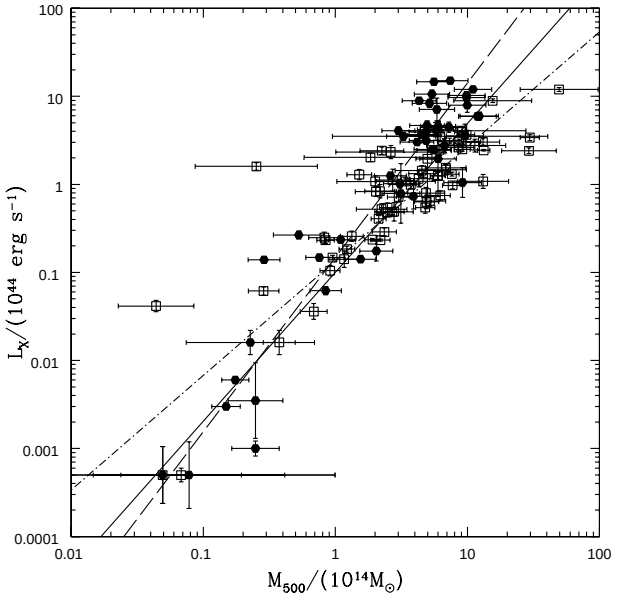

Fig. 6. $L_X - M_{500}$ relation for the RASS-SDSS galaxy cluster sample. The empty squares in the figure are clusters with mass estimated from the dynamical analysis of the Sloan spectroscopic data. The filled points are systems with mass estimated from the $M - T_X$ relation. The dot-dashed line is the best fit line obtained for the O sample. The dashed line is the best fit line for the X sample and the solid line is the result obtained from the E sample.

the sample with masses derived from the $M - T_X$ relation (49 systems). Then we analyse the correlations obtained using all the clusters of the RASS-SDSS galaxy cluster sample with known mass (either the virial estimate from optical data, or, when this is not available, the mass derived from the X-ray temperature) for a total number of 102 systems (69 clusters with known optical mass + 49 clusters with mass estimated from the temperature, with an overlap of 16 clusters). In the following tables, "O" (Optical sample) refers to the sample with optical masses, the "X" (X-ray sample) to the sample with mass derived from T_X and, finally, the "E" (Enlarged sample) refers to the sample of all the clusters with known mass.

Throughout the following analysis we consider only the relation obtained with the optical luminosity calculated in the *i* Sloan band. All the results obtained in the other three SDSS optical bands (g, r and z) are listed in the Appendix.

5.1. Correlations of the optical and X-ray luminosities with the cluster mass

Both the optical and the X-ray luminosity show a tight relation with the cluster mass (see Figs. 5 and 6, respectively for the $L_{op} - M_{500}$ and $L_X - M_{500}$ relations). The optical luminosity is estimated within the same radius as the mass, while L_X is the *total* X-ray luminosity of the system. The total L_X is not estimated within a fixed aperture but is calculated from the X-ray luminosity radial profile. Table 1 lists the best fit values of the correlation for the different samples. In both the $L_{op} - M$ and $L_X - M$ relations the slope is flatter for the O sample than for the X sample. As a consequence, the best fit values of the correlation obtained with the enlarged sample are the mean of the previous values. However, all the derived values of slope and normalization are in agreement within 1.5σ. The slope of 0.75 ± 0.02 of the $L_{op} - M$ relation in the *B* band studied by Girardi et al. (2002) is in very good agreement (within 1σ) with the slope of 0.81 ± 0.04 obtained with the O sample. The agreement is less good (within 3σ) for the slope obtained with the X and E samples. The values of slope and normalization of the $L_X - M$ relation lie in the range of values given in R02. To recalibrate the $L_X - M$ relation we add our enlarged sample to the sample of clusters of R02, obtaining a final sample of 198 clusters (106 from R02 + 102 from this work, with an overlap of 10) with known mass and X-ray luminosity. The best fit values of the correlation obtained with this sample are indicated by "R+E" in Table 1. The resulting slope of 1.5 ± 0.05 is in good agreement with the value obtained from the E sample. The correlation is shown in Fig. 7.

It is particularly interesting to compare the scatter of the $L_{op} - M$ and $L_X - M$ relations in order to understand which of the two observables, L_{op} and L_X, shows the best correlation with the cluster mass. Table 1 lists three kinds of scatters evaluated for each correlation: the orthogonal scatter, which gives an estimate of the dispersion along the direction orthogonal to the best fit line, and the scatter in both variables. The orthogonal scatter in the $L_{op} - M$ relation has a minimum value of 20% and a maximum of 30% in all the analysed correlations. The observable L_{op} can be used to predict the cluster mass within r_{500} or r_{200} with an accuracy in the range 40−50%. The X-ray luminosity shows a less tight relation with the cluster mass for all the analysed correlations. In fact, the orthogonal scatter of the $L_X - M$ relations lies in the range 38–50%, while the mass can

Table 1. The table lists the best fit parameters for the $L_{op} - M$, $L_X - M$, $L_{op} - L_X$ and $L_{op} - r_{500/200}$ relations respectively for different samples of galaxy clusters and for different methods. O refers to the sample with masses estimated from the dynamical analysis performed with the optical spectroscopic data. X refers to the sample with masses estimated from the $M - T_X$ relation. E refers to the enlarged sample, which comprises all the clusters in the RASS-SDSS galaxy cluster catalog with known mass. $R + E$ refers to the enlarged sample plus the sample of R02. The left side of the table lists the results obtained performing the dynamical analysis only for the red members od the system. The right side lists the best fit values of the correlations obtained using the results of the dynamical analysis applied to all the cluster members. The table lists three estimations of the scatter for each relation: σ is the orthogonal scatter of the A–B relation, σ_A is the scatter in the A variable and σ_B is the scatter in the B variable. All the scatter values in the table are expressed in dex and all the errors are given at the 95% confidence level.

$A-B$ relation		Sample	Red members					All members				
A	B		α	β	σ	σ_B	σ_A	α	β	σ	σ_B	σ_A
M_{500}	L_{op}	O	0.80 ± 0.04	-0.03 ± 0.03	0.12	0.16	0.16	0.81 ± 0.04	-0.09 ± 0.03	0.10	0.16	0.15
		X	0.96 ± 0.05	0.01 ± 0.04	0.09	0.15	0.16					
		E	0.91 ± 0.04	-0.03 ± 0.03	0.11	0.19	0.17	0.90 ± 0.05	-0.06 ± 0.03	0.11	0.17	0.16
M_{200}	L_{op}	O	0.79 ± 0.04	0.12 ± 0.03	0.13	0.16	0.15	0.79 ± 0.04	-0.05 ± 0.04	0.10	0.16	0.14
		X	1.05 ± 0.07	-0.04 ± 0.06	0.10	0.17	0.16					
		E	0.91 ± 0.04	0.05 ± 0.04	0.11	0.17	0.16	0.91 ± 0.04	-0.08 ± 0.04	0.12	0.19	0.17
M_{500}	L_X	O	1.30 ± 0.09	-0.77 ± 0.09	0.15	0.19	0.30	1.41 ± 0.12	-0.92 ± 0.06	0.18	0.19	0.32
		X	1.87 ± 0.12	-0.83 ± 0.06	0.14	0.19	0.29					
		E	1.68 ± 0.09	-0.88 ± 0.06	0.17	0.22	0.36	1.69 ± 0.10	-1.00 ± 0.06	0.19	0.23	0.43
		R+E	1.50 ± 0.05	-0.38 ± 0.03	0.17	0.22	0.27					
M_{200}	L_X	O	1.30 ± 0.09	-0.95 ± 0.07	0.15	0.19	0.30	1.32 ± 0.08	-1.08 ± 0.07	0.17	0.18	0.30
		X	1.98 ± 0.13	-1.24 ± 0.10	0.16	0.20	0.29					
		E	1.71 ± 0.09	-1.18 ± 0.07	0.17	0.21	0.35	1.66 ± 0.09	-1.27 ± 0.07	0.17	0.21	0.39
		R+E	1.58 ± 0.07	-0.92 ± 0.06	0.16	0.26	0.30					
L_X	L_{op}	O	0.60 ± 0.05	0.40 ± 0.02	0.12	0.30	0.16	0.63 ± 0.04	0.41 ± 0.02	0.14	0.29	0.17
	(r_{500})	X	0.53 ± 0.03	0.39 ± 0.03	0.16	0.33	0.19					
		E	0.54 ± 0.03	0.40 ± 0.03	0.14	0.33	0.18	0.55 ± 0.03	0.41 ± 0.02	0.15	0.33	0.18
L_X	L_{op}	O	0.59 ± 0.05	0.55 ± 0.02	0.13	0.28	0.16	0.64 ± 0.04	0.57 ± 0.02	0.15	0.27	0.17
	(r_{200})	X	0.55 ± 0.04	0.56 ± 0.03	0.19	0.35	0.22					
		E	0.56 ± 0.03	0.56 ± 0.03	0.16	0.32	0.18	0.58 ± 0.03	0.57 ± 0.02	0.17	0.31	0.19
r_{500}	L_{op}	O	2.28 ± 0.14	0.31 ± 0.02	0.05	0.05	0.15	2.26 ± 0.13	0.33 ± 0.04	0.05	0.06	0.14
		X	2.95 ± 0.15	0.43 ± 0.02	0.04	0.05	0.14					
		E	2.53 ± 0.12	0.36 ± 0.02	0.05	0.07	0.17	2.50 ± 0.13	0.38 ± 0.05	0.05	0.06	0.17
r_{200}	L_{op}	O	2.25 ± 0.13	0.07 ± 0.04	0.06	0.07	0.14	2.28 ± 0.14	0.08 ± 0.04	0.06	0.08	0.14
		X	2.88 ± 0.18	0.06 ± 0.05	0.06	0.08	0.17					
		E	2.49 ± 0.12	0.06 ± 0.04	0.07	0.09	0.17	2.52 ± 0.11	0.07 ± 0.04	0.07	0.08	0.17

be predicted from the X-ray luminosity with an accuracy in the range 55–65%. These values are in agreement with the results of R02 and are confirmed by the correlation obtained with the "R+E" sample, as indicated in Table 1. The dispersion along the L_X axis is much larger (more than 90%) and is due to the propagation of the errors, since $\sigma_{L_X} \sim \alpha \times \sigma_M$. The difference in the scatter observed in the two relations cannot be explained by the measurement errors, since the average error in the L_{op} measure is around 15% and is comparable to the average measurement error in L_X (around 10%).

5.2. The scatter in the $L_{op} - M$ and $L_X - M$ relations

A possible explanation for the large scatter of the $L_X - M$ relation is the presence of a large number of groups in our samples. In fact measuring the mass and the X-ray luminosity for low-mass systems is not an easy task. However, the low-mass systems do not increase the scatter in the $L_{op} - M$ relation, as they should if their masses were not measured correctly. Moreover, the scatter of the $L_X - M$ relation is the same in all the mass ranges, since including or excluding the groups in our analysis does not change the amount of scatter in the correlations. A more plausible explanation for the larger scatter in the $L_X - M$ relation in comparison to the $L_{op} - M$ relation, is the presence of a large number of cool-core (once named "cooling flow") clusters in the analysed sample. In fact, the presence of a cool core in a cluster could cause an increase of the observed X-ray luminosity for a given cluster mass. In principle even the mass estimated from the ICM temperature could be affected by this effect. In fact, Markevitch (1998, hereafter M98) has shown that the presence of a cool core in a system can significantly affect the temperature estimation if the cool core region

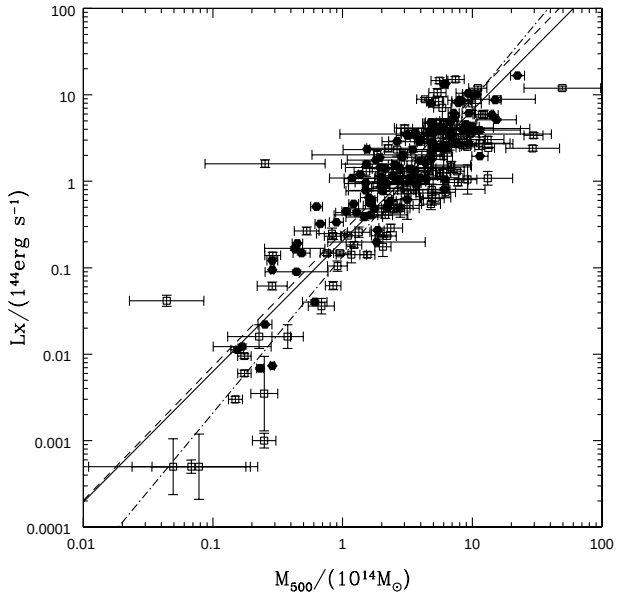

Fig. 7. $L_X - M_{500}$ relation for the RASS-SDSS galaxy cluster sample plus the cluster sample of R02. The empty squares are the E clusters and the filled hexagons are the clusters of R02. The dot-dashed line is the best fit line obtained for the E sample. The dashed line is the best fit line for the R02 sample and the solid line is the result obtained from the "E+R" sample.

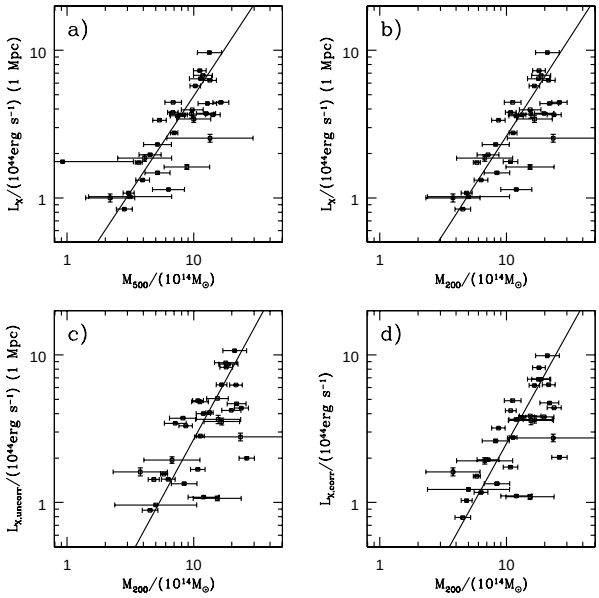

Fig. 8. $L_X - M_{500}$ relation for the sample of M98. The $L_X - M$ relation is obtained using a cool-core-corrected X-ray luminosity. Panels **a)** and **b)** show the $L_X - M$ relation given by the X-ray luminosity calculated in the 0.1−2.4 keV energy band within 1.4 Mpc from the cluster center with M_{500} and M_{200} respectively. The X-ray luminosity is taken from M98, while the mass is taken from R02. R02 used the cool-core-corrected temperature of M98 to calculate the mass. Panels **c)** and **d)** show the same relation given by the total X-ray luminosity of the system (calculated within the physical size of the system) in the 0.1−2.4 keV energy band and M_{200}. The total L_X is taken from R02 and is calculated with the same method used to estimate the X-ray luminosity in the RASS-SDSS sample. Panel **c)** shows the $L_X - M$ relation with uncorrected X-ray luminosity, while panel **d)** shows the $L_X - M$ relation obtained using the X-ray luminosity corrected for the cool-core effect. The correction is obtained comparing the corrected and uncorrected L_X retrieved in M98.

is not excised. However, the scatter observed in the $L_X - M$ relation obtained with the X sample and with the R02 sample, in which the mass is calculated using the temperature, is exactly the same as the scatter observed in the $L_X - M$ relation obtained with the O sample, in which the mass estimation is not influenced by the presence of a cool core. Thus, we do not expect that the presence of a cool core affects the mass in our correlation. Therefore, in Fig. 7 the cool-core clusters should move to higher X-ray luminosity but not to higher mass. We call this effect the "cool core" effect throughout the paper.

Unfortunately our data are not able to fully explore this effect. To calculate the amount of scatter due to the cool-core effect on the X-ray luminosity we must use the cluster sample of M98. In this sample the X-ray luminosities and temperatures have been corrected for the cool core effect. We retrieve the masses of 33 of the 35 clusters of that sample from R02. The masses taken from R02 have all been calculated with the corrected temperature of M98. In Fig. 8 we show the $L_X - M$ relation obtained using a cool-core-corrected X-ray luminosity. Panels *a* and *b* show the $L_X - M$ relation given by the X-ray luminosity calculated in the 0.1−2.4 keV energy band within 1.4 Mpc from the cluster center with M_{500} and M_{200} respectively. Panels *c* and *d* show the same relation given by the total X-ray luminosity of the system in the same energy band and M_{200}. The total L_X is taken from R02 and is calculated within r_{200} with a method similar to the method used to estimate the X-ray luminosity in the RASS-SDSS sample. Therefore, it should give a robust estimate of the total X-ray emission of the system. Panel *c* shows the $L_X - M$ relation with uncorrected X-ray luminosity, while panel *d* shows the $L_X - M$ relation obtained using the X-ray luminosity corrected for the cool core effect. The correction is obtained by comparing the corrected and uncorrected L_X calculated by M98. M98 removed the effect due to the presence of a cool core by the excision of the cool core region. They assumed that a 70 kpc radius contains most of the cool core emission in clusters that do not have an extremely cool core, like those in the sample considered here. Therefore, to do the excision in a uniform manner, for all clusters, regions of 70 kpc radius centered on the main brightness peak were masked, and the resulting fluxes and luminosities were multiplied by 1.06 to account for the flux inside the masked region, assuming an average β model for the cluster X-ray brightness. Therefore, subtracting the corrected from the uncorrected X-ray luminosity gives the amount of cool-core correction applied by M98. We use the same amount to correct the total X-ray luminosities given by R02.

As shown in Table 2, applying the correction for cool-core effect does not change the scatter of the relation. In fact, in the relation obtained using the total X-ray luminosity, the scatter along the M_{200} axis is 0.13 dex before the correction and 0.12 dex after that. This means that the cool core correction reduces the scatter by only 3%. As a matter of fact, for most of the clusters in the M98 sample the correction is of the same order. Moreover, it is important to stress here that even the

Table 2. The table lists the best fit values for the $L_X - M$ relations. The first three lines list the relations obtained with the M98 data: $L_X - M_{500}$ with L_X calculated in 0.1–2.4 keV energy band, within 1.4 Mpc from the cluster center and corrected for cool-core effect, $L_X - M_{200}$ (L_X before), L_X(Bol) $- M_{200}$ with the bolometric X-ray luminosity calculated within 1.4 Mpc from the cluster center and corrected for cool-core effect. The last two lines list the correlations obtained with the total X-ray luminosity taken from R02 corrected and uncorrected for the cool-core effect respectively. The table lists three estimations of the scatter for each relation: σ is the orthogonal scatter of the $A - B$ relation, σ_A is the scatter in the A variable and σ_B is the scatter in the B variable. All the scatter values in the table are expressed in dex and all the errors are given at the 95% confidence level.

	α	β	σ	σ_B	σ_A
L_X(0.1−2.4 keV) − M_{500} (1.4 Mpc)	1.30 ± 0.12	−0.61 ± 0.10	0.10	0.11	0.20
L_X(0.1−2.4 keV) − M_{200} (1.4 Mpc)	1.33 ± 0.13	−0.91 ± 0.14	0.10	0.11	0.14
L_X(Bol) − M_{200} (1.4 Mpc)	2.01 ± 0.20	−1.35 ± 0.22	0.10	0.11	0.20
$L_{X,\,\mathrm{corr}}$(0.1−2.4 keV) − M_{200} (tot)	1.55 ± 0.19	−1.15 ± 0.20	0.11	0.12	0.17
$L_{X,\,\mathrm{uncorr}}$(0.1−2.4 keV) − M_{200} (tot)	1.58 ± 0.23	−1.15 ± 0.24	0.11	0.13	0.18

scatter of the $L_X - M$ relation obtained in this analysis with the uncorrected X-ray luminosity is much lower than the dispersion obtained with the the RASS-SDSS galaxy cluster catalog, which is a sample more than 3 times as large. In fact, the sample of M98 covers a very small range in mass and X-ray luminosity, only one order of magnitude in both variables. Hence, the statistical significance of the result is very low and it cannot be taken as a robust result, since it does not seem to represent the behavior of the $L_X - M$ relation obtained with much larger samples of clusters. Therefore, it is not clear if the presence of a large number of cool core clusters in our sample and in the sample of R02 could really contribute to the scatter in the $L_X - M$ relation. As a last point, we note that replacing the L_X calculated in the ROSAT energy band (0.1–2.4 keV) with the bolometric luminosity does not change at all the scatter in the relation. The bolometric X-ray luminosity is taken from M98. The slope of the $L_{X,\,\mathrm{bol}} - M_{200}$ relation is steeper than the $L_{X,\,\mathrm{ROSAT}} - M_{200}$ relation, as expected (the bolometric correction is smaller for the faint X-ray clusters than in the bright ones), while the orthogonal scatter and the dispersion along the M_{200} axis are unchanged. The scatter in L_X changes because of the slope, since $\sigma_B \sim \alpha \times \sigma_A$. In conclusion, to really understand the nature of the scatter in the $L_X - M$ relation and its connection to the cool core correction to the X-ray luminosity, the analysis should be done with a cluster sample much larger than the M98 sample and with a much more extended range in mass and L_X.

Finally, let us consider the possibility that the better behavior of the optical luminosity as a mass predictor, in comparison with L_X could be due to the fact that L_{op} is calculated within the same aperture as the mass (r_{500} and r_{200}) while L_X is estimated within a variable aperture. R02 calculate the mass within r_{200} and yet obtain the same scatter we observe in the $L_X - M$ relation. Therefore, the scatter in the $L_X - M$ relation does not seem to depend on the limiting radius used to compute L_X. The observed dispersion in the $L_X - M$ relation is most probably due to variations in the compactness of clusters. The dichotomy of compact cD clusters (often associated with the cooling flow signatures) and less compact non-cD clusters is more pronounced than just an excess of X-ray flux in the central 70 kpc region (as used in the above correction for cooling flows). This is indicated for example by the work of Jones & Forman (1984) and Ota & Mitsuda (2002) and has been discussed by Fabian et al. (1994). Because of the strong quadratic dependence of the X-ray emission on the gas density this variation in compactness is observed in an amplified way in the X-ray luminosity variation.

The most important and interesting conclusion of this analysis is that both the optical and the X-ray luminosity show extremely good relations with the cluster mass within r_{500} and r_{200}. The $L_{op} - M$ relation is tighter than the $L_X - M$ relation and the optical luminosity can be used as mass estimator with an average accuracy of 40%. The X-ray luminosity can predict the cluster mass with an accuracy of 55% on average. The presence of a large number of cool core clusters in our sample does not seem to be the cause of the larger scatter in the $L_X - M$ relation than in the $L_{op} - M$ relation.

Our result is in excellent agreement with that obtained by Lin et al. (2003), who used the K-band luminosity as a mass predictor, and found an average accuracy of 45%.

On the basis of these results the scatter of the $L_{op} - L_X$ relation has a natural explanation. As shown in Table 1 the values of all the estimated scatter values are very close to the values calculated for the $L_X - M$ relation. Therefore, we conclude that the scatter in the $L_{op} - L_X$ relation (Fig. 9) is mostly derived from the scatter in the $L_X - M$ relation.

5.3. The mass-to-light ratio

To conclude the analysis of the relation between the optical luminosity and the cluster mass, we consider the mass-to-light ratio, M/L, as a function of the cluster mass.

Previous analyses have shown that, in general, M/L increases with the cluster mass. Assuming a relation of the type $M/L \propto M^{\alpha}$, and adopting the usual scaling relations between mass and X-ray temperature or velocity dispersion, when needed, most authors have found $\alpha \simeq 0.25 \pm 0.1$, in both optical and near-infrared bands, and over a very large mass range, from loose groups to rich clusters of galaxies (Adami et al. 1998; Bahcall & Comerford 2002; Girardi et al. 2002; Lin et al. 2003, 2004; Rines et al. 2004; Ramella et al. 2004; see however Kochanek et al. 2003, for a discordant result).

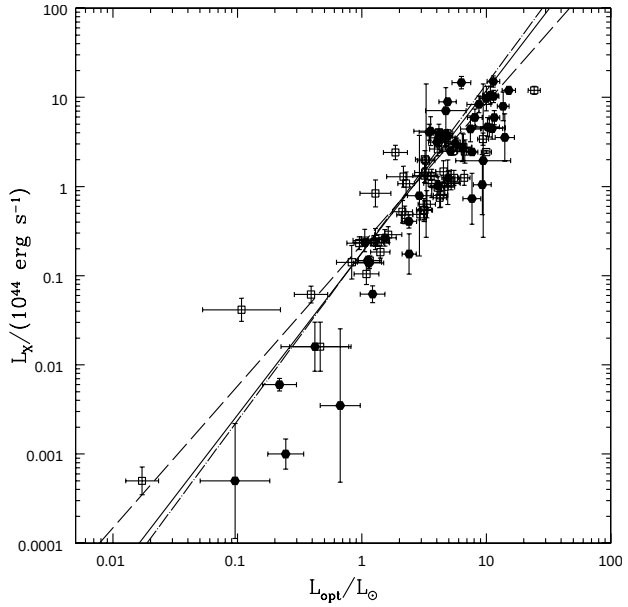

Fig. 9. $L_{op} - L_X$ relation. The optical luminosities are calculated within r_{500}. The empty squares in the figure are clusters with mass estimated from the dynamical analysis of the Sloan spectroscopic data. The filled points are systems with r_{500} estimated from mass obtained with the $M - T_X$ relation. The dot-dashed line is the best fit line obtained for the O sample. The dashed line is the best fit line for the X sample and the solid line is the result obtained from the E sample.

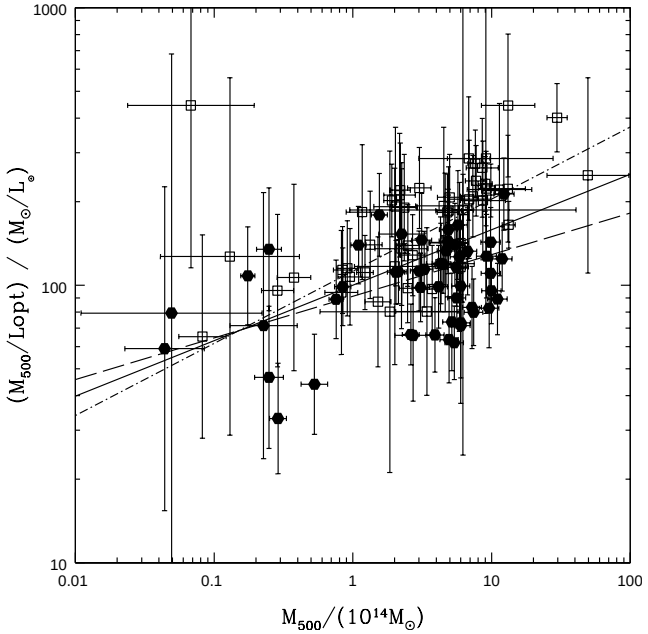

Fig. 10. $M/L - M$ relation. The mass-to-light ratio is calculated in the *i* Sloan band. Masses and optical luminosities are calculated within r_{500}. The empty squares in the figure are clusters with masses estimated from the dynamical analysis of the Sloan spectroscopic data. The filled points are systems with masses estimated from the $M - T_X$ relation. The dot-dashed line is the best fit line obtained for the O sample. The dashed line is the best fit line for the X sample and the solid line is the result obtained from the E sample.

Our result is shown in Fig. 10, where we plot M/L (in the *i* band) calculated within r_{500}, versus M_{500}. An increase of the mass-to-light ratio with the mass is clearly visible. The existence of a correlation is confirmed by a Spearman correlation analysis (the correlation cofficient is 0.42, corresponding to a probability of only 7×10^{-6} that the two quantities are not correlated). In order to quantify the relation between mass and luminosity, we prefer to use the $L_{op} - M$ relation directly. In fact, since M/L is defined as a function of M and L, it is not correct to search for the best-fitting relation of M/L versus M or L. The $L_{op} - M$ relation implies $M/L \propto M^{0.2\pm0.08}$. Therefore the mass-to-light ratio of galaxy clusters is not constant, but (slightly) increases with the cluster mass. Our relation (derived in the *i* band) is clearly consistent with the relations found in other bands (*B*-band, Girardi et al. 2002; *V*-band, Bahcall & Comerford 2002; *R*-band, Adami et al. 1998; *K*-band, Lin et al. 2003, 2004; Rines et al. 2004; Ramella et al. 2004), and, as a matter of fact, we checked that similar M/L vs. M dependencies are found in the other bands of the SDSS.

The fact that the M/L vs. M relation is wavelength independent clearly rules out the explanation provided by Bahcall & Comerford (2002), namely that more massive clusters have a larger M/L because their galaxies contain older stellar populations, on average, than galaxies that are members of less massive clusters. The most likely explanation for this M/L variation with M has been provided by Lin et al. (2003): the overall star formation efficiency must be a decreasing function of the cluster mass.

5.4. Correlations of the optical and the X-ray luminosities with the cluster temperature and velocity dispersion.

The X-ray temperature, T_X, and the cluster velocity dispersion, σ_V, have both been used as key measures of cluster properties and in particular of the cluster mass. Given the excellent correlation of the optical luminosity with the mass, L_{op} should also correlate with, and have predictive power for, these two quantities. Table 3 summarizes the results obtained by correlating the optical luminosity in the *i* Sloan band within r_{500} and r_{200} with T_X and σ_V. As shown by Figs. 11 and 12, the optical luminosity correlates very well with both T_X and σ_V with an orthogonal scatter of 22% and 15% respectevely. Moreover, L_{op} can predict T_X with 23–28% accuracy and σ_V with 17–23% accuracy. Table 3 contains the best fit results also for the $L_X - T_X$ and $L_X - \sigma_V$ relations. The best fit values of the relations are in perfect agreement with the results of Ortiz-Gil et al. (2004), who used a subsample of the REFLEX sample.

The X-ray luminosities defined in the REFLEX catalog are calculated with the same method as used for the RASS-SDSS cluster catalog. The orthogonal scatter of the $L_X - \sigma_V$ relation (17%) is also in good agreement with Ortiz-Gil et al. (2004), if we consider the relation obtained in that work using only clusters with accurate σ_V estimation. As shown by Figs. 13 and 14, the X-ray luminosity also shows a tight correlation with both quantities and the scatter of the best fit line (25–30% accuracy in the T_X prediction and 20–23% accuracy in the σ_V prediction) is very close to the results obtained for the optical

Table 3. The table lists the best fit values for several correlations: $L_{op} - \sigma_V$, $L_X - \sigma_V$, $L_{op} - T_X$ and $L_X - T_X$. The table shows the results obtained with the dynamical analysis performed for the red members of the systems ("red m." in the table) and for the complete cluster membership ("all m". in the table). The table lists three estimations of the scatter for each relation: σ is the orthogonal scatter of the $A - B$ relation, σ_A is the scatter in the A variable and σ_B is the scatter in the B variable. All the scatter values in the table are expressed in dex and all the errors are given at the 95% confidence level.

		α	β	σ	σ_B	σ_A
$L_{op} - \sigma_V$ (r_{500})	red m.	2.26 ± 0.13	−6.04 ± 0.38	0.06	0.07	0.16
	all m.	2.36 ± 0.13	−6.29 ± 0.37	0.06	0.07	0.17
$L_{op} - \sigma_V$ (r_{200})	red m.	2.33 ± 0.16	−6.02 ± 0.45	0.06	0.08	0.17
	all m.	2.33 ± 0.15	−6.05 ± 0.42	0.07	0.09	0.17
$L_X - \sigma_V$	red m.	3.60 ± 0.29	−10.22 ± 0.80	0.07	0.09	0.38
	all m.	3.68 ± 0.25	−10.53 ± 0.80	0.08	0.08	0.40
$L_{op} - T_X$	r_{500}	1.68 ± 0.08	−0.50 ± 0.06	0.08	0.09	0.15
	r_{200}	1.66 ± 0.09	−0.41 ± 0.07	0.09	0.12	0.17
$L_X - T_X$		3.06 ± 0.10	−1.77 ± 0.07	0.07	0.10	0.29

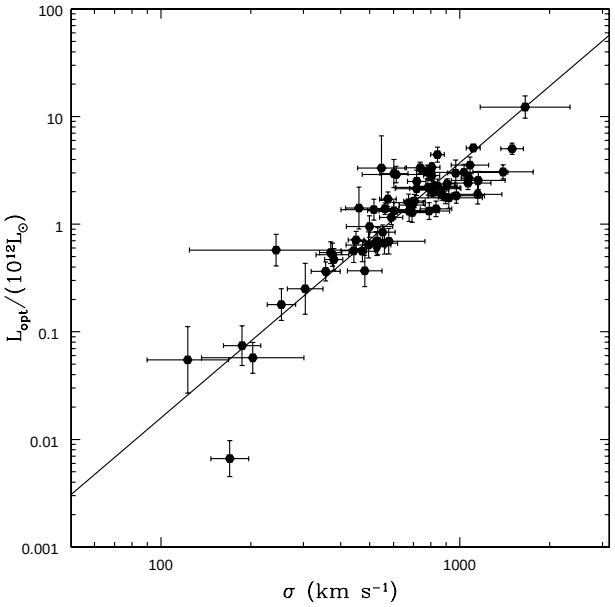

Fig. 11. $L_{op} - \sigma_V$ relation. The optical luminosities are calculated within r_{500}. The best-fit line is also shown.

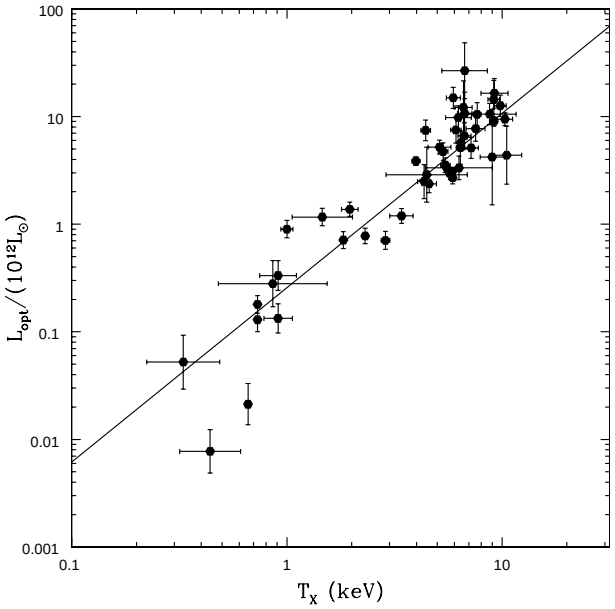

Fig. 12. $L_{op} - T_X$ relation. The optical luminosities are calculated within r_{500}. The best-fit line is also shown.

luminosity. L_{op} is a slightly better predictor than L_X with a 5% difference in the scatter. Note that, while L_{op} is a much better predictor of the cluster mass in comparison to L_X, optical and X-ray luminosities can predict approximately with the same accuracy (20%) the intracluster temperature and the galaxy velocity dispersion. This different behavior of the scatter in the relations involving L_X could be due to the dependence of the X-ray luminosity and temperature on the cluster compactness. The cluster temperature is proportional to M/R, where M is the cluster mass and R is a characteristic radius of the system. Thus, T_X is related to mass with a weighting for compactness. As explained in the previous paragraph, L_X is proportional to the gas density squared. This implies that, at given mass, a compact cluster is much more X-ray bright than a less compact one. Therefore, the cluster compactness could enter the $L_X - M$ relation as a third parameter, explaining the observed large scatter. However, since both L_X and T_X have a similar dependence on the compactness, the dispersion in the $L_X - T_X$ relation would not be affected. This would explain why L_{op} is a better estimator of the cluster mass than L_X, while optical and X-ray luminosities have similar scatter in their relation with T_X and σ_V.

As in the case of the luminosity-mass relation, we investigate in more details the luminosity-temperature relation to understand which of the two luminosities is the best predictor of the other cluster parameters. We use the X-ray luminosity

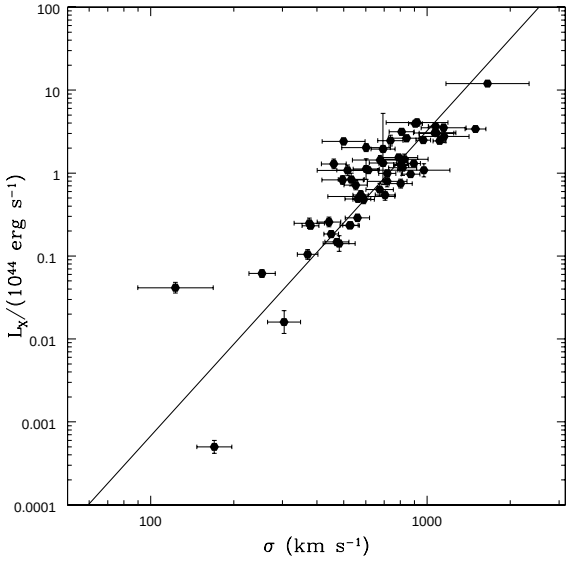

Fig. 13. $L_X - \sigma_V$ relation. The best-fit line is also shown.

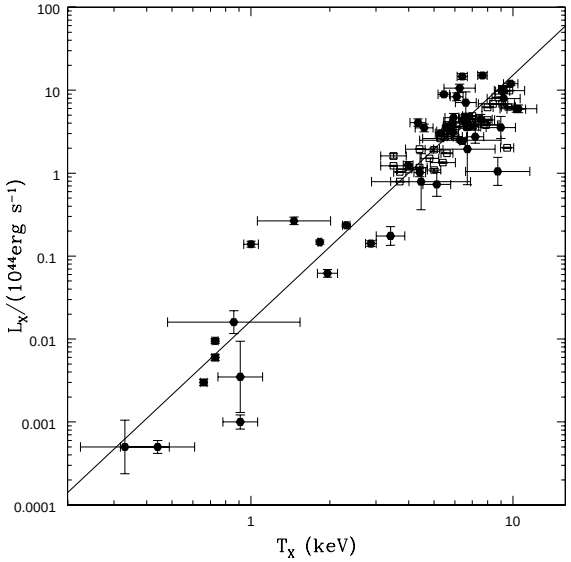

Fig. 14. $L_X - T_X$ relation. The filled points are the RASS-SDSS clusters with known ASCA temperature and the empty squares are the clusters of M98. The best-fit line is also shown.

(calculated within 1.4 Mpc) and the temperature from M98 to check the influence of the cool-core correction in the $L_X - T_X$ relation (Fig. 15). As shown in Table 4, using the cool-core-corrected X-ray luminosity and temperature lowers the scatter in the T_X variable by 6%. We analyse the relation using also the total X-ray luminosity of R02 with and without the cool-core correction (panel *c* and *d*, respectively, in Fig. 15), as we did for the $L_X - M$ relation. In both cases, using the total L_X not only affects the slope of the relation, but also increases the scatter by 6% in comparison to the relations obtained using L_X values from M98.

The slope of the $L_X - T_X$ relation obtained applying the cool-core-correction to the total luminosity and temperature is in perfect agreement with the results obtained previously with the subsample of "uncorrected" RASS-SDSS clusters, while the scatter is lower by 5%. Such a reduction of the

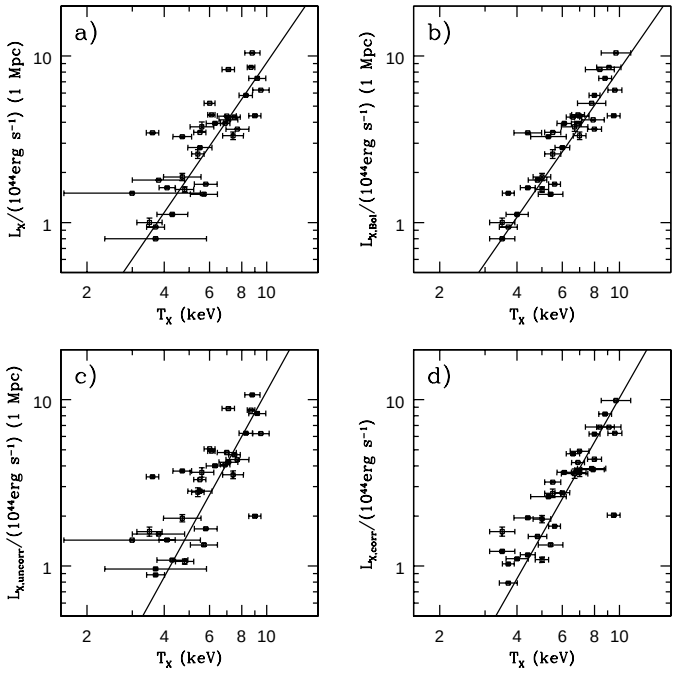

Fig. 15. The same as in Fig. 8 but for the $L_X - T_X$ relation.

scatter makes the X-ray luminosity a predictor of the X-ray temperature that is at least as good as the optical luminosity. However, a similar scatter reduction could in principle be expected for the $L_{op} - T_X$ relation also, since the cool-core correction affects X-ray temperatures more strongly than X-ray luminosities (M98). Unfortunately only few of the clusters of the M98 sample are in the sky region covered by the SDSS. Thus, we cannot check this possibility directly.

6. Summary and conclusions

We used the RASS-SDSS galaxy cluster sample to compare the quality of the optical and X-ray luminosity as predictors of other cluster properties such as the mass within r_{500} and r_{200}, the velocity dispersion and the ICM temperature. The optical luminosity turns out to be a better predictor of the cluster mass than the X-ray luminosity. The knowledge of L_{op} make it possible to estimate the cluster mass with an average accuracy of 40%, while L_X can be used to predict the mass with an average accuracy of 55%. We investigated the nature of the scatter of the $L_X - M$ relation using a sample of clusters with X-ray luminosity corrected for the effect of a cool core at the center of the system. We concluded that this kind of effect can affect the scatter of the relation by at most 3% and, thus, it cannot explain the dispersion in the observed $L_X - M$ relation, which is probably related to the variation in the compactness of the galaxy clusters. We conclude that a cluster optical luminosity is a better estimator of its mass than its X-ray luminosity. The optical luminosity is clearly a very useful and rather cheap estimator (in terms of observational resources required) given that it can be determined from ground-based photometric data only.

We also analysed the relations of the optical and X-ray luminosities with cluster velocity dispersions and X-ray temperatures. We found that both luminosities are strongly correlated

Table 4. The table lists the best fit values for the $L_X - T_X$ relations. The first two lines list the relations obtained with the M98 data: $L_X - T_X$ with L_X calculated in the 0.1–2.4 keV energy band, within 1 Mpc from the cluster center and the temperature uncorrected for cool core effect, $L_X - T_X$ with the X-ray luminosity and temperature corrected for cool core effect. The last two lines list the correlations obtained with the total X-ray luminosity taken from R02 and the temperature of M98 corrected and uncorrected for cool core effect respectively. All the scatter values in the table are expressed in dex and have the same meaning as in the previous table.

	α	β	σ	σ_A	σ_B
$L_X(0.1-2.4$ keV$) - T_X$ (1.4 Mpc, uncorr)	2.59 ± 0.38	-1.48 ± 0.31	0.06	0.07	0.18
$L_X(0.1-2.4$ keV$) - T_X$ (1.4 Mpc, corr)	2.26 ± 0.19	-1.30 ± 0.15	0.04	0.05	0.11
$L_{X,\,corr}(0.1-2.4$ keV$) - T_X$ (tot, uncorr)	3.30 ± 0.67	-2.06 ± 0.54	0.06	0.09	0.24
$L_{X,\,uncorr}(0.1-2.4$ keV$) - T_X$ (tot, corr)	2.80 ± 0.38	-1.75 ± 0.30	0.05	0.07	0.15

with these cluster properties, and can be used to predict them with an average accuracy of 20%. Using a sample of clusters with L_X and T_X corrected for the cool core effect, we find that the scatter in the $L_X - T_X$ relation is decreased by 5%. Such a decrease is almost exclusively due to the correction applied to the X-ray temperature, since the cool-core correction has a negligible effect on the X-ray luminosity. Therefore, we expect a similar decrease of the scatter of the $L_{op} - T_X$ relation, when the X-ray temperatures are corrected for the same cool-core effect. Unfortunately we cannot verify this expectation from our sample, since we lack the information to apply the cool-core correction to the clusters with known L_{op}. We conclude that L_{op} and L_X can be used to predict the ICM temperature and the cluster velocity dispersion, at a similar level of accuracy.

The most important conclusion from our analysis is that the optical luminosity is a key measure of the fundamental properties of a galaxy cluster, such as its mass, velocity dispersion, and temperature. In this respect, the optical luminosity performs even better than the X-ray luminosity, which suggests that the mass distribution of a cluster is better traced by cluster galaxies than by intracluster gas (see, e.g., the discussion in Biviano & Girardi 2003). The poorer performance of L_X as a cluster mass predictor, relative to L_{op}, is probably related to the variation in the compactness of the galaxy clusters.

Our conclusion is clearly in agreement with Lin et al.'s (2003) result, namely that the K-band luminosity is a good estimator of the cluster mass. On the other hand, our conclusion is at odds with the generally accepted view that the main physical properties of a cluster are more easily revealed in the X-ray than in the optical (e.g. Donahue et al. 2002). Such a view was established at an epoch when the lack of optical wide field surveys precluded a reliable determination of the optical luminosities of a large sample of clusters. With the advent of the Sloan Digital Sky survey, this problem is now overcome, and L_{op} can now be used to infer the fundamental physical properties of the many clusters being discovered within large optical surveys with improved cluster finding techniques (such as, e.g., the Red-Sequence Cluster Survey, Barrientos et al. 2003). In this context L_{op} becomes a very powerful means to do cosmological studies with galaxy clusters without the need of optical or X-ray spectroscopy.

Finally, we showed that the relation between mass and luminosity implies an increasing mass-to-light ratio, M/L, with increasing cluster mass. The dependence we found is in excellent agreement with previous results (Adami et al. 1998; Bahcall & Comerford 2002; Girardi et al. 2002; Lin et al. 2003, 2004; Rines et al. 2004; Ramella et al. 2004), and confirms the achromaticity of the effect. Hence, the effect cannot be explained by the different ages of the stellar populations of the galaxies in clusters of different masses (Bahcall & Comerford 2002), but, rather, seems to indicate that the star formation efficiency decreases as the cluster mass increases (Lin et al. 2003).

The results obtained in this paper are applicable to nearby clusters since the RASS-SDSS galaxy cluster catalog comprises only X-ray clusters at $z \leq 0.3$. It would be very interesting to conduct the same analysis for a sample of high redshift clusters to study the evolution of the analysed relations and to compare again the quality of L_{op} and L_X as predictors of the other cluster properties.

The analysis conducted in this paper is based on a sample of clusters all detected in the X-ray, 90% of which are taken from X-ray-selected galaxy cluster catalogs. It seems that optically bright clusters exist which are faint in the X-ray (Donahue et al. 2002). Hence, the selection criteria of the RASS-SDSS galaxy cluster catalog could in principle affect our results (see, e.g., Gilbank et al. 2004). To check how the selection criteria affect the correlations studied in this paper, we plan to repeat the same analyses for a sample of optically-selected clusters.

Acknowledgements. Funding for the creation and distribution of the SDSS Archive has been provided by the Alfred P. Sloan Foundation, the Participating Institutions, the National Aeronautics and Space Administration, the National Science Foundation, the US Department of Energy, the Japanese Monbukagakusho, and the Max Planck Society. The SDSS web site is `http://www.sdss.org/`. The SDSS is managed by the Astrophysical Research Consortium (ARC) for the Participating Institutions. The Participating Institutions are The University of Chicago, Fermilab, the Institute for Advanced Study, the Japan Participation Group, The Johns Hopkins University, Los Alamos National Laboratory, the Max-Planck-Institute for Astronomy (MPIA), the Max-Planck-Institute for Astrophysics (MPA), New Mexico State University, University of Pittsburgh, Princeton University, the United States Naval Observatory, and the University of Washington.

Appendix A: Correlation of L_{op} in the Sloan *g*, *r* and *z* bands with the cluster parameters

We list in the table all the results obtained using the optical luminosity calculated in the g, r and z SDSS Sloan bands. The structure of the three tables in this appendix is similar to the tables in the text of the paper. For each analysed correlation we

	g band					*r* band					z band				
						$L_{\rm op} - M_{500}$									
	α	β	σ	$\sigma_{M_{500}}$	$\sigma_{L_{\rm op}}$	α	β	σ	$\sigma_{M_{500}}$	$\sigma_{L_{\rm op}}$	α	β	σ	$\sigma_{M_{500}}$	$\sigma_{L_{\rm op}}$
O	0.81 ± 0.05	−0.30 ± 0.03	0.12	0.18	0.16	0.80 ± 0.04	−0.22 ± 0.03	0.11	0.16	0.16	0.91 ± 0.04	0.00 ± 0.03	0.13	0.18	0.19
X	1.06 ± 0.06	−0.26 ± 0.04	0.14	0.22	0.17	1.08 ± 0.06	−0.18 ± 0.04	0.12	0.18	0.16	1.04 ± 0.05	0.07 ± 0.04	0.10	0.16	0.14
E	0.90 ± 0.04	−0.31 ± 0.03	0.15	0.21	0.20	0.92 ± 0.04	−0.24 ± 0.03	0.13	0.20	0.20	0.79 ± 0.04	0.01 ± 0.03	0.10	0.16	0.15
						$L_{\rm op} - M_{200}$									
	α	β	σ	$\sigma_{M_{200}}$	$\sigma_{L_{\rm op}}$	α	β	σ	$\sigma_{M_{200}}$	$\sigma_{L_{\rm op}}$	α	β	σ	$\sigma_{M_{200}}$	$\sigma_{L_{\rm op}}$
O	0.81 ± 0.04	−0.27 ± 0.04	0.13	0.18	0.15	0.80 ± 0.04	−0.18 ± 0.04	0.12	0.17	0.14	0.79 ± 0.04	0.06 ± 0.04	0.12	0.16	0.14
X	1.08 ± 0.08	−0.25 ± 0.06	0.14	0.23	0.20	1.05 ± 0.07	−0.17 ± 0.06	0.12	0.20	0.17	1.02 ± 0.06	0.08 ± 0.06	0.10	0.18	0.16
E	0.94 ± 0.05	−0.31 ± 0.04	0.16	0.23	0.20	0.94 ± 0.04	−0.24 ± 0.04	0.15	0.21	0.19	0.93 ± 0.04	0.00 ± 0.04	0.14	0.21	0.19
						$L_{\rm op} - L_{\rm X}\ (r_{500})$									
	α	β	σ	$\sigma_{L_{\rm X}}$	$\sigma_{L_{\rm op}}$	α	β	σ	$\sigma_{L_{\rm X}}$	$\sigma_{L_{\rm op}}$	α	β	σ	$\sigma_{L_{\rm X}}$	$\sigma_{L_{\rm op}}$
O	0.62 ± 0.05	0.21 ± 0.02	0.15	0.31	0.18	0.63 ± 0.04	0.28 ± 0.02	0.14	0.29	0.17	0.63 ± 0.04	0.52 ± 0.02	0.13	0.28	0.16
X	0.51 ± 0.03	0.19 ± 0.03	0.19	0.38	0.20	0.53 ± 0.03	0.27 ± 0.03	0.18	0.33	0.20	0.52 ± 0.03	0.49 ± 0.03	0.15	0.32	0.18
E	0.55 ± 0.03	0.21 ± 0.02	0.17	0.35	0.19	0.56 ± 0.03	0.28 ± 0.02	0.15	0.32	0.18	0.56 ± 0.03	0.51 ± 0.02	0.14	0.31	0.17
						$L_{\rm op} - L_{\rm X}\ (r_{200})$									
	α	β	σ	$\sigma_{L_{\rm X}}$	$\sigma_{L_{\rm op}}$	α	β	σ	$\sigma_{L_{\rm X}}$	$\sigma_{L_{\rm op}}$	α	β	σ	$\sigma_{L_{\rm X}}$	$\sigma_{L_{\rm op}}$
O	0.63 ± 0.05	0.37 ± 0.02	0.17	0.28	0.18	0.64 ± 0.04	0.45 ± 0.02	0.15	0.26	0.17	0.64 ± 0.04	0.68 ± 0.02	0.15	0.25	0.16
X	0.54 ± 0.04	0.37 ± 0.03	0.22	0.39	0.23	0.54 ± 0.04	0.44 ± 0.03	0.20	0.36	0.22	0.54 ± 0.04	0.67 ± 0.03	0.19	0.35	0.21
E	0.57 ± 0.03	0.37 ± 0.02	0.19	0.34	0.19	0.58 ± 0.03	0.45 ± 0.02	0.17	0.31	0.19	0.58 ± 0.03	0.68 ± 0.02	0.16	0.30	0.18
						$L_{\rm op} - r_{500}$									
	α	β	σ	$\sigma_{r_{500}}$	$\sigma_{L_{\rm op}}$	α	β	σ	$\sigma_{r_{500}}$	$\sigma_{L_{\rm op}}$	α	β	σ	$\sigma_{r_{500}}$	$\sigma_{L_{\rm op}}$
O	2.24 ± 0.15	0.11 ± 0.02	0.06	0.06	0.16	2.24 ± 0.14	0.19 ± 0.02	0.05	0.06	0.15	2.27 ± 0.14	0.42 ± 0.02	0.05	0.05	0.15
X	2.95 ± 0.16	0.23 ± 0.03	0.06	0.07	0.17	2.97 ± 0.16	0.31 ± 0.02	0.05	0.06	0.15	2.93 ± 0.15	0.54 ± 0.02	0.04	0.05	0.14
E	2.44 ± 0.12	0.14 ± 0.02	0.07	0.09	0.18	2.50 ± 0.12	0.23 ± 0.02	0.06	0.08	0.18	2.50 ± 0.12	0.47 ± 0.02	0.06	0.07	0.17
						$L_{\rm op} - r_{200}$									
	α	β	σ	$\sigma_{r_{200}}$	$\sigma_{L_{\rm op}}$	α	β	σ	$\sigma_{r_{200}}$	$\sigma_{L_{\rm op}}$	α	β	σ	$\sigma_{r_{200}}$	$\sigma_{L_{\rm op}}$
O	2.27 ± 0.15	−0.14 ± 0.04	0.07	0.07	0.15	2.24 ± 0.13	−0.06 ± 0.04	0.06	0.07	0.14	2.26 ± 0.13	0.17 ± 0.04	0.06	0.06	0.14
X	2.27 ± 0.15	−0.14 ± 0.04	0.07	0.07	0.15	2.85 ± 0.18	−0.05 ± 0.05	0.06	0.09	0.17	2.81 ± 0.18	0.19 ± 0.05	0.06	0.08	0.16
E	2.44 ± 0.13	−0.14 ± 0.04	0.08	0.11	0.18	2.47 ± 0.12	−0.06 ± 0.04	0.07	0.09	0.17	2.45 ± 0.12	0.18 ± 0.04	0.07	0.09	0.17
						$L_{\rm op} - \sigma_V$									
	α	β	σ	σ_{σ_V}	$\sigma_{L_{\rm op}}$	α	β	σ	σ_{σ_V}	$\sigma_{L_{\rm op}}$	α	β	σ	σ_{σ_V}	$\sigma_{L_{\rm op}}$
r_{500}	2.37 ± 0.15	−6.54 ± 0.41	0.06	0.07	0.18	2.35 ± 0.14	−6.39 ± 0.39	0.06	0.07	0.17	2.35 ± 0.13	−6.17 ± 0.38	0.06	0.06	0.17
r_{200}	2.38 ± 0.16	−6.39 ± 0.46	0.07	0.09	0.18	2.29 ± 0.15	−6.06 ± 0.41	0.07	0.08	0.16	2.29 ± 0.15	−5.84 ± 0.42	0.07	0.08	0.17
						$L_{\rm op} - T_{\rm X}$									
	α	β	σ	$\sigma_{T_{\rm X}}$	$\sigma_{L_{\rm op}}$	α	β	σ	$\sigma_{T_{\rm X}}$	$\sigma_{L_{\rm op}}$	α	β	σ	$\sigma_{T_{\rm X}}$	$\sigma_{L_{\rm op}}$
r_{500}	1.66 ± 0.08	−0.82 ± 0.06	0.10	0.09	0.17	1.69 ± 0.08	−0.77 ± 0.06	0.09	0.08	0.16	1.65 ± 0.08	−0.50 ± 0.06	0.08	0.08	0.14
r_{200}	1.62 ± 0.10	−0.59 ± 0.08	0.12	0.13	0.20	1.64 ± 0.09	−0.53 ± 0.07	0.10	0.12	0.17	1.62 ± 0.10	−0.28 ± 0.07	0.09	0.12	0.16

report the values of the best fit parameters plus the error at 95% confidence level and three values of the scatter: the orthogonal scatter of the relation and the scatters in both variables (in the logarithmic space). All the scatter values are expressed in dex. All the results are obtained using the mass and velocity dispersion derived from the dynamical analysis of the red members of the clusters.

References

Akritas, M. G., & Bershady, M. A. 1996, ApJ, 470, 706
Abazajian, K., Adelman, J., Agueros, M., et al. 2003, AJ, 126, 2081 (Data Release One)
Adami, C., Mazure, A., Biviano, A., Katgert, P., & Rhee, G. 1998, A&A, 331, 493
Bahcall, N. A., & Comerford, J. M. 2002, ApJ, 565, L5
Barrientos, F., Gladders, M., Yee, H., et al. 2003, Messenger, 112, 40
Beers, T. C., Geller, M. J., Huchra, J. P., et al. 1984, ApJ, 283, 33
Beers, T. C., Flynn, K., & Gebhardt, K. 1990, AJ, 100, 32
Biviano, A., & Girardi, M. 2003, ApJ, 585, 205
Biviano, A., & Katgert, P. 2003, Ap&SS, 285, 25
Biviano, A., Katgert, P., Mazure, A., et al. 1997, A&A, 321, 84
Biviano, A., Katgert, P., Thomas, T., et al. 2002, A&A, 387, 8
Blanton, M. R., Lupton, R. H., Maley, F. M., et al. 2003, AJ, 125, 2276 (Tiling Algorithm)
Böhringer, H., Voges, W., Huchra, J. P., et al. 2000, ApJS, 129, 435
Böhringer, H., Schuecker, P., Guzzo, L., et al. 2001, A&A, 369, 826
Böhringer, H., Collins, C. A., Guzzo, L., et al. 2002, ApJ, 566, 93
Borgani, S., Murante, G., Springel, V., et al. 2004, MNRAS, 348, 1078
Carlberg, R. G., Yee, H. K., & Ellingson, E. 1997a, ApJ, 478, 462
Carlberg, R. G., Yee, H. K. C., Ellingson, E., et al. 1997b, ApJ, 476, L7
den Hartog, R., & Katgert, P. 1996, MNRAS, 279, 349
Dolag, K., Bartelmann, M., Perrotta, F., et al. 2004, A&A, 416, 853
Donahue, M., Scharf, C. A., Mack, J., et al. 2002, ApJ, 569, 689
Eisenstein, D. J., Annis, J., Gunn, J. E., et al. 2001, AJ, 122, 2267
Ettori, S., Borgani, S., Moscardini, L., et al. 2004, MNRAS, 322
Evrard August, E., Metzler Christopher, A., & Navarro Julio, F. 1996, ApJ, 469, 494
Fabian, A. C., Crawford, C. S., Edge, A. C., & Mushotzky, R. F. 1994, MNRAS, 267, 779
Finoguenov, A., Reiprich, T., & Böhringer, H. 2001, A&A, 368, 749 (F01)
Fukugita, M., Ichikawa, T., & Gunn, J. E. 1996, AJ, 111, 1748
Fujita, Y., & Takahara, F. 1999, ApJ, 519, 55F
Gilbank, D. G., Bower, R. G., Castander, F. J., & Ziegler, B. L. 2004, MNRAS, 348, 551
Girardi, M., Biviano, A., Giuricin, G., et al. 1993, ApJ, 404, 38
Girardi, M., Biviano, A., Giuricin, G., et al. 1995, ApJ, 438, 527
Girardi, M., Giuricin, G., Mardirossian, F., Mezzetti, M., et al. 1998, ApJ, 505, 74
Girardi, M., Borgani, S., Giuricin, G., et al. 2000, ApJ, 530, 62
Girardi, M., Manzato, P., Mezzetti, M., et al. 2002, ApJ, 569, 720
Gunn, J. E., Carr, M. A., Rockosi, C. M., et al. 1998, AJ, 116, 3040 (SDSS Camera)
den Hartog, R., & Katgert, P. 1996, MNRAS, 279, 349
Hogg, D.W., Finkbeiner, D. P., Schlegel, D. J., & Gunn, J. E. 2001, AJ, 122, 2129
Horner, D. 2001, Ph.D. Thesis, University of Maryland
Jones, C., & Forman, W. 1984, ApJ, 276, 38
Katgert, P., Biviano, A., & Mazure, A. 2004, ApJ, 600, 657
Kochanek, C. S., White, M., Huchra, J., et al. 2003, ApJ, 585, 161
Lin, Y.-T., Mohr, J. J., & Stanford, S. A. 2003, ApJ, 591, 749
Lin, Y.-T., Mohr, J. J., & Stanford, S. A. 2004, ApJ, 610, 745
Lupton, R. H., Gunn, J. E., & Szalay, A. S. 1999, AJ, 118, 1406
Lupton, R., Gunn, J. E., Ivezić, Z., et al. 2001, in Astronomical Data Analysis Software and Systems X, ed. F. R. Harnden, Jr., F. A. Primini, & H. E. Payne (San Francisco: ASP), ASP Conf. Ser., 238, 269 [arXiv:astro-ph/0101420]
Markevitch, M. 1998, ApJ, 504, 27 (M98)
Moss, C., & Dickens, R. J. 1977, MNRAS, 178, 701
Mulchaey, J. S., Davis, D. S., Mushotzky, R. F., & Burstein, D. 2003, ApJS, 145, 39
Navarro, J. F., Frenk, C. S., & White, S. D. M. 1996, ApJ, 462, 563
Navarro, J. F., Frenk, C. S., & White, S. D. M. 1997, ApJ, 490, 493
Oort, J. H. 1958, in La structure et l'evolution de l'univers, ed. R. Stoopes (Brussels: Solvay Inst.), 163
Ortiz-Gil, A., Guzzo, L., Schücker, P., et al. 2004, MNRAS, 348, 325
Ota, N., & Mitsuda, K. 2002, ApJ, 567, L23
Popesso, P., Böhringer, H., Brinkmann, J., et al. 2004, A&A, 423, 449
Ramella, M., Boschin, W., Geller, M. J., Mahdavi, A., & Rines, K. 2004, AJ, in press [arXiv:astro-ph/0407640]
Reiprich, T., & Böhringer, H. 2002, ApJ, 567, 740 (R02)
Rines, K., Geller, M. J., Diaferio, A., et al. 2004, AJ, 128, 1078
Rines, K., Geller, M. J., Kurtz, M. J., & Diaferio, A. 2003, AJ, 126, 2152
Retzlaff, J. 2001, XXIst Moriond Astrophysics Meeting, March 10–17, 2001 Savoie, France ed. D. M. Neumann, & J. T. T. Van
Rines, K., Geller, M. J., Diaferio, A., Kurtz, M. J., & Jarrett, T. H. 2004, AJ, 128, 1078
Schaeffer, R., Maurogordato, S., Cappi, A., et al. 1993, MNRAS, 263L, 21S
Smail, I., Ellis, R. S., Dressler, A., et al. 1997, ApJ, 479, 70S
Smith, S. 1936, ApJ, 83, 23S
Smith, J. A., Tucker, D. L., Kent, S. M., et al. 2002, AJ, 123, 2121
Stoughton, C., Lupton, R. H., Bernardi, M., et al. 2002, AJ, 123, 485
Strauss, M. A., Weinberg, D. H., Lupton, R. H., et al. 2002, AJ, 124, 1810
The, L. S., & White, S. D. M. 1986, AJ, 92, 1248
Tegmark, M., Strauss, M., Blanton, M., et al. 2004, PhRvD
Voges, W., Aschenbach, B., Boller, T., et al. 1999, A&A, 349, 389
Wu, X.-P. 2000, MNRAS, 316, 299
Yasuda, N., Fukugita, M., Narayanan, V. K., et al. 2001, AJ, 122, 1104
Yee, H. K. C., & Ellingson, E. 2003, ApJ, 585, 226
York, D. G., Adelman, J., Anderson, J. E., et al. 2000, AJ, 120, 1579
Zwicky, F. 1933, Helv. Phys. Acta, 6, 110
Zwicky, F. 1937, ApJ, 86, 127

A&A 445, 29–42 (2006)
DOI: 10.1051/0004-6361:20052954

Astronomy & Astrophysics

RASS-SDSS Galaxy cluster survey

IV. A ubiquitous dwarf galaxy population in clusters

P. Popesso[1], A. Biviano[2], H. Böhringer[1], and M. Romaniello[3]

[1] Max-Planck-Institut fur extraterrestrische Physik, 85748 Garching, Germany
e-mail: ppopesso@eso.org
[2] INAF – Osservatorio Astronomico di Trieste, via G. B. Tiepolo 11, 34131, Trieste, Italy
[3] European Southern Observatory, Karl Scharzschild Strasse 2, 85748, Germany

Received 1 March 2005 / Accepted 8 June 2005

ABSTRACT

We analyze the Luminosity Functions (LFs) of a subsample of 69 clusters from the RASS-SDSS galaxy cluster catalog. When calculated within the cluster physical sizes, given by r_{200} or r_{500}, all the cluster LFs appear to have the same shape, well fitted by a composite of two Schechter functions with a marked upturn and a steepening at the faint-end. Previously reported cluster-to-cluster variations of the LF faint-end slope are due to the use of a metric cluster aperture for computing the LF of clusters of different masses.

We determine the composite LF for early- and late-type galaxies, where the typing is based on the galaxy $u - r$ colors. The late-type LF is well fitted by a single Schechter function with a steep slope ($\alpha = -2.0$ in the r band, within r_{200}). The early-type LF instead cannot be fitted by a single Schechter function, and a composite of two Schechter functions is needed. The faint-end upturn of the global cluster LF is due to the early-type cluster galaxies. The shape of the bright-end tail of the early-type LF does not seem to depend upon the local galaxy density or the distance from the cluster center. The late-type LF shows a significant variation only very near the cluster center. On the other hand, the faint-end tail of the early-type LF shows a significant and continuous variation with the environment.

We provide evidence that the process responsible for creating the excess population of dwarf early type galaxies in clusters is a threshold process that occurs when the density exceeds ∼500 times the critical density of the Universe.

We interpret our results in the context of the "harassment" scenario, where faint early-type cluster galaxies are predicted to be the descendants of tidally-stripped late-type galaxies.

Key words. galaxies: clusters: general – galaxies: luminosity function, mass function

1. Introduction

The galaxy Luminosity Function (LF) is a fundamental tool for understanding galaxy evolution and faint galaxy populations. The shape of the cluster LF provides information on the initial formation and subsequent evolution of galaxies in clusters while the slope of the faint-end indicates how steeply the dwarf number counts rise as a function of magnitude.

Much work has been done on the cluster LF, with various groups finding differences in its shape and the faint-end slope. Different techniques have been used to measure LFs of individual clusters or to make a composite LF from individual clusters LFs (e.g. Dressler 1978; Lugger 1986, 1989; Colless 1989; Biviano et al. 1995; Lumsden et al. 1997; Valotto et al. 1997; Rauzy et al. 1998; Garilli et al. 1999; Paolillo et al. 2001; Goto et al. 2002; Yagi et al. 2002; Popesso et al. 2004a). Whether the LF of cluster galaxies is universal or not, and whether it is different from the LF of field galaxies are still debated issues. Several authors (Dressler 1978; Lumdsen et al. 1997; Valotto et al. 1997; Garilli et al. 1999; Goto et al. 2002; Christlein & Zabludoff 2003) have found significant differences between the LFs of different clusters as well as between the LFs of cluster and field galaxies, while others (Lugger 1986, 1989; Colless 1989; Rauzy et al. 1998; Trentham 1998; Paolillo et al. 2001; Andreon 2004) have concluded that the galaxy LF is universal in all environments. Another debated issue is the slope of the faint end of the LF of cluster galaxies (see, e.g., Driver et al. 1994; De Propris et al. 1995; Lobo et al. 1997; Smith et al. 1997; Phillipps et al. 1998; Boyce et al. 2001; Beijersbergen et al. 2001; Trentham et al. 2001; Sabatini et al. 2003; Cortese et al. 2003). The LF of cluster galaxies is typically observed to steepen faint-ward of $M_g \sim -18$, with power-law slopes $\alpha \sim -1.8 \pm 0.4$. This corresponds to the debated upturn of the cluster LF due to an excess of dwarf galaxies relative to the field LF. The effect may be real, and due to cluster environmental effects, but it could also be generated by systematics in the detection techniques of faint, low surface-brightness galaxies.

In Popesso et al. (2004a, hereafter Paper II) we have recently analyzed the LF of clusters from the RASS-SDSS

(ROSAT All Sky Survey – Sloan Digital Sky Survey) galaxy clusters survey down to −14 mag. We concluded that the composite cluster LF is characterized by an upturn and a clear steepening at faint magnitudes, in all SDSS photometric bands. Different methods of background subtraction were shown to lead to the same LF. The observed upturn of the LF at faint magnitudes was shown in particular not to be due to background contamination by large scale structures or multiple clusters along the same line of sight. We concluded that the observed steepening of the cluster LF is due to the presence of a real population of faint cluster galaxies.

The composite LF was well fitted by the sum of two Schechter (1976) functions. The LF at its bright-end was shown to be characterized by the classical slope of −1.25 in all photometric bands, and a decreasing M^* from the z to the g band. The LF at its faint-end was found to be much steeper than the LF at its bright-end, and characterized by a power-law slope $-2.5 \leq \alpha \leq -1.6$. The observed upturn of the LF was found to occur at −16 in the g band, and at −18.5 in the z band.

A steep mass function of galactic halos is a robust prediction of currently popular hierarchical clustering theories for the formation and evolution of cosmic structure (e.g. Kauffmann et al. 1993; Cole et al. 1994). This prediction conflicts with the flat galaxy LF measured in the field and in local groups, but is in agreement with the steep LF measured in the RASS-SDSS clusters. Two models have been proposed to explain the observed environmental dependence of the LF. According to Menci et al. (2002), merging processes are responsible for the flattening of the LF; the environmental dependence arises because mergers are more common in the field (or group) environment than in clusters, where they are inhibited by the high velocity dispersion of galaxies. According to Tully et al. (2002), instead, the LF flattening is due to inhibited star formation in dark matter halos that form late, i.e. after photoionization of the intergalactic medium has taken place. Since dark matter halos form earlier in higher density environments, a dependence of the observed LF slope on the environment is predicted. On the other hand, if reionization happens very early in the Universe, this scenario may not work (Davies et al. 2005). Other physical processes are however at work in the cluster environment, such as ram-pressure stripping (Gunn & Gott 1972) and galaxy harassment (e.g. Moore et al. 1996, 1998), which are able to fade cluster galaxies, particularly the less massive ones. Whether the outcome of these processes should be a steepening or a flattening of the LF faint-end is still unclear.

In Paper II it was also shown that the bright-end of the LF is independent from the cluster environment, and the same in all clusters. On the other hand, the LF faint-end was found to vary from cluster to cluster. In the present paper (IV in the series of the RASS-SDSS galaxy cluster survey) we show that the previously found variations of the faint end of the cluster LF are due to aperture effects. In other words, when measured within the physical size of the system, given by either r_{200} or r_{500}, the LF is invariant for all clusters, both at the bright and at the faint end. We also analyze how the number ratio of dwarf to giant galaxies in galaxy clusters depends on global cluster properties such as the velocity dispersion, the mass, and the X-ray and optical luminosities. Finally, we investigate the nature of the dwarf galaxies in clusters by studying their color distribution and suggest a possible formation scenario for this population.

The paper is organized as follows. In Sect. 2 of the paper we describe our dataset. In Sect. 3 we summarize the methods used to calculate the individual and the composite cluster LFs. In Sect. 4 we summarize our methods for measuring the clusters characteristic radii. In Sect. 5 we analyze the resulting composite and individual LFs. In Sect. 6 we determine the cluster composite LF per galaxy type. In Sect. 7 we analyse the environmental dependence of the LF, and compare the cluster and field LFs. In Sect. 8 we provide our discussion, suggesting a possible formation scenario for the faint galaxy population in clusters. Finally, in Sect. 9 we draw our conclusions.

For consistency with Paper II and with previous works, we use $H_0 = 100\ h$ km s^{-1} Mpc^{-1}, $\Omega_{\rm m} = 0.3$ and $\Omega_\Lambda = 0.7$ throughout the paper.

2. The data

In order to study the variation of the cluster LF from system to system, the analysis has to be applied to a large statistical sample of clusters, covering the whole spectrum of properties (in mass, richness, X-ray luminosity and optical luminosity) of the systems considered. Since the X-ray observations provide a robust method of identification of galaxy clusters and the X-ray luminosity is a good estimator of the system total mass and optical luminosity (see Paper I; and Popesso et al. 2004c, hereafter Paper III), we have used for our purpose the RASS-SDSS galaxy cluster sample, which is an X-ray selected sample of objects in a wide range of X-ray luminosity. The updated version of the RASS-SDSS galaxy cluster catalog comprises 130 systems detected in the RASS and in the SDSS sky region (16 clusters more than in the first version of the catalog released in Paper I due to the larger sky area available in the SDSS DR2). The X-ray cluster properties and the cluster redshifts have been taken from a variety of X-ray catalogs, that allow to cover the whole L_X spectrum. The X-ray intermediate and bright clusters have been selected from three ROSAT based cluster samples: the ROSAT-ESO flux limited X-ray cluster sample (REFLEX, Böhringer et al. 2002), the Northern ROSAT All-sky cluster sample (NORAS, Böhringer et al. 2000), the NORAS 2 cluster sample (Retzlaff 2001). The X-ray faint clusters and the groups have been selected from two catalogs of X-ray detected objects: the ASCA Cluster Catalog (ACC) from Horner (2001) and the Group Sample (GS) of Mulchaey et al. (2003). The RASS-SDSS galaxy cluster sample comprises only nearby systems at the mean redshift of 0.1. The sample covers the entire range of masses and X-ray luminosities, from very low-mass and X-ray faint groups ($10^{13}\ M_\odot$ and 10^{42} erg s^{-1}) to very massive and X-ray bright clusters ($5\times10^{15}\ M_\odot$ and 5×10^{44} erg s^{-1}).

The optical photometric data are taken from the 2nd data release of the SDSS (Fukugita et al. 1996; Gunn et al. 1998; Lupton et al. 1999; York et al. 2000; Hogg et al. 2001; Eisenstein et al. 2001; Smith et al. 2002; Strauss et al. 2002; Stoughton et al. 2002; Blanton et al. 2003; and Abazajian et al. 2003). The SDSS consists of an imaging survey of π steradians of the northern sky in the five passbands u, g, r, i, z,. The imaging data are processed with a photometric pipeline (PHOTO)

specially written for the SDSS data. For each cluster we defined a photometric galaxy catalog as described in Sect. 3 of Popesso et al. (2004b, Paper I). For the analysis in this paper we only use SDSS Model magnitudes (see Paper II for details).

In this paper we consider a subsample of 69 clusters of the RASS-SDSS sample for which the masses, velocity dispersion, r_{200} and r_{500} (see Sect. 4) were derived through the virial analysis (see Paper III) applied to the spectroscopic galaxy members of each systems.

Since throughout the paper the results obtained with the current analysis of the cluster LF are often compared with the results obtained in Paper II, it is important to notice that the cluster sample used here is a subsample of the dataset used in Paper II.

3. Determination of the individual and composite Luminosity Functions

We here summarize the methods by which we measure the individual and composite cluster LFs. Full details can be found in Papers I and II.

We consider two different approaches to the statistical subtraction of the galaxy background. As a first approach, we calculate a local background in an annulus centered on the X-ray cluster center with an inner radius of 3 h^{-1} Mpc and a width of 0.5 deg.

As a second approach we derive a global background correction. We define as $N^{g}_{bg}(m)\mathrm{d}m$ the mean of the galaxy number counts determined in five different SDSS sky regions, randomly chosen, each with an area of 30 deg^2. A detailed comparison of the local and global background estimates can be found in Paper I. The results shown in this paper are obtained using a global background subtraction.

We derive the LFs of each cluster by subtracting from the galaxy counts measured in the cluster region, the field counts rescaled to the cluster area. Following previous literature suggestions, we exclude the brightest cluster galaxies from the clusters LFs.

In order to convert from apparent to absolute magnitudes we use the cluster luminosity distance, correct the magnitudes for the Galactic extinction (obtained from the maps of Schlegel et al. 1998), and apply the K-correction of Fukugita et al. (1995) for elliptical galaxies, which are likely to constitute the main cluster galaxy population.

The composite LF is obtained following Colless (1989) prescriptions. A detailed description of the method can be found in Paper II.

3.1. Low surface brightness selection effect

It is well known that magnitude-limited surveys may be biased against low-surface brightness galaxies (e.g. Phillips & Driver 1995). An assessment of this bias for the SDSS-EDR and SDSS-DR1 has been done by Cross et al. (2004), who compared these catalogs with the Millennium Galaxy Catalog (Liske et al. 2003), a deep survey limited in surface brightness to 26 mag arcsec^{-2}. Cross et al. (2004) concluded that the incompleteness of SDSS-EDR is less than 5% in the range of effective surface-brightness $21 \leq \mu_e \leq 25$ mag arcsec^{-2}, and it is around 10% in the range $25 \leq \mu_e \leq 26$ mag arcsec^{-2}. In this paper, galaxies contributing to the faint-end of the cluster LFs have magnitudes $18 \leq r \leq 21$. In this magnitude range, 65% of the objects have $\mu_e \leq 23$ mag arcsec^{-2}, 30% have $23 < \mu_e \leq 24$ mag arcsec^{-2}, and 5% have $mu_e \geq 25$ mag arcsec^{-2}. Hence, from the results of Cross et al. (2004), we do not expect that the bias against low surface-brightness galaxies results in an incompleteness above ∼5%. The faint-end of the cluster LFs derived in this paper should thus be quite unaffected by this selection effect.

4. The characteristic radii of galaxy clusters

We here describe the methods by which we measure the characteristic radii r_{500} and r_{200}. r_{200} is the radius where the mass density of the system is 200 times the critical density of the Universe and it is considered as a robust measure of the virial radius of the cluster. Similarly, r_{500} is defined setting 500 instead of 200 in the previous definition and it samples the central region of the cluster. Full details can be found in Paper III.

We estimate a cluster characteristic radius through the virial analysis applied on the redshifts of its member galaxies. We use the redshifts provided in the SDSS spectroscopic catalog to define the galaxy membership of each considered system. The SDSS spectroscopic sample comprises all the objects observed in the Sloan r band with pretrosian magnitude $r_P \leq 17.77$ mag and half-light surface brightness $\mu_{50} \leq 24.5$ mag arcsec^{-2}. The SDSS DR2 spectrocsopic sample used for this analysis counts more tha 250 000 galaxies.

Cluster members are selected following the method of Girardi et al. (1993). First, among the galaxies contained in a circle of radius equal to the Abell radius, those with redshift $|cz - cz_{\mathrm{cluster}}| > 4000$ km s^{-1} are removed, where z_{cluster} is the mean cluster redshift. Then, the gapper procedure (see also Beers et al. 1990) is used to define the cluster limits in velocity space. Galaxies outside these limits are removed. Finally, on the remaining galaxies we apply the interloper-removal method of Katgert et al. (2004; see Appendix A in that paper for more details).

The virial analysis (see, e.g., Girardi et al. 1998) is then performed on the clusters with at least 10 member galaxies. The velocity dispersion is computed using the biweight estimator (Beers et al. 1990). The virial masses are corrected for the surface-pressure term (The & White 1986), using a Navarro et al. (1996, 1997) mass density profile, with concentration parameter $c = 4$. This profile provides a good fit to the observationally determined average mass profile of rich clusters (see Katgert et al. 2004).

Our clusters span a wide range in mass; since clusters of different masses have different concentrations (see, e.g. Dolag et al. 2004) we should in principle compute the cluster masses, M's, using a different concentration parameter c for each cluster. According to Dolag et al. (2004), $c \propto M^{-0.102}$. Taking $c = 4$ for clusters as massive as those analysed by Katgert et al. (2004), $M \simeq 2 \times 10^{15}\ M_{\odot}$, Dolag et al.'s scaling implies our clusters span a range $c \simeq 3$–6. Using $c = 6$ instead of $c = 4$ makes the mass estimates 4% and 10% higher at, respectively,

r_{200} and r_{500}, while using $c = 3$ makes the mass estimates lower by the same factors. This effect being clearly much smaller than the observational uncertainties, we assume the same $c = 4$ in the analysis for all clusters.

If $M_{\rm vir}$ is the virial mass (corrected for the surface-pressure term) contained in a volume of radius equal to the clustercentric distance of the most distant cluster member in the sample, i.e. the aperture radius $r_{\rm ap}$, then, the radius r_{200} is then given by:

$$r_{200} \equiv r_{\rm ap}\,[\rho_{\rm vir}/(200\rho_{\rm c})]^{1/2.4} \quad (1)$$

where $\rho_{\rm vir} \equiv 3M_{\rm vir}/(4\pi r_{\rm ap}^3)$ and $\rho_{\rm c}(z)$ is the critical density at redshift z in the adopted cosmology. The exponent in Eq. (1) is the one that describes the average cluster mass density profile near r_{200}, as estimated by Katgert et al. (2004) for an ensemble of 59 rich clusters. Similarly, r_{500} is estimated by setting 500 instead of 200 in Eq. (1).

5. Analysis of the individual and composite LFs

In order to analyze the behavior of the composite LF faint-end as a function of waveband and clustercentric distance, we define the number ratio of dwarf to giant galaxies, DGR, as the ratio between the number of faint ($-18 \leq M \leq -16.5$) and bright ($M < -20$) galaxies in the cluster LF. The DGR is found to vary from cluster to cluster, more than expected from statistical errors. These variations are not random however. As shown in Fig. 1, when the DGRs are computed within a fixed metric radius, they are significantly anti-correlated with several cluster global properties, i.e. the cluster velocity dispersions, masses, and X-ray and optical luminosities (velocity dispersions, virial masses, and X-ray luminosities for our cluster sample were derived in Paper III). All the correlations are very significant ($1-5\times10^{-5}$, according to a Spearman correlation test). The more massive a cluster, the lower its fraction of dwarf galaxies.

The correlation between cluster DGRs and cluster masses is most likely due to the choice of a fixed metric aperture for all the clusters. In fact, a fixed metric aperture samples larger (smaller) fractions of the virialized regions of clusters of smaller (respectively, larger) masses, and DGR is known to increase with clustercentric distance (Paper II).

Because of this effect, the different cluster physical sizes must be taken into account before comparing different cluster LFs. We then determine the individual and composite LFs within r_{500} and r_{200} for the subsample of 69 clusters of the RASS-SDSS galaxy cluster sample for which these parameters are known (see Paper III).

The composite LF calculated within r_{200} is shown in Fig. 2 for four SDSS photometric bands. The u-band LF is not shown; in this band, there is no evidence for an upturn at faint magnitude levels (see Paper II). For all the other bands LFs, a single Schechter function does not provide acceptable fits, and a composite of two Schechter functions is needed:

$$\phi(L) = \phi^* \left[\left(\frac{L}{L^*_{\rm b}}\right)^{\alpha_b} \exp\left(\frac{-L}{L^*_{\rm b}}\right) + \left(\frac{L^*_{\rm b}}{L^*_{\rm f}}\right) \times \left(\frac{L}{L^*_{\rm f}}\right)^{\alpha_{\rm f}} \exp\left(\frac{-L}{L^*_{\rm f}}\right)\right] \quad (2)$$

where b and f label the Schechter parameters of the bright and faint end respectively. From the reduced-χ^2 values given in Table 1 we conclude that a double-Schechter function does provide adequate fits to the 4-bands composite LFs. Alternatively, we fit the composite LFs with a function of this form:

$$\phi(L) = \phi^* \left(\frac{L}{L^*}\right)^{\alpha} \exp\left(\frac{-L}{L^*}\right)\left[1 + \left(\frac{L}{L_{\rm t}}\right)^{\beta}\right]. \quad (3)$$

In this function, ϕ^*, L^* and α are the standard Schechter parameters, $L_{\rm t}$ is a transition luminosity between the two power laws and β is the power law slope of the very faint end (Loveday 1997). Both functions require the same number of fit parameters. However, the double Schechter component function provides slightly better fits than the Schechter+power-law function in all the Sloan bands (see Table 1).

The Double Schechter function has been used for the first time by Driver et al. (1994), while Thompson & Gregory (1993) and Biviano et al. (1995) suggested a Gaussian+Schechter function, to fit respectively the bright and the faint end of the LF. More recently, Hilker et al. (2003) used a double Schechter Function to fit the LF of the Fornax cluster.

The confidence-level contours of the best-fit parameters of the bright- and faint-end Schechter components are shown in Figs. 3 and 4, respectively. Both results for the composite LF within r_{500} (dotted contours) and r_{200} (solid contours) are shown. Clearly, the best-fit Schechter function to the LF bright-end does not change significantly from r_{500} to r_{200} (see Fig. 3) confirming the findings of Paper II. However, the faint-end LF steepens significantly (by 0.1–0.15 dex) from r_{500} to r_{200}, and the characteristic magnitude correspondingly brightens by 0.3–0.4 magnitudes (see Fig. 4), thereby indicating an increasing DGR with radius. Our result is in agreement with the findings of Paper II, and several other works in the literature, which were however mostly based on single cluster studies (e.g. Lobo et al. 1997; Durret et al. 2002; Mercurio et al. 2003; Pracy et al. 2004; see however Trentham et al. 2001, for a discordant result).

While our conclusions on the composite LF agree with those of Paper II, we find here different results concerning the individual cluster LFs. While in Paper II we claimed significant LF variations from cluster to cluster, we discover that such variations disappear when the individual cluster LFs are computed within the physical sizes of each cluster (defined by r_{500} or r_{200}). This can be seen in Fig. 5a, where we plot the individual LFs of 15 clusters (those with the faintest absolute magnitude limits) and, superposed, the composite LF, all measured within r_{200} and in the r-band. The agreement between the composite and individual LFs is very good. Fitting the composite LF to the individual cluster LFs result in the reduced-χ^2 distribution shown in Fig. 5b. For 90% of the clusters the probability that the composite and individual LFs are drawn from the same parent distribution is larger than 95%.

In Fig. 5c we also show the z-band DGR-distribution. When compared to the DGR distribution found in Paper II, the new DGR distribution is much narrower. In this paper we considered the DGR within r_{200} of 29 clusters, those with known mass, r_{200} and r_{500}, out of the 35 systems considered in Paper II. The mean value of the DGR is 3.5 and its dispersion is indeed very close to the mean DGR statistical error of 1.4, as expected

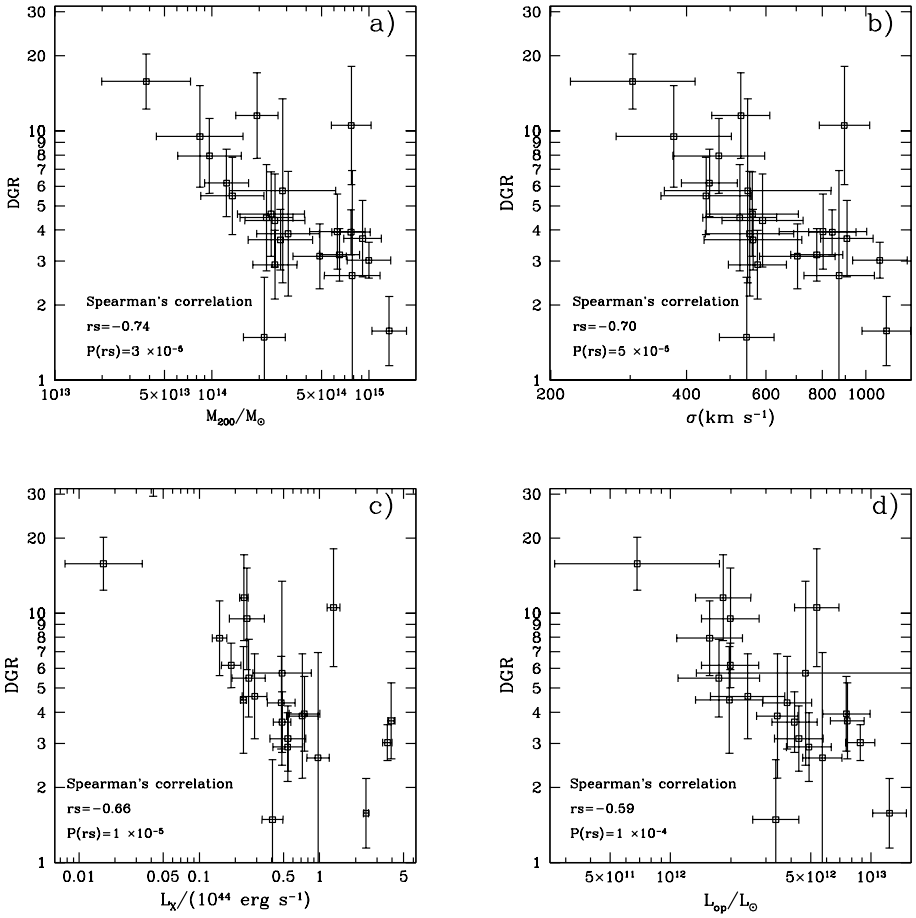

Fig. 1. The *z*-band DGR vs. the cluster mass (panel **a)**), the velocity dispersion σ (panel **b)**), the X-ray luminosity (panel **c)**), and the optical luminosity (panel **d)**). The DGR is calculated within a circle of 1 Mpc radius centered on the X-ray cluster center. In each panel, we list the value of the Spearman's rank correlation coefficient and the implied probability of no correlation.

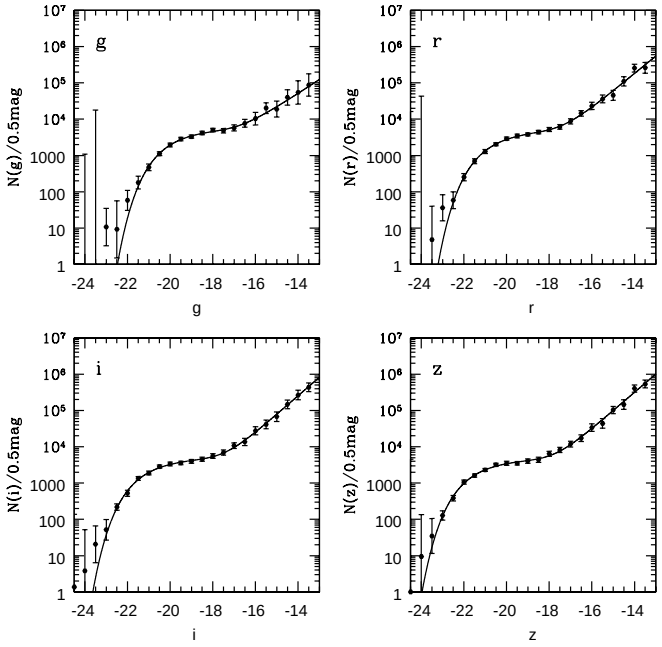

Fig. 2. The 4 panels show the composite LFs in the 4 Sloan bands. The individual LFs used to calculate the composite LFs are measured within the physical sizes of the clusters, as given by r_{200}.

if the individual cluster LFs are indeed all rather similar when computed within a cluster-related physical radius.

Finally, in Fig. 6 we show DGR within r_{200} as a function of the cluster mass M_{200} (panel a) and the velocity dispersion (panel b). There is no hint of the relation previously found (compare with Fig. 1a): the Spearman correlation coefficient is −0.08, which is not statistically significant. Similar results are found also for the $DGR - L_X$ and $DGR - L_{op}$ relations.

Hence we conclude that the cluster to cluster LF variation seen in Paper II are entirely due to the use of a fixed metric aperture for all clusters, rather than an aperture sampling the same fraction of the virialized region of each cluster.

6. The cluster LF per galaxy type

In order to better understand the nature of the cluster galaxies responsible for the LF upturn at low luminosities, we examine their color distribution. In particular, we use the $u - r$ color, since the $u - r$ distribution of Sa and earlier-type galaxies is well separated from the $u - r$ distribution of Sb and later-type galaxies (Strateva et al. 2001), thereby allowing to distinguish the two morphological samples down to very faint magnitudes.

To define the color distribution of the cluster galaxies we statistically subtract the contribution of field galaxies

Table 1. Schechter parameters of the composite LF.

	g	r	i	z
Double Schechter components function within r_{200}				
α_b	-1.07 ± 0.12	-1.09 ± 0.09	-1.08 ± 0.08	-1.07 ± 0.08
M^*_b	-20.18 ± 0.21	-20.94 ± 0.16	-21.35 ± 0.16	-21.69 ± 0.15
α_f	-1.98 ± 0.16	-2.19 ± 0.09	-2.26 ± 0.07	-2.25 ± 0.07
M^*_f	-17.37 ± 0.21	-18.14 ± 0.15	-18.43 ± 0.15	-18.66 ± 0.14
χ^2/ν	0.89	1.05	1.15	1.16
Double Schechter components function within r_{500}				
α_b	-0.97 ± 0.09	-1.05 ± 0.07	-1.06 ± 0.06	-1.05 ± 0.05
M^*_b	-20.04 ± 0.15	-20.84 ± 0.13	-21.36 ± 0.14	-21.67 ± 0.13
α_f	-1.84 ± 0.11	-2.02 ± 0.06	-2.17 ± 0.05	-2.19 ± 0.06
M^*_f	-16.61 ± 0.22	-17.38 ± 0.13	-17.49 ± 0.12	-17.58 ± 0.12
χ^2/ν	0.87	0.98	1.11	1.09
Schechter+exponential function within r_{200}				
α	-0.88 ± 0.25	-1.26 ± 0.12	-1.16 ± 0.13	-1.16 ± 0.12
M^*	-19.95 ± 0.29	-21.16 ± 0.26	-21.41 ± 0.22	-21.71 ± 0.20
β	-1.40 ± 0.05	-1.30 ± 0.07	-1.26 ± 0.08	-1.25 ± 0.07
M^*_t	-17.27 ± 0.22	-16.99 ± 0.43	-17.65 ± 0.41	-17.80 ± 0.39
χ^2/ν	1.10	1.15	1.38	1.40
Schechter+exponential function within r_{500}				
α	-0.88 ± 0.25	-1.05 ± 0.16	-1.22 ± 0.14	-1.00 ± 0.14
M^*	-19.94 ± 0.29	-20.91 ± 0.28	-21.40 ± 0.25	-21.54 ± 0.21
β	-1.33 ± 0.14	-1.33 ± 0.09	-1.22 ± 0.06	-1.28 ± 0.08
M^*_t	-16.95 ± 0.63	-17.28 ± 0.50	-17.43 ± 0.52	-17.93 ± 0.45
χ^2/ν	1.13	1.15	1.41	1.43

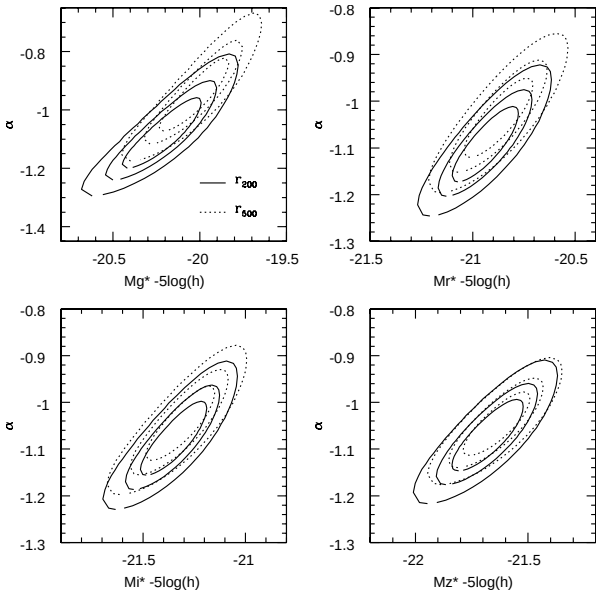

Fig. 3. Contour plots of the 68%, 95%, and 99% confidence levels of the parameters of the bright-end component of the double-Schechter function fit to the 4 SDSS bands composite LFs. Solid (dotted) contours show the results for the composite LF computed within r_{200} (respectively r_{500}).

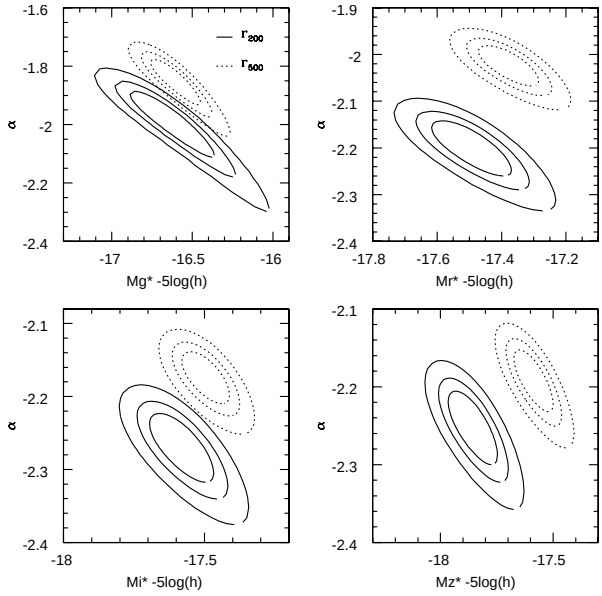

Fig. 4. Same as Fig. 3, but for the faint-end component.

(Boyce et al. 2001), using the same method applied for the statistical subtraction of the background from the magnitude number counts. We determine the background color distribution of field galaxies in an annulus around the cluster with inner radius larger than r_{200}; significantly under- or over-dense regions (e.g. voids and background clusters) are excluded. By subtracting the background color distribution from the color distribution of galaxies in the cluster region, we obtain the $u-r$ distribution of cluster galaxies. The validity of the method is confirmed by its application to the spectroscopic subsample, for which cluster membership can be established from the galaxy redshifts.

Figure 7 shows the (background-subtracted) $u-r$ distribution of cluster galaxies in the range $-18 \leq r \leq -16.5$ (panel a) and $-16.5 \leq r \leq -15$ (panel b) for the subsample of 15 clusters with the faintest absolute magnitude limit in the r band

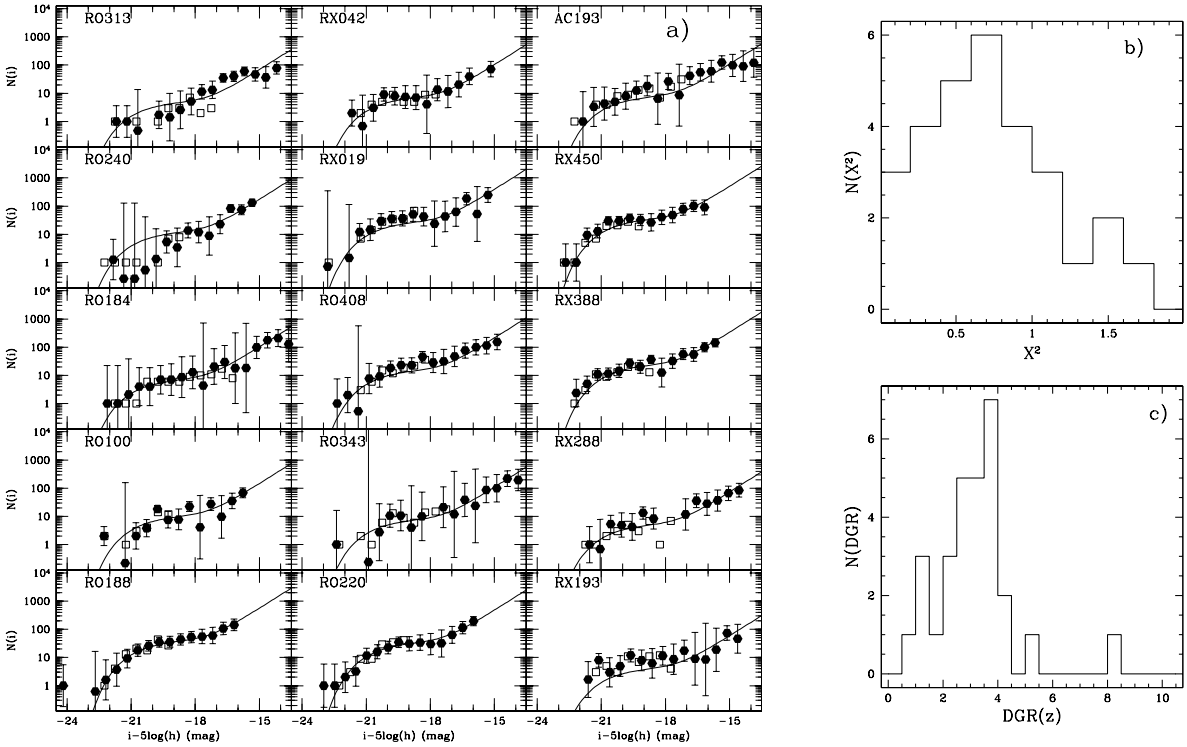

Fig. 5. Panel **a)**: the individual r-band LFs within r_{200} of a subsample of 15 clusters with the faintest absolute magnitude limit ($M_{r,\rm lim} \leq -15.5$). Empty squares and filled points distinguish the LFs computed from cluster members only (down to the SDSS spectroscopic completeness magnitude, $r \leq 17.77$), and using a statistical background subtraction, respectively. The solid line is the composite LF. Cluster names are indicated. Panel **b)**: the distribution of the χ^2 values obtained from the comparison of the composite and the 29 individual LFs of clusters with $M_{z,\rm lim} \geq -16.5$ mag. Panel **c)**): the z-band DGR distribution of the 29 clusters.

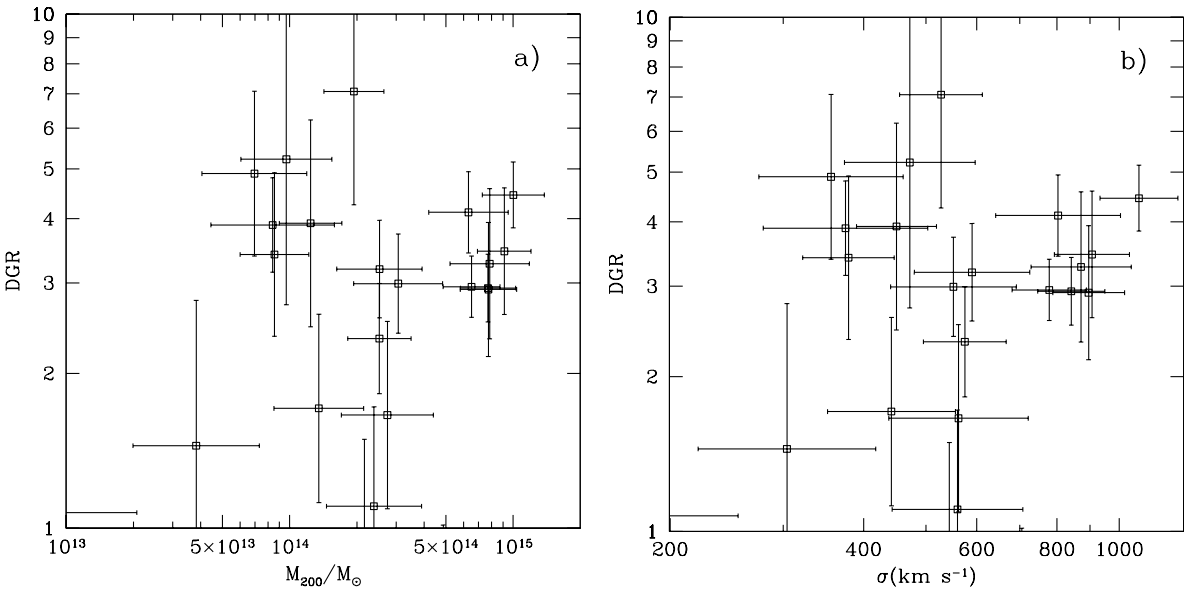

Fig. 6. The z-band DGR within r_{200} as a function of cluster mass (panel **a)**) and the cluster velocity dispersion (panel **b)**). If DGR is calculated within r_{200} the anti-correlation with mass (σ, $L_{\rm X}$ and $L_{\rm op}$) disappears.

($M_{r,\rm lim} \geq -15$). The error bars shown in the figure take into account the galaxy counts Poisson statistics as well as the error due to the background subtraction.

At the redshifts of the 15 clusters considered ($0.02 \leq z \leq 0.05$) early-type galaxies have $u-r$ colors in the range 2.6–2.9 (Fukugita et al. 1995), and galaxies redder than $u-r = 3$ are probably in the background. Hence, we can see from Fig. 7a that the residual background contamination after the statistical background subtraction, is generally small (≤10%) and in fact not significant in the bright magnitude range. The contamination is higher for the two clusters RO313 and RX 288, and probably due to the presence of another cluster along the same

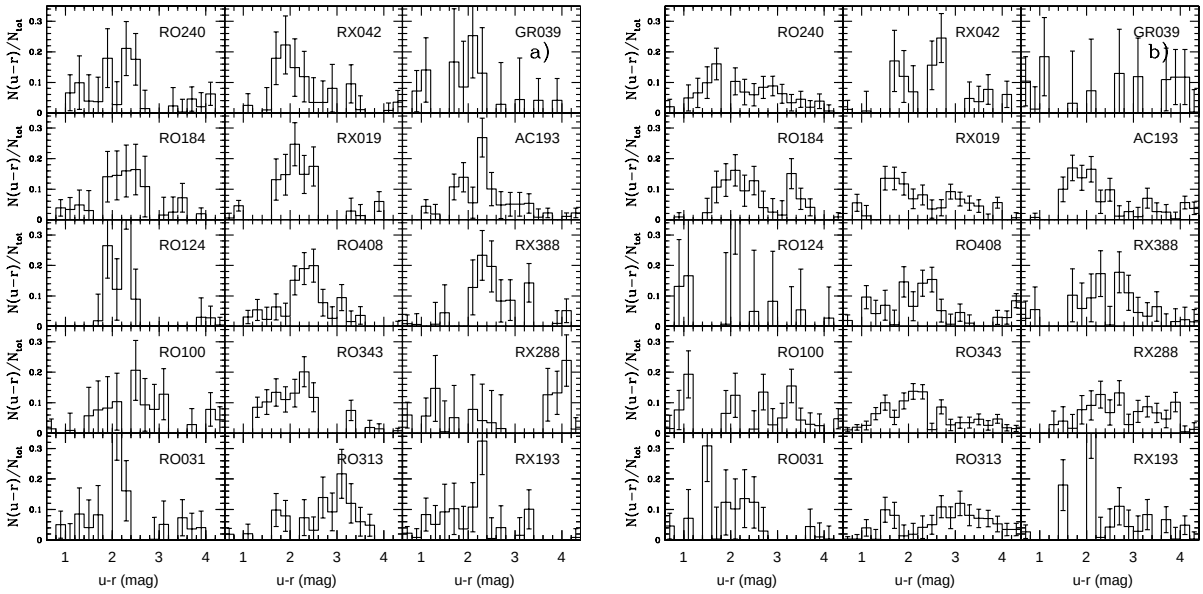

Fig. 7. The background-subtracted $u-r$ distribution of the galaxy members of the 15 clusters with the faintest absolute magnitude limit ($M_{r,\rm lim} \geq -15$). **a)**: Color distribution in the magnitude range $-18 \leq M_r \leq -16.5$; **b)**: color distribution in the magnitude range $-16.5 \leq M_r \leq -15$.

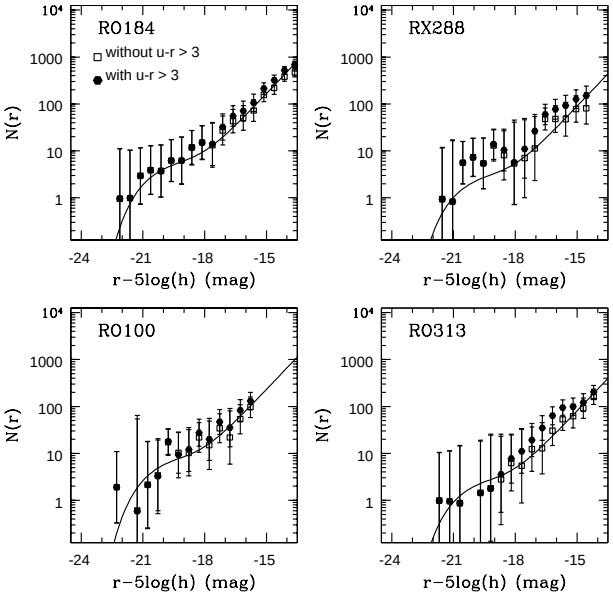

Fig. 8. The LFs of 4 clusters computed as for Fig. 5 (filled points), and by additionally excluding all galaxies with $u-r \geq 3$ (empty squares).

line-of-sight. In the fainter magnitude range, the average background contamination increases to 25–35%, but is still not significant (see Fig. 7b).

If we exclude galaxies with $u-r \geq 3$ from our cluster samples, and recalculate the cluster LFs as before (see Sect. 3), the modifications are marginal (compare filled points and empty squares in Fig. 8). If anything, a better agreement is now found between the composite LF and the individual LF of the cluster R0313, for which the background contamination is more severe, clearly suggesting that the $u-r \geq 3$ color cut helps in cleaning the cluster sample from background contamination.

We therefore adopt the $u-r < 3$ color cut to select cluster members, and, following Strateva et al. (2001) we distinguish between cluster early- and late-type galaxies using a color-cut $u-r = 2.22$. We restrict our analysis to the very nearby clusters ($z \leq 0.1$) to minimize the effects of an uncertain K-correction on the derived colors. The composite LFs of the early- and late-type galaxies (defined on the basis of their $u-r$ colors) are shown in Fig. 9 for four SDSS photometric bands. The late-type galaxy LF is well fitted by a single Schechter function and does not show any evidence of an upturn at the faint end. On the other hand, the early-type LF looks quite different from the late-type LF. It shows a marked bimodal behavior with a pronounced upturn in the faint magnitude region. The best fit parameters are listed in Table 2. Such an upturn is then reflected in the complete (early+late) LF, with the late-type dwarf galaxies contributing to make the faint-end of the complete LF even steeper. This result is in agreement with Yagi et al. (2002). They determine the total LF of 10 clusters within 1 h^{-1} Mpc radius circle. They find that the early-type LF cannot be fitted by a single Schechter function in the magnitude range from -23 to -15, because it flattens at $M_R = -18$ and then rises again.

7. The environmental dependence of the LFs

In order to gain insight into the processes responsible for the shaping of the LF in clusters, we here examine the dependence of the LF on the environmental conditions. In particular we analyze how the LF shape, and the relative fraction of red and blue dwarf galaxies, vary as a function of the clustercentric distance. Figure 10 shows the behavior of the cluster LF calculated within different clustercentric apertures, separately for the early-type (panel a) and late-type (panel b) galaxy populations. Distances are in units of r_{200}. For simplicity we only plot the best fitting functions and not the data-points. The early-type LF is close to a Schechter function at the center of the cluster (within 0.2 r_{200}) and shows a marked upturn afterwards. The location of the upturn varies from -16.2 ± 0.3 mag at distances $\leq 0.3\ r_{200}$ to -17.4 ± 0.4 at distances $\leq r_{200}$.

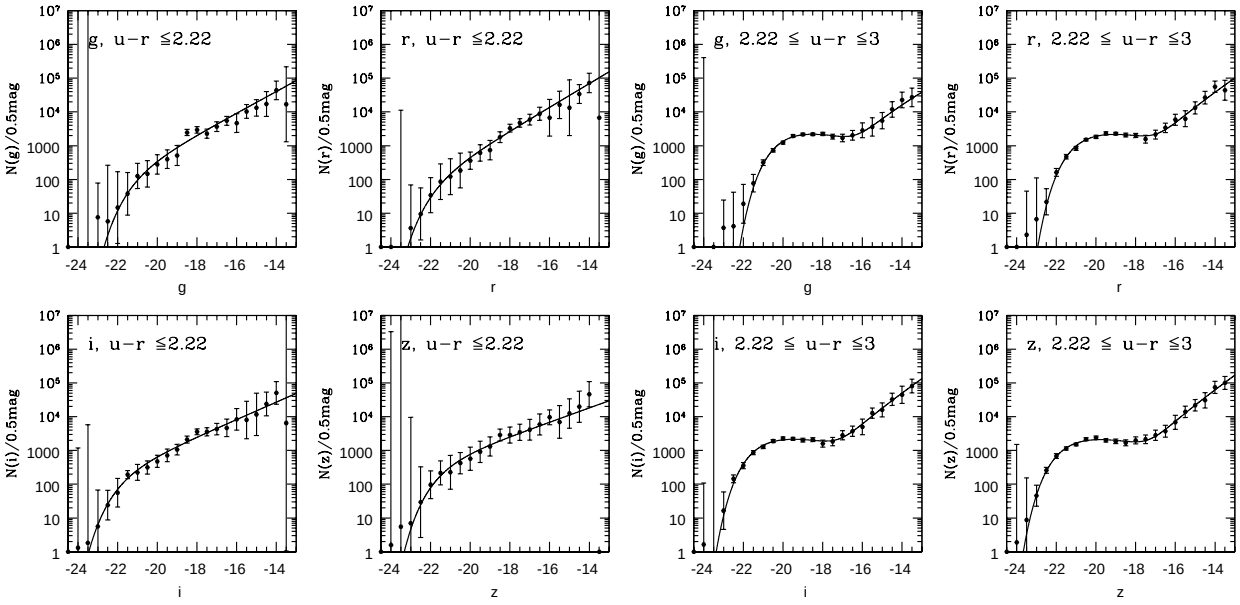

Fig. 9. The composite late-type and early-type LFs in four SDSS photometric bands. The late-type (early-type) LFs are displayed in the four panels on the left (respectively, right).

Table 2. Schechter parameters of the early and late type galaxies composite LFs.

	g	r	i	z
Double Schechter components (r_{200}) for early type galaxies				
α_b	-0.69 ± 0.10	-0.75 ± 0.09	-0.76 ± 0.09	-0.76 ± 0.08
M^*_b	-19.79 ± 0.16	-20.57 ± 0.14	-21.03 ± 0.15	-21.30 ± 0.14
α_f	-1.86 ± 0.15	-2.01 ± 0.11	-2.03 ± 0.08	-2.05 ± 0.09
M^*_f	-17.37 ± 0.21	-18.14 ± 0.15	-18.43 ± 0.15	-18.66 ± 0.14
χ^2/ν	0.72	1.04	1.03	0.90
Single Schechter (r_{200}) for late type galaxies				
α	-1.80 ± 0.04	-1.87 ± 0.04	-1.64 ± 0.02	-1.52 ± 0.05
M^*	-21.13 ± 0.40	-21.71 ± 0.52	-21.79 ± 0.35	-21.52 ± 0.47
χ^2/ν	0.87	0.75	0.90	0.98

The late-type LF is well fitted by a single Schechter function at any clustercentric distance. We do not observe blue galaxies within 0.1 r_{200}. Moreover, the central late-type LF at 0.2 r_{200} is flatter than the LFs in the outer regions and shows a fainter M^*. Since red galaxies are mostly high surface-brightness objects (Blanton et al. 2004), the surface brightness selection effect should be more important for the late-type LF, which, once corrected, would become steeper at the faint-end. If anything, the difference in slope between the faint-ends of the early- and late-type LFs should thus be even larger than observed.

These results are confirmed by the analysis of the early-type LFs in independent clustercentric rings. We consider the region at distances $r \leq 0.3\ r_{200}$ (the central ring), $0.3 \leq r/r_{200} \leq 0.7$ (the intermediate ring) and $0.7 \leq r/r_{200} \leq 1$ (the outer ring). The best fitting functions of the cluster early-type LFs within these regions are shown in Fig. 11. In order to emphasize the *shape* variation of the LF, all three LFs are renormalized to the same value. The upturn at the faint end is brighter in the outer ring than in the central one, confirming the previous analysis. Moreover, the shape of the bright end of the cluster LF seems to be absolutely independent from the faint end. The values of M^* and the slope of the bright end are consistent within the errors in the three regions (as found in Paper II). This suggests that the process of formation of the bright cluster galaxies (with magnitude brighter that $M^* - 2$ mag) is the same in all the cluster environments. Therefore, it seems unlikely that the lack of dwarf systems observed at the center of the cluster is due to a hierarchical process of formation of the bright central galaxies. Indeed, in that case we should observe also a lack of bright galaxies in the outer ring in favor of large amount of dwarf systems, which is not observed.

The analysis so far provides only results about the LF *shape*. In order to quantify the relative contribution of the early- and late-type dwarf galaxy populations to the faint end of the LF, and its dependence on the environment, we analyse the radial (cumulative and differential) profile of the dwarf systems in the clusters. For this, we consider the galaxies with $-18 \leq M_r \leq -15$, and to improve the statistics, we stack the clusters with $M_{r,\rm lim} \geq -15$ mag, by rescaling the clustercentric distances in units of r_{200}. The cumulative profiles of the fractions of dwarf galaxies of both the early- and the late-type are shown in Fig. 12a. The center ($\leq 0.4\ r_{200}$) contains less than 30% of dwarf galaxies (half of them are red systems), in the selected magnitude range. Dwarf galaxies are more

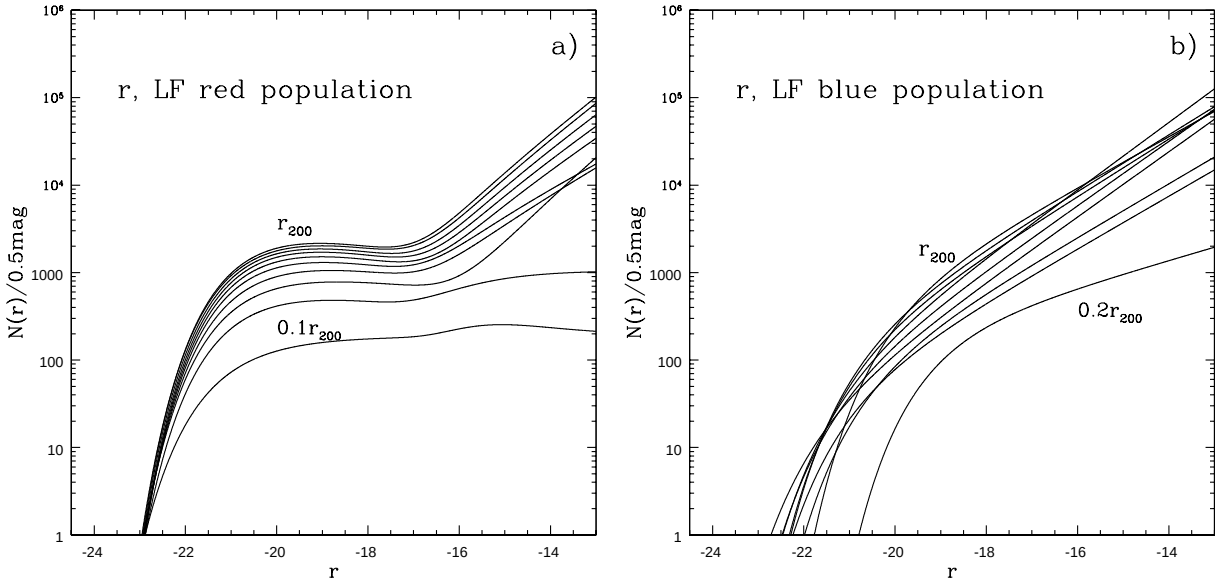

Fig. 10. The cluster LFs within different cluster apertures in the r band per morphological type. The increment of the apertures is $0.1 \times r_{200}$. The normalization of the fitting function is increasing at larger apertures. Panel **a)** shows the LF of the cluster red galaxy population, calculated within different clustercentric apertures expressed in unit of r_{200}. Panel **b)** shows the same for the cluster blue galaxy population. For simplicity we only plot the best fitting functions and not the data points.

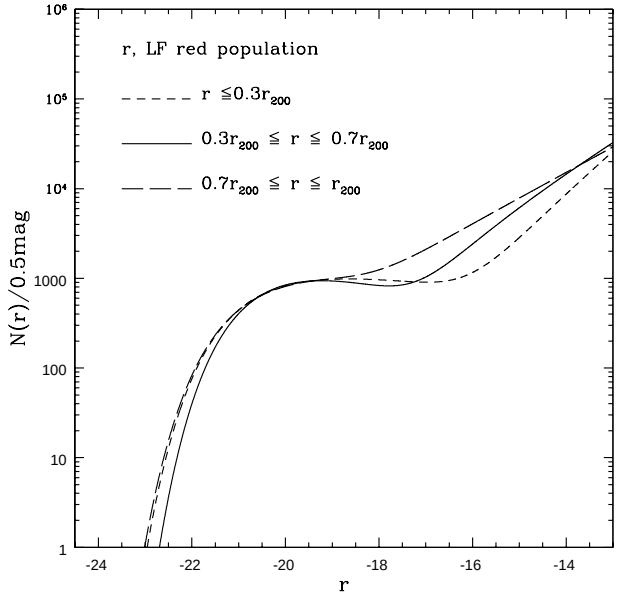

Fig. 11. The early-type LF calculated within three different cluster regions. Only the best fitting functions are plotted, for simplicity, and not the data points. The LFs are renormalized to the same value to emphasize the shape variations.

abundant in the cluster outskirts; the high-density environment in the cluster cores is hostile to dwarf galaxies. This phenomenology has already been observed in several individual clusters (see e.g. Lobo et al. 1997; Boyce et al. 2001; Mercurio et al. 2003; Dahlen et al. 2004).

The early-type dwarf galaxies represents 35% of the whole dwarf population within r_{200}, i.e. most of the dwarf galaxies are of late-type. However, the dwarf early-type galaxies are the dominant dwarf population region within 0.4 r_{200}, their relative fraction reaching a plateau at $\simeq$0.6 r_{200}, while the late-type dwarf galaxies are more abundant in clusters outskirts. This is confirmed also by the ratio between early- and late-type dwarf galaxies calculated in contiguous clustercentric rings (differential profile, see Fig. 12b). The number of early-type dwarf galaxies is twice the number of late-type dwarf galaxies within 0.2 r_{200} and then decreases to 1/2 at larger distances.

The relation between dwarf morphology and clustercentric distance translates into a morphology-density relation. In Fig. 12d we show the ratio between early- and late-type dwarf galaxies as a function of the number density of galaxies brighter than $M_r \leq -18$ (the bright galaxies number density profile is shown in panel c of the same figure). As expected, the early-type dwarf galaxies dominate in high density regions, while the late-type dwarf galaxies are frequent in low density regions. Clearly, the well known morphology density relation for cluster galaxies (Dressler 1980) has an extension into the dwarf regime.

7.1. Comparison with the field

In order to extend the morphology-density relation for dwarf cluster galaxies outside clusters, we extract a subsample of galaxies from the SDSS spectroscopic sample. We select a fairly complete sample of galaxies in the redshift range $z \leq 0.02$ and in the magnitude range $-18 \leq M_r \leq -16$. The late-type galaxies ($u - r \leq 2.22$) represent the 93% of the galactic population in that range of magnitude, in agreement with the results of Blanton et al. (2004). We then calculate for each galaxy in the sample the local density of galaxy neighbors, by counting the number of systems with $M_r \leq -18$ mag, within 2.5 Mpc projected radius and ± 500 km s^{-1} of the galaxy position and redshift. We divide the subsample in late and early-type galaxies using the color cut of Strateva et al. (2001). Figure 13 shows the number of galaxies per bin of local density for the two

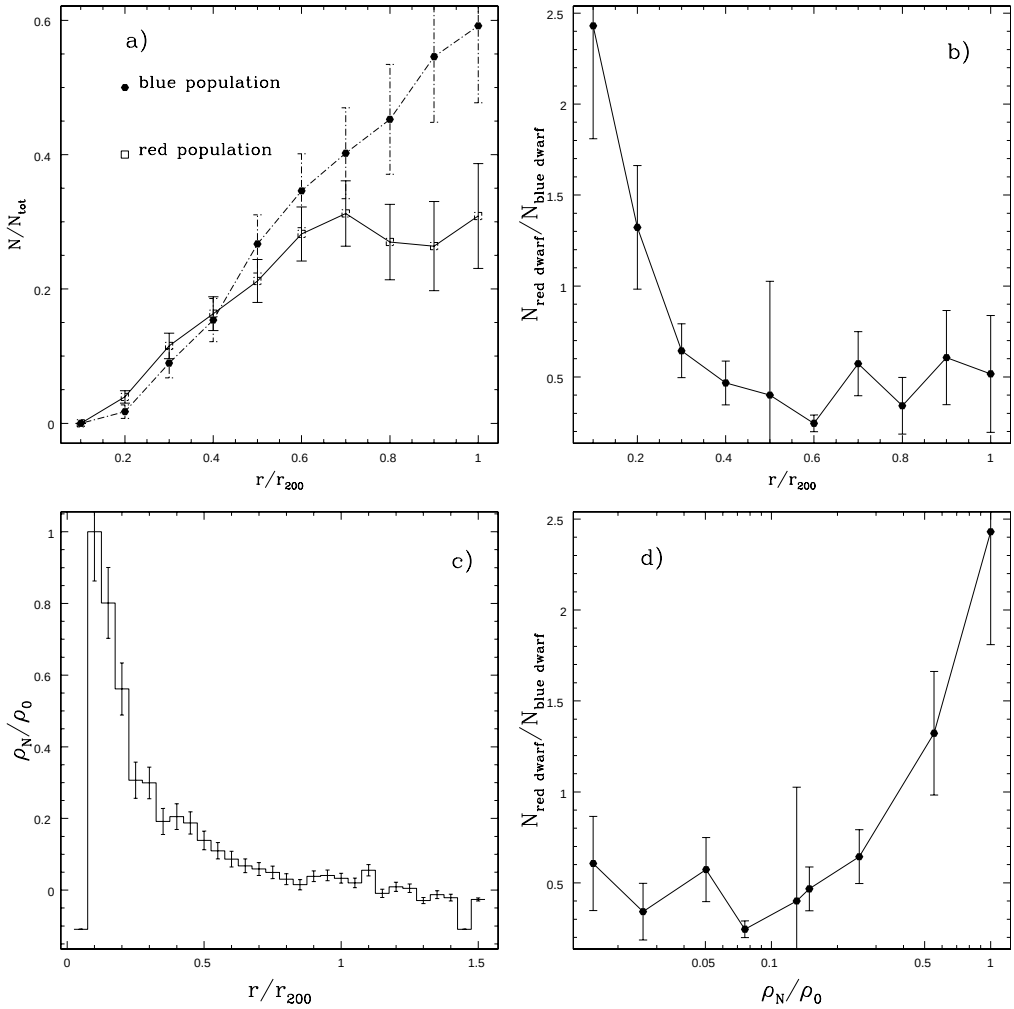

Fig. 12. The fraction of red and blue dwarf galaxies as a function of the cluster environments. Panel **a)** shows the cumulative radial profile of the fraction of blue (filled points) and red (empty squared) dwarf galaxies ($-18 \leq M_r \leq -15$ mag). The fraction is defined on the total number of cluster dwarf galaxies in the considered magnitude range. Panel **b)** shows the differential radial profile of the ratio between red and blue dwarf galaxies. Panel **c)** shows the differential radial profile of the surface density of the bright cluster galaxies in clusters ($M_r \leq -18$ mag). Panel **d)** shows the relation between the surface density of bright galaxies and the fraction of red and blue dwarf galaxies calculated in the same clustercentric ring.

galaxy types. It is clear that late-type galaxies (dashed dotted histogram) populate the very low density regions, while the early-type galaxies distribution (solid histogram) has a much larger spread, with 50% of the systems located in regions with more than 10 galaxy neighbors.

It is also interesting to compare our composite cluster LFs with the LF of field galaxies. Blanton et al. (2005) have recently derived the LF of field SDSS galaxies down to −12 mag. Their LF have a very weak upturn, much shallower and at a fainter carachteristic magnitude than in our cluster LF. The faint-end slope of their LF is −1.3, but could be steeper (−1.5) if a correction is applied to account for low surface-brightness selection effects. The LF of *blue* field galaxies is even steeper, but the authors do not report the value of the faint-end slope. A similar faint-end slope (−1.5) has also been found by Madgwick et al. (2002) for the LF of field galaxies from the 2dF survey. They also noticed an upturn in the LF, due to an overabundance of early-type galaxies, making it impossible to fit the LF adequately with a single Schechter function. A previous determination of the SDSS field LF was obtained by Nakamura et al. (2003). They found a slope of ∼−1.9 for dIrr, consistent with the value found by Marzke et al. (1994) for the CfA survey.

The faint-end slope of our late-type cluster galaxies LF is steeper than most field LFs for the same galaxy type (see Table 3 in Paper II) but consistent with those of Nakamura et al. (2003) and Marzke et al. (1994). Given the large variance of results for the field LFs, possibly due to the different magnitude limits adopted, or to poor statistics in the fainter bins of the LF (see de Lapparent 2003 for a thorough discussion on this topic), we conclude there is no significant difference between the late-type LF in clusters and the field.

8. Discussion

There are many observations and theoretical models in the literature (see, e.g., De Propris et al. 2003) that try to explain the formation and evolution of cluster galaxies, red dwarf galaxies in particular. According to the hierarchical picture for structure

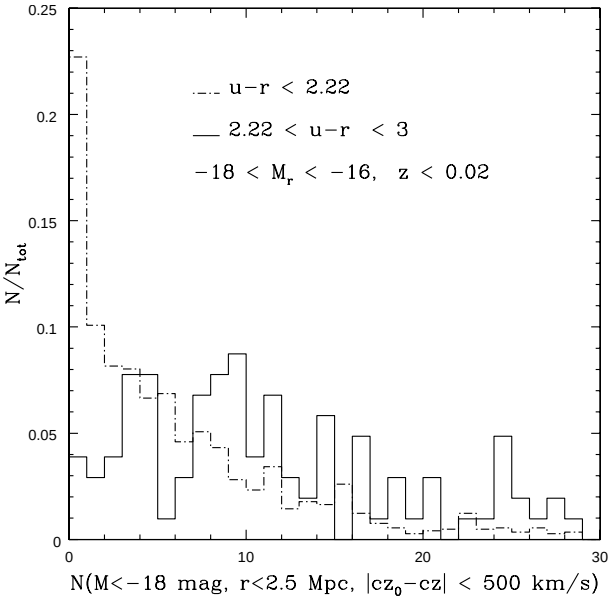

Fig. 13. The density distribution of neighbors of late (dotted histogram) and early (solid histogram) galaxies in the field. We select a fairly complete sample of nearby galaxies ($z \leq 0.02$) from the Sloan spectroscopic sample in the magnitude region $-18 \leq M_R \leq -16$. We calculate for each galaxy in the sample the local density of neighbor galaxies counting the number of systems with $M_R \leq -18$ mag, within 2.5 Mpc projected radius and ± 500 km s^{-1} of the galaxy position and redshift. The sample comprises 1561 systems.

formation, small dark matter haloes form before large ones. If one identifies the dwarf galaxies with the small dark matter haloes, they are predicted to origin soon after the structure formation began. Dwarf ellipticals would then be old, passively evolved galaxies. This scenario seems to be inconsistent with the observations of a large spread in age and metallicity in the clusters dwarf early-type galaxies (Conselice et al. 2001, 2003; Rakos et al. 2001). Hence, dwarf ellipticals must have had a delayed star formation epoch. The delay could be originated by the intense ultraviolet background intensity at high redshift, keeping the gas of the dwarf galaxies photoionized until $z \sim 1$, or, perhaps by the intra-cluster medium confinement. The intra-cluster medium pressure could avoid dwarf galaxies losing their gas content by SN ejecta. However, this possibility would require a much more centrally concentrated distribution of dwarf ellipticals in clusters than is observed.

In alternative, the excess of dwarf early-type galaxies in clusters could origin from the evolution of field dIrr when they are accreted by the clusters. The evolution of dIrr into dwarf early-type galaxies is supported by the result of van Zee et al. (2004), namely that there is significant similarity in the scaling relations and properties of dIrr and dEs. A scenario where *all* dwarf early-type galaxies evolve from dIrr via disk fading does not however seem possible, because many dEs in the Virgo and Fornax clusters are brighter than the dIrr (Conselice et al. 2001).

Perhaps, some dwarf early-type galaxies evolve from dIrr and some evolve from spirals. The evolution of spirals into dwarf spheroidals can occur via the process of "galaxy harassment" proposed by Moore et al. (1996, 1998). In this scenario, close, rapid encounters between galaxies can lead to a radical transformation of a galaxy morphology. Gas and stars are progressively stripped out of the disk systems, eventually leaving a spheroidal remnant, that resembles an S0 galaxy or a dwarf spheroidal, depending on the size of the progenitor. Direct support for the harassment scenario comes from the discoveries of disks or even spiral arms in dwarf early-type cluster galaxies (Jerjen et al. 2000; Barazza et al. 2002; Graham et al. 2003). Indirect support comes from the similar velocity distribution of dwarf cluster galaxies (Drinkwater et al. 2001) and gas-rich spirals and irregulars (Biviano et al. 1997), both suggesting infalling orbits.

Is the harassment scenario still viable in view of our results? We can draw the following conclusions from our observational results. First, the universality of the cluster LF suggests that whatever shapes the cluster LF is not strictly dependent on the cluster properties. Second, the difference between the cluster and field LF seems to be related to an excess of dwarf early-type galaxies in clusters. Hence, there is a cluster-related process that leads to the formation of dwarf early-type galaxies, regardless of the cluster intrinsic properties. The process cannot be related, e.g., to the intra-cluster gas density, or the cluster velocity dispersion, or the cluster mass, hence, a process like ram-pressure would seem to be ruled out.

The density dependence of the relative number of early- and late-type dwarfs suggests that the shaping of the cluster LF is related to the excess mean density relative to the field, which is the same for all clusters if, as we have done, the cluster regions are defined within a fixed overdensity radius (r_{200} in our case). In other words, the transformation of spirals, and perhaps, dIrr, into dwarf spheroidals or dEs, seems to be a threshold process that occurs when the local density exceeds a given threshold. Judging from Fig. 12, this threshold seems to occur at a clustercentric distance of $\sim$0.6–0.7 r_{200}.

We have also found that the relative number of dwarf early- and late-type galaxies increases with decreasing clustercentric distance (and increasing density). Galaxies near the cluster center are probably an older cluster population, accreted when the cluster was smaller, according to the hierarchical picture of cluster formation and evolution. Hence, these centrally located galaxies have had more time to accomplish the morphology transformation than galaxies located in the cluster outskirts, which are more recent arrivals.

On the other hand, very near the cluster center, an additional process must be at work to explain our observed fading of the upturn of the cluster early-type LF, and the decrease of both the early- and the late-type dwarf-to-giant galaxy ratio with decreasing clustercentric distance. High-velocity dispersions in clusters inhibit merging processes (e.g. Mihos 2004), hence it is unlikely that dwarf galaxies merge to produce bigger galaxies at the cluster centers. Consistently, we find that the shape of the bright-end of the early-type LF does not depend on the environment, which suggests that bright early-type galaxies are not a recent product of the cluster environment. In fact, the luminosity density profile of bright early-type galaxies has not evolved significantly since redshift $z \sim 0.5$ (Ellingson 2003).

The most likely explanation for the lack of dwarf galaxies near the cluster center is tidal or collisional disruption of the

dwarf galaxies. The fate of the disrupted dwarfs is probably to contribute to the intra-cluster diffuse light (e.g. Feldmeier et al. 2004; Murante et al. 2004; Willman et al. 2004).

The difference between the cluster and field LF could thus be explained as a difference in morphological mix, plus a density-dependent dwarf early-type galaxies LF, that, added to an invariant bright early-type LF, produces a more or less important and bright upturn, depending on the density of the environment.

9. Conclusion

We have presented a detailed analysis of the cluster individual and composite luminosity functions down to -14 mag in all the Sloan photometric bands. All the luminosity functions are calculated within the physical size of the systems given by r_{500} and r_{200}. The main conclusions of our analysis are as follows:

- We confirm that the composite LF shows a bimodal behavior with a marked upturn at the faint magnitude range. A double Schechter component function is the best fit for the cluster LF. We show that calculating the individual and the composite LF within a fixed aperture for all the systems introduces selection effects. These selection effects justify the differences observed in the faint end of the individual cluster LFs studied in Paper II and the anti-correlations between DGR and the global cluster properties (mass, velocity dispersion, optical and X-ray luminosities) observed in this work. If the cluster LF is calculated within the physical size of the system (r_{500} or r_{200}), the differences due to aperture effects disappear and the individual cluster LF is well represented by the composite LF. Therefore, we conclude that the shape of the cluster LF is universal in all the magnitude ranges.
- We use the $u-r$ color to study the color distribution of the faint cluster galaxies. The color distribution confirms that the contamination due to background galaxies is due to field-to-field variance of the background. We apply the color cut at $u-r=2.22$ suggested by Strateva et al. (2001) to separate early-type from late-type galaxies and study the composite LF by morphological type. We observe that the upturn at the faint magnitudes shown by the complete LF is due to early-type galaxies while the late-type LF is well represented by a single Schechter function.
- We study the cumulative and the differential radial profile of the faint early- and late-type galaxies in clusters. The faint early-type galaxies are concentrated in the central regions while the faint late-type galaxies dominate the outskirts of the systems. The analysis of the color-density relation in a reference sample of nearby galaxies selected from the SDSS spectroscopic sample suggests that red galaxies could be a typical cluster galaxy population. Our analysis show that the bright red population seems to have a luminosity distribution absolutely independent from the behavior of the faint red galaxies in different environments. We observe a fading of the LF upturn toward the cluster core.
- We propose to interpret our results in term of a combination of two processes, transformation of spirals and dIrr into dwarf early-type galaxies via harassment, and disruption of dwarf galaxies near the cluster center by collisions and/or tidal effects.

Whether galaxies evolve from one type to another, in response to the local density, to create the morphology-density relation, or whether the relation is established when the galaxies form, is still an open issue (see, e.g., Dressler 2004). Photometric data alone cannot provide conclusive indications about the nature and the origin of the dwarf population in cluster. In this respect, it would be very useful to sample the velocity distributions of a large set of dwarf galaxies in clusters, in order to constrain their orbital characteristics as it has recently been done for bright cluster galaxies (Biviano & Katgert 2004). If the dwarf early-type galaxies evolve from spirals, radially elongated orbits are expected, while if dwarf early-type galaxies are a more pristine cluster population, their orbits should resemble the isotropic orbits of ellipticals. Additional insights may come from higher accuracy spectroscopy of the dwarf galaxies, allowing to deduce information about their internal velocity dispersion and metallicity, which could be used to put constraints on their age (see, e.g., Kauffmann et al. 2004; Carretero et al. 2004).

Acknowledgements. We would like to thank Gwenael Boué and the anonymous referee for the usefull comments which significantly improved the paper.
Funding for the creation and distribution of the SDSS Archive has been provided by the Alfred P. Sloan Foundation, the Participating Institutions, the National Aeronautics and Space Administration, the National Science Foundation, the US Department of Energy, the Japanese Monbukagakusho, and the Max Planck Society. The SDSS Web site is `http://www.sdss.org/`. The SDSS is managed by the Astrophysical Research Consortium (ARC) for the Participating Institutions. The Participating Institutions are The University of Chicago, Fermilab, the Institute for Advanced Study, the Japan Participation Group, The Johns Hopkins University, Los Alamos National Laboratory, the Max-Planck-Institute for Astronomy (MPIA), the Max-Planck-Institute for Astrophysics (MPA), New Mexico State University, University of Pittsburgh, Princeton University, the United States Naval Observatory, and the University of Washington.

References

Abazajian, K., Adelman-McCarthy, J., Agüeros, M., et al. 2003, AJ, 126, 2081
Andreon, S. 2004, A&A, 416, 865
Barazza, F. D., Binggeli, B., & Jerjen, H. 2002, A&A, 391, 823
Beers, T. C., Flynn, K., & Gebhardt, K. 1990, AJ, 100, 32
Beijersbergen, M., Hoekstra, H., van Dokkum, P. G., & van der Hulst, T. 2002, MNRAS, 329, 385
Biviano, A., & Girardi, M. 2003, ApJ, 585, 205
Biviano, A., & Katgert, P. 2004, A&A, 424, 779
Biviano, A., Durret, F., Gerbal, D., et al. 1995, A&A, 297, 610
Biviano, A., Katgert, P., Mazure, A., et al. 1997, A&A, 321, 84
Blanton, M. R., Lin, H., Lupton, R. H., et al. 2003, AJ, 125, 2276
Blanton, M. R., Lupton, R. H., Schlegel, D. J., et al. 2005, ApJ, 631, 208
Böhringer, H., Voges, W., Huchra, J. P., et al. 2000, ApJS, 129, 435
Böhringer, H., Collins, C. A., Guzzo, L., et al. 2002, ApJ, 566, 93
Boyce, P. J., Phillips, S., Jones, J. B., et al. 2001, MNRAS, 328, 277

Carretero, C., Vazdekis, A., Beckman, J. E., Sánchez-Blázquez, P., & Gorgas, J. 2004, ApJ, 609, L45
Christlein, D., & Zabludoff, A. 2003, ApJ, 591, 764
Cole, S., Aragon-Salamanca, A., Frenk, C. S., Navarro, J. F., & Zepf, S. E. 1994, MNRAS, 271, 781
Colless, M. 1989, MNRAS, 237, 799
Conselice, C. J., Gallagher, J. S. III, & Wyse, R. F. G. 2001, ApJ, 559, 791
Conselice, C. J., Gallagher, J. S. III, & Wyse, R. F. G. 2003, AJ, 125, 66
Cortese, L., Gavazzi, G., Boselli, A., et al. 2003, A&A, 410, L25
Cross, N. J. G., Driver, S. P., Liske, J., et al. 2004, MNRAS, 349, 576
Dahlén, T., Fransson, C., Östlin, G., & Näslund, M. 2004, MNRAS, 350, 253
Davies, J. I., Roberts, S., & Sabatini, S. 2005, MNRAS, 356, 794
de Lapparent, V. 2003, A&A, 408, 845
De Propris, R., Colless, M., Driver, S. P., et al. 2003, MNRAS, 342, 725
De Propris, R., Pritchet, C. J., Harris, W. E., & McClure, R. D. 1995, ApJ, 450, 534
Dolag, K., Bartelmann, M., Perrotta, F., et al. 2004, A&A, 416, 853
Dressler, A. 1978, ApJ, 223, 765
Dressler, A. 1980, ApJ, 236, 351
Dressler, A. 2004, in Clusters of Galaxies: Probes of Cosmological Structure and Galaxy Evolution ed. J. S. Mulchaey, A. Dressler, & A. Oemler Jr. (Cambridge University Press), 206
Drinkwater, M. J., Gregg, M. D., & Colless, M. 2001, ApJ, 548, L139
Driver, S. P., Phillips, S., Davies, J. I., Morgan, I., & Disney, M. J. 1994, MNRAS, 268, 393
Durret, F., Slezak, E., Lieu, R., Dos Santos, S., & Bonamente, M. 2002, A&A, 390, 397
Eisenstein, D. J., Annis, J., Gunn, J. E., et al. 2001, AJ, 122, 2267
Ellingson, E. 2003, Ap&SS, 285, 9
Feldmeier, J. J., Ciardullo, R., Jacoby, G. H., & Durrell, P. R. 2004, ApJ, 615, 196
Fukugita, M., Shimasaku, K., & Ichikawa, T. 1995, PASP, 107, 945
Fukugita, M., Ichikawa, T., Gunn, J. E., et al. 1996, AJ, 111, 1748
Garilli, B., Maccagni, D., & Andreon, S. 1999, A&A, 342, 408
Girardi, M., Biviano, A., Giuricin, G., Mardirossian, F., & Mezzetti, M. 1993, ApJ, 404, 38
Girardi, M., Giuricin, G., Mardirossian, F., Mezzetti, M., & Boschin, W. 1998, ApJ, 505, 74
Goto, T., Sekiguchi, M., Nichol, R. C., et al. 2002, AJ, 123, 1807
Graham, A. W., Jerjen, H., & Guzmán, R. 2003, AJ, 126, 1787
Gunn, J. E., & Gott, J. R. III 1972, ApJ, 176, 1
Gunn, J. E., Carr, M., Rockosi, C., et al. 1998, AJ, 116, 3040
Hilker, M., Mieske, S., & Infante, L. 2003, A&A, 397, L9
Hogg, D. W., Finkbeiner, D. P., Schlegel, D. J., & Gunn, J. E. 2001, AJ, 122, 2129
Horner, D. 2001, Ph.D. Thesis, University of Maryland
Jerjen, H., Kalnajs, A., & Binggeli, B. 2000, A&A, 358, 845
Katgert, P., Biviano, A., & Mazure, A. 2004, ApJ, 600, 657
Kauffmann, G., White, S. D. M., & Guiderdoni, B. 1993, MNRAS, 264, 201
Kauffmann, G., White, S. D. M., Heckman, T. M., et al. 2004, MNRAS, 353, 713
Liske, J., Lemon, D. J., Driver, S. P., et al. 2003, MNRAS, 344, 307
Lobo, C., Biviano, A., Durret, F., et al. 1997, A&A, 317, 385
Loveday, J. 1997, ApJ, 489, 29
Lugger, P. M. 1986, ApJ, 303, 535
Lugger, P. M. 1989, ApJ, 343, 572
Lumsden, S. L., Collins, C. A., Nichol, R. C., Eke, V. R., & Guzzo, L. 1997, MNRAS, 290, 119
Lupton, R. H., Gunn, J. E., & Szalay, A. S. 1999, AJ, 118, 1406
Madgwick, D. S., Lahav, O., Baldry, I. K., et al. 2002, MNRAS, 333, 133
Marzke, R. O., Geller, M. J., Huchra, J. P., & Corwin, H. G. Jr. 1994, AJ, 108, 437
Menci, N., Cavaliere, A., Fontana, A., Giallongo, E., & Poli, F. 2002, ApJ, 575, 18
Mercurio, A., Massarotti, M., Merluzzi, P., et al. 2003, A&A, 408, 57
Mihos, J. C. 2004, in Clusters of Galaxies: Probes of Cosmological Structure and Galaxy Evolution ed. J. S. Mulchaey, A. Dressler, & A. Oemler Jr. (Cambridge University Press), 277
Mobasher, B., Colless, M., Carter, D., et al. 2003, ApJ, 587, 605
Moore, B., Katz, N., Lake, G., Dressler, A., & Oemler, A. Jr. 1996, Nature, 379, 613
Moore, B., Lake, G., & Katz, N. 1998, ApJ, 495, 139
Mulchaey, J. S., Davis, D. S., Mushotzky, R. F., & Burstein, D. 2003, ApJS, 145, 39
Murante, G., Arnaboldi, M., Gerhard, O., et al. 2004, ApJ, 607, L83
Nakamura, O., Fukugita, M., Yasuda, N., et al. 2003, AJ, 125, 1682
Navarro, J. F., Frenk, C. S., & White, S. D. M. 1996, ApJ, 462, 563
Navarro, J. F., Frenk, C. S., & White, S. D. M. 1997, ApJ, 490, 493
Paolillo, M., Andreon, S., Longo, G., et al. 2001, A&A, 367, 59
Phillips, S., & Driver, S. 1995, MNRAS, 274, 832
Phillips, S., Driver, S. P., Couch, W. J., & Smith, R. M. 1998, ApJ, 498, L119
Popesso, P., Böhringer, H., Brinkmann J., Voges, W., & York, D. G. 2004b, A&A, 423, 449 (Paper I)
Popesso, P., Böhringer, H., Romaniello, M., & Voges, W. 2004a, A&A, accepted [arXiv:astro-ph/0410011] (Paper II)
Popesso, P., Biviano, A., Böhringer, Romaniello, M., & Voges, W. 2004c, A&A, accepted [arXiv:astro-ph/0411536] (Paper III)
Pracy, M. B., De Propris, R., Driver, S. P., Couch, W. J., & Nulsen, P. E. J. 2004, MNRAS, 352, 1135
Rakos, K., Schombert, J., Maitzen, H. M., Prugovecki, S., & Odell, A. 2001, AJ, 121, 1974
Rauzy, S., Adami, C., & Mazure, A. 1998, A&A, 337, 31
Retzlaff, J. 2001, in Clusters of galaxies and the high redshift universe in X-rays. Recent results of XMM-Newtomn and Chandra, XXIst Moriond Astrophysics Meeting, March 10–17, 2001 Savoie, France, ed. D. M. Neumann, & J. T. T. Van
Sabatini, S., Davies, J., Scaramella, R., et al. 2003, MNRAS, 341, 981
Schechter, P. 1976, ApJ, 203, 297
Schlegel, D., Finkbeiner, D. P., & Davis, M. 1998, ApJ, 500, 525
Smith, R. M., Driver, S. P., & Phillips, S. 1997, MNRAS, 287, 415
Smith, J. A., Tucker, D. L., Kent, S., et al. 2002, AJ, 123, 2121
Stoughton, C., Lupton, R. H., Bernardi, M., et al. 2002, AJ, 123, 485
Strateva, I., Ivezić, Z., Knapp, G., et al. 2001 AJ, 122, 1861
Strauss, M. A., Weinberg, D. H., Lupton, R. H., et al. 2002, AJ, 124, 1810
The, L. S., & White, S. D .M. 1986, AJ, 92, 1248
Thompson, L. A., & Gregory, S. A. 1993, AJ, 106, 2197
Trentham, N. 1998, MNRAS, 295, 360
Trentham, N., Tully, R. B., & Verheijen, M. A. W. 2001, MNRAS, 325, 385
Tully, R. B., Somerville, R. S., Trentham, N., & Verheijen, M. A. 2002, ApJ, 569, 573
Ulmer, M. P., Bernstein, G. M., Martin, D. R., et al. 1996, AJ, 112, 2517
Valotto, C., Nicotra, M. A., Muriel, H., & Lambas, D. G. 1997, ApJ, 479, 90
van Zee, L., Skillman, E. D., & Haynes, M. P. 2004, AJ, 128, 121
Willman, B., Governato, F., Wadsley, J., & Quinn, T. 2004, MNRAS, 355, 159
Yagi, M., Kashikawa, N., Sekiguchi, M., et al. 2002, AJ, 123, 87
York, D. G., Adelman, J., Anderson, J. E. Jr., et al. 2000, AJ, 120, 1579

A&A 461, 397–410 (2007)
DOI: 10.1051/0004-6361:20054493

Astronomy & Astrophysics

RASS-SDSS galaxy cluster survey⋆

V. The X-ray-underluminous Abell clusters

P. Popesso[1], A. Biviano[2], H. Böhringer[3], and M. Romaniello[1]

[1] European Southern Observatory, Karl Scharzschild Strasse 2, 85748, Germany
e-mail: ppopesso@eso.org
[2] INAF - Osservatorio Astronomico di Trieste, via G. B. Tiepolo 11, 34131, Trieste, Italy
[3] Max-Planck-Institut fur extraterrestrische Physik, 85748 Garching, Germany

Received 8 November 2005 / Accepted 26 May 2006

ABSTRACT

Aims. In this paper we consider a large sample of optically selected clusters, in order to elucidate the physical reasons for the existence of X-ray underluminous clusters.
Methods. For this purpose we analyzed the correlations of the X-ray and optical properties of a sample of 137 spectroscopically confirmed Abell clusters in the SDSS database. We searched for the X-ray counterpart of each cluster in the ROSAT All Sky Survey. We find that 40% of our clusters have a marginal X-ray detection or remain undetected in X-rays. These clusters appear too X-ray faint on average for their mass as determined by velocity dispersion; i.e. they do not follow the scaling relation between X-ray luminosity and virial mass traced by the other clusters. On the other hand, they do follow the general scaling relation between optical luminosity and virial mass. We refer to these clusters as the X-ray-underluminous Abell clusters (AXU clusters, for short) and designate as "normal" the X-ray detected Abell systems. We separately examined the distributions and properties of the galaxy populations of the normal and the AXU clusters.
Results. The AXU clusters are characterized by leptokurtic (more centrally concentrated than a Gaussian) velocity distribution of their member galaxies in the outskirts ($1.5 < r/r_{200} \leq 3.5$), as expected for the systems in accretion. In addition, the AXU clusters have a higher fraction of blue galaxies in the external region and show a marginally significant paucity of galaxies at the center. Our results seem to support the interpretation that the AXU clusters are systems in formation undergoing a phase of mass accretion. Their low X-ray luminosity should be due to the still accreting intracluster gas or to an ongoing merging process.

Key words. galaxies: clusters: general

1. Introduction

Clusters of galaxies are extremely important astrophysical tools for many reasons. They are the most massive gravitationally bound systems in the universe. Since they sample the high-mass end of the mass function of collapsed systems, they can be used to provide tight constraints on cosmological parameters such as Ω_m, σ_8, and Λ (Eke et al. 1996; Donahue & Voit 1999). Moreover, they are extremely powerful laboratories for studying galaxy formation and evolution. To investigate the global properties of the cosmological background, it is necessary to construct and study a large sample of clusters (Borgani & Guzzo 2001).

Several techniques exist for building cluster samples, each based on different cluster properties. The first attempts at a large, homogeneous survey for galaxy clusters was conducted by Abell (1958) with the visual identification of clusters on the Palomar Observatory Sky Survey (POSS) photographic plates. Similar catalogs were constructed by Zwicky and collaborators (Zwicky et al. 1968). Since then, a large number of optically selected samples have been constructed with automated methods: EDCC (Edimburgh Durham Cluster Catalog: Lumdsen et al. 1992), APM (Automatic Plate measuring; Dalton et al. 1994), PSCS (Palomar Distant Cluster Survey; Postman et al. 1996), EIS (ESO Imaging Cluster Survey; Olsen et al. 1999), ENACS (ESO Nearby Abell Cluster Survey, Katgert et al. 1996; Mazure et al. 1996), RCS (Red sequence Cluster Survey; Gladders & Yee 2000), and the samples derived from the Sloan Digital Sky Survey (Goto et al. 2002; Bahcall et al. 2003). The advantage of using optical data is that it is relatively easy to build large optically-selected cluster catalogs that allow one to investigate cluster properties with a statistically solid database. On the other hand, the main disadvantage of the optical selection is that the selection procedure can be seriously affected by projection effects. Only a very observationally expensive spectroscopic campaign can confirm the overdensities in 3 dimensions.

In 1978, the launch of the first X-ray imaging telescope, the *Einstein* observatory, began a new era of cluster discovery, as clusters proved to be luminous ($\geq 10^{42-45}$ erg s^{-1}), extended ($r \gtrsim 1$ Mpc) X-ray sources, which are readily identified in the X-ray sky. Therefore, X-ray observations of galaxy clusters provided an efficient and physically motivated method of identification of these structures. The X-ray selection is more robust against contamination along the line-of-sight than traditional optical methods, because the X-ray emission, unlike galaxy overdensities, is proportional to the square of the (gas) density. The ROSAT satellite, with its large field of view and better sensitivity, allowed a leap forward in X-ray cluster astronomy, producing large samples of both nearby and distant clusters (Castander et al. 1995; Ebeling et al. 1996a,b; Scharf et al. 1997; Ebeling et al. 2000; Böhringer et al. 2001, 2002; Gioia et al. 2001;

⋆ Appendix A is only available in electronic form at
http://www.aanda.org

Rosati et al. 2002, and references therein). The disadvantage of X-ray cluster surveys is their lower efficiency and higher observational cost as compared to optical surveys.

It is clear that understanding the selection effects and the biases due to the different cluster selection techniques is crucial for interpreting the scientific results obtained from such different cluster samples. Castander et al. (1994) used ROSAT to observe cluster candidates in the redshift range 0.7−0.9 from the 3.5 square degree subsample of the Gunn et al. (1986) optical cluster catalog and found surprisingly weak X-ray emission. Bower et al. (1994) undertook ROSAT X-ray observations of optically selected clusters from the Couch et al. (1991) 46 deg^2 catalog. Bower et al. (1994) selected a random subset of the full catalog in the redshift range 0.15−0.66. The X-ray luminosity of almost all the selected clusters was found to be surprisingly low, suggesting, on the one hand, substantial evolution of the X-ray luminosity function between redshift $z = 0$ and $z \sim 0.4$ and, on the other, overestimated velocity dispersions for the nearby X-ray underluminous clusters, perhaps as a consequence of the contamination by galaxy filaments and of radial infall of field galaxies into the clusters. Similar results were obtained by Holden et al. (1997).

With the ROSAT Optical X-ray Survey (ROXS), Donahue et al. (2002) conclude that there is little overlap of the samples of X-ray-selected and optically-selected galaxy clusters. Only ∼20% of the optically selected clusters were found in X-rays, while ∼60% of the X-ray clusters were also identified in the optical sample. Furthermore, not all of the X-ray detected clusters had a prominent red-sequence, something that could introduce a selection bias in those cluster surveys based on color information (Goto et al. 2002; Gladders & Yee 2000). Ledlow et al. (2003) analyzed the X-ray properties of a sample of nearby bright Abell clusters, using the ROSAT All-Sky Survey (RASS). They find an X-ray detection rate of 83%. Gilbank et al. (2004) explored the biases due to optical and X-ray cluster selection techniques in the X-ray Dark Cluster Survey (XDCS). They find that a considerable fraction of the optically selected clusters do not have a clear X-ray counterpart, yet spectroscopic follow-up of a subsample of X-ray underluminous systems confirms their physical reality. Lubin et al. (2004) analyzed the X-ray properties of two optically selected clusters at $z \geq 0.7$ with XMM-Newton. They find that the two clusters are characterized by too small X-ray luminosities and temperatures, given their measured velocity dispersions. Similar results were obtained in the XMM-2dF Survey of Basilakos et al. (2004). They find many more optical cluster candidates than X-ray ones. Deeper XMM data confirmed that their X-ray undetected cluster candidates intrinsically have very low X-ray luminosities.

In this paper we consider a large sample of optically- and X-ray-selected clusters, in order to elucidate the physical reasons for the existence of underluminous optical/X-ray clusters. The starting point of this work was the analysis we conducted on a sample of X-ray selected clusters (Popesso et al. 2005a, Paper III of this series). Ninety percent of those systems were taken from the REFLEX and NORAS catalogs, which are X-ray flux-limited cluster catalogs entirely built upon the ROSAT-All-Sky Survey (RASS). The remaining 10% of that sample are groups or faint clusters with X-ray fluxes below the flux limits of REFLEX and NORAS. In Paper III we found an optical counterpart for each of the X-ray selected clusters of the RASS. Using optical data from the Sloan Digital Sky Survey (SDSS, see, e.g., Abazajian et al. 2003) for these clusters, we then studied the scatter of the correlations between several optical and X-ray cluster properties: X-ray and optical luminosities, mass, velocity dispersion, and temperature. In this paper we extend our analysis to a sample of *optically* selected clusters.

The paper is organized as follows. In Sect. 2 we describe the data and the sample of optically selected clusters used for the analysis. We also describe how we measure the optical luminosity, the velocity dispersion, the mass and the X-ray luminosity of the clusters. In Sect. 3 we analyze the correlation of both the X-ray and the optical cluster luminosities with their masses. In Sect. 4 we describe the optical properties of the Abell clusters without clear X-ray detection and compare them with those of normal X-ray emitting Abell systems. In Sect. 5 we discuss our results and give our conclusions.

We adopt a Hubble constant $H_0 = 70\ h$ km s^{-1} Mpc^{-1} and a flat geometry of the Universe, with $\Omega_m = 0.3$ and $\Omega_\Lambda = 0.7$ throughout this paper.

2. The data

The optical data used in this paper are taken from the SDSS (Fukugita et al. 1996; Gunn et al. 1998; Lupton et al. 1999; York et al. 2000; Hogg et al. 2001; Eisenstein et al. 2001; Smith et al. 2002; Strauss et al. 2002; Stoughton et al. 2002; Blanton et al. 2003; and Abazajian et al. 2003). The SDSS is still ongoing and consists of an imaging survey of π steradians of the northern sky in the five passbands u, g, r, i, z, covering the entire optical range. The imaging survey is being taken in drift-scan mode. The imaging data are being processed with a photometric pipeline specially written for the SDSS data (PHOTO, Lupton et al. 2001). For each cluster we defined a photometric galaxy catalog as described in Sect. 3 of Popesso et al. (2004, Paper I of this series, see also Yasuda et al. 2001). For the analysis in this paper we used only SDSS Model magnitudes.

The spectroscopic component of the survey is being carried out using two fiber-fed double spectrographs, covering the wavelength range 3800−9200 Å, over 4098 pixels. They have a resolution $\Delta\lambda/\lambda$ varying between 1850 and 2200, and together they are fed by 640 fibers, each with an entrance diameter of 3 arcsec.

The X-ray data were taken from the RASS. The RASS was conducted mainly during the first half year of the ROSAT mission in 1990 and 1991 (Trümper 1988). The ROSAT mirror system and the Position-Sensitive Proportional Counter (PSPC) operating in the soft X-ray regime (0.1−2.4 keV) provided optimal conditions for studying celestial objects with low surface brightness, in particular, due to the unlimited field of view of the RASS and the low background of the PSPC, this dataset is ideal for investigating the properties of nearby clusters of galaxies.

2.1. The cluster samples

2.1.1. The X-ray selected cluster sample

As reference X-ray cluster sample for the comparison between X-ray and optically selected clusters, we considered a subsample of the X-ray selected RASS-SDSS galaxy cluster sample of Popesso et al. (2005b, Paper II). The RASS-SDSS galaxy cluster catalog comprises 130 systems detected in the ROSAT All Sky Survey (RASS). The X-ray cluster properties and the redshifts were taken from different catalogs of X-ray selected clusters: the ROSAT-ESO flux limited X-ray cluster sample (REFLEX, Böhringer et al. 2001, 2002), the Northern ROSAT All-sky cluster sample (NORAS, Böhringer et al. 2000), the NORAS 2 cluster sample (Retzlaff 2001), the ASCA Cluster Catalog (ACC) from Horner et al. (2001), and the Group Sample (GS) of

Mulchaey et al. (2003). The subsample considered in this paper comprises the RASS-SDSS galaxy clusters with known mass (either the virial estimate from optical data or, when this is not available, the mass derived from the X-ray temperature) for a total number of 102 systems (69 clusters with known optical mass + 33 clusters with mass derived from the mass-temperature relation). The sample is drawn from the SDSS DR2 imaging data which cover 3324 square degrees. The considered cluster sample covers the entire range of masses and X-ray/optical luminosities, from very low-mass and X-ray/optical faint groups (10^{13} $M_{\odot}$) to very massive and X-ray/optical bright clusters (5×10^{15} $M_{\odot}$). The cluster sample comprises mainly nearby systems at the mean redshift of 0.1 and a few objects (10) in the range $0.25 \leq z \leq 0.37$. The redshift distribution of the cluster sample is shown in Fig. 1.

2.1.2. The optically selected cluster sample

The optically selected cluster sample considered in this paper is a subsample of the Abell cluster catalog (Abell 1958). We selected all the Abell clusters in the region covered by the 3rd data release (DR3) of the SDSS (5282 deg^{-2}). The Abell catalog is based on a visual inspection of galaxy overdensities. It is, therefore, affected by the presence of spurious detections due to projection effects. To exclude the spurious clusters from the catalog, we considered only the clusters with a spectroscopic confirmation of the galaxy overdensity. For this, we used the SDSS spectroscopic catalog, which provides spectra and redshifts for more than 250 000 galaxies with Petrosian magnitude $r_{\rm Petro} \leq 17.77$.

We estimated the mean cluster spectroscopic redshift $z_{\rm c}$ as the peak of the overdensity in the redshift distribution of the galaxies around the cluster coordinates. Since the purpose of this paper is to compare optical and X-ray properties of galaxy clusters, it is extremely important to avoid misclassification between the optical and the X-ray sources. Therefore, we checked our estimations of the mean cluster redshift with those available in the literature, as well as with the photometric $z_{\rm c}$ estimate obtained from the relation that links the mean redshift of a cluster with the apparent magnitude of its tenth brightest galaxy (Abell et al. 1989). Clusters for which discrepancies are found among the different $z_{\rm c}$ estimates were excluded from the final sample used in this paper.

Cluster members were selected among SDSS galaxies with available redshifts, as follows. First, we selected only galaxies within a circle of 2.15 Mpc radius (the Abell radius). We then grouped together those galaxies with intergalaxy velocity differences less than a critical value that depends on the total number of galaxies along the line-of-sight, according to the relation adopted by Adami et al. (1998a). This allowed us to define the cluster limits in velocity space. As an additional step, we applied the membership selection algorithm of Katgert et al. (2004) to *all* the galaxies (also outside an Abell radius) with velocities within the limits defined with the gapper procedure. This algorithm takes both the velocities and the clustercentric positions of the galaxies into account. The method is identical to that of den Hartog & Katgert (1996) where the cluster sample contains at least 45 galaxies, and it is a simplified version of it for smaller samples (for more details, see Appendix A in Katgert et al. 2004). It requires a cluster center to be defined. When possible, we adopted the X-ray center for this. However some clusters do not have secure X-ray detection, in which case the X-ray center cannot be accurately defined. In those cases we took the position of the brightest cluster member as the cluster center (see, e.g., Biviano et al. 1997). Analysis of clusters identified in cosmological numerical simulations indicates that the choice of the center is not critical for a correct performance of the membership selection algorithm (Biviano et al. 2006).

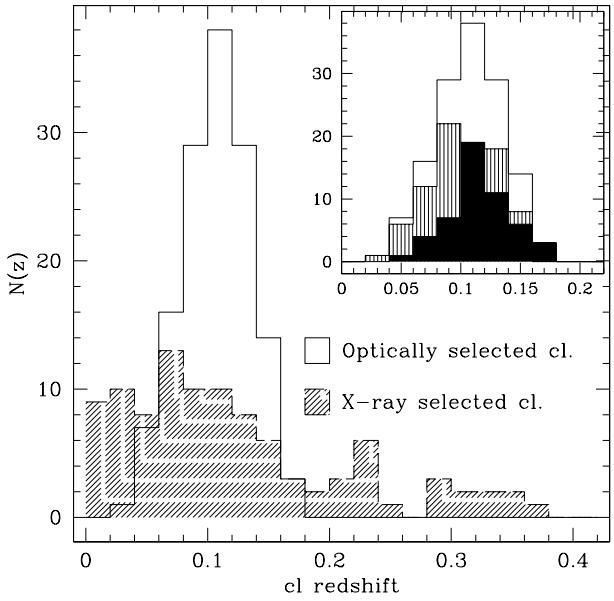

Fig. 1. Redshift distribution of the X-ray and optically selected cluster samples used in this paper. The solid line in the main panel shows the redshift distribution of the optically selected cluster sample, and the shaded histogram is the redshift distribution of the X-ray clusters. The small panel in the figure shows the redshift distribution of the X-ray detected (grey histogram) and the X-ray undetected (black histogram) optically selected clusters. The solid line in the small panel shows the redshift distribution of the whole optically selected cluster sample for comparison.

Only Abell clusters with at least 10 galaxy members were selected, since 10 is the minimum number of cluster members needed to calculate the cluster mass and velocity dispersion in a reasonable way (Girardi et al. 1993). Among the 280 Abell clusters in the region covered by DR3, 179 fulfil this requirement. Among these clusters, 38 are affected by problems of contamination, due to the presence of a close companion or a second system along the same line-of-sight but at different redshifts and 4 show large discrepancies between our estimate of $z_{\rm c}$ and the value derived from the literature or the $z_{\rm c} - m_{10}$ relation (Postman et al. 1985). Those systems were excluded from our final sample. Hence we were left with a sample of 138 Abell clusters, listed in the Appendix, along with their global properties. As shown in Fig. 1, the considered cluster sample comprises only nearby systems ($z < 0.25$) at the mean redshift of 0.1. As the X-ray reference sample, the optically selected cluster sample covers the entire range of masses and X-ray/optical luminosities, from the low-mass (faint X-ray/optical luminosity) regime (2×10^{13} $M_{\odot}$) to the high-mass (high X-ray/optical luminosity) regime (3×10^{15} $M_{\odot}$). We point out that the two cluster samples (X-ray and optically selected) considered in this work are not complete. However, for the purpose of this work we do not need complete cluster samples but clean X-ray and optically selected cluster samples spanning the whole cluster mass and luminosity range. The X-ray and optically selected cluster samples used in this work fulfil these requirements.

2.2. Optical luminosities

The estimate of the optical luminosity of a cluster, $L_{\rm op}$, requires subtraction of the foreground and background galaxy contamination. We considered two different approaches to the statistical subtraction of the galaxy background. We computed the local background number counts in an annulus around the cluster and global background number counts from the mean of the magnitude number counts determined in five different SDSS sky regions, each with an area of 30 deg^2. From our analysis we show the results obtained using the optical luminosity estimated with the second method, since the two methods produce only marginal differences in the $L_{\rm op}$ estimates. The cluster magnitude number counts in the virial region were obtained by subtracting from the galaxy counts measured within r_{200}, the local (global) field counts rescaled to the cluster area. The cluster magnitude number counts were converted in luminosity number counts after dereddening, K-correcting and transforming the apparent magnitudes in absolute magnitudes. The cluster optical luminosities were then obtained simply by summing up the luminosity number counts multiplied by the mean luminosity of the bin. The reader is referred to Paper I of this series for details of the comparison between optical luminosities obtained with different background subtraction methods and for the other technical details.

2.3. Velocity dispersions and virial masses

The virial analysis (see, e.g., Girardi et al. 1998) is performed on those clusters with at least 10 member galaxies. The velocity dispersion is computed on the cluster members, using the biweight estimator (Beers et al. 1990). The virial masses are corrected for the surface pressure term (The & White 1986) by adopting a profile of Navarro et al. (1996, 1997; NFW hereafter) with a concentration parameter, c, that depends on the initial estimate of the cluster virial mass itself. The c-mass relation is given by $c = 4 \times (M/M_{\rm KBM})^{-0.102}$ where the slope of the relation is taken from Dolag et al. (2004), and the normalization $M_{\rm KBM} \simeq 2 \times 10^{15}\ M_\odot$ from Katgert et al. (2004). The clusters in our sample span a range $c \simeq 3$–6.

The surface-pressure term correction requires knowledge of the r_{200} radius, for which we adopt the Carlberg et al. (1997) definition (see Eq. (8) in that paper) as a first guess. After the virial mass is corrected for the surface-pressure term, we refine our r_{200} estimate using the virial mass density itself. Let $M_{\rm vir}$ be the virial mass (corrected for the surface term) contained in a volume of radius equal to a chosen observational aperture, $r_{\rm ap}$, that we have set equal to the Abell radius, 2.15 Mpc. The radius r_{200} is then given by:

$$r_{200} \equiv r_{\rm ap}\,[\rho_{\rm vir}/(200\rho_{\rm c})]^{1/2.4} \qquad (1)$$

where $\rho_{\rm vir} \equiv 3M_{\rm vir}/(4\pi r_{\rm ap}^3)$ and $\rho_{\rm c}(z)$ is the critical density at redshift z in the adopted cosmology. The exponent in Eq. (1) is the one that describes the average cluster mass density profile near r_{200}, as estimated by Katgert et al. (2004) for an ensemble of 59 rich clusters.

For consistency the c-mass relation is used to interpolate (or, in a few cases, extrapolate) the virial mass $M_{\rm vir}$ from $r_{\rm ap}$ to r_{200}, yielding M_{200}. From M_{200} the final estimate of r_{200} is obtained, using the definition of M_{200} itself.

Even if the completeness level of the SDSS spectroscopic sample is very high, in the central regions of galaxy clusters such a level is likely to drop because fibers cannot be placed closer than 55 arcsec. We estimate that the spectroscopic completeness drops to ∼70% in the central ∼0.1 Mpc cluster regions. This affects the observed number-density profile of a cluster, and hence our virial mass estimates (see, e.g., Beers et al. 1984). Using the average cluster number-density profile, we estimate that this effect of incompleteness translates into an average over-estimate of the virial mass of only ∼5% (see Paper III of the series for more details about this estimate). Since the effect is very small, and much smaller than the observational uncertainties, we neglect this correcting factor in the following analysis.

2.4. X-ray luminosities

In order to create a homogeneous catalog of X-ray cluster properties, we searched for the X-ray counterparts of all the 137 Abell clusters, and compute their X-ray luminosity, $L_{\rm X}$, using only RASS data.

The X-ray luminosities are calculated with the growth curve analysis (GCA) method used for the NORAS and REFLEX cluster surveys (Böhringer et al. 2000) based on the RASS3 data base (Voges et al. 1999). The GCA method is optimized for the detection of the extended emission of clusters by assessing the plateau of the background subtracted cumulative count rate curve. We use as a final result the total flux inside the radius r_{200}, which is corrected for the missing flux estimated via the assumption of a standard β-model for the X-ray surface brightness (see Böhringer et al. 2000, for more details). The correction is typically only 8–10%, illustrating the high effectiveness of the GCA method for sampling the flux of extended sources.

We checked by eye all the X-ray sources associated to the Abell clusters. We found a secure X-ray detection for 86 systems out of the 137 isolated and well classified Abell clusters. Another 27 have a marginally significant detection (between 2 and 3σ), and another 24 do not have clear X-ray emission (detection level $\sim 1\sigma$ or no detection at all). The GCA method provides an estimate of the X-ray detection also in the case of dubious X-ray detection, but the percentage error is higher than 80%, and the estimate has to be considered as an upper limit. In 7 cases out of the 24 systems without X-ray detection, the GCA method failed completely to provide an estimate of $L_{\rm X}$. The X-ray luminosity ended up to be negative after the background subtraction. For those systems, the X-ray luminosity was set equal to zero. We discuss in detail the nature of these 27 + 24 clusters with marginal or no X-ray detection in the following sections. We refer to these 51 systems in the next paragraph as "clusters without secure X-ray detection".

3. X-ray versus optical properties

In this section we present the relations among the bolometric X-ray luminosity, the cluster mass, M_{200}, and the optical i-band luminosity, $L_{\rm op}$. The bolometric X-ray luminosity was derived by correcting the X-ray luminosity in the ROSAT energy band (0.1–2.4 keV) with the bolometric correction corresponding to the cluster temperature. The cluster temperature was estimated from the cluster mass using the $T_{\rm X} - M_{200}$ relation given in Paper III. We performed an orthogonal linear regression in logarithmic space for each of the analyzed relations. The orthogonal regression was performed with the software package ODRPACK (Akritas & Bershady 1996). Table 1 lists the values of the best fit parameters and the scatter for all the analyzed correlations. In the table, "X-ray" refers to the X-ray selected systems with known mass, taken from the RASS-SDSS galaxy cluster catalog (Paper III), "Abell" refers to the whole Abell sample considered in this work, and "A+X-ray" refers to the Abell sample

plus the X-ray selected cluster sample. "A($P_{DS} > 0.1$)+X-ray" refers to the X-ray selected clusters plus the Abell sample without the clusters with unsecure X-ray detection and the systems with high level of subclustering. The table lists three estimations of the scatter for each relation: σ is the orthogonal scatter of the A-B relation (where $A = 10^{\beta} \times B^{\alpha}$), σ_A is the scatter in the A variable and σ_B is the scatter in the B variable. All the scatter values in the table are expressed in dex, while all the errors are given at the 95% confidence level.

3.1. The $M - L_X$ relation and the Abell X-ray underluminous clusters

Panel a of Fig. 2 shows the $L_X - M_{200}$ relation obtained from the X-ray selected RASS-SDSS galaxy cluster sample. The RASS-SDSS galaxy cluster sample comprises 102 systems. For 69 of them the mass, M_{200}, was calculated through the dynamical analysis as explained in Sect. 2.3. For the remaining 33 objects, the mass was calculated using the known ICM temperature in the M-T relation given in Paper III. The solid line in panel a of Fig. 2 shows the best-fit line obtained with the whole sample (102 clusters) and the dashed line shows the best fit line obtained using the 69 clusters for which the mass is calculated as for the Abell Clusters.

Panel b of Fig. 2 shows the location of the 86 Abell clusters with clear X-ray detection in RASS relative to the best fit obtained on the X-ray selected sample. Panel c shows the behavior of the Abell systems without secure X-ray detection in the RASS in the same diagram.

As shown by panel d of Fig. 2, the scatter of the $L_X - M_{200}$ relation increases significantly when the Abell clusters are added to the sample of RASS-SDSS clusters. The best-fit parameters of the $L_X - M_{200}$ relation obtained by considering the Abell and RASS-SDSS clusters together is consistent with the relation found for only the RASS-SDSS clusters (see Table 1). However, the orthogonal scatter increases from 44 to 65%. The RASS-SDSS clusters sample comprises several clusters (10 objects) at redshifts higher than the redshift range of the Abell clusters. Thus, to check the possible effect of evolution on the scatter of the considered relation, we perform the analysis by considering the RASS-SDSS clusters in the same redshift range as the Abell clusters. The resulting correlations are perfectly consistent with the results listed in Table 1 for all the considered cluster sample. The scatter increase is not only due to the Abell clusters without clear X-ray detection. Instead, a large contribution to the increase in the scatter is given by the normal Abell clusters, which show a high level of subclustering. In fact, the presence of substructures causes the cluster mass to be overestimated. Therefore the systems presenting subclustering should deviate from the relation. We quantify the presence of galaxy substructures in the whole Abell cluster sample through the Dressler & Shectman (1988) statistical test. This test looks for deviations in the local velocity mean and dispersion from the global values. Here we adopt the slightly modified version of the test introduced by Biviano et al. (2002). We call P_{DS} the probability that a cluster does *not* contain substructures according to the Dressler & Shectman test. We find that the fraction of clusters with a probability >0.90 ($P_{DS} < 0.1$) of having significant substructure is somewhat low (20%) compared to the results of previous studies (e.g. Dressler & Shectman 1988; Biviano et al. 1997). This is not surprising. We remind the reader that the 137 Abell clusters in our sample were selected to be relatively isolated and free of major contaminations along the line-of-sight (see Sect. 2.1). As shown in Fig. 3 the cluster with values of P_{DS} lower than 0.1 have the largest negative residuals from the best fit line. When the clusters with a high level of subclustering (20% of the total), together with the Abell systems with unsecure X-ray detection, are excluded from the linear regression, the best-fit parameters and the scatter of the relation are consistent with the values found in the case of the RASS-SDSS cluster sample. Table 1 lists the results of this linear regression in the line corresponding to the A($P_{DS} > 0.1$) + X-ray sample, which refers to the Abell clusters with $P_{DS} > 0.1$ plus the RASS-SDSS systems.

In order to cahracterize the different behaviors of the normal Abell clusters and the Abell systems without secure X-ray detection, we analyzed the distribution of the residuals of the Abell clusters relatively to the RASS-SDSS $L_X - M_{200}$ relation, along the $\log(L_X)$ axis. The residuals were defined as $\Delta \log(L_X) = \log(L_{X,m}) - \log(L_{X,p})$, where $L_{X,m}$ is the measured cluster X-ray luminosity and $L_{X,p} = 0.0776\, M_{200}^{2.04}$ is the L_X predicted by the $L_X - M_{200}$ relation (see Table 1). Hence, a negative value of the residual indicates that the cluster has a low X-ray luminosity for its mass.

Panel e of Fig. 2 shows the distribution of the residuals of the normal Abell clusters. The median of the distribution is at -0.3 ± 0.3, and it moves to -0.1 ± 0.3 when the clusters with a high level of subclustering are excluded. This confirms that those systems obey the same $L_X - M_{200}$ relation as the RASS-SDSS clusters.

Panel f of Fig. 2 shows the same distribution for the Abell clusters without secure X-ray detection (except clusters with zero L_X). The median of the distribution is at -0.9 ± 0.4, which indicates that those clusters are *not* on the same $L_X - M_{200}$ relation. Seventy percent of those systems have an X-ray luminosity that is more than 3 times lower than what is expected at their mass, and 50% of them have L_X one order of magnitude lower than the expectation. Hence, the Abell clusters without secure X-ray detection appear to be clearly X-ray underluminous for their mass. What causes this effect? Are those systems real clusters? The poor significance of the X-ray detection of these systems would suggest that it is a question of spurious detections in the redshift distribution. That is, the observed 3D galaxy overdensity of those systems is not due to a unique massive cluster but to the superposition of two interacting small groups. In fact, in this case a double-peaked velocity distribution of the two systems could be misclassified as a unique Gaussian distribution with a large velocity dispersion. As a consequence, the low X-ray luminosity of the two groups would be associated to the mass of a spurious massive cluster. To check this possibility we performed several tests. A double-peaked velocity distribution misclassified as a Gaussian should appear as a platikurtic distribution (more flat-topped than a Gaussian). This effect can be quantified with the the robust scaled tail index (T.I. herafter, Beers et al. 1991). Values of the T.I. higher than unity indicate a leptokurtic distribution (i.e. more centrally peaked than a Gaussian), while values lower than unity indicate a platikurtic distribution. Values close to unity indicate consistency with a Gaussian distribution. First, we computed the T.I. values of the individual cluster velocity distributions for those clusters with unsecure X-ray detection with at least 10 member galaxies within r_{200}. Out of 51 systems, 37 fulfill this requirement. Three out of 37 have platikurtic distributions and one has a leptokurtic one, while all the remaining distributions are consistent with a Gaussian. The confidence level used in the test is 99%; therefore, less than 10% of the clusters are suspected of being spurious detections. We perform the same analysis on the normal Abell clusters finding the same percentage of platikurtic distributions.

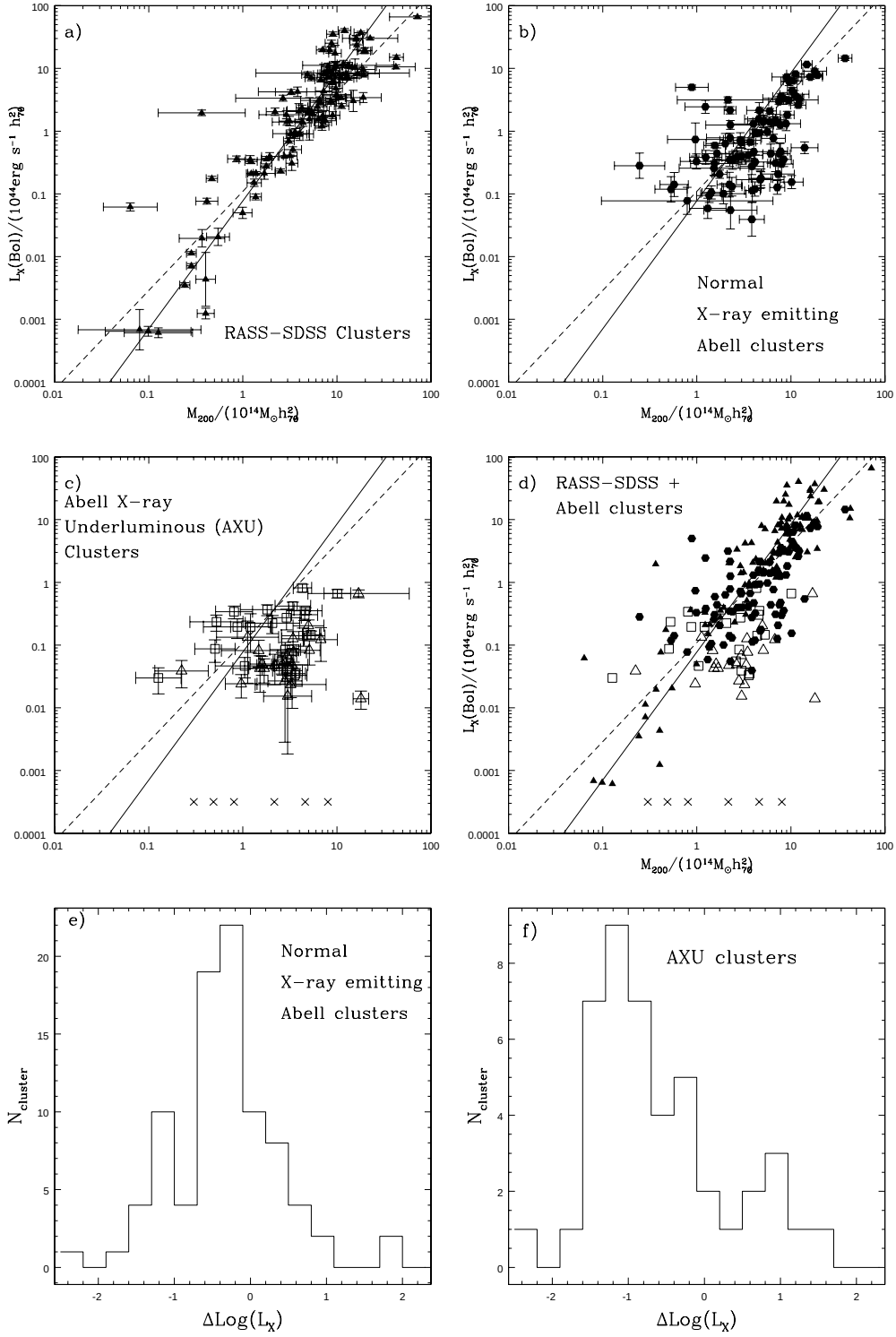

Fig. 2. $L_X - M_{200}$ relation. Panel **a)** shows the $L_X - M_{200}$ of the X-ray selected RASS-SDSS cluster sample (filled triangles). Panel **b)** shows the location of the Normal X-ray emitting Abell clusters (filled dots) relative to the best fit obtained in the X-ray selected sample. Panel **c)** shows the location of the AXU systems in the same diagram. The empty squares are the Abell clusters with marginally significant X-ray emission, and the empty triangles are the Abell clusters without X-ray emission (upper limits, see text for the explanation), the crosses are the Abell clusters for which the GCA method was not able to calculate the L_X upper limit (they are all plotted at $L_X = 10^{-40.5}$ erg s^{-1}). Panel **d)** shows the $L_X - M_{200}$ relation for the RASS-SDSS plus the whole Abell sample. The symbols in the panel have the same meaning as in the previous three panels. The solid line in the 4 panels is the best-fit line obtained in the whole X-ray selected sample of panel **a)** and the dashed line is the best fit obtained from the subsample of 69 RASS-SDSS clusters for which the mass was calculated as for the Abell clusters. Panel **e)** shows the distribution of the residuals of the normal X-ray emitting clusters. Panel **f)** shows the same distribution for the AXU clusters. The residuals are defined as $\Delta \log(L_X) = \log(L_{X,m}) - \log(L_{X,p})$, where $L_{X,m}$ is the measured cluster X-ray luminosity and $L_{X,p}$ the L_X predicted by the $L_X - M_{200}$ X-ray relation.

Table 1. The best fit parameters for the relations between several global cluster quantities, i.e. the bolometric X-ray luminosity, L_X(Bol), the virial mass, M_{200}, and the *i*-band optical luminosity L_{op}, for different samples of galaxy clusters.

A-*B* relation		sample					
A	*B*		α	β	σ	σ_B	σ_A
L_X(Bol)	M_{200}	X-ray	2.04 ± 0.08	−1.11 ± 0.06	0.16	0.21	0.43
		Abell	2.19 ± 0.14	−1.67 ± 0.14	0.23	0.32	0.48
		A+X-ray	2.12 ± 0.08	−1.32 ± 0.07	0.22	0.29	0.48
		A(P_{DS} > 0.1)+X-ray	2.06 ± 0.08	−1.21 ± 0.06	0.18	0.23	0.46
L_X(Bol)	L_{op}	X-ray	1.72 ± 0.08	−0.98 ± 0.07	0.17	0.19	0.31
		Abell	2.01 ± 0.15	−1.17 ± 0.09	0.20	0.28	0.35
		A+X-ray	1.87 ± 0.08	−1.08 ± 0.06	0.19	0.25	0.35
L_{op}	M_{200}	X-ray	0.88 ± 0.03	−0.08 ± 0.02	0.13	0.18	0.16
		Abell	0.80 ± 0.07	−0.01 ± 0.04	0.14	0.21	0.22
		A+X-ray	0.83 ± 0.03	−0.05 ± 0.03	0.14	0.20	0.19

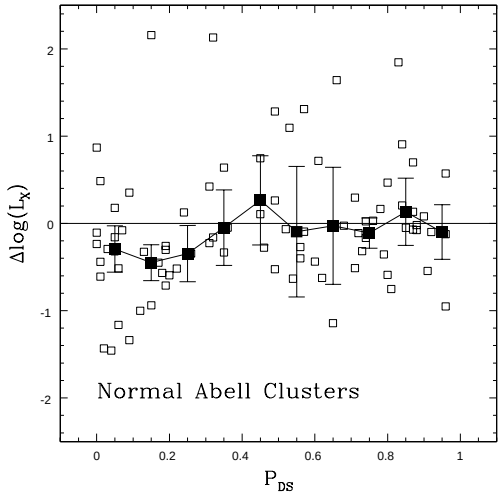

Fig. 3. The X-ray luminosity residuals $\Delta\log(L_X)$ from the best-fit $L_X - M_{200}$ relation of normal Abell clusters, vs. the Dressler & Shectman parameter P_{DS}. Systems with $P_{DS} < 0.1$ are considered to be characterized by subclustering. Filled squares with error bars represent the mean and dispersion of all points in bins of P_{DS}.

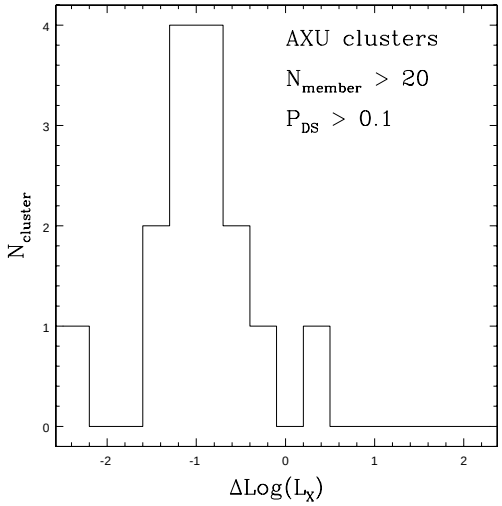

Fig. 4. Distribution of the residuals along the $\log(L_X)$ axis for the Abell clusters without secure X-ray detection with more than 20 spectroscopic members within 1 abell radius and with $P_{DS} > 0.1$. The residuals are defined as $\Delta\log(L_X) = \log(L_{X,m}) - \log(L_{X,p})$, where $L_{X,m}$ is the measured cluster X-ray luminosity and $L_{X,p}$ is the L_X predicted by the $L_X - M_{200}$ X-ray relation.

As a further test we used the Dressler & Shectman parameter to estimate the level of subclustering of those objects. Also this test is sensitive to the presence of different peaks in the redshift distribution and could reveal misclassifications. Only 5 clusters out of 51 systems without secure X-ray detection have values of P_{DS} lower than 0.1 (they comprise the 3 clusters with T.I lower than 1). Hence whether a cluster is detected or not in X-ray does not seem to be related to subclustering in the distribution of cluster galaxies.

An additional cause of uncertainties in the mass estimation is the use of a small number of spectroscopic members in the measurement. To check this point, we analyzed the residuals along the $\log(L_X)$ axis for the systems with a high number of members. Figure 4 shows the distribution of the residuals along the $\log(L_X)$ axis for the Abell clusters without secure X-ray detection with more than 20 spectroscopic members within 1 Abell radius and with $P_{DS} > 0.1$. The mass estimation of these clusters with a high number of member galaxies should be less affected by the systematics considered so far. That the distribution still peaks at -1.0 ± 0.3 confirms that these systems do not lie on the RASS-SDSS $M - L_X$ relations and that they are on average one order of magnitude fainter in the X-ray band than what is expected for their mass. Moreover, in Paper III of this series, we show that in the case of low level of subclustering, the masses obtained from the dynamical analysis of the cluster members are consistent with the hydrodynamical mass estimates.

On the basis of these analyses we conclude that the Abell clusters without secure X-ray detection are not spurious objects and that their difference with regard to the normal Abell systems and the RASS-SDSS clusters is physical. Due to their location relative to the X-ray $M - L_X$ relation, these objects are on average one order of magnitude fainter than what is expected for their mass. Their marginal detection or non-detection in X-rays suggests that RASS is too shallow to reveal the (probably weak) X-ray emission of these systems. Moreover, the detection depends on parameters that are not related to cluster properties like local RASS exposure, galactic N_H, and cluster distance. This conclusion is supported by the fact that several of these underluminous X-ray clusters are confirmed to be very faint X-ray systems by other independent analyses (Donahue et al. 2002; Ledlow et al. 2003), based on RASS PSPC-pointed observations with longer exposure times. For these reasons a better physical distinction between these systems and the normal Abell clusters is the underluminosity in X-rays of the cluster compared to the RASS-SDSS relation. However, since the errors on L_X for these clusters is so large our chosen subdivision is more

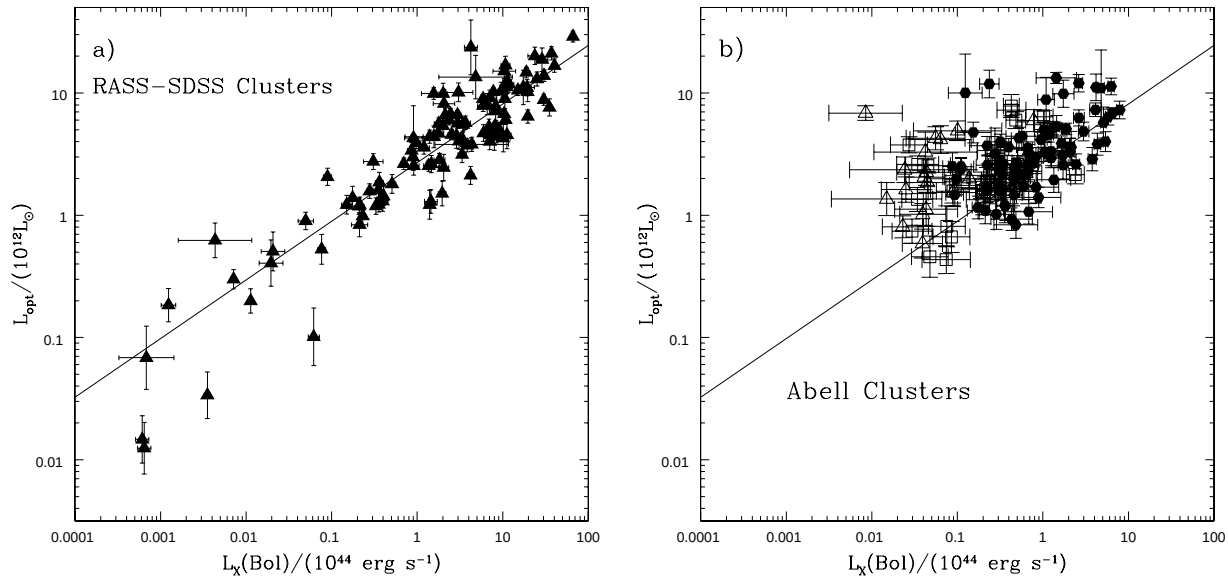

Fig. 5. $L_X - L_{op}$ relation. in panel **a)** the filled triangles are the X-ray selected clusters of the RASS-SDSS sample of Paper III. In panel **b)** the filled points are the normal X-ray emitting Abell clusters, the empty triangles are the AXU clusters with a marginally significant X-ray detection, the empty squares are the AXU clusters with no detection. The solid line is the best fit obtained from the RASS-SDSS clusters. The optical luminosity is computed in the *i*-band.

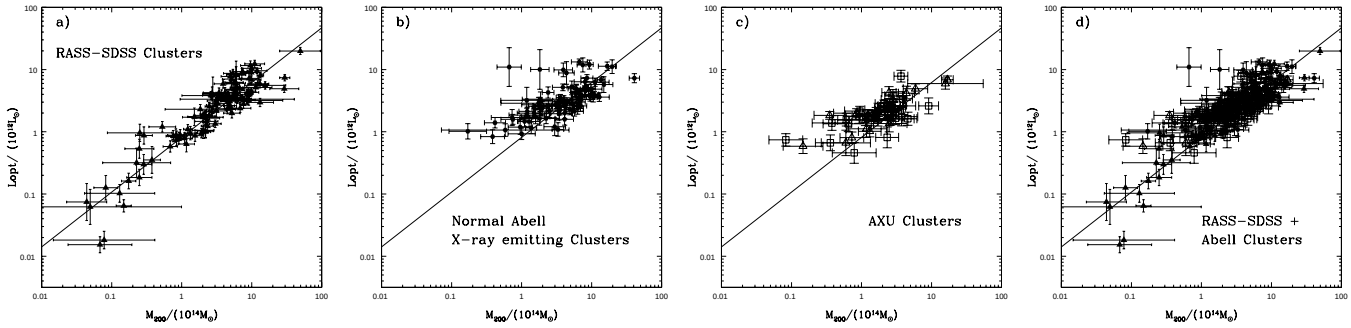

Fig. 6. $L_{op} - M_{200}$ relation. Panel **a)** shows the $L_{op} - M_{200}$ of the X-ray selected RASS-SDSS cluster sample (filled triangles). Panel **b)** shows the location of the normal X-ray emitting Abell clusters (filled dots) relatively to the best fit obtained in the X-ray selected sample. Panel **c)** shows the behavior of the AXU systems in the same relation. The empty squares are the AXU clusters with marginally significant X-ray emission, and the empty triangles are the totally underluminous AXU clusters. Panel **d)** shows the $L_{op} - M_{200}$ relation for the RASS-SDSS plus the whole Abell sample. Symbols in this panel have the same meaning as in the previous three panels. The solid line in all 4 panels is the best-fit line obtained in the X-ray-selected sample of panel **a)**. The optical luminosity was computed in the *i*-band.

practical. We call these objects X-ray underluminous Abell clusters (AXU clusters for short) throughout the paper.

3.2. The $L_X - L_{op}$ and the $L_{op} - M$ relations

Panel a of Fig. 5 shows the $L_X - L_{op}$ relation for the RASS-SDSS clusters (the optical luminosity is computed in the *i*-band). Panel b of the same figure shows the $L_X - L_{op}$ relation for the Abell sample. Similar to what was found for the $L_X - M_{200}$ relation, the best-fit regression lines obtained using the RASS-SDSS sample, or the combined RASS-SDSS and Abell samples, are not significantly different (see Table 1). Also in this case, the inclusion of the Abell clusters increases the scatter in the fitted relation. The AXU clusters are the main source of scatter, but the normal Abell clusters with high level of subclustering also contribute to increasing the scatter. The AXU clusters are significantly offset from the RASS-SDSS $L_X - L_{op}$ relation, while the normal Abell clusters are not. The mean residual of the normal Abell clusters along the $\log(L_{op})$ axis is 0.12 ± 0.25, while that of the AXU clusters is 0.54 ± 0.20. Thus, the AXU clusters are significantly underluminous in X-ray at a given optical luminosity compared to both the normal Abell clusters and the X-ray-selected RASS-SDSS systems.

Panel a of Fig. 6 shows the $L_{op} - M_{200}$ relation for the RASS-SDSS sample. Table 1 lists the best-fit parameters obtained performing a linear regression in the logarithmic space. Note that the slope of the relations and their scatter are not significantly different in other SDSS bands compared to the *i*-band. Panels b and c of Fig. 6 show the location of the normal Abell clusters and, respectively, of the AXU clusters, compared to the RASS-SDSS sample best-fit line. Clearly, both the normal Abell clusters and the AXU clusters obey the same $L_{op} - M_{200}$ relation as the X-ray selected clusters. The mean residual from the RASS-SDSS relation is ∼0 for both Abell cluster samples. Panel d of Fig. 6 shows that adding the Abell clusters to the sample of RASS-SDSS clusters does not alter the slope and the scatter of the relation (see also Table 1). The slope of the $L_{op} - M_{200}$ relation is confirmed to be less than 1. Therefore, we confirm the

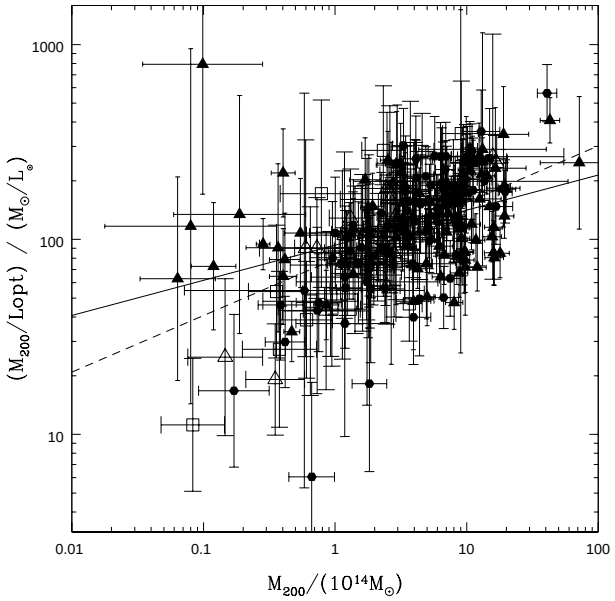

Fig. 7. The mass-to-light ratio versus the mass in the Sloan *i* band. The filled points are the normal Abell clusters, the empty triangles are the AXU clusters with a marginally significant X-ray detection, the empty squares are the AXU clusters without X-ray detection, the filled triangles are the X-ray-selected clusters of the RASS-SDSS galaxy cluster sample of Paper III. The solid line is the best fit obtained from the RASS-SDSS clusters, and the dashed line is the best fit obtained from the Abell plus the RASS-SDSS clusters.

result of Paper III that the cluster mass-to-light ratio M/L is an increasing function of the cluster mass, as shown in Fig. 7.

4. Nature of the AXU clusters

As shown in the previous section, the AXU clusters are not a source of scatter in the $L_{\rm op} - M_{200}$ relation; therefore, their optical luminosity does not differ from that of the normal X-ray emitting clusters of the same mass. On the other hand, they are significantly offset from the $L_{\rm X} - L_{\rm op}$ and $L_{\rm X} - M_{200}$ relations. In this section we try to elucidate the physical reason for this, in respect to whether the AXU clusters are different from normal X-ray emitting galaxy clusters. For this purpose, hereafter we compare the galaxy luminosity functions, the relative fractions of red and blue galaxies, galaxy number density profiles, and velocity distributions of both AXU and normal clusters. We also look for the presence of optical substructures, in order to see whether AXU clusters are more unrelaxed systems than normal clusters.

4.1. Luminosity functions

We used the SDSS photometric data to compute a composite galaxy luminosity function (LF) for the AXU systems by stacking the individual cluster LFs calculated within r_{200}. The individual LFs were obtained by subtracting the field number counts calculated within an annulus around the cluster, from the number counts in the cluster region, as described in Paper II. As in Popesso et al. (2006, Paper IV), we distinguished between early and late type galaxies using a color cut at $u - r = 2.22$, as suggested by Strateva et al. (2001). Figure 8 shows the composite LF of the AXU clusters for the whole (left-hand panel), the red (middle panel), and the blue (right-hand panel) cluster galaxy populations. For comparison we also plot the corresponding composite LFs of the normal Abell clusters, suitably renormalized to ease the comparison with the LFs of the AXU custers. The solid lines in the three panels of Fig. 8 are the best-fit double-Schechter (Schechter 1976) functions, obtained in Paper IV on the corresponding populations of the X-ray selected RASS-SDSS galaxy clusters. It is clear that there are no significant differences among the LFs of the three cluster samples, for any of the galaxy populations.

4.2. Blue galaxy fractions

In order to study the relative fraction of blue and red galaxies in the different cluster samples, we stacked the galaxy color distributions of all the clusters of each given sample together. Note that in this case we only considered spectroscopically confirmed cluster members, down to an absolute Petrosian magnitude $r_{\rm Petro} \leq -20$, and within $1.5\,r_{200}$. We find that there is no difference between the global color distributions of the normal Abell clusters and the AXU clusters. The AXU clusters do seem to have a larger fraction of blue galaxies than normal Abell clusters in the outer regions (see Fig. 9), but the statistical significance of this difference is marginal.

4.3. Galaxy number-density profiles

As in the analyses presented above, we computed the composite galaxy number-density profiles of the AXU clusters and the normal Abell clusters. These are shown in Fig. 10. In order to characterize these profiles, we fit two models to them. One is a King (1962) profile, $\Sigma(x) = \Sigma_0(1 + x^2)^{-1}$, where $x = r/r_{\rm c}$ and $r_{\rm c}$ is the core radius. The other model is the projected NFW profile, which in 3-dimensions reads $n(x) = n_0 x^{-1}(1 + x^2)^{-1}$, where $x = c_{\rm g} r/r_{200}$ and $c_{\rm g}$ is the concentration parameter. The surface density is then an integral of the 3D profile (see Bartelmann 1996, for more details).

For both the AXU and the normal Abell cluster samples, the composite radial profiles are better fit by a King profile (according to a standard χ^2 test). This agrees with previous results in the literature (Adami et al. 1998b; Díaz et al. 2005). The best-fit values of the core radii for the two samples of clusters are $r_{\rm c}/r_{200} = 0.209 \pm 0.006$ Mpc (normal Abell clusters) and $r_{\rm c}/r_{200} = 0.218 \pm 0.009$ Mpc (AXU clusters). Therefore the two profiles are perfectly consistent. However, we note that in the case of the AXU clusters an NFW profile also provides an acceptable fit to the data. This is, however, not due to a cuspier profile than that of the normal Abell clusters, but to the large error bar in the first bin of the number-density profile. Such a large error bar is due to a paucity of galaxies in the very center of AXU clusters. Hence AXU clusters, compared to normal Abell clusters, seem to have a lower central galaxy number-density. This is consistent with their larger fraction of blue galaxies (see the previous section) when we convolve this information with the morphology-density relation (Dressler 1980).

4.4. Galaxy velocity distributions

In this subsection we analyze the composite galaxy velocity distributions of the AXU clusters and the normal X-ray emitting clusters. The differences between the mean cluster velocity and the velocities of its member galaxies were normalized by $\sigma_{\rm c}$, the global cluster velocity dispersion. Each individual cluster velocity distribution was then normalized to the total number of cluster members in the region of the cluster being considered.

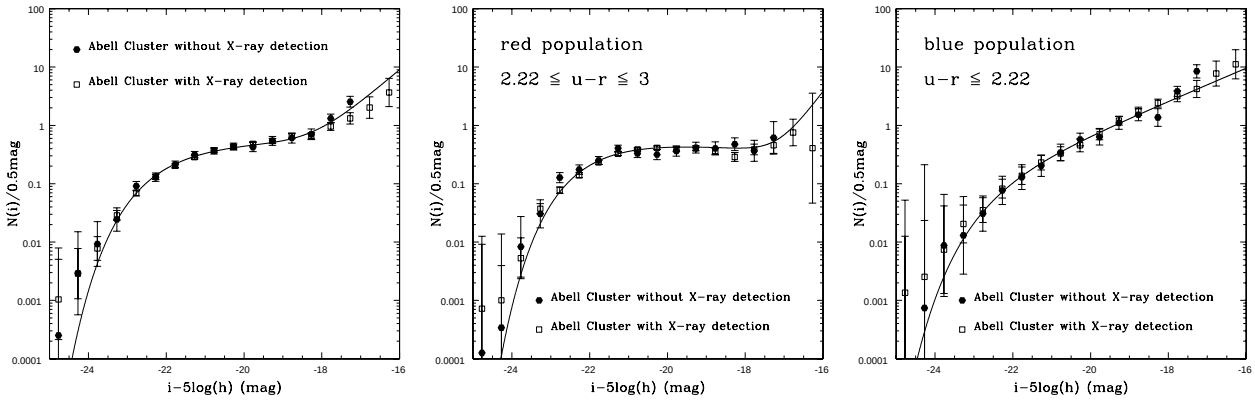

Fig. 8. The luminosity function of the normal Abell clusters and the AXU clusters. *Left panel*: composite cluster LFs of the whole galaxy population; filled dots, AXU clusters; open squares, normal Abell clusters; solid line, best-fit double Schechter LF obtained on the X-ray selected RASS-SDSS cluster sample (see Paper IV). *Middle panel*: same as left panel, but for the red galaxies only ($u - r \geq 2.22$). *Right panel*: same as left panel, but for the blue galaxies only ($u - r < 2.22$).

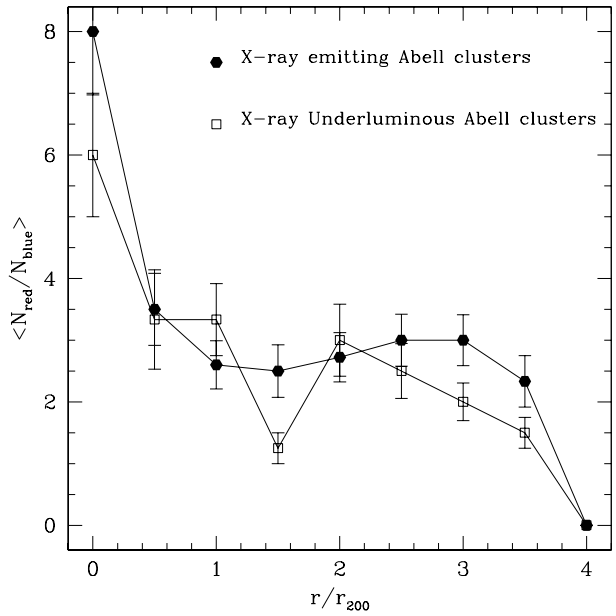

Fig. 9. The ratio of the numbers of red and blue cluster galaxies as a function of the clustercentric distance in units of r_{200}.

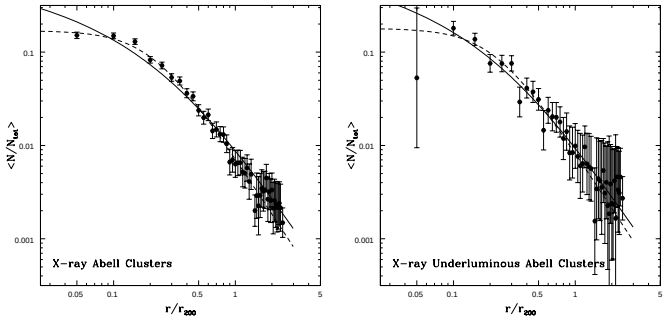

Fig. 10. The composite galaxy number density profiles of the normal Abell clusters (*left panel*) and of the AXU clusters (*right panel*). The solid and dashed lines are the best fits given by a projected NFW, and, respectively, a King density profile.

We considered only member galaxies with absolute Petrosian magnitude $r_{\rm Petro} \leq -20$ mag, which is brighter than the limiting magnitude of any cluster in our sample. We estimated the incompleteness of cluster spectroscopic samples by comparing the number of cluster spectroscopic members found within $3.5\,r_{200}$ and within the chosen absolute magnitude limit, with the number of cluster members obtained from the photometric data. The photometric sample is not affected by incompleteness down to the chosen magnitude limit. The number of photometric cluster members was obtained by subtracting the number of background galaxies at the same magnitude limit, rescaled by the cluster area, from the number of galaxies (cluster+field) in the cluster region. From this analysis we conclude that all the clusters have a spectroscopic completeness ≥80% down to $r_{\rm Petro} \leq -20$ mag.

Figure 11 shows the composite cluster velocity distributions of the normal Abell clusters and the AXU clusters, for two clustercentric distance intervals, $r/r_{200} \leq 1.5$ ("inner" sample hereafter) and $1.5 < r/r_{200} \leq 3.5$ ("outer" sample hereafter). The best-fit Gaussian dispersion decreases from 1.00 ± 0.01 to 0.96 ± 0.02 from the inner to the outer velocity distribution of the normal Abell clusters. The decrease is much stronger for the AXU clusters, from 1.00 ± 0.05 to 0.80 ± 0.07. Hence, the velocity dispersion profile is much steeper for the AXU clusters than for the normal Abell clusters. It is reminiscent of the steep velocity dispersion profile of late-type cluster galaxies (Biviano et al. 1997; Adami et al. 1998c; Biviano & Katgert 2004).

In order to gain more insight into the meaning of this result, we considered statistics that address the *shape* of the velocity distributions. A classical shape estimator, the kurtosis, is not recommended because it is very much influenced by the tails of the distribution. Instead, we consider the more robust T.I. The values of the T.I. for the considered distribution are 1.05, 0.88, 1.16, 1.45 for the four subsamples (inner normal, outer normal, inner AXU, outer AXU, respectively). As explained above, values higher than unity indicate a leptokurtic distribution (i.e. more centrally peaked than a Gaussian), while values lower than unity indicate a platikurtic distribution (i.e. more flat-topped than a Gaussian). Only the T.I. value 1.45 is significantly different from unity at >99% confidence level. We conclude that the outer velocity distribution of the AXU clusters is not only significantly narrower than all other velocity distributions, but it is also significantly non-Gaussian, leptokurtic in particular. Leptokurtic

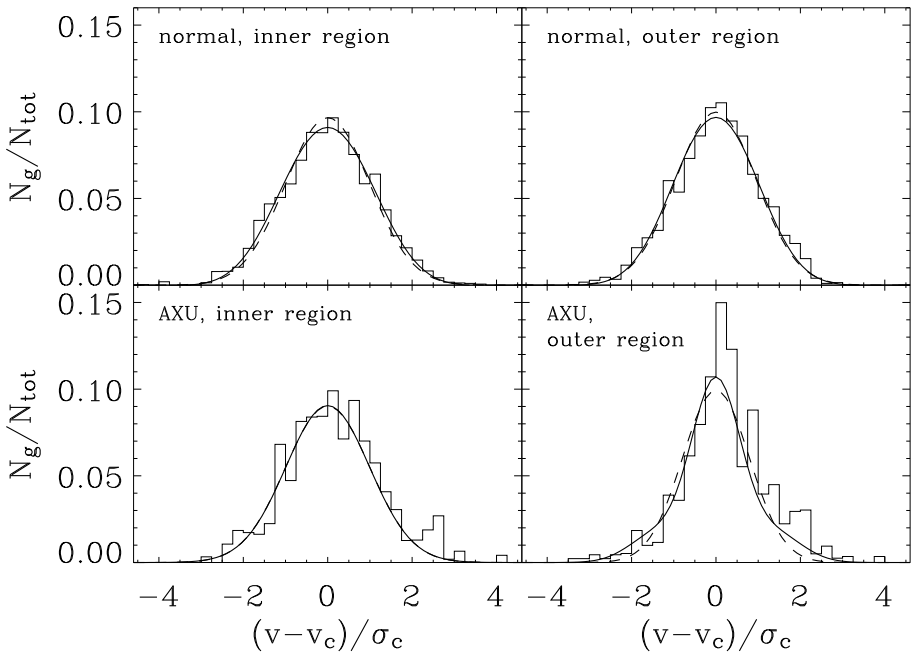

Fig. 11. The composite cluster velocity distributions. *Top-left panel*: the velocity distribution of galaxies in normal Abell clusters (histogram), within $1.5\,r_{200}$. *Top-right panel*: the velocity distribution of galaxies in normal Abell clusters (histogram), at clustercentric distances in the range $1.5{-}3.5\,r_{200}$. *Bottom-left panel*: the velocity distribution of galaxies in AXU clusters (histogram), within $1.5\,r_{200}$. *Bottom-right panel*: the velocity distribution of galaxies in AXU clusters (histogram), at clustercentric distances in the range $1.5{-}3.5\,r_{200}$. In each panel, the dashed line represents the best-fit Gaussian, and the solid line the best-fit obtained with a GH polynomial of order 4.

velocity distributions occur in the outer cluster regions when the external cluster members are characterized by radially elongated orbits (Merritt 1987; van der Marel et al. 2000). Cosmological simulations predict that haloes should display leptokurtic velocity distributions in their infall regions, characterized by ordered flows (Wojtak et al. 2005).

In order to estimate the amount of radial anisotropy required to fit the shape of the outer velocity distribution of AXU clusters, we determined the value of the Gauss-Hermite (GH hereafter) moment of order four (see, e.g., van der Marel et al. 2000). For completeness we determined the GH moments also for the velocity distributions of the other three subsamples. As expected from the T.I. analysis above, the GH polynomial fits to the velocity distributions of the normal Abell cluster galaxies and of the inner AXU cluster galaxies are very similar to the Gaussian fits, and only for the velocity distribution of the outer AXU cluster galaxies is there a clear difference between the GH polynomial fit and the Gaussian fit (see Fig. 11).

We then compared the values of the 4th-order GH moments of these velocity distributions with the predictions of the dynamical models of van der Marel et al. (2000, see their Fig. 8). While these predictions do depend on the number density distribution of the considered galaxy population, such a dependence is not strong. Hence, direct comparisons with van der Marel et al. dynamical models should provide useful information on the orbital anisotropy of the galaxy populations.

The 4th-order GH moments are −0.018 and −0.012 for the inner and outer velocity distributions of normal Abell cluster galaxies, respectively, and 0.002 and 0.106 for the inner and outer velocity distributions of AXU cluster galaxies, respectively. These values are all consistent with isotropic orbits, except that of the outer velocity distribution of the AXU cluster galaxies. For this population, we find $\sigma_r/\sigma_t \sim 2$, where σ_r and σ_t are the radial and tangential velocity dispersions of the galaxy population.

Analysis of the galaxy velocity distributions reveals a clear difference between normal Abell clusters and AXU clusters. The characteristics of the velocity distribution of AXU cluster galaxies is reminiscent of an infalling galaxy population, such as the one seen in numerical simulations in the external regions of dark matter haloes (Wojtak et al. 2005). The higher fraction of blue galaxies seen in AXU clusters, compared to that seen in normal Abell clusters, is certainly consistent with a higher fraction of infalling galaxies, since these must be part of the field galaxy population.

5. Discussion and conclusions

We have studied the X-ray and optical properties of 137 isolated Abell clusters. Each object has a confirmed 3D overdensity of galaxies. We looked for the X-ray counterpart of each system in the RASS data. Three classes of objects have been identified, where the classification is based on the quality of the X-ray detection. Eighty-six clusters out of the 137 Abell systems have a clear X-ray detection and are considered normal X-ray emitting clusters (the "normal Abell clusters"), 27 systems have a X-ray detection of low significance (less than 3σ), and 24 do not have clear X-ray detection (a rough estimate of L_X is provided but with huge statistical errors).

The normal Abell clusters follow the same scaling relations as observed in the X-ray-selected RASS-SDSS clusters. The 24 + 27 Abell clusters with unsecure X-ray detection appear to be outliers in the $L_X - M_{200}$ relation determined for X-ray luminous clusters. Their X-ray luminosity is on average one order of magnitude fainter than would be expected for their mass. A careful analysis of the 3D galaxy overdensity of these systems reveals that the individual galaxy velocity distributions in the virial region are Gaussian in 90% of the clusters and cannot be ascribed to the superposition of smaller interacting systems. We conclude that these Abell clusters with unsecure X-ray

detection in RASS are not spurious detections in the redshift distribution, but are a distinct class of objects. Due to their location with regard to the RASS-SDSS $M - L_X$ relation, we call them "Abell X-ray underluminous clusters", or AXU clusters for short. Several AXU clusters are confirmed to be very faint X-ray objects in the literature. Their X-ray flux is probably too low to be detected in the RASS survey, and yet, AXU clusters are not outliers from the $L_{\rm op} - M_{200}$ relation; i.e. they have a normal optical luminosity, given their mass. Hence, the distinctive signature of AXU clusters seems to lie in an X-ray luminosity that is unexpectedly low.

We looked for other properties of AXU clusters that make them different from normal Abell clusters. We have shown that AXU clusters do not have more substructures than normal Abell clusters. The galaxy luminosity functions within the virial region of the two cluster samples are very similar to each other. Also fairly similar are their galaxy number density profiles, even if the AXU clusters seem to lack galaxies near the core, relative to normal Abell clusters (but the significance of this result is low). The fractions of blue galaxies in the two kinds of clusters are only marginally different, since AXU clusters are characterized by a higher fraction.

The main difference between the two classes of objects lies in the velocity distribution of their member galaxies. The galaxy velocity distribution of the normal Abell clusters is perfectly fitted by a Gaussian both in the inner, virialized region ($\leq 1.5\,r_{200}$) and in the external region ($1.5\,r_{200} \leq r \leq 3.5\,r_{200}$). The AXU clusters instead only have a Gaussian velocity distribution within the virial region. In the external region, their velocity distribution is significantly more peaked than a Gaussian. The analysis of its shape by comparison with dynamical models available in the literature (van der Marel et al. 2000), suggests a radially anisotropic galaxy orbital distribution. However, the galaxies in this external region need not be in dynamical equilibrium with the cluster potential. As a matter of fact, a leptokurtic shape of the velocity distribution is a typical signature of the external, infall regions of dark matter haloes (Wojtak et al. 2005).

Analysis of the velocity distribution of the AXU clusters in their outer regions therefore suggests the presence of an unvirialized component of the galaxy population, still in the process of accretion onto the cluster. This infalling population would be mainly composed of field, hence blue, galaxies, which could then explain the excess of blue galaxies in AXU clusters, compared to normal Abell clusters. On the other hand, the Gaussian velocity distribution in the inner region suggests that there the galaxy population is dynamically more evolved, and probably virialized.

By a similar analysis of a different sample of X-ray underluminous clusters, Bower et al. (1997) proposed two different scenarios. AXU clusters could be severely affected by projection effects arising from surrounding large-scale structure filaments elongated along the line-of-sight. Their velocity dispersion, hence their virial masses would then be severely overestimated by interlopers in the filaments. In the alternative scenario, AXU clusters could be clusters that are not yet formed, or in the phase of forming, or, at least, caught at a particular stage of their evolution, while they are undergoing rapid mass growth.

Should the former of the two scenarios apply, we would expect AXU clusters to be X-ray underluminous for their mass, but they could still be optically luminous because we partly see the light of the filament projected onto the cluster. However, contamination by interlopers does affect the optical luminosity estimate, but not so much as the virial mass estimate and not so much in the *i* band, where contamination by the field (hence

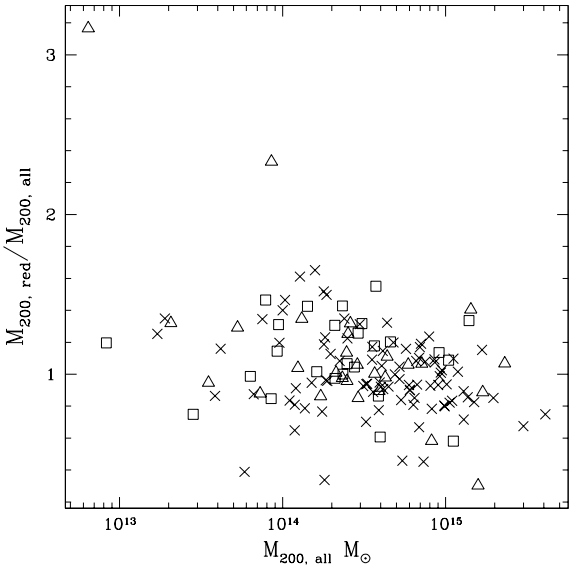

Fig. 12. Ratio of M_{200} calculated only with the red cluster members ($M_{200,\,\rm red}$) and M_{200} calculated with all the cluster members ($M_{200,\,\rm all}$) versus $M_{200,\,\rm all}$. The crosses are the "normal" Abell clusters, the empty triangles and squares are the AXU systems with marginally significant and without X-ray detection, respectively.

blue) galaxies should be small. Therefore, in such a scenario, it would be surprising that the clusters obey the $L_{\rm op} - M_{200}$ relation so well, which requires that the effects of the filament on the dynamical mass estimate and the optical light in the aperture both conspire not to produce an offset from the relation. It would also be surprising that the AXU clusters show a galaxy LF perfectly consistent with the steep LF found in galaxy clusters (see Papers II and IV) and not the flat LF observed in the field (Blanton et al. 2005). Instead, AXU clusters are not outliers from the $L_{\rm op} - M_{200}$ relation. If anything, AXU clusters are overluminous in the optical for their mass. In fact, the biweight-average (see Beers et al. 1990), *i*-band, mass-to-light ratios of normal Abell clusters and AXU clusters are $150 \pm 10\,M_\odot/L_\odot$ and $110 \pm 10\,M_\odot/L_\odot$, respectively.

As a further test, we have re-calculated the virial masses of all clusters by considering only red cluster members belonging to the red sequence in the $u - i$ vs. i color–magnitude diagram. In this way contamination by interlopers is strongly reduced (see, e.g., Biviano et al. 1997, 2006). Masses computed using all cluster members are compared to masses computed using only red-sequence members in Fig. 12. The cluster masses do not change significantly when only red-sequence members are used to calculate them, suggesting a low level of contamination by interlopers.

The results of our analyses therefore support the Bower et al. alternative scenario; namely, AXU clusters are systems in the stage of formation and/or of significant mass accretion. If AXU clusters are still forming, the intra-cluster gas itself may still be infalling or may not yet have reached the virial temperature. In addition, for AXU clusters undergoing massive accretion, it is to some degree possible that the continuous collisions of infalling groups is affecting the gas distribution, lowering its central density (such as in the case of the so-called "bullet cluster", see Barrena et al. 2002 and Clowe et al. 2004). In both cases the X-ray luminosity would be substantially lower than predicted for the virial mass of the system, because of its dependence on the square of the gas density. We note, however, that a virialized cluster undergoing a strong collision with an infalling group

would show up as a substructured cluster, yet the AXU clusters do not show an increased level of substructures when compared to normal Abell clusters. In summary, we know that the X-ray emission is very dominated by the central region, whereas the optical properties are more global. Therefore it could well be that we see a rough relaxation on the large scale (within $1.5r_{200}$) of the galaxy system reflected by a rough Gaussian galaxy velocity distribution, while the central region has not yet settled to reach the high density and temperatures of the luminous X-ray clusters.

In order to explore this further, we need much more detailed information on the distribution of the density and temperature of the intracluster gas in AXU clusters, something that cannot be done with the RASS data but that requires the spatial resolution and sensitivity of XMM-Newton.

Our results support the conclusion of Donahue et al. (2002) concerning the biases inherent in the selection of galaxy clusters in different wavebands. Although the optical selection is prone to substantial projection effects, the X-ray selection is also not perfect or not simple to characterize. The existence of X-ray underluminous clusters, even with large masses, makes it difficult to reach the needed completeness in mass for cosmological studies. Moreover, as discussed in Paper III, the relation between the X-ray luminosity and mass is not very tight even for the X-ray bright clusters, and the relation between cluster masses and optical luminosities is as tight or perhaps even tighter. Clearly, a multi-waveband approach is needed for optimizing the completeness and reliability of cluster samples.

On the other hand, it becomes clear that, for precision cosmology, we also need a more observationally oriented prescription for cluster selection from theory, rather than a mere counting of "relaxed" dark-matter haloes. Predicted distribution functions closer to the observational parameters, like temperature or velocity dispersion distribution functions and their relations to X-ray and optical luminosity, are needed.

Acknowledgements. We thank the referee F. Castander for the useful comments that helped in improving the paper. We thank Alain Mazure for useful discussions. Funding for the creation and distribution of the SDSS Archive has been provided by the Alfred P. Sloan Foundation, the Participating Institutions, the National Aeronautics and Space Administration, the National Science Foundation, the US Department of Energy, the Japanese Monbukagakusho, and the Max Planck Society. The SDSS Web site is `http://www.sdss.org/`. The SDSS is managed by the Astrophysical Research Consortium (ARC) for the Participating Institutions. The Participating Institutions are The University of Chicago, Fermilab, the Institute for Advanced Study, the Japan Participation Group, The Johns Hopkins University, Los Alamos National Laboratory, the Max-Planck-Institute for Astronomy (MPIA), the Max-Planck-Institute for Astrophysics (MPA), New Mexico State University, University of Pittsburgh, Princeton University, the United States Naval Observatory, and the University of Washington.

References

Abell, G. O. 1958, ApJ, 3, 211
Abell, G. O., Corwin, H. G. Jr., & Olowin, R. P. 1989, ApJ, 70, 1
Abazajian, K., Adelman, J., Agueros, M., et al. 2003, AJ, 126, 2081 (Data Release One)
Adami, C., Mazure, A., Biviano, A., Katgert, P., & Rhee, G. 1998a, A&A, 331, 493
Adami, C., Mazure, A., Katgert, P., & Biviano, A. 1998b, A&A, 336, 63
Adami, C., Biviano, A., & Mazure, A. 1998c, A&A, 331, 439
Akritas, M. G., & Bershady, M. A. 1996, ApJ, 470, 706
Bahcall, N. A., McKay, T. A,, Annis, J., et al. 2003, ApJ, 148, 243
Barrena, R., Biviano, A., Ramella, M., Falco, E. E., & Seitz, S. 2002, A&A, 386, 816
Bartelmann, M. 1996, A&A, 313, 697
Basilakos, S., Plionis, M., Georgakakis, A., & Georgantopoulos, I. 2004, MNRAS, 351, 989
Beers, T. C., Geller, M. J., Huchra, J. P., Latham, D. W., & Davis, R. J. 1984, ApJ, 283, 33
Beers, T. C., Flynn, K., & Gebhardt 1990, AJ, 100, 32
Beers, T. C., Forman, W., Huchra, J. P., Jones, C., & Gebhardt, K. 1991, AJ, 102, 1581
Biviano, A., & Katgert, P. 2004, A&A, 424, 779
Biviano, A., Katgert, P., Mazure, A., et al. 1997, A&A, 321, 84
Biviano, A., Katgert, P., Thomas, T., & Adami, C. 2002, A&A, 387, 8
Biviano, A., Murante, G., Borgani, S., et al. 2006, A&A, 456, 23
Blanton, M. R., Lupton, R. H., Maley, F. M., et al. 2003, AJ, 125, 2276
Blanton, M. R., Lupton, R. H., Schlegel, D. J., et al. 2005, ApJ, 631, 208
Böhringer, H., Voges, W., Huchra, J. P., et al. 2000, ApJS, 129, 435
Böhringer, H., Schuecker, P., Guzzo, L., et al. 2001, A&A, 369, 826
Böhringer, H., Collins, C. A., Guzzo, L., et al. 2002, ApJ, 566, 93
Borgani, S., & Guzzo, L. 2001, Nature, 409, 39
Bower, R. G., Bohringer, H., Briel, U. G., et al. 1994, MNRAS, 268, 345
Bower, R. G., Castander, F. J., Ellis, R. S., et al. 1997, MNRAS, 291, 353
Carlberg, R. G., Yee, H. K., & Ellingson, E. 1997, ApJ, 478, 462
Castander, F. J., Ellis, R. S., Frenk, C. S., Dressler, A., & Gunn, J. E. 1994, ApJ, 424, 79
Castander, F. J., Bower, R. G., & Ellis, R. S. 1995, Nature, 377, 39
Clowe, D., De Lucia, G., & King, L. 2004, MNRAS, 350, 1038
Couch, W. J., Ellis, R. S., MacLaren, I., & Malin, D. F. 1991, MNRAS, 249, 606
Dalton, G. B., Efstathiou, G., Maddox, S. J., & Sutherland, W. J. 1994, MNRAS, 269, 151
den Hartog, R., & Katgert, P. 1996, MNRAS, 279, 349
Díaz, E., Zandivarez, A., Merchán, M. E., & Muriel, H. 2005, ApJ, 629, 158
Dolag, K., Bartelmann, M., Perrotta, F., et al. 2004, A&A, 416, 853
Donahue, M., & Voit, M. 1999, ApJ, 523, 137
Donahue, M., Scharf, C. A., Mack, J., et al. 2002, ApJ, 569, 689
Dressler, A. 1980, ApJ, 236, 351
Dressler, A., & Shectman, S. A. 1988, AJ, 95, 985
Ebeling, H., Voges, W., Bohringer, H., et al. 1996a, MNRAS, 281, 799
Ebeling, H., Voges, W., Bohringer, H., et al. 1996b, MNRAS, 283, 1103
Ebeling, H., Edge, A. C., Allen, S. W., et al. 2000, MNRAS, 318, 333
Eisenstein, D. J., Annis, J., Gunn, J. E., et al. 2001, AJ, 122, 2267
Eke, V. R., Cole, S., Frenk, C. S., et al. 1996, MNRAS, 282, 263
Fukugita, M., Ichikawa, T., & Gunn, J. E. 1996, AJ, 111, 1748
Gilbank, D. G., Bower, R. G., Castander, F. J., & Ziegler, B. L. 2004, MNRAS, 348, 551
Gioia, I. M., Henry, J. P., Mullis, C. R., et al. 2001, ApJ, 553, 105
Girardi, M., Biviano, A., Giuricin, G., Mardirossian, F., & Mezetti, M. 1993, ApJ, 404, 38
Girardi, M., Giuricin, G., Mardirossian, F., Mezzetti, M., & Boschin, W. 1998, ApJ, 505, 74
Gladders, M. D., & Yee, H. K. C. 2000, AJ, 120, 2148
Goto, T., Sekiguchi, M., Nichol, R. C., et al. 2002, AJ, 123, 1807
Gunn, J. E., Hoessel, J. G., & Oke, J. B. 1986, ApJ, 306, 30
Gunn, J. E., Carr, M. A., Rockosi, C. M., et al. 1998, AJ, 116, 3040 (SDSS Camera)
Holden, B. P., Romer, A. K., Nichol, R. C., & Ulmer, M. P. 1997, AJ, 114, 1701
Hogg, D. W., Finkbeiner, D. P., Schlegel, D. J., & Gunn, J. E. 2001, AJ, 122, 2129
Horner, D. 2001, Ph.D. Thesis, University of Maryland
Katgert, P., Mazure, A., Perea, J., et al. 1996, A&A, 310, 8
Katgert, P., Biviano, A., & Mazure, A. 2004, ApJ, 600, 657
King, I. 1962, AJ, 67, 471
Ledlow, M. J., Voges, W., Owen, F. N., & Burns, J. O. 2003, AJ, 126, 2740
Lubin, L. M., Mulchaey, J. S., & Postman, M. 2004, ApJ, 601, 9
Lumsden, S. L., Collins, C. A., Nichol, R. C., et al. 1992, MNRAS, 258, 1
Lupton, R. H., Gunn, J. E., & Szalay, A. S. 1999, AJ, 118, 1406
Lupton, R., Gunn, J. E., Ivezić, Z., et al. 2001, in Astronomical Data Analysis Software and Systems X, ed. F. R. Harnden, Jr., F. A. Primini, & H. E. Payne (San Francisco: Astr. Soc. Pac.), ASP Conf. Ser., 238, 269 [arXiv:astro-ph/0101420]
Mazure, A., Katgert, P., den Hartog, R., et al. 1996, A&A, 310, 31
Merritt, D. R. 1987, ApJ, 313, 121
Mulchaey, J. S., Davis, D. S., Mushotzky, R. F., & Burstein, D. 2003, ApJS, 145, 39
Navarro, J. F., Frenk, C. S., & White, S. D. M. 1996, ApJ, 462, 563
Navarro, J. F., Frenk, C. S., & White, S. D. M. 1997, ApJ, 490, 493 (NFW)
Olsen, L. F., Scodeggio, M., da Costa, L., et al. 1999, A&A, 345, 681
Popesso, P., Böhringer, H., Brinkmann J., Voges, W., & York, D. G. 2004, A&A, 423, 449 (Paper I)

Popesso, P., Biviano, A., Böhringer, H., Romaniello, M., & Voges, W. 2005a, A&A, 433, 431 (Paper III)
Popesso, P., Böhringer, H., Romaniello, M., & Voges, W. 2005b, A&A, 433, 415 (Paper II)
Popesso, P., Biviano, A., Böhringer, H., & Romaniello, M. 2006, A&A, 445, 29 (Paper IV)
Postman, M. 1985, Huchra, J. P., Geller, M. J., & Henry, J. P. 1985, AJ, 90, 1400
Postman, M., Lubin, L. M., Gunn, J. E., et al. 1996, AJ, 111, 615
Retzlaff, J. 2001, XXIst Moriond Astrophysics Meeting, March 10−17, 2001 Savoie, France, ed. D. M. Neumann, & J. T. T. Van
Rosati, P., Borgani, S., & Norman, C. 2002, ARA&A, 40, 539
Scharf, C. A., Jones, L. R., Ebeling, H., et al. 1997, ApJ, 477, 79
Schechter, P. 1976, ApJ, 203, 297
Smith, J. A., Tucker, D. L., Kent, S. M., et al. 2002, AJ, 123, 2121
Stoughton, C., Lupton, R. H., Bernardi, M., et al. 2002, AJ, 123, 485
Strateva, I., Ivezić, Z., Knapp, G., et al. 2001, AJ, 122, 1861
Strauss, M. A., Weinberg, D. H., Lupton, R. H., et al. 2002, AJ, 124, 1810
The, L. S., & White, S. D. M. 1986, AJ, 92, 1248
Trümper, J. 1988, NATO Advanced Science Institutes (ASI) Series C, 249, 355
van der Marel, R. P., Magorrian, J., Carlberg, R. G., Yee, H. K. C., & Ellingson, E. 2000, AJ, 119, 2038
Voges, W., Aschenbach, B., Boller, T., et al. 1999, A&A, 349, 389
Wojtak, R., Łokas, E. L., Gottlöber, S., & Mamon, G. A. 2005, MNRAS, 361, L1
Yasuda, N., Fukugita, M., Narayanan, V. K., et al. 2001, AJ, 122, 1104
York, D. G., Adelman, J., Anderson, J. E., et al. 2000, AJ, 120, 1579
Zwicky, F., Herzog, E., Wild, P., Karpowicz, M., & Kowal, C. 1961−1968, Catalog of Galaxies and Clusters of Galaxies 1−6 (Pasadena: Caltech)

Online Material

Appendix A: The Abell Cluster Catalog

Table A.1. Here we list the properties of the 137 spectroscopically confi rmed Abell systems extracted from the SDSS DR3, used in this paper. The meaning of the individual columns is the following: Col. 1: the name of the Abell cluster; Col. 2: the number of cluster members within 1 Abell radius; Col. 3: the cluster mean redshift; Col. 4: the cluster velocity dispersion and its error Col. 5: the cluster mass within r_{200}, M_{200}, in units of 10^{14} $M_{\odot}$; Col. 6: the cluster mass within r_{200} calculated using only the cluster red members, $M_{200,\mathrm{red}}$, in units of 10^{14} $M_{\odot}$; $M_{200,\mathrm{red}}$ is given only for the clusters with at least 10 red members; Col. 7: the fractional error on M_{200} and $M_{200,\mathrm{red}}$; Col. 8: the cluster virial radius, r_{200}, in Mpc; Col. 9: the cluster optical luminosity L_{op} and its error, in unit of 10^{12} $L_{\odot}$; Col. 10: the cluster X-ray luminosity in the ROSAT energy band (0.1−2.4 erg s^{-1}), in unit of 10^{44} erg s^{-1}; Col. 11: the fractional error on the X-ray luminosity; Col. 12: the Dressler & Shectman probability that a cluster does not contain substructures, P_{DS} (values <0.1 indicate clusters that are likely to contain substructures); Col. 13: the X-ray class: 0 for the normal X-ray emitting cluster, 1 for the Abell systems with less the 3σ X-ray detection, 2 for the X-ray non-detected Abell Clusters.

Name	N_{mem}	z_{c}	σ_{c}	M_{200}	$M_{200,\mathrm{red}}$	er_M	r_{200}	L_{op}	L_{X}	$er_{L_{\mathrm{X}}}$	P_{DS}	X-class
a0116	24	0.0661	582 ± 73	4.66	4.71	0.29	1.6	1.59 ± 0.35	0.090	0.25	0.19	0
a0117	95	0.0550	559 ± 41	4.03	3.85	0.15	1.5	2.52 ± 0.64	0.064	0.26	0.96	0
a0129	19	0.1501	749 ± 119	8.78	9.80	0.36	2.0	5.03 ± 1.87	0.548	0.26	0.62	0
a0130	21	0.1106	447 ± 84	2.81	2.34	0.37	1.4	2.12 ± 0.48	0.161	0.61	0.13	1
a0152	69	0.0589	729 ± 59	7.04	5.12	0.19	1.8	2.38 ± 0.52	0.057	0.25	0.09	0
a0168	110	0.0450	559 ± 36	3.57	2.89	0.14	1.5	2.70 ± 0.36	0.370	0.09	0.57	0
a0175	37	0.1285	606 ± 60	4.47	3.73	0.31	1.6	9.88 ± 2.53	1.114	0.29	0.84	0
a0190	17	0.1021	431 ± 122	2.19	0.61	0.66	1.2	1.64 ± 0.41	0.034	0.70	0.00	0
a0208	31	0.0793	499 ± 60	2.60	2.42	0.29	1.3	1.64 ± 0.32	0.237	0.22	0.68	0
a0243	32	0.1125	469 ± 50	2.52	2.04	0.30	1.3	2.83 ± 0.39	0.000	0.00	0.40	1
a0315	16	0.1740	636 ± 96	6.61	6.24	0.41	1.8	4.91 ± 0.91	0.056	1.20	0.50	2
a0351	14	0.1108	510 ± 118	2.70	2.27	0.42	1.3	2.35 ± 0.57	0.016	1.50	0.99	2
a0412	31	0.1092	585 ± 50	3.29	3.04	0.28	1.4	2.20 ± 0.69	0.071	0.53	0.11	2
a0441	25	0.1443	907 ± 554	17.17	4.80	1.25	2.5	5.95 ± 1.24	0.218	0.44	0.00	2
a0607	34	0.0962	501 ± 88	2.88	2.65	0.37	1.4	2.61 ± 0.42	0.023	0.57	0.56	1
a0620	14	0.1323	518 ± 76	2.17	2.78	0.61	1.2	3.34 ± 0.91	0.787	0.17	0.35	0
a0626	15	0.1168	757 ± 158	7.16	5.48	0.40	1.8	3.30 ± 0.83	0.092	0.44	0.32	0
a0628	61	0.0834	642 ± 63	5.98	4.46	0.19	1.7	2.81 ± 0.44	0.208	0.35	0.81	0
a0631	48	0.0826	577 ± 48	3.77	3.11	0.19	1.5	1.09 ± 0.27	0.061	0.42	0.49	0
a0646	29	0.1266	738 ± 96	10.45	9.72	0.24	2.1	3.82 ± 0.80	2.487	0.09	0.92	0
a0655	47	0.1276	736 ± 78	9.47	9.21	0.20	2.0	7.29 ± 0.94	2.527	0.16	0.88	0
a0660	26	0.0642	752 ± 138	7.91	7.61	0.43	1.9	1.62 ± 0.32	0.000	0.00	0.27	2
a0667	17	0.1441	512 ± 85	2.05	1.33	1.25	1.2	2.88 ± 0.63	1.998	0.11	0.53	0
a0682	17	0.1147	266 ± 242	0.75	0.22	2.12	0.9	1.07 ± 0.25	0.057	0.50	0.57	0
a0685	16	0.1464	496 ± 56	4.47	3.49	0.26	1.6	3.46 ± 0.88	0.000	0.00	0.07	2
a0714	29	0.1392	574 ± 78	4.97	4.86	0.26	1.6	4.16 ± 1.10	0.041	0.83	0.86	2
a0716	17	0.1188	494 ± 144	2.88	2.37	0.59	1.4	1.36 ± 0.43	0.009	1.50	0.46	2
a0729	28	0.0978	688 ± 87	3.38	3.90	0.36	1.4	1.21 ± 0.40	0.232	0.22	0.19	0
a0733	11	0.1156	392 ± 78	0.91	–	0.69	0.9	1.69 ± 0.51	0.535	0.62	0.49	0
a0736	42	0.0619	826 ± 98	10.11	9.08	0.29	2.1	4.66 ± 0.77	0.061	0.25	0.04	0
a0847	16	0.1508	704 ± 115	5.03	4.11	0.40	1.6	2.94 ± 0.54	0.730	0.21	0.87	0
a0856	19	0.1393	450 ± 69	1.92	2.61	0.48	1.2	1.74 ± 0.45	0.407	0.38	0.01	0
a0860	31	0.0965	941 ± 95	12.98	12.0	0.36	2.2	2.13 ± 0.46	0.313	0.23	0.00	0
a0861	17	0.1259	468 ± 104	3.29	2.88	0.44	1.4	2.51 ± 0.51	0.237	0.27	0.67	1
a0866	10	0.1435	266 ± 106	0.83	–	0.84	0.9	1.34 ± 0.39	0.143	0.47	0.12	1
a0869	12	0.1198	381 ± 127	1.74	2.02	0.66	1.2	1.81 ± 0.39	0.241	0.30	0.29	1
a0892	23	0.0943	470 ± 148	1.45	0.76	0.86	1.1	3.20 ± 1.56	0.175	0.26	0.09	0
a0912	28	0.0906	590 ± 82	3.72	3.05	0.31	1.5	3.01 ± 0.60	0.021	0.62	0.75	0
a0917	11	0.1370	403 ± 76	0.76	–	0.46	0.9	1.57 ± 0.37	0.252	0.31	0.24	1
a0919	12	0.0954	136 ± 37	0.21	–	0.66	0.6	0.59 ± 0.16	0.033	0.55	0.18	2
a0933	56	0.0965	455 ± 46	2.86	3.22	0.20	1.4	4.28 ± 0.89	0.387	0.21	0.87	0
a0975	14	0.1192	208 ± 58	0.48	–	0.50	0.8	0.67 ± 0.19	0.068	0.50	0.96	1
a1038	13	0.1275	253 ± 48	0.55	0.48	0.35	0.8	1.40 ± 0.27	0.108	0.44	0.83	0
a1064	17	0.1318	485 ± 93	2.30	2.21	0.34	1.3	2.39 ± 0.59	0.211	0.33	0.74	0
a1066	100	0.0690	731 ± 52	6.63	5.55	0.15	1.8	4.15 ± 0.60	0.657	0.17	0.35	0
a1072	11	0.1173	364 ± 83	1.45	–	0.67	1.1	1.12 ± 0.36	0.029	0.86	0.10	2
a1076	18	0.1168	418 ± 77	1.57	2.06	0.37	1.1	1.46 ± 0.30	0.295	0.21	0.96	0
a1078	11	0.1242	249 ± 51	0.50	–	0.66	0.8	1.38 ± 0.38	0.182	0.37	0.60	1
a1092	26	0.1058	449 ± 64	2.07	1.47	0.34	1.2	1.55 ± 0.35	0.000	0.00	0.02	2
a1107	15	0.1508	792 ± 104	10.03	10.3	0.33	2.1	2.61 ± 0.78	0.265	0.38	0.03	1
a1132	27	0.1358	880 ± 138	8.90	7.48	0.36	2.0	6.37 ± 0.95	3.038	0.07	0.45	0
a1139	89	0.0395	376 ± 34	1.68	1.07	0.19	1.2	1.16 ± 0.25	0.136	0.16	0.24	0
a1143	13	0.1379	459 ± 86	2.10	–	0.45	1.2	2.25 ± 0.56	0.030	0.80	0.10	2
a1164	19	0.1057	609 ± 144	4.24	5.79	0.54	1.6	1.75 ± 0.60	0.074	0.61	0.15	1
a1171	16	0.0577	161 ± 40	0.12	0.09	0.56	0.5	0.74 ± 0.17	0.024	0.55	0.01	1
a1189	37	0.0969	654 ± 196	4.58	4.26	0.59	1.6	2.63 ± 0.44	0.087	0.32	0.20	0

Table A.1. continued.

Name	N_{mem}	z_c	σ_c	M_{200}	$M_{200,red}$	er_M	r_{200}	L_{op}	L_X	er_{L_X}	P_{DS}	X-class
a1205	80	0.0761	865 ± 73	11.99	9.13	0.19	2.2	3.88 ± 0.54	0.976	0.09	0.01	0
a1218	23	0.0801	364 ± 75	0.91	0.63	0.39	0.9	0.81 ± 0.17	0.017	0.56	0.58	2
a1221	11	0.1103	289 ± 132	0.77	–	0.82	0.9	0.66 ± 0.32	0.000	0.00	0.66	2
a1236	38	0.1021	533 ± 59	3.72	2.27	0.29	1.5	2.57 ± 0.45	0.150	0.30	0.06	0
a1302	47	0.1153	691 ± 80	7.35	7.14	0.25	1.9	3.61 ± 1.08	1.307	0.09	0.72	0
a1346	74	0.0983	709 ± 54	7.64	4.59	0.18	1.9	3.98 ± 0.59	0.208	0.30	0.15	0
a1364	41	0.1066	553 ± 59	2.85	2.80	0.24	1.4	4.27 ± 0.94	0.040	0.80	0.55	2
a1366	42	0.1164	691 ± 70	7.72	8.13	0.20	1.9	2.61 ± 0.53	1.550	0.10	0.88	0
a1368	27	0.1293	735 ± 92	7.84	8.40	0.28	1.9	3.71 ± 0.65	0.130	0.47	0.06	0
a1376	16	0.1179	461 ± 204	3.11	3.43	0.88	1.4	1.62 ± 0.39	0.013	0.67	0.31	2
a1387	35	0.1310	692 ± 73	6.73	5.44	0.27	1.8	4.91 ± 0.66	0.693	0.20	0.05	0
a1392	11	0.1361	517 ± 146	3.86	–	0.61	1.5	3.11 ± 0.71	0.707	0.19	0.49	0
a1399	23	0.0910	251 ± 59	0.46	0.33	0.52	0.8	1.83 ± 0.27	0.000	0.00	0.03	2
a1406	14	0.1170	337 ± 97	1.48	0.96	0.59	1.1	1.85 ± 0.48	0.207	0.47	0.31	0
a1407	10	0.1349	561 ± 142	2.78	–	0.51	1.4	2.64 ± 0.50	0.423	0.28	0.78	0
a1411	10	0.1327	377 ± 98	1.41	–	0.92	1.1	1.54 ± 0.31	0.056	0.67	0.44	2
a1419	19	0.1077	504 ± 89	2.89	3.06	0.31	1.4	2.14 ± 0.50	0.233	0.30	0.96	0
a1424	83	0.0754	662 ± 45	5.49	4.88	0.14	1.7	2.32 ± 0.50	0.476	0.13	0.13	0
a1437	33	0.1341	1497 ± 13	39.89	30.5	0.17	3.2	7.27 ± 1.24	3.461	0.08	0.12	0
a1456	35	0.1346	540 ± 54	4.18	4.30	0.23	1.6	7.82 ± 1.72	0.431	0.27	0.63	1
a1457	17	0.0626	177 ± 42	0.29	0.27	0.61	0.6	0.40 ± 0.13	0.000	0.00	0.29	2
a1468	49	0.0869	361 ± 92	1.80	1.49	0.19	1.5	1.86 ± 0.94	0.004	1.00	0.33	2
a1496	56	0.0958	347 ± 46	1.53	1.29	0.30	1.1	1.85 ± 0.38	0.033	0.50	0.00	2
a1501	15	0.1336	406 ± 57	1.18	1.14	0.40	1.0	1.19 ± 0.32	0.268	0.26	0.61	0
a1507	65	0.0600	374 ± 42	1.36	0.92	0.23	1.1	1.47 ± 0.30	0.072	0.24	0.76	0
a1516	72	0.0765	705 ± 71	8.30	8.08	0.19	1.9	11.88 ± 3.12	0.151	0.27	0.65	0
a1518	23	0.1065	628 ± 118	4.49	2.40	0.41	1.6	2.61 ± 0.85	0.182	0.23	0.14	1
a1539	17	0.1072	510 ± 60	3.35	2.47	0.32	1.4	2.35 ± 0.61	0.043	0.55	0.30	2
a1559	45	0.1058	863 ± 124	14.06	11.5	0.33	2.3	3.61 ± 0.59	0.193	0.21	0.02	0
a1564	57	0.0790	633 ± 57	5.17	5.51	0.21	1.7	1.62 ± 0.40	0.072	0.29	0.11	1
a1566	28	0.1015	561 ± 69	3.52	4.04	0.24	1.5	1.65 ± 0.40	0.019	0.67	0.24	1
a1577	16	0.1388	359 ± 123	1.07	1.99	0.77	1.0	1.99 ± 0.34	0.095	1.14	0.72	2
a1579	15	0.1033	286 ± 86	1.00	1.15	0.73	1.0	0.46 ± 0.18	0.033	0.50	0.23	1
a1581	16	0.1503	521 ± 92	4.85	4.17	0.38	1.6	3.97 ± 0.61	0.103	0.46	0.22	2
a1599	30	0.0855	322 ± 38	0.84	0.58	0.40	0.9	10.98 ± 7.96	3.660	0.09	0.15	0
a1620	67	0.0846	782 ± 53	9.90	8.39	0.15	2.1	4.76 ± 0.94	0.002	4.00	0.04	0
a1621	32	0.1037	551 ± 61	2.12	2.24	0.31	1.2	10.03 ± 7.43	0.088	0.46	0.03	0
a1646	27	0.1055	573 ± 88	2.14	1.77	0.39	1.2	2.57 ± 0.86	0.219	0.23	0.71	0
a1650	70	0.0839	799 ± 87	11.14	9.51	0.22	2.1	4.00 ± 0.75	3.134	0.06	0.36	0
a1659	15	0.1067	383 ± 79	1.61	1.76	0.38	1.1	1.02 ± 0.21	0.028	0.62	0.80	2
a1663	86	0.0830	703 ± 60	7.62	7.57	0.17	1.9	3.01 ± 0.52	0.548	0.15	0.22	0
a1674	17	0.1051	549 ± 98	4.05	4.15	0.46	1.5	2.24 ± 0.41	0.172	0.26	0.46	0
a1678	16	0.1689	390 ± 124	1.98	1.64	0.67	1.2	1.90 ± 0.50	0.143	0.50	0.14	1
a1692	54	0.0845	561 ± 65	4.69	3.75	0.24	1.6	2.00 ± 0.42	0.090	0.35	0.56	0
a1701	21	0.1239	413 ± 54	1.15	1.0	0.49	1.0	1.76 ± 0.45	0.138	0.86	0.49	1
a1750	115	0.0858	784 ± 41	10.27	9.43	0.12	2.1	12.05 ± 2.00	1.770	0.10	0.00	0
a1767	127	0.0705	884 ± 55	11.57	8.68	0.14	2.2	3.59 ± 0.64	1.329	0.05	0.17	0
a1773	82	0.0773	779 ± 74	9.07	6.43	0.17	2.0	4.57 ± 0.66	0.753	0.13	0.71	0
a1780	55	0.0776	450 ± 46	2.51	2.72	0.22	1.3	2.55 ± 0.36	0.033	0.61	0.17	1
a1809	99	0.0795	716 ± 52	5.83	5.05	0.16	1.7	5.30 ± 1.13	1.002	0.09	0.85	0
a1872	12	0.1480	694 ± 138	3.89	–	0.43	1.5	1.95 ± 0.47	0.253	0.30	0.05	0
a1882	55	0.1396	733 ± 99	7.44	6.25	0.26	1.9	13.29 ± 1.42	0.192	0.39	0.19	0
a1918	20	0.1402	935 ± 129	16.26	12.3	0.30	2.4	5.73 ± 1.68	2.448	0.08	0.60	0
a1937	13	0.1380	223 ± 50	0.23	0.21	0.62	0.6	1.02 ± 0.29	0.239	0.47	0.32	0
a1938	18	0.1376	601 ± 70	4.95	5.78	0.26	1.6	8.82 ± 3.74	0.714	0.22	0.52	0
a2026	51	0.0908	753 ± 59	6.73	5.43	0.19	1.8	4.44 ± 1.20	0.141	0.31	0.80	0
a2030	51	0.0915	460 ± 54	2.27	1.80	0.25	1.3	2.50 ± 0.40	0.081	0.35	0.79	0
a2050	34	0.1193	826 ± 165	10.84	7.89	0.36	2.1	4.85 ± 0.87	1.505	0.14	0.26	0
a2082	31	0.0862	380 ± 111	1.84	1.42	0.56	1.2	1.99 ± 0.33	0.065	0.38	0.56	0
a2094	36	0.1446	606 ± 110	4.41	3.01	0.35	1.6	5.18 ± 0.65	0.815	0.24	0.90	0
a2118	24	0.1416	572 ± 91	4.41	3.34	0.32	1.6	3.39 ± 0.91	0.158	0.37	0.32	1
a2149	60	0.0650	330 ± 46	1.49	1.09	0.28	1.1	2.13 ± 0.33	0.400	0.08	0.87	0
a2196	19	0.1340	422 ± 131	2.17	2.71	0.58	1.2	2.72 ± 0.45	0.492	0.17	0.80	0
a2211	15	0.1361	493 ± 100	2.71	3.32	0.38	1.4	0.81 ± 0.32	0.050	0.50	0.92	1
a2235	15	0.1492	855 ± 195	12.24	12.2	0.47	2.2	6.26 ± 0.96	1.176	0.14	0.91	0
a2243	36	0.1067	759 ± 85	6.37	6.62	0.29	1.8	2.13 ± 0.38	0.357	0.15	0.18	0
a2244	83	0.0993	1062 ± 61	14.89	11.7	0.13	2.3	6.84 ± 0.71	4.005	0.04	0.05	0

Table A.1. continued.

Name	$N_{\rm mem}$	$z_{\rm c}$	$\sigma_{\rm c}$	M_{200}	$M_{200,\rm red}$	er_M	r_{200}	$L_{\rm op}$	$L_{\rm X}$	$er_{L_{\rm X}}$	$P_{\rm DS}$	X-class
a2255	176	0.0801	1121 ± 67	19.56	16.7	0.12	2.6	11.14 ± 2.83	2.443	0.02	0.54	0
a2259	16	0.1600	1080 ± 15	18.15	19.2	0.30	2.5	11.32 ± 1.78	2.913	0.09	0.01	0
a2356	23	0.1195	716 ± 85	5.84	5.45	0.25	1.7	3.30 ± 0.59	0.670	0.18	0.31	0
a2379	14	0.1234	531 ± 105	3.23	–	0.39	1.4	3.29 ± 1.24	0.027	1.40	0.44	2
a2399	111	0.0579	569 ± 37	4.09	3.19	0.14	1.5	3.54 ± 0.43	0.490	0.12	0.07	0
a2428	42	0.0839	420 ± 23	2.17	2.12	0.15	1.2	2.57 ± 0.67	1.351	0.14	0.84	0
a2433	16	0.1195	257 ± 44	0.50	0.33	0.40	0.8	0.84 ± 0.22	0.092	0.47	0.66	0
a2448	38	0.0820	447 ± 62	2.56	2.14	0.28	1.3	2.05 ± 0.49	0.029	0.54	0.64	2
a2505	21	0.1100	366 ± 57	0.94	1.01	0.40	1.0	1.58 ± 0.29	0.238	0.28	0.00	0
a2561	13	0.1634	405 ± 91	1.17	1.23	0.50	1.0	2.16 ± 0.38	1.720	0.25	0.72	1
a2564	20	0.0828	339 ± 70	1.25	1.40	0.45	1.0	0.93 ± 0.20	0.041	0.38	0.45	0
a2593	167	0.0419	570 ± 55	4.53	3.68	0.18	1.6	3.24 ± 0.53	0.485	0.07	0.74	0
a2670	109	0.0761	804 ± 51	9.40	9.32	0.13	2.0	5.08 ± 0.56	1.255	0.10	0.73	0
a2705	33	0.1165	452 ± 64	3.45	3.65	0.30	1.5	3.77 ± 0.58	0.018	0.50	0.03	1

A&A 461, 411–421 (2007)
DOI: 10.1051/0004-6361:20065357

Astronomy & Astrophysics

RASS-SDSS galaxy cluster survey

VI. The dependence of the cluster SFR on the cluster global properties

P. Popesso[1], A. Biviano[2], M. Romaniello[1], and H. Böhringer[3]

[1] European Southern Observatory, Karl Schwarzschild Strasse 2, 85748 Garching, Germany
e-mail: ppopesso@eso.org
[2] INAF - Osservatorio Astronomico di Trieste, via G. B. Tiepolo 11, 34131 Trieste, Italy
[3] Max-Planck-Institut fur extraterrestrische Physik, 85748 Garching, Germany

Received 4 April 2006 / Accepted 1 September 2006

ABSTRACT

We aim at quantifying the relationships between star formation in cluster galaxies and global cluster properties. Using a subsample of 79 nearby clusters from the RASS-SDSS galaxy cluster catalogue of Popesso et al. (2005, A&A, 433, 431), we perform a regression analysis between the cluster integrated star formation rate (ΣSFR), the cluster total stellar mass ($M_\star$), the fractions of star forming ($f_{\rm SF}$) and blue ($f_{\rm b}$) galaxies and other cluster global properties, namely its richness ($N_{\rm gal}$, i.e. the total number of cluster members within the cluster virial radius, corrected for incompleteness), velocity dispersion (σ_v), virial mass (M_{200}), and X-ray luminosity ($L_{\rm X}$). All cluster global quantities are corrected for projection effects before the analysis. Galaxy *SFR*s and stellar masses are taken from the catalog of Brinchmann et al. (2004), which is based on SDSS spectra. We only consider galaxies with $M_r \leq -20.25$ in our analysis, and exclude AGNs. We find that both ΣSFR and $M_\star$ are correlated with all the cluster global quantities. A partial correlation analysis shows that all the correlations are induced by the fundamental one between ΣSFR and $N_{\rm gal}$, hence there is no evidence that the cluster properties affect the mean *SFR* or $M_\star$ per galaxy. The relations between ΣSFR and $M_\star$, on the one side, and both $N_{\rm gal}$ and M_{200}, on the other side, are linear, i.e. we see no evidence that different clusters have different *SFR* or different $M_\star$ per galaxy and per unit mass. The fraction $f_{\rm SF}$ does not depend on any cluster property considered, while $f_{\rm b}$ does depend on $L_{\rm X}$. We note that a significant fraction of star-forming cluster galaxies are red (~25% of the whole cluster galaxy population). We conclude that the global cluster properties are unable to affect the *SF* properties of cluster galaxies, but the presence of the X-ray luminous intra-cluster medium can affect their colors, perhaps through the ram-pressure stripping mechanism.

Key words. galaxies: clusters: general – galaxies: formation

1. Introduction

What role does the environment play in the evolution of cluster galaxies? The dependence of the morphological mix from the environmental conditions was qualitatively illustrated in the early study of the Virgo cluster by Hubble & Humason (1931) and has been confirmed in many studies (e.g. Oemler 1974; Dressler 1980; Postman & Geller 1984; Dressler et al. 1997). The clear observational evidence is that the high density regions, such as the massive galaxy clusters, are dominated by a quiescent early type galaxy population, while the late type star forming galaxies more likely populate low density regions such as the field. A recently proposed way to study the relation between galaxy population and environmental conditions is the analysis of the ongoing star formation (SF) in galaxies of different environments (see, e.g., Christlein & Zabludoff 2005). The SF rate (SFR) is an important measure of the evolutionary state of a galaxy, and a sensitive indicator of the environmental interactions. Previous studies of cluster galaxy SFRs have sometimes reached conflicting conclusions. The SFRs of cluster galaxies have been found to be reduced (Kennicutt 1983; Bicay & Giovanelli 1987; Kodaira et al. 1990; Moss & Whittle 1993; Abraham et al. 1996; Balogh et al. 1998, 2002; Koopmann & Kenney 1998; Hashimoto et al. 1998; Gavazzi et al. 2002; Pimbblet et al. 2006), comparable (Kennicutt et al. 1984; Donas et al. 1990; Gavazzi et al. 1991, 1998; Biviano et al. 1997; Moss & Whittle 2005), or in some case enhanced (Moss & Whittle 1993; Bennet & Moss 1998) relative to the SFRs of field galaxies of the same classes.

Several cluster-related environmental processes can affect the SFRs of galaxies. Some processes mainly affect the gaseous content of a galaxy, such as the ram-pressure stripping (Gunn & Gott 1972; Kenney et al. 2004; van Gorkom 2004), re-accretion of the stripped gas (Vollmer et al. 2001), turbulence and viscosity (e.g. Quilis et al. 2001), and starvation/strangulation (Larson et al. 1980). Gravitational processes, which affect both the gaseous and the stellar properties of a galaxy, range from low-velocity tidal interactions and mergers (e.g. Mamon 1996; Barnes & Hernquist 1996; Conselice 2006), to high-velocity interactions between galaxies and/or clusters (Moore et al. 1998, 1999; Struck 1999; Mihos 2004). Despite a number of recent studies of nearby and distant clusters, it is not yet clear which of these processes, if any, are dominant.

Clues on the relative importance of the cluster-related environmental processes can be obtained by investigating the evolution of the star-forming properties of cluster galaxies. In this context, the most important evolutionary phenomenon is the Butcher-Oemler (BO hereafter) effect (Butcher & Oemler 1978, 1984), i.e. the increasing fraction of blue cluster members with redshift. The BO effect has been confirmed and detailed by many studies since the original works of Butcher & Oemler (e.g. Ellingson et al. 2001; Margoniner et al. 2001;

Alexov et al. 2003; De Propris et al. 2003; Rakos & Shombert 2005), although Andreon et al. (2004, 2006) have argued that no cluster-dependent evolution is required to explain the BO effect, which is entirely compatible with the normal color evolution of galaxies in an ageing universe. The BO-effect is purely photometrical. The spectroscopic version of the BO-effect is an excess of emission-line and star-forming galaxies in distant, relative to nearby, clusters, first suggested by Dressler & Gunn (1982) and later confirmed by several authors (e.g. Postman et al. 1998, 2001; Dressler et al. 1999; Finn et al. 2004, 2005; Homeier et al. 2005; Poggianti et al. 2006, P06 hereafter)

Most of the analyses so far have concentrated on the comparison of the star-forming properties of individual cluster galaxies with those of field galaxies, and on the variation of the galaxy SFRs on the local density of their environment. However, it is also important to assess the dependence (if any) of the star-forming properties of cluster galaxies on their cluster global properties, such as the mass, velocity dispersion and X-ray luminosity. Should the SFRs of cluster galaxies depend on global properties of their host cluster, results obtained for different individual clusters would not be straightforward to compare, thereby producing apparently discrepant results. Moreover, the relative efficiency of the different evolutionary processes depends on several cluster properties, and investigating the SFRs of cluster galaxies as a function of these properties can help understanding this issue (see, e.g., Pimbblet 2003). Also the evolution of the star forming properties of cluster galaxies must be studied in close connection with the evolution of their host cluster properties. In fact, evolutionary studies of cluster galaxy SFRs may be affected by selection biases if the SFRs depend on global cluster properties, such as their masses. Since in flux-limited surveys more massive clusters are preferentially selected with increasing redshift, a biased estimate of the evolution of the star-forming properties of cluster galaxies may result (see, e.g., Newberry et al. 1998; Andreon & Ettori 1999).

Recently, several studies have addressed the dependence of the star-forming properties of cluster galaxies on their host global properties. Several studies have found that the cluster global properties do not affect the star-forming properties of cluster galaxies. In particular, no dependence has been found of either the blue or the late-type galaxy fraction in clusters on cluster velocity dispersions (σ_vs) and masses (Goto 2005), nor of the blue fraction with cluster richness, concentration, and degree of subclustering (De Propris et al. 2004). On the other hand, both Margoniner et al. (2001) and Goto et al. (2003) had previously found a dependence of the blue or late-type galaxy fractions on the cluster richness. Goto (2005) has also claimed no dependence on the cluster σ_vs and masses of either the total cluster SFR or of the total cluster SFR normalized by the cluster mass, in disagreement with Finn et al. (2005) who have shown that the integrated SFR per cluster mass decreases with increasing cluster mass. Lea & Henry (1988), Fairley et al. (2002), and Wake et al. (2005) have all failed to find any dependence of the fraction of blue cluster galaxies with the cluster X-ray luminosity, L_X. Similarly, Balogh et al. (2002) have compared the galaxy SFRs in high-L_X and low-L_X clusters and have found no differences. In the sample of Homeier et al. (2005) there are hints of correlations between the total cluster SFRs and cluster L_Xs and intra-cluster gas temperatures, T_Xs, but the trends are not really significant. Most recently, P06 have found that the fraction of emission-line galaxies (ELGs hereafter) decreases with increasing cluster σ_v. The trend is continuous at high-z, but is characterized by a break at $\sigma_v \sim 500$–600 km s^{-1} in nearby clusters, where the relation they find is consistent with the results obtained by Biviano et al. (1997).

In this paper we re-address the issue of the dependence of the SFR and the fraction of star forming galaxies on the cluster global properties. At variance with most previous studies, we consider both optical and X-ray cluster global properties, namely the mass, σ_v, and L_X. While these quantities are correlated (Popesso et al. 2005, Paper III of this series), it is worthwhile to consider them all, since the star-forming properties of cluster galaxies may show a stronger dependence on one of these properties, thereby pointing to a different physical mechanism affecting their SFRs. E.g., Postman et al. (2005) have recently shown that the fraction of early-type galaxies in distant clusters does depend on L_X, but not on σ_v, nor on T_X. In our analysis we use a sample of 79 low-redshift clusters taken from the X-ray selected RASS-SDSS galaxy cluster catalog (Popesso et al. 2004, Paper I) and the optically selected Abell cluster sample (Popesso et al. 2006a, Paper V). Besides providing further constraints on the mechanisms of galaxy evolution in clusters, our investigation should be useful for assessing the possible selection effects in the comparison of the star-forming properties of galaxies in nearby vs. distant clusters, as well as in clusters at similar redshifts but with different global properties.

In Sect. 2 of the paper we describe our dataset. In Sect. 3 we analyze the relation between the cluster integrated star formation rate and the global properties of the systems. In Sect. 5 we apply the same analysis to the fraction of blue cluster galaxies and the fraction of cluster star forming galaxies. Section 7 contains our conclusions.

Throughout this paper, we use $H_0 = 70$ km s^{-1} Mpc^{-1} in a flat cosmology with $\Omega_0 = 0.3$ and $\Omega_\Lambda = 0.7$ (e.g. Tegmark et al. 2004).

2. The data

The optical data used in this paper are taken from the Sloan Digital Sky Survey (SDSS, Fukugita et al. 1996; Gunn et al. 1998; Lupton et al. 1999; York et al. 2000; Hogg et al. 2001; Eisenstein et al. 2001; Smith et al. 2002; Strauss et al. 2002; Stoughton et al. 2002; Blanton et al. 2003; and Abazajian et al. 2003). The SDSS consists of an imaging survey of π steradians of the northern sky in the five passbands u, g, r, i, z, in the entire optical range. The imaging survey is taken in drift-scan mode. The imaging data are processed with a photometric pipeline (PHOTO, Lupton et al. 2001) specially written for the SDSS data. For each cluster we defined a photometric galaxy catalog as described in Sect. 3 of Paper I (see also Yasuda et al. 2001). For the analysis in this paper we use only SDSS Model magnitudes.

The spectroscopic component of the survey is carried out using two fiber-fed double spectrographs, covering the wavelength range 3800–9200 Å, over 4098 pixels. They have a resolution $\Delta\lambda/\lambda$ varying between 1850 and 2200, and together they are fed by 640 fibers, each with an entrance diameter of 3 arcsec. The fibers are manually plugged into plates inserted into the focal plane; the mapping of fibers to plates is carried out by a tiling algorithm (Blanton et al. 2003) that optimizes observing efficiency in the presence of large-scale structure.

The X-ray data are taken from the ROSAT All Sky Survey. The RASS was conducted mainly during the first half year of the ROSAT mission in 1990 and 1991 (Trümper 1988). The ROSAT mirror system and the Position Sensitive Proportional counter (PSPC) operating in the soft X-ray regime (0.1–2.4 keV) provided optimal conditions for the studies of celestial objects

with low surface brightness. In particular, due to the unlimited field of view of the RASS and the low background of the PSPC, the properties of nearby clusters of galaxies can be ideally investigated.

2.1. The cluster sample

In this paper we use a combined sample of X-ray selected galaxy clusters and optically selected systems. The X-ray selected clusters are taken from the RASS-SDSS galaxy cluster catalog of Paper III, and the optically selected clusters are taken from the sample of Abell clusters spectroscopically confirmed using SDSS DR3 data of Paper V. Of these clusters, we only consider those with available X-ray center, in order to minimize possible centering errors. There is partial overlap between the X-ray and optical samples. In Paper V we have recently compared the properties and scaling relations of optically- and X-ray selected clusters. We have found no difference among the two samples, except for a larger scatter of the L_X-mass relation when derived on the optically-selected clusters rather than on the X-ray selected ones (see Paper V for details). We can thus safely combine the two samples together in the present analysis.

We have determined the cluster membership by studying the redshifts distribution of the galaxies in the cluster region (see next section for details). In order to analyze the SFR and the blue fraction of galaxies in the same magnitude range for all the clusters, we have selected only those clusters for which the limiting magnitude of the SDSS spectroscopic catalog, $r_{\rm Petro} \leq 17.77$, corresponds to an absolute magnitude limit fainter than -20.25 (and hence to a redshift limit $z \sim 0.1$). This magnitude is about 0.7 mag fainter than the value of $M^\star$ of the Schechter (1976) function that provides the best-fit to the RASS-SDSS clusters luminosity function (Popesso et al. 2006b, Paper IV). Among these clusters, we finally select only those containing at least 5 cluster members brighter than -20.25 in the r-band. Note that the σ_vs and masses of these clusters are estimated using all cluster members, irrespectively of their magnitude, and hence are generally based on at least 10 cluster members. Studying clusters extracted from cosmological simulations, Biviano et al. (2006) have recently shown that 10 cluster members are sufficient to obtain an unbiased estimate of a cluster σ_v. The final catalog contains 79 clusters, spanning a large mass range (10^{13}–5×10^{15} $M_\odot$).

2.2. Cluster masses, velocity dispersions and X-ray luminosities

We here provide a summary of the methods by which we measure the cluster global properties, σ_vs, masses, and L_Xs. Full details can be found in Papers III and IV.

We define the cluster membership of a galaxy on the basis of its location in the projected phase-space diagram, velocity with respect to the cluster mean vs. clustercentric distance. Specifically, we combine the methods of Girardi et al. (1993) and Katgert et al. (2004). Using the cluster members, the virial analysis (see, e.g., Girardi et al. 1998) is then performed on the clusters with at least 10 member galaxies. The line-of-sight velocity dispersion is computed in the cluster rest-frame (Harrison 1974) using the biweight estimator (Beers et al. 1990). By multiplying it by a factor $\sqrt{3}$ we obtain the 3D σ_v. The virial masses, M_{200} are corrected for the surface pressure term (The & White 1986) and estimated at the virial radius, r_{200}, using an iterative procedure. Namely, we start by using Carlberg et al.'s 1997 r_{200} definition as a first guess, then extrapolate or interpolate the virial mass estimate obtained within the observational aperture to r_{200} using a Navarro et al. (1997) mass profile. This mass estimate is used to obtain a new estimate of r_{200} and the virial mass is finally re-estimated by extrapolating or interpolating the observed value to the new estimate of r_{200} (see Biviano et al. 2006, for a thorough description of our procedure).

Cluster L_Xs are calculated from RASS data using the growth curve analysis method (Böhringer et al. 2000). This method is optimized for the detection of the extended emission of clusters by assessing the plateau of the background subtracted cumulative count rate curve. The X-ray luminosity estimate we adopt corresponds to the total flux inside the radius r_{200}, corrected for the missing flux by using a standard β-model for the X-ray surface brightness (see Böhringer et al. 2000, for more details). The correction is typically only 8–10%.

2.3. Galaxy star formation rates

We take the SFR-estimates for our cluster members from Brinchmann et al. (2004, hereafter, B04). In addition to SFRs, we also take from B04 the SFRs normalized to the stellar masses, SFR/m^*. They provide mainly H_α-derived SFR, based on SDSS spectra, for all the SDSS DR2 spectroscopic catalog. B04 divided their galaxy sample in three subsamples on the basis of the Baldwin et al. (1981) log[OIII]5007/Hβ vs. log[NII]6584/Hα diagram. B04 distinguish the following galaxy categories: star-forming galaxies, composite galaxies, AGNs, and unclassifiable objects. For all the star-forming galaxies and the unclassifiable objects the SFR is calculated directly from the emission lines (see B04 for details).

B04 provide three estimators of the galaxy SFR, the median, the mode and the average of the likelihood distribution. Since the average and the mode of the distribution are somewhat binning sensitive, we adopt the median of the distribution as our SFR estimator. B04's SFRs are derived from spectra taken within the 3 arcsec diameter fibers of the SDSS, which generally sample only a fraction of the total galaxy light. B04 correct their SFRs for these aperture effects (see B04 for details), and we adopt their corrected (total) SFRs. We have checked that our results do not change when instead of the median we use the mode, and when instead of the corrected SFRs we use the uncorrected ones.

2.4. Cluster star formation rates

In order to estimate the integrated cluster SFRs we first sum up the SFRs of their cluster members, AGNs and composite-spectrum galaxies excluded. I.e. we consider all the galaxies classified star-forming by B04, as well as the unclassifiable objects. The unclassifiable objects among our cluster members have extremely low SFR (as estimated by B04) and their summed contribution to the cluster integrated SFR is not significant.

Since our spectroscopic sample is not complete down to the chosen magnitude limit, we need to multiply the sum of the cluster member SFRs by an incompleteness correction factor. In order to estimate the incompleteness correction for each cluster we compare the number of cluster spectroscopic members, $N_{\rm spec}$, within r_{200} and with $r_{\rm petro} \leq -20.25$, with the corresponding number of cluster galaxies estimated from the photometric data, $N_{\rm phot}$, since the photometric sample is complete for $r_{\rm petro} \leq -20.25$. In order to estimate $N_{\rm phot}$ we first estimate the density of foreground and background galaxies from the counts of $r_{\rm petro} \leq -20.25$ galaxies in an annulus outside the virialized

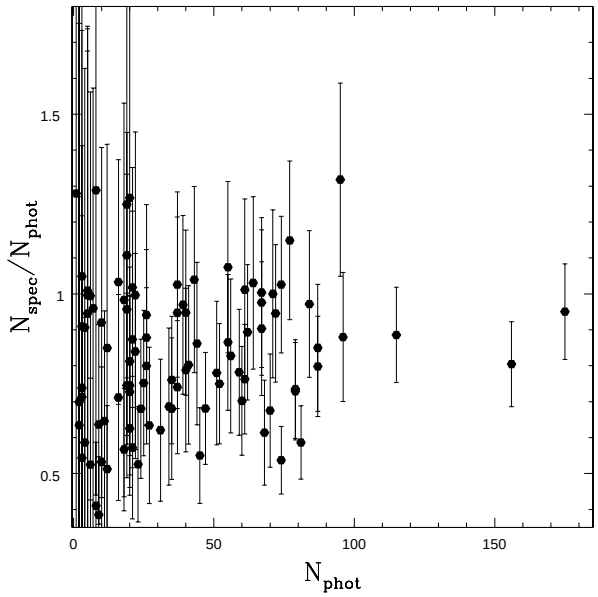

Fig. 1. Comparison between the number of cluster spectroscopic members (N_{spec}) within r_{200} and with $r_{petro} \leq -20.25$ with the number of cluster photometric members (N_{phot}) in the same region and magnitude range. The inverse of the N_{spec}/N_{phot} ratio gives the incompleteness correction factor to apply to the ΣSFR. When this factor is lower than 1, we set it to 1.

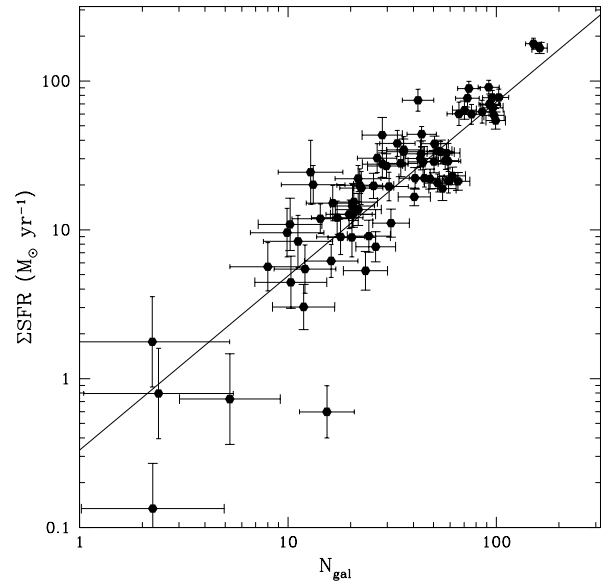

Fig. 2. Correlation of the integrated cluster SFR calculated within r_{200} and with $r_{petro} \leq -20.25$ with the total number of galaxies in the same region and magnitude range. We define N_{gal} by subtracting statistically the background and foreground galaxies.

area (at radii $> r_{200}$) centered on the cluster center. We then subtract the number of background galaxies expected in the cluster area from the number of galaxies (down to the same magnitude limit) in the cluster region. In Fig. 1 we show the number ratios of spectroscopic and photometric members as a function of N_{phot}. 80% of our clusters have a completeness level higher than 80%. We calculate the incompleteness correction factor as the maximum between N_{phot}/N_{spec} and 1.

Another correction we need to apply to the sum of cluster member SFRs is the de-projection correction since the global cluster quantities we want to compare the integrated SFR with, are all de-projected quantities. When we sum up the SFRs of cluster members with a clustercentric projected distance $\leq r_{200}$, we include the contribution of galaxies outside the virial sphere, but within the cylinder of same radius. In Fig. 2 we shows the relation between the integrated SFR within r_{200} and N_{spec}. Because of the strict proportionality between these two quantities, and because the relation is linear within the errors (see Table 2), we can estimate the de-projection correction for the number of cluster members, and apply the same correction to the integrated SFR. In order to estimate the de-projection correction for N_{spec}, we build the number density profiles of our clusters, and fit them with the King (1962) cored profile, and the NFW cuspy profile (Navarro et al. 1997). We then de-project these profiles, and take the ratio between the integrals from the center to r_{200} of the de-projected and the projected profiles. This ratio provides the correction factor.

The number density profiles of our clusters are built by stacking together our clusters after rescaling their galaxy clustercentric distances by their cluster r_{200}s (see also Popesso et al. 2006c, Paper VII, where we perform the same analysis). We use the SDSS r-band photometric data down to the completeness limit $r = 21$, and consider a common absolute magnitude limit of -18.5 for all our clusters. The cluster galaxy distributions are normalized to the total number of galaxies within r_{200}, after subtraction of the mean background galaxy density, evaluated within the $2.5-3.5 \times r_{200}$ annulus. We split our sample of clusters in 6 mass bins ($M_{200}/10^{14}\ M_\odot \leq 1$, $1 < M_{200}/10^{14}\ M_\odot \leq 3$, $3 < M_{200}/10^{14}\ M_\odot \leq 7$, $7 < M_{200}/10^{14}\ M_\odot \leq 10$,$10 < M_{200}/10^{14}\ M_\odot \leq 30$, and $M_{200}/10^{14}\ M_\odot > 30$) and determine the number density profile for each of these subsamples. Each bin contains at least 10 clusters. We find that the number density profiles become steeper near the center as the cluster mass increases. This is true independently for the red and blue cluster members ($u - r \geq 2.22$ and, respectively, <2.22, see Strateva et al. 2001), so this is not an effect due to the population of cluster galaxies, but it is a mass-related effect. More massive clusters have more centrally concentrated galaxy distributions. The best fit parameters of the King profiles for different cluster mass bins and galaxy populations are listed in Table 1. In Fig. 3 we show the number density profiles in the lowest and highest mass bins for the whole (left panel), the red (central panel) and the blue (right panel) cluster galaxy populations.

Since the galaxy number density profiles depend on the mass of the cluster, also the de-projection corrections are mass dependent. In Table 1 we list the correction factors determined for each mass bin by using the best-fit King profiles for the whole cluster population. We apply these mass-dependent de-projection correction factors to the integrated SFRs. In the following, ΣSFR refers to the incompleteness- and de-projection-corrected values of the integrated SFRs within a sphere of radius r_{200}.

3. The dependence of the cluster ΣSFR on the cluster global properties

In order to analyse the relation between ΣSFR and M_{200} we perform an orthogonal linear regression in the logarithmic space, using the software package ODRPACK (Akritas & Bershady 1996). We find a significant correlation between these two quantities (as quantified by the Spearman correlation coefficient, see Table 2). The slope of the relation is consistent with unity (see Table 2). Figure 4 shows the $\Sigma SFR - M_{200}$ relation. Note that the slope of the relation would have been found to be

Table 1. King's profile best fit parameters for different cluster mass bins ($m = M_{200}/(10^{14}\ M_{\odot})$) and different cluster galaxy population. r_c is the core radius of the King profile expressed in units of r_{200}. σ_0 is the central number density of galaxy normalized to the total number of galaxies. "cf" is the de-projection correction factor to be applied to the observed number of cluster members within a projected clustercentric distance r_{200}.

	$m \leq 1$	$1 < m \leq 3$	$3 < m \leq 7$	$7 < m \leq 10$	$10 < m \leq 30$	$m > 30$
The whole cluster galaxy population						
r_c	0.40 ± 0.08	0.20 ± 0.02	0.22 ± 0.01	0.16 ± 0.01	0.15 ± 0.01	0.15 ± 0.01
σ_0	0.08 ± 0.01	0.12 ± 0.01	0.14 ± 0.01	0.20 ± 0.01	0.19 ± 0.01	0.19 ± 0.01
cf	0.72	0.79	0.81	0.81	0.85	0.85
The red galaxy population ($u - r > 2.22$)						
r_c	0.37 ± 0.03	0.23 ± 0.01	0.20 ± 0.01	0.17 ± 0.01	0.17 ± 0.01	0.15 ± 0.01
σ_0	0.08 ± 0.01	0.13 ± 0.01	0.16 ± 0.01	0.19 ± 0.01	0.20 ± 0.01	0.23 ± 0.01
The blue galaxy population ($u - r < 2.22$)						
r_c	1.03 ± 0.13	0.65 ± 0.06	0.46 ± 0.05	0.36 ± 0.08	0.34 ± 0.04	0.46 ± 0.06
σ_0	0.03 ± 0.01	0.05 ± 0.01	0.07 ± 0.01	0.08 ± 0.01	0.09 ± 0.01	0.08 ± 0.01

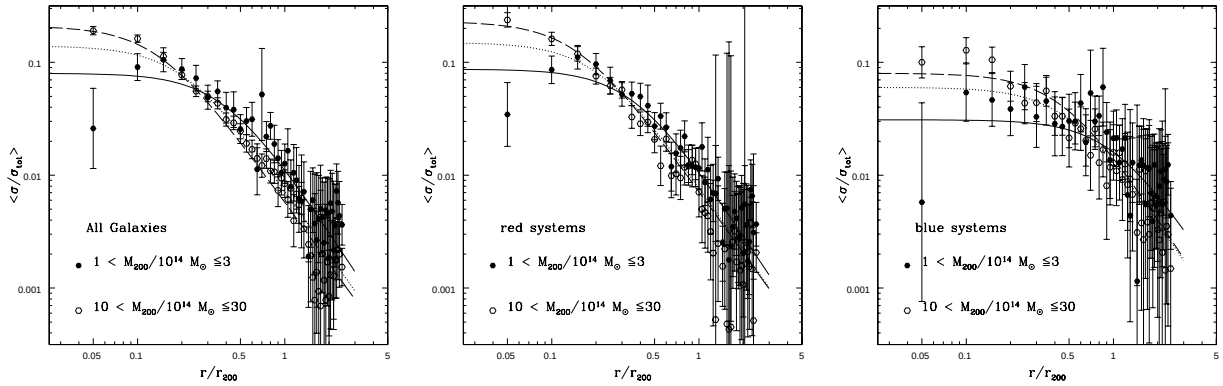

Fig. 3. The stacked surface number density profiles of clusters in lowest and highest mass bins for the whole (*left panel*), red (*central panel*) and the blue (*right panel*) cluster galaxy population. The individual cluster profiles are obtained by considering all the galaxies with $r_{petro} < -18.5$. In each panel the open circles are the density profile of the highest mass bin and the filled circles are the profile of the lowest mass bin. The dashed line is the best-fit King profile of the highest mass bin, the dotted line is the best-fit King profile of the mean surface number density distribution (obtained stacking all the clusters in the sample) and the solid line is the best-fit King profile of the lowest mass bin.

Table 2. Best-fit parameters of the correlations between global cluster quantities, A vs. B, with $A = 10^{\beta} \times B^{\alpha}$, and the estimate of the orthogonal scatter, expressed in dex. Errors on the best-fit parameters are given at the 95% confidence level. Units are: $M_{\odot}$ yr^{-1} for ΣSFR, $M_{\odot}$ for M_{200} and $M_{\star}$, km s^{-1} for σ_v and 10^{44} erg s^{-1} for L_X (f_b is unit-less).

A	B	α	β	σ	r_S	$P(r_S)$
ΣSFR	N_{gal}	1.08 ± 0.08	−0.32 ± 0.12	0.13	0.84	2×10^{-21}
ΣSFR	M_{200}	1.11 ± 0.10	−15.36 ± 1.57	0.20	0.74	1×10^{-16}
ΣSFR	σ_v	2.18 ± 0.23	−4.96 ± 0.62	0.15	0.76	2×10^{-18}
ΣSFR	L_X	0.62 ± 0.09	1.62 ± 0.07	0.27	0.46	2×10^{-5}
$\Sigma SFR/M_{200}$	σ_v	−0.67 ± 0.19	−11.63 ± 0.54	0.24	−0.30	4×10^{-3}
$M_{\star}$	ΣSFR	1.09 ± 0.06	−11.77 ± 0.73	0.12	0.80	2×10^{-17}
$M_{\star}$	N_{gal}	1.01 ± 0.07	10.86 ± 0.07	0.07	0.85	2×10^{-21}
$M_{\star}$	M_{200}	1.08 ± 0.09	−3.50 ± 1.12	0.16	0.75	4×10^{-16}
$M_{\star}$	σ_v	2.31 ± 0.23	5.55 ± 0.63	0.09	0.84	3×10^{-20}
$M_{\star}$	L_X	0.61 ± 0.06	12.47 ± 0.04	0.25	0.49	2×10^{-5}
f_b	L_X	−0.13 ± 0.04	0.91 ± 0.04	0.19	−0.41	2×10^{-4}
$\Sigma SFR_{blue}/\Sigma SFR$	L_X	−0.19 ± 0.05	0.78 ± 0.04	0.22	−0.41	4×10^{-4}

significantly smaller than unity, had we not applied the de-projection correction to ΣSFR.

ΣSFR is also significantly correlated with σ_v. The best-fit parameters of the regression line are listed in Table 2.

To check the robustness of our results we have re-analyzed the $\Sigma SFR - M_{200}$ and $\Sigma SFR - \sigma_v$ relations by considering in turn only the clusters with more than 20, 30 and 40 cluster members. The correlations remain significant, and the values of the best-fit parameters of the regression lines are consistent, within errors, with those obtained when considering the whole cluster sample.

The correlation between ΣSFR and L_X is less well defined than in the previous cases due to the larger scatter, but the correlation is very significant also in this case (see Fig. 5 and Table 2). The large scatter is at least partially due to the Abell X-ray-Underluminous (AXU) clusters (see Fig. 5). These systems are similar to the normal X-ray emitting clusters in all their optically-derived properties but are generally X-ray underluminous for their mass and optical luminosity (see Paper V for further details).

The significant correlations between ΣSFR and the cluster global quantities may not all be independent from one another.

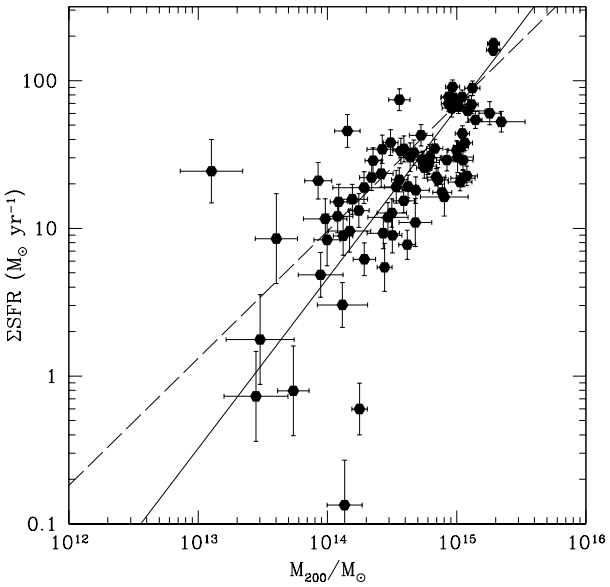

Fig. 4. Σ*SFR* vs. M_{200}. The solid line is the best fit obtained using the de-projected quantities. The dashed line is the best fit we would obtain without correcting the integrated cluster SFR for the projection effects.

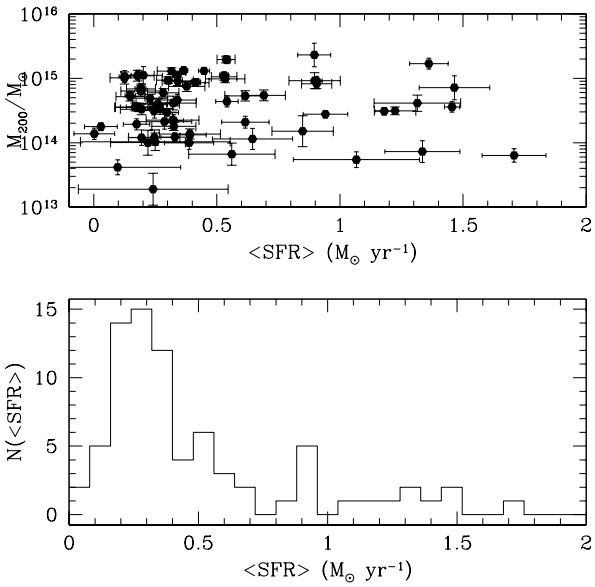

Fig. 6. *Upper panel*: M_{200} vs. the mean cluster SFR, ⟨*SFR*⟩. *Lower panel*: the distribution of ⟨*SFR*⟩.

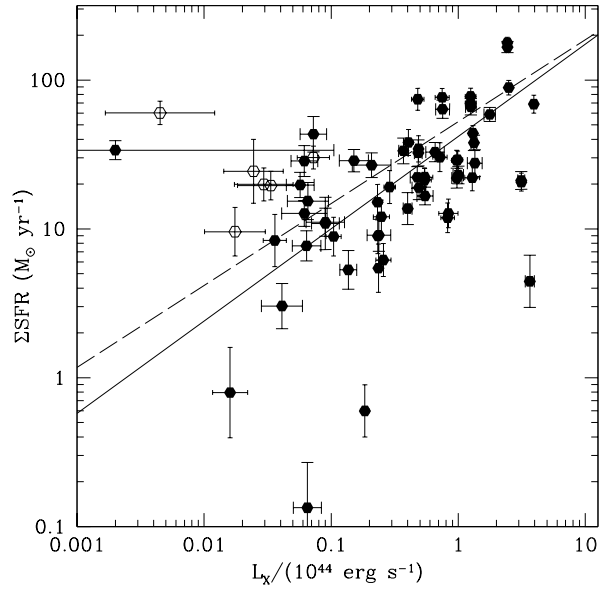

Fig. 5. Σ*SFR* vs. L_X relation. Open points are the Abell X-ray-Underluminous (AXU) clusters (for details, see Paper V of this series). The solid line is the best fit obtained after correction for projection effects. The dashed line is the best fit we would obtain had we not applied the de-projection correction.

In fact, σ_v, M_{200}, and L_X are all correlated quantities (see, e.g., Paper III). They are also correlated with N_{gal} (see Paper VII), as it is Σ*SFR* (see Fig. 2, and Table 2 – note that the same de-projection correction applies to both Σ*SFR* and N_{gal}, so the relation between the two quantities does not vary after applying this correction). We perform a multiple regression analysis (e.g. Flury & Riedwyl 1988; see also Biviano et al. 1991, for another application of the method in an astrophysical context) to try to understand which (if any) of these correlations is the most fundamental one. We take Σ*SFR* as the dependent variable and consider N_{gal}, σ_v, M_{200}, and L_X as independent variables (regressors). We then adopt the method of backward elimination (Flury & Riedwyl 1988) in order to identify the fundamental regressors for the dependent variable Σ*SFR*. Namely, we compute the coefficient of determination, R_p^2, using all p regressors first, then eliminate each regressor one at a time and look at the variation in R_p^2. The regressor giving the smallest contribution to R_p^2 is eliminated, and we proceed until only one regressor is left. When fundamental regressors are eliminated, R_p^2 is substantially reduced.

We find that the only fundamental regressor of Σ*SFR* is N_{gal}. I.e., Σ*SFR* depends on M_{200} (but also on σ_v and L_X) only because the more massive a cluster, the larger its number of cluster galaxies and, proportionally, of star-forming galaxies.

Not only N_{gal} is the fundamental regressor of Σ*SFR*, the relation between the two quantities is linear. This may come as a surprise if clusters of different richness contain different fraction of star-forming galaxies within their virial radius. However, this is not seen in our cluster sample (see Sect. 5). Since the Σ*SFR* vs. N_{gal} is linear (see Table 2), the mean SFR of cluster galaxies is constant (and equal to $0.47 \pm 0.13\ M_\odot$/yr). This is illustrated in Fig. 6, where we show M_{200} vs. $\langle SFR\rangle = \Sigma SFR/N_{gal}$ (upper panel) and the ⟨*SFR*⟩ distribution among our clusters. No significant relation is found between ⟨*SFR*⟩ and M_{200} (nor in fact between ⟨*SFR*⟩ and either σ_v, or L_X). The scatter in the ⟨*SFR*⟩ distribution is at least partly due to the uncertainties in the incompleteness correction factors (see Sect. 2.4).

In lieu of normalizing Σ*SFR* by the number of cluster members, for the sake of comparison with other works in the literature, we also normalize it by the cluster mass, $\Sigma SFR/M_{200}$. As expected from the Σ*SFR* vs. M_{200} relation, there is no significant trend of $\Sigma SFR/M_{200}$ with M_{200}, i.e. $\Sigma SFR/M_{200}$ is constant[1]. Similarly, there is no correlation between $\Sigma SFR/M_{200}$ and L_X. The evidence for a significant anti-correlation of $\Sigma SFR/M_{200}$ with σ_v (see Table 2) is somewhat surprising, given that the slopes of the regression lines between Σ*SFR* and M_{200}, on the one side, and σ_v, on the other side, are consistent with each-other (2.18 ± 0.23 and 2.5 ± 0.05, respectively, see Table 2 and Paper III). We note, however, that the slope of the

[1] Note that we would have obtained a significant anti-correlation of $\Sigma SFR/M_{200}$ with cluster mass, had we not applied the de-projection correction.

$\Sigma SFR/M_{200} - \sigma_v$ relation is still consistent within 2σ with the value inferred from the $\Sigma SFR - \sigma_v$ and $M_{200} - \sigma_v$ relations.

We conclude that the increase of ΣSFR as a function of the cluster mass is due to the proportionality between ΣSFR and $N_{\rm gal}$ and that the mean SFR per galaxy or per unit mass is nearly constant throughout our cluster sample, except perhaps for a residual dependence on the cluster velocity dispersion.

4. The total cluster stellar mass vs. the cluster global properties

We have performed a similar analysis as that described in the previous Section using the total cluster stellar mass, $M_\star$, in lieu of ΣSFR. $M_\star$ is computed by summing up the stellar mass of all the cluster spectroscopic members within r_{200} and with $M_r \leq -20.25$ (we use the median values of the stellar masses in the B04 catalog). As for ΣSFR, we correct $M_\star$ for the incompleteness and for the projection effects (see Sect. 2.4). As shown by the results listed in Table 2, the cluster $M_\star$ is proportional to ΣSFR. As a consequence, the slopes of the relations of $N_{\rm gal}$, M_{200}, σ_v, and $L_{\rm X}$ with $M_\star$ are all consistent with those of the corresponding relations of these quantities with ΣSFR. A multiple regression analysis shows that, also in this case, the fundamental regressor of $M_\star$ is $N_{\rm gal}$.

5. The fractions of blue and star-forming galaxies vs. the cluster global properties

We analyze the relations between the fractions of blue ($f_{\rm b}$) and star-forming ($f_{\rm SF}$) galaxies in clusters with the cluster global properties. We define $f_{\rm b}$ as the ratio between the number of spectroscopic cluster members with $u - r < 2.22$ (see Strateva et al. 2001), and the number of all spectroscopic cluster members, within r_{200}. We do not need to apply an incompleteness correction here, since we find that the blue and the whole cluster galaxy populations have similar incompleteness levels for $r_{\rm Petro} \leq -20.25$, within the statistical uncertainties, as shown in Fig. 7 (the incompleteness are estimated as in Sect. 2.4, but taking into account the color cuts). We do not apply the de-projection correction either, since the de-projection correction factor for the blue galaxies is very uncertain and in any case consistent with that for the whole population.

The correlations of $f_{\rm b}$ with M_{200}, σ_v, and $N_{\rm gal}$ are not significant. On the other hand, there is a significant anti-correlation of $f_{\rm b}$ with $L_{\rm X}$ (see Table 2 and Fig. 8).

The $f_{\rm b}$ vs. $L_{\rm X}$ relation deserves a closer look. Another way of looking at it is through the use of the fractional contribution of blue galaxies to ΣSFR, $\Sigma SFR_{\rm blue}/\Sigma SFR_{\rm tot}$. $\Sigma SFR_{\rm blue}/\Sigma SFR_{\rm tot}$ is anti-correlated with $L_{\rm X}$ (see Fig. 9), and the slopes of the $f_{\rm b} - L_{\rm X}$ and $\Sigma SFR_{\rm blue}/\Sigma SFR_{\rm tot} - L_{\rm X}$ relations are consistent within the errors (see Table 2).

The color cut of Strateva et al. (2001) is used to separate blue from red galaxies, but not all the star-forming galaxies are bluer than $u - r = 2.22$. Figure 10 shows the SFR/m^* in a sample of 2680 cluster galaxies versus the color $u-r$. The dashed line in the plot is the color cut of Strateva et al. (2001) at $u-r = 2.22$. In addition to the usual populations of star-forming blue galaxies and of no star-forming (quiescent) red galaxies, there is a third population of red, star-forming red galaxies at $SFR/m^* \geq 10^{-10.5}$ yr^{-1}. Hence, the color cut by itself does not distinguish between star-forming and quiescent galaxies. For this we need a cut in SFR/m^*, that we set at $SFR/m^* = 10^{-10.5}$ yr^{-1}. We then define $f_{\rm SF}$ as the fractional number of galaxies with mass normalized SFR above this limit. There is no significant correlation of $f_{\rm SF}$ with any cluster global quantity, M_{200}, σ_v, $N_{\rm gal}$, and $L_{\rm X}$. Thus, while $f_{\rm b}$ is anti-correlated with $L_{\rm X}$, $f_{\rm SF}$ is not. This is due to the inclusion of the red star-forming galaxies in the sample. In fact, the fraction of red star-forming galaxies do not correlate with any of the global cluster properties, not even $L_{\rm X}$, and among the star-forming galaxies the red ones outnumber the blue ones. This can be seen in Fig. 11: the median fractions of blue star-forming, red star-forming, and red quiescent galaxies are 0.15 ± 0.05, 0.26 ± 0.07 and 0.63 ± 0.05.

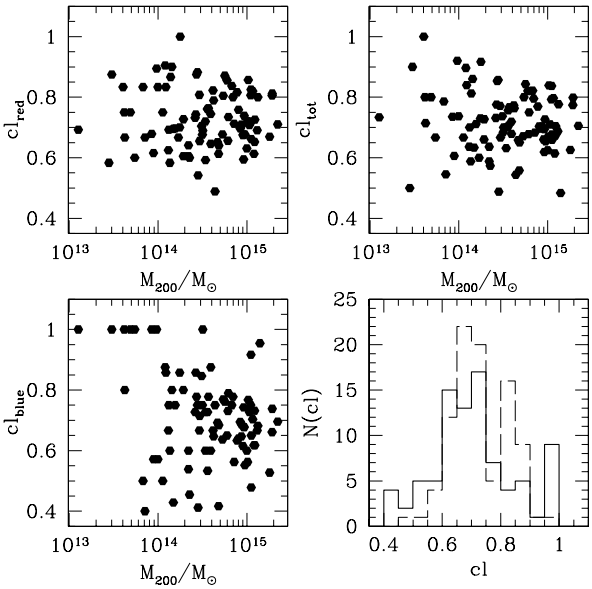

Fig. 7. Spectroscopic completeness of the total (*top-right panel*), red (*top-left panel*), and blue (*bottom-left panel*) cluster galaxy populations as a function of the cluster mass. The *bottom-right panel* shows the distributions of the whole (solid histogram) and blue (dashed histogram) cluster galaxy populations.

6. Discussion

Our results show that the cluster global properties (M_{200}, σ_v, $L_{\rm X}$) do not influence the SF properties of cluster galaxies. While ΣSFR *does* increase with increasing cluster M_{200}, σ_v and $L_{\rm X}$, all these trends can be totally explained as a richness effect, $\Sigma SFR \propto N_{\rm gal}$. The more galaxies in a cluster, the larger its mass, and the higher its number of star-forming galaxies. Since the relation between ΣSFR and $N_{\rm gal}$ is linear, the average cluster SFR is essentially constant throughout our cluster sample. Consistently, we do not find any dependence of $f_{\rm SF}$ with any cluster global property. We do however find a residual correlation of the mass normalized integrated SFR, $\Sigma SFR/M_{200}$ with σ_v, and a significant anti-correlation of $f_{\rm b}$ with $L_{\rm X}$.

Also the total stellar mass, $M_\star$, depends linearly on $N_{\rm gal}$, i.e. the average stellar mass per cluster galaxy does not depend on cluster properties. This is consistent with the universality of the shape of the cluster luminosity function found in Paper IV. It suggests that not only the average *current* star formation but also the average *history* of star formation in clusters is independent on the cluster properties.

How do our results compare with previous findings? The lack of correlations we find between $f_{\rm b}$ and σ_v, M_{200}, and $N_{\rm gal}$ confirm previous negative results by Goto (2005) and De Propris et al. (2004) but disagree with the claimed trend of $f_{\rm b}$ with cluster richness (Margoniner et al. 2001; Goto et al. 2003). We agree

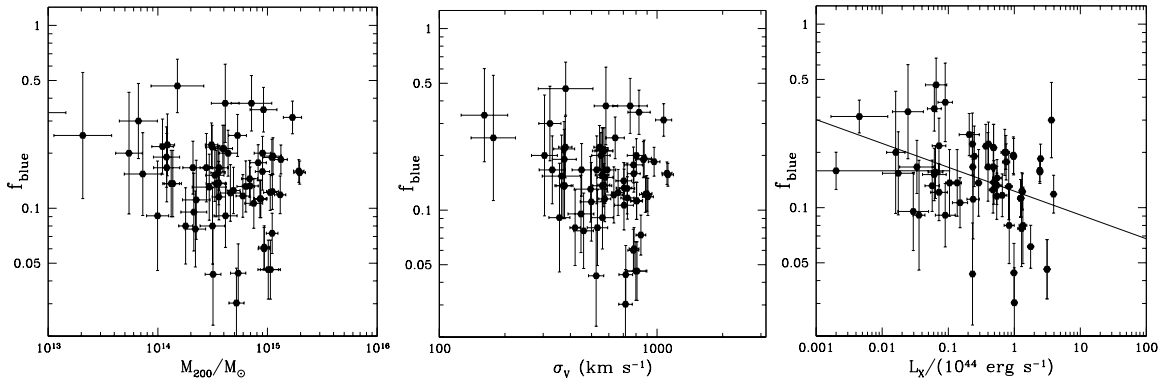

Fig. 8. Relations between the fraction of blue cluster galaxies and cluster global properties: M_{200}, σ_v, and L_X. The best-fit regression lines are shown for the statistically significant correlations only.

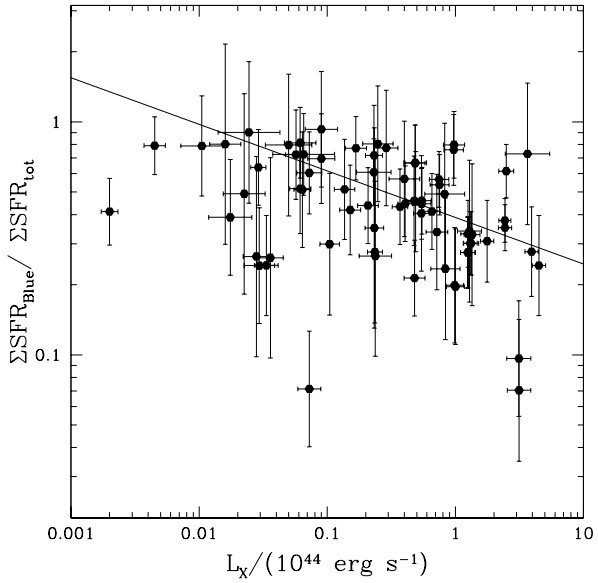

Fig. 9. The relation between the fraction of ΣSFR due to blue cluster galaxies and L_X. The best-fit regression line is shown.

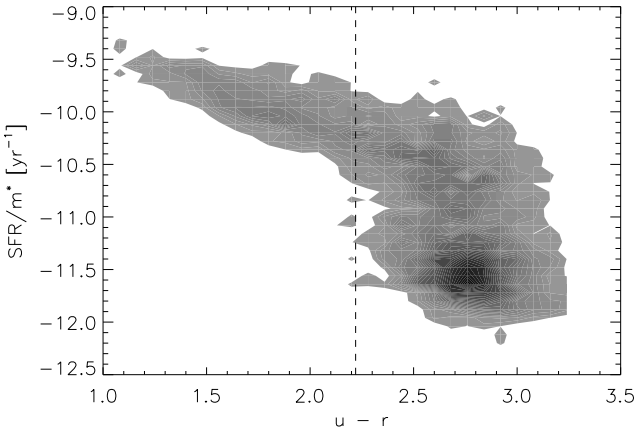

Fig. 10. Star formation rate per unit of stellar mass versus the $u-r$ color for the cluster spectroscopic members. The grey shading intensity is proportional to the logarithm of the density of galaxies in the diagram. The dashed line in the plot is the color cut of Strateva et al. (2001) at $u-r = 2.22$, used to separate red from blue galaxies. Note that in addition to the usual populations of star-forming blue galaxies and of no star-forming red galaxies, there is a third population of red, star-forming red galaxies at $SFR/m^* \geq 10^{-10.5}$ yr^{-1}.

with Goto (2005) that there is no dependence of $\Sigma SFR/M_{200}$ on M_{200}, but, at variance with his findings, we do find a correlation between $\Sigma SFR/M_{200}$ and σ_v, as well as between ΣSFR and either M_{200} or σ_v, in broad agreement with the tentative correlations found by Homeier et al. (2005).

Our results disagree with those of Finn et al. (2005), since, unlike them, we do *not* find that the integrated SFR per cluster mass decreases with increasing cluster mass. Our results disagree also with those of Lin et al. (2003), since they find $M_\star/M_{500} \propto M_{500}^{-0.26}$, while we find a linear relation between $M_\star$ and M_{200}, meaning that the fraction of mass in form of stars, $M_\star/M_{200}$, is constant among different clusters. Remarkably, however, our result would have been consistent with both Finn et al.'s and Lin et al.'s had we also neglected to apply the mass-dependent de-projection correction to ΣSFR and $M_\star$ (see Sect. 2.4) as they did.

The anti-correlation we find between f_b and L_X is in disagreement with previous claims of no correlations by Lea & Henry (1988), Fairley et al. (2002), and Wake et al. (2005). Such a correlation, as well as the lack of correlation between f_b and other cluster global quantities, is however consistent with the result of Postman et al. (2005). Postman et al. have recently shown that the fraction of early-type galaxies in distant clusters increases with L_X, but does not depend on either σ_v, or T_X. We actually checked that the fraction of *red*, rather than blue, galaxies in our clusters does show a relation with L_X which is consistent (within 2σs) with the relation found by Postman et al. for their distant cluster sample.

The lack of correlation we find between f_{SF} and L_X confirms the results of Balogh et al. (2002), but the lack of correlation we find between f_{SF} and σ_v is in disagreement with the recent findings of P06. In their nearby cluster sample, they find a decreasing fraction of ELGs with increasing σ_v for $\sigma_v \leq 500$ km s^{-1}.

It is difficult to explore in detail the reasons for all the apparent discrepancies among different results. One important issue is the de-projection correction that we have introduced (see Sect. 2.4) and that has not been applied before. Another important issue is the limiting absolute magnitudes adopted in different studies. Yet another relevant point could be the difference among different cluster samples, since different samples span different redshift and mass ranges, and none of the samples studied so far can be claimed to be a volume-complete sample down to a given cluster mass limit. Since there is a significant overlap of the sample with P06, and we both use data from the SDSS, we deem nevertheless worthwhile to investigate further the reason why our results are in disagreement.

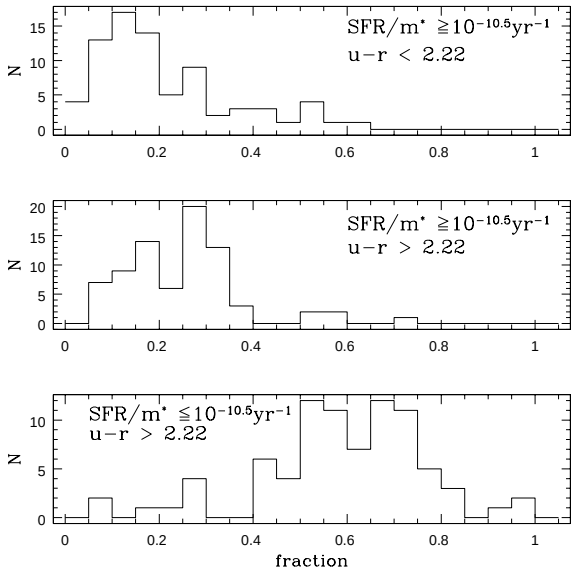

Fig. 11. Distributions of the fractions of blue star-forming galaxies (*top panel*), red star-forming galaxies (*central panel*) and quiescent galaxies (*bottom panel*) in our cluster sample.

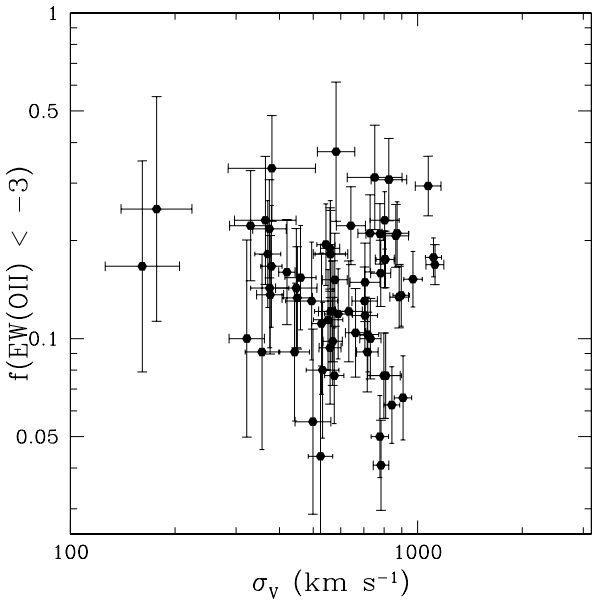

Fig. 12. The fraction of ELGs vs. σ_v in our cluster sample. Note that AGNs and composite-spectra galaxies are not included in our ELG galaxy sample. No significant correlation exists.

We first compared the values for the σ_vs of 22 clusters in common. P06's and our values are very nicely correlated, and obey a regression relation with a slope close to unity (although their values are systematically higher than ours by $\sim$50 km s^{-1}). The result discrepancy must origin in the different definition of the fraction of star-forming galaxies. P06 define the star-forming galaxies as those cluster members with a [OII] emission-line with equivalent width (*EW*) smaller than −3 Å. For the sake of comparison we show in Fig. 12 the relation between the fraction of ELGs (with *EW* smaller than −3 Å) and σ_v in our sample. At variance with P06 we do exclude AGNs and composite-spectra galaxies from our sample. There is no significant correlation, no trend is evident. Including AGNs in our sample we instead recover the trend found by P06. Hence we conclude that the trend reported by P06 is due to their including AGNs among the star-forming galaxies. We will pursue the investigation of this topic in a forthcoming paper (Popesso & Biviano 2006).

Two relations that we find cannot be simply explained by the linear relation between ΣSFR and $N_{\rm gal}$. These are the observed decrease of $f_{\rm b}$ with increasing $L_{\rm X}$, and the observed decrease of $\Sigma SFR/M_{200}$ with σ_v. The fact that $f_{\rm b}$ does not correlate with M_{200} excludes the possibility that the $f_{\rm b} - L_{\rm X}$ anti-correlation reflects a dependence of the fraction of blue galaxies on cluster mass, as suggested by Postman et al. (2005). As a matter of fact, $L_{\rm X}$ is not a very good proxy for the cluster mass (Reiprich & Böhringer 2002; Paper III). The anti-correlation $f_{\rm b} - L_{\rm X}$ may be telling us more about the cluster and galaxy formation processes than about the cluster evolution process. A possible physical mechanism that could be responsible for this anti-correlation is ram-pressure stripping (Gunn & Gott 1972). The ram -pressure force is proportional to $\rho_{\rm ICM}\sigma_v^2$, where $\rho_{\rm ICM}$ is the density of the IC diffuse gas, and also $L_{\rm X}$ is proportional to $\rho_{\rm ICM}^2$. If ram-pressure stripping is indeed responsible for the $f_{\rm b}$–$L_{\rm X}$ anti-correlation, its strength should depend on the clustercentric radius. Unfortunately our data are not sufficient to test such a dependence.

The fact that the same anti-correlation is seen in high-z clusters (Postman et al. 2005) would argue for little evolution in the properties of the IC gas out to $z \sim 1$, if ram-pressure stripping is really the main process at work. Timescale is not a problem, since ram-pressure stripping is a rapid process (Vollmer et al. 2001). Because of the proportionality with σ_v^2, ram-pressure stripping is also our best candidate for explaining the anti-correlation of $\Sigma SFR/M_{200}$ with σ_v.

Although models of galaxy evolution in clusters tend to assign little importance to the ram-pressure stripping mechanism (e.g. Okamoto & Nagashima 2003; Lanzoni et al. 2005), direct evidence for ongoing ram-pressure stripping in cluster galaxies exist (e.g. Gavazzi et al. 2003; Kenney et al. 2004). Ram-pressure is thought to induce gas stripping from cluster galaxies, thereby reddening their colors. However, the stripped gas can eventually fall back into the aged galaxy, producing a short and mild burst of SF (Vollmer et al. 2001; Fujita 2004), and this could explain why we observe an anti-correlation between $f_{\rm b}$ and $L_{\rm X}$ but not between $f_{\rm SF}$ and $L_{\rm X}$.

As a matter of fact, $f_{\rm SF}$ differs from $f_{\rm b}$ because of the presence of a red star-forming cluster galaxy population making up a significant portion of the cluster star forming members, on average 25% of the whole cluster galaxy population. The red colors ($u - r > 2.22$) of these galaxies suggest that they are dominated by an old stellar population, unless there is a significant amount of dust extinction. The spectra of our red star-forming cluster galaxies are similar to those of early-type spirals (Sa–Sb). Evidence for such a population of red star-forming galaxies has already been found in other studies (Demarco et al. 2005; Homeier et al. 2005; Jørgensen et al. 2005; Tran et al. 2005a,b; Weinmann et al. 2006). Their spectra are characterized as $k + a$ (Franx 1993) with [OII] or Hα (Miller et al. 2002) in emission. Their morphologies are disklike (Tran et al. 2003), and their concentrations are intermediate between those of the blue star-forming and of those of the red and passive populations (Weinmann et al. 2006).

We can interpret these red star-forming galaxies as objects in the process of accomplishing their transformation from late- to early-type galaxies. This transformation process may be identified by the ram-pressure stripping because of the above mentioned correlations. Another process able to induce bursts of SF

in otherwise quiescent galaxies is the merger of two quiescent galaxies. While the process could occur in distant, low-σ_v clusters (Tran et al. 2005b), it is very unlikely to be effective in nearby ones (e.g. Mamon 1996). Fast encounters between galaxies in clusters rather produce the "harassment" mechanism described by Moore et al. (1996, 1998).

Recently, these red star-forming galaxies have also been found outside clusters. According to Franzetti et al. (2006), ∼35–40% of all the red field galaxies have ongoing SF. This fraction is comparable, if not higher, than the fraction we observe in our sample of nearby clusters, and suggest that we do not actually need a cluster-related phenomenon to explain the presence of red star-forming galaxies. Perhaps these galaxies are simply more dusty than the blue star-forming galaxies (e.g. Tran et al. 2005a). Red-sequence mid-infrared emitters, with significant levels of inferred SF, have indeed already been detected in some clusters (Miller et al. 2002; Biviano et al. 2004; Coia et al. 2005).

In conclusion, we feel that a more detailed analysis of the morphology of the red star-forming systems and a careful study of their properties within and outside the cluster environment, are mandatory for understanding their nature.

7. Conclusion

We have analyzed the relationships between SF in cluster galaxies and global cluster properties, such as cluster M_{200}, σ_v, L_X, and N_{gal}. For our analysis we have used a sample of 79 nearby clusters extracted from the RASS-SDSS galaxy cluster catalogue of Paper III and Paper V. Galaxy *SFR*s and stellar masses are taken from the catalog of Brinchmann et al. (2004), which is based on SDSS spectra. We only consider galaxies with $M_r \leq -20.25$ in our analysis, and exclude AGNs and composite-spectra galaxies.

All the cluster quantities considered are corrected for incompleteness, when needed, and for projection effects. The deprojection correction is of particular importance in our analysis, since we find that it depends on the cluster mass.

ΣSFR is correlated with all the cluster global quantities mentioned above. By performing a multiple regression analysis that the main correlation is that between ΣSFR and N_{gal}. Since this relation is linear the average SFR of cluster galaxies is the same in different clusters, and is unaffected by either the cluster mass, or its velocity dispersion, or its X-ray luminosity. We come to essentially the same conclusion when $M_\star$ is considered in lieu of ΣSFR. If instead of normalizing ΣSFR with N_{gal} we normalize it with M_{200}, we still find $\Sigma SFR/M_{200}$ does not depend on any cluster global property, except σ_v, which we suggest could be evidence of the effect of ram-pressure stripping on the cluster galaxy properties.

Ram-pressure could also be the mechanism able to explain the observed anti-correlation of f_b with L_X, since f_b is *not* correlated with either M_{200} or with σ_v. On the other hand, the fact that we do not observe any correlation between L_X and f_{SF} is due to the presence of a dominant fraction of *red* star-forming galaxies. They could also be the result of the ram-pressure mechanism, or, in alternative, they could be star-forming galaxies with an anomalous amount of dust.

If global cluster properties affect the star-forming properties of cluster galaxies, their effect is rather marginal, except perhaps on galaxy colors, which seem to be influenced by the presence of the IC diffuse gas.

Acknowledgements. We thank the anonymous referee for useful suggestions which helped us improving the quality of this paper. Funding for the creation and distribution of the SDSS Archive has been provided by the Alfred P. Sloan Foundation, the Participating Institutions, the National Aeronautics and Space Administration, the National Science Foundation, the US Department of Energy, the Japanese Monbukagakusho, and the Max Planck Society. The SDSS Web site is `http://www.sdss.org/`. The SDSS is managed by the Astrophysical Research Consortium (ARC) for the Participating Institutions. The Participating Institutions are The University of Chicago, Fermilab, the Institute for Advanced Study, the Japan Participation Group, The Johns Hopkins University, Los Alamos National Laboratory, the Max-Planck-Institute for Astronomy (MPIA), the Max-Planck-Institute for Astrophysics (MPA), New Mexico State University, University of Pittsburgh, Princeton University, the United States Naval Observatory, and the University of Washington.

References

Abazajian, K., Adelman, J., Agueros, M., et al. 2003, AJ, 126, 2081 (Data Release One)
Abraham, R. G., Smecker-Hane, T. A., Hutchings, J. B., et al. 1996, ApJ, 471, 694
Akritas, M. G., & Bershady, M. A. 1996, ApJ, 470, 706
Alexov, A., Silva, D. R., & Pierce, M. J. 2003, AJ, 126, 2644
Andreon, S., & Ettori, S. 1999, ApJ, 516, 647
Andreon, S., Lobo, C., & Iovino, A. 2004, MNRAS, 349, 889
Andreon, S., Quintana, H., Tajer, M., Galaz, G., & Surdej, J. 2006, MNRAS, 365, 915
Baldwin, J. A., Phillips, M. M., & Terlevich, R. 1981, PASP, 93, 5
Balogh, M. L., Shade, D., Morris, S., et al. 1998, ApJ, 504, 75
Balogh, M., Bower, R. G., Smail, I., et al. 2002, MNRAS, 337, 256
Barnes, J. E., & Hernquist, L. 1996, ApJ, 471, 115
Beers, T. C., Flynn, K., & Gebhardt 1990, AJ, 100, 32
Bennett, S. M., & Moss, C. 1998, A&A, 132, 55
Bicay, M. D., & Giovanelli, R. 1987, ApJ, 321, 645
Biviano, A., Katgert, P., Mazure, A., et al. 1997, A&A, 321, 84
Biviano, A., Metcalfe, L., McBreen, B., et al. 2004, A&A, 425, 33
Biviano, A., Murante, G., Borgani, S., et al. 2006, A&A, 456, 23
Blanton, M. R., Lupton, R. H., Maley, F. M., et al. 2003, AJ, 125, 2276
Böhringer, H., Voges, W., Huchra, J. P., et al. 2000, ApJS, 129, 435
Brinchmann, J., White, S. D. M., Tremonti, C., et al. 2004, MNRAS, 351, 1151
Butcher, H., & Oemler, A. Jr. 1978, ApJ, 226, 559
Butcher, H., & Oemler, A. Jr. 1984, ApJ, 285, 426
Carlberg, R. G., Yee, H. K. C., & Ellingson, E. 1997, ApJ, 478, 462
Christlein, D., & Zabludoff, A. I. 2005, ApJ, 621, 201
Coia, D., McBreen, B., Metcalfe, L., et al. 2005, A&A, 431, 433
Conselice, C. J. 2006, ApJ, 638, 686
Demarco, R., Blakeslee, J. P., Ford, H. C., et al. 2005 [arXiv:astro-ph/0509575]
De Propris, R., Stanford, S. A., Eisenhardt, P. R., & Dickinson, M. 2003, ApJ, 598, 20
De Propris, R., Colless, M., Peacock, J. A., et al. 2004, MNRAS, 351, 125
Donas, J., Buat, V., Milliard, B., et al. 1990, A&A, 235, 60
Dressler, A. 1980, ApJ, 236, 351
Dressler, A., & Gunn, J. E. 1982, ApJ, 263, 563
Dressler, A., Oemler, A., Couch, W. J., et al. 1997, ApJ, 490, 577
Dressler, A., Smail, I., Poggianti, B. M., et al. 1999, ApJS, 122, 51
Eisenstein, D. J., Annis, J., Gunn, J. E., et al. 2001, AJ, 122, 2267
Ellingson, E., Lin, H., Yee, H. K. C., & Carlberg, R. G. 2001, ApJ, 547, 609
Fairley, B. W., Jones, L. R., Wake, D. A., et al. 2002, MNRAS, 330, 755
Finn, R. A., Zaritsky, D., & McCarthy D. W. Jr. 2004, ApJ, 604, 141
Finn, R. A., Zaritsky, D., McCarthy, D. W., et al. 2005, ApJ, 630, 206
Franx, M. 1993, ApJ, 407, L5
Franzetti, P., Scodeggio, M., Maccagni, D., et al. 2006 [arXiv:astro-ph/0607075]
Fujita, Y. 2004, PASJ, 56, 29
Fukugita, M., Ichikawa, T., & Gunn, J. E. 1996, AJ, 111, 1748
Gavazzi, G., Boselli, A., Kennicutt, R., et al. 1991, AJ, 101, 1207
Gavazzi, G., Catinella, B., Carrasco, L., et al. 1998, AJ, 115, 1745
Gavazzi, G., Boselli, A., Pedotti, P., et al. 2002, A&A, 396, 449
Gavazzi, G., Cortese, L., Boselli, A., et al. 2003, ApJ, 597, 210
Girardi, M., Biviano, A., Giuricin, G., et al. 1993, ApJ, 404, 38
Girardi, M., Giuricin, G., Mardirossian, F., Mezzetti, M., & Boschin, W. 1998, ApJ, 505, 74
Goto, T. 2005, MNRAS, 356, L6
Goto, T., Okamura, S., Yagi, M., et al. 2003, PASJ, 55, 739
Gunn, J. E., & Gott, J. 1972, ApJ, 176, 1
Gunn, J. E., Carr, M. A., Rockosi, C. M., et al. 1998, AJ, 116, 3040
Harrison, E. R. 1974, ApJ, 191, L51
Hashimoto, Y., Oemler, A. Jr., Lin, H., & Tucker, D. L. 1998, ApJ, 499, 589

Hogg, D. W., Finkbeiner, D. P., Schlegel, D. J., & Gunn, J. E. 2001, AJ, 122, 2129
Homeier, N. L., Demarco, R., Rosati, P., et al. 2005, ApJ, 621, 651
Hubble, E., & Humason, M. L. 1931, ApJ, 74, 43
Jørgensen, I., Bergmann, M., Davies, et al. 2005, AJ, 129, 1249
Katgert, P., Biviano, A., & Mazure, A. 2004, ApJ, 600, 657
Kenney, J. D. P., van Gorkom, J. H., & Vollmer, B. 2004, AJ, 127, 3361
Kennicutt, R. C. 1983, AJ, 88, 483
Kennicutt, R. C., Bothun, G. D., & Schommer, R. A. 1984, AJ, 89, 179
King, I. 1962, AJ, 67, 471
Kodaira, K., Watanabe, T., Onaka, T., et al. 1990, ApJ, 363, 422
Koopmann, R. A., & Kenney, J. D. P. 1998, ApJ, 497, L75
Lanzoni, B., Guiderdoni, B., Mamon, G. A., Devriendt, J., & Hatton, S. 2005, MNRAS, 361, 369
Larson, R. B., Tinsley, B. M., & Caldwell, C. N. 1980, ApJ, 237, 692
Lea, S. M., & Henry, J. P. 1988, ApJ, 332, 81
Lin, Y.-T., Mohr, J. J., & Stanford, S. A. 2003, ApJ, 591, 749
Lupton, R., Gunn, J. E., Ivezić, Z., et al. 2001, in Astronomical Data Analysis Software and Systems X, ed. F. R. Harnden, Jr., F. A. Primini, & H. E. Payne (San Francisco: ASP), ASP Conf. Ser., 238, 269 [arXiv:astro-ph/0101420]
Lupton, R. H., Gunn, J. E., & Szalay, A. S. 1999, AJ, 118, 1406
Mamon, G. A. 1996, in The Dynamics of Groups and Clusters of Galaxies and Links to Cosmology, ed. H. de Vega, & N. Sanchez (Singapore: World Scientifi c), 95
Margoniner, V. E., de Carvalho, R. R., Gal, R. R., et al. 2001, ApJ, 548, L143
Mihos, J. C. 2004, in Clusters of Galaxies: Probes of Cosmological Structure and Galaxy Evolution, ed. J. S. Mulchaey, A. Dressler, & A. Oemler (Cambridge: Cambridge Univ. Press), 278
Miller, N. A., & Owen, F. N. 2002, AJ, 124, 2453
Moore, B., Katz, N., Lake, G., Dressler, A., & Oemler, A. Jr. 1996, Nature, 379, 613
Moore, B., Lake, G., & Katz, N. 1998, ApJ, 495, 139
Moore, B., Lake, G., Quinn, T., & Stadel, J. 1999, MNRAS, 304, 465
Moss, C., & Whittle, M. 1993, ApJ, 407, L17
Moss, C., & Whittle, M. 2005, MNRAS, 357, 1337
Navarro, J. F., Frenk, C. S., & White, S. D. M. 1997, ApJ, 490, 493
Newberry, M. V., Kirshner, R. P., & Boroson, T. A. 1988, ApJ, 335, 629
Oemler, A. Jr. 1974, ApJ, 194, 1
Okamoto, T., & Nagashima, M. 2003, ApJ, 587, 500
Pimbblet, K. A. 2003, PASA, 20, 294
Pimbblet, K. A., Smail, I., Edge, A. C., et al. 2006, MNRAS, 366, 645
Poggianti, B. M., von der Linden, A., De Lucia, G., et al. 2006, ApJ, 642, 188 (P06)
Popesso, P., & Biviano, A. 2006, A&A, 460, L23
Popesso, P., Böhringer, H., Brinkmann, J., Voges, W., & York, D. G. 2004, A&A, 423, 449 (Paper I)
Popesso, P., Biviano, A., Böhringer, H., Romaniello, M., & Voges, W. 2005, A&A, 433, 431 (Paper III)
Popesso, P., Biviano, A., Böhringer, H., & Romaniello, M. 2006a, A&A, 461, 397 (Paper V)
Popesso, P., Biviano, A., Böhringer, H., & Romaniello, M. 2006b, A&A, 445, 29 (Paper IV)
Popesso, P., Biviano, A., Böhringer, H., & Romaniello, M. 2006c, A&A, in press, [arXiv:astro-ph/0606260] (Paper VII)
Postman, M., & Geller, M. J. 1984, ApJ, 281, 95
Postman, M., Lubin, L. M., & Oke, J. B. 1998, AJ, 116, 560
Postman, M., Lubin, L. M., & Oke, J. B. 2001, AJ, 122, 1125
Postman, M., Franx, M., Cross, N. J. C., et al. 2005, ApJ, 623, 721
Quilis, V., Moore, B., & Bower, R. 2000, Science, 288, 5471
Rakos, K., & Schombert, J. 2005, AJ, 130, 1002
Reiprich, T. H., & Böhringer, H. 2002, ApJ, 567, 716
Schechter, P. 1976, ApJ, 203, 297
Smith, J. A., Tucker, D. L., Kent, S. M., et al. 2002, AJ, 123, 2121
Stoughton, C., Lupton, R. H., Bernardi, M., et al. 2002, AJ, 123, 485
Strateva, I., Ivezic, Z., Knapp, G., et al. 2001, AJ, 122, 1861
Strauss, M. A., Weinberg, D. H., Lupton, R. H., et al. 2002, AJ, 124, 1810
Struck, C. 1999, Phys. Rep., 321, 1
Tegmark, M., Strauss, M., Blanton, M., et al. 2004, PhRvD, 69, 103501
The, L. S., & White, S. D. M. 1986, AJ, 92, 1248
Tran, K.-V. H., Simard, L., Illingworth, G., & Franx, M. 2003, ApJ, 590, 238
Tran, K.-V. H., van Dokkum, P., Illingworth, G. D., et al. 2005a, ApJ, 619, 134
Tran, K.-V. H., van Dokkum, P., Franx, M., et al. 2005b, ApJ, 627, L25
Trümper, J. 1988, Hot Thin Plasmas in Astrophysics, Proceedings of a NATO Advanced Study Institute, held at Cargese, Corsica, September 8–18, 1987 (Dordrecht: Kluwer), ed. R. Pallavicini, NATO Advanced Science Institutes (ASI) Ser. C, 249, 355
van Gorkom, J. H. 2004, in Clusters of Galaxies: Probes of Cosmological Structure and Galaxy Evolution, ed. J. S. Mulchaey, A. Dressler, & A. Oemler (Cambridge: Cambridge Univ. Press), 306
Vollmer, B., Cayatte, V., & Balkowski, C. 2001, ApJ, 561, 708
Wake, D. A., Collins, C. A., Nichol, R. C., Jones, L. R., & Burke, D. J. 2005, ApJ, 627, 186
Weinmann, S. M., van den Bosch, F. C., Yang, X., & Mo, H. J. 2006, MNRAS, 366, 2
Yasuda, N., Fukugita, M., Narayanan, V. K., et al. 2001, AJ, 122, 1104
York, D. G., Adelman, J., Anderson, J. E., et al. 2000, AJ, 120, 1579

A&A 464, 451–464 (2007)
DOI: 10.1051/0004-6361:20054708

Astronomy & Astrophysics

RASS-SDSS galaxy cluster survey

VII. On the cluster mass-to-light ratio and the halo occupation distribution

P. Popesso[1], A. Biviano[2], H. Böhringer[3], and M. Romaniello[1]

[1] European Southern Observatory, Karl Scharzschild Strasse 2, 85748 Garching, Germany
e-mail: ppopesso@eso.org
[2] INAF – Osservatorio Astronomico di Trieste, via G.B. Tiepolo 11, 34131 Trieste, Italy
[3] Max-Planck-Institut für Extraterrestrische Physik, 85748 Garching, Germany

Received 16 December 2005 / Accepted 8 June 2006

ABSTRACT

Aims. We explore the mass-to-light ratio in galaxy clusters and its relation to the cluster mass.
Methods. We study the relations among the optical luminosity ($L_{\rm op}$), the cluster mass (M_{200}) and the number of cluster galaxies within r_{200} ($N_{\rm gal}$) in a sample of 217 galaxy clusters with confirmed 3D overdensity. We correct for projection effect, by determining the galaxy surface number density profile in our cluster sample. This is best fitted by a cored King profile in low and intermediate mass systems. The core radius decreases with cluster mass, and, for the highest mass clusters, the profile is better represented by a generalized King profile or a cuspy Navarro, Frenk & White profile.
Results. We find a very tight proportionality between $L_{\rm op}$ and $N_{\rm gal}$, which, in turn, links the cluster mass-to-light ratio to the Halo Occupation Distribution $N_{\rm gal}$ vs. M_{200}. After correcting for projection effects, the slope of the $L_{\rm op}-M_{200}$ and $N_{\rm gal}-M_{200}$ relations is found to be 0.92 ± 0.03, close, but still significantly less than unity. We show that the non-linearity of these relations cannot be explained by variations of the galaxy luminosity distributions and of the galaxy M/L with the cluster mass.
Conclusions. We suggest that the nonlinear relation between number of galaxies and cluster mass reflects an underlying nonlinear relation between number of subhaloes and halo mass.

Key words. galaxies: clusters: general – galaxies: luminosity function, mass function

1. Introduction

Clusters of galaxies are the most massive gravitationally bound systems in the universe. The cluster mass function and its evolution provide constraints on the evolution of large-scale structure and important cosmological parameters such as $\Omega_{\rm m}$ and σ_8. Cluster mass-to-light ratios (M/L hereafter) provide one of the most robust determination of $\Omega_{\rm m}$ in connection with the observed luminosity density in the Universe via the Oort (1958) method. In this method, a fundamental assumption is that the average M/L of clusters is a fair representation of the universal value. For this reason, many works have focused on the dependence of the cluster M/L on the mass of the systems. In general, M/L has been found to increase with the cluster mass. Assuming a power-law relation $M/L \propto M^{\alpha}$, and adopting the usual scaling relations between mass and X-ray temperature or velocity dispersion, when needed, most authors have found α in the range 0.2–0.4, in both optical and near-infrared bands, and over a large mass range (Adami et al. 1998a; Bahcall & Comerford 2002; Girardi et al. 2002; Lin et al. 2003, 2004; Rines et al. 2004; Ramella et al. 2004; see however Kochanek et al. 2003, for a discordant result). Why does the cluster M/L increase with the mass? Based on the results of numerical simulations, Bahcall & Comerford (2002) have proposed that the trend of M/L with mass is caused by the stellar populations of galaxies in more massive systems being older than the stellar populations of galaxies in less massive systems. In this scenario, the slope of the $M/L-M$ relation should be steeper in the B and V bands, dominated by the young stellar populations, than at longer wavelengths, eventually becoming flat in the infrared K band, dominated by the light of the old stellar population. Such a scenario is not consistent with the results of the semi-analytical modeling of Kauffmann et al. (1999), where the M/L is predicted to increase with mass with approximately the same slope in the B and I band. Also observationally, the slope of the $M/L-M$ relation is found to be the same in different bands, the B-band (Girardi et al. 2002) the V-band (Bahcall & Comerford 2002), the R-band (Adami et al. 1998a; Popesso et al. 2005b, 2007) and the K-band (Lin et al. 2003, 2004; Rines et al. 2004; Ramella et al. 2004). An alternative interpretation of the increasing M/L with system mass is provided by Springel & Hernquist (2003). They analyze the star formation efficiency within halos extracted from cosmological simulations, with masses in the range 10^8–10^{15} $M_{\odot}$, and find that the integrated star formation efficiency decreases with increasing halo mass by a factor 5–10 over the cluster mass range. This scenario is investigated by Lin et al. (2003), who convert the 2MASS K-band cluster luminosities into cluster stellar masses. They find that the fraction of mass in stars is a decreasing function of the cluster mass ($M_{\rm star}/M_{\rm tot} \propto M_{\rm tot}^{-0.26}$).

In this paper we address the above issues by studying M/L for a sample of 217 clusters, which span the entire cluster mass range. In particular, we study the relations among the cluster optical luminosity $L_{\rm op}$, the mass M_{200}, and the number of cluster galaxies $N_{\rm gal}$, within the virial radius r_{200}. We find a very tight relation between $L_{\rm op}$ and $N_{\rm gal}$, which links the $L_{\rm op}-M_{200}$ relation (and therefore, the cluster M/L), to the Halo Occupation Distribution (HOD hereafter) $N_{\rm gal}-M_{200}$. The HOD is a powerful tool for describing galaxy bias and modelling galaxy

clustering (e.g. Ma & Fry 2000; Peacock & smith 2000; Seljak 2000; Scoccimarro et al. 2001; Berlind & Weinberg 2002). It characterizes the bias between galaxies and mass in terms of the probability distribution $P(N|M)$ that a halo of virial mass M contains N galaxies of a given type, together with relative spatial and velocity distributions of galaxies and dark matter within halos. The HOD is a fundamental prediction of galaxy formation theory (e.g. Kauffmann et al. 1997, 1999; White et al. 2001; Yoshikawa et al. 2001; Berlind et al. 2003; Kravtsov et al. 2004; Zheng et al. 2005) and it can be extremely useful to compare the observational results with the theoretical models.

This paper is organized as follows. In Sect. 2 we describe our dataset. In Sect. 3 we describe the methods we use to calculate several cluster properties, like the characteristic radius, the virial mass, the optical luminosity, and the number density profile of cluster galaxies. In Sect. 4 we analyze the $L_{\rm op} - M_{200}$ and the $N_{\rm gal}-M_{200}$ relations, and find that the number of galaxies per given halo mass decreases as the halo mass increases. In Sect. 5 we seek a physical explanation of this trend by comparing our results with theoretical predictions. In Sect. 6 we provide our conclusions.

Throughout this paper, we use $H_0 = 70$ km s^{-1} Mpc^{-1} in a flat cosmology with $\Omega_0 = 0.3$ and $\Omega_\Lambda = 0.7$ (e.g. Tegmark et al. 2004).

2. The data

The optical data used in this paper are taken from the Sloan Digital Sky Survey (SDSS, Fukugita 1996; Gunn et al. 1998; Lupton et al. 1999; York et al. 2000; Hogg et al. 2001; Eisenstein et al. 2001; Smith et al. 2002; Strauss et al. 2002; Stoughton et al. 2002; Blanton et al. 2003, and Abazajian et al. 2003). The SDSS consists of an imaging survey of π steradians of the northern sky in the five passbands u, g, r, i, z, in the entire optical range. The imaging survey is taken in drift-scan mode. The imaging data are processed with a photometric pipeline (PHOTO, Lupton et al. 2001) specially written for the SDSS data. For each cluster we defined a photometric galaxy catalog as described in Sect. 3 of Popesso et al. (2004; see also Yasuda et al. 2001). For the analysis in this paper we use only SDSS Model magnitudes. The discussion about completeness limits in magnitude and surface brightness of the SDSS galaxy photometric sample can be found in Popesso et al. (2005a,b, Papers II and IV of this series).

The spectroscopic component of the survey is carried out using two fiber-fed double spectrographs, covering the wavelength range 3800–9200 Å, over 4098 pixels. They have a resolution $\Delta\lambda/\lambda$ varying between 1850 and 2200, and together they are fed by 640 fibers, each with an entrance diameter of 3 arcsec. The fibers are manually plugged into plates inserted into the focal plane; the mapping of fibers to plates is carried out by a tiling algorithm (Blanton et al. 2003) that optimizes observing efficiency in the presence of large-scale structure.

2.1. The cluster sample

In this paper we use a combined sample of X-ray selected galaxy clusters and optically selected systems. The X-ray selected clusters are taken from the RASS-SDSS galaxy cluster catalog of Popesso et al. (2005b, hereafter Paper III), which comprises 130 systems selected mainly from the REFLEX and NORAS X-ray cluster catalogs. The optically selected clusters are taken from Popesso et al. (2007), who selected a subsample of 130 Abell clusters with confirmed 3-dimensional galaxy overdensity in the third release of the SDSS galaxy spectroscopic catalog. The two samples overlap with 43 clusters. The combined sample with the exclusion of the double detections comprises 217 clusters and covers the entire range of masses and X-ray/optical luminosities, from very low-mass and X-ray/optical faint groups ($10^{13}\ M_\odot$) to very massive and X-ray/optical bright clusters ($5 \times 10^{15}\ M_\odot$). The cluster sample comprises only nearby systems at the mean redshift of 0.1. The redshift distribution of the cluster sample is shown in Fig. 1.

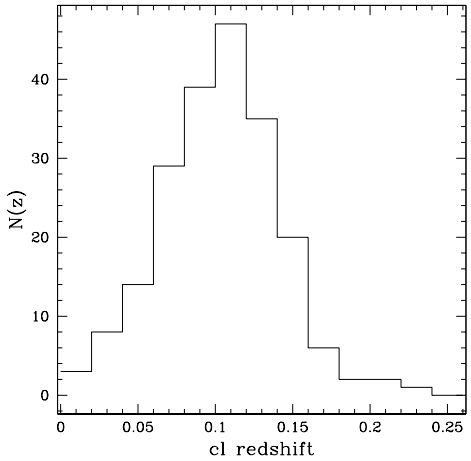

Fig. 1. Redshift distribution of the cluster sample used in this paper.

3. The cluster properties

In this section we explain the methods used to calculate the cluster properties as the characteristic radius, the virial mass, the optical luminosity and the parameters of the radial profile of the cluster galaxies.

3.1. Characteristic radii and masses

Here we describe the methods by which we measure the characteristic cluster radii r_{200} and mass M_{200}. r_{200} and M_{200} are the radius and the mass, respectively, where the mass density of the system is 200 times the critical density of the Universe and it is considered as a robust measure of the virial radius of the cluster.

Estimates of cluster velocity dispersion, mass, and characteristic radius requires knowledge of the redshifts of its member galaxies. We have used the redshifts provided in the SDSS spectroscopic catalog.

Cluster members are selected following the method of Adami et al. (1998a) or Girardi et al. (1993), depending on whether the mean cluster redshift $z_{\rm cluster}$ is known in advance (from previous studies) or not, respectively. Girardi et al. (1993) method requires in fact that a preliminary cut be done in the line-of-sight velocity space, ± 4000 km s^{-1} around $cz_{\rm cluster}$, before searching for significant weighted-gaps in the velocity distribution. On the other hand, the density-gap technique of Adami et al. does not require such a preliminary cut. If $z_{\rm cluster}$ is known already, we select among the groups identified by the gapping technique that one closest in velocity space to $cz_{\rm cluster}$, otherwise we select the most populated one. After the initial group selection, we apply the interloper-removal method of Katgert et al. (2004; see Appendix A in that paper for more details) on the remaining galaxies, using the X-ray center when available, or else

the position of the brightest cluster galaxy on the cluster colour-magnitude sequence.

The virial analysis (see, e.g., Girardi et al. 1998) is then performed on the clusters with at least 10 member galaxies. The velocity dispersion is computed on the cluster members, using the biweight estimator (Beers et al. 1990). The virial masses are corrected for the surface pressure term (The & White 1986) by adopting a profile of Navarro et al. (1996, 1997, NFW hereafter) with a concentration parameter, c, that depends on the initial estimate of the cluster virial mass itself. The c-mass relation is given by $c = 4 \times (M/M_{\rm KBM})^{-0.102}$ where the slope of the relation is taken from Dolag et al. (2004), and the normalization $M_{\rm KBM} \simeq 2 \times 10^{15}\ M_{\odot}$ from Katgert et al. (2004). The clusters in our sample span a range $c \simeq 3$–6.

Correction for the surface pressure term requires knowledge of the r_{200} radius, for which we adopt the Carlberg et al. (1997) definition (see Eq. (8) in that paper) as a first guess. After the virial mass is corrected for the surface pressure term, we refine our r_{200} estimate using the virial mass density itself. Let $M_{\rm vir}$ be the virial mass (corrected for the surface term) contained in a volume of radius equal to a chosen observational aperture, $r_{\rm ap}$. The radius r_{200} is then given by:

$$r_{200} \equiv r_{\rm ap}\,[\rho_{\rm vir}/(200\rho_{\rm c})]^{1/2.4} \qquad (1)$$

where $\rho_{\rm vir} \equiv 3M_{\rm vir}/(4\pi r_{\rm ap}^3)$ and $\rho_{\rm c}(z)$ is the critical density at redshift z in the adopted cosmology. The exponent in Eq. (1) is the one that describes the average cluster mass density profile near r_{200}, as estimated by Katgert et al. (2004) for an ensemble of 59 rich clusters.

A NFW profile is used to interpolate (or, in a few cases, extrapolate) the virial mass $M_{\rm vir}$ from $r_{\rm ap}$ to r_{200}, yielding M_{200}. As before, we scale the concentration parameter of the used NFW profile according to a preliminary estimate of the mass of the system. From M_{200} the final estimate of r_{200} is obtained, using the definition of M_{200} itself.

3.2. Optical luminosities

The total optical luminosity of a cluster has to be computed after the subtraction of the foreground and background galaxy contamination. We consider two different approaches to the statistical subtraction of the galaxy background. We compute the local background number counts in an annulus around the cluster and a global background number counts from the mean of the magnitude number counts determined in five different SDSS sky regions, randomly chosen, each with an area of 30 deg^2. In our analysis we show the results obtained using the optical luminosity estimated with the second method. The optical luminosity is then computed within r_{200} following the prescription of Popesso et al. (2004). The reader is referred to that paper for a detailed discussion about the comparison between optical luminosities calculated with different methods. To avoid selection effects due to the slightly different redshifts of the clusters, the optical luminosity has been calculated in the same absolute magnitude range for all the clusters. The adopted range has been varied to check the robustness of the results of the regression analyses.

3.3. Number density profiles and projection effects

The observed cluster optical luminosity, $L_{\rm op}$, is contributed not only by galaxies within the virial sphere of radius r_{200}, but also by galaxies outside the virial sphere yet within the cylinder of same radius. It is therefore necessary to correct the observed optical luminosity for the contribution of cluster galaxies outside the virial sphere (the following analysis is based on photometric data and the field galaxies contribution is removed statistically as described in the previous section).

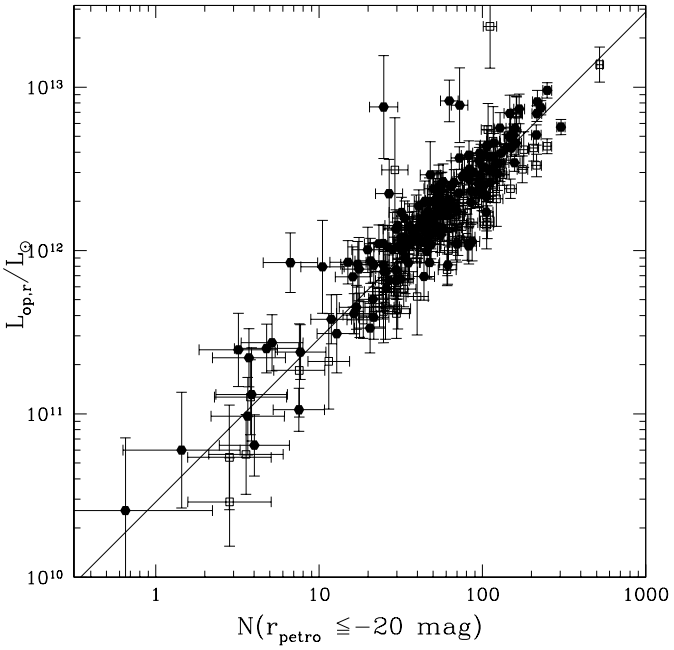

Fig. 2. Relation between the optical luminosity calculated in the SDSS r band within r_{200} and the number of cluster galaxies contributing to $L_{\rm op}$. The solid line is the best fit line with slope 1.00 ± 0.03.

Figure 2 shows the proportionality between the cluster r-band optical luminosity within r_{200} and the number of cluster galaxies ($N_{\rm gal}$), contributing to the luminosity itself, i.e. the background-subtracted galaxy counts within the same radius, down to the magnitude limit used to estimate $L_{\rm op}$. Because of the strict proportionality between $L_{\rm op}$ and $N_{\rm gal}$, we can use the ratio between the number of cluster galaxies within the cylindrical volume and the number of galaxies within the virial sphere, to correct the observed $L_{\rm op}$ for the contribution of cluster galaxies outside the virial sphere. In order to estimate this ratio, we build the surface number density profiles of our clusters, and fit them with two widely-used analytical functions, the King (1962) cored profile, and the NFW cuspy profile. The 3D and projected King profiles are given by, respectively:

$$\rho(r) = \frac{n_0}{(1 + (r/r_{\rm c})^2)^{3/2}} \qquad (2)$$

and:

$$\sigma(b) = \frac{\sigma_0}{(1 + (b/r_{\rm c})^2)} \qquad (3)$$

where $r_{\rm c}$ is the core radius and $\sigma_0 = 2n_0 r_{\rm c}$ is the normalization (see also Sarazin 1980). The NFW profile in 3D is given by:

$$\rho(r) = \frac{\delta_0}{r/r_{\rm s}(1 + (r/r_{\rm s})^2)} \qquad (4)$$

where $r_{\rm s}$ is the characteristic radius ($r_{\rm s} = r_{200}/c$ with c the concentration parameter) and δ_0 is the normalization. The projected surface density profile is then obtained from an integration of the three-dimensional profile (see Bartelmann et al. 1996).

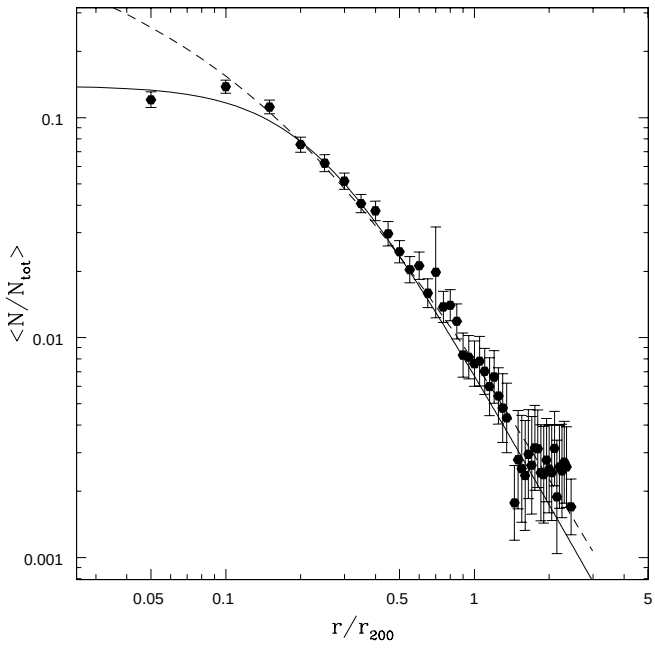

Fig. 3. The stacked mean surface number density profile of all the cluster galaxies with magnitude $r < -18.5$. The solid curve is the best fit King profile, the dashed curve is the best fit NFW profile.

As a first step we explore the the mean surface density galaxy distribution within our cluster sample, by stacking the projected galaxy distributions of the individual systems. Note that in this analysis we only consider the clusters with available X-ray centers, in order to reduce possible mis-centering when adopting the positions of brightest cluster galaxies as cluster centers (not all brightest cluster galaxies lie at centers of their parent clusters, see, e.g., Lin & Mohr 2004). The clustercentric distances are rescaled to the cluster r_{200} before the stacking. The cluster galaxy distributions are normalized to the total number of galaxies within r_{200}, after subtraction of the mean background galaxy density, evaluated within the 2.5–3.5 $\times$ r_{200} annulus. Figure 3 shows the stacked surface density profile of all the 217 clusters. The best fit is given by a King profile with core radius $r_c/r_{200} = 0.224 \pm 0.005$, while a NFW profile provides a poor fit near the centre. We then split our sample of clusters in 6 mass bins: $M_{200}/10^{14}\ M_\odot \leq 1$, $1 < M_{200}/10^{14}\ M_\odot \leq 3$, $3 < M_{200}/10^{14}\ M_\odot \leq 7$, $7 < M_{200}/10^{14}\ M_\odot \leq 10$, $10 < M_{200}/10^{14}\ M_\odot \leq 30$, and $M_{200}/10^{14}\ M_\odot > 30$. Each bin contains at least 10 clusters.

Figure 4 shows the surface density profiles in each cluster mass bin. The solid line in each plot shows the King profile that provides the best-fit to the surface density profile of all galaxies in all clusters, already shown in Fig. 3. The dashed line in each panel is the best-fit King profile for the surface density profile of each cluster mass bin. The NFW profiles provide poor fits for most cluster mass bins, and are not plotted. From Fig. 4 one can clearly see how the cluster galaxy distribution changes with cluster mass. The surface density profiles become steeper near the centre as the cluster mass increases. Note that the surface number density profile in the low mass bin ($M_{200}/10^{14}\ M_\odot \leq 1$) is not completely consistent with a King profile since it shows a deficit of galaxies near the center. The core radius is quite large, $r_c/r_{200} = 0.40 \pm 0.08$. The core radius becomes smaller as the cluster mass increases, and it is $r_c/r_{200} = 0.16 \pm 0.01$ for clusters in the mass interval $7 < M_{200}/10^{14}\ M_\odot \leq 10$. In the last two mass bins, the galaxy distributions become so concentrated that the simple King profile no longer provides a good fit, and a generalized King profile is needed, of the form:

$$\sigma(b) = \frac{\sigma_0}{(1 + (b/r_c)^2)^\beta}. \quad (5)$$

The dotted lines in the panels of Fig. 4 corresponding to the highest cluster mass bins, show the best fit given by the generalized King profile, where $\beta = 0.91 \pm 0.01$. Finally, in the highest mass bin ($M_{200} > 3 \times 10^{15}$) the projected NFW profile also provides a good fit to the galaxy distributions. This is shown in Fig. 5, where the best-fit generalized King profile is shown as a solid curve, and the best-fit NFW profile is shown as a dashed curve. In this case, the best-fit value of the NFW concentration parameter is $c = 4.2 \pm 0.3$, and is consistent with the value found for the dark matter distribution in similarly massive clusters (e.g. Biviano & Girardi 2003; Katgert et al. 2004).

Lin et al. (2004) perform the same analysis on a smaller sample of 93 X-ray selected clusters observed in the 2 MASS all sky survey. Their conclusion is that the surface density profile of cluster galaxies is consistent with a NFW profile with concentration parameter 2.90 ± 0.22. They study the galaxy distribution in 2 mass bins with mean mass $\langle M_{500} \rangle = 7.9 \times 10^{13}\ M_\odot$ for the groups, and $\langle M_{500} \rangle = 5.3 \times 10^{14}\ M_\odot$, for the massive clusters, and claim that the spatial profiles are consistent with the mean profile in both mass bins. However, by fitting their data (taken from Fig. 8 of Lin et al. 2004) with both a King, a generalized King, and a NFW profile, we find that a King profile provides the best fit, in agreement with our findings.

Our results are further supported by the analysis of the surface brightness profile of our clusters. Figure 6 shows the composite surface brightness profile of two cluster subsamples: the low-mass systems with $M_{200} \leq 10^{14}\ M_\odot$ and the high-mass clusters with $M_{200} > 3 \times 10^{15}\ M_\odot$. The profile of the low-mass objects displays a core, and is less centrally concentrated than that of the high-mass clusters which is in fact rather cuspy. As expected, due to the presence of the Brightest Cluster Galaxies at the center of the systems, the luminosity profiles are generally more cuspy than the density profiles in the same cluster mass bins (Adami et al. 2001).

In stacking clusters, we have assumed circularity, because the number of galaxies per cluster is generally too small to allow a precise determination of individual cluster shapes and orientations. Adami et al. (1998b) have shown that enforcing circularity could create a central artificial cusp in the number density profile of the stacked cluster. However, lower mass clusters are more elongated than higher mass clusters (see Fasano et al. 1993; de Theije et al. 1995; Plionis et al. 2004), so the effect of assuming circularity should lead to more cuspy density profiles for lower mass clusters, which is opposite to what we find. Indeed, the effect reported by Adami et al. does not seem to be strong enough to account for the differences seen in the density profiles of the stacked clusters of different masses (compare Fig. 4 with Fig. 7 in Adami et al. 1998b).

Hence we conclude that there is a significant variation of the number density and luminosity density profiles of clusters, as a function of cluster mass, with higher mass clusters displaying more concentrated profiles. As a consequence, also the correction needed to convert the number of galaxies contained in the cylindrical volume to that in the virial sphere depends on the cluster mass. Using the volume and the surface density King profile given in Eqs. (2) and (3), respectively, we estimate that

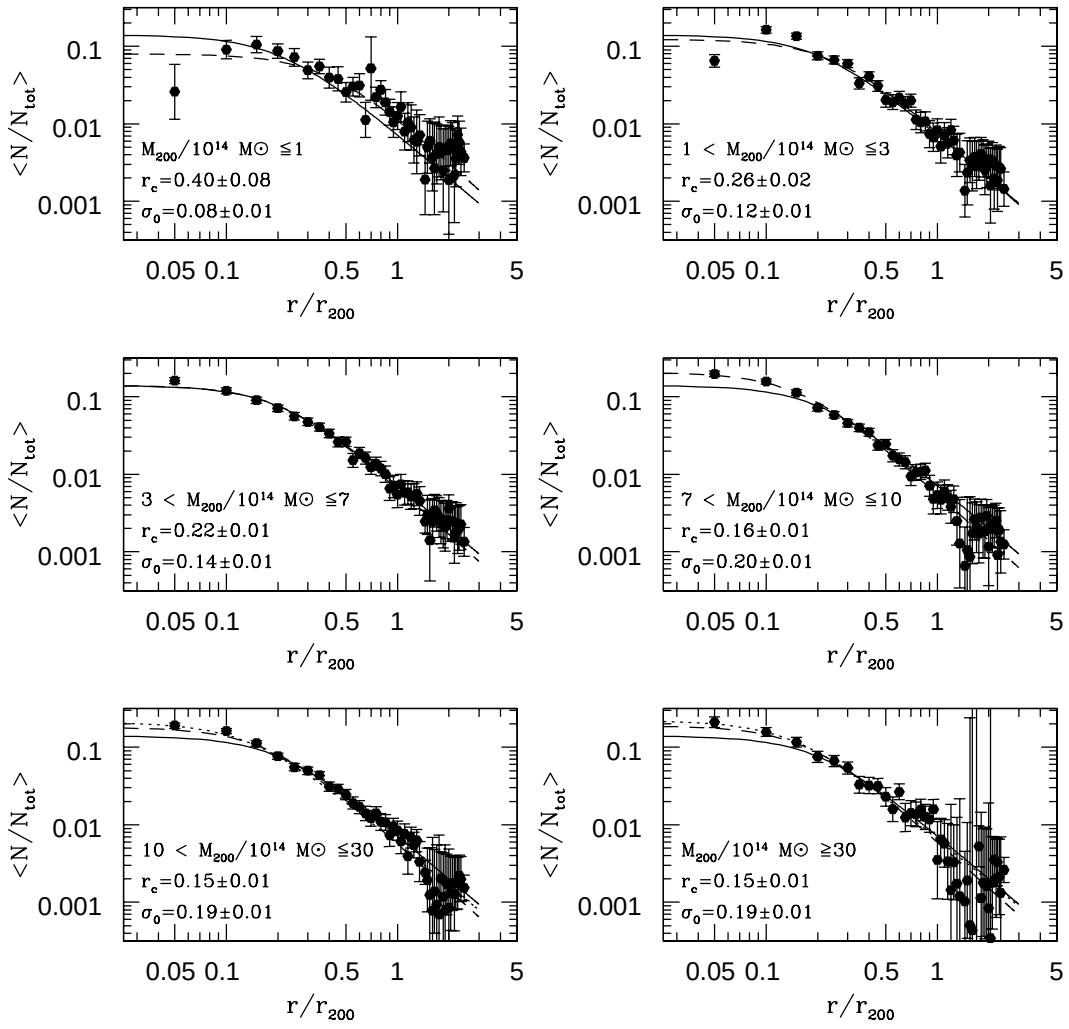

Fig. 4. The stacked surface number density profiles of clusters in different cluster mass bins. The individual cluster profiles are obtained by considering all the galaxies with $r_{\rm petro} < -18.5$. The dashed curve in each panel is the King profile that provides the best-fit to the surface density profile shown in that same panel, while the solid curve is the King profile that provides the best-fit to the mean stacked surface density profile (same as the solid line in Fig. 3). The dotted line in the bottom panels (corresponding to the highest-mass bin clusters) is the best fit provided by a generalized King profile.

the ratio between the number of galaxies in the virial sphere of radius r_{200} and the number of galaxies actually observed in the cylinder of same radius is 0.69–0.76 for clusters in the lowest-mass bin, 0.78–0.80 for clusters in the $1–3 \times 10^{14}$ $M_\odot$ mass bin, 0.81 in the $3–7 \times 10^{14}$ $M_\odot$ mass bin, and 0.85 in the highest mass bins.

We performed the same analysis separately for the red (early-type) and blue (late-type) cluster galaxy populations. The colour separation between the two population is based on the SDSS galaxy color $u-r$ (Strateva et al. 2001; Popesso et al. 2006). For both the red and the blue galaxy populations, the core radius of the best-fit King profile monotonically decreases from the low-mass systems to the more massive clusters (see Figs. 7 and 8).

Since there is a significant mass-dependence of the number density profiles, a mass-dependent deprojection correction needs to be applied to the observed values of $L_{\rm op}$. In the following, we only consider the deprojection-corrected values of $L_{\rm op}$, obtained by adopting the correction factors per mass bin derived above.

4. The $L_{\rm op}$–M_{200} and the $N_{\rm gal}$–M_{200} relations

In Fig. 9 we show the r-band $L_{\rm op}-M_{200}$ relation after correcting $L_{\rm op}$ for the projection effects (see Sect. 3.3). The solid line in the figure is the best-fit linear regression in logarithmic space, and the dotted line is the best-fit we would have obtained had $L_{\rm op}$ not been corrected for the projection effects. The best-fit relation for the corrected $L_{\rm op}$ is:

$$L_{\rm op}/(10^{12}\,L_\odot) = 10^{-0.29\pm0.03}(M_{200}/(10^{14}\,M_\odot))^{0.92\pm0.03}. \quad (6)$$

The slope of this relation is steeper than the slope of the uncorrected relation, which is 0.85 ± 0.03. The two values are anyhow marginally consistent within 2.5σ. As a consequence, also the $M/L-M$ relation is flatter. The slope of the corrected relation is 0.18 ± 0.04 instead of 0.27 ± 0.04 for the uncorrected relation. Remarkably, we find that the slopes of the best-fit $L-M$ and $M/L-M$ relations do not depend on the chosen photometric SDSS band.

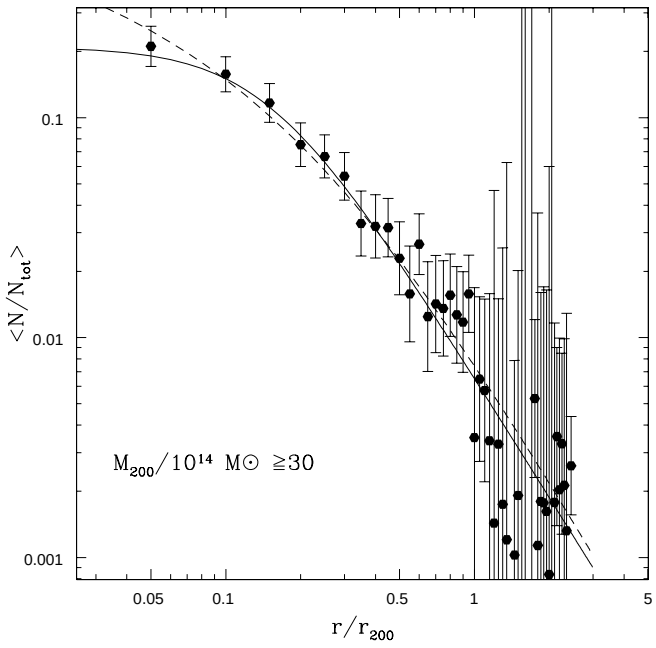

Fig. 5. The surface number density profile of all the cluster galaxies with $r < -18.5$ in the highest of our considered cluster mass bins. The solid curve is the best fit provided by the generalized King profile. The dashed curve is the best fit provided by the NFW profile. Both profiles are consistent with the data.

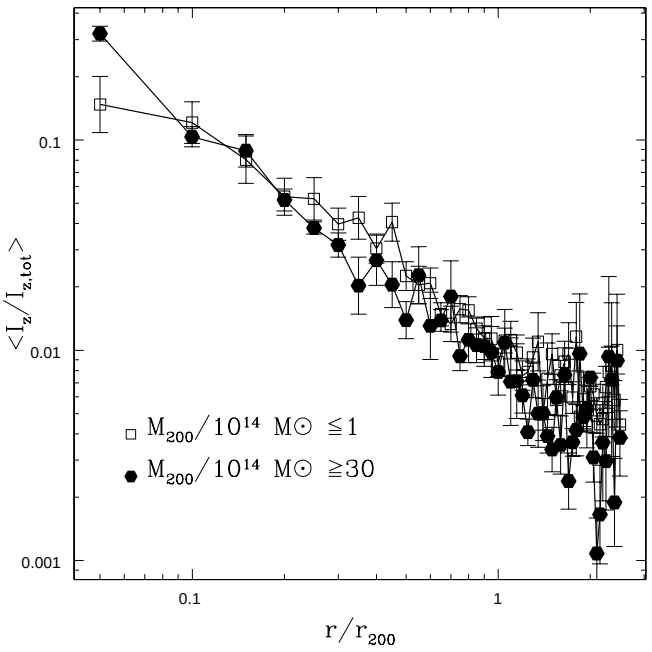

Fig. 6. Composite surface brightness profile of two cluster samples: the low mass systems at $M_{200} \leq 10^{14}\ M_{\odot}$ (empty squares) and the massive clusters at $M_{200} > 3 \times 10^{15}\ M_{\odot}$ (filled dots).

Due to the strict proportionality observed between the cluster optical luminosity and the number of cluster galaxies (see Fig. 2), it is clear that the $L_{\rm op}-M_{200}$ relation is strictly connected to the $N_{\rm gal}-M_{200}$ relation. In other words, the cluster mass-to-light ratio M/L is strictly related to the Halo Occupation Number γ of the Halo Occupation Distribution (HOD) $N \propto M^{\gamma}$. It is then useful to study the cluster M/L in terms of the HOD since this allows an easier comparison with the predictions of models of structure formation.

We study the HOD with two approaches. First we use the $N_{\rm gal}$ calculated using the photometric data ($N_{\rm phot}$), by summing the background-subtracted cluster number counts used to calculate $L_{\rm op}$. As a second approach we estimate the number of spectroscopically-confirmed cluster members ($N_{\rm spec}$). Both estimates are corrected for projection effects in the same way as we did for $L_{\rm op}$. Both $N_{\rm phot}$ and $N_{\rm spec}$ are computed down to the same absolute magnitude, in order to allow comparison of the two estimates. The SDSS spectroscopic and photometric catalogs have two different apparent magnitude limits ($r = 17.77$ for the spectroscopic catalog and $r \sim 21$ mag for the photometric one). We apply an absolute magnitude cut of $M_r \leq -20$, which allows us to sample the cluster luminosity function (LF hereafter) down to $M^* + 2$ (Popesso et al. 2005a). With such a cut, $N_{\rm spec}$ can be measured for a significant fraction of our cluster sample, those 90 clusters for which $M_r \leq -20$ is brighter than the apparent magnitude limit of $r = 17.77$.

In Fig. 10 we show the $N_{\rm gal}-M_{200}$ relation, using $N_{\rm gal} \equiv N_{\rm phot}$. We also plot the best fit relations

$$N_{\rm gal} = 10^{-11.60\pm0.59}(M_{200}/M_{\odot})^{0.91\pm0.04} \quad (7)$$

for $N_{\rm gal} \equiv N_{\rm phot}$, and

$$N_{\rm gal} = 10^{-11.43\pm0.76}(M_{200}/M_{\odot})^{0.89\pm0.05} \quad (8)$$

for $N_{\rm gal} \equiv N_{\rm spec}$. The two estimates of the halo occupation number γ are consistent, while the different normalizations reflect the incompleteness of the spectroscopic samples (see Popesso et al. 2006). The orthogonal scatter in both relations is 35%, and M_{200} can be predicted from $N_{\rm gal}$ with an accuracy of 55%.

Had we not corrected $N_{\rm gal}$ for the projection effects, we would have underestimated the slope for the $N_{\rm gal}-M_{200}$ relation, obtaining 0.79 ± 0.04. Clearly, applying an average, mass independent, correction to the observed value of $N_{\rm gal}$ and $L_{\rm op}$ leads to underestimate the slope of the considered relations.

We check also if different cluster selection techniques introduce biases in our analysis. For this purpose we perform the same analysis separately on the optically and X-ray selected cluster samples, respectively. The observed best fit values are consistent within the statistical errors. Moreover, we perform the analysis by adopting different magnitude cuts to check for vatiation of the Halo Occupation number in different magnitude regimes. We consider the following magnitude cuts: -20, -17 and -16 mag in the i band. While the normalization of the relation is obviously changing, the best fit values of the Halo Occupation number are cosistent within the errors in all the magniture ranges.

The Halo Occupation Number γ has been measured with several different methods in the literature. Most of these come from assuming a form of the HOD, and adjusting the parameters until the prediction from the halo model matches the observed galaxy clustering (e.g. Seljak et al. 2004; Peacock & Smith 2000; Yang et al. 2003; Zehavi et al. 2004; Magliocchetti & Porciani 2003). Pisani et al. (2003) used the velocity dispersion in the groups of the Zwicky catalog and obtained $\gamma = 0.70 \pm 0.04$, while Marinoni & Hudson (2002) used the LF of the Nearby Optical Galaxy sample and obtained $\gamma = 0.55 \pm 0.043$.

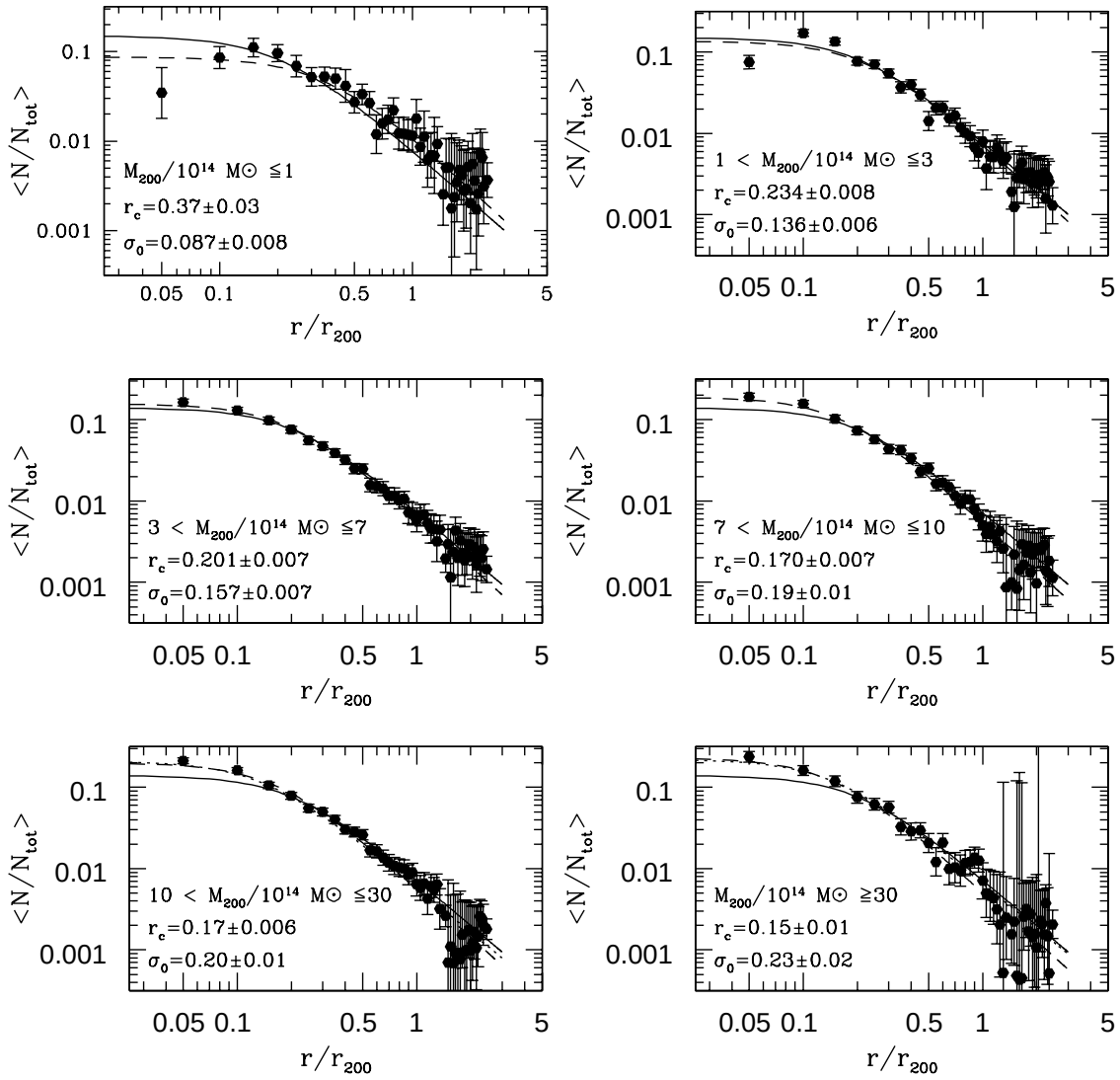

Fig. 7. The stacked surface number density profile of the *red* cluster galaxies with magnitude $r < -18.5$, separately for clusters of different masses. The meaning of the lines is the same as in Fig. 4.

Many other works in the literature used an approach similar to ours. Kochanek et al. (2003) used a sample of clusters identified in the 2MASS all sky survey, and obtained $\gamma = 1.11 \pm 0.09$ on a sample of 84 clusters. Lin et al. (2004) used a sample of 93 X-ray clusters observed in 2MASS, and found $\gamma = 0.84 \pm 0.04$. Similar results were obtained by Yang et al. (2005) who used a large sample of groups identified in the 2-degree Field Galaxy Redshift Survey.

With the exclusion of Kochanek et al. (2003), all other studies agree on the fact that the exponent in the $N-M$ relation, and consequently in the $L-M$ relation, is not consistent with unity (see Lin et al. 2004, for a discussion about the discrepancy with the results of Kochanek et al. 2003). However, with the mass-dependent correction applied to our clusters to clean the $N-M$ ($L-M$) relation from projection effects, the estimated value of γ becomes closer to unity. Nevertheless, a direct proportionality between cluster mass and number of cluster galaxies is still excluded by our analysis at the ∼2–2.5σ level.

5. Luminosity function shape and cluster mass

In this section we investigate whether the lack of galaxies observed in the high-mass systems is related to a different shape of the LFs of clusters of different masses. The universality of the cluster LF has been analysed in two papers of the RASS-SDSS Galaxy Cluster Survey Series (Popesso et al. 2005a, 2006). When measured within the cluster virial radius (r_{200}), the shape of the LF does not change from cluster to cluster both at the faint and at the bright end (Popesso et al. 2006). Moreover, we observed that the cluster to cluster variations of the LF found in the literature are due to choice of a fixed metric apertures for all the systems. This is due to the fact that fraction of dwarf galaxies in clusters is an increasing function of the clustercentric distance (see also Durret et al. 2002). To keep under control also the possible dependence between the shape of the LF and the cluster mass, we divided our cluster sample (with mass ranges from 10^{13} $M_\odot$ to 4×10^{15} $M_\odot$) in three mass bins ($M_{200}/10^{14}$ $M_\odot \leq 1$, $1 < M_{200}/10^{14}$ $M_\odot \leq 10$ and $M_{200}/10^{14}$ $M_\odot > 10$). To increase

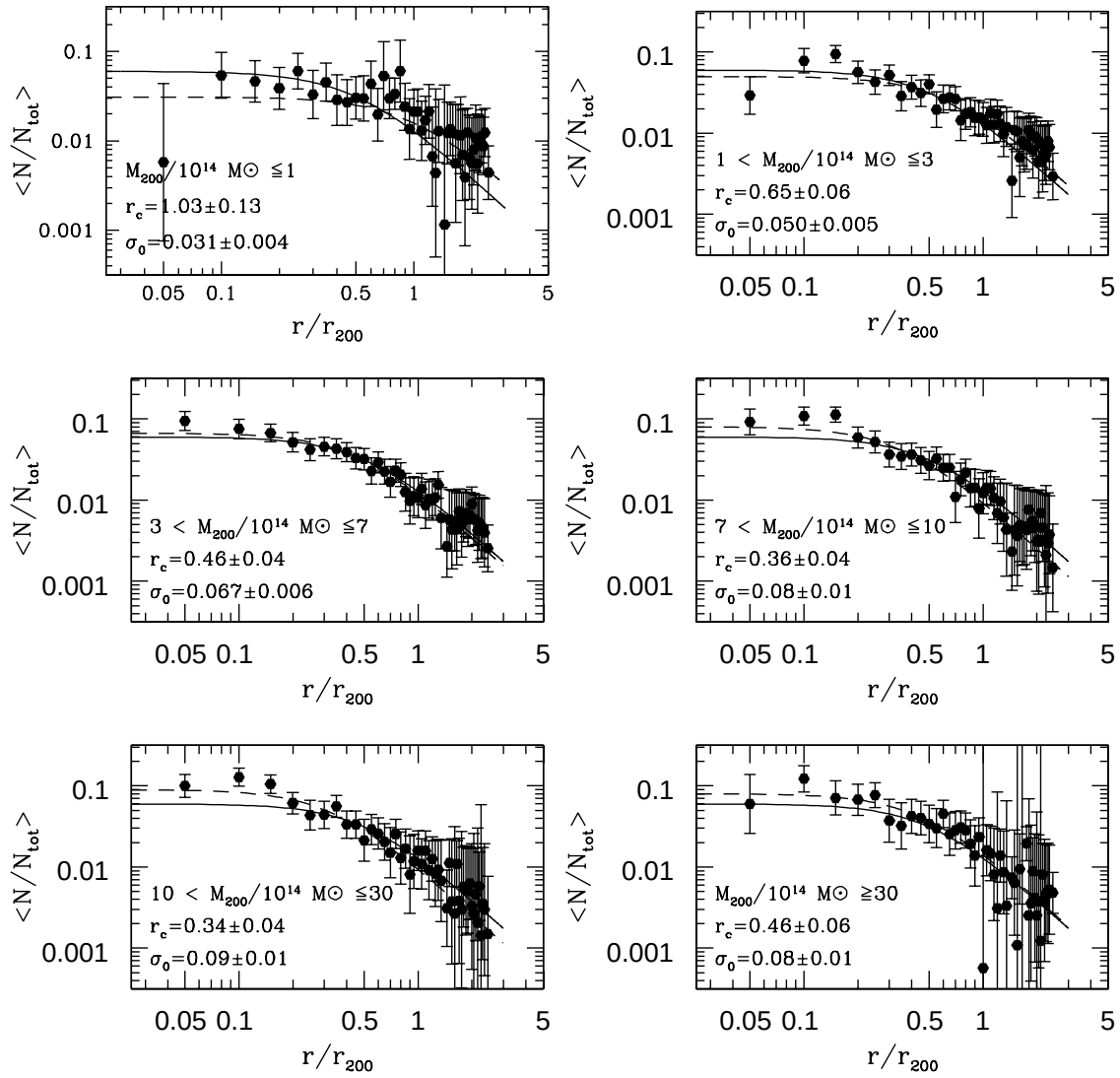

Fig. 8. The stacked surface number density profile of the *blue* cluster galaxies with magnitude $r < -18.5$, separately for clusters of different masses. The meaning of the lines is the same as in Fig. 4.

the statistics and study the average luminosity distribution of the galaxies in each mass bin, we have used the SDSS photometric data to compute a composite luminosity function (LF) by stacking the individual cluster LFs calculated within r_{200}. The individual LFs are obtained by subtracting the field number counts calculated within an annulus around the cluster (0.2 deg with), from the number counts in the cluster region, as described in Popesso et al. (2005a). Following previous works, we exclude from the individual cluster LFs the Brightest Cluster Galaxies (BCGs). The composite LF in each mass bin is calculated by following the prescriptions of Colless (1989; see also Popesso et al. 2005a for more details about this method). We require at least 10 clusters contributing to each magnitude bin of the composite LF. This requirement is fulfilled at magnitudes brighter than the absolute magnitude limit $i - 5\log(h) \leq -16.7$ mag in all the cluster mass bins considered, while 95% of our clusters have magnitude limits brighter than −18.25 mag in the i band. Thus, we consider galaxies down to 5.5 mag fainter than the cluster M^* in this SDSS band (Popesso et al. 2006). Moreover, we use the stellar masses estimated by Kauffmann et al. (2003) for the DR2 spectroscopic sample to evaluate the stellar mass range sampled within this magnitude limit. As shown in Fig. 11, although the scatter is large (0.18 dex), the magnitude cut at −16.7 mag corresponds roughly to a galaxy stellar mass of $1.5 \times 10^8\ M_\odot$. As in Sect. 3.3, we distinguish between early and late type galaxies using a SDSS color cut at $u-r = 2.22$. In Fig. 12 we show the composite LF for the whole (left panel) and the red (right panel) cluster galaxies populations. In both panel the filled points are the low-mass clusters ($M_{200}/10^{14}\ M_\odot \leq 1$), the empty squares the intermediate-mass systems ($1 < M_{200}/10^{14}\ M_\odot \leq 10$) and the empty triangles are the high-mass clusters ($M_{200}/10^{14}\ M_\odot > 10$). The different mass-bin LFs are renormalized so as to ease the comparisons among them. The solid lines in the panels are the best fits obtained in Popesso et al. (2006) from the X-ray selected RASS-SDSS galaxy clusters for the corresponding whole and red cluster galaxy populations. From Fig. 12 it is clear that,

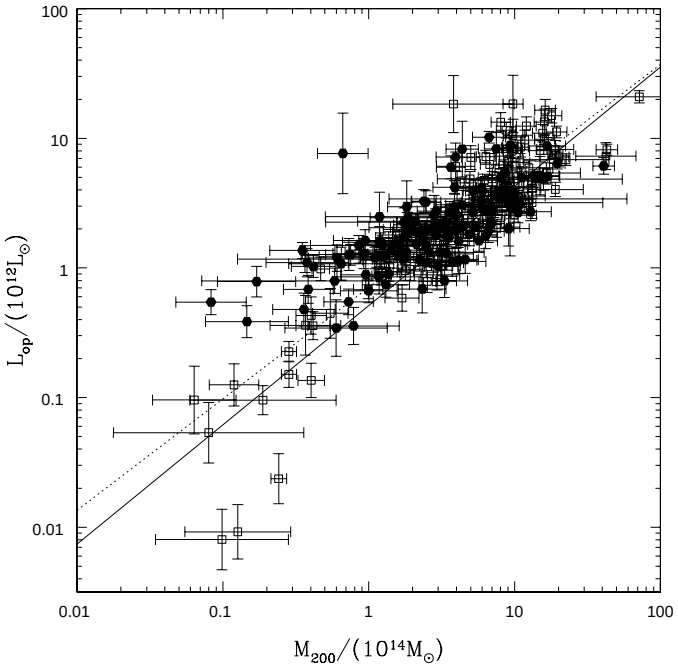

Fig. 9. $L_{op}-M_{200}$ relation. The optical luminosity is calculated within r_{200} and is corrected for contamination due to projection effect. The empty squares in the plot are the X-ray selected clusters. The filled points are the optically selected clusters. The solid line in the plot is the best fit line of the corrected $L_{op}-M_{200}$ relation. The dashed line is the best fit line of the uncorrected $L_{op}-M_{200}$ relation.

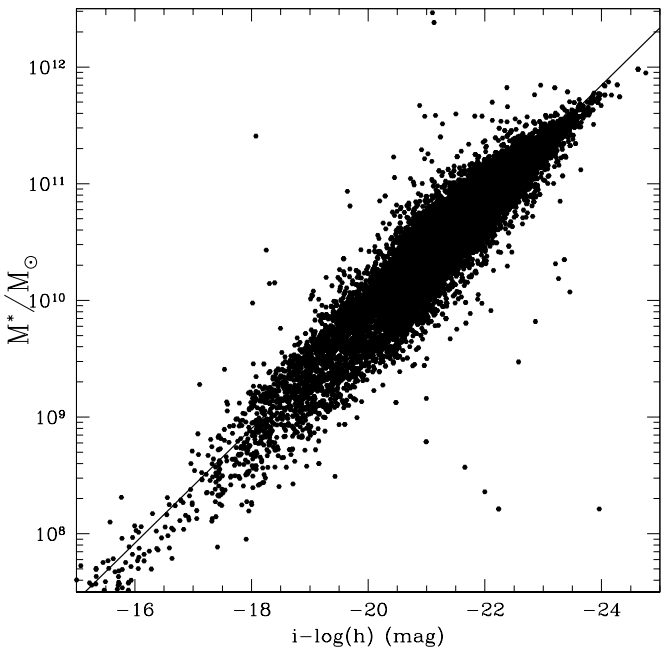

Fig. 11. Relation between the *i* band Petrosian absolute magnitude and the galaxy stellar mass. The galaxy stellar masses are taken by Kauffmann et al. (2003).

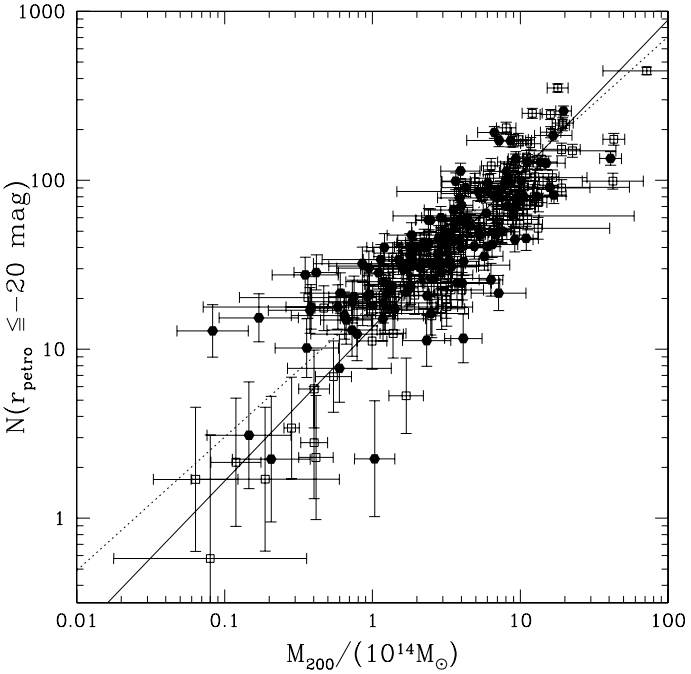

Fig. 10. $N_{gal}-M_{200}$ relation. The number of cluster galaxies is calculated within r_{200} and is corrected for contamination due to projection effect. The empty squares in the plot are the X-ray selected clusters. The filled points are the optically selected clusters. The solid line in the plot is the best fit line of the corrected $N_{gal}-M_{200}$ relation. The dashed line is the best fit line of the uncorrected $N_{gal}-M_{200}$ relation.

at magnitudes brither than −16.7 mag (alternatively, for galaxy stellar masses above 1.5×10^8 $M_{\odot}$), there are no significant differences among the LFs in the different mass bins. Moreover, the best fit of the composite LF of the X-ray selected RASS-SDSS sample provides a very good fit to any of the considered LFs. We conclude that the cluster LF does not depend on the cluster mass. This conclusion is consistent with our previous findings (Popesso et al. 2006).

The previous analysis is based on LFs with the BCGs excluded. Here we examine to what extent can the BCG luminosities be considered the high-end tail extension of the overall cluster LFs. This has been shown *not* to be the case by previous investigations (e.g. Schechter 1976; Bhavsar & Barrow 1985). The Schechter function was generally found to provide a good fit to the observed galaxy magnitude distribution as long as the very brightest galaxies, the cD galaxies, were excluded from the fit (Schechter 1976). The exceptional luminosities of these galaxies have often been interpreted as arising from special processes that are not common to all galaxies, and are particularly effective at the bottom of cluster potential wells. Nevertheless, Lugger (1986) did not find significantly different best-fits to the observed cluster galaxy LFs using Schechter functions, when BCGs were or were not included in the sample.

Following Colless (1989), we normalize the cluster LFs to the number of cluster galaxies in a common magnitude region ($r \leq -18.5$ mag in the present case, see Popesso et al. 2005a for details). Given the number of cluster galaxies in that magnitude region and the best-fit Schechter function of the composite LF, it is possible to calculate the magnitude M_r of the nth brightest cluster member as the magnitude corresponding to $N(M_r) = n$, where $N(M_r)$ is the analytical form of the cluster integral LF. For this we use the best-fit obtained with a composite of two Schechter functions, after excluding the BCGs.

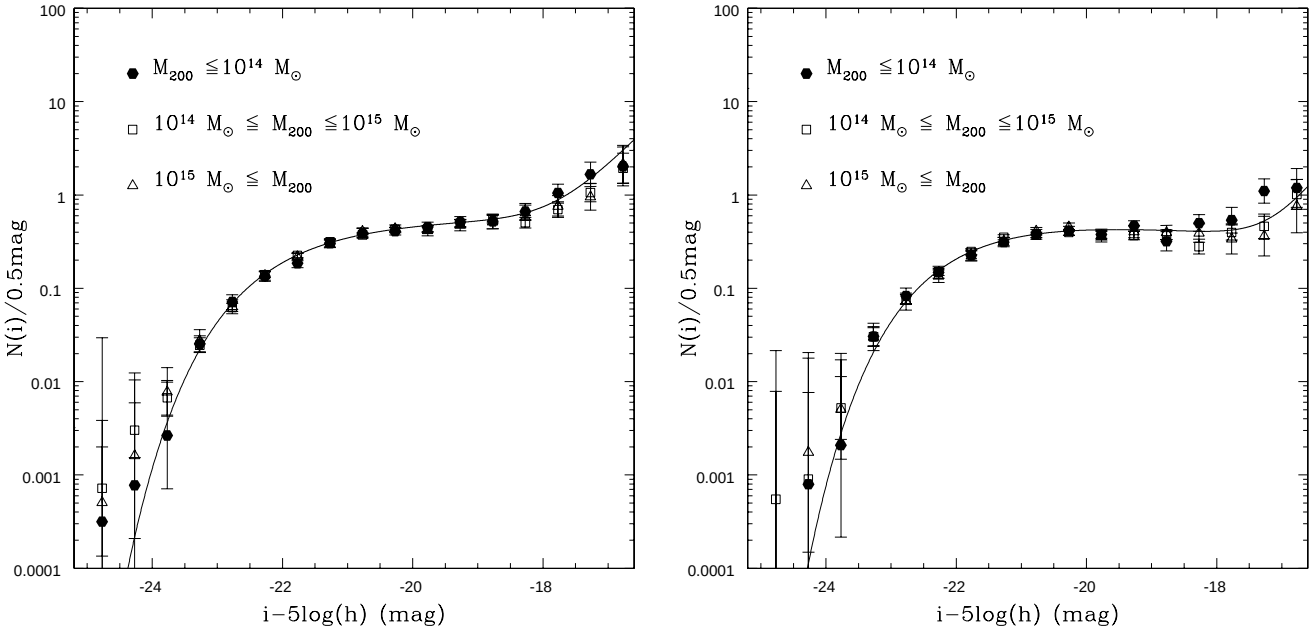

Fig. 12. The composite LF for the whole (*left panel*) and the red (*right panel*) cluster galaxy populations. In both panels the filled points are the low-mass clusters ($M_{200}/10^{14}\ M_\odot \leq 1$), the empty squares the intermediate-mass systems ($1 \leq M_{200}/10^{14}\ M_\odot \leq 10$) and the empty triangles are the high-mass clusters ($M_{200}/10^{14}\ M_\odot \geq 10$). The different mass-bin LFs are renormalized so as to ease the comparisons among them. The solid lines in the panels are the best fits obtained in Popesso et al. (2006) from the X-ray selected RASS-SDSS galaxy clusters for the corresponding whole and red cluster galaxy populations.

The left panel of Fig. 13 shows the magnitude of the brightest spectroscopically-confirmed cluster members within r_{200}, as a function of the number of cluster galaxies within r_{200} and with $r \leq -18.5$ mag. The solid line shows the expected magnitude of the brightest galaxies, as estimated from the best-fit LF, vs. the cluster normalization. The dashed line are the statistical uncertainties in the location of the brightest cluster member. Clearly, the estimated magnitudes of the 1st ranked galaxies are consistent with the observed values, as can be judged by considering the median of the 1st-ranked galaxy magnitudes per $N_{\rm gal}$ bin (filled squares in the plot), and by the fact that 95% of the BCGs lie within the statistical uncertainties of the expected relation. The middle and the right panel of Fig. 13 are similar to the left panel, but for the 2nd and 3rd brightest cluster galaxies respectively. Again, the agreement between the expected and observed magnitudes is extremely good, and the similarity of these three plots argues against the BCG magnitudes being an anomaly of the cluster LF.

The reason why our result disagrees with previous findings (Postman & Lauer 1995) must be related to the use of a double (instead of a single) Schechter function for the fit of the observed LF, which allows a better representation of the LF bright end. This was first pointed out by Biviano et al. (1995) in their study of the Coma cluster LF (see also Thompson & Gregory 1993). The deviation of the cluster LF from a single Schecter function was also found in the clusters extracted from the *N*-body simulations combined with semi-analytical models analysed by Diaferio et al. (1999). They interpreted the LF shape as the effect of the large merger cross-section of the bright and massive central galaxies.

Our result is in agreement with the recent findings of Lin & Mohr (2004) and Yang et al. (2005) of a tight correlation between the BCG luminosity and the cluster mass. In particular, in the mass range $10^{13} \leq M_{200}/M_\odot \leq 10^{15}$, $L_{\rm BCG} \propto M_{200}^{0.25}$. The excellent agreement between Lin & Mohr's result and ours is demonstrated in Fig. 14. There we show the relation between the BCG luminosity and the cluster mass of our cluster sample, where we transformed the cluster $N_{\rm gal}$ into cluster masses using the HOD we derived in Sect. 4. The solid line in the plot is the best-fit obtained with an orthogonal linear regression, $L_{\rm BCG} \propto M_{200}^{0.33\pm0.04}$, and it is in excellent agreement with the Lin & Mohr (2004) relation (the dashed line in the plot).

6. The fundamental plane of cluster ellipticals

The elliptical galaxies are the dominant population in clusters and therefore any variation of their mass-to-light ratio as a function of the cluster mass could contribute to affecting the slope of the $N-M$ and the $L-M$ relations. Thus, one could still have a constant ratio between the total cluster mass and the total mass in galaxies, even for $\gamma < 1$ (see Sect. 4), if galaxies of given luminosity have higher masses in higher-mass clusters.

To investigate whether elliptical galaxies in high mass clusters have a higher average M/L than their counterparts in low mass systems, we determine the fundamental plane (FP hereafter) of ellipticals as traced by the spectroscopic members of each cluster within r_{200}. The FP relates the effective radius of the luminosity distribution of ellipticals, $r_{\rm e}$, with their internal velocity dispersion, σ, and their surface brightness (Djorgovsky & Davis 1987). If the virial radius of ellipticals is linearly proportional to $r_{\rm e}$ and their internal velocity dispersion to the virial value, the FP effectively can be used to constrain the mass-to-light ratio of elliptical galaxies.

For this analysis, as before, we have divided our cluster sample in three subsamples of low-, intermediate-, and high-mass. Ellipticals are identified within each cluster using the selection

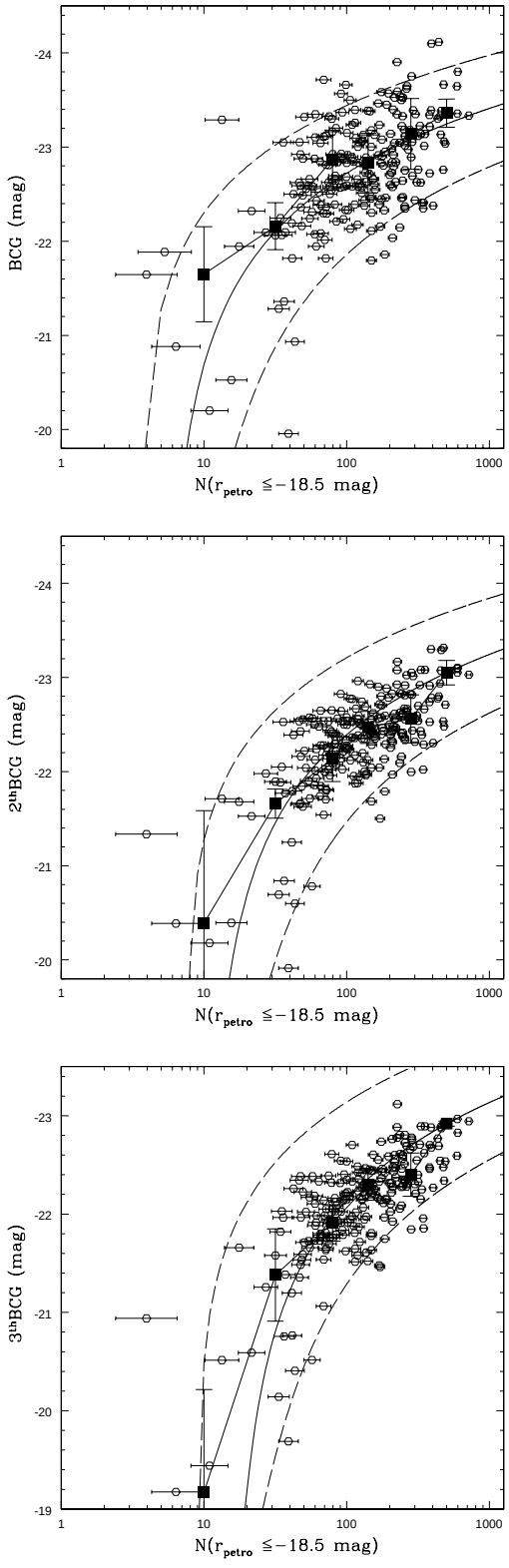

Fig. 13. *Upper panel*: the magnitude of the BCGs (empty squares) within r_{200} as a function of the number of cluster galaxies within the same radius, and with $r \leq -18.5$ mag. The solid line in the plot shows the expected BCG magnitude as estimated from the best-fitting composite LF, as a function of the cluster normalization. The dashed lines are the statistical uncertainties in the relation represented by the solid line. The filled squares are the median magnitudes per bin of $N_{\rm gal}$. *Middle panel*: same as the left panel, but for the second brightest cluster galaxies. *Bottom panel*: same as the left panel, but for the third brightest cluster galaxies.

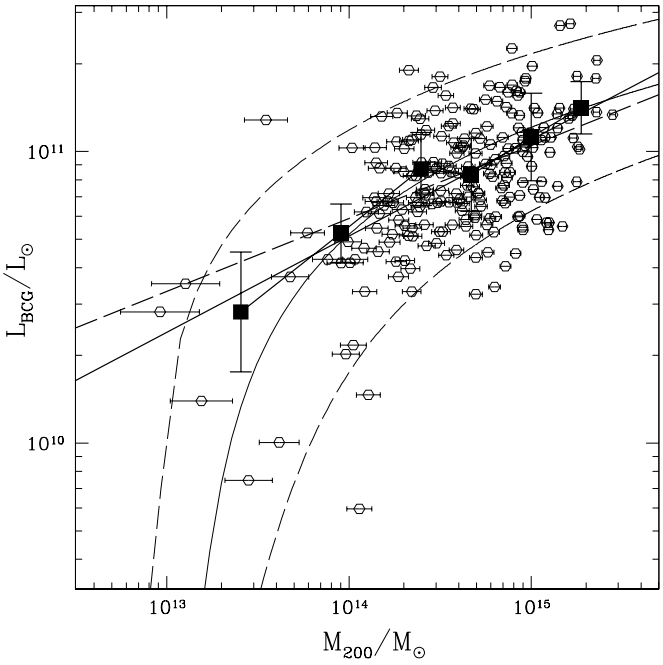

Fig. 14. The relation between BCG luminosity and cluster mass for our cluster sample. Cluster masses are computed from $N_{\rm gal}$s using our derived HOD. The solid line in the plot is the best-fit line obtained with an orthogonal linear regression, $L_{\rm BCG} \propto M_{200}^{0.33\pm0.04}$, and the dashed line is Lin & Mohr's (2004) relation. Other symbols have the same meaning as in the Fig. 13.

criteria of Bernardi et al. (2003a). As a measure of the effective radius we use the Petrosian radius r_{50}, which encloses 50% of the total Petrosian luminosity, multiplied by the square root of the ratio b/a of the lengths of the minor and major axes of the observed surface brightness profile. The SDSS spectroscopic catalog contains a measure of the line of sight velocity dispersion which has been corrected for aperture effects as in Bernardi et al. (2003a). In what follows, we show the best correlation between the variables $r_{\rm e}$, σ and $\mu = -2.5\log[(L/2)/r_{\rm e}^2]$ in the SDSS r-band. Data are fitted with the ODRPACK routine (Akritas & Bershady 1996).

The left-hand side panel of Fig. 15 shows the best-fit FP relating the three variables σ, $r_{\rm e}$ and μ; our result is consistent with Bernardi et al. (2003b). The different symbols in the plot indicate elliptical galaxies of clusters in different mass bins. We do not find any variation of the best-fit FP for the different mass samples. In the right panel of the same figure we show the mean residuals from the FP of the elliptical populations of individual clusters as a function of the cluster masses. The scatter around the FP is ∼10% as in Bernardi et al. (2003b) and the mean residual is consistent with zero independent of the cluster mass.

Any variation of the average mass-to-light ratio of the ellipticals would result in a variation of their FP. The constancy of the FP across the cluster mass range therfore implies a constant mass-to-light ratio of the cluster ellipticals.

7. Discussion

Using a large sample of galaxy clusters we have shown that the number of galaxies per unit mass is lower in clusters of higher masses, i.e. the slope of the relation $N \propto M^{\gamma}$ is $\gamma < 1$ at the 2.5σ

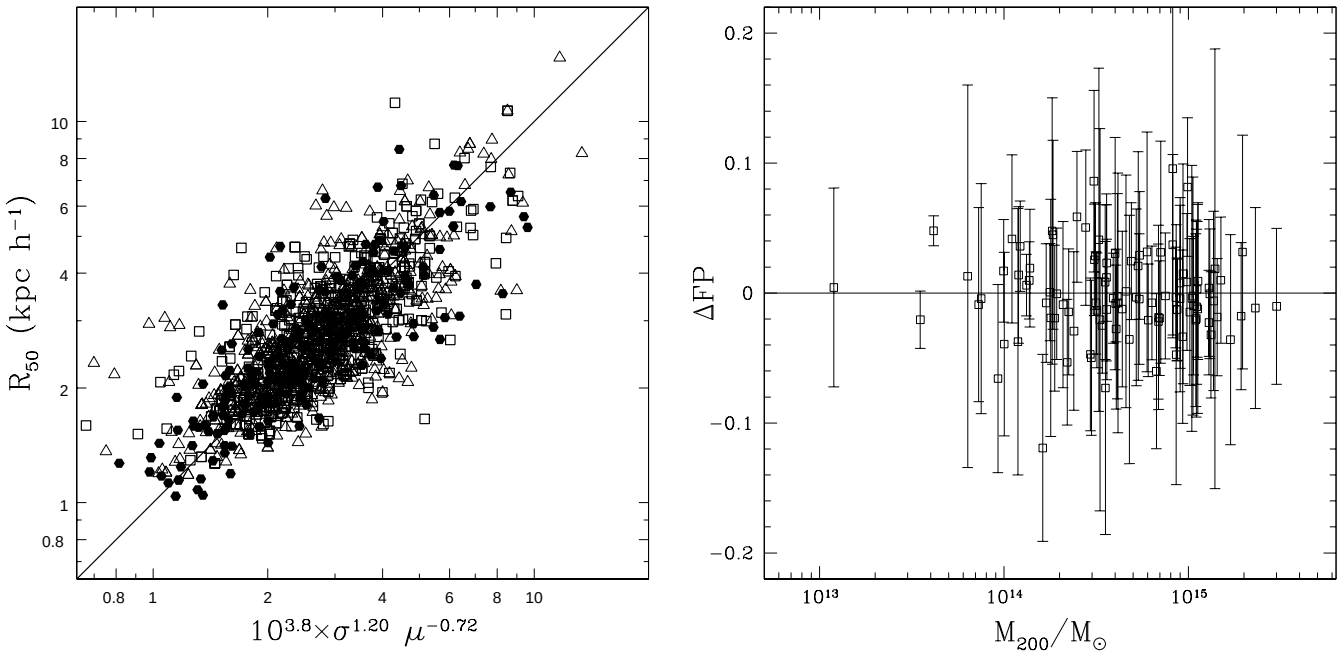

Fig. 15. *Left panel*: the best-fit FP of cluster ellipticals, relating their internal velocity dispersions (σ), effective radii (r_e), and surface brightnesses within r_e (μ). The different symbols in the plot indicate elliptical galaxies of clusters in different mass bins. The right-hand side panel shows the mean residuals from the global FP of the elliptical populations of individual clusters as a function of the cluster mass.

level. Our result is thus in agreement with previous findings (see, e.g., Lin et al. 2004, and references therein) although we find a somewhat steeper $N-M$ relation (γ closer to unity), because of our mass-dependent correction for projection effects.

From the theoretical point of view, $\gamma < 1$ is expected. On one hand, hierarchical models of structure formation predict a universal mass distributions of the subhalos (see, e.g., De Lucia et al. 2004; and Gao et al. 2004), independent of the mass of the parent halo. As a consequence, the number of subhalos is directly proportional to the parent halo mass ($N \propto M$). On the other hand, including baryons in the simulations leads to a decreasing number of galaxies per given mass in halos of higher masses (i.e. $\gamma < 1$, see, e.g., Benson et al. 2000a,b; White et al. 2001; Berlind et al. 2003), and of an increasing M/L as a function of mass (e.g. Kauffmann et al. 1999). This could happen as the consequence of a decreasing efficiency of gas cooling and star formation (see, e.g., Springel & Hernquist 2003; Berlind et al. 2003; Borgani et al. 2004; Kravtsov et al. 2004), or because of an increased merger rate (White et al. 2001), or of an increased destruction rate of galaxies (Lin et al. 2003), as the mass of the parent halo increases.

Although we observe $\gamma < 1$ as predicted, a deeper look at other properties of our clusters seems to be at odds with theoretical predictions. If mergers and/or tidal effects are responsible for reducing the number of galaxies per given mass in clusters of higher masses, we expect to see these processes to leave an imprint into the cluster LFs. Instead, we find that the LF is universal, with no dependence on the cluster mass. Our result is at odds with Lin et al. (2004). The reason for this difference is unclear, but it could be related to the different photometric bands (Lin et al. use the K-band), although it is difficult to see why the LFs of clusters of different masses should look identical in four SDSS photometric bands and different in the K-band.

Another result argues against galaxy-destruction via tidal stripping being more efficient in higher mass clusters. Higher mass clusters are characterized by a more concentrated number density profile (see Sect. 3.3) and a less concentrated mass density profile (NFW, Katgert et al. 2004; Pratt & Arnaud 2005) near the centre. If anything, this is consistent with a picture where galaxies are more likely to survive near the centre of higher mass clusters, while galaxies in lower-mass clusters are destroyed when crossing the cluster core, because of the efficient tidal stripping resulting from a more concentrated halo mass profile.

A lower efficiency of star formation in galaxies of higher mass clusters would also lead to observing $\gamma < 1$ in the HOD. A consequence of this process should be visible in a decreased M/L for the galaxies of higher mass clusters, as compared to the galaxies of lower mass clusters. We have explored this possibility by the analysis of the FP of cluster ellipticals. No evidence for a variation of the FP as a function of cluster mass was found. This result argues for a constant M/L and hence a similar star formation efficiency of cluster ellipticals in clusters of different masses, in agreement with the predictions of Diaferio et al. (2001), based on numerical simulations combined with semi-analytical models of galaxy formation. Note, however, that Springel et al. (2001) have argued that even heavily stripped cluster galaxies obey the Faber-Jackson relation, since the internal velocity dispersion of a stripped subhalo remains relatively stable until it is fully disrupted. Hence the constancy of the FP does not rule out the possibility of subhalos stripping.

Bahcall & Comerford (2002) have suggested that the observed increasing M/L of clusters as a function of cluster masses is a consequence of a higher fraction of galaxies with evolved stellar populations in higher mass clusters. There is no evidence for this in our data (Popesso et al. 2005e). Moreover, Bahcall & Comerford's prediction that M/L vs. M would become flatter

when the photometric band is moved to longer wavelengths, is also ruled out by our data, where we see that the relation does not change by changing the SDSS photometric band, in agreement with the results of numerical simulations combined with semi-analytical modelling (Kauffmann et al. 1999).

How can we, then, reconcile the observed $N - M$ with the predictions for a universal subhalo mass distribution? It is hard to find physical processes capable of reducing the number of observed galaxies per given mass, while at the same time leaving the subhalo mass distribution, the galaxy LF, and the average galaxy mass-to-light ratios unchanged. Hence, the most likely explanation is that the mass distribution of the subhalos is not universal and the observed $\gamma < 1$ for galaxies simply reflect an underlying $\gamma < 1$ for subhalos.

Our correction for projection effects does work in the sense of changing the observed γ of the $N \propto M^{\gamma}$ closer to unity. The resulting γ is still found to be below unity, but the significance of this is not overwhelming (2.5σ level). Hence it is well possible that other insofar unapplied corrections, or, perhaps, an improved correction for the projection effects, could make γ consistent with unity, thus reconciling theory and observations.

8. Conclusions

We have studied the $L-M$ and the $N-M$ relations in the 4 SDSS bands *g*, *r*, *i*, *z* for a sample of 217 galaxy clusters with confirmed 3D overdensity in the SDSS DR3 spectroscopic catalog. All the quantities are measured within the characteristic cluster radius r_{200}. We have remarked upon the direct connection between the two relations due to the proportionality of the cluster optical luminosity and the number of cluster galaxies.

We have studied the galaxy surface number density profile in five bins of cluster mass and discovered that the profile has a strong dependence on the cluster mass. In the low and intermediate mass systems the best fit is provided by a King profile. The core radius of the best fit decreases as a function of the cluster mass, while the central galaxy density increases. In the highest mass bins a more concentrated generalized King profile or a cuspy NFW profile provide the best fits. Using the best fit profile in each mass bin, we have converted the observed number of cluster galaxies to the value within the virial sphere. Since clusters of different masses exhibit different surface density profiles, the deprojection correction decreases with the cluster mass. Applying this mass-dependent correction affects the $L-M$ and $N-M$ relations, by increasing the slope of these relations to the value of 0.92 ± 0.03. Similarly, the slope of the $M/L-M$ relation also is affected and becomes 0.18 ± 0.04. Hence, neglecting the dependence of the deprojection correction on the cluster mass leads one to underestimate the slope of the $L_{\rm op}-M_{200}$ and $N_{\rm gal}-M_{200}$ relations. Despite the deprojection correction, the derived $N-M$ and the $L-M$ relations are still only marginally consistent with unity, at the 2.5σ level, i.e. direct proportionality between cluster mass and number of cluster galaxies is not supported.

We have compared the properties of our clusters with the prediction of the hierarchical models of structure formation. These models naturally predict that $N \propto M^{\gamma}$ with $\gamma < 1$. This result is generally interpreted as an indication that the galaxies in the low mass systems are older and more luminous per unit mass than the galaxies in high mass clusters. As a consequence, variations of the shape of the cluster LF and of the elliptical FP with the cluster mass are also expected. Such predicted variations are however not seen in our data. Not only we have found the LF to be the same for clusters of different masses, but we also proved that this universal LF can be used to accurately predict the magnitudes of the three brightest cluster galaxies, given the LF-normalization of the clusters in which they are located. In other words, the BCG magnitudes are consistent with being drawn from the best-fit magnitude distribution of other cluster galaxies. Moreover we have shown that the FP of cluster ellipticals has the same slope in all the clusters and does not depend on the cluster mass.

From the observational point of view, the mean cluster luminosity function and the $N-M$ or the $L-M$ relation determine completely the luminosity distribution of cluster galaxies. The mean cluster LF constrains with high accuracy the shape of the luminosity distribution in clusters, while the $N-M$ relation, calculated in a given magnitude range, fixes the normalization of the LF as a function of the cluster mass. Forthcoming cosmological models of galaxy formation should aim at reproducing this characteristic of the cluster galaxy population, in order to understand the processes of galaxy formation and evolution in the cluster enviroment.

Acknowledgements. We thank the referee, Christophe Adami, for the useful comments which helped in improving the paper. We acknowledge useful discussions with Stefano Borgani and Simon White. Funding for the creation and distribution of the SDSS Archive has been provided by the Alfred P. Sloan Foundation, the Participating Institutions, the National Aeronautics and Space Administration, the National Science Foundation, the US Despartment of Energy, the Japanese Monbukagakusho, and the Max Planck Society. The SDSS Web site is `http://www.sdss.org/`. The SDSS is managed by the Astrophysical Research Consortium (ARC) for the Participating Institutions. The Participating Institutions are The University of Chicago, Fermilab, the Institute for Advanced Study, the Japan Participation Group, The Johns Hopkins University, Los Alamos National Laboratory, the Max-Planck-Institute for Astronomy (MPIA), the Max-Planck-Institute for Astrophysics (MPA), New Mexico State University, University of Pittsburgh, Princeton University, the United States Naval Observatory, and the University of Washington.

References

Abazajian, K., Adelman, J., Agueros, M., et al. 2003, AJ, 126, 2081 (Data Release One)
Adami, C., Mazure, A., Biviano A., Katgert, P., & Rhee, G. 1998a, A&A, 331, 493
Adami, C., Mazure, A., Katgert, P., & Biviano A. 1998b, A&A, 336, 63
Adami, C., Mazure, A., Ulmer, M. P., Savine, C. 2001, A&A, 371, 11
Akritas, M. G., & Bershady, M. A. 1996, ApJ, 470, 706
Bahcall, N. A., & Comerford, J. M. 2002, ApJ, 565, L5
Bartelmann, M. 1996, A&A, 313, 697
Beers, T. C., Flynn, K., & Gebhardt 1990, AJ, 100, 32
Benson, A. J., Baugh, C. M., Cole, S., Frenk, C. S., & Lacey, C. G. 2000a, MNRAS, 316, 107
Benson, A. J., Cole, S., Frenk, C. S., Baugh, C. M., & Lacey, C. G. 2000b, MNRAS, 311, 793
Berlind, A. A., & Weinberg, D. H. 2002, ApJ, 575, 587
Berlind, A. A., Weinberg, D. H., Benson, A. J., et al. 2003, ApJ, 593, 1
Bernardi, M., Sheth, R. K., Annis, J., et al. 2003a, AJ, 125, 1817
Bernardi, M., Sheth, R. K., Annis, J., et al. 2003b, AJ, 125, 1866
Bhavsar S. P., & Barrow, J. D 1985, MNRAS, 213, 857
Biviano A., Durret F., Gerbal D., et al. 1995, A&A, 297, 610
Biviano, A., & Girardi, M. 2003, ApJ, 585, 205
Blanton, M. R., Lupton, R. H., Maley, F. M., et al. 2003, AJ, 125, 2276 (Tiling Algorithm)
Borgani, S., Murante, G., Springel, V., et al. 2004, MNRAS, 348, 1078
Carlberg, R. G., Yee, H. K., & Ellingson, E. 1997, ApJ, 478, 462
Colless, M. 1989, MNRAS, 237, 799
De Lucia, G., Kauffmann, G., Springel, V., et al. 2004, MNRAS, 348, 333
de Theije, P. A. M., Katgert, P., & van Kampen, E. 1995, MNRAS, 273, 30
Diaferio, A., Kauffmann, G., Balogh, M. L., et al. 2001, MNRAS, 323, 999
Diaferio, A., Kauffmann, G., Colberg, J. M., & White, S. D. M. 1999, MNRAS, 307, 537
Dolag, K., Bartelmann, M., Perrotta, F., et al. 2004, A&A, 416, 853
Djorgovski S., & Davis M. 1987, ApJ, 313, 59

Durret, F., Adami, C., & Lobo, C. 2002, A&A, 393, 439
Eisenstein, D. J., Annis, J., Gunn, J. E., et al. 2001, AJ, 122, 2267
Fasano, G., Pisani, A., Vio, R., & Girardi, M. 1993, ApJ, 416, 546
Fukugita, M., Ichikawa, T., & Gunn, J. E. 1996, AJ, 111, 1748
Gao, L., White, S. D. M., Jenkins, A., et al. 2004, MNRAS, 355, 819
Girardi, M., Biviano, A., Giuricin, G., et al. 1995, ApJ, 438, 527
Girardi, M., Giuricin, G., Mardirossian F., et al. 1998, ApJ, 505, 74
Girardi, M., Manzato, P., Mezzetti, M., et al. 2002, ApJ, 569, 720
Gunn, J. E., Carr, M. A., Rockosi, C. M., et al 1998, AJ, 116, 3040 (SDSS Camera)
Hogg, D. W., Finkbeiner, D. P., Schlegel, D. J., & Gunn, J. E. 2001, AJ, 122, 2129
Katgert, P., Biviano, A., & Mazure, A. 2004, ApJ, 600, 657
Kauffmann, G., Nusser, A., & Steinmetz, M. 1997, MNRAS, 286, 795
Kauffmann, G., Colberg, J. M., Diaferio, A., & White, Simon D. M. 1999, MNRAS, 303, 188
Kauffmann, G., Heckman, T. M., White, S. D. M., et al. 2003, MNRAS, 341, 33
King, I. 1962, AJ, 67, 274
Kochanek, C. S., White, M., Huchra, J., et al. 2003, ApJ, 585, 161
Kravtsov, A. V., Berlind, A. A., Wechsler, R. H., et al. 2004, ApJ, 609, 35
Lin, Y.-T., Mohr, J. J., & Stanford, S. A. 2003, ApJ, 591, 749
Lin Y. T., & Mohr J. J. 2004, ApJ, 617, 879
Lin Y. T., Mohr J. J., & Stanford, S. A. 2004, ApJ, 610, 745
Lugger, P. M. 1986, ApJ, 303, 535
Lupton, R. H., Gunn, J. E., & Szalay, A. S. 1999, AJ, 118, 1406
Lupton, R., Gunn, J. E., Ivezić, Z., et al. 2001, in Astronomical Data Analysis Software and Systems X, ed. F. R. Harnden, Jr., F. A. Primini, & H. E. Payne (San Francisco: Astr. Soc. Pac.), ASP Conf. Ser., 238, 269 [arXiv:astro-ph/0101420]
Ma, C., & Fry, J. N. 2000, ApJ, 538, L107
Magliocchetti, M., & Porciani, C. 2003, MNRAS, 346, 186
Marinoni, C., & Hudson, M. J 2002, ApJ, 569, 101
Navarro, J. F., Frenk, C. S., & White, S. D. M. 1996, ApJ, 462, 563
Navarro, J. F., Frenk, C. S., & White, S. D. M. 1997, ApJ, 490, 493
Oort, J H 1958, in La structure et l'évolution de l'univers, ed. R. Stoopes (Brussels: Solvay Inst), 163
Peacock, J. A., & Smith, R. E. 2000, MNRAS, 318, 1144
Pisani, A., Ramella, M., & Geller, M. J. 2003, AJ, 126, 1677
Plionis, M., Basilakos, S., & Tovmassian, H. M. 2004, MNRAS, 352, 1323
Popesso, P., Böhringer, H., Brinkmann J., et al. 2004, A&A, 423, 449 (Paper I)
Popesso, P., Biviano, A., Böhringer, H., et al. 2005a, A&A, 433, 415 (Paper II)
Popesso, P., Biviano, A., Böhringer, H., & Romaniello, M. 2005b, A&A, 433, 431 (Paper III)
Popesso, P., Biviano, A., Böhringer, H., & Romaniello, M. 2006, A&A, 445, 29 (Paper IV)
Popesso, P., Biviano, A., Böhringer, H., & Romaniello, M. 2007, A&A, 461, 397 (Paper V)
Postman M., & T. Lauer 1995, ApJ, 440, 28
Pratt G. W., & Arnaud M. 2005, A&A, 429, 791
Rines, K., Geller, M. J., Diaferio, A., et al. 2004, AJ, 128, 1078
Ramella, M., Boschin, W., Geller, M. J., Mahdavi, A., & Rines, K. 2004, AJ, in press [arXiv:astro-ph/0407640]
Sarazin, C. L. 1988, X-Ray Emission from Clusters of Galaxies, British Astron. Assoc. J., 98, 212
Schechter, P. 1976, ApJ, 203, 297
Scoccimarro, R., Sheth, R. K., Hui, L., et al. 2001, ApJ, 546, 20
Seljak, U. 2000, MNRAS, 318, 203
Smith, J. A., Tucker, D. L., Kent, S. M., et al. 2002, AJ, 123, 2121
Springel, V., & Hernquist, L. 2003, MNRAS, 339, 312
Springel, V., White, S. D. M., Tormen, G., & Kauffmann, G. 2001, MNRAS, 328, 726
Stoughton, C., Lupton, R. H., Bernardi, M., et al. 2002, AJ, 123, 485
Strateva, I., Ivezić, Z., Knapp, G., et al. 2001, AJ, 122, 1861
Strauss, M. A., Weinberg, D. H., Lupton, R. H., et al. 2002, AJ, 124, 1810
Tegmark, M., Strauss, M., Blanton, M., et al. 2004, PhRvD
The L. S., & White, S. D. M. 1986, AJ, 92, 1248
Thompson, L. A., & Gregory, S. A. 1993, AJ, 106, 2197
White, M., Hernquist, L., & Springel, V. 2001, ApJ, 550, 129
Yang, X., Mo, H. J., & van den Bosch, F. C. 2003, MNRAS, 339, 1057
Yasuda, N., Fukugita, M., Narayanan, V. K., et al. 2001, AJ, 122, 1104
Yoshikawa, K., Taruya, A., Jing, Y. P., & Suto, Y. 2001, ApJ, 558, 520
York, D. G., Adelman, J., Anderson, J. E., et al. 2000, AJ, 120, 1579
Zehavi, I., Weinberg, D. H., Zheng, Z., et al. 2004, ApJ, 608, 16
Zheng Z., Berlind A. A., Weinberg D. H., et al. 2005 [arXiv:astro-ph/0408564]